Numerical Methods in Contact Mechanics

To Alexandra, Andrey and Daniel

Numerical Methods in Contact Mechanics

Vladislav A. Yastrebov

Series Editor
Piotr Breitkopf

ISTE WILEY

First published 2013 in Great Britain and the United States by ISTE Ltd and John Wiley & Sons, Inc.

ISTE Ltd
27-37 St George's Road
London SW19 4EU
UK

www.iste.co.uk

John Wiley & Sons, Inc.
111 River Street
Hoboken, NJ 07030
USA

www.wiley.com

Library of Congress Control Number: 2012954082

British Library Cataloguing-in-Publication Data
A CIP record for this book is available from the British Library
ISBN: 978-1-84821-519-1

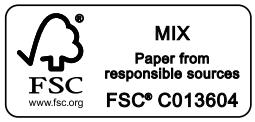

Printed and bound in Great Britain by CPI Group (UK) Ltd., Croydon, Surrey CR0 4YY

Table of Contents

Foreword xi

Preface xiii

Notations xv

Chapter 1. Introduction to Computational Contact 1

1.1. Historical remark 5
1.1.1. The augmented Lagrangian method 7
1.2. Basics of the numerical treatment of contact problems 9
1.2.1. Contact detection 9
1.2.2. Contact discretization 10
1.2.3. Contact resolution 13

Chapter 2. Geometry in Contact Mechanics 15

2.1. Introduction 15
2.2. Interaction between contacting surfaces 19
2.2.1. Some notations 19
2.2.2. Normal gap 21
2.2.3. Closest point on a surface 26
2.2.4. Closest point on a curve 28
2.2.5. Shadow-projection method 32
2.2.6. Tangential relative sliding 35
2.3. Variations of geometrical quantities 38
2.3.1. First-order variations 38
2.3.2. Second-order variations 40
2.4. Numerical validation 42
2.5. Discretized geometry 44
2.5.1. Shape functions and finite elements 44

2.5.2. Geometry of contact elements 45
2.6. Enrichment of contact geometry 51
2.6.1. Derivation of enriched quantities 53
2.6.2. Variations of geometrical quantities 58
2.6.3. Example of enrichment 65
2.6.4. Concluding remarks 68

Chapter 3. Contact Detection 71

3.1. Introduction 71
3.2. All-to-all detection 76
3.2.1. Preliminary phase 76
3.2.2. Detection phase 79
3.3. Bucket sort detection 84
3.3.1. Preliminary phase 86
3.3.2. Numerical tests 87
3.3.3. Detection phase 90
3.3.4. Multi-face contact elements 91
3.3.5. Improvements 92
3.4. Case of unknown master–slave 93
3.5. Parallel contact detection 97
3.5.1. General presentation 97
3.5.2. Single detection, multiple resolution approach 97
3.5.3. Multiple detection, multiple resolution approach 99
3.5.4. Scalability test 100
3.6. Conclusion 101

Chapter 4. Formulation of Contact Problems 103

4.1. Contact of a deformable solid with a rigid plane 103
4.1.1. Unilateral contact with a rigid plane 104
4.1.2. Interpretation of contact conditions 109
4.1.3. Friction 111
4.1.4. An analogy with plastic flow 117
4.1.5. Interpretation of frictional conditions 121
4.2. Contact of a deformable solid with an arbitrary rigid surface 124
4.2.1. Non-penetration condition 125
4.2.2. Hertz–Signorini–Moreau's contact conditions 129
4.2.3. Interpretation of contact conditions 130
4.2.4. Frictional conditions and their interpretation 132
4.2.5. Example: rheology of a one-dimensional frictional system on a sinusoidal rigid substrate 133
4.3. Contact between deformable solids 135
4.3.1. General formulation and variational inequality 135
4.3.2. Remarks on Coulomb's frictional law 142

4.4. Variational equality and resolution methods 144
4.5. Penalty method 145
4.5.1. Frictionless case 145
4.5.2. Example 148
4.5.3. Nonlinear penalty functions 151
4.5.4. Frictional case 153
4.6. Method of Lagrange multipliers 157
4.6.1. Frictionless case 158
4.6.2. Frictional case 161
4.6.3. Example 164
4.7. Augmented Lagrangian Method 170
4.7.1. Introduction 170
4.7.2. Application to contact problems 174
4.7.3. Example 183

Chapter 5. Numerical Procedures 189

5.1. Newton's method 189
5.1.1. One-dimensional Newton's method 190
5.1.2. Multidimensional Newton's method 193
5.1.3. Application to non-differentiable functions 195
5.1.4. Subdifferentials and subgradients 196
5.1.5. Generalized Newton method 200
5.2. Return mapping algorithm 203
5.3. Finite element method 210
5.3.1. Introduction 211
5.3.2. Contact elements 216
5.3.3. Discretization of the contact interface 219
5.3.4. Virtual work for discretized contact interface 220
5.3.5. Linearization of equations 223
5.3.6. Example 225
5.4. Residual vectors and tangent matrices for contact elements 225
5.4.1. Penalty method: frictionless case 226
5.4.2. Penalty method: frictional case 228
5.4.3. Augmented Lagrangian method: frictionless case 237
5.4.4. Augmented Lagrangian method: frictional case 240
5.5. Method of partial Dirichlet–Neumann boundary conditions 248
5.5.1. Description of the numerical technique 248
5.5.2. Frictionless case 250
5.5.3. Frictional case 254
5.5.4. Remarks 255
5.6. Technical details 255
5.6.1. Rigid master surface 256
5.6.2. Multi-face contact elements and smoothing techniques 257

5.6.3. Heterogeneous friction 260
5.6.4. Short remarks 261

Chapter 6. Numerical Examples 265

6.1. Two dimensional problems 265
6.1.1. Indentation by a rigid flat punch 265
6.1.2. Elastic disk embedded in an elastic bored plane 269
6.1.3. Indentation of an elastic rectangle by a circular indenter 272
6.1.4. Axisymmetric deep cup drawing 274
6.1.5. Shallow ironing 278
6.1.6. Axisymmetric post-buckling of a thin-walled cylinder 279
6.2. Three-dimensional problems 286
6.2.1. Accordion post-buckling folding of a thin-walled tube 286
6.2.2. Hydrostatic extrusion of a square plate through a circular hole . . . 288
6.2.3. Frictional sliding of a cube on a rigid plane 292

Appendix 1. Vectors, Tensors and s-Structures 297

A1.1. Fundamentals 298
A1.2. Vector space basis 303
A1.2.1. Transformation matrices, covariant and contravariant objects . . . 306
A1.2.2. Gradient operator or Hamilton's operator 308
A1.3. Sub-basis, vector function of v-scalar argument 311
A1.4. Tensors 314
A1.5. Tensor as a linear operator on vector space 322
A1.6. S-structures 325
A1.6.1. Formal definition, notations and types 327
A1.6.2. Simple operations 331
A1.6.3. Invariant s-structures 333
A1.6.4. Scalar products of v-vectors 336
A1.6.5. Inverse v-vector 341
A1.6.6. Isomorphism of s-space and tensor space 343
A1.6.7. Tensor product of v-vectors 348
A1.7. Reduced form of s-structures 349

Appendix 2. Variations of Geometrical Quantities 353

A2.1. First-order variations 353
A2.1.1. Normal projection case 354
A2.1.2. Shadow-projection case: infinitely remote emitter 356
A2.1.3. Shadow-projection case: close emitter 361

A2.2. Second-order variations 362
A2.2.1. Normal projection case 362
A2.2.2. Shadow-projection case: infinitely remote emitter 369
A2.2.3. Shadow-projection case: close emitter 370

Bibliography 375

Index 387

Foreword

The area of contact mechanics has become a vivid research field since the modeling of engineering problems has become a lot more sophisticated. This is due to the available computing power that has led to more refined models including contact constraints. This book by Vladislav Yastrebov is related to this still emerging area of contact mechanics. It starts from the basic principles and geometrical relations of contact mechanics and then moves to the essential issue, the detection of contact constraints. Here, the book includes valuable help for those who want to implement contact algorithms since the detection procedures are described in detail, including many exceptions. The formulation of contact problems, again, provides many insights into the complex contact behavior and gives a complete overview with respect to frictionless and frictional contact. This is also true for the chapter that describes the numerical procedures for contact problems. These are discussed in detail and well presented such that the reader will understand the different approaches that can be applied to solve nonlinear contact.

The book will be useful as an introduction to contact mechanics and related algorithms for graduate students who have the necessary background in mathematics and continuum mechanics. However, the book is also a reliable and comprehensive source for researchers who are interested in implementing algorithms and discretization schemes for the solution of nonlinear contact problems. Last but not least, design engineers from industry can use this book as background information for contact analyses related to, e.g. forming, forging and other problems that involve contact and friction.

Prof. Dr. Ing. Peter WRIGGERS

December 2012
Institute of Continuum Mechanics
Leibniz Universität
Hannover

Preface

Nowadays, contact and friction are particularly important for our civilization. Think, for example, about car brakes, wheel–rail contact, assembled pieces in engines and turbines, bearings and gears in mechanical devices and electromechanical contacts. Numerical simulations permit us to study and improve these complex systems involving contact, friction and wear. This book answers the question of what is behind these simulations and uncovers for readers the underlying machinery of the finite element analysis in contact mechanics.

Regardless of the prevalence of contact and friction, these phenomena are hard to study experimentally because of their multiscale/multiphysical nature and the inaccessibility of contact interfaces to direct observations. Likewise, these problems are challenging for numerical treatment due to the particularity of contact and friction conditions and complexity of involved algorithms. Moreover, the mathematics and non-trivial notions introduced in this branch of computational mechanics are hard to comprehend for beginners. Thus, the first motivation of this book is to introduce new people to this field. The second motivation is to expose all involved components of computational contact in its integrity and interconnection: geometry, detection and resolution. And finally, I would like to expose some original developments in computational contact mechanics.

I address this book to students, engineers and researchers who solve contact problems by means of the finite element method. Also, I am aiming at developers wishing to implement or improve contact algorithms in their commercial or in-house finite element software. To make the book accessible to people unfamiliar with basics of the computational contact, I shall introduce all terms and notions and give many examples. For all developments in contact geometry I used a new tensor algebra, so some effort are needed from the reader to “get used to it”. But I believe that for readers familiar with programming, this novelty should not present a difficulty, because the main concept is transparent – array of arrays.

Contact algorithms are rich in details that are seemingly negligible but are crucial for the robustness and accuracy of the code. So, based on our experience, I made an attempt to expose most of them. Furthermore, as the implementation of contact algorithms is delicate (both for contact detection and resolution steps), it requires an extended validation and testing. For that purpose, I standardized and exposed many tests from the literature and suggested some new ones.

I hope that this book will introduce new people to the field of computational contact mechanics and that the ideas expressed here will engender the development of new methods and approaches to make the simulation of contact more reliable and accurate.

This book would not be possible without the help and encouragement of Georges Cailletaud, Frédéric Feyel and the financial support of CNRS and SNECMA, which I gratefully acknowledge. I express my thanks to my dear wife Alexandra, my sons, Andrey and Daniel, my parents and my brother for their love, patience and comprehension. I am grateful to my colleagues Djamel Missoum-Benziane and Nikolay Osipov for their constant support, help and friendship. I also acknowledge André Pineau, Jacques Besson and Samuel Forest for creating a stimulating scientific atmosphere. I thank also Liliane Locicero, Konaly Sar, Odile Adam, and Anne Piant for their permanent administrative help, empathy and friendly attention.

Vladislav A. YASTREBOV

Centre des Matériaux
MINES ParisTech
Evry
December 2012

Notations

Vectors and tensors

– *Scalar* (zero-order tensor) – small Latin and Greek letters:

$$a, \alpha, b, \ldots$$

– *Vector* (first-order tensor) – underlined small bold Latin and Greek letters:

$$\underline{\boldsymbol{c}}, \underline{\boldsymbol{\beta}}, \underline{\boldsymbol{d}}, \ldots$$

– *Second-order tensor* – capital bold Latin letters underlined twice:

$$\underline{\underline{\boldsymbol{E}}}, \underline{\underline{\boldsymbol{F}}}, \ldots$$

– *Higher order tensor* – capital bold Latin letters underlined twice with upper left index of order:

$$^{3}\underline{\underline{\boldsymbol{G}}}, \; ^{4}\underline{\underline{\boldsymbol{H}}}, \ldots$$

V-Vectors and V-tensors

– *V-scalar* (“vector of scalars”) – small Latin and Greek letters underlined by a wave:

$$\underset{\sim}{\mathrm{i}}, \underset{\sim}{\gamma}, \cdots \in {}^{m}_{1}\mathbb{S}^{n}_{0}$$

– *V-vector* (“vector of vectors”) – small Latin and Greek letters underlined by a line and a wave:

$$\underline{\underset{\sim}{\boldsymbol{j}}}, \underline{\underset{\sim}{\boldsymbol{\varepsilon}}}, \cdots \in {}^{m}_{1}\mathbb{S}^{n}_{1}$$

– *V-tensor* ("vector of tensors") – capital bold Latin letters underlined by a double line and a wave:

$$\underset{\sim}{\underline{\boldsymbol{K}}}, \underset{\sim}{\underline{\boldsymbol{L}}}, \cdots \in {}^{m}_{1}\mathbb{S}^{n}_{2}$$

T-Vectors and T-tensors

– *T-scalar* ("tensor of scalars") – capital bold Latin letter underlined by a double wave:

$$\underset{\approx}{\mathrm{M}}, \underset{\approx}{\mathrm{N}}, \cdots \in {}^{m}_{2}\mathbb{S}^{n}_{0}$$

– *T-vector* ("tensor of vectors") – small Latin and Greek letters underlined by a line and a double wave:

$$\underset{\approx}{\underline{\boldsymbol{o}}}, \underset{\approx}{\underline{\boldsymbol{\eta}}}, \cdots \in {}^{m}_{2}\mathbb{S}^{n}_{1}$$

– *T-tensor* ("tensor of tensors") – capital bold Latin letters underlined by a double line and a double wave:

$$\underset{\approx}{\underline{\underline{\boldsymbol{P}}}}, \underset{\approx}{\underline{\underline{\boldsymbol{Q}}}}, \cdots \in {}^{m}_{2}\mathbb{S}^{n}_{2}$$

Vector and tensor operations

– $\| \underline{\boldsymbol{a}} \|$: Euclidean norm of a vector;

– $\det \underline{\underline{\boldsymbol{A}}}$: determinant of a tensor;

– $\underline{\underline{\boldsymbol{I}}}$: unit tensor;

– $\underset{\approx}{\mathrm{I}}$: unit t-scalar;

– $\mathrm{tr}\underline{\underline{\boldsymbol{A}}}$: trace of a tensor;

– $\underline{\underline{\boldsymbol{A}}}^{-1}$: inverse of a tensor;

– $\underline{\underline{\boldsymbol{A}}}^{T}$: transpose of a tensor;

– ${}^{i}\underline{\underline{\boldsymbol{A}}} \cdot {}^{j}\underline{\underline{\boldsymbol{B}}} = {}^{i+j-2}\underline{\underline{\boldsymbol{C}}}$: scalar or dot product;

– ${}^{i}\underline{\underline{\boldsymbol{A}}} \times {}^{j}\underline{\underline{\boldsymbol{B}}} = {}^{i+j-1}\underline{\underline{\boldsymbol{C}}}$: vector or cross product;

– $\overset{i}{\underline{\underline{\boldsymbol{A}}}} \otimes \overset{j}{\underline{\underline{\boldsymbol{B}}}} = \overset{i}{\underline{\underline{\boldsymbol{A}}}}\overset{j}{\underline{\underline{\boldsymbol{B}}}} = \overset{i+j}{\underline{\underline{\boldsymbol{C}}}}$: tensor product;

– $\overset{i}{\underline{\underline{\boldsymbol{A}}}} \cdot \cdot \overset{j}{\underline{\underline{\boldsymbol{B}}}} = \overset{i+j-4}{\underline{\underline{\boldsymbol{C}}}}$: tensor contraction.

Other operations

– $(\bullet)^{\cdot} = \frac{d\bullet}{dt}$: full time derivative;

– $\delta(\bullet),\ \Delta(\bullet)$: first variations;

– $\bar{\delta}(\bullet),\ \bar{\Delta}(\bullet)$: full first variations;

– $\Delta\delta(\bullet)$: second variation;

– $\bar{\Delta}\bar{\delta}(\bullet)$: full second variation;

– $\nabla \otimes (\bullet)$: gradient;

– $\nabla \cdot (\bullet)$: divergence;

– $\nabla \times (\bullet)$: rotor.

Miscellaneous

– δ_i^j: Kronecker's delta $\delta_i^j = 1$, if $i = j$ else $\delta_i^j = 0$;

– $\langle x \rangle = \frac{1}{2}(x + |x|)$: Macaulay brackets;

– $[\bullet,\ \bullet];\ (\bullet,\ \bullet);\ (\bullet,\ \bullet]$: closed, open, open-closed intervals;

– $\forall$, $\exists$, $\exists!$, $\exists!!$, $\nexists$: for all, exists, exists only one, exists infinitely many, does not exist;

– $\Rightarrow$, $\Leftarrow$, $\Leftrightarrow$: sufficient, necessary, sufficient and necessary conditions;

– $\min$, $\max$, ext, $\sup$, $\inf$: minimum, maximum, extremum, supremum, infimum;

– $\widetilde{\min}$, $\widetilde{\max}$: global minimum, global maximum;

– $i = 1, n$: i changes from 1 to n.

Abbreviations

– PM: penalty method;

– LMM: Lagrange multiplier method;

– ALM: augmented Lagrangian method;

– FEM: finite element method;

– FEA: finite element analysis;

– CAD: computer-aided design;

– NTN: node-to-node;

– NTS: node-to-segment discretizations;

– MPC: multi-point constraints;

– PDN: partial dirichlet–neumann;

– SDMR: single detection multiple resolution;

– MDMR: multiple detection multiple resolution.

Remark. Macaulay brackets, dist$(.,.)$ and $\theta(.)$ functions.

Throughout the book, we use the notation of Macaulay brackets.

$$\langle x\rangle = \begin{cases} x, & x \geq 0, \\ 0, & x < 0 \end{cases}; \qquad \langle -x\rangle = \begin{cases} -x, & x \leq 0, \\ 0, & x > 0 \end{cases}$$

The θ function is a similar notation widely used in both engineering and mathematical literature:

$$\theta(x) = \max(x,0) = \begin{cases} x, & x \geq 0, \\ 0, & x < 0 \end{cases}; \quad \theta(-x) = \min(x,0) = \begin{cases} -x, & x \leq 0, \\ 0, & x > 0 \end{cases}$$

or a more general dist$(,)$ function:

$$dist(x,\Omega) = \begin{cases} dist(x,\partial\Omega), & x \notin \Omega \\ 0, & x \in \Omega, \end{cases}$$

where $dist(x,\partial\Omega)$ is a somehow defined distance from point x to the closure of the set Ω. For example, in the simplest case $\Omega = \mathbb{R}_-$, $x \in \mathbb{R}$, then $\partial\mathbb{R}_- = 0$:

$$dist(x,\mathbb{R}_-) = \begin{cases} x, & x \geq 0, \\ 0, & x < 0 \end{cases}; \qquad dist(x,\mathbb{R}_+) = \begin{cases} -x, & x \leq 0, \\ 0, & x > 0. \end{cases}$$

All these functions are equivalent for the considered case and interchangeable, so the reader is invited to interpret the Macaulay brackets as one of the above-mentioned functions to which he/she is more accustomed.

Chapter 1

Introduction to Computational Contact

From a mechanical point of view, at macroscopic scale, contact is the notion for the interaction between bodies coming in to touch and exchanging load and energy (heat and electric charge). The physics of contact – rich and complex – is hard to study because of its multiscale and multiphysical nature and also because of the contact zone's inaccessibility for direct observations[1]. Both experimental and numerical investigations of the contact experience difficulties. Tribology is an experimental science that describes and characterizes the contact, adhesion, friction, wear and lubrification as well as the involved mechanical, physical and chemical effects at different scales. Mathematics formalizes these descriptions by some measurable quantities (the coefficient of friction, the real contact area, the heat transfer coefficient, etc.). On the basis of observations, we suggest some models for the evolution of these quantities and then integrate them in complete numerical models to study particular systems at a common basis. The simulations thus imply strong simplifications[2] that may be crucial for their validity. On the other hand, even the simplest models appear complicated for numerical simulations both from mathematical and programming points of view. All together, the oversimplification of the phenomenon and the imperfect implementation of established models may easily lead to incorrect results. The aim of this book is to resolve some of these problems, provide a consistent basis for the numerical treatment of contact problems at all stages, avoid unnecessary simplifications and enhance existing numerical models. The book focuses on the mechanics of contact and its numerical treatment by the

1 The contact zone is visible only if one of the contact bodies is transparent.

2 Sometimes these simplifications result from the limited computer resources or programming skills, so may be partly avoided in many cases.

finite element method (FEM). The underlying physics and mathematics are covered only partly and superficially[3].

We suppose that the reader is unfamiliar with this field, so from the very beginning we provide the reader with the vocabulary and all the basic notions of computational contact mechanics. Many notions are very technical and complex, so we explain them in many ways throughout the book[4] and often enhance these explanation with figures and examples. The material covers three subjects: geometry, detection and resolution. However, these parts are hard to comprehend independently. To ensure the readability of the book, this chapter introduces the subject, provides the global context of the numerical treatment and briefly discusses every component.

Contact problems in mechanics of deformable solids can be singled out into a particular class. First, they imply a discontinuity: the contact occurs at the interface between two *separate* continuous bodies. Second, the contact constraints at this interface cannot be replaced by ordinary boundary conditions imposed on both the contacting surfaces. Third, the contact interface itself cannot be simply considered as an internal surface. In an idealized case, the contact interface is a zero thickness layer, which sustains only compressive stress in the direction orthogonal to the contact interface (Figure 1.1(a)); any stretching leads to the vanishing of the contact interface (Figure 1.1(b)). In the case of frictionless contact, the contact interface contrary to an ordinary internal surface, does not sustain any tangential efforts, which allows two solids to slide relative to each other (Figure 1.1(a)). In the case of frictional contact, things become more complex. For example, in case of the classic Coulomb's friction law, in stick state, the contact interface under pressure is similar to an internal interface – no separation, no sliding – locally both surfaces remain glued to each other (Figure 1.1(c)). However, if locally we reach a critical shear stress, the surfaces start to slip relatively to each other (Figure 1.1(d)). It follows from this simple representation that the contribution of the contact interface to the energy of the system is always zero except in the case of frictional slip.

Many mechanical problems can be formulated as boundary value problems, where governing differential equations should be fulfilled within the domain Ω under ordinary boundary conditions imposed on its closure $\partial\Omega$. This formulation is called the *strong form*. By writing the balance of virtual works, we obtain a *weak (integral) form* of this boundary value problem. This weak form presents a basis on which the structural FEM is constructed. Contact constraints are formulated as sets of

3 We refer the reader interested in the physics and mechanics of contact to [RAB 65, BOW 50]; and those who prefer to gain a solid mathematical basis to [KIK 88].

4 It implies some repetitions and reformulations of all the notions, which hopefully will help the reader to better visualize them.

inequalities, which are not trivial to incorporate in the weak form. The rigorous construction leads to a *variational inequality* instead of a classical weak form formulated as a *variational equality*. This new mathematical structure requires new solution approaches. The problem becomes even more complex when we introduce a friction. Coulomb's friction law states that tangential resistance depends upon the normal contact pressure that is known only if the solution is known. Roughly speaking, the boundary conditions depend on the solution, which naturally leads to difficulties in the formulation of the frictional contact problem. Moreover, the Coulomb's friction law yields a non-smooth energy functional making the problem even more difficult from a numerical point of view. In summary:

> *"Frictional contact problem between continuous deformable solids involves formidable mathematical difficulties."*
>
> N. Kikuchi and J.T. Oden [KIK 88]

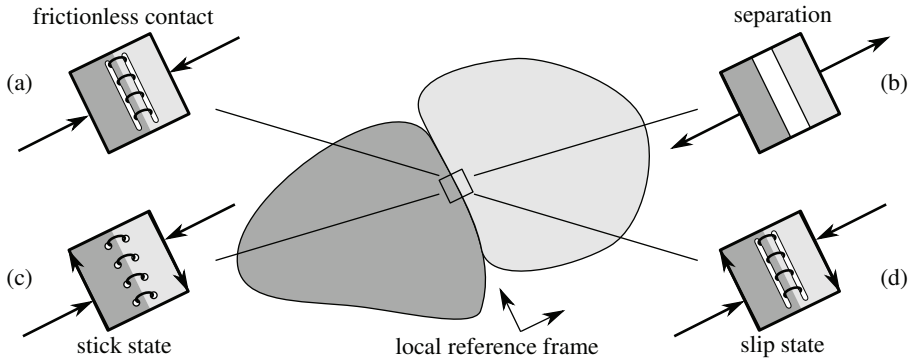

Figure 1.1. *Analogy between contact and internal interfaces: (a) frictionless contact sustains compressive stress in the local reference frame, (b) any stretching leads to the vanishing of contact interface, (c) frictional contact interface can transfer shear stress, (d) in Coulomb's friction law, in stick state there is no relative sliding up to reaching a critical shear stress*

Another mathematical difficulty in contact mechanics arises from a rigorous description of continuous interacting surfaces. First, contacting bodies may penetrate each other or be separated: in both cases, a one-to-one correspondence between points of the contacting surfaces does not always exist. Second, the finite element discretization renders only piecewise-smooth surfaces, which leads to mathematical and numerical difficulties. Third, a considerable effort has to be undertaken to find variations of the weak form, which requires second-order variations of the normal

gap and the tangential sliding, which is not an easy task. We need a basic knowledge of the differential geometry to obtain the relevant quantities.

The discretization of the contact interface[5] is the third challenge in computational contact mechanics. A simple and stable *node-to-node* (NTN) discretization for conforming meshes[6] can be established only in the case of small deformations and infinitely small relative sliding. A less simple but multipurpose *node-to-segment* (NTS) *discretization* implies the creation of contact pairs consisting of a node belonging to one surface and a corresponding segment of another surface. However, this discretization does not fulfill the so called Babuška–Brezzi conditions and leads to an unstable discretization. It means, for example, that a uniform contact pressure cannot be obtained at the interface between non-matching meshes. Recently, new techniques based on *segment-to-segment* (STS) *discretizations – Nitsche* and *mortar methods* – have been successfully introduced in computational contact mechanics; however, the computer implementation of these methods for a general case presents a challenge both from algorithmic and technical points of view. Seeking for a stable and relatively simple contact discretization is still in progress.

All aforementioned difficulties are related to the resolution phase of the contact algorithm. This phase follows the detection that determines the contacting pairs on discretized surfaces. At first glance, the contact detection phase is a standalone task, but in reality it appears to be strongly connected with the contact discretization, the definition of the gap and with the type of contact (e.g. simple contact or self-contact). The detection may present a bottleneck for the numerical treatment of contact problems both in terms of rapidity and robustness. The contact detection becomes one of the crucial points for an efficient parallelization of the whole resolution scheme. Elaboration and implementation of an efficient contact detection algorithm is an absolute necessity for a robust and fast finite element analysis (FEA) of large contact problems.

First, we make a short historical remark on contact and computational contact mechanics. In the coming sections, we present the general concept of contact treatment in the framework of the FEM and implicit integration. To provide the reader with a general understanding of the numerical treatment, we expose, here, in a first approximation, the contact detection, contact discretization and contact resolution.

---

5 By contact discretization or discretization of the contact interface we mean the establishment of contact elements over which the transferred forces are transmitted. Even though two contacting surfaces are already discretized, there are different ways to discretize the interface between them.

6 By *conforming* or *matching* meshes we understand a situation where each node on one contacting surface matches a corresponding node on another surface.

1.1. Historical remark

Modern contact mechanics is about 130 years old. It started in 1882 with the publication of Hertz's famous paper *On the Contact of Elastic Solids* [HER 82], which gives the solution for frictionless contact between two ellipsoidal bodies. This problem came from the optical interference between glass lenses. Further developments in contact theory appear only at the beginning of 20^{th} Century in application to railways, reduction gears and rolling contact bearings. Progress in contact mechanics was associated with removing the restrictions of the Hertz theory: linear elasticity, frictionless contact and small deformations. The Russian school of mechanicians, starting from Galin [GAL 53, GAL 76] and Muskhelishvili [MUS 66], made a significant contribution to this development. A synthesis of analytical solutions and approaches for contact problems can be found, for example, in monographs by [LUR 70, ALE 83, JOH 94, GOR 98, GOR 01, VOR 01].

Since the analytical solution is achievable only for a few simple geometries, boundary conditions and mostly for linear materials, it can only provide rough approximations for complex industrial contact problems, which include complex geometries, friction, wear, adhesion, large deformations and nonlinear materials. More powerful tools are needed to fulfill the industrial demand for a fast and accurate solution of these problems.

Since 1965 (NASTRAN), the FEM becomes one of the most usable and efficient tools for the treatment of problems in structural mechanics. To answer the requirements from industry, the scientific community worked out a rigorous mathematical framework valid for incorporation of the contact in the FEM, which required formidable efforts from mathematicians and mechanicians. First, the frictionless Signorini's problem (unilateral contact between a deformable body and a rigid foundation) has been treated, further the developed approaches were extended to the case of unilateral frictional contact in small and large deformations and finally to bilateral[7] or multibody contact. At the same time, engineering practice tested the solution schemes and proposed new challenging tasks. The work on an accurate and reliable method to treat large-sliding frictional contact is still in progress.

The history of computational contact began in 1933 with the works of Signorini. He was the first who formulated the general problem of the equilibrium of a linearly elastic body in frictionless contact with a rigid foundation [SIG 33, SIG 59]. The works of Fichera represent the first treatment of the questions of existence and uniqueness of the solution of *variational inequalities* arising from the minimization of functionals on convex subsets of Banach spaces, which yields from his rigorous

7 *Bilateral* contact – contact between two or more deformable solids, in contrast to *unilateral* contact – contact between a deformable and a rigid solid.

analysis of a class of Signorini's problems [FIC 63, FIC 64, FIC 72]. Variational inequality is a new structure in the field of optimization theory; new approaches are required to use such a formulation for practical problems in physics and mechanics. "Inequalities in mechanics and physics" by Duvaut and Lions (first published in French and translated in English [DUV 76]) was a scientific breakthrough in this direction, the authors investigated the solution of frictional contact problems and large deformation contact. Among the early relevant contributions, we can enumerate Cocu [COC 84], Panagiotopoulos [PAN 85] and Rabier *et al.* [RAB 86]. A consistent description of the variational inequality approach to contact problems is given in the book by Kikuchi and Oden [KIK 88], where among other important results the existence and uniqueness of the solution of Signorini's problem is proven. The questions of stability of contact problem's solution were discussed by Klarbring [KLA 88]; the examples of non-uniqueness or non-existence were demonstrated by Klarbring [KLA 90] and by Martins *et al.* [MAR 94]. The existence and uniqueness results for dynamic contact problems can be found in Martins and Oden [MAR 87], Jarusek and Eck [JAR 99] and others.

The *frictionless* contact problem formulated as a variational inequality presents a special type of minimization problem with inequality constraints, which can be efficiently treated in a standard manner (penalty method (PM), Lagrange multiplier method (LMM), augmented Lagrangian method (ALM)). Unfortunately, there is no associated minimization principle for the *frictional* contact problem [KIK 88, MIJ 00]. Such a problem is complicated and unusual for optimization theory as the energy of the system (objective function in optimization) depends on the frictional status, which in turn depends on the normal contact pressure, which itself depends on the displacements, finally the energy depends on the solution of the problem, which is unknown. As there is no smooth energy functional associated with the frictional contact problem, its formulation and resolution present real challenges.

The assumption of a known *a priori* contact interface on the current computational step results in a reformulation of the variational inequality into a variational equality problem with a special contact term; the form of this term depends on the method chosen to enforce the contact constraints. Among the well-known and widely used methods, there are barrier and penalty methods, LMMs and their combinations. Another branch of methods makes use of different techniques from mathematical programming: application of the simplex method to contact problems can be found in [CHA 76], parametric quadratic programming method is used in [KLA 86, ZHO 88]. Separately from these two branches, there is a group of direct methods, which treats the contact problem independently from the structural problem. The *flexibility method* proposed by Francavilla and Zienkiewicz [FRA 75] and modified and improved by Jean [JEA 95] is rarely mentioned in the scientific literature on computational contact. In practice [WRO 94], this method demonstrates a higher robustness and rapidity in

comparison to ordinary methods if the number of nodes in contact remains moderate. But it is not applicable for large contact problems and the parallelization of the method is hardly possible. A complete list of methods used for the numerical treatment of contact problems can be found in [WRI 06, LAU 02].

1.1.1. *The augmented Lagrangian method*

As mentioned in the previous section, the assumption of a known *a priori* contact surface allows us to replace the variational inequality by a variational equality with an additional contact term. The form of this contact term depends upon the choice of the optimization method; the most usable in contact mechanics are the LMM, the linear PM and an ALM, the two latter methods are implemented in leading modern FEA softwares: ANSYS [BHA 02, OAT 07, ANS 05], ABAQUS [ABA 07], COMSOL [COM 10] and others. In this chapter, all aforementioned methods are considered, but particular attention is paid to the ALM, possessing several advantages in comparison to other methods.

Within the framework of classical LMM, contact conditions are exactly satisfied by the introduction of extra degrees of freedom (dof) called Lagrange multipliers. The constrained minimization problem converts into an unconstrained saddle point problem often called the min–max problem. Because of inequality constraints, this formulation has to be considered in combination with an active set strategy [LUE 03, MUR 88], that is a check and update of active and passive constraints should be integrated in the convergence loop. Moreover, the additional dof of the LMM introduce supplementary computational efforts. PM is simple to implement and interpret from the physical point of view, but, on the other hand, the contact conditions are fulfilled exactly only in case of the infinite penalty parameter that results in ill-conditioning of the numerical problem. The ALM is a sort of Lagrange multiplier formulation regularized by penalty functions. It yields a smooth energy functional and fully unconstrained problem, resulting in exact fulfillment of contact constraints with a finite value of the penalty parameter. In this section, a few historical remarks concerning the ALM are given. For a more detailed background, the reader is referred to the articles and books cited below.

The ALM has been proposed in the first raw approximation by Arrow and Solow in 1958 [ARR 58b]. Further a more elaborated version of the ALM method for optimization problems subjected to equality constraints has been independently proposed by Hestenes [HES 69] and Powell [POW 69] in 1969. As mentioned by Pietrzak [PIE 97], it was proposed “rather in an intuitive way” and a lot of questions have not been considered. The way to apply the ALM method to optimization problems with inequality constraints has been developed by Rockafellar [ROC 70, ROC 73b] and Wierzbick [WIE 71].

Using the ALM as well as the LMM leads to the saddle point problem, that is the objective function is to be minimized by "ordinary" primal variables (e.g. displacement dof in the displacement-based FEM) and is to be maximized by dual variables – Lagrange multipliers that represent contact stresses. All aforementioned authors approach this min–max (saddle point) problem by an independent consecutive updating of the primal and dual dof. An algebraic formula is used to update the Lagrange multipliers at each iteration step and consequently a standard minimization procedure is used to update the primal dof. This idea has been worked out by Powell [POW 69]. Nowadays such an approach is used under the name of Uzawa's algorithm and the full method is referred to as a nested augmented Lagrangian algorithm. Another approach has been developed by Fletcher [FLE 70]. It consists of a continuous minimization of the resulting saddle problem with a simultaneous update of both primal and dual variables.

One of the first applications of the ALM to frictionless contact problem can be found in Glowinski and Le Tallec [GLO 89] and Wriggers, Simo and Taylor [MID 85]. The first application of the ALM with Uzawa's algorithm to frictional problems has been reported by Simo and Laursen [SIM 92]. The first successful attempt to apply the coupled ALM to frictional contact problems has been undertaken by Alart [ALA 88], and Alart and Curnier [ALA 91]. The augmented Lagrangian approach has been elaborated by developing the perturbation approach to convex minimization as proposed in [ROC 70] and first applied by Fortin [FOR 76] to visco-plastic flow problems (rather similar to frictional contact problems).

Further developments of the ALM method to large deformations, large sliding and nonlinear materials can be found in [HEE 93, MIJ 04a, MIJ 04b], etc. A comprehensive investigation on the implementation of the ALM method in the framework of the FEM to large deformation frictional contact problems has been carried out by Pietrzak and Curnier [PIE 97, PIE 99]. The attempts to work out a technique for penalty parameter updating are worth mentioning, since it became a crucial factor for convergence of the ALM. A direction was proposed in early works [HES 69] and [POW 69]. The need was mentioned by Rockafellar [ROC 73b], discussed in [ALA 97] and an approach has been proposed by Mijar and Arora [MIJ 04a, MIJ 04b]; another phenomenological approach has been proposed in [BUS 09]. An early attempt to parallelize the ALM has been undertaken by Barboteu [BAR 99] for particular structures.

The ALM combines advantages of both methods LMM and PM and avoids their drawbacks, it converges precisely to the exact solution for a finite value of the penalty coefficient and if a nested update of dual variables is used, there are almost no additional computational efforts. Following Pietrzak, we would like to emphasis the smoothing effect of the ALM, which is not the only advantage over ordinary LMM. Even in the case of a smooth objective function, the ALM method shows its superiority. The ordinary LMM does not fully reduce the optimization problem with inequality constraints to an unconstrained problem, since the condition of positivity

of the Lagrange multipliers $\lambda \geq 0$ has to be satisfied. The ALM method does not have this restriction and therefore is better for practical use. An elaborated presentation of the method will be given in section 4.7.

1.2. Basics of the numerical treatment of contact problems

A finite element code – capable of treating contact problems – should include the following steps: detection of contact, construction and update of "contact elements", their incorporation in associated residual vectors and tangential matrices and finally resolution of the resulting problem. Here, we give basic ideas and a general view of these steps, which will be presented in detail in the corresponding chapters.

Contact elements[8] are a sort of "bridge elements" between locally separated but potentially interacting bodies. Each contact element contains components (nodes, edges, faces) of both surfaces; the composition of these components depends upon the *contact discretization* method. Besides structural dof contact element may have their proper dof. These unknowns and the structure of the residual vector and the tangential matrix are determined by the *resolution method*. For example, in addition to primal or structural dof (e.g. displacements) contact elements may contain dual dof (Lagrange multipliers) representing contact forces.

The *contact detection* is a step preceding all others. The aim of this step is to create contact elements containing the proximal components of both surfaces that *may* come into contact during the current solution step. Thus, the detection is an algorithmic task that relies on the search for the closest components. The criterion of proximity is either provided by the user or is chosen automatically based on boundary conditions and/or discretization of contacting surfaces. If we use an *implicit integration*, then to incorporate contact elements in the resolution cycle, they should be created before a contact occurs and if needed should be removed and recreated at each solution step. In the case of *explicit integration*, generally, the searching step should ensure only the detection of already occurred penetrations.

1.2.1. *Contact detection*

The development of numerical methods and the increasing demands on complexity (large deformation/sliding, self-contact, remeshing) and size of problems

8 Contact elements are similar to ordinary structural finite elements in the way that they are assembled with the latter in the global residual vector and the global tangential matrix. But their elemental residual vectors and the tangential matrices are very different from structural elements; normally, contact elements do not need shape functions and they are not visualized in the graphical user interface; also they are generally created and removed "on flight" during the solution.

in computational contact mechanics entail the progress in contact detection techniques. Construction of an efficient technique, which is based on the notion of proximity, presents a purely algorithmic problem and depends upon the contact discretization. For example, in the case of NTN discretization, the contact detection consists simply of establishing close pairs of nodes: nodes of one surface form pairs with their closest opponents from another surface. As the NTN discretization is limited to small deformations and slidings, once created contact pairs do not change during the solution steps. NTS discretization requires a more elaborated detection procedure: for nodes of one surface (slave), we have to find the closest point on another surface (master), the master segment possessing this point complemented by the slave node forms an NTS contact element.

This simple detection procedure contains several difficulties. First, the detection of the closest point on the master segments may be ambiguous if the slave node is not sufficiently close to the master surface or if the latter is not smooth – the case of finite element discretization of the surface. The numerical scheme of the closest point detection is based on the looking for a minimum of the distance function, but on the one hand this minimum does not always exist, and on the other hand there may be several or infinitely many minimum points. Second, the detection has to be organized in a smart way. Large contact problems imply a large number of contacting nodes on both surfaces, that is why a simple detection technique, based on a comparison of distances from each slave node to all components of the master surface, leads to an excessive time consumption, especially if contact elements must be frequently updated.

STS discretization requires totally different detection algorithms based on surface topologies. In this book, we confine ourself to consideration of the NTS contact discretization, so we omit the detection for other discretizations. In Chapter 2, we discuss the geometrical aspects of the closest point search and in Chapter 3, the detection algorithms.

1.2.2. *Contact discretization*

The contact discretization predetermines the structure of contact elements that transfer efforts from one contacting surface to another. We distinguish three types of discretization:

– Node-to-node (NTN);

– Node-to-segment, (NTS);

– Segment-to-segment, (STS).

The simplest and the oldest NTN discretization [FRA 75] introduces restrictions on mesh generation and does not permit any finite sliding or large deformations (see

Figure 1.2(a)). But it passes the contact patch test [TAY 91] – contact pressure is transferred correctly through the conforming contact interface. The NTN discretization is applicable for linear and quadratic elements in the two-dimensional case and to linear elements in the three-dimensional case. The NTN technique smoothes the asymmetry between contacting surfaces. However, the normal vector for each pair of nodes is usually determined[9] according to one of the surfaces.

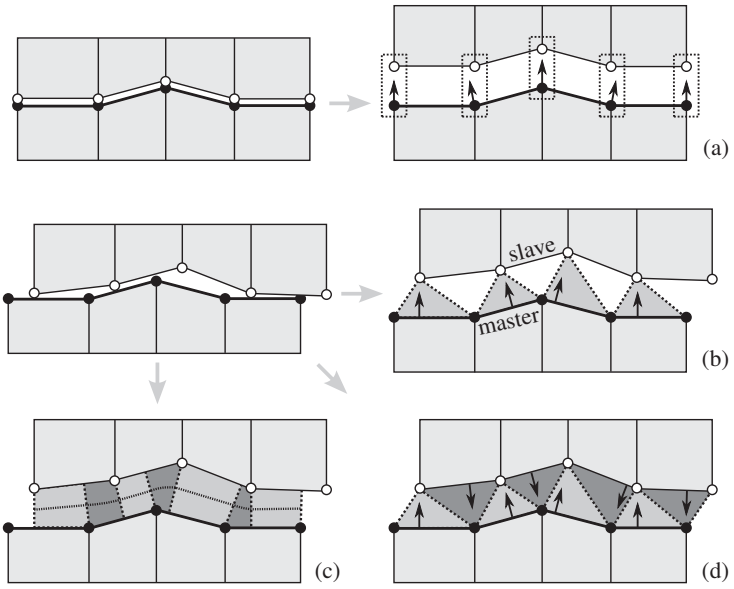

Figure 1.2. *Graphical representation of different contact discretizations: for small deformations/sliding (a) node-to-node, associated pairs of nodes and normals; for large deformations/slidings (b) node-to-segment, slave nodes and associated master segments; (c) segment-to-segment, contact elements and intermediate integration line; (d) contact domain discretization, contact elements*

NTS (Figure 1.2(b)) is a multipurpose discretization technique [HUG 77], valid for non-conforming meshes and large deformations/sliding. But this discretization is not stable and does not pass the contact patch test [TAY 91] for non-conforming meshes – a uniform contact pressure cannot be transferred correctly through the contact interface. This drawback can be omitted in the method of Lagrange multipliers using a "two-pass" technique [HAL 85], which means that at each solution step both surfaces serve as slave and master to create two layers of contact

9 Different possibilities of normal definition are presented in remark 3.2 in section 3.4.

elements. However, it may lead to locking problems [KIK 88]. A comprehensive discussion of the contact patch test for NTS discretizations can be found in [CRI 00c], where a new approach combining linear and quadratic shape functions is also suggested. Recently, a modification of the NTS discretization has been proposed for the PM [ZAV 09a], which also passes the patch test. Besides these drawbacks, the NTS discretization is simple and robust. Contact detection and resolution techniques that we present in this book are suitable for this discretization.

Another technique *contact domain method* proposed in [OLI 09, HAR 09] is based on a symmetric NTS discretization and contact element shape functions. The discretization of the contact interface is based on a full triangulation of the zone between contacting surfaces based on surface nodes (Figure 1.2(c)). This formulation seems to be rather stable and passes the patch test, but its three-dimensional implementation reported in [OLI 10] is not applicable for arbitrary discretizations of the contacting surfaces.

STS discretization (Figure 1.2(d)) has been first proposed by Simo *et al.* [SIM 85] for the two-dimensional case (see also [ZAV 98]). Recently such a discretization has been efficiently applied to two- and three-dimensional problems coupled with the *mortar method* for non-conforming meshes, inspired by the domain decomposition methods [WOH 01]. This technique is stable and passes the patch test but its implementation for a general case presents a great challenge, "a nightmare", according to Tod A. Laursen, one of the authors of the mortar method's implementation for both two- and three-dimensional structural and contact problems [PUS 03, PUS 04, YAN 05, YAN 08b, MCD 00]. A standalone discretization technique is needed for the *Nitsche* method [BEC 03, WRI 08], the Gauss points of one surface play the role of slave nodes. The comparison of Nitsche and mortar techniques can be found in [FRI 04].

The basic idea of the mortar method appeared in the second half of the 1980s and in the beginning of the 1990s for domain decomposition techniques between non-conforming subdomains, see, for example, [BER 90]. In 1998, Belgacem *et al.* [BEL 98] adapted the mortar method for the multibody (bilateral) frictionless contact problem. Further at the beginning of 2000s, the rigorous formulation adapted to the frictional contact problem subjected to large deformations/slidings has been established by McDevitt and Laursen [MCD 00]. The mortar method consists of either introducing an intermediate contact surface, where contact pressure is defined, or using one of the contacting surfaces as mortar surface, for details see [WRI 06]. The mortar-based formulation leads to a consistent formulation of the frictional contact problem for large sliding and large deformations. It allows us to pass the contact patch test for non-conforming meshes and, contrary to the NTS, does not suffer from locking and spurious penetrations.

1.2.3. *Contact resolution*

The rigorous formulation of a variational principle for contact problems results in a variational inequality subjected to geometrical constraints [KIK 88]. These constraints can be brought as additional terms in the weak form by means of PM, LMM or other optimization methods [BER 84, BER 03, LUE 03, BON 06], etc. Such an operation converts the constrained optimization problem, where constraints are given as inequalities, into an unconstrained or partly unconstrained problem. If we suppose the active contact zone to be known, then the variational inequality can be replaced by a variational equality, which finally results in an unconstrained problem written in a standard form of variational equality [WRI 06]. This problem can be treated as a standard nonlinear minimization problem by the means available in a finite element code. A solver for systems of linear equations and a method for the treatment of nonlinear problems are needed. Note that since the contact constraints are given as inequalities, a special attention has to be paid to the definition of the active contact zone. For PM and ALM, this task is trivial. For the LMM, an active set strategy should be used (e.g. see, [LUE 03]).

The resulting unconstrained minimization problem is not sufficiently smooth, which may result in a slow convergence or even divergence of the resolution scheme. The stability of the numerical scheme depends upon the discretization and on the solution parameters. The frictional contact renders a non-symmetric tangent matrix, which presents a problem for several solvers (like conjugate gradient method) and for the parallel treatment of the problem: the Schwarz theory for non-symmetric problems is less satisfactory than for positive definite symmetric problems [TOS 05]. The way out has been proposed in [LAU 92, LAU 93] for ALM with Uzawa's algorithm – governing equations of Coulomb's friction have been linearized by the operator splitting technique, first recognized in [GLO 89], where is the entire problem is recast in two subproblems, that are solved once at each solution step. ALM and LMM derive non-symmetric tangent matrices only for the slip state. This is due to the non-associativity of Coulomb's friction law, that is slip occurs in the plane of the constant contact pressure. The PM suffers from a non-symmetry both in stick and slip states. A solution has been proposed in [WRI 06], which consists of a similar treatment of normal and tangential deviations from the stick state. Another approach yielding a symmetric tangent matrix in stick state has been proposed in [KON 05], based on a rigorous covariant description of the contact geometry. The same author proposed a symmetrization of different friction models based on the ALM coupled with Uzawa's algorithm [KON 07b].

Chapter 2

Geometry in Contact Mechanics

2.1. Introduction

Contact phenomenon takes place at the interface between solids. This fact implies a strong connection of the contact problem with a geometrical description of contacting surfaces. The first continuum-based description of the contact problem, valid for a numerical treatment, was given by Laursen and Simo [LAU 93] and Laursen [LAU 94]. Such a geometrical description still presents an interesting topic for research in computational contact mechanics, see; for example, recent articles by Konyukhov and Schweizerhof [KON 06a, KON 06b, KON 09]. The mathematical formulation of frictionless contact conditions leads to equations connecting the *contact pressure* σ_n with the *mutual penetration* of bodies, expressed by a signed *gap function*; frequently a *normal gap* function g_n is used. The formulation of frictional contact leads to the connection between *shear or tangential contact stress vector* $\underline{\boldsymbol{\sigma}}_t$ and the *relative tangential sliding velocity* $\underline{\boldsymbol{v}}_t$. The contact stresses have to be integrated over the *contact surface* Γ_c^i of each solid, where the lower index denotes the solid's ID.

Let us show how the geometrical description may predetermine methods and approaches that are used in the numerical treatment of contact. The first problem, which we usually encounter, is an ambiguity in the definition of the normal gap between contacting surfaces. It seems easy to determine the normal gap for each point of one surface as a distance to the closest point of another surface: for a point M of the first surface ∂A we look for the closest point N on the other surface ∂B. Three problems arise from such a definition:

P1. *Asymmetry of the gap (Figure 2.1(a))*
If instead of looking for the closest point $N \in \partial B$ to the point $M \in \partial A$, we invert the problem and search for the point $M' \in \partial A$ closest to the $N \in \partial B$, then the points M and M' do not coincide as soon as the contacting surfaces are not parallel at least locally or if they are not in contact. It means that there is no one-to-one correspondence between surface points. It implies an asymmetry in the gap function and consequently in the entire geometrical description.

P2. *Non-uniqueness of the closest point (Figure 2.1(b))*
For example, the center of a circle does not have a single closest point on the circle, but all the points on the circle are equally close to its center. All other points have a unique closest point on the circle. The uniqueness of the closest point refers to the curvature of the considered curve or surface and has been discussed in detail by Heergaard and Curnier [HEE 96] Pietrzak [PIE 97] and Konyukhov and Schweizerhof [KON 08]. The limit case of an infinite curvature leads to the third problem.

P3. *Requirement of smoothness (Figure 2.1(c))*
The smoothness of at least one of the contacting surfaces (master) is not sufficient but is a necessary condition for the existence of the normal projection[1]. Smooth surfaces allow a rigorous mathematical description of contact, a robust detection procedure and a reliable convergence of numerical schemes. However, surfaces in the finite element framework are only piecewise-smooth due to the discretization.

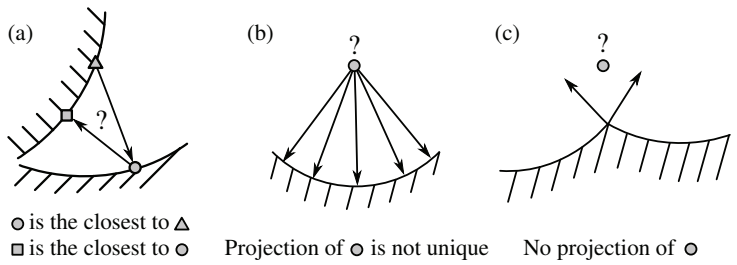

Figure 2.1. *Geometry-related problems: (a) asymmetry of the closest point definition; (b) non-uniqueness of the closest point; (c) non-existence of the normal projection point*

1 Normal projection $\underline{\boldsymbol{p}}$ of a point $\underline{\boldsymbol{r}}_s$ on a surface is a point at which the normal vector is collinear to the vector $\underline{\boldsymbol{r}}_s - \underline{\boldsymbol{p}}$.

All these difficulties affect the geometrical description of the contact. The asymmetry of the closest point detection (P1) results in an asymmetric treatment of contact surfaces, which leads to the so-called "master–slave" approach (also called "target-impactor" or "target-contactor"). For each point of the slave surface $\underline{\boldsymbol{r}}_i \in \Gamma_s$, the closest point on the master surface $\underline{\boldsymbol{\rho}}_i \in \Gamma_m$ has to be determined, that is:

$$\underline{\boldsymbol{\rho}}_i = \left\{ \underline{\boldsymbol{\rho}}_i \in \Gamma_m \;\middle|\; \forall \underline{\boldsymbol{\rho}} \in \Gamma_m \;:\; \|\underline{\boldsymbol{\rho}}_i - \underline{\boldsymbol{r}}_i\| \leq \|\underline{\boldsymbol{\rho}} - \underline{\boldsymbol{r}}_i\| \right\}$$

The problem of non-uniqueness (P2) is not so important for the detection, as it is improbable to have several equivalently close points. The non-uniqueness may present a problem for the convergence. So instead of using a normal projection, we can use a different projection fulfilling the conditions on the uniqueness and continuity (see section 2.2.5). That allows us to improve the convergence and to avoid non-physical discontinuities in the sliding path, which is crucial for a rigorous description of frictional contact.

The non-smoothness of the surface (P3) results in multiple closest points and generates blind angles in normal projection domains, which renders the detection procedure complex. Also, it engenders a discontinuous normal-vector field and, as a result, oscillations and possible divergence of the numerical solution. The main remedy consists of smoothing the master surface over several segments [PIE 97, WRI 01, KRS 02].

These revealed difficulties demonstrate the need in a well-founded geometrical approach for an accurate treatment of contact problems. As the definition of the closest point is closely connected with the contact detection (see Chapter 3), many results obtained in this chapter will be used for the establishment of reliable detection techniques.

The aim of this chapter is as an elaborated analysis of geometry-related questions in computational contact mechanics in the framework of the FEM and the node-to-segment (NTS) discretization. To provide a multipurpose framework independent of the finite element discretization, we start from a *continuous description* of the contact geometry. Such an approach is valid for NTS discretization (any order of finite elements and arbitrary shape functions), for *smoothed* or enriched master surface and for *unilateral* contact, where the contact surface may be given analytically or via a computer-aided design (CAD) model [HAN 90, HEE 96] For many reasons, it is advantageous to replace a piecewise-smooth master by a globally C^1-smooth surface based on information from several adjacent master segments. This procedure ensures a continuous projection on the master surface and leads to a better convergence [PIE 97, PAD 01, PUS 02, WRI 01, KRS 02, WRI 06, CHA 04]. All smoothing procedures (NURBS, Bézier, Gregory patches, etc.) enrich the geometry and require an adapted geometrical description, which can be easily

derived from the continuous description given here. The unilateral contact normally demonstrate a better convergence than a *bilateral* contact[2] and has many applications in engineering: metal forming and metal processing, rubber–metal and tire–road contact, etc.

Our geometrical description is confined to the interaction between a point (slave) and a surface (master), which is well adapted to the NTS contact discretization. We introduce the key geometrical quantities: the gap g and the tangential sliding velocity $\underline{\boldsymbol{v}}_t$. Complementarily, we give a rigorous definition of the closest point and introduce a new technique, which renders a continuous and unique projection of a slave point onto non-smooth surfaces.

The next section discusses the incorporation of contact terms into the weak form arising from the application of the principle of virtual works in the finite element method (FEM). To include the contribution of the contact interface into the balance of virtual works, we need variations of geometrical quantities – gap g and tangential relative slip $\underline{\boldsymbol{v}}_t$:

$$\delta g, \quad \delta \underline{\boldsymbol{v}}_t$$

The resulting equation is nonlinear, and thus we need its linearized form to obtain an approximative solution using Newton's method. For that purpose, the second variations of these geometrical quantities are needed:

$$\Delta\delta g, \quad \Delta\delta \underline{\boldsymbol{v}}_t$$

We compute these values in sections 2.3.1 and 2.3.2 for continuous geometry and we adapt them for the FEM in section 2.5.

Initially, the geometrical variations were obtained for particular finite element discretizations in [PAR 89]; they can also be found in a recent book [WRI 06]. Laursen and Simo [LAU 93] established a new standard in computational contact mechanics by deriving all equations in continuous form, which can then be easily applied to any discretization of the contact interface and different element types. Different forms of these expressions can be found, for example, in [PIE 97, PIE 99]. Simplified expressions using the assumption of a zero normal gap can be found in [KON 05]. Here, we obtain all required variations without any assumption.

2 By a *unilateral* contact we mean a contact between a rigid surface and a deformable solid; a *bilateral* or *many-body* contact implies a contact between deformable solids.

Moreover, we use a new mathematical formalism that simplifies some derivatives (see Appendix 1). We derive all the expressions needed for two projection types: the classical normal projection and the original shadow-projection. Section 2.6 introduces a new concept – enrichment of the contact geometry – which is used for simulating wear and contact between solids with complex submesh geometries.

2.2. Interaction between contacting surfaces

2.2.1. *Some notations*

– Time: t

– Radius vector of the slave point: $\underline{\boldsymbol{r}}_s = \underline{\boldsymbol{r}}_s(t) \in \Gamma_s$

– Master-surface parametrization by v-scalar:

$$\underset{\sim}{\xi} = \underset{\sim}{\xi}(t) \sim \begin{bmatrix} \xi_1(t) \\ \xi_2(t) \end{bmatrix}$$

– Surface coordinates of the slave point's projection onto the master surface:

$$\underset{\sim}{\xi}_\pi = \underset{\sim}{\xi}_\pi(t)$$

– Radius vector of the slave point's projection onto the master surface:

$$\underline{\boldsymbol{\rho}} = \underline{\boldsymbol{\rho}}(t, \underset{\sim}{\xi}_\pi) \in \Gamma_m$$

– v-Vector of covariant tangential vectors on the surface (covariant surface basis at the projection point):

$$\nabla_{\underset{\sim}{\xi}} \underline{\boldsymbol{\rho}}(t, \underset{\sim}{\xi}_\pi) = \left. \frac{\partial \underline{\boldsymbol{\rho}}}{\partial \underset{\sim}{\xi}} \right|_{\underset{\sim}{\xi}_\pi} \sim \begin{bmatrix} \frac{\partial \underline{\boldsymbol{\rho}}}{\partial \xi_1} \\ \frac{\partial \underline{\boldsymbol{\rho}}}{\partial \xi_2} \end{bmatrix}$$

– v-Vector of contravariant tangential basis vectors on the surface (contravariant surface basis at the projection point):

$$\overline{\frac{\partial \underline{\boldsymbol{\rho}}}{\partial \underset{\sim}{\xi}}} = \underset{\approx}{\bar{\mathrm{A}}} \frac{\partial \underline{\boldsymbol{\rho}}}{\partial \underset{\sim}{\xi}}$$

– First covariant fundamental surface metric matrix (t-scalar):

$$\underset{\approx}{\mathrm{A}} = \frac{\partial \underline{\boldsymbol{\rho}}}{\partial \underset{\sim}{\xi}} \cdot \frac{\partial \underline{\boldsymbol{\rho}}^{\mathsf{T}}}{\partial \underset{\sim}{\xi}}$$

– First contravariant fundamental surface metric matrix (t-scalar):

$$\underset{\approx}{\bar{\mathrm{A}}} = \underset{\approx}{\mathrm{A}}^{-1} = \overline{\frac{\partial \underline{\boldsymbol{\rho}}}{\partial \underset{\sim}{\xi}}} \cdot \overline{\frac{\partial \underline{\boldsymbol{\rho}}}{\partial \underset{\sim}{\xi}}}^{\mathsf{T}}$$

– Second covariant fundamental surface matrix (t-scalar):

$$\underset{\approx}{\mathrm{H}} = \underline{\boldsymbol{n}} \cdot \frac{\partial^2 \underline{\boldsymbol{\rho}}}{\partial \underset{\sim}{\xi}^2}$$

– Unit vector, normal to the master surface at the projection point:

$$\underline{\boldsymbol{n}} = \underline{\boldsymbol{n}}(t, \underset{\sim}{\xi}_{\pi}) = \frac{\frac{\partial \underline{\boldsymbol{\rho}}}{\partial \xi_1} \times \frac{\partial \underline{\boldsymbol{\rho}}}{\partial \xi_2}}{\left\| \frac{\partial \underline{\boldsymbol{\rho}}}{\partial \xi_1} \times \frac{\partial \underline{\boldsymbol{\rho}}}{\partial \xi_2} \right\|}$$

– Normal gap:

$$g_n = g_n(t) = (\underline{\boldsymbol{r}}_s - \underline{\boldsymbol{\rho}}) \cdot \underline{\boldsymbol{n}} \qquad [2.1]$$

– Tangential sliding velocity: $\underline{\boldsymbol{v}}_t = \frac{\partial \underline{\boldsymbol{\rho}}}{\partial \underset{\sim}{\xi}} \dot{\underset{\sim}{\xi}}$

Remark 2.1. On s-structures (v- and t-notations)

S-structures (set-structures or s-tensors) – a new notion in mechanics – are helpful in describing the geometry, which involves different dimensions (see section A1.6). The description of spatial interaction between surfaces requires both three-dimensional (3D) and two- dimensional (2D) quantities, associated with the space and the surface, respectively. In this case, the use of indices and Einstein summation is ambiguous, because for some quantities an index takes values from 1 to 3, for others – from 1 to 2. In differential geometry, this ambiguity is avoided by the use of Greek and Roman letters to distinguish summation limits. However, I wished to get rid of indices and to express everything in shorter and more transparent notations of the direct tensor language. Moreover, a consistent formulation of s-structures over the space of vectors and tensors leads to an improvement and simplification of the tensor apparatus in many cases as shown in Appendix 1. In this chapter, a simplified form of s-structures is used (see section A1.7).

2.2.2. *Normal gap*

The *gap*[3] between contacting surfaces and the *closest point* are important quantities for computational contact mechanics. But, as mentioned in the introduction, it is hard to define them properly. The gap is the central notion in frictionless contact mechanics; it is responsible for preserving the non-penetration condition. The closest point projection allows us to determine contacting pairs and to track the relative sliding between surfaces. This sliding – crucial for frictional contact – is described by *relative tangential sliding*, another important geometrical quantity.

Formally, the absolute value of the normal gap $|g_n|$ is defined as the closest distance from the slave node to the master surface. It can be interpreted as the minimal radius $0 \leq R < \infty$ of a sphere (circle in 2D) with its center placed in the slave point $\underline{\boldsymbol{r}}_s$ and touching (but not intersecting) the master surface. It is not important if this sphere touches the master surface in one, several or infinitely many points. The gap is positive if the slave point is outside the solid enveloped by the master surface, otherwise it is negative. The sign of the normal gap implies the following:

– $g_n > 0$, solids are locally separated;

– $g_n = 0$, solids are locally in contact;

– $g_n < 0$, solids locally penetrate each other.

The normal gap can be equivalently defined using the closest-point concept: the absolute value of the normal gap is then the distance between the slave node and the closest point on the master surface. It is considered positive $g_n > 0$ if the dot product of the vector connecting the slave node and the closest point $\underline{\boldsymbol{\rho}}$ with a normal vector[4] at the surface is positive $\left(\underline{\boldsymbol{r}}_s - \underline{\boldsymbol{\rho}}\right) \cdot \underline{\boldsymbol{n}}\left(\underline{\boldsymbol{\rho}}\right) > 0$; otherwise $g_n < 0$. For shell structures, each point has two opposite normals, thus to define the sign of the gap we need to track the history of the master-slave interaction. Formally, the point $\underline{\boldsymbol{\rho}}$ on the master surface is called the closest point to the slave point $\underline{\boldsymbol{r}}_s$ if all other points are not closer than $\left\| \underline{\boldsymbol{\rho}} - \underline{\boldsymbol{r}}_s \right\|$. According to this definition for any *closed* master surface, the closest point always exists, but it is not always unique.

---

3 By *gap* between contacting surfaces, we understand is as any scalar function of the slave point and the master surface, which is positive if there is no contact, zero if there is a contact and negative if there is a penetration. By *normal gap*, we understand the signed distance between the slave point and its normal projection (if it exists); the sign rules are the same.

4 The normal vector at the master surface is oriented outwards the bulk.

We suggest a definition of the normal gap and the closest point, which is valid for a piecewise C^1-smooth master surface and for an arbitrary location of the slave point[5]. An absolute value of the *normal gap* $|g_n|$ between the slave point $\underline{\boldsymbol{r}}_s$ and the master surface Γ_m is related to the infimum of the distance functional $F\left(\underline{\boldsymbol{\rho}}\right)$ on the closed set of the master surface $\underline{\boldsymbol{\rho}} \in \Gamma_m$ in the following way:

$$F\left(\underline{\boldsymbol{\rho}}\right) = \frac{1}{2}\left(\underline{\boldsymbol{r}}_s - \underline{\boldsymbol{\rho}}\right)^2,\ |g_n| = \sqrt{2 \inf_{\underline{\boldsymbol{\rho}}' \in \Gamma_m} \left\{F\left(\underline{\boldsymbol{\rho}}'\right)\right\}} \qquad [2.2]$$

The *normal gap* is positive if the slave point is outside of the solid enveloped by the master surface, and negative otherwise. The only difference between the definition used here and the classical definition consists of replacing $\min$ by $\inf$, but this difference matters (see remark 2.2).

Remark 2.2. On the difference between infimum and minimum

Frequently, we use a minimum *of the distance functional for the definition of the normal gap and the closest point. But often we neglect non-smooth regions on the surface and confuse the definition of the minimum for smooth and non-smooth functionals. This imprecision may lead to a wrong definition of contact pairs (see figure below). In many cases, the use of* infimum *instead of minimum solves some problems. Rigorously, we can seek for a minimum of a function only on an open set* $\underline{\boldsymbol{\rho}} \in \Gamma_m \backslash \partial\Gamma_m$*; and the function must be at least* continuous*, the smoothness is not required (see definitions below). A function may have infinitely many minima or does not have them at all. Infimum is defined both for an open or a closest set; it is unique and always existing. On an open set, the minimum point* x^* *(if it exists) belongs to the set, it is not always the case for the infimum* M*; it does for a closed set. Consider below the definitions of the minimum and the infimum:*

– *Minimum of a function* $F(x) \in C^0_{(x_0;x_1)}$

$$F(x^*) = \min_{x \in (x_0;x_1)} [F(x)] \Leftrightarrow \exists \varepsilon,\ \forall x \in (x_0; x_1)$$
$$\textit{and } \|x - x^*\| < \varepsilon :\ F(x) \geq F(x^*)$$

5 Konyukhov and Schweizerhof [KON 08] undertook an attempt to summarize different approaches and to overcome the difficulties related to the definition of the normal gap and the closest point; however, the resulting technique based on “continuous projection domain” and the “generalized closest point procedure” is not fully satisfactory because it does not cover all the cases and requires a proximity of the slave node to the master surface.

– *Minimum of a function* $F(x) \in C^1_{(x_0;x_1)}$

$$F(x^*) = \min_{x\in(x_0;x_1)} [F(x)] \Leftrightarrow \left.\frac{\partial F}{\partial x}\right|_{x^*} = 0 \text{ and } \left.\frac{\partial^2 F}{\partial x^2}\right|_{x^*-} > 0 \text{ and } \left.\frac{\partial^2 F}{\partial x^2}\right|_{x^*+} > 0$$

– *Minimum of a function* $F(x) \in C^2_{(x_0;x_1)}$

$$F(x^*) = \min_{x\in(x_0;x_1)} [F(x)] \Leftrightarrow \left.\frac{\partial F}{\partial x}\right|_{x^*} = 0 \text{ and } \left.\frac{\partial^2 F}{\partial x^2}\right|_{x^*} > 0$$

– *Infimum of a function* $F(x) \in C^0_{(x_0;x_1)}$

$$M = \inf_{x\in(x_0;x_1)} [F(x)] \Leftrightarrow \begin{cases} \forall x \in (x_0;x_1) : F(x) \geq M \\ \forall M' > M, \exists x \in (x_0;x_1) : F(x) \leq M' \end{cases}$$

In the literature, we often encounter the definition of the closest point assuming the C^2*-smoothness of the surface, but we know that the master surface is only* C^0*-continuous, so rigorously, the first definition of the* min *should be used. Moreover, we generally have to take into account edges and to look for a global minimum, for this purpose it is better to use the* inf*. Note that by edges we mean not only global edges of the master surface, but also edges of each master face; remember that the detection procedure proceeds face-by-face and never deals with the entire master surface.*

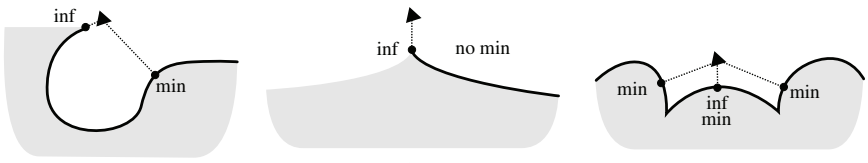

(a) (b) (c)

*Difference between "*inf*" and "*min*" definition of the closest point: (a) wrong "min" closest point, (b) "min" closest point does not exist and (c) multiple "min" closest points*

According to this definition, the normal gap always exists without any requirements on the master surface's smoothness. It follows from the remark that the infimum and the global minimum $\widetilde{\min}$ are equivalent for a closed set Γ_m except edges (see figure in remark 2.2 and Figure 2.2).

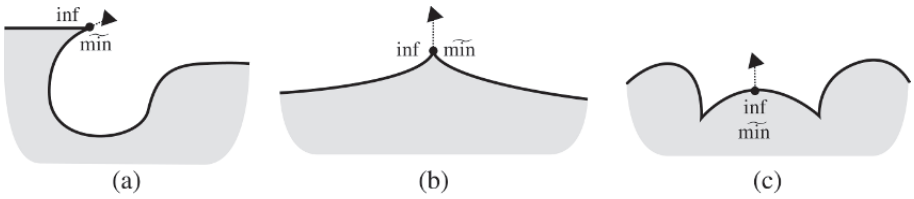

Figure 2.2. *Equivalence between* $\inf$ *and* $\widetilde{\min} = \inf_i [\min_i]$ *of the distance functional for continuous surface far from edges*

From a numerical point of view, it is inconvenient to solve directly equation [2.2] for the entire non-smooth master surface. It is better to split it into many smooth open sets and points of non-differentiability: the master surface Γ_m is the union of smooth open parametrized surfaces Γ_s^i, smooth open parametrized edges Γ_e^j and vertices Γ_v^k (Figure 2.3):

$$\Gamma_m = \left\{ \bigcup_{i=1,N_s} \Gamma_s^i \right\} \cup \left\{ \bigcup_{i=1,N_e} \Gamma_e^j \right\} \cup \left\{ \bigcup_{i=1,N_v} \Gamma_v^k \right\}.$$

Surfaces in the 3D case are parametrized by a v-scalar $\underset{\sim}{\xi} \in I_\xi$; segment in the 2D case by a scalar $\xi \in I_\xi$; edges by a scalar $\zeta \in I_\zeta$ in both the cases I_ξ and I_ζ are open sets. So in the 3D case, a master surface consists of:

– N_s connected parametrized open and C^2-smooth surfaces (segments)

$$\underline{\boldsymbol{\rho}}^i(\underset{\sim}{\xi}) \in \Gamma_s^i,\ i \in [1, N_s],\ \underset{\sim}{\xi} \in I_\xi,\ \frac{\partial^3 \underline{\boldsymbol{\rho}}}{\partial \underset{\sim}{\xi}^3} < \infty$$

– N_e C^2-smooth open parametrized edges

$$\underline{\boldsymbol{\rho}}^j(\zeta) \in \Gamma_e^j,\ j \in [1; N_e], \zeta \in I_\zeta,\ \frac{\partial^3 \underline{\boldsymbol{\rho}}}{\partial \zeta^3} < \infty$$

– N_v vertices

$$\underline{\boldsymbol{\rho}}_k \in \Gamma_v^k,\ k \in [1; N_v].$$

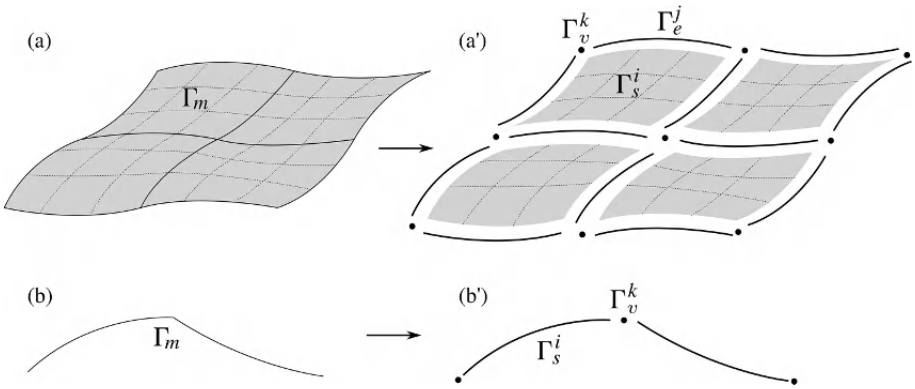

Figure 2.3. *(a) Split of the three-dimensional master surface (a') into sets of surfaces, edges and vertices; and (b) two-dimensional master curve (b') into sets of segments and vertices*

The absolute value of the normal gap can be expressed in a more appropriate form from a numerical point of view:

$$|g_n| = \sqrt{2 \inf_{\underline{\boldsymbol{\rho}} \in \Gamma_m} \left\{ F(\underline{\boldsymbol{\rho}}) \right\}}, \quad \text{where}$$

$$\inf_{\underline{\boldsymbol{\rho}} \in \Gamma_m} \left\{ F\left(\underline{\boldsymbol{\rho}}\right) \right\} = \left[\begin{array}{l} \text{3D: } \inf \left\{ \begin{array}{ll} \inf\limits_{\underline{\boldsymbol{\rho}}^i \in \Gamma_s^i, i \in [1;N_s]} \left\{ \operatorname{ext}\limits_{\underset{\sim}{\xi} \in I_\xi} F\left(\underline{\boldsymbol{\rho}}^i\left(\underset{\sim}{\xi}\right)\right) \right\} & \text{term 3D.1} \\ \inf\limits_{\underline{\boldsymbol{\rho}}^j \in \Gamma_e^j, j \in [1;N_e]} \left\{ \operatorname{ext}\limits_{\zeta \in I_\zeta} F\left(\underline{\boldsymbol{\rho}}^j(\zeta)\right) \right\} & \text{term 3D.2} \\ \inf\limits_{\underline{\boldsymbol{\rho}}^k \in \Gamma_v^k, k \in [1;N_v]} \left\{ F\left(\underline{\boldsymbol{\rho}}^k\right) \right\} & \text{term 3D.3} \end{array} \right. \\ \\ \text{2D: } \inf \left\{ \begin{array}{ll} \inf\limits_{\underline{\boldsymbol{\rho}}^i \in \Gamma_s^i, i \in [1;N_s]} \left\{ \operatorname{ext}\limits_{\xi \in I_\xi} F(\underline{\boldsymbol{\rho}}^i(\xi)) \right\} & \text{term 2D.1} \\ \inf\limits_{\underline{\boldsymbol{\rho}}^k \in \Gamma_v^k, k \in [1;N_v]} \left\{ F\left(\underline{\boldsymbol{\rho}}^k\right) \right\} & \text{term 2D.2} \end{array} \right. \end{array} \right. \qquad [2.3]$$

Remark that there is neither local nor global minimum in the definition, they have been replaced by extremum (ext). It does not change the result, but may facilitate the numerical treatment, because the investigation of the sign of second- or higher order derivatives of the functional F is no longer needed. A sufficient and necessary condition for extremum of a smooth function is the vanishing of the first derivative:

$$F(x) \in C^1(\Omega),\ F(x^*) = \operatorname*{ext}_{x \in \Omega} F(x) \ \Leftrightarrow\ \left.\frac{\partial F}{\partial x}\right|_{x^*} = 0.$$

According to Equation [2.3] the infimum can correspond to one, several or infinitely many points on the master surface Γ_m. One of them may be assigned as the closest point.

2.2.3. *Closest point on a surface*

We analyze equation [2.3], term-by-term. The extremum of the distance function [2.2] on the i th face (smooth and open) Γ_s^i (Figure 2.4, equation [2.3] term 3D.1):

$$\underline{\boldsymbol{\rho}}' \in \Gamma_m^i,\ F(\underset{\sim}{\xi}) \in C^2(I_\xi), \quad \underset{\underset{\sim}{\xi} \in I_\xi}{\text{ext}} \left[F\left(\underline{\boldsymbol{\rho}}'(\underset{\sim}{\xi}) \right) \right] \Leftrightarrow$$

gives the following equation for the closest projection point:

$$\Leftrightarrow \frac{\partial F}{\partial \underset{\sim}{\xi}} = 0 \Leftrightarrow (\underline{\boldsymbol{r}}_s - \underline{\boldsymbol{\rho}}) \cdot \frac{\partial \underline{\boldsymbol{\rho}}}{\partial \underset{\sim}{\xi}} = 0 \qquad [2.4]$$

The last equality in equation [2.4] means that in an extremum point $\underline{\boldsymbol{\rho}}(\underset{\sim}{\xi}^j)$, the vectors of the local basis are orthogonal to the vector connecting $\underline{\boldsymbol{\rho}}(\underset{\sim}{\xi}^j)$ with the slave point. The unit normal at the master surface is evaluated through a normalized cross product of the local basis vectors:

$$\underline{\boldsymbol{n}} = \frac{\frac{\partial \underline{\boldsymbol{\rho}}}{\partial \xi_1} \times \frac{\partial \underline{\boldsymbol{\rho}}}{\partial \xi_2}}{\left\| \frac{\partial \underline{\boldsymbol{\rho}}}{\partial \xi_1} \times \frac{\partial \underline{\boldsymbol{\rho}}}{\partial \xi_2} \right\|} \qquad [2.5]$$

From [2.4] and [2.5], $\underline{\boldsymbol{r}}_s - \underline{\boldsymbol{\rho}}(\underset{\sim}{\xi}^j) = \alpha \underline{\boldsymbol{n}}(\underset{\sim}{\xi}^j)$, where α is the distance between the slave point and its projection taken with an appropriate sign:

$$\underline{\boldsymbol{r}}_s - \underline{\boldsymbol{\rho}}(\underset{\sim}{\xi}^j) = \pm \left\| \underline{\boldsymbol{r}}_s - \underline{\boldsymbol{\rho}}(\underset{\sim}{\xi}^j) \right\| \underline{\boldsymbol{n}}(\underset{\sim}{\xi}^j) \qquad [2.6]$$

If $\underset{\sim}{\xi}^j$ is a point of the global minimum on the current surface Γ_s^j, then the norm in [2.6] represents the local normal gap g_n^j:

$$\underline{\boldsymbol{r}}_s - \underline{\boldsymbol{\rho}}(\underset{\sim}{\xi}^j) = g_n^j \, \underline{\boldsymbol{n}}(\underset{\sim}{\xi}^j) \qquad [2.7]$$

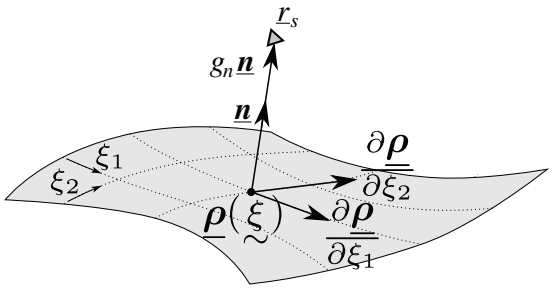

Figure 2.4. *Geometry of a smooth master surface with a close slave point*

To solve nonlinear equation [2.4], we use Newton's method, so we linearize it in a proximity of $\underset{\sim}{\xi}$:

$$\left[(\underline{\boldsymbol{r}}_s - \underline{\boldsymbol{\rho}})\cdot\frac{\partial\underline{\boldsymbol{\rho}}}{\partial\underset{\sim}{\xi}}\right]\Bigg|_{\underset{\sim}{\xi}+\delta\underset{\sim}{\xi}} = \left[(\underline{\boldsymbol{r}}_s - \underline{\boldsymbol{\rho}})\cdot\frac{\partial\underline{\boldsymbol{\rho}}}{\partial\underset{\sim}{\xi}}\right]\Bigg|_{\underset{\sim}{\xi}} + \left[-\frac{\partial\underline{\boldsymbol{\rho}}}{\partial\underset{\sim}{\xi}}\cdot\frac{\partial\underline{\boldsymbol{\rho}}^{\mathsf{T}}}{\partial\underset{\sim}{\xi}} + (\underline{\boldsymbol{r}}_s - \underline{\boldsymbol{\rho}})\cdot\frac{\partial^2\underline{\boldsymbol{\rho}}}{\partial\underset{\sim}{\xi}^2}\right]\Bigg|_{\underset{\sim}{\xi}}\cdot\delta\underset{\sim}{\xi} = 0 \qquad [2.8]$$

The increment of the surface parameter is then:

$$\delta\underset{\sim}{\xi} = \left[\frac{\partial\underline{\boldsymbol{\rho}}}{\partial\underset{\sim}{\xi}}\cdot\frac{\partial\underline{\boldsymbol{\rho}}^{\mathsf{T}}}{\partial\underset{\sim}{\xi}} - (\underline{\boldsymbol{r}}_s - \underline{\boldsymbol{\rho}})\cdot\frac{\partial^2\underline{\boldsymbol{\rho}}}{\partial\underset{\sim}{\xi}^2}\right]^{-1}\cdot\left[(\underline{\boldsymbol{r}}_s - \underline{\boldsymbol{\rho}})\cdot\frac{\partial\underline{\boldsymbol{\rho}}}{\partial\underset{\sim}{\xi}}\right] \qquad [2.9]$$

Remark that we cannot substitute $(\underline{\boldsymbol{r}}_s - \underline{\boldsymbol{\rho}})$ in [2.9] according to [2.7], as it is valid only at the extremum point. Newton's method cannot provide multiple extrema, so to find all solutions of equation [2.4], the master surface Γ_m^i has to be divided into regions containing only one extremum or a more advanced method has to be used.

In case of a 2D geometry, the term 2D.1 from equation [2.3] gives the following equation for the increment of ξ:

$$\delta\xi = \frac{(\underline{\boldsymbol{r}}_s - \underline{\boldsymbol{\rho}})\cdot\frac{\partial\underline{\boldsymbol{\rho}}}{\partial\xi}}{\frac{\partial\underline{\boldsymbol{\rho}}}{\partial\xi}\cdot\frac{\partial\underline{\boldsymbol{\rho}}}{\partial\xi} - (\underline{\boldsymbol{r}}_s - \underline{\boldsymbol{\rho}})\cdot\frac{\partial^2\underline{\boldsymbol{\rho}}}{\partial\xi^2}} \qquad [2.10]$$

Different simple and non-trivial cases of extremum location are presented in Figure 2.5 for 2D and in Figure 2.6 for 3D geometries. Within the chosen numerical scheme, it is complicated to analyze cases when the functional F has several or infinitely many extrema (Figures 2.5 (b) (c) and (d) and Figures 2.6 (b) (c) and (d)).

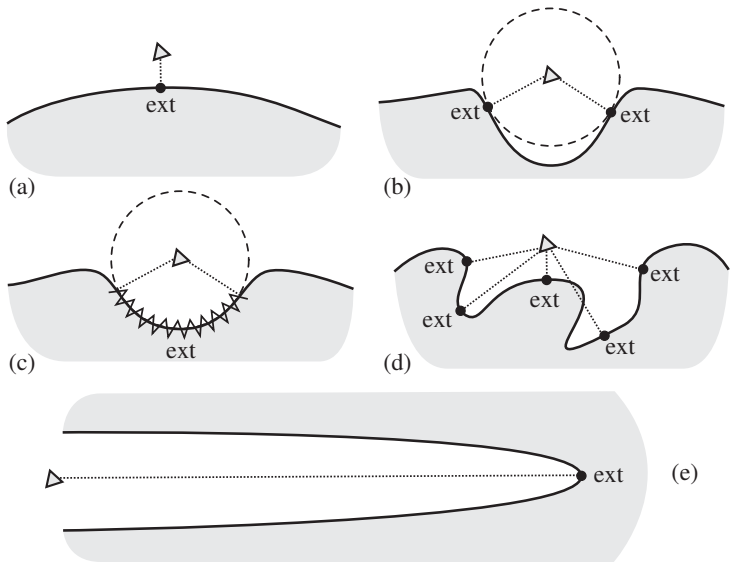

Figure 2.5. *Different cases of extremum location in 2D: (a) unique extremum (global minimum), (b) several extrema located at the same distance from the slave point, (c) case of infinite number of extrema, slave point is situated in the local center of curvature of the master surface, (d) case of several different extrema and (e) unique extremum (global maximum)*

2.2.4. *Closest point on a curve*

An extremum point on the jth smooth curve Γ_e^j (term 3D.2) (Figure 2.7) is given by:

$$\begin{aligned} &\underline{\boldsymbol{\rho}}' \in \Gamma_e^j,\ F(\zeta) \in C^2(I_\zeta),\quad \underset{\zeta \in I_\zeta}{\text{ext}} \left[F\left(\underline{\boldsymbol{\rho}}'(\zeta)\right)\right] \Leftrightarrow \\ &\Leftrightarrow \frac{dF}{d\zeta} = 0 \Leftrightarrow (\underline{\boldsymbol{r}}_s - \underline{\boldsymbol{\rho}}) \cdot \frac{\partial \underline{\boldsymbol{\rho}}}{\partial \zeta} = 0 \Leftrightarrow (\underline{\boldsymbol{r}}_s - \underline{\boldsymbol{\rho}}) \cdot \frac{\partial \underline{\boldsymbol{\rho}}}{\partial s(\zeta)} = 0 \end{aligned} \qquad [2.11]$$

where s is a classical parametrization of the curve and it denotes the curve's length

$$ds = \sqrt{\frac{\partial \underline{\boldsymbol{\rho}}}{\partial \zeta} \cdot \frac{\partial \underline{\boldsymbol{\rho}}}{\partial \zeta}} d\zeta$$

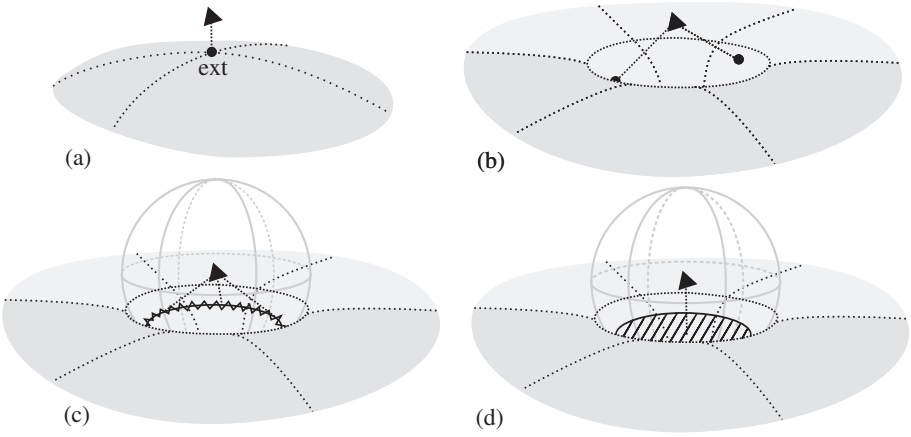

Figure 2.6. *Different cases of extremum location in 3D: (a) unique extremum (global minimum), (b) several extrema located at the same distance from the slave point, (c) case of infinite number of extrema (curve) and (d) case of infinite number of extrema (surface)*

Three normalized basis vectors associated with a curve are:

– a unit tangential vector

$$\underline{\boldsymbol{\tau}} = \frac{\partial \underline{\boldsymbol{\rho}}}{\partial s}$$

– a unit normal vector pointing to a center of curvature of the curve

$$\underline{\boldsymbol{\nu}} = \frac{1}{\kappa} \frac{\partial^2 \underline{\boldsymbol{\rho}}}{\partial s^2}$$

– a unit binormal vector defined as the cross product of the first two vectors

$$\underline{\boldsymbol{\beta}} = \underline{\boldsymbol{\tau}} \times \underline{\boldsymbol{\nu}}$$

where κ is the curve's curvature defined as

$$\kappa(\zeta) = \frac{\left\| \frac{\partial \underline{\boldsymbol{\rho}}}{\partial \zeta} \times \frac{\partial^2 \underline{\boldsymbol{\rho}}}{\partial \zeta^2} \right\|}{\left\| \frac{\partial \underline{\boldsymbol{\rho}}}{\partial \zeta} \right\|^3}.$$

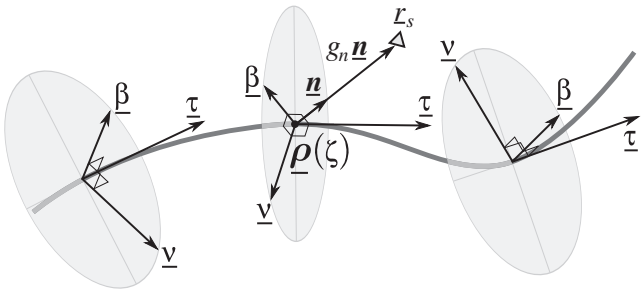

Figure 2.7. *Point-curve interaction in three-dimensional space*

The numerical scheme to find an extremum point is derived just like for a surface. The linearization of equation [2.11] gives:

$$\left[(\underline{\boldsymbol{r}}_s - \underline{\boldsymbol{\rho}}) \cdot \frac{\partial \underline{\boldsymbol{\rho}}}{\partial \zeta}\right]\Bigg|_{\zeta^0+\delta\zeta} = \left[(\underline{\boldsymbol{r}}_s - \underline{\boldsymbol{\rho}}) \cdot \frac{\partial \underline{\boldsymbol{\rho}}}{\partial \zeta}\right]\Bigg|_{\zeta^0} + \left[-\frac{\partial \underline{\boldsymbol{\rho}}}{\partial \zeta} \cdot \frac{\partial \underline{\boldsymbol{\rho}}}{\partial \zeta} + (\underline{\boldsymbol{r}}_s - \underline{\boldsymbol{\rho}}) \cdot \frac{\partial^2 \underline{\boldsymbol{\rho}}}{\partial \zeta^2}\right]\Bigg|_{\zeta^0} \cdot \delta\zeta = 0 \qquad [2.12]$$

So the increment $\delta\zeta$ of the curve parameter is given by:

$$\delta\zeta = \frac{(\underline{\boldsymbol{r}}_s - \underline{\boldsymbol{\rho}}) \cdot \underline{\boldsymbol{t}}}{\underline{\boldsymbol{t}} \cdot \underline{\boldsymbol{t}} - \kappa \underline{\boldsymbol{\nu}} \cdot (\underline{\boldsymbol{r}}_s - \underline{\boldsymbol{\rho}})}, \quad \text{where } \underline{\boldsymbol{t}} = \frac{\partial \underline{\boldsymbol{\rho}}}{\partial \zeta} \qquad [2.13]$$

Terms (3D.3) and (2D.2) in [2.3] are trivial: the distance from the slave point has to be measured to each vertex of the master surface, no iterations are needed. Finally, equations [2.9], [2.13] in 3D and [2.10] in 2D allow us to determine an extremum on surfaces Γ_m^i and edges Γ_e^j in 3D and on curves Γ_e^j in 2D, respectively. Next, the infimum over all extrema has to be determined. However, as already mentioned, the infimum may correspond to several or infinitely many points. A remedy for that is a selection procedure: for example, we can choose the new closest point according to the previous position of the closest point and/or according to the relative motion of bodies.

Let us demonstrate the closest point projection procedure for a specific master geometry and a slave point's path [Figure 2.8(a)]. The master surface is $ABCD$ curve; the slave point follows the path 1–6–10–1. In Figure 2.8(b), the following projection zones are presented: all points in the "K" zone are projected on the arc BC; in "L"–on

the segment AB; in "M"–on the vertex B; in "N"–on the vertex C and in "P"–on the segment CD. Some projection zones are separated by dashed lines, they correspond to discontinuities in the closest point projection, that is if a slave point crosses such a line, its projection (closest point on the master surface) makes a finite jump from one segment to another. For example, on path $1-2$, the slave point moves in the projection zone "K" and has a projection on the segment BC. At point 2, as shown in Figure 2.8(c), the slave point has two projections: point P on the arc BC and point Q on the segment AB. Next, on path 2–3–4–5–6, there are no discontinuities in the closest point projection. At point 6, the closest point jumps from vertex B to C. Point 7 is a special point on the path, all points of the segment BC are closest points; so in compliance with the aforementioned, any starting point in Newton's procedure will be chosen as the closest point, so sometimes the continuity of the projection point can be retained if the starting point is chosen appropriately. However, in the presented case, there is no way for that, so there is a discontinuity at point 7. On path 7–8–9–10, the projection is continuous. At point 10, there are two closest points on different segments. At path 10–1, the projection is continuous.

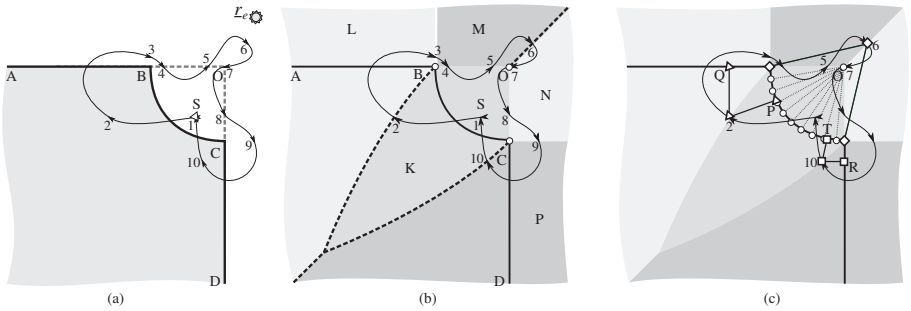

Figure 2.8. *Illustration projection zones and related problems of the closest point projection; path of a slave point close to a piecewise-smooth master surface*

From a numerical point of view, it is not crucial that on the dashed lines several closest points exist, because the probability to find a slave node exactly on these lines is zero. What is important is that, when such a line is crossed, the projection point jumps relatively far from its position at the previous step. Decreasing the time step to zero does not decrease the size of this jump. Another observation can be made: in domains M and N, any change of position of the slave point does not result in the change of position of the closest point.

A small change in position of the slave point does not always result in a small change in the closest point projection, i.e. the closest point motion over the master surface is discontinuous. As seen from the example, this difficulty is sometimes related to the fact that the slave point is relatively far from the master surface

(points 6 and 7 in Figure 2.8), but it may also be crucial even for sufficiently close slave nodes (points 2 and 10). In the case of a distant slave point, the jump can be huge even if the master surface is C^2-smooth. The energy dissipation within one computational iteration in frictional contact problems is related to the sliding distance. If a small change in geometry results in a jump of the projection point (the sliding distance changes abruptly), then the corresponding dissipated energy will also experience a jump, i.e. the virtual work of frictional forces becomes non-continuous. In this case, the convergence of Newton's method cannot be ensured. These consequences cannot be avoided in the classical approach, when the gap and sliding distance are measured with respect to the *closest projection point* on the master surface. That is why in the next section, we suggest a new approach.

2.2.5. *Shadow-projection method*

Idea 2.1. Shadow-projection method

As an alternative to the closest point projection, we propose to determine the gap and the relative sliding according to a new technique – shadow-projection. It establishes the relation between a slave point and its shadow or "back-shadow" on the master surface. This shadow is cast by an imaginary light-emitting point (emitter) placed at some distance from the system of contacting surfaces. This technique has been inspired from a unique and continuous aircraft's shadow cast by the Sun on the Earth's surface. Also, this shadow-projection point may serve as a starting point for Newton's procedure to detect the closest projection point for complex surfaces.

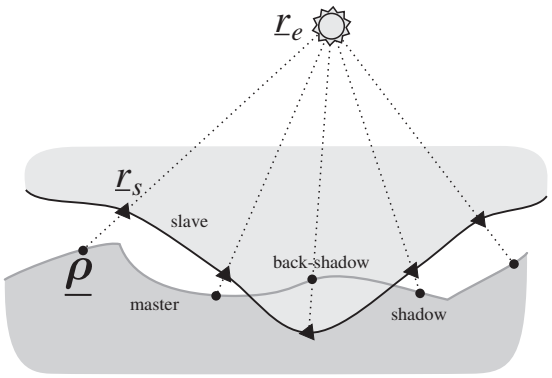

Figure 2.9. *An imaginary light-emitting-point (emitter) $\underline{\mathbf{r}}_e$ casts shadows and back-shadows $\underline{\boldsymbol{\rho}}$ of slave nodes $\underline{\mathbf{r}}_s$ onto a non-smooth master surface*

If a shadow exists, then it is unique, if the master surface does not cast "shadows" on its own. To find a shadow or a "back-shadow" $\underline{\boldsymbol{\rho}}$ (see Figure 2.9) of a slave point $\underline{\boldsymbol{r}}_s$ due to an imaginary point $\underline{\boldsymbol{r}}_e$ emitting light, we have to solve a nonlinear equation:

$$\underline{\boldsymbol{F}}(\underset{\sim}{\xi}, \alpha) = \underline{\boldsymbol{\rho}}(\underset{\sim}{\xi}) - \underline{\boldsymbol{r}}_e - \alpha(\underline{\boldsymbol{r}}_s - \underline{\boldsymbol{r}}_e) = 0 \qquad [2.14]$$

where $\alpha > 0$ is an unknown coefficient. To solve equation [2.14] by Newton's method, it should be linearized:

$$\underline{\boldsymbol{F}}(\underset{\sim}{\xi}, \alpha) + \begin{bmatrix} \frac{\partial \underline{\boldsymbol{F}}}{\partial \underset{\sim}{\xi}} \\ \frac{\partial \underline{\boldsymbol{F}}}{\partial \alpha} \end{bmatrix}^{\mathsf{T}} \begin{bmatrix} \delta \underset{\sim}{\xi} \\ \delta\alpha \end{bmatrix} = 0 \Leftrightarrow \underline{\boldsymbol{\rho}} - \underline{\boldsymbol{r}}_e - \alpha(\underline{\boldsymbol{r}}_s - \underline{\boldsymbol{r}}_e) + \begin{bmatrix} \frac{\partial \underline{\boldsymbol{\rho}}}{\partial \underset{\sim}{\xi}} \\ -(\underline{\boldsymbol{r}}_s - \underline{\boldsymbol{r}}_e) \end{bmatrix}^{\mathsf{T}} \begin{bmatrix} \delta \underset{\sim}{\xi} \\ \delta\alpha \end{bmatrix} = 0$$

We take the dot product of the latter expression with the v-vector $\begin{bmatrix} \frac{\partial \underline{\boldsymbol{F}}}{\partial \underset{\sim}{\xi}} & \frac{\partial \underline{\boldsymbol{F}}}{\partial \alpha} \end{bmatrix}^{\mathsf{T}}$ and extract the increments $\delta \underset{\sim}{\xi}^{\,i}$ and $\delta\alpha^i$:

$$\begin{bmatrix} \delta \underset{\sim}{\xi}^{\,i} \\ \delta\alpha^i \end{bmatrix} = - \begin{bmatrix} \frac{\partial \underline{\boldsymbol{\rho}}}{\partial \underset{\sim}{\xi}} \cdot \frac{\partial \underline{\boldsymbol{\rho}}}{\partial \underset{\sim}{\xi}}^{\mathsf{T}} & -(\underline{\boldsymbol{r}}_s - \underline{\boldsymbol{r}}_e) \cdot \frac{\partial \underline{\boldsymbol{\rho}}}{\partial \underset{\sim}{\xi}} \\ -(\underline{\boldsymbol{r}}_s - \underline{\boldsymbol{r}}_s) \cdot \frac{\partial \underline{\boldsymbol{\rho}}}{\partial \underset{\sim}{\xi}}^{\mathsf{T}} & (\underline{\boldsymbol{r}}_s - \underline{\boldsymbol{r}}_e)^2 \end{bmatrix}^{-1} \Bigg|_{\underset{\sim}{\xi}^{\,i}, \alpha^i} \begin{bmatrix} \frac{\partial \underline{\boldsymbol{\rho}}}{\partial \underset{\sim}{\xi}} \cdot \left(\underline{\boldsymbol{\rho}} - \underline{\boldsymbol{r}}_e - \alpha(\underline{\boldsymbol{r}}_s - \underline{\boldsymbol{r}}_e) \right) \\ -(\underline{\boldsymbol{r}}_s - \underline{\boldsymbol{r}}_e) \cdot \left(\underline{\boldsymbol{\rho}} - \underline{\boldsymbol{r}}_e - \alpha(\underline{\boldsymbol{r}}_s - \underline{\boldsymbol{r}}_e) \right) \end{bmatrix} \Bigg|_{\underset{\sim}{\xi}^{\,i}, \alpha^i} \qquad [2.15]$$

It can be easily shown that the inverse matrix always exists. The unknowns at ith increment become:

$$\underset{\sim}{\xi}^{\,i+1} = \underset{\sim}{\xi}^{\,i} + \delta \underset{\sim}{\xi}^{\,i}, \quad \alpha^{i+1} = \alpha^i + \delta\alpha^i$$

and $\{\underset{\sim}{\xi}^{\,0}; \alpha^0\}$ is the starting point. In this method, there is no need to split the master surface into faces/segments, edges and vertices as has been done for the closest point projection. The shadow-projection point is assumed to be always located on one of

the master faces/segments $\underline{\boldsymbol{\rho}} \in \Gamma_m^i$. This is because the probability is zero[6] to obtain a shadow-projection on an edge or a vertex.

The proposed method has some drawbacks:

– it is complicated to check that for a given light emitter, there are no self-shadows (see Figure 2.10(c)), that is there are no master points for which equation [2.14] has more than one solution;

– it is hard to determine whether for a given surface, an emitter, which does not cast self-shadows, exists (see Figure 2.10(d)).

But the advantages of the method are important:

– If a master surface allows us to find an emitter that does not cast self-shadows, it is rather simple to find the shadow-projection point and moreover such a point is unique.

– The shadow-projection on the master surface is continuous and does not depend on smoothness of the master surface; one can carry out an imaginary test given in Figure 2.8(a) with an emitter $\underline{\boldsymbol{r}}_e$. This statement is valid if slave nodes remain closer to the master surface than the emitter, which is always the case if the emitter is chosen to be infinitely remote from the master (see Figure 2.10(b)).

– If the emitting point is placed infinitely far from the master surface (recall an aircraft's shadow cast by the Sun), equation [2.14] becomes simpler:

$$\underline{\boldsymbol{F}}(\underset{\sim}{\xi}, \alpha) = \underline{\boldsymbol{\rho}}(\underset{\sim}{\xi}) + \alpha \underline{\boldsymbol{e}} - \underline{\boldsymbol{r}}_s = 0 \qquad [2.16]$$

where $\underline{\boldsymbol{e}}$ is a constant unit vector pointing in the direction of the infinitely remote emitter – a pointer to the emitter. The resulting equation for increments $\delta\underset{\sim}{\xi}, \delta\alpha$ in Newton's method can be constructed as in equation [2.15]:

$$\begin{bmatrix} \delta\underset{\sim}{\xi}^i \\ \delta\alpha^i \end{bmatrix} = - \left[\begin{matrix} \frac{\partial \underline{\boldsymbol{\rho}}}{\partial \underset{\sim}{\xi}} \cdot \frac{\partial \underline{\boldsymbol{\rho}}^{\mathsf{T}}}{\partial \underset{\sim}{\xi}} & \underline{\boldsymbol{e}} \cdot \frac{\partial \underline{\boldsymbol{\rho}}}{\partial \underset{\sim}{\xi}} \\ \underline{\boldsymbol{e}} \cdot \frac{\partial \underline{\boldsymbol{\rho}}^{\mathsf{T}}}{\partial \underset{\sim}{\xi}} & 1 \end{matrix} \right]^{-1}_{\underset{\sim}{\xi}^i, \alpha^i} \left[\begin{matrix} \frac{\partial \underline{\boldsymbol{\rho}}}{\partial \underset{\sim}{\xi}} \cdot \left(\underline{\boldsymbol{\rho}} + \alpha \underline{\boldsymbol{e}} - \underline{\boldsymbol{r}}_s \right) \\ \underline{\boldsymbol{e}} \cdot \left(\underline{\boldsymbol{\rho}} + \alpha \underline{\boldsymbol{e}} - \underline{\boldsymbol{r}}_s \right) \end{matrix} \right]_{\underset{\sim}{\xi}^i, \alpha^i} \qquad [2.17]$$

6 This is because the projection zones of edges and vertices are simply surfaces and lines, respectively. Their measures (in the sense of the set theory) are zero in comparison to the measure of any volume that corresponds to projection zones of a face.

where at the solution point, the coefficient α is nothing, but a "shadow" gap g_s (different from the normal gap g_n). And the slave point can be expressed as:

$$\underline{\boldsymbol{r}}_s = \underline{\boldsymbol{\rho}} + g_s \underline{\boldsymbol{e}}$$

As it will be demonstrated later, it is much easier to work with this expression than with the similar expression for the normal projection:

$$\underline{\boldsymbol{r}}_s = \underline{\boldsymbol{\rho}} + g_n \underline{\boldsymbol{n}}$$

In Figure 2.10, different positions of the emitter and different master surfaces are depicted.

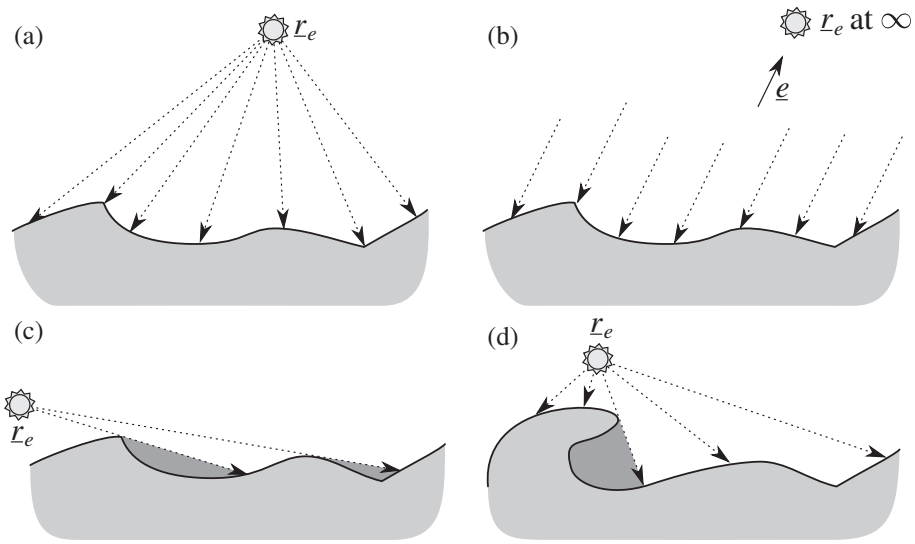

Figure 2.10. *Possible configuration of the master–emitter systems: unique projection of slave nodes possessing a shadow: (a) close emitter; (b) infinitely remote emitter; invalid configurations: (c) incorrectly chosen emitter (there are self-shadows on the master surface); (d) the emitter deriving a unique projection for the given master surface does not exist (self-shadows are always present)*

2.2.6. *Tangential relative sliding*

Consideration of frictional contact requires the tracking of the relative motion of two surfaces both in normal and tangential directions. As shown later, the variation of

the tangential relative velocity $\underline{\boldsymbol{v}}_t$[7] enters in to the main equations governing frictional contact (see Chapter 4). To obtain an accurate expression for $\underline{\boldsymbol{v}}_t$, we have to take into account two independent motions, those of the slave point and of the master surface, moreover we have to consider the deformation of the latter.

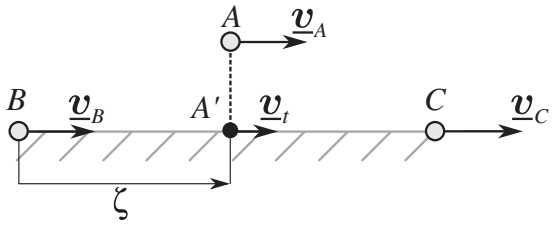

Figure 2.11. *Scheme for definition of the relative tangential velocity in one-dimensional*

2.2.6.1. *One-dimensional example of the relative sliding velocity*

A simple one-dimensional (1D) example depicted in Figure 2.11 demonstrates the relative motion of a point A over a straight segment BC. Absolute velocities $\underline{\boldsymbol{v}}_A$, $\underline{\boldsymbol{v}}_B$ and $\underline{\boldsymbol{v}}_C$ correspond to points A, B and C, respectively. Let us express the relative tangential velocity $\underline{\boldsymbol{v}}_t$ of the point A' (projection of the point A on the segment BC). If the segment BC is parametrized with $\zeta \in [0; 1]$, then the point A' can be expressed as:

$$\underline{\boldsymbol{\rho}}(A') = \zeta \underline{\boldsymbol{\rho}}(C) + (1 - \zeta)\underline{\boldsymbol{\rho}}(B) \qquad [2.18]$$

As the problem is 1D

$$\underline{\boldsymbol{\rho}}(A) = \underline{\boldsymbol{\rho}}(A') \qquad [2.19]$$

and the parameter ζ can be expressed as:

$$\zeta = \frac{(\underline{\boldsymbol{\rho}}(A) - \underline{\boldsymbol{\rho}}(B)) \cdot (\underline{\boldsymbol{\rho}}(C) - \underline{\boldsymbol{\rho}}(B))}{\|\underline{\boldsymbol{\rho}}(C) - \underline{\boldsymbol{\rho}}(B)\|^2}$$

7 For the relative tangential sliding velocity, we intentionally use $\underline{\boldsymbol{v}}_t$ and omit a dot notation $\underline{\dot{\boldsymbol{g}}}_t$ because of its ambiguity. Some authors [PIE 97, PIE 99] use a $\underline{\overset{\circ}{\boldsymbol{g}}}_t$ notation to emphasize the fact that there is no such vector whose time derivative is equal to the tangential relative sliding velocity between two deformable bodies.

Then the absolute velocity of the projection point is calculated as:

$$\underline{\boldsymbol{v}}_{A'} = \underbrace{\zeta\underline{\boldsymbol{v}}_C + (1-\zeta)\underline{\boldsymbol{v}}_B}_{=\frac{\partial\underline{\boldsymbol{\rho}}(A')}{\partial t}} + \underbrace{[\underline{\boldsymbol{\rho}}(C) - \underline{\boldsymbol{\rho}}(B)]\dot{\zeta}}_{\frac{\partial\underline{\boldsymbol{\rho}}(A')}{\partial\zeta}\dot{\zeta}}$$

To get the relative tangential velocity, we have to subtract from this expression the velocity of the material at the projection point $\frac{\partial\underline{\boldsymbol{\rho}}(A')}{\partial t} = \underline{\boldsymbol{v}}_{A'}(\zeta)$ for a fixed ζ:

$$\underline{\boldsymbol{v}}_t = \underline{\boldsymbol{v}}_{A'} - \frac{\partial\underline{\boldsymbol{\rho}}(A')}{\partial t} = [\underline{\boldsymbol{\rho}}(C) - \underline{\boldsymbol{\rho}}(B)]\dot{\zeta} + \underbrace{\zeta\underline{\boldsymbol{v}}_C + (1-\zeta)\underline{\boldsymbol{v}}_B - \frac{\partial\underline{\boldsymbol{\rho}}(A')}{\partial t}}_{=0}$$

The expression for the relative tangential sliding is then:

$$\underline{\boldsymbol{v}}_t = \frac{\partial\underline{\boldsymbol{\rho}}(A')}{\partial\zeta}\dot{\zeta} \qquad [2.20]$$

The velocity of the parameter $\dot{\zeta}$ can be computed by taking the derivative of equation [2.18], substituting [2.19] and evaluating the dot product with vector $\underline{\boldsymbol{t}} = \underline{\boldsymbol{\rho}}(C) - \underline{\boldsymbol{\rho}}(B)$:

$$\dot{\zeta} = \frac{[\underline{\boldsymbol{v}}_A - \zeta\underline{\boldsymbol{v}}_C - (1-\zeta)\underline{\boldsymbol{v}}_B] \cdot \underline{\boldsymbol{t}}}{\|\underline{\boldsymbol{t}}\|^2}$$

equation [2.20] is the derivative of the projection point vector $\underline{\boldsymbol{\rho}}(A')$ along the changing vector field $\underline{\boldsymbol{\rho}}$ of the master segment BC.

In the general case, the tangential relative sliding velocity is given as:

$$\underline{\boldsymbol{v}}_t = \frac{\partial\underline{\boldsymbol{\rho}}^{\mathsf{T}}}{\partial\underset{\sim}{\xi}}\,\dot{\underset{\sim}{\xi}} \qquad [2.21]$$

where $\frac{\partial\underline{\boldsymbol{\rho}}}{\partial\underset{\sim}{\xi}}$ is a v-vector of the local basis and $\underset{\sim}{\xi}$ is a convective parameter of the master surface. The required velocity vector is obtained as the Lie derivative of the vector connecting slave point $\underline{\boldsymbol{r}}_s$ and its projection $\underline{\boldsymbol{\rho}}_\pi$. The Lie derivative evaluates the change of a tensor field[8] along the change of a vector field. The objective

8 By a *tensor field* here, we mean any order tensor field.

expression for the relative tangential sliding velocity has been obtained by Laursen and Simo [LAU 93, LAU 94] and by Curnier *et al.* [CUR 95]. A critical discussion of different forms for the tangential relative velocity can be found in [PIE 97]. Below, we will use the following form for the variation of the tangential relative sliding:

$$\delta \underline{\boldsymbol{g}}_t = \frac{\partial \underline{\boldsymbol{\rho}}^{\mathsf{T}}}{\partial \underset{\sim}{\xi}} \delta \underset{\sim}{\xi} \qquad [2.22]$$

The length of the sliding path is computed as the following integral:

$$\underline{\boldsymbol{g}}_t = \int_{t_0}^{t} \|\underline{\boldsymbol{v}}_t\| \, dt' = \int_{t_0}^{t} \left\| \frac{\partial \underline{\boldsymbol{\rho}}^{\mathsf{T}}}{\partial \underset{\sim}{\xi}} \underset{\sim}{\xi} \right\| dt' = \int_{t_0}^{t} \sqrt{\underset{\sim}{\xi}^{\mathsf{T}} \underset{\approx}{\mathrm{A}} \underset{\sim}{\xi}} \, dt'$$

where t_0 is the time of the switch to the slip state, t is the actual time and $\underset{\approx}{\mathrm{A}}$ is the first fundamental t-scalar of the surface.

2.3. Variations of geometrical quantities

Here, we present the first- and second-order variations of the normal and shadow gaps (δg_n and δg_s) and also the variations of the projection-point coordinates $\delta \underset{\sim}{\xi}$ for normal and shadow-projections. We recall that the first variations are needed to incorporate the contact in the weak form whereas the second variations are needed to obtain its linearized form for Newton's method (see Chapter 4). Here, we only give the final expressions, all technical details are given in Appendix 2.

2.3.1. *First-order variations*

2.3.1.1. *Normal projection case*

The first variation of the normal gap is:

$$\delta g_n = \underline{\boldsymbol{n}} \cdot (\delta \underline{\boldsymbol{r}}_s - \delta \underline{\boldsymbol{\rho}}) \qquad [2.23]$$

The first variation of the local coordinate is:

$$\delta \underset{\sim}{\xi} = \left[\underset{\approx}{\mathrm{A}} - g_n \underset{\approx}{\mathrm{H}} \right]^{-1} \left(\frac{\partial \underline{\boldsymbol{\rho}}}{\partial \underset{\sim}{\xi}} \cdot (\delta \underline{\boldsymbol{r}}_s - \delta \underline{\boldsymbol{\rho}}) + g_n \underline{\boldsymbol{n}} \cdot \delta \frac{\partial \underline{\boldsymbol{\rho}}}{\partial \underset{\sim}{\xi}} \right) \qquad [2.24]$$

where $\underset{\approx}{\mathrm{A}}$ and $\underset{\approx}{\mathrm{H}}$ are the first and the second fundamental surface metric matrices (t-scalars), respectively:

$$\underset{\approx}{\mathrm{A}} = \frac{\partial \underline{\boldsymbol{\rho}}}{\partial \underset{\sim}{\xi}} \cdot \frac{\partial \underline{\boldsymbol{\rho}}^{\mathsf{T}}}{\partial \underset{\sim}{\xi}}, \qquad \underset{\approx}{\mathrm{H}} = \frac{\partial^2 \underline{\boldsymbol{\rho}}}{\partial \underset{\sim}{\xi}^2} \cdot \underline{\boldsymbol{n}} \qquad [2.25]$$

Often, the normal gap is assumed to be relatively small and is neglected, which gives a simpler expression:

$$\delta \underset{\sim}{\xi} = \bar{\underset{\approx}{\mathrm{A}}} \frac{\partial \underline{\boldsymbol{\rho}}}{\partial \underset{\sim}{\xi}} \cdot (\delta \underline{\boldsymbol{r}}_s - \delta \underline{\boldsymbol{\rho}}) = \overline{\frac{\partial \underline{\boldsymbol{\rho}}}{\partial \underset{\sim}{\xi}}} \cdot (\delta \underline{\boldsymbol{r}}_s - \delta \underline{\boldsymbol{\rho}}) \qquad [2.26]$$

Note also that using this form [2.26] for huge separations/penetrations makes the numerical procedure stable [WRI 06].

2.3.1.2. *Shadow-projection case: infinitely remote emitter*

The first variation of the shadow gap is:

$$\delta g_s = \frac{\underline{\boldsymbol{n}}}{\underline{\boldsymbol{n}} \cdot \underline{\boldsymbol{e}}} \cdot (\delta \underline{\boldsymbol{r}}_s - \delta \underline{\boldsymbol{\rho}}) \qquad [2.27]$$

where $\underline{\boldsymbol{e}}$ is a unit vector pointing to the infinitely remote emitter. The first variation of the local coordinate is:

$$\delta \underset{\sim}{\xi} = \overline{\frac{\partial \underline{\boldsymbol{\rho}}}{\partial \underset{\sim}{\xi}}} \cdot \left[\underline{\underline{\boldsymbol{I}}} - \frac{\underline{\boldsymbol{e}} \otimes \underline{\boldsymbol{n}}}{\underline{\boldsymbol{e}} \cdot \underline{\boldsymbol{n}}} \right] \cdot (\delta \underline{\boldsymbol{r}}_s - \delta \underline{\boldsymbol{\rho}}) \qquad [2.28]$$

2.3.1.3. *Shadow-projection case: close emitter*

The first variation of the shadow gap is:

$$\delta g_s = \frac{\underline{\boldsymbol{n}}}{\underline{\boldsymbol{e}} \cdot \underline{\boldsymbol{n}}} \cdot \left[\left(1 + \frac{g_s}{d_{se}} \right) \delta \underline{\boldsymbol{r}}_s - \delta \underline{\boldsymbol{\rho}} \right] - \frac{g_s}{d_{se}} \underline{\boldsymbol{e}} \cdot \delta \underline{\boldsymbol{r}}_s \qquad [2.29]$$

where the unit vector $\underline{\boldsymbol{e}}$ pointing to the emitter is given by:

$$\underline{\boldsymbol{e}} = \frac{\underline{\boldsymbol{r}}_e - \underline{\boldsymbol{r}}_s}{d_{se}} \quad \text{and} \quad d_{se} = \| \underline{\boldsymbol{r}}_e - \underline{\boldsymbol{r}}_s \|$$

where $\underline{\boldsymbol{r}}_e$ is the position of the emitter. The first variation of the local coordinate is:

$$\delta\underset{\sim}{\xi} = \overline{\frac{\partial\underline{\boldsymbol{\rho}}}{\partial\underset{\sim}{\xi}}} \cdot \left[\underline{\underline{\boldsymbol{I}}} - \frac{\underline{\boldsymbol{e}} \otimes \underline{\boldsymbol{n}}}{\underline{\boldsymbol{e}} \cdot \underline{\boldsymbol{n}}}\right] \cdot \left[\left(1 + \frac{g_s}{d_{se}}\right)\delta\underline{\boldsymbol{r}}_s - \delta\underline{\boldsymbol{\rho}}\right] \qquad [2.30]$$

For a far emitter $d_{se} \gg 1$ or for small gaps $g_s \approx 0$, expressions [2.29] and [2.30] reduce to [2.27] and [2.28], respectively.

2.3.2. *Second-order variations*

2.3.2.1. *Normal projection case*

The second variation of the normal gap is:

$$\begin{aligned}\Delta\delta g_n = \quad & -\underline{\boldsymbol{n}} \cdot \left(\delta\frac{\partial\underline{\boldsymbol{\rho}}^{\intercal}}{\partial\underset{\sim}{\xi}}\Delta\underset{\sim}{\xi} + \Delta\frac{\partial\underline{\boldsymbol{\rho}}^{\intercal}}{\partial\underset{\sim}{\xi}}\delta\underset{\sim}{\xi}\right) - \Delta\underset{\sim}{\xi}^{\intercal}\underset{\approx}{\mathrm{H}}\delta\underset{\sim}{\xi} + \\ & + g_n\left(\Delta\underset{\sim}{\xi}^{\intercal}\underset{\approx}{\mathrm{H}} + \underline{\boldsymbol{n}} \cdot \Delta\frac{\partial\underline{\boldsymbol{\rho}}^{\intercal}}{\partial\underset{\sim}{\xi}}\right)\underset{\approx}{\bar{\mathrm{A}}}\left(\underline{\boldsymbol{n}} \cdot \delta\frac{\partial\underline{\boldsymbol{\rho}}}{\partial\underset{\sim}{\xi}} + \underset{\approx}{\mathrm{H}}\delta\underset{\sim}{\xi}\right)\end{aligned} \qquad [2.31]$$

By assuming small gaps $g_n \approx 0$, we reduce significantly the number of arithmetical operations in the program, but loose the quadratic convergence rate. Moreover, as already mentioned, the assumption of small gaps is needed to ensure convergence in the case of huge separations/penetrations.

$$\Delta\delta g_n = -\underline{\boldsymbol{n}} \cdot \left(\delta\frac{\partial\underline{\boldsymbol{\rho}}^{\intercal}}{\partial\underset{\sim}{\xi}}\Delta\underset{\sim}{\xi} + \Delta\frac{\partial\underline{\boldsymbol{\rho}}^{\intercal}}{\partial\underset{\sim}{\xi}}\delta\underset{\sim}{\xi}\right) - \Delta\underset{\sim}{\xi}^{\intercal}\underset{\approx}{\mathrm{H}}\delta\underset{\sim}{\xi} \qquad [2.32]$$

The second variation of the surface parameter is:

$$\begin{aligned}\Delta\delta\underset{\sim}{\xi} = {} & (g_n\underset{\approx}{\mathrm{H}} - \underset{\approx}{\mathrm{A}})^{-1}\left\{\frac{\partial\underline{\boldsymbol{\rho}}}{\partial\underset{\sim}{\xi}} \cdot \left(\delta\frac{\partial\underline{\boldsymbol{\rho}}^{\intercal}}{\partial\underset{\sim}{\xi}}\Delta\underset{\sim}{\xi} + \Delta\frac{\partial\underline{\boldsymbol{\rho}}^{\intercal}}{\partial\underset{\sim}{\xi}}\delta\underset{\sim}{\xi}\right) + \right. \\ & + \Delta\underset{\sim}{\xi}^{\intercal}\left(\frac{\partial\underline{\boldsymbol{\rho}}}{\partial\underset{\sim}{\xi}} \cdot \frac{\partial^2\underline{\boldsymbol{\rho}}}{\partial\underset{\sim}{\xi}^2}\right)\delta\underset{\sim}{\xi} - g_n\underline{\boldsymbol{n}} \cdot \left(\delta\frac{\partial^2\underline{\boldsymbol{\rho}}}{\partial\underset{\sim}{\xi}^2}\Delta\underset{\sim}{\xi} + \Delta\frac{\partial^2\underline{\boldsymbol{\rho}}}{\partial\underset{\sim}{\xi}^2}\delta\underset{\sim}{\xi}\right) - g_n\Delta\underset{\sim}{\xi}^{\intercal}\left(\underline{\boldsymbol{n}} \cdot \frac{\partial^3\underline{\boldsymbol{\rho}}}{\partial\underset{\sim}{\xi}^3}\right)\delta\underset{\sim}{\xi} + \\ & + \left[g_n\left(\delta\frac{\partial\underline{\boldsymbol{\rho}}}{\partial\underset{\sim}{\xi}} + \frac{\partial^2\underline{\boldsymbol{\rho}}}{\partial\underset{\sim}{\xi}^2}\delta\underset{\sim}{\xi}\right) \cdot \frac{\partial\underline{\boldsymbol{\rho}}^{\intercal}}{\partial\underset{\sim}{\xi}}\underset{\approx}{\bar{\mathrm{A}}} - \delta g_n\underset{\approx}{\mathrm{I}}\right]\left(\underline{\boldsymbol{n}} \cdot \Delta\frac{\partial\underline{\boldsymbol{\rho}}}{\partial\underset{\sim}{\xi}} + \underset{\approx}{\mathrm{H}}\Delta\underset{\sim}{\xi}\right) + \\ & \left. + \left[g_n\left(\Delta\frac{\partial\underline{\boldsymbol{\rho}}}{\partial\underset{\sim}{\xi}} + \frac{\partial^2\underline{\boldsymbol{\rho}}}{\partial\underset{\sim}{\xi}^2}\Delta\underset{\sim}{\xi}\right) \cdot \frac{\partial\underline{\boldsymbol{\rho}}^{\intercal}}{\partial\underset{\sim}{\xi}}\underset{\approx}{\bar{\mathrm{A}}} - \Delta g_n\underset{\approx}{\mathrm{I}}\right]\left(\underline{\boldsymbol{n}} \cdot \delta\frac{\partial\underline{\boldsymbol{\rho}}}{\partial\underset{\sim}{\xi}} + \underset{\approx}{\mathrm{H}}\delta\underset{\sim}{\xi}\right)\right\}\end{aligned} \qquad [2.33]$$

The assumption of small gaps $g_n \approx 0$ leads to a simpler form:

$$\begin{aligned}\Delta\delta\underset{\sim}{\xi} \;&=\; \bar{\underset{\approx}{\mathrm{A}}}\left\{\delta g_n\left(\underline{\boldsymbol{n}}\cdot\Delta\frac{\partial\underline{\boldsymbol{\rho}}}{\partial\underset{\sim}{\xi}}+\underset{\approx}{\mathrm{H}}\Delta\underset{\sim}{\xi}\right)+\Delta g_n\left(\underline{\boldsymbol{n}}\cdot\delta\frac{\partial\underline{\boldsymbol{\rho}}}{\partial\underset{\sim}{\xi}}+\underset{\approx}{\mathrm{H}}\delta\underset{\sim}{\xi}\right)-\right.\\ &\left.-\frac{\partial\underline{\boldsymbol{\rho}}}{\partial\underset{\sim}{\xi}}\cdot\left(\delta\frac{\partial\underline{\boldsymbol{\rho}}}{\partial\underset{\sim}{\xi}}^{\mathsf{T}}\Delta\underset{\sim}{\xi}+\Delta\frac{\partial\underline{\boldsymbol{\rho}}}{\partial\underset{\sim}{\xi}}^{\mathsf{T}}\delta\underset{\sim}{\xi}\right)-\Delta\underset{\sim}{\xi}^{\mathsf{T}}\left(\frac{\partial\underline{\boldsymbol{\rho}}}{\partial\underset{\sim}{\xi}}\cdot\frac{\partial^2\underline{\boldsymbol{\rho}}}{\partial\underset{\sim}{\xi}^2}\right)\delta\underset{\sim}{\xi}\right\}\end{aligned} \tag{2.34}$$

2.3.2.2. *Shadow-projection case: infinitely remote emitter*

The second variation of the shadow gap is:

$$\Delta\delta g_s=-\frac{\underline{\boldsymbol{n}}}{\underline{\boldsymbol{e}}\cdot\underline{\boldsymbol{n}}}\cdot\left(\delta\frac{\partial\underline{\boldsymbol{\rho}}}{\partial\underset{\sim}{\xi}}^{\mathsf{T}}\Delta\underset{\sim}{\xi}+\Delta\frac{\partial\underline{\boldsymbol{\rho}}}{\partial\underset{\sim}{\xi}}^{\mathsf{T}}\delta\underset{\sim}{\xi}+\Delta\underset{\sim}{\xi}^{\mathsf{T}}\frac{\partial^2\underline{\boldsymbol{\rho}}}{\partial\underset{\sim}{\xi}^2}\delta\underset{\sim}{\xi}\right) \tag{2.35}$$

The second variation of the surface parameter is:

$$\Delta\delta\underset{\sim}{\xi}=-\overline{\frac{\partial\underline{\boldsymbol{\rho}}}{\partial\underset{\sim}{\xi}}}\cdot\left[\underline{\underline{\boldsymbol{I}}}-\frac{\underline{\boldsymbol{e}}\otimes\underline{\boldsymbol{n}}}{\underline{\boldsymbol{e}}\cdot\underline{\boldsymbol{n}}}\right]\cdot\left(\delta\frac{\partial\underline{\boldsymbol{\rho}}}{\partial\underset{\sim}{\xi}}^{\mathsf{T}}\Delta\underset{\sim}{\xi}+\Delta\frac{\partial\underline{\boldsymbol{\rho}}}{\partial\underset{\sim}{\xi}}^{\mathsf{T}}\delta\underset{\sim}{\xi}+\Delta\underset{\sim}{\xi}^{\mathsf{T}}\frac{\partial^2\underline{\boldsymbol{\rho}}}{\partial\underset{\sim}{\xi}^2}\delta\underset{\sim}{\xi}\right) \tag{2.36}$$

Note that the value of the shadow gap does not enter in these expressions.

2.3.2.3. *Shadow-projection case: close emitter*

The second variation of the shadow gap is:

$$\begin{aligned}\Delta\delta g_s \;=\; &-\frac{\underline{\boldsymbol{n}}}{\underline{\boldsymbol{n}}\cdot\underline{\boldsymbol{e}}}\cdot\left(\delta\frac{\partial\underline{\boldsymbol{\rho}}}{\partial\underset{\sim}{\xi}}^{\mathsf{T}}\Delta\underset{\sim}{\xi}+\Delta\frac{\partial\underline{\boldsymbol{\rho}}}{\partial\underset{\sim}{\xi}}^{\mathsf{T}}\delta\underset{\sim}{\xi}+\Delta\underset{\sim}{\xi}^{\mathsf{T}}\frac{\partial^2\underline{\boldsymbol{\rho}}}{\partial\underset{\sim}{\xi}^2}\delta\underset{\sim}{\xi}-\right.\\ &-\frac{\underset{\sim}{\boldsymbol{s}}^{\mathsf{T}}\otimes\underset{\sim}{\boldsymbol{s}}}{d_{se}}\cdot(\Delta g_s\delta\underline{\boldsymbol{r}}_s+\delta g_s\Delta\underline{\boldsymbol{r}}_s)+\frac{g_s}{d_{se}^2}\underset{\sim}{\boldsymbol{s}}^{\mathsf{T}}\left(\underset{\sim}{\boldsymbol{s}}\cdot\Delta\underline{\boldsymbol{r}}_s\underline{\boldsymbol{e}}\cdot\delta\underline{\boldsymbol{r}}_s+\right.\\ &\left.\left.+\;\underset{\sim}{\boldsymbol{s}}\cdot\delta\underline{\boldsymbol{r}}_s\otimes\underline{\boldsymbol{e}}\cdot\Delta\underline{\boldsymbol{r}}_s\right)\right)+\frac{g_s}{d_{se}^2}(\delta\underline{\boldsymbol{r}}_s\cdot\underset{\sim}{\boldsymbol{s}}^{\mathsf{T}})(\underset{\sim}{\boldsymbol{s}}\cdot\Delta\underline{\boldsymbol{r}}_s)\end{aligned} \tag{2.37}$$

The second variation of the surface parameter is:

$$\begin{aligned}\Delta\delta\underset{\sim}{\xi}\;=&-\overline{\frac{\partial\underline{\boldsymbol{\rho}}}{\partial\underset{\sim}{\xi}}}\cdot\left[\underline{\underline{\boldsymbol{I}}}-\frac{\underline{\boldsymbol{e}}\otimes\underline{\boldsymbol{n}}}{\underline{\boldsymbol{e}}\cdot\underline{\boldsymbol{n}}}\right]\cdot\left\{\delta\frac{\partial\underline{\boldsymbol{\rho}}}{\partial\underset{\sim}{\xi}}^{\mathsf{T}}\Delta\underset{\sim}{\xi}+\Delta\frac{\partial\underline{\boldsymbol{\rho}}}{\partial\underset{\sim}{\xi}}^{\mathsf{T}}\delta\underset{\sim}{\xi}+\Delta\underset{\sim}{\xi}^{\mathsf{T}}\frac{\partial^2\underline{\boldsymbol{\rho}}}{\partial\underset{\sim}{\xi}^2}\delta\underset{\sim}{\xi}-\right.\\ &\left.-\frac{1}{d_{se}}(\Delta g_s\delta\underline{\boldsymbol{r}}_s+\delta g_s\Delta\underline{\boldsymbol{r}}_s)+\frac{g_s}{d_{se}^2}(\Delta\underline{\boldsymbol{r}}_s\otimes\underline{\boldsymbol{e}}\cdot\delta\underline{\boldsymbol{r}}_s+\delta\underline{\boldsymbol{r}}_s\otimes\underline{\boldsymbol{e}}\cdot\Delta\underline{\boldsymbol{r}}_s)\right\}\end{aligned} \tag{2.38}$$

Assuming small gaps $g_s \approx 0$ results in a shorter expression:

$$\begin{aligned}\Delta\delta g_s \quad = & -\frac{\underline{\boldsymbol{n}}}{\underline{\boldsymbol{n}}\cdot\underline{\boldsymbol{e}}}\cdot\left(\delta\frac{\partial\underline{\boldsymbol{\rho}}^{\mathsf{T}}}{\partial\underset{\sim}{\xi}}\Delta\underset{\sim}{\xi}+\Delta\frac{\partial\underline{\boldsymbol{\rho}}^{\mathsf{T}}}{\partial\underset{\sim}{\xi}}\delta\underset{\sim}{\xi}+\Delta\underset{\sim}{\xi}^{\mathsf{T}}\frac{\partial^2\underline{\boldsymbol{\rho}}}{\partial\underset{\sim}{\xi}^2}\delta\underset{\sim}{\xi}-\right.\\ & \left.-\frac{\underset{\approx}{\boldsymbol{s}}^{\mathsf{T}}\otimes\underset{\approx}{\boldsymbol{s}}}{d_{se}}\cdot(\Delta g_s\delta\underline{\boldsymbol{r}}_s+\delta g_s\Delta\underline{\boldsymbol{r}}_s)\right)\end{aligned} \qquad [2.39]$$

In the case of an infinitely remote emitter $(d_{se}\to\infty)$, we get the same expressions as in the previous section both for the shadow gap [2.35] and the surface parameter [2.36].

Remark 2.3. On variations in two-dimensional problems

In order to get all variations for 2D geometries, we have to replace simply all quantities by their 2D homologues:

$$\underset{\sim}{\xi}\to\xi,\qquad \frac{\partial^n\underline{\boldsymbol{\rho}}}{\partial\underset{\sim}{\xi}^n}\to\frac{\partial^n\underline{\boldsymbol{\rho}}}{\partial\xi^n},\qquad \underset{\approx}{\mathrm{I}}=1,$$

$$\underset{\approx}{\mathrm{A}}\to A=\frac{\partial\underline{\boldsymbol{\rho}}}{\partial\xi}\cdot\frac{\partial\underline{\boldsymbol{\rho}}}{\partial\xi},\qquad \underset{\approx}{\bar{\mathrm{A}}}\to\frac{1}{A},\qquad \underset{\approx}{\mathrm{H}}\to H=\underline{\boldsymbol{n}}\cdot\frac{\partial^2\underline{\boldsymbol{\rho}}}{\partial\xi^2},\qquad \overline{\frac{\partial\underline{\boldsymbol{\rho}}}{\partial\underset{\sim}{\xi}}}\to\frac{1}{A}\frac{\partial\underline{\boldsymbol{\rho}}}{\partial\xi}$$

2.4. Numerical validation

Here, we demonstrate briefly how to validate numerically the expressions presented in the previous section. At the same time, this validation allows us to estimate the errors that we introduce in the incremental solution by approximating the first and the second variations by analytical expressions obtained within the assumption of infinitely small perturbations of the contact geometry.

The numerical validation technique can be summarized as follows: for a randomly generated biquadratic master surface in 3D $\underline{\boldsymbol{\rho}}(\underset{\sim}{\xi})$ and a slave point at a random position $\underline{\boldsymbol{r}}$, perturbations $\underline{\boldsymbol{\pi}}'(\underset{\sim}{\xi})$ and $\underline{\boldsymbol{p}}'$ are applied, respectively:

$$\underline{\boldsymbol{\rho}}\to\underline{\boldsymbol{\rho}}+\underline{\boldsymbol{\pi}}',\quad \underline{\boldsymbol{r}}\to\underline{\boldsymbol{r}}+\underline{\boldsymbol{p}}'$$

The direction of the perturbation is arbitrary and its value, for example, is given in fraction of the master segment dimension (maximal length):

$$\|\pi'(\underset{\sim}{\xi})\| = \varepsilon_p \dim(\underline{\boldsymbol{\rho}}), \quad \|\underline{\boldsymbol{p}}'\| = \varepsilon_p \dim(\underline{\boldsymbol{\rho}})$$

The initial normal gap g_n between the slave-node and its projection is prescribed, its value is also expressed in fraction of the master segment dimension:

$$g_n = \varepsilon_g \dim(\underline{\boldsymbol{\rho}})$$

Applied perturbations $\underline{\boldsymbol{\pi}}$ and $\underline{\boldsymbol{p}}$ result in change of all geometrical quantities:

$$g_n \to g_n'; \underset{\sim}{\xi} \to \underset{\sim}{\xi}{}'$$

The real variation of these quantities is evaluated as the difference between the perturbed state quantities and the initial quantities:

$$\delta g_n = g_n' - g_n, \quad \delta \underset{\sim}{\xi} = \underset{\sim}{\xi}{}' - \underset{\sim}{\xi}$$

At the same time, these variations can be estimated according to analytical formulas [2.23] and [2.24] as functions of the initial geometry and its perturbation:

$$\delta^a g_n = \delta^a g_n(\underline{\boldsymbol{\rho}}, \underline{\boldsymbol{r}}, \underline{\boldsymbol{\pi}}', \underline{\boldsymbol{p}}'), \quad \delta^a \underset{\sim}{\xi} = \delta^a \underset{\sim}{\xi}(\underline{\boldsymbol{\rho}}, \underline{\boldsymbol{r}}, \underline{\boldsymbol{\pi}}', \underline{\boldsymbol{p}}')$$

To evaluate the second variations, another perturbation is imposed to the initial geometry $\underline{\boldsymbol{\rho}}, \underline{\boldsymbol{r}}$. The value of this perturbation is the same ε_p, but direction is different:

$$\underline{\boldsymbol{\rho}} \to \underline{\boldsymbol{\rho}}'', \quad \underline{\boldsymbol{r}} \to \underline{\boldsymbol{r}}''$$

The corresponding real change in geometrical quantities is denoted with Δ:

$$\Delta g_n = g_n'' - g_n, \quad \Delta \underset{\sim}{\xi} = \underset{\sim}{\xi}{}'' - \underset{\sim}{\xi}$$

To evaluate the second variations, the geometry should be perturbed once again. The perturbation is fully determined by two previous perturbations:

$$\underline{\boldsymbol{\rho}} \to \underline{\boldsymbol{\rho}} + \underline{\boldsymbol{\pi}}' + \underline{\boldsymbol{\pi}}'', \quad \underline{\boldsymbol{r}} \to \underline{\boldsymbol{r}} + \underline{\boldsymbol{p}}' + \underline{\boldsymbol{p}}''$$

The corresponding change in geometrical quantities will be:

$$D\, g_n = g_n''' - g_n, \quad D\underset{\sim}{\xi} = \underset{\sim}{\xi}''' - \underset{\sim}{\xi}$$

From these three perturbed states, the real second variations of geometrical quantities can be deduced as:

$$\Delta\delta g_n = D\, g_n - \delta g_n - \Delta g_n, \quad \Delta\delta\underset{\sim}{\xi} = D\underset{\sim}{\xi} - \delta\underset{\sim}{\xi} - \Delta\underset{\sim}{\xi}$$

These variations can be estimated by the full analytical expressions:

$$\Delta\delta^a g_n = \Delta\delta^a g_n(\underline{\boldsymbol{\rho}}, \underline{\boldsymbol{r}}, \underline{\boldsymbol{\pi}}', \underline{\boldsymbol{p}}', \underline{\boldsymbol{\pi}}'', \underline{\boldsymbol{p}}''), \quad \Delta\delta^a\underset{\sim}{\xi} = \quad \Delta\delta^a\underset{\sim}{\xi}(\underline{\boldsymbol{\rho}}, \underline{\boldsymbol{r}}, \underline{\boldsymbol{\pi}}', \underline{\boldsymbol{p}}', \underline{\boldsymbol{\pi}}'', \underline{\boldsymbol{p}}'')$$

Using this technique, we can compare the full and truncated analytical estimations ($g_n \approx 0$) with the real variations computed for a given negative initial normal gap $g_n = -\varepsilon_g \dim(\underline{\boldsymbol{\rho}})$ and the given values of the perturbation $\|\underline{\boldsymbol{\pi}}\| = \varepsilon_p \dim(\underline{\boldsymbol{\rho}})$, $\|\underline{\boldsymbol{p}}\| = \varepsilon_p \dim(\underline{\boldsymbol{\rho}})$. For a statistically meaningful result, several thousand tests can be performed.

2.5. Discretized geometry

2.5.1. *Shape functions and finite elements*

To introduce the variations of the geometrical quantities in a simulation code, we first give some basic notions of the FEM. The FEM approximates the real geometry by the so-called *finite element mesh*. Such a mesh consists of *nodes* that are connected in order to form *elements* that are coupled together into a structure. We deal with coordinates of nodes $\boldsymbol{x}$ and their displacements. The displacement of points inside the element is determined by an interpolation of nodal displacements by means of the so-called *shape functions*:

$$\phi_i(\underset{\sim}{\xi}), \quad i = 1, N$$

where N is the number of nodes, which determines the geometry of the given element and $\underset{\sim}{\xi}$ is a vector (v-scalar) of normalized parameters ($\xi_j \in [-1; 1]$), which determine the coordinates of points $\underline{\boldsymbol{r}}$ in the "parent space":

$$\underline{\boldsymbol{r}} = \sum_{i=1}^{N} \phi_i(\underset{\sim}{\xi})\underline{\boldsymbol{x}}_i \qquad [2.40]$$

where $\underline{\boldsymbol{x}}_i$ are nodal coordinates or, in general, any tensor field values at nodes. Shape functions must verify the following equality:

$$\phi_i(\underset{\sim}{\xi}^j) = \delta_i^j$$

where $\underset{\sim}{\xi}^j$ is the coordinate of the jth node in the local frame and δ_i^j is Kronecker's delta.

Structural finite elements can be classified by the order of shape functions – linear and quadratic – which in general correspond to the number of nodes. In the following subsections, we will consider an abstract 3D element, whose contacting surface is formed by N nodes with the corresponding order of approximation. A more detailed presentation of the finite element formalism will be given in section 5.3.

2.5.2. *Geometry of contact elements*

To describe the contact geometry, let us create an abstract *contact-element*, which consists of one slave node $\underline{\boldsymbol{x}}_0(t)$ and several master nodes $\underline{\boldsymbol{x}}_i(t)$, $i = 1, \ldots, N$ associated with the master surface of one structural element. This surface is parametrized by $\underset{\sim}{\xi}$, a point $\underline{\boldsymbol{\rho}}$ on the surface is given by:

$$\underline{\boldsymbol{\rho}} = \sum_{i=1}^{N} \phi_i(\underset{\sim}{\xi})\underline{\boldsymbol{x}}_i = \sum_{i=1}^{N} \phi_i(\xi_1, \xi_2)\underline{\boldsymbol{x}}_i \qquad [2.41]$$

The last equality is valid for 3D geometries, for which the two surface parameters ξ_1 and ξ_2 are assembled in the v-scalar $\underset{\sim}{\xi} = [\xi_1,\ \xi_2]^{\mathsf{T}}$.

First, we derive all the quantities to express the first- and second-order variations in the frame of the contact element.

– $[\underline{\boldsymbol{X}}]_{\dim \times N+1}$ is an array or v-vector, which contains coordinate vectors of the contact-element's nodes: the slave node first and next all master nodes:

$$\underset{\sim}{\boldsymbol{X}} \sim [\underline{\boldsymbol{X}}] = [\underline{\boldsymbol{X}}(t)] = [\underline{\boldsymbol{x}}_0(t),\ \underline{\boldsymbol{x}}_1(t),\ \ldots,\ \underline{\boldsymbol{x}}_N(t)]^{\intercal}$$

– $[\Phi]_{1\times N+1}$ is an array or v-scalar, which contains zero in the first position and next the shape functions of the master surface:

$$\underset{\sim}{\phi} \sim [\Phi] = \left[\Phi(\underset{\sim}{\xi})\right] = \left[0,\ \phi_1(\underset{\sim}{\xi}),\ \ldots,\ \phi_N(\underset{\sim}{\xi})\right]^{\intercal}$$

– $[\Phi'_i]_{1\times N+1}$ is an array or v-scalar of derivatives of the shape functions by the surface parameter ξ_i with zero in the first position:

$$\underset{\sim}{\phi}'_i \sim [\Phi'_i] = \left[\frac{\partial \Phi(\underset{\sim}{\xi})}{\partial \xi_i}\right] = \left[0,\ \frac{\partial \phi_1(\underset{\sim}{\xi})}{\partial \xi_i},\ \ldots,\ \frac{\partial \phi_N(\underset{\sim}{\xi})}{\partial \xi_i}\right]^{\intercal} = [0,\ \phi_{1,i}\ ,\ \ldots,\ \phi_{N,i}]^{\intercal}$$

– and so on for the higher order derivations:

$$\underset{\sim}{\phi}''_{ij} \sim \left[\Phi''_{ij}\right] = \left[\frac{\partial^2 \Phi(\underset{\sim}{\xi})}{\partial \xi_i \partial \xi_j}\right] = [0,\ \phi_{1,ij}\ ,\ \ldots,\ \phi_{N,ij}]^{\intercal}$$

$$\underset{\sim}{\phi}'''_{ijk} \sim \left[\Phi'''_{ijk}\right] = \left[\frac{\partial^3 \Phi(\underset{\sim}{\xi})}{\partial \xi_i \partial \xi_j \partial \xi_k}\right] = [0,\ \phi_{1,ijk}\ ,\ \ldots,\ \phi_{N,ijk}]^{\intercal}$$

Next, we express all the kinematic quantities and their variations, which appear in section 2.2, in a form adapted for the finite element formalism.

– slave node:

$$\boxed{\underline{\boldsymbol{r}}_s} = \underline{\boldsymbol{r}}_s(t) = \underline{\boldsymbol{x}}_0(t) = \boxed{[S_0]^{\intercal}\,[\underline{\boldsymbol{X}}]}$$

where $[S_0]_{N+1}$ is nothing but a selection vector for the slave nodes component:

$$[S_0] = [1,\ 0,\ \ldots\ ,\ 0]^{\intercal}$$

– projection point on the master surface:

$$\boxed{\underline{\boldsymbol{\rho}}} = \underline{\boldsymbol{\rho}}(t, \underset{\sim}{\xi_\pi}) = \sum_{i=1}^{N} \phi_i(\underset{\sim}{\xi_\pi})\underline{\boldsymbol{x}}_i = \left[\Phi(\underset{\sim}{\xi_\pi})\right]^{\intercal}[\underline{\boldsymbol{X}}(t)] = \boxed{[\Phi]^{\intercal}\,[\underline{\boldsymbol{X}}]} = \underset{\sim}{\phi}^{\intercal}\underset{\sim}{\boldsymbol{X}}$$

where $\underset{\sim}{\xi}_\pi$ stands for the coordinate of the projection point:

– local surface basis at the projection point:

$$\boxed{\frac{\partial \underline{\boldsymbol{\rho}}}{\partial \xi_i}} = \left.\frac{\partial \underline{\boldsymbol{\rho}}(t, \underset{\sim}{\xi})}{\partial \xi_i}\right|_{\underset{\sim}{\xi}_\pi} = \left[\left.\frac{\partial \Phi(\underset{\sim}{\xi})}{\partial \xi_i}\right|_{\underset{\sim}{\xi}_\pi}\right]^{\intercal} [\underline{\boldsymbol{X}}(t)] = \boxed{[\Phi_i']^{\intercal}\,[\underline{\boldsymbol{X}}]} = \underset{\sim}{\phi}_i'^{T}\,\underline{\underline{\boldsymbol{X}}}$$

– unit normal to the master surface at the projection point:

$$\boxed{\underline{\boldsymbol{n}}} = \underline{\boldsymbol{n}}(t, \underset{\sim}{\xi}_\pi) = \frac{\frac{\partial \underline{\boldsymbol{\rho}}(t,\xi_\pi)}{\partial \xi_1} \times \frac{\partial \underline{\boldsymbol{\rho}}(t,\xi_\pi)}{\partial \xi_2}}{\left\|\frac{\partial \underline{\boldsymbol{\rho}}(t,\xi_\pi)}{\partial \xi_1} \times \frac{\partial \underline{\boldsymbol{\rho}}(t,\xi_\pi)}{\partial \xi_2}\right\|} = \boxed{\frac{\left([\Phi_1']^{\intercal}\,[\underline{\boldsymbol{X}}]\right) \times \left([\Phi_2']^{\intercal}\,[\underline{\boldsymbol{X}}]\right)}{\|([\Phi_1']^{\intercal}\,[\underline{\boldsymbol{X}}]) \times ([\Phi_2']^{\intercal}\,[\underline{\boldsymbol{X}}])\|}}$$

hereinafter we will use simply $\underline{\boldsymbol{n}}$ to denote the normal, as variations or derivative of the normal are not needed.

The variations of the kinematic quantities can be derived in the finite element formalism. We start with the *first-order variation of the normal gap* δg_n. From [2.23] we get:

$$\delta g_n = \underline{\boldsymbol{n}} \cdot (\delta \underline{\boldsymbol{r}}_s - \delta \underline{\boldsymbol{\rho}}) = \underline{\boldsymbol{n}} \cdot (\delta\,[\underline{\boldsymbol{X}}]_0 - [\Phi]^{\intercal}\,\delta\,[\underline{\boldsymbol{X}}]) = ([S_0]^{\intercal} - [\Phi]^{\intercal})\,\underline{\boldsymbol{n}} \cdot \delta\,[\underline{\boldsymbol{X}}] \qquad [2.42]$$

or in a component form:

$$\boxed{\delta g_n = \begin{bmatrix} \underline{\boldsymbol{n}} \\ -\phi_1 \underline{\boldsymbol{n}} \\ \vdots \\ -\phi_N \underline{\boldsymbol{n}} \end{bmatrix}^{\intercal} \cdot \begin{bmatrix} \delta \underline{\boldsymbol{x}}_0 \\ \delta \underline{\boldsymbol{x}}_1 \\ \vdots \\ \delta \underline{\boldsymbol{x}}_N \end{bmatrix} = [\nabla g_n]^{\intercal} \cdot \delta\,[\underline{\boldsymbol{X}}]} \qquad [2.43]$$

The *first-order variation of the surface parameter* $\delta \underset{\sim}{\xi}$ is expressed from [2.24]

$$\delta \xi_i = \left[(\underset{\approx}{\mathrm{A}} - g_n \underset{\approx}{\mathrm{H}})^{-1}\right]_{ij} \left(\frac{\partial \underline{\boldsymbol{\rho}}}{\partial \xi_j} \cdot (\delta \underline{\boldsymbol{r}}_s - \delta \underline{\boldsymbol{\rho}}) + g_n \delta \frac{\partial \underline{\boldsymbol{\rho}}}{\partial \xi_j} \cdot \underline{\boldsymbol{n}}\right). \qquad [2.44]$$

If we denote $\underset{\approx}{\mathrm{C}} = (\underset{\approx}{\mathrm{A}} - g_n \underset{\approx}{\mathrm{H}})^{-1}$, we get:

$$\delta \xi_i = C_{ij} \left(([S_0]^{\intercal} - [\Phi]^{\intercal})\,\frac{\partial \underline{\boldsymbol{\rho}}}{\partial \xi_j} + g_n \left[\Phi_j'\right]^{\intercal} \underline{\boldsymbol{n}}\right) \cdot \delta\,[\underline{\boldsymbol{X}}] \qquad [2.45]$$

or in a component form:

$$\boxed{\delta\xi_i = C_{ij} \begin{bmatrix} \frac{\partial \underline{\boldsymbol{\rho}}}{\partial \xi_j} \\ -\frac{\partial \underline{\boldsymbol{\rho}}}{\partial \xi_j}\phi_1 + g_n \underline{\boldsymbol{n}}\phi_{1,j} \\ \vdots \\ -\frac{\partial \underline{\boldsymbol{\rho}}}{\partial \xi_j}\phi_N + g_n \underline{\boldsymbol{n}}\phi_{N,j} \end{bmatrix}^{\intercal} \cdot \begin{bmatrix} \delta \underline{\boldsymbol{x}}_0 \\ \delta \underline{\boldsymbol{x}}_1 \\ \vdots \\ \delta \underline{\boldsymbol{x}}_N \end{bmatrix} = [\boldsymbol{\nabla}\xi_i]^{\intercal} \cdot \delta\,[\underline{\boldsymbol{X}}]} \qquad [2.46]$$

where the basis vectors $\frac{\partial \underline{\boldsymbol{\rho}}}{\partial \xi_j}$ may be either inserted explicitly in this expression or expressed through the shape functions:

$$\frac{\partial \underline{\boldsymbol{\rho}}}{\partial \xi_i} = [\Phi_i']^{\intercal}\,[\underline{\boldsymbol{X}}]$$

To express the *second-order variation of the normal gap* $\Delta\delta g_n$ we rewrite [2.31]

$$\begin{aligned} \Delta\delta g_n = & \underbrace{-\underline{\boldsymbol{n}} \cdot \delta\frac{\partial \underline{\boldsymbol{\rho}}}{\partial \xi_i}\Delta\xi_i - \underline{\boldsymbol{n}} \cdot \Delta\frac{\partial \underline{\boldsymbol{\rho}}}{\partial \xi_i}\delta\xi_i}_{\text{term 1}} \underbrace{-\delta\xi_i(H_{ij} - g_n H_{ik}A^{km}H_{mj})\Delta\xi_j}_{\text{term 2}} + \\ & + \underbrace{g_n \left(\underline{\boldsymbol{n}} \cdot \delta\frac{\partial \underline{\boldsymbol{\rho}}}{\partial \xi_i}\right) A^{ij} \left(\Delta\frac{\partial \underline{\boldsymbol{\rho}}}{\partial \xi_j} \cdot \underline{\boldsymbol{n}}\right)}_{\text{term 3}} \end{aligned} \qquad [2.47]$$

To express $\Delta\underset{\sim}{\xi}$ and $\delta\underset{\sim}{\xi}$, we use [2.46]; other terms are replaced by their discretized homologues:

$$\begin{aligned} \Delta\delta g_n = & \underbrace{-\delta\,[\underline{\boldsymbol{X}}]^{\intercal} \cdot \left\{\underline{\boldsymbol{n}}\,[\Phi_i'] \otimes [\boldsymbol{\nabla}\xi_i]^{\intercal} + [\boldsymbol{\nabla}\xi_i] \otimes [\Phi_i']^{\intercal}\,\underline{\boldsymbol{n}}\right\} \cdot \Delta\,[\underline{\boldsymbol{X}}]}_{\text{term 1}} \\ & \underbrace{-\delta\,[\underline{\boldsymbol{X}}]^{\intercal} \cdot \left\{(H_{ij} - g_n H_{ik}A^{km}H_{mj})[\boldsymbol{\nabla}\xi_i] \otimes [\boldsymbol{\nabla}\xi_j]^{\intercal}\right\} \cdot \Delta\,[\underline{\boldsymbol{X}}]}_{\text{term 2}} \\ & \underbrace{+\delta\,[\underline{\boldsymbol{X}}]^{\intercal} \cdot \left\{g_n A^{ij}\underline{\boldsymbol{n}}\,[\Phi_i'] \otimes \left[\Phi_j'\right]^{\intercal}\underline{\boldsymbol{n}}\right\} \cdot \Delta\,[\underline{\boldsymbol{X}}]}_{\text{term 3}} \end{aligned} \qquad [2.48]$$

By grouping the terms, we obtain the final expression for the second variation of the normal gap:

$$\boxed{\begin{array}{c}\Delta\delta g_n = \delta\left[\underline{\boldsymbol{X}}\right]^{\intercal}\cdot\left\{-\underline{\boldsymbol{n}}\left[\Phi_i'\right]\otimes\left[\boldsymbol{\nabla}\xi_i\right]^{\intercal}-\left[\boldsymbol{\nabla}\xi_i\right]\otimes\left[\Phi_i'\right]^{\intercal}\underline{\boldsymbol{n}}-\right.\\ \left.-\left(H_{ij}-g_n H_{ik}A^{km}H_{mj}\right)\left[\boldsymbol{\nabla}\xi_i\right]\otimes\left[\boldsymbol{\nabla}\xi_j\right]^{\intercal}+g_n A^{ij}\underline{\boldsymbol{n}}\left[\Phi_i'\right]\otimes\left[\Phi_j'\right]^{\intercal}\underline{\boldsymbol{n}}\right\}\cdot\Delta\left[\underline{\boldsymbol{X}}\right]=\\ =\delta\left[\underline{\boldsymbol{X}}\right]^{\intercal}\cdot\left[\nabla\nabla g_n\right]\cdot\Delta\left[\underline{\boldsymbol{X}}\right]\end{array}} \qquad [2.49]$$

where $[\boldsymbol{\nabla}\xi_i]$ should be substituted from equation [2.46].

The *second-order variation of the surface parameter* $\Delta\delta\underset{\sim}{\xi}$ is derived from its continuous form [2.33].

$$\begin{aligned}\Delta\delta\xi_i = -C_{ij}\Bigg[&\underbrace{\frac{\partial\underline{\boldsymbol{\rho}}}{\partial\xi_j}\cdot\left(\delta\frac{\partial\underline{\boldsymbol{\rho}}}{\partial\xi_k}\Delta\xi_k+\Delta\frac{\partial\underline{\boldsymbol{\rho}}}{\partial\xi_k}\delta\xi_k+\delta\xi_k\frac{\partial^2\underline{\boldsymbol{\rho}}}{\partial\xi_k\partial\xi_m}\Delta\xi_m\right)}_{\text{term 1}}\\ &\underbrace{-g_n\underline{\boldsymbol{n}}\cdot\left(\delta\frac{\partial^2\underline{\boldsymbol{\rho}}}{\partial\xi_j\partial\xi_k}\Delta\xi_k+\Delta\frac{\partial^2\underline{\boldsymbol{\rho}}}{\partial\xi_j\partial\xi_k}\delta\xi_k+\delta\xi_k\frac{\partial^3\underline{\boldsymbol{\rho}}}{\partial\xi_k\partial\xi_j\partial\xi_m}\Delta\xi_m\right)}_{\text{term 2}}\\ +\ &\underbrace{\left(-\delta g_n\delta_{kj}+g_nA^{km}\frac{\partial\underline{\boldsymbol{\rho}}}{\partial\xi_m}\cdot\left\{\delta\frac{\partial\underline{\boldsymbol{\rho}}}{\partial\xi_j}+\frac{\partial^2\underline{\boldsymbol{\rho}}}{\partial\xi_j\partial\xi_l}\delta\xi_l\right\}\right)\left\{\Delta\frac{\partial\underline{\boldsymbol{\rho}}}{\partial\xi_k}\cdot\underline{\boldsymbol{n}}+H_{ks}\Delta\xi_s\right\}}_{\text{term 3}}\\ +\ &\underbrace{\left(-\Delta g_n\delta_{kj}+g_nA^{km}\frac{\partial\underline{\boldsymbol{\rho}}}{\partial\xi_m}\cdot\left\{\Delta\frac{\partial\underline{\boldsymbol{\rho}}}{\partial\xi_j}+\frac{\partial^2\underline{\boldsymbol{\rho}}}{\partial\xi_j\partial\xi_l}\Delta\xi_l\right\}\right)\left\{\delta\frac{\partial\underline{\boldsymbol{\rho}}}{\partial\xi_k}\cdot\underline{\boldsymbol{n}}+H_{ks}\delta\xi_s\right\}}_{\text{term 4}}\Bigg]\end{aligned} \qquad [2.50]$$

Recall that $C_{ij}=\left[\left(\underset{\approx}{\mathrm{A}}-g_n\underset{\approx}{\mathrm{H}}\right)^{-1}\right]_{ij}$, next we replace all the continuous quantities by their discretized analogs.

Term 1.

$$\begin{aligned}&\frac{\partial\underline{\boldsymbol{\rho}}}{\partial\xi_j}\cdot\left\{\delta\left[\underline{\boldsymbol{X}}\right]^{\intercal}\left[\Phi_k'\right]\left[\boldsymbol{\nabla}\xi_k\right]^{\intercal}\cdot\Delta\left[\underline{\boldsymbol{X}}\right]+\left(\delta\left[\underline{\boldsymbol{X}}\right]^{\intercal}\cdot\left[\boldsymbol{\nabla}\xi_k\right]\right)\left[\Phi_k'\right]^{\intercal}\Delta\left[\underline{\boldsymbol{X}}\right]+\right.\\ &\qquad\left.+\frac{\partial^2\underline{\boldsymbol{\rho}}}{\partial\xi_k\partial\xi_m}\left(\delta\left[\underline{\boldsymbol{X}}\right]^{\intercal}\cdot\left[\boldsymbol{\nabla}\xi_k\right]\right)\left(\left[\boldsymbol{\nabla}\xi_m\right]^{\intercal}\cdot\Delta\left[\underline{\boldsymbol{X}}\right]\right)\right\}=\\ &=\delta\left[\underline{\boldsymbol{X}}\right]^{\intercal}\cdot\left\{\left[\Phi_k'\right]\frac{\partial\underline{\boldsymbol{\rho}}}{\partial\xi_j}\otimes\left[\boldsymbol{\nabla}\xi_k\right]^{\intercal}+\left[\boldsymbol{\nabla}\xi_k\right]\otimes\frac{\partial\underline{\boldsymbol{\rho}}}{\partial\xi_j}\left[\Phi_k'\right]^{\intercal}+\right.\\ &\qquad\left.+\left(\frac{\partial\underline{\boldsymbol{\rho}}}{\partial\xi_j}\cdot\frac{\partial^2\underline{\boldsymbol{\rho}}}{\partial\xi_k\partial\xi_m}\right)\left[\boldsymbol{\nabla}\xi_k\right]\otimes\left[\boldsymbol{\nabla}\xi_m\right]^{\intercal}\right\}\cdot\Delta\left[\underline{\boldsymbol{X}}\right]\end{aligned} \qquad [2.51]$$

Term 2.

$$
\begin{aligned}
& g_n \left\{ \delta\left[\underline{\underline{X}}\right]^{\intercal} \cdot \underline{\underline{n}} \left[\Phi''_{jk}\right] \left[\nabla\xi_k\right]^{\intercal} \cdot \Delta\left[\underline{\underline{X}}\right] + \delta\left[\underline{\underline{X}}\right]^{\intercal} \cdot \left[\nabla\xi_k\right] \left[\Phi''_{jk}\right]^{\intercal} \underline{\underline{n}} \cdot \Delta\left[\underline{\underline{X}}\right] \right. \\
& \left. + \delta\left[\underline{\underline{X}}\right]^{\intercal} \cdot \left[\nabla\xi_k\right] \left(\underline{\underline{n}} \cdot \frac{\partial^3 \underline{\underline{\rho}}}{\partial\xi_k \partial\xi_j \partial\xi_m} \right) \left[\nabla\xi_m\right]^{\intercal} \cdot \Delta\left[\underline{\underline{X}}\right] \right\} = \\
& = \delta\left[\underline{\underline{X}}\right]^{\intercal} \cdot \left\{ g_n \left[\Phi''_{jk}\right] \underline{\underline{n}} \otimes \left[\nabla\xi_k\right]^{\intercal} + g_n \left[\nabla\xi_k\right] \otimes \underline{\underline{n}} \left[\Phi''_{jk}\right]^{\intercal} \right. \\
& \qquad \left. + g_n \left(\underline{\underline{n}} \cdot \frac{\partial^3 \underline{\underline{\rho}}}{\partial\xi_k \partial\xi_j \partial\xi_m} \right) \left[\nabla\xi_k\right] \otimes \left[\nabla\xi_m\right]^{\intercal} + \right\} \cdot \Delta\left[\underline{\underline{X}}\right]
\end{aligned}
\qquad [2.52]
$$

Term 3.

$$
\begin{aligned}
& \left(- \left[\nabla g_n\right]^{\intercal} \cdot \delta\left[\underline{\underline{X}}\right] \delta_{kj} + g_n A^{km} \frac{\partial \underline{\underline{\rho}}}{\partial\xi_m} \cdot \left\{ \left[\Phi'_j\right]^{\intercal} \delta\left[\underline{\underline{X}}\right] + \frac{\partial^2 \underline{\underline{\rho}}}{\partial\xi_j \partial\xi_l} \left[\nabla\xi_l\right]^{\intercal} \cdot \delta\left[\underline{\underline{X}}\right] \right\} \right) \otimes \\
& \qquad \otimes \left\{ \left[\Phi'_k\right]^{\intercal} \Delta\left[\underline{\underline{X}}\right] \cdot \underline{\underline{n}} + H_{ks} \left[\nabla\xi_s\right]^{\intercal} \cdot \Delta\left[\underline{\underline{X}}\right] \right\} = \\
& - \left(\delta\left[\underline{\underline{X}}\right]^{\intercal} \cdot \left[\nabla g_n\right] \delta_{kj} \right) \left(\left[\Phi'_k\right]^{\intercal} \underline{\underline{n}} \cdot \Delta\left[\underline{\underline{X}}\right] + H_{ks} \left[\nabla\xi_s\right]^{\intercal} \cdot \Delta\left[\underline{\underline{X}}\right] \right) + \\
& + \left(\delta\left[\underline{\underline{X}}\right]^{\intercal} \cdot \frac{\partial \underline{\underline{\rho}}}{\partial\xi_m} \left[\Phi'_j\right] g_n A^{km} \right) \left(\left[\Phi'_k\right]^{\intercal} \underline{\underline{n}} \cdot \Delta\left[\underline{\underline{X}}\right] + H_{ks} \left[\nabla\xi_s\right]^{\intercal} \cdot \Delta\left[\underline{\underline{X}}\right] \right) + \\
& + \left(\delta\left[\underline{\underline{X}}\right]^{\intercal} \cdot \left[\nabla\xi_l\right] \right) \left(g_n A^{km} \frac{\partial \underline{\underline{\rho}}}{\partial\xi_m} \cdot \frac{\partial^2 \underline{\underline{\rho}}}{\partial\xi_j \partial\xi_l} \right) \left(\left[\Phi'_k\right]^{\intercal} \underline{\underline{n}} \cdot \Delta\left[\underline{\underline{X}}\right] + H_{ks} \left[\nabla\xi_s\right]^{\intercal} \cdot \Delta\left[\underline{\underline{X}}\right] \right) \\
& = \delta\left[\underline{\underline{X}}\right]^{\intercal} \cdot \left\{ -\delta_{kj} \left[\nabla g_n\right] \otimes \left(\underline{\underline{n}} \left[\Phi'_k\right]^{\intercal} + H_{ks} \left[\nabla\xi_s\right]^{\intercal} \right) + g_n A^{km} \left[\Phi'_j\right] \frac{\partial \underline{\underline{\rho}}}{\partial\xi_m} \otimes \right. \\
& \qquad \otimes \left(\underline{\underline{n}} \left[\Phi'_k\right]^{\intercal} + H_{ks} \left[\nabla\xi_s\right]^{\intercal} \right) + g_n A^{km} \left(\frac{\partial \underline{\underline{\rho}}}{\partial\xi_m} \cdot \frac{\partial^2 \underline{\underline{\rho}}}{\partial\xi_j \partial\xi_l} \right) \left[\nabla\xi_l\right] \otimes \\
& \qquad \left. \otimes \left(\underline{\underline{n}} \left[\Phi'_k\right]^{\intercal} + H_{ks} \left[\nabla\xi_s\right]^{\intercal} \right) \right\} \cdot \Delta\left[\underline{\underline{X}}\right]
\end{aligned}
\qquad [2.53]
$$

Term 4 is the same as term 3, but Δ is replaced by δ and vice versa.

The final expression for the second-order variation of the surface parameter is the sum of terms 1–4 multiplied by t-scalar $\underset{\approx}{\mathrm{C}}$ with minus sign:

$$
\begin{aligned}
& \Delta\delta\xi_i = \delta\left[\underline{\underline{X}}\right]^{\intercal} \cdot \left\{ -C_{ij} \left[\left[\Phi'_k\right] \frac{\partial \underline{\underline{\rho}}}{\partial\xi_j} \otimes \left[\nabla\xi_k\right]^{\intercal} + \left[\nabla\xi_k\right] \otimes \frac{\partial \underline{\underline{\rho}}}{\partial\xi_j} \left[\Phi'_k\right]^{\intercal} + \right. \right. \\
& + \left(\frac{\partial \underline{\underline{\rho}}}{\partial\xi_j} \cdot \frac{\partial^2 \underline{\underline{\rho}}}{\partial\xi_k \partial\xi_m} - g_n \underline{\underline{n}} \cdot \frac{\partial^3 \underline{\underline{\rho}}}{\partial\xi_k \partial\xi_j \partial\xi_m} \right) \left[\nabla\xi_k\right] \otimes \left[\nabla\xi_m\right]^{\intercal} - g_n \left[\Phi''_{jk}\right] \underline{\underline{n}} \otimes \left[\nabla\xi_k\right]^{\intercal} - \\
& - g_n \left[\nabla\xi_k\right] \otimes \underline{\underline{n}} \left[\Phi''_{jk}\right]^{\intercal} - \left[\nabla g_n\right] \otimes \left(\underline{\underline{n}} \left[\Phi'_j\right]^{\intercal} + H_{js} \left[\nabla\xi_s\right]^{\intercal} \right) - \\
& - \left(\left[\Phi'_j\right] \underline{\underline{n}} + H_{js} \left[\nabla\xi_s\right] \right) \otimes \left[\nabla g_n\right]^{\intercal} + g_n A^{km} \left(\left[\Phi'_j\right] \frac{\partial \underline{\underline{\rho}}}{\partial\xi_m} \otimes \left(\underline{\underline{n}} \left[\Phi'_k\right]^{\intercal} + H_{ks} \left[\nabla\xi_s\right]^{\intercal} \right) + \right. \\
& \left. + \left(\underline{\underline{n}} \left[\Phi'_k\right] + H_{ks} \left[\nabla\xi_s\right] \right) \otimes \frac{\partial \underline{\underline{\rho}}}{\partial\xi_m} \left[\Phi'_j\right]^{\intercal} \right) + g_n A^{km} \left(\frac{\partial \underline{\underline{\rho}}}{\partial\xi_m} \cdot \frac{\partial^2 \underline{\underline{\rho}}}{\partial\xi_j \partial\xi_l} \right) \\
& \left. \left. \left(\left[\nabla\xi_l\right] \otimes \left(\underline{\underline{n}} \left[\Phi'_k\right]^{\intercal} + H_{ks} \left[\nabla\xi_s\right]^{\intercal} \right) + \left(\underline{\underline{n}} \left[\Phi'_k\right] + H_{ks} \left[\nabla\xi_s\right] \right) \otimes \left[\nabla\xi_l\right]^{\intercal} \right) \right] \right\} \cdot \Delta\left[\underline{\underline{X}}\right] = \\
& = \delta\left[\underline{\underline{X}}\right]^{\intercal} \cdot \left[\nabla\nabla\xi_i\right] \cdot \Delta\left[\underline{\underline{X}}\right]
\end{aligned}
\qquad [2.54]
$$

where expressions $[\nabla g_n]$ and $[\boldsymbol{\nabla}\xi_i]$ should be substituted from [2.43] and [2.46], respectively. All derivatives of the projection vector are evaluated through the shape functions:

$$\left.\frac{\partial \underline{\boldsymbol{\rho}}}{\partial \xi_i}\right|_{\underset{\sim}{\xi}_\pi} = [\Phi_i']^{\mathsf{T}}\,[\underline{\boldsymbol{X}}]\,, \quad \left.\frac{\partial^2 \underline{\boldsymbol{\rho}}}{\partial \xi_i \xi_j}\right|_{\underset{\sim}{\xi}_\pi} = \left[\Phi_{ij}''\right]^{\mathsf{T}}\,[\underline{\boldsymbol{X}}]\,, \quad \left.\frac{\partial^3 \underline{\boldsymbol{\rho}}}{\partial \xi_i \xi_j \xi_k}\right|_{\underset{\sim}{\xi}_\pi} = \left[\Phi_{ijk}'''\right]^{\mathsf{T}}\,[\underline{\boldsymbol{X}}]$$

In [2.49] and [2.54] the matrices connecting $\Delta\delta\underset{\sim}{\xi}$ and $\Delta\delta g_n$ with $\delta[\underline{\boldsymbol{X}}]$ and $\Delta[\underline{\boldsymbol{X}}]$ are symmetric.

2.6. Enrichment of contact geometry

In the second half of the 1990s, several approaches based on the enriching of the element interpolation functions have been proposed for different problems [HEY 89], [BAB 95].

$$\underline{\boldsymbol{r}}(t,\zeta) = \underset{\sim}{\phi}^{\mathsf{T}}(\zeta)\underline{\underline{\boldsymbol{x}}}(t) \longrightarrow \underline{\boldsymbol{r}}_e(t,\zeta) = \left(\underset{\sim}{\phi}^{\mathsf{T}}(\zeta) + \underset{\sim}{\psi}_e^{\mathsf{T}}(\zeta)\right)\underline{\underline{\boldsymbol{x}}}(t)$$

where $\underline{\boldsymbol{r}}_e$ denotes the enriched vector and $\underset{\sim}{\psi}_e$ denotes the enriching shape functions. The entire class of enriched or extended finite element methods got the name XFEM (extended finite element method) [MOË 99], GFEM (generalized finite element method FEM) or PUM (partition of unity method) [MEL 96]. The method is used for modeling of dislocations, solidification, two-fluid flows, cracks and cohesive cracks; for example, the last two examples are based on enriching by the Heaviside function.

Idea 2.2. On enrichment of contact geometry

Inspired by these techniques, we propose an enrichment method for contact problems [YAS 11a]. The method consists of enriching the master surface (Figure 2.12) with an arbitrary enriching function h_e:

$$\underline{\boldsymbol{\rho}} \longrightarrow \boxed{\underline{\boldsymbol{\rho}}_e = \underline{\boldsymbol{\rho}} + h_e\underline{\boldsymbol{n}}} \Leftrightarrow \underline{\boldsymbol{\rho}}_e(\underset{\sim}{\xi}) = \underline{\boldsymbol{\rho}}(\underset{\sim}{\xi}) + h_e(\underset{\sim}{\xi}, \underset{\sim}{\Theta})\underline{\boldsymbol{n}}(\underset{\sim}{\xi}) \quad [2.55]$$

where the enriching function $h_e(\underset{\sim}{\xi}, \underset{\sim}{\Theta})$ may depend on the surface parameter $\underset{\sim}{\xi}$ and/or on the local stress–strain state, its history, time, loading cycle, etc., which are included in parameter $\underset{\sim}{\Theta}$. So we can take into account the submesh features of the contact geometry and its evolution without an excessive remeshing and complex material models. These features may include roughness, geometry change due to wear, dislocation escape, oxidation, etc.

To keep the formulation consistent, we impose two conditions on the enriching function:

1) $h_e(\underset{\sim}{\xi}, \underset{\sim}{\Theta})$ is at least C^2-smooth by $\underset{\sim}{\xi}$ and C^1-smooth by $\underset{\sim}{\Theta}$;

2) to avoid self-intersection of the enriched surface, we require that the value of enriching function remains smaller than the minimal local curvature radius of the surface $|h_e(\underset{\sim}{\xi})| < \min\limits_i \left\{ 1/\kappa_i(\underset{\sim}{\xi}) \right\}$.

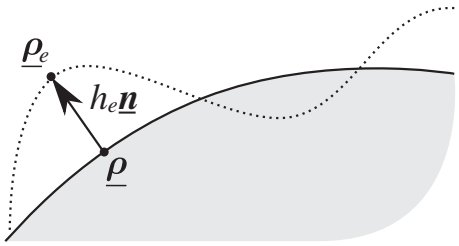

Figure 2.12. *Enriched geometry $\underline{\boldsymbol{\rho}}_e$ of the master surface $\underline{\boldsymbol{\rho}}$*

If the enriching function depends on only the surface parameter or it depends weakly on the loading and time, then the kinematic quantity's variations (see sections 2.3.1 and 2.3.2) retain their form; simply the quantities related to the master surface have to be replaced by their enriched variants $\bullet_e$, which are given below:

a) $\boxed{\underline{\boldsymbol{\rho}} \longrightarrow \underline{\boldsymbol{\rho}}_e}$: $\underline{\boldsymbol{\rho}}_e = \underline{\boldsymbol{\rho}} + h_e\underline{\boldsymbol{n}}$

b) $\boxed{\underline{\boldsymbol{n}} \longrightarrow \underline{\boldsymbol{n}}_e}$: $\underline{\boldsymbol{n}}_e = \dfrac{\frac{\partial \underline{\boldsymbol{\rho}}_e}{\partial \xi_1} \times \frac{\partial \underline{\boldsymbol{\rho}}_e}{\partial \xi_2}}{\left\| \frac{\partial \underline{\boldsymbol{\rho}}_e}{\partial \xi_1} \times \frac{\partial \underline{\boldsymbol{\rho}}_e}{\partial \xi_2} \right\|}$

c) $\boxed{\bar{\delta}\underline{\boldsymbol{\rho}} \longrightarrow \bar{\delta}\underline{\boldsymbol{\rho}}_e}$: $\bar{\delta}\underline{\boldsymbol{\rho}}_e = \delta\underline{\boldsymbol{\rho}}_e + \frac{\partial \underline{\boldsymbol{\rho}}_e^{\mathsf{T}}}{\partial \underset{\sim}{\xi}}\delta\underset{\sim}{\xi}$

d) $\boxed{\delta\underline{\boldsymbol{\rho}} \longrightarrow \delta\underline{\boldsymbol{\rho}}_e}$: $\delta\underline{\boldsymbol{\rho}}_e = \delta\underline{\boldsymbol{\rho}} + h_e\delta\underline{\boldsymbol{n}}$

e) $\boxed{\frac{\partial \underline{\boldsymbol{\rho}}}{\partial \underset{\sim}{\xi}} \longrightarrow \frac{\partial \underline{\boldsymbol{\rho}}_e}{\partial \underset{\sim}{\xi}}}$: $\frac{\partial \underline{\boldsymbol{\rho}}_e}{\partial \underset{\sim}{\xi}} = \frac{\partial \underline{\boldsymbol{\rho}}}{\partial \underset{\sim}{\xi}} + \underline{\boldsymbol{n}}\frac{\partial h_e}{\partial \underset{\sim}{\xi}} + h_e\frac{\partial \underline{\boldsymbol{n}}}{\partial \underset{\sim}{\xi}}$ [2.56]

f) $\boxed{\frac{\partial^2 \underline{\boldsymbol{\rho}}}{\partial \underset{\sim}{\xi}^2} \longrightarrow \frac{\partial^2 \underline{\boldsymbol{\rho}}_e}{\partial \underset{\sim}{\xi}^2}}$: $\frac{\partial^2 \underline{\boldsymbol{\rho}}_e}{\partial \underset{\sim}{\xi}^2} = \frac{\partial^2 \underline{\boldsymbol{\rho}}}{\partial \underset{\sim}{\xi}^2} + \frac{\partial \underline{\boldsymbol{n}}}{\partial \underset{\sim}{\xi}}\frac{\partial h_e}{\partial \underset{\sim}{\xi}}^{\mathsf{T}} + \frac{\partial h_e}{\partial \underset{\sim}{\xi}}\frac{\partial \underline{\boldsymbol{n}}}{\partial \underset{\sim}{\xi}}^{\mathsf{T}} + h_e\frac{\partial^2 \underline{\boldsymbol{n}}}{\partial \underset{\sim}{\xi}^2} + \underline{\boldsymbol{n}}\frac{\partial^2 h_e}{\partial \underset{\sim}{\xi}^2}$

g) $\boxed{\underset{\approx}{\mathrm{A}} \longrightarrow \underset{\approx}{\mathrm{A}}_e}$: $\underset{\approx}{\mathrm{A}}_e = \frac{\partial \underline{\boldsymbol{\rho}}_e}{\partial \underset{\sim}{\xi}} \cdot \frac{\partial \underline{\boldsymbol{\rho}}_e^{\mathsf{T}}}{\partial \underset{\sim}{\xi}}$

h) $\boxed{\underset{\approx}{\mathrm{H}} \longrightarrow \underset{\approx}{\mathrm{H}}_e}$: $\underset{\approx}{\mathrm{H}}_e = \underline{\boldsymbol{n}}_e \cdot \frac{\partial^2 \underline{\boldsymbol{\rho}}_e}{\partial \underset{\sim}{\xi}^2}$

2.6.1. *Derivation of enriched quantities*

The unit normal to the enriched surface can be obtained by substituting [2.56.e] in [2.56.b]. Then, the numerator takes the form:

$$\frac{\partial \underline{\underline{\boldsymbol{\rho}}}_e}{\partial \xi_1} \times \frac{\partial \underline{\underline{\boldsymbol{\rho}}}_e}{\partial \xi_2} = \left(\frac{\partial \underline{\underline{\boldsymbol{\rho}}}}{\partial \xi_1} + \underline{\boldsymbol{n}} \frac{\partial h_e}{\partial \xi_1} + h_e \frac{\partial \underline{\boldsymbol{n}}}{\partial \xi_1} \right) \times \left(\frac{\partial \underline{\underline{\boldsymbol{\rho}}}}{\partial \xi_2} + \underline{\boldsymbol{n}} \frac{\partial h_e}{\partial \xi_2} + h_e \frac{\partial \underline{\boldsymbol{n}}}{\partial \xi_2} \right) \quad [2.57]$$

where, according to A2.2.43[9]:

$$\frac{\partial \underline{\boldsymbol{n}}}{\partial \underset{\sim}{\xi}} = - \underset{\approx}{\mathrm{H}} \underset{\approx}{\bar{\mathrm{A}}} \frac{\partial \underline{\underline{\boldsymbol{\rho}}}}{\partial \underset{\sim}{\xi}}, \text{ where } \underset{\approx}{\mathrm{H}} \underset{\approx}{\bar{\mathrm{A}}} = \begin{bmatrix} \underset{\sim}{\gamma}_1^{\mathsf{T}} \\ \underset{\sim}{\gamma}_2^{\mathsf{T}} \end{bmatrix} \Rightarrow \frac{\partial \underline{\boldsymbol{n}}}{\partial \underset{\sim}{\xi}} = - \begin{bmatrix} \underset{\sim}{\gamma}_1^{\mathsf{T}} \\ \underset{\sim}{\gamma}_2^{\mathsf{T}} \end{bmatrix} \frac{\partial \underline{\underline{\boldsymbol{\rho}}}}{\partial \underset{\sim}{\xi}} = - \begin{bmatrix} \underset{\sim}{\gamma}_1^{\mathsf{T}} \frac{\partial \underline{\underline{\boldsymbol{\rho}}}}{\partial \underset{\sim}{\xi}} \\ \underset{\sim}{\gamma}_2^{\mathsf{T}} \frac{\partial \underline{\underline{\boldsymbol{\rho}}}}{\partial \underset{\sim}{\xi}} \end{bmatrix} \quad [2.58]$$

Expanding [2.57] and carrying [2.58] gives:

$$\begin{aligned} &\left(\frac{\partial \underline{\underline{\boldsymbol{\rho}}}}{\partial \xi_1} + \underline{\boldsymbol{n}} \frac{\partial h_e}{\partial \xi_1} - h_e \underset{\sim}{\gamma}_1^{\mathsf{T}} \frac{\partial \underline{\underline{\boldsymbol{\rho}}}}{\partial \underset{\sim}{\xi}} \right) \times \left(\frac{\partial \underline{\underline{\boldsymbol{\rho}}}}{\partial \xi_2} + \underline{\boldsymbol{n}} \frac{\partial h_e}{\partial \xi_2} - h_e \underset{\sim}{\gamma}_2^{\mathsf{T}} \frac{\partial \underline{\underline{\boldsymbol{\rho}}}}{\partial \underset{\sim}{\xi}} \right) = \\ &= \frac{\partial \underline{\underline{\boldsymbol{\rho}}}}{\partial \xi_1} \times \frac{\partial \underline{\underline{\boldsymbol{\rho}}}}{\partial \xi_2} + \frac{\partial \underline{\underline{\boldsymbol{\rho}}}}{\partial \xi_1} \times \underline{\boldsymbol{n}} \frac{\partial h_e}{\partial \xi_2} - h_e \frac{\partial \underline{\underline{\boldsymbol{\rho}}}}{\partial \xi_1} \times \frac{\partial \underline{\underline{\boldsymbol{\rho}}}^{\mathsf{T}}}{\partial \underset{\sim}{\xi}} \underset{\sim}{\gamma}_2 + \underline{\boldsymbol{n}} \times \frac{\partial \underline{\underline{\boldsymbol{\rho}}}}{\partial \xi_2} \frac{\partial h_e}{\partial \xi_1} - h_e \underline{\boldsymbol{n}} \times \\ &\times \frac{\partial \underline{\underline{\boldsymbol{\rho}}}^{\mathsf{T}}}{\partial \underset{\sim}{\xi}} \underset{\sim}{\gamma}_2 \frac{\partial h_e}{\partial \xi_1} - h_e \underset{\sim}{\gamma}_1^{\mathsf{T}} \frac{\partial \underline{\underline{\boldsymbol{\rho}}}}{\partial \underset{\sim}{\xi}} \times \frac{\partial \underline{\underline{\boldsymbol{\rho}}}}{\partial \xi_2} + h_e \underline{\boldsymbol{n}} \times \frac{\partial \underline{\underline{\boldsymbol{\rho}}}^{\mathsf{T}}}{\partial \underset{\sim}{\xi}} \underset{\sim}{\gamma}_1 \frac{\partial h_e}{\partial \xi_2} + h_e^2 \underset{\sim}{\gamma}_1^{\mathsf{T}} \frac{\partial \underline{\underline{\boldsymbol{\rho}}}}{\partial \underset{\sim}{\xi}} \times \frac{\partial \underline{\underline{\boldsymbol{\rho}}}^{\mathsf{T}}}{\partial \underset{\sim}{\xi}} \underset{\sim}{\gamma}_2 \end{aligned} \quad [2.59]$$

where the cross product of the basis v-vectors can be expressed through a special antisymmetric t-scalar $\underset{\approx}{\mathrm{J}}$:

$$\underset{\approx}{\mathrm{J}} = \begin{bmatrix} 0 & 1 \\ -1 & 0 \end{bmatrix}, \quad \underset{\approx}{\mathrm{J}}^{\mathsf{T}} = - \underset{\approx}{\mathrm{J}}, \quad \underset{\approx}{\mathrm{J}} \underset{\approx}{\mathrm{J}}^{\mathsf{T}} = \underset{\approx}{\mathrm{I}}, \quad \underset{\approx}{\mathrm{J}} \underset{\approx}{\mathrm{J}} = - \underset{\approx}{\mathrm{I}}, \quad [2.60]$$

$$\frac{\partial \underline{\underline{\boldsymbol{\rho}}}}{\partial \underset{\sim}{\xi}} \times \frac{\partial \underline{\underline{\boldsymbol{\rho}}}^{\mathsf{T}}}{\partial \underset{\sim}{\xi}} = \underline{\hat{\boldsymbol{n}}} \underset{\approx}{\mathrm{J}} \quad [2.61]$$

9 Here, it is more convenient to use the components of s-structures.

where $\underline{\hat{\boldsymbol{n}}}$ denotes non-normalized vector normal to the initial master surface. Some terms of [2.59] can be simplified in the following manner:

$$h_e \frac{\partial \underline{\boldsymbol{\rho}}}{\partial \xi_1} \times \frac{\partial \underline{\boldsymbol{\rho}}}{\partial \underset{\sim}{\xi}}^{\mathsf{T}} \underset{\sim}{\gamma}_2 + h_e \underset{\sim}{\gamma}_1^{\mathsf{T}} \frac{\partial \underline{\boldsymbol{\rho}}}{\partial \underset{\sim}{\xi}} \times \frac{\partial \underline{\boldsymbol{\rho}}}{\partial \xi_2} = h_e \underline{\hat{\boldsymbol{n}}} \, (\gamma_{22} + \gamma_{11}) = h_e \underline{\hat{\boldsymbol{n}}} \, \mathrm{tr}[\underset{\approx}{\mathrm{H}} \, \underset{\approx}{\bar{\mathrm{A}}}] \tag{2.62}$$

$$\underset{\sim}{\gamma}_1^{\mathsf{T}} \frac{\partial \underline{\boldsymbol{\rho}}}{\partial \underset{\sim}{\xi}} \times \frac{\partial \underline{\boldsymbol{\rho}}}{\partial \underset{\sim}{\xi}}^{\mathsf{T}} \underset{\sim}{\gamma}_2 = \underline{\hat{\boldsymbol{n}}} \, \underset{\sim}{\gamma}_1^{\mathsf{T}} \underset{\approx}{\mathrm{J}} \underset{\sim}{\gamma}_2 = \underline{\hat{\boldsymbol{n}}} \, (\gamma_{11}\gamma_{22} - \gamma_{12}\gamma_{21}) = \underline{\hat{\boldsymbol{n}}} \, \det[\underset{\approx}{\mathrm{H}} \, \underset{\approx}{\bar{\mathrm{A}}}] \tag{2.63}$$

From [2.59], [2.62] and [2.63], the cross product of the basis v-vectors of the enriched surface becomes:

$$\begin{cases} \frac{\partial \underline{\boldsymbol{\rho}}_e}{\partial \xi_1} \times \frac{\partial \underline{\boldsymbol{\rho}}_e}{\partial \xi_2} = \underline{\hat{\boldsymbol{n}}} \, (1 - h_e \, \mathrm{tr}[\underset{\approx}{\mathrm{H}} \, \underset{\approx}{\bar{\mathrm{A}}}] + h_e^2 \det[\underset{\approx}{\mathrm{H}} \, \underset{\approx}{\bar{\mathrm{A}}}]) + \\ \qquad + \underline{\boldsymbol{n}} \times \left(\frac{\partial \underline{\boldsymbol{\rho}}}{\partial \xi_2} \frac{\partial h_e}{\partial \xi_1} - \frac{\partial \underline{\boldsymbol{\rho}}}{\partial \xi_1} \frac{\partial h_e}{\partial \xi_2} \right) - h_e \underline{\boldsymbol{n}} \times \frac{\partial \underline{\boldsymbol{\rho}}}{\partial \underset{\sim}{\xi}}^{\mathsf{T}} \left(\underset{\sim}{\gamma}_2 \frac{\partial h_e}{\partial \xi_1} - \underset{\sim}{\gamma}_1 \frac{\partial h_e}{\partial \xi_2} \right) \end{cases} \tag{2.64}$$

The last two brackets in [2.63] can be transformed using $\underset{\approx}{\mathrm{J}}$ t-scalar:

$$\begin{aligned} &\frac{\partial \underline{\boldsymbol{\rho}}}{\partial \xi_2} \frac{\partial h_e}{\partial \xi_1} - \frac{\partial \underline{\boldsymbol{\rho}}}{\partial \xi_1} \frac{\partial h_e}{\partial \xi_2} = - \frac{\partial \underline{\boldsymbol{\rho}}}{\partial \underset{\sim}{\xi}}^{\mathsf{T}} \underset{\approx}{\mathrm{J}} \frac{\partial h_e}{\partial \underset{\sim}{\xi}} \\ &\underset{\sim}{\gamma}_2 \frac{\partial h_e}{\partial \xi_1} - \underset{\sim}{\gamma}_1 \frac{\partial h_e}{\partial \xi_2} = - \underset{\approx}{\mathrm{H}} \, \underset{\approx}{\bar{\mathrm{A}}} \, \underset{\approx}{\mathrm{J}} \frac{\partial h_e}{\partial \underset{\sim}{\xi}}, \quad \text{as} \quad \begin{bmatrix} \underset{\sim}{\gamma}_1^{\mathsf{T}} \\ \underset{\sim}{\gamma}_2^{\mathsf{T}} \end{bmatrix} = \underset{\approx}{\mathrm{H}} \, \underset{\approx}{\bar{\mathrm{A}}} \end{aligned} \tag{2.65}$$

Now it is necessary to express the cross product of the normal vector with the basis v-vector. This cross product lies in the tangent plane to the master surface, moreover:

$$\underline{\boldsymbol{n}} \times \frac{\partial \underline{\boldsymbol{\rho}}}{\partial \xi_1} = \alpha_1 \overline{\frac{\partial \underline{\boldsymbol{\rho}}}{\partial \xi_2}} \text{ and } \underline{\boldsymbol{n}} \times \frac{\partial \underline{\boldsymbol{\rho}}}{\partial \xi_2} = \alpha_2 \overline{\frac{\partial \underline{\boldsymbol{\rho}}}{\partial \xi_1}}$$

which can be rewritten as:

$$\underline{\boldsymbol{n}} \times \frac{\partial \underline{\boldsymbol{\rho}}}{\partial \underset{\sim}{\xi}} = \underset{\approx}{\alpha} \overline{\frac{\partial \underline{\boldsymbol{\rho}}}{\partial \underset{\sim}{\xi}}}$$

The right dot product of this expression with the covariant basis v-vector gives:

$$\left(\underline{\boldsymbol{n}} \times \frac{\partial \underline{\boldsymbol{\rho}}}{\partial \underset{\sim}{\xi}}\right) \cdot \frac{\partial \underline{\boldsymbol{\rho}}^{\intercal}}{\partial \underset{\sim}{\xi}} = \underset{\approx}{\alpha}\,\underset{\approx}{\mathrm{I}} \quad \Leftrightarrow \quad \left(\frac{\partial \underline{\boldsymbol{\rho}}}{\partial \underset{\sim}{\xi}} \times \frac{\partial \underline{\boldsymbol{\rho}}^{\intercal}}{\partial \underset{\sim}{\xi}}\right) \cdot \underline{\boldsymbol{n}} = \underset{\approx}{\alpha} \quad \Leftrightarrow \quad \underset{\approx}{\alpha} = \|\,\underline{\hat{\boldsymbol{n}}}\,\|\,\underset{\approx}{\mathrm{J}} = \hat{n}\,\underset{\approx}{\mathrm{J}}$$

consequently:

$$\underline{\boldsymbol{n}} \times \frac{\partial \underline{\boldsymbol{\rho}}}{\partial \underset{\sim}{\xi}} = \hat{n}\,\underset{\approx}{\mathrm{J}}\,\overline{\frac{\partial \underline{\boldsymbol{\rho}}}{\partial \underset{\sim}{\xi}}} \quad \text{and} \quad \underline{\boldsymbol{n}} \times \frac{\partial \underline{\boldsymbol{\rho}}^{\intercal}}{\partial \underset{\sim}{\xi}} = \hat{n}\,\overline{\frac{\partial \underline{\boldsymbol{\rho}}}{\partial \underset{\sim}{\xi}}}^{\intercal}\,\underset{\approx}{\mathrm{J}}^{\intercal} \qquad [2.66]$$

Substituting [2.65] and [2.66] in the last two terms of [2.64] gives:

$$\begin{aligned} &\underline{\boldsymbol{n}} \times \left(\frac{\partial \underline{\boldsymbol{\rho}}}{\partial \underset{\sim}{\xi}_2}\frac{\partial h_e}{\partial \underset{\sim}{\xi}_1} - \frac{\partial \underline{\boldsymbol{\rho}}}{\partial \underset{\sim}{\xi}_1}\frac{\partial h_e}{\partial \underset{\sim}{\xi}_2}\right) - h_e \underline{\boldsymbol{n}} \times \frac{\partial \underline{\boldsymbol{\rho}}^{\intercal}}{\partial \underset{\sim}{\xi}} \left(\underset{\sim}{\gamma}_2 \frac{\partial h_e}{\partial \underset{\sim}{\xi}_1} - \underset{\sim}{\gamma}_1 \frac{\partial h_e}{\partial \underset{\sim}{\xi}_2}\right) = \\ &= -\underline{\boldsymbol{n}} \times \frac{\partial \underline{\boldsymbol{\rho}}^{\intercal}}{\partial \underset{\sim}{\xi}} \left(\underset{\approx}{\mathrm{J}}\frac{\partial h_e}{\partial \underset{\sim}{\xi}} - h_e \underset{\approx}{\mathrm{H}}\,\underset{\approx}{\bar{\mathrm{A}}}\,\underset{\approx}{\mathrm{J}}\frac{\partial h_e}{\partial \underset{\sim}{\xi}}\right) = -\hat{n}\,\overline{\frac{\partial \underline{\boldsymbol{\rho}}}{\partial \underset{\sim}{\xi}}}^{\intercal} (\underset{\approx}{\mathrm{I}} - h_e \underset{\approx}{\mathrm{J}}^{\intercal}\,\underset{\approx}{\mathrm{H}}\,\underset{\approx}{\bar{\mathrm{A}}}\,\underset{\approx}{\mathrm{J}})\frac{\partial h_e}{\partial \underset{\sim}{\xi}} \end{aligned} \qquad [2.67]$$

Finally, from [2.64] and [2.67] (replacement of the contravariant basis by the covariant), we get the following expression for the numerator of the unit normal vector to the enriched master surface:

$$\begin{aligned} \frac{\partial \underline{\boldsymbol{\rho}}_e}{\partial \xi_1} \times \frac{\partial \underline{\boldsymbol{\rho}}_e}{\partial \xi_2} \quad = \quad & \left(1 - h_e\,\mathrm{tr}[\underset{\approx}{\mathrm{H}}\,\underset{\approx}{\bar{\mathrm{A}}}] + h_e^2\,\det[\underset{\approx}{\mathrm{H}}\,\underset{\approx}{\bar{\mathrm{A}}}]\right) \times \\ & \times \underline{\hat{\boldsymbol{n}}} - \hat{n}\frac{\partial h_e}{\partial \underset{\sim}{\xi}}^{T} (\underset{\approx}{\mathrm{I}} - h_e \underset{\approx}{\mathrm{J}}^{\intercal}\,\underset{\approx}{\mathrm{H}}\,\underset{\approx}{\bar{\mathrm{A}}}\,\underset{\approx}{\mathrm{J}})\,\underset{\approx}{\bar{\mathrm{A}}}\,\frac{\partial \underline{\boldsymbol{\rho}}}{\partial \underset{\sim}{\xi}} \end{aligned} \qquad [2.68]$$

Note that the t-scalar $\underset{\approx}{\mathrm{J}}^{\intercal}\,\underset{\approx}{\mathrm{H}}\,\underset{\approx}{\bar{\mathrm{A}}}\,\underset{\approx}{\mathrm{J}} = (\underset{\approx}{\mathrm{J}}^{\intercal}\,\underset{\approx}{\mathrm{H}}\,\underset{\approx}{\bar{\mathrm{A}}}\,\underset{\approx}{\mathrm{J}})^{\intercal}$ is symmetric.

Now we can write the expression for the normal to the enriched surface:

$$\underline{\boldsymbol{n}}_e = \frac{\left(\alpha \underline{\boldsymbol{n}} - \underset{\sim}{\beta}^{\intercal}\frac{\partial \underline{\boldsymbol{\rho}}}{\partial \underset{\sim}{\xi}}\right)}{\sqrt{\alpha^2 + \underset{\sim}{\beta}^{\intercal}\,\underset{\approx}{\mathrm{A}}\,\underset{\sim}{\beta}}}$$

where

$$\alpha = 1 - h_e\,\mathrm{tr}[\underset{\approx}{\mathrm{H}}\,\underset{\approx}{\bar{\mathrm{A}}}] + h_e^2\,\det[\underset{\approx}{\mathrm{H}}\,\underset{\approx}{\bar{\mathrm{A}}}]$$

$$\underset{\sim}{\beta}^{\intercal} = \frac{\partial h_e}{\partial \underset{\sim}{\xi}}^{\intercal} (\underset{\approx}{\mathrm{I}} - h_e \underset{\approx}{\mathrm{J}}^{\intercal}\,\underset{\approx}{\mathrm{H}}\,\underset{\approx}{\bar{\mathrm{A}}}\,\underset{\approx}{\mathrm{J}})\,\underset{\approx}{\bar{\mathrm{A}}}$$

[2.69]

It follows naturally from this expression that an adequate enriched geometry (without singularities and self-intersections) is retained if and only if:

$$\frac{\partial h_e}{\partial \underset{\sim}{\xi}} < \infty, \quad \alpha > 0 \text{ and } \underset{\approx}{\mathrm{I}} - h_e \underset{\approx}{\mathrm{J}}^{\intercal} \underset{\approx}{\mathrm{H}}\, \underset{\approx}{\bar{\mathrm{A}}}\, \underset{\approx}{\mathrm{J}} > 0$$

The last two conditions[10] imply that:

$$\det(\underset{\approx}{\mathrm{I}} - h_e \underset{\approx}{\mathrm{H}}\, \underset{\approx}{\bar{\mathrm{A}}}) = 1 - h_e \,\mathrm{tr}[\underset{\approx}{\mathrm{H}}\, \underset{\approx}{\bar{\mathrm{A}}}] + h_e^2 \,\det[\underset{\approx}{\mathrm{H}}\, \underset{\approx}{\bar{\mathrm{A}}}] > 0$$

which is equivalent to the requirement that $h_e < \min\left\{\frac{1}{\kappa_1}, \frac{1}{\kappa_2}\right\}$, where κ_1 and κ_2 are local curvatures of the surface and consequently are the solutions of the following equation (e.g. see [KON 08]):

$$\kappa^2 - \kappa \mathrm{tr}[\underset{\approx}{\mathrm{H}}\, \underset{\approx}{\bar{\mathrm{A}}}] + \det[\underset{\approx}{\mathrm{H}}\, \underset{\approx}{\bar{\mathrm{A}}}] = 0$$

To compute the explicit forms for two fundamental surface t-scalars ($\underset{\approx}{\mathrm{A}}$ and $\underset{\approx}{\mathrm{H}}$) of the enriched surface; starting from [2.56.g] and using [2.56.e], we get:

$$\begin{aligned}
\underset{\approx}{\mathrm{A}}_e &= \frac{\partial \underline{\boldsymbol{\rho}}_e}{\partial \underset{\sim}{\xi}} \cdot \frac{\partial \underline{\boldsymbol{\rho}}_e}{\partial \underset{\sim}{\xi}}^{\intercal} = \left(\frac{\partial \underline{\boldsymbol{\rho}}}{\partial \underset{\sim}{\xi}} + \underline{\boldsymbol{n}} \frac{\partial h_e}{\partial \underset{\sim}{\xi}} + h_e \frac{\partial \underline{\boldsymbol{n}}}{\partial \underset{\sim}{\xi}}\right) \cdot \left(\frac{\partial \underline{\boldsymbol{\rho}}}{\partial \underset{\sim}{\xi}}^{\intercal} + \underline{\boldsymbol{n}} \frac{\partial h_e}{\partial \underset{\sim}{\xi}}^{\intercal} + h_e \frac{\partial \underline{\boldsymbol{n}}}{\partial \underset{\sim}{\xi}}^{\intercal}\right) = \\
&= \underset{\approx}{\mathrm{A}} + \frac{\partial h_e}{\partial \underset{\sim}{\xi}} \frac{\partial h_e}{\partial \underset{\sim}{\xi}}^{\intercal} + 2h_e \frac{\partial \underline{\boldsymbol{\rho}}}{\partial \underset{\sim}{\xi}} \cdot \frac{\partial \underline{\boldsymbol{n}}}{\partial \underset{\sim}{\xi}}^{\intercal} + h_e^2 \frac{\partial \underline{\boldsymbol{n}}}{\partial \underset{\sim}{\xi}} \cdot \frac{\partial \underline{\boldsymbol{n}}}{\partial \underset{\sim}{\xi}}^{\intercal} = \\
&= \underset{\approx}{\mathrm{A}} + \frac{\partial h_e}{\partial \underset{\sim}{\xi}} \frac{\partial h_e}{\partial \underset{\sim}{\xi}}^{\intercal} - 2h_e \underset{\approx}{\mathrm{H}} + h_e^2 \underset{\approx}{\mathrm{H}}\, \underset{\approx}{\bar{\mathrm{A}}}\, \underset{\approx}{\mathrm{H}}
\end{aligned} \qquad [2.70]$$

so

$$\boxed{\underset{\approx}{\mathrm{A}}_e = \underset{\approx}{\mathrm{A}} + \frac{\partial h_e}{\partial \underset{\sim}{\xi}} \frac{\partial h_e}{\partial \underset{\sim}{\xi}}^{\intercal} - 2h_e \underset{\approx}{\mathrm{H}} + h_e^2 \underset{\approx}{\mathrm{H}}\, \underset{\approx}{\bar{\mathrm{A}}}\, \underset{\approx}{\mathrm{H}}} \qquad [2.71]$$

10 It is easy to show that: $\det(\underset{\approx}{\mathrm{I}} - h_e \underset{\approx}{\mathrm{J}}^{\intercal} \underset{\approx}{\mathrm{H}}\, \underset{\approx}{\bar{\mathrm{A}}}\, \underset{\approx}{\mathrm{J}}) = \det(\underset{\approx}{\mathrm{I}} - h_e \underset{\approx}{\mathrm{H}}\, \underset{\approx}{\bar{\mathrm{A}}})$.

To derive the second fundamental surface t-scalar, we make use of the equations obtained for the enriched normal vector [2.69] and [2.56.f]:

$$\begin{aligned}\underset{\approx}{\mathrm{H}}_e &= \underline{\boldsymbol{n}}_e \cdot \frac{\partial^2 \underline{\boldsymbol{\rho}}_e}{\partial \underset{\sim}{\xi}^2} = \frac{\left(\alpha \underline{\boldsymbol{n}} + \underset{\sim}{\beta}^T \frac{\partial \underline{\boldsymbol{\rho}}}{\partial \underset{\sim}{\xi}}\right)}{\sqrt{\alpha^2 + \underset{\sim}{\beta}^T \underset{\approx}{\bar{\mathrm{A}}} \underset{\sim}{\beta}}} \cdot \left(\frac{\partial^2 \underline{\boldsymbol{\rho}}}{\partial \underset{\sim}{\xi}^2} + \frac{\partial \underline{\boldsymbol{n}}}{\partial \underset{\sim}{\xi}} \frac{\partial h_e^T}{\partial \underset{\sim}{\xi}} + \frac{\partial h_e}{\partial \underset{\sim}{\xi}} \frac{\partial \underline{\boldsymbol{n}}^T}{\partial \underset{\sim}{\xi}} + h_e \frac{\partial^2 \underline{\boldsymbol{n}}}{\partial \underset{\sim}{\xi}^2} + \underline{\boldsymbol{n}} \frac{\partial^2 h_e}{\partial \underset{\sim}{\xi}^2} \right) \\ &= \frac{1}{\sqrt{\alpha^2 + \underset{\sim}{\beta}^{\intercal} \underset{\approx}{\bar{\mathrm{A}}} \underset{\sim}{\beta}}} \left(\alpha \underset{\approx}{\mathrm{H}} - \alpha h_e \underset{\approx}{\mathrm{H}} \underset{\approx}{\bar{\mathrm{A}}} \underset{\approx}{\mathrm{H}} + \alpha \frac{\partial^2 h_e}{\partial \underset{\sim}{\xi}^2} + \underset{\sim}{\beta}^{\intercal} \frac{\partial \underline{\boldsymbol{\rho}}}{\partial \underset{\sim}{\xi}} \cdot \frac{\partial^2 \underline{\boldsymbol{\rho}}}{\partial \underset{\sim}{\xi}^2} - \right. \\ &\quad \left. - \underset{\sim}{\beta}^{\intercal} \underset{\approx}{\mathrm{H}} \frac{\partial h_e^T}{\partial \underset{\sim}{\xi}} - \underset{\sim}{\beta}^{\intercal} \frac{\partial \underline{\boldsymbol{\rho}}}{\partial \underset{\sim}{\xi}} \cdot \frac{\partial h_e}{\partial \underset{\sim}{\xi}} \frac{\partial \underline{\boldsymbol{\rho}}^{\intercal}}{\partial \underset{\sim}{\xi}} \underset{\approx}{\mathrm{H}} \underset{\approx}{\bar{\mathrm{A}}} + h_e \underset{\sim}{\beta}^{\intercal} \frac{\partial \underline{\boldsymbol{\rho}}}{\partial \underset{\sim}{\xi}} \cdot \frac{\partial^2 \underline{\boldsymbol{n}}^T}{\partial \underset{\sim}{\xi}^2} \right)\end{aligned} \quad [2.72]$$

where the last term can be expressed in the following way (in order to exclude the derivative of the normal vector):

$$\begin{aligned}&\frac{\partial \underline{\boldsymbol{\rho}}}{\partial \underset{\sim}{\xi}} \cdot \underline{\boldsymbol{n}} = 0 \Rightarrow \frac{\partial}{\partial \underset{\sim}{\xi}} \left(\frac{\partial \underline{\boldsymbol{\rho}}}{\partial \underset{\sim}{\xi}} \cdot \underline{\boldsymbol{n}} \right) = 0 \Leftrightarrow \frac{\partial^2 \underline{\boldsymbol{\rho}}}{\partial \underset{\sim}{\xi}^2} \cdot \underline{\boldsymbol{n}} + \frac{\partial \underline{\boldsymbol{\rho}}}{\partial \underset{\sim}{\xi}} \cdot \frac{\partial \underline{\boldsymbol{n}}^T}{\partial \underset{\sim}{\xi}} = 0 \Leftrightarrow \\ \Leftrightarrow &\frac{\partial}{\partial \underset{\sim}{\xi}} \left(\frac{\partial^2 \underline{\boldsymbol{\rho}}}{\partial \underset{\sim}{\xi}^2} \cdot \underline{\boldsymbol{n}} + \frac{\partial \underline{\boldsymbol{\rho}}}{\partial \underset{\sim}{\xi}} \cdot \frac{\partial \underline{\boldsymbol{n}}^T}{\partial \underset{\sim}{\xi}} \right) = 0 \Leftrightarrow \frac{\partial^3 \underline{\boldsymbol{\rho}}}{\partial \underset{\sim}{\xi}^3} \cdot \underline{\boldsymbol{n}} + 2 \frac{\partial^2 \underline{\boldsymbol{\rho}}}{\partial \underset{\sim}{\xi}^2} \cdot \frac{\partial \underline{\boldsymbol{n}}^T}{\partial \underset{\sim}{\xi}} + \frac{\partial \underline{\boldsymbol{\rho}}^T}{\partial \underset{\sim}{\xi}} \cdot \frac{\partial^2 \underline{\boldsymbol{n}}}{\partial \underset{\sim}{\xi}^2} = 0 \\ &\Leftrightarrow \frac{\partial \underline{\boldsymbol{\rho}}^T}{\partial \underset{\sim}{\xi}} \cdot \frac{\partial^2 \underline{\boldsymbol{n}}}{\partial \underset{\sim}{\xi}^2} = - \frac{\partial^3 \underline{\boldsymbol{\rho}}}{\partial \underset{\sim}{\xi}^3} \cdot \underline{\boldsymbol{n}} + 2 \frac{\partial^2 \underline{\boldsymbol{\rho}}}{\partial \underset{\sim}{\xi}^2} \cdot \frac{\partial \underline{\boldsymbol{\rho}}^T}{\partial \underset{\sim}{\xi}} \underset{\approx}{\mathrm{H}} \underset{\approx}{\bar{\mathrm{A}}}\end{aligned} \quad [2.73]$$

Substituting [2.73] in [2.72] gives the final expression for the second fundamental tensor of the enriched surface:

$$\begin{aligned}\underset{\approx}{\mathrm{H}}_e \quad &= \frac{1}{\sqrt{\alpha^2 + \underset{\sim}{\beta}^T \underset{\approx}{\bar{\mathrm{A}}} \underset{\sim}{\beta}}} \left(\alpha \underset{\approx}{\mathrm{H}} - \alpha h_e \underset{\approx}{\mathrm{H}} \underset{\approx}{\bar{\mathrm{A}}} \underset{\approx}{\mathrm{H}} + \alpha \frac{\partial^2 h_e}{\partial \underset{\sim}{\xi}^2} + \underset{\sim}{\beta}^T \frac{\partial \underline{\boldsymbol{\rho}}}{\partial \underset{\sim}{\xi}} \cdot \frac{\partial^2 \underline{\boldsymbol{\rho}}}{\partial \underset{\sim}{\xi}^2} - \underset{\sim}{\beta}^T \underset{\approx}{\mathrm{H}} \frac{\partial {h_e}^T}{\partial \underset{\sim}{\xi}} - \right. \\ &\quad \left. - \beta^{\intercal} \frac{\partial \underline{\boldsymbol{\rho}}}{\partial \underset{\sim}{\xi}} \cdot \frac{\partial h_e}{\partial \underset{\sim}{\xi}} \frac{\partial \underline{\boldsymbol{\rho}}^T}{\partial \underset{\sim}{\xi}} \underset{\approx}{\mathrm{H}} \underset{\approx}{\bar{\mathrm{A}}} - h_e \underset{\sim}{\beta}^T \frac{\partial^3 \underline{\boldsymbol{\rho}}}{\partial \underset{\sim}{\xi}^3} \cdot \underline{\boldsymbol{n}} + 2 h_e \underset{\sim}{\beta}^{\intercal} \frac{\partial^2 \underline{\boldsymbol{\rho}}}{\partial \underset{\sim}{\xi}^2} \cdot \frac{\partial \underline{\boldsymbol{\rho}}^T}{\partial \underset{\sim}{\xi}} \underset{\approx}{\mathrm{H}} \underset{\approx}{\bar{\mathrm{A}}} \right)\end{aligned} \quad [2.74]$$

As we can see, the third derivative of vector $\underline{\boldsymbol{\rho}}$ appears, which requires that $\underline{\boldsymbol{\rho}}(\underset{\sim}{\xi}) \in C^3(\underset{\sim}{\xi})$. This condition is satisfied for classic shape functions (linear, quadratic) of the FEM within master faces, but not on their edges.

2.6.2. *Variations of geometrical quantities*

The form of the geometrical variations does not change. The master quantities have to be simply replaced by their enriched analogs, and the variations of the geometrical quantities are expressed through the basic variations of the master and slave vectors:

$$\delta g_n^e,\ \delta\underset{\sim}{\xi},\ \Delta\delta g_n^e,\ \Delta\delta\underset{\sim}{\xi} \quad \longleftarrow \quad \delta\underline{\boldsymbol{r}}_s,\ \ \delta\underline{\boldsymbol{\rho}}_e,\ \ \delta\frac{\partial\underline{\boldsymbol{\rho}}_e}{\partial\underset{\sim}{\xi}},\ \ \delta\frac{\partial^2\underline{\boldsymbol{\rho}}_e}{\partial\underset{\sim}{\xi}^2}$$

But from the point of view of the FEM, all variations in the right part are not basic, except only $\delta\underline{\boldsymbol{r}}_s$; some efforts have to be undertaken to convert them in to a suitable form for the FEM. We start from the variation of the projection vector on the enriched surface, according to [2.56.d and [A2.45]:

$$\delta\underline{\boldsymbol{\rho}}_e = \delta\underline{\boldsymbol{\rho}} + h_e\delta\underline{\boldsymbol{n}} \Rightarrow \boxed{\delta\underline{\boldsymbol{\rho}}_e = \delta\underline{\boldsymbol{\rho}} - h_e\left(\underline{\boldsymbol{n}}\cdot\delta\frac{\partial\underline{\boldsymbol{\rho}}}{\partial\underset{\sim}{\xi}}\right)^{\mathsf{T}}\underset{\approx}{\bar{\mathrm{A}}}\frac{\partial\underline{\boldsymbol{\rho}}}{\partial\underset{\sim}{\xi}}} \qquad [2.75]$$

The variation of the covariant basis v-vector $\delta\frac{\partial\underline{\boldsymbol{\rho}}_e}{\partial\underset{\sim}{\xi}}$ does not stand alone in expressions of variations, only its dot product with the normal $\underline{\boldsymbol{n}}_e$ or the basis v-vector $\frac{\partial\underline{\boldsymbol{\rho}}_e}{\partial\underset{\sim}{\xi}}$ of the enriched surface appears, since both of them can be expressed through the normal $\underline{\boldsymbol{n}}$ and the basis v-vector $\frac{\partial\underline{\boldsymbol{\rho}}}{\partial\underset{\sim}{\xi}}$ of the original master surface (see [2.56.e] and [A2.45]:

$$\begin{aligned}\underline{\boldsymbol{n}}_e &= \mathrm{a}_1\underline{\boldsymbol{n}} + \underset{\sim}{\mathrm{a}}_2^T\frac{\partial\underline{\boldsymbol{\rho}}}{\partial\underset{\sim}{\xi}}\\ \frac{\partial\underline{\boldsymbol{\rho}}_e}{\partial\underset{\sim}{\xi}} &= \underset{\sim}{\mathrm{b}}_1\underline{\boldsymbol{n}} + \underset{\approx}{\mathrm{b}}_2\frac{\partial\underline{\boldsymbol{\rho}}}{\partial\underset{\sim}{\xi}}\end{aligned} \qquad [2.76]$$

where

$$\begin{gathered}\mathrm{a}_1 = \frac{\alpha}{\sqrt{\alpha^2 + \underset{\sim}{\beta}^{\mathsf{T}}\underset{\approx}{\mathrm{A}}\underset{\sim}{\beta}}};\quad \underset{\sim}{\mathrm{a}}_2^T = \frac{-\underset{\sim}{\beta}^{\mathsf{T}}}{\sqrt{\alpha^2 + \underset{\sim}{\beta}^{\mathsf{T}}\underset{\approx}{\mathrm{A}}\underset{\sim}{\beta}}}\\ \alpha = 1 - h_e\,\mathrm{tr}[\underset{\approx}{\mathrm{H}}\,\underset{\approx}{\bar{\mathrm{A}}}] + h_e^2\,\det[\underset{\approx}{\mathrm{H}}\,\underset{\approx}{\bar{\mathrm{A}}}];\quad \underset{\sim}{\beta} = \frac{\partial h_e}{\partial\underset{\sim}{\xi}}^{\mathsf{T}}(\underset{\approx}{\mathrm{I}} - h_e\underset{\approx}{\mathrm{J}}^{\mathsf{T}}\underset{\approx}{\mathrm{H}}\,\underset{\approx}{\bar{\mathrm{A}}}\,\underset{\approx}{\mathrm{J}})\,\underset{\approx}{\bar{\mathrm{A}}}\\ \underset{\sim}{\mathrm{b}}_1 = \frac{\partial h_e}{\partial\underset{\sim}{\xi}};\quad \underset{\approx}{\mathrm{b}}_2 = \underset{\approx}{\mathrm{I}} - h_e\underset{\approx}{\mathrm{H}}\,\underset{\approx}{\bar{\mathrm{A}}}\end{gathered} \qquad [2.77]$$

Let us derive the expression for the dot product of the basis vectors $\underline{\boldsymbol{n}}$ and $\frac{\partial \underline{\underline{\boldsymbol{\rho}}}}{\partial \underset{\sim}{\xi}}$ with variations of the enriched quantities:

$$\underline{\boldsymbol{n}} \cdot \delta \frac{\partial \underline{\underline{\boldsymbol{\rho}}_e}^{\intercal}}{\partial \underset{\sim}{\xi}} = \underline{\boldsymbol{n}} \cdot \left(\delta \frac{\partial \underline{\underline{\boldsymbol{\rho}}}^{\intercal}}{\partial \underset{\sim}{\xi}} + \delta \underline{\boldsymbol{n}} \frac{\partial h_e}{\partial \underset{\sim}{\xi}}^{\intercal} + h_e \delta \frac{\partial \underline{\boldsymbol{n}}^{\intercal}}{\partial \underset{\sim}{\xi}} \right) = \underline{\boldsymbol{n}} \cdot \delta \frac{\partial \underline{\underline{\boldsymbol{\rho}}}^{\intercal}}{\partial \underset{\sim}{\xi}} + \underline{\boldsymbol{n}} \cdot \delta \frac{\partial \underline{\boldsymbol{n}}^{\intercal}}{\partial \underset{\sim}{\xi}} h_e \quad [2.78]$$

where according to [A2.43] and [A2.45] the last term is:

$$\underline{\boldsymbol{n}} \cdot \delta \frac{\partial \underline{\boldsymbol{n}}^T}{\partial \underset{\sim}{\xi}} = -\delta \underline{\boldsymbol{n}} \cdot \frac{\partial \underline{\boldsymbol{n}}^T}{\partial \underset{\sim}{\xi}} = -\left(\underline{\boldsymbol{n}} \cdot \delta \frac{\partial \underline{\underline{\boldsymbol{\rho}}}}{\partial \underset{\sim}{\xi}} \right)^T \underset{\approx}{\bar{\mathrm{A}}} \frac{\partial \underline{\underline{\boldsymbol{\rho}}}}{\partial \underset{\sim}{\xi}} \cdot \frac{\partial \underline{\underline{\boldsymbol{\rho}}}^T}{\partial \underset{\sim}{\xi}} \underset{\approx}{\mathrm{H}} \underset{\approx}{\bar{\mathrm{A}}} = -\underset{\approx}{\mathrm{H}} \underset{\approx}{\bar{\mathrm{A}}} \left(\underline{\boldsymbol{n}} \cdot \delta \frac{\partial \underline{\underline{\boldsymbol{\rho}}}^T}{\partial \underset{\sim}{\xi}} \right) \quad [2.79]$$

Finally, we get:

$$\boxed{\underline{\boldsymbol{n}} \cdot \delta \frac{\partial \underline{\underline{\boldsymbol{\rho}}_e}^T}{\partial \underset{\sim}{\xi}} = \underline{\boldsymbol{n}} \cdot \delta \frac{\partial \underline{\underline{\boldsymbol{\rho}}}^T}{\partial \underset{\sim}{\xi}} \left(\underset{\approx}{\mathrm{I}} - h_e \underset{\approx}{\mathrm{H}} \underset{\approx}{\bar{\mathrm{A}}} \right)} \quad [2.80]$$

The dot product of the covariant basis v-vector with the first variation of its enriched analog gives:

$$\frac{\partial \underline{\underline{\boldsymbol{\rho}}}}{\partial \underset{\sim}{\xi}} \cdot \delta \frac{\partial \underline{\underline{\boldsymbol{\rho}}_e}^T}{\partial \underset{\sim}{\xi}} = \frac{\partial \underline{\underline{\boldsymbol{\rho}}}}{\partial \underset{\sim}{\xi}} \cdot \left(\delta \frac{\partial \underline{\underline{\boldsymbol{\rho}}}^T}{\partial \underset{\sim}{\xi}} + \delta \underline{\boldsymbol{n}} \frac{\partial h_e^T}{\partial \underset{\sim}{\xi}} + h_e \delta \frac{\partial \underline{\boldsymbol{n}}^T}{\partial \underset{\sim}{\xi}} \right) = \frac{\partial \underline{\underline{\boldsymbol{\rho}}}}{\partial \underset{\sim}{\xi}} \cdot \delta \frac{\partial \underline{\underline{\boldsymbol{\rho}}}^T}{\partial \underset{\sim}{\xi}} - \underline{\boldsymbol{n}} \cdot \delta \frac{\partial \underline{\underline{\boldsymbol{\rho}}}}{\partial \underset{\sim}{\xi}} \frac{\partial h_e^T}{\partial \underset{\sim}{\xi}} + h_e \frac{\partial \underline{\underline{\boldsymbol{\rho}}}}{\partial \underset{\sim}{\xi}} \cdot \delta \frac{\partial \underline{\boldsymbol{n}}^T}{\partial \underset{\sim}{\xi}} \quad [2.81]$$

where the last term can be derived from:

$$\delta \frac{\partial}{\partial \underset{\sim}{\xi}} \left(\underline{\boldsymbol{n}} \cdot \frac{\partial \underline{\underline{\boldsymbol{\rho}}}}{\partial \underset{\sim}{\xi}} \right) = 0 \Leftrightarrow \frac{\partial \underline{\underline{\boldsymbol{\rho}}}}{\partial \underset{\sim}{\xi}} \cdot \delta \frac{\partial \underline{\boldsymbol{n}}^T}{\partial \underset{\sim}{\xi}} = -\underline{\boldsymbol{n}} \cdot \delta \frac{\partial^2 \underline{\underline{\boldsymbol{\rho}}}}{\partial \underset{\sim}{\xi}^2} + \left(\underline{\boldsymbol{n}} \cdot \delta \frac{\partial \underline{\underline{\boldsymbol{\rho}}}^T}{\partial \underset{\sim}{\xi}} \right) \underset{\approx}{\bar{\mathrm{A}}} \frac{\partial \underline{\underline{\boldsymbol{\rho}}}}{\partial \underset{\sim}{\xi}} \cdot \frac{\partial^2 \underline{\underline{\boldsymbol{\rho}}}}{\partial \underset{\sim}{\xi}^2} + \delta \frac{\partial \underline{\underline{\boldsymbol{\rho}}}}{\partial \underset{\sim}{\xi}} \cdot \frac{\partial \underline{\underline{\boldsymbol{\rho}}}^T}{\partial \underset{\sim}{\xi}} \underset{\approx}{\mathrm{H}} \underset{\approx}{\bar{\mathrm{A}}} \quad [2.82]$$

Substituting the last expression in [2.81] yields a non-symmetric t-scalar $\delta \underset{\approx}{\mathrm{Q}}$:

$$\boxed{\begin{aligned}\delta \underset{\approx}{\mathrm{Q}} \;&= \frac{\partial \underline{\boldsymbol{\rho}}}{\partial \underset{\sim}{\xi}} \cdot \delta \frac{\partial \underline{\boldsymbol{\rho}}_e^T}{\partial \underset{\sim}{\xi}} = \frac{\partial \underline{\boldsymbol{\rho}}}{\partial \underset{\sim}{\xi}} \cdot \delta \frac{\partial \underline{\boldsymbol{\rho}}^T}{\partial \underset{\sim}{\xi}} - \underline{\boldsymbol{n}} \cdot \delta \frac{\partial \underline{\boldsymbol{\rho}}}{\partial \underset{\sim}{\xi}} \frac{\partial h_e^T}{\partial \underset{\sim}{\xi}} - h_e \underline{\boldsymbol{n}} \cdot \delta \frac{\partial^2 \underline{\boldsymbol{\rho}}}{\partial \underset{\sim}{\xi}^2} + \\ &+ h_e \left(\underline{\boldsymbol{n}} \cdot \delta \frac{\partial \underline{\boldsymbol{\rho}}^T}{\partial \underset{\sim}{\xi}} \right) \underset{\approx}{\bar{\mathrm{A}}} \frac{\partial \underline{\boldsymbol{\rho}}}{\partial \underset{\sim}{\xi}} \cdot \frac{\partial^2 \underline{\boldsymbol{\rho}}}{\partial \underset{\sim}{\xi}^2} + h_e \delta \frac{\partial \underline{\boldsymbol{\rho}}}{\partial \underset{\sim}{\xi}} \cdot \frac{\partial \underline{\boldsymbol{\rho}}^T}{\partial \underset{\sim}{\xi}} \underset{\approx}{\mathrm{H}} \underset{\approx}{\bar{\mathrm{A}}}\end{aligned}} \qquad [2.83]$$

The same procedure has to be carried out with the variation of the derivatives of the basis v-vector. Let us compute $\underline{\boldsymbol{n}} \cdot \delta \frac{\partial^2 \underline{\boldsymbol{\rho}}_e}{\partial \underset{\sim}{\xi}^2}$ and $\frac{\partial \underline{\boldsymbol{\rho}}}{\partial \underset{\sim}{\xi}} \cdot \delta \frac{\partial^2 \underline{\boldsymbol{\rho}}_e}{\partial \underset{\sim}{\xi}^2}$. According to [2.56.f]:

$$\begin{aligned}\underline{\boldsymbol{n}} \cdot \delta \frac{\partial^2 \underline{\boldsymbol{\rho}}_e}{\partial \underset{\sim}{\xi}^2} \;&= \underline{\boldsymbol{n}} \cdot \left(\delta \frac{\partial^2 \underline{\boldsymbol{\rho}}}{\partial \underset{\sim}{\xi}^2} + \delta \frac{\partial \underline{\boldsymbol{n}}}{\partial \underset{\sim}{\xi}} \frac{\partial h_e^T}{\partial \underset{\sim}{\xi}} + \frac{\partial h_e}{\partial \underset{\sim}{\xi}} \delta \frac{\partial \underline{\boldsymbol{n}}^T}{\partial \underset{\sim}{\xi}} + h_e \delta \frac{\partial^2 \underline{\boldsymbol{n}}}{\partial \underset{\sim}{\xi}^2} + \delta \underline{\boldsymbol{n}} \frac{\partial^2 h_e}{\partial \underset{\sim}{\xi}^2} \right) = \\ &= \underline{\boldsymbol{n}} \cdot \delta \frac{\partial^2 \underline{\boldsymbol{\rho}}}{\partial \underset{\sim}{\xi}^2} - \delta \underline{\boldsymbol{n}} \cdot \frac{\partial \underline{\boldsymbol{n}}}{\partial \underset{\sim}{\xi}} \frac{\partial h_e^T}{\partial \underset{\sim}{\xi}} - \frac{\partial h_e}{\partial \underset{\sim}{\xi}} \frac{\partial \underline{\boldsymbol{n}}^T}{\partial \underset{\sim}{\xi}} \cdot \delta \underline{\boldsymbol{n}} + h_e \underline{\boldsymbol{n}} \cdot \delta \frac{\partial^2 \underline{\boldsymbol{n}}}{\partial \underset{\sim}{\xi}^2}\end{aligned} \qquad [2.84]$$

carrying equation [2.79]:

$$\begin{aligned}\underline{\boldsymbol{n}} \cdot \delta \frac{\partial^2 \underline{\boldsymbol{\rho}}_e}{\partial \underset{\sim}{\xi}^2} \;&= \underline{\boldsymbol{n}} \cdot \delta \frac{\partial^2 \underline{\boldsymbol{\rho}}}{\partial \underset{\sim}{\xi}^2} - \underset{\approx}{\mathrm{H}} \underset{\approx}{\bar{\mathrm{A}}} \left(\underline{\boldsymbol{n}} \cdot \delta \frac{\partial \underline{\boldsymbol{\rho}}}{\partial \underset{\sim}{\xi}} \right) \frac{\partial h_e^T}{\partial \underset{\sim}{\xi}} - \frac{\partial h_e}{\partial \underset{\sim}{\xi}} \left(\underline{\boldsymbol{n}} \cdot \delta \frac{\partial \underline{\boldsymbol{\rho}}^T}{\partial \underset{\sim}{\xi}} \right) \underset{\approx}{\mathrm{H}} \underset{\approx}{\bar{\mathrm{A}}} + \\ &+ h_e \underline{\boldsymbol{n}} \cdot \delta \frac{\partial^2 \underline{\boldsymbol{n}}}{\partial \underset{\sim}{\xi}^2}\end{aligned} \qquad [2.85]$$

where the last term is quite long. First, we evaluate the following expression:

$$\begin{aligned}&\delta \frac{\partial}{\partial \underset{\sim}{\xi}} \left(\underline{\boldsymbol{n}} \cdot \frac{\partial \underline{\boldsymbol{n}}}{\partial \underset{\sim}{\xi}} \right) = 0 \Leftrightarrow \delta \frac{\partial \underline{\boldsymbol{n}}}{\partial \underset{\sim}{\xi}} \cdot \frac{\partial \underline{\boldsymbol{n}}^T}{\partial \underset{\sim}{\xi}} + \frac{\partial \underline{\boldsymbol{n}}}{\partial \underset{\sim}{\xi}} \cdot \delta \frac{\partial \underline{\boldsymbol{n}}^T}{\partial \underset{\sim}{\xi}} + \delta \underline{\boldsymbol{n}} \cdot \frac{\partial^2 \underline{\boldsymbol{n}}}{\partial \underset{\sim}{\xi}^2} + \underline{\boldsymbol{n}} \cdot \delta \frac{\partial^2 \underline{\boldsymbol{n}}}{\partial \underset{\sim}{\xi}^2} = 0 \Leftrightarrow \\ &\Leftrightarrow \quad \underline{\boldsymbol{n}} \cdot \delta \frac{\partial^2 \underline{\boldsymbol{n}}}{\partial \underset{\sim}{\xi}^2} = - \underbrace{\delta \frac{\partial \underline{\boldsymbol{n}}}{\partial \underset{\sim}{\xi}} \cdot \frac{\partial \underline{\boldsymbol{n}}^T}{\partial \underset{\sim}{\xi}}}_{\text{term 1}} - \underbrace{\frac{\partial \underline{\boldsymbol{n}}}{\partial \underset{\sim}{\xi}} \cdot \delta \frac{\partial \underline{\boldsymbol{n}}^T}{\partial \underset{\sim}{\xi}}}_{\text{term 2}} - \underbrace{\delta \underline{\boldsymbol{n}} \cdot \frac{\partial^2 \underline{\boldsymbol{n}}}{\partial \underset{\sim}{\xi}^2}}_{\text{term 3}}\end{aligned} \qquad [2.86]$$

Replacing $\frac{\partial \underline{\boldsymbol{n}}}{\partial \underset{\sim}{\xi}}$ in terms 1 and 2 in [2.86] and carrying [2.82] yields:

$$
\begin{aligned}
&\text{term 1:} \qquad \delta\frac{\partial \underline{\boldsymbol{n}}}{\partial \underset{\sim}{\xi}} \cdot \frac{\partial \underline{\boldsymbol{n}}^T}{\partial \underset{\sim}{\xi}} = -\delta\frac{\partial \underline{\boldsymbol{n}}}{\partial \underset{\sim}{\xi}} \cdot \frac{\partial \underline{\boldsymbol{\rho}}^T}{\partial \underset{\sim}{\xi}} \underset{\approx}{\mathrm{H}}\, \underset{\approx}{\bar{\mathrm{A}}} = \\
&= \underline{\boldsymbol{n}} \cdot \delta\frac{\partial^2 \underline{\boldsymbol{\rho}}}{\partial \underset{\sim}{\xi}^2} \underset{\approx}{\mathrm{H}}\, \underset{\approx}{\bar{\mathrm{A}}} - \left(\underline{\boldsymbol{n}} \cdot \delta\frac{\partial \underline{\boldsymbol{\rho}}^T}{\partial \underset{\sim}{\xi}}\right) \underset{\approx}{\bar{\mathrm{A}}}\, \frac{\partial \underline{\boldsymbol{\rho}}}{\partial \underset{\sim}{\xi}} \cdot \frac{\partial^2 \underline{\boldsymbol{\rho}}}{\partial \underset{\sim}{\xi}^2} \underset{\approx}{\mathrm{H}}\, \underset{\approx}{\bar{\mathrm{A}}} - \frac{\partial \underline{\boldsymbol{\rho}}}{\partial \underset{\sim}{\xi}} \cdot \delta\frac{\partial \underline{\boldsymbol{\rho}}^T}{\partial \underset{\sim}{\xi}} \underset{\approx}{\mathrm{H}}^2\, \underset{\approx}{\bar{\mathrm{A}}}^2 \\
&\text{term 2:} \qquad \frac{\partial \underline{\boldsymbol{n}}}{\partial \underset{\sim}{\xi}} \cdot \delta\frac{\partial \underline{\boldsymbol{n}}^T}{\partial \underset{\sim}{\xi}} = -\underset{\approx}{\mathrm{H}}\, \underset{\approx}{\bar{\mathrm{A}}}\, \frac{\partial \underline{\boldsymbol{\rho}}}{\partial \underset{\sim}{\xi}} \cdot \delta\frac{\partial \underline{\boldsymbol{n}}^T}{\partial \underset{\sim}{\xi}} = \\
&= \underline{\boldsymbol{n}} \cdot \delta\frac{\partial^2 \underline{\boldsymbol{\rho}}}{\partial \underset{\sim}{\xi}^2} \underset{\approx}{\mathrm{H}}\, \underset{\approx}{\bar{\mathrm{A}}} - \left(\underline{\boldsymbol{n}} \cdot \delta\frac{\partial \underline{\boldsymbol{\rho}}^T}{\partial \underset{\sim}{\xi}}\right) \underset{\approx}{\bar{\mathrm{A}}}\, \frac{\partial \underline{\boldsymbol{\rho}}}{\partial \underset{\sim}{\xi}} \cdot \frac{\partial^2 \underline{\boldsymbol{\rho}}}{\partial \underset{\sim}{\xi}^2} \underset{\approx}{\mathrm{H}}\, \underset{\approx}{\bar{\mathrm{A}}} - \underset{\approx}{\mathrm{H}}\, \underset{\approx}{\bar{\mathrm{A}}}\, \delta\frac{\partial \underline{\boldsymbol{\rho}}}{\partial \underset{\sim}{\xi}} \cdot \frac{\partial \underline{\boldsymbol{\rho}}^T}{\partial \underset{\sim}{\xi}} \underset{\approx}{\mathrm{H}}\, \underset{\approx}{\bar{\mathrm{A}}}
\end{aligned}
\qquad [2.87]
$$

The variation of the normal $\delta\underline{\boldsymbol{n}}$ in the third term in [2.86] has to be replaced by a combination of the basis vectors:

$$
\delta\underline{\boldsymbol{n}} \cdot \frac{\partial^2 \underline{\boldsymbol{n}}}{\partial \underset{\sim}{\xi}^2} = -\left(\underline{\boldsymbol{n}} \cdot \delta\frac{\partial \underline{\boldsymbol{\rho}}^T}{\partial \underset{\sim}{\xi}}\right) \underset{\approx}{\bar{\mathrm{A}}}\, \frac{\partial \underline{\boldsymbol{\rho}}}{\partial \underset{\sim}{\xi}} \cdot \frac{\partial^2 \underline{\boldsymbol{n}}}{\partial \underset{\sim}{\xi}^2}, \qquad [2.88]
$$

where the last product can be derived from:

$$
\frac{\partial^2}{\partial \underset{\sim}{\xi}^2}\left(\frac{\partial \underline{\boldsymbol{\rho}}}{\partial \underset{\sim}{\xi}} \cdot \underline{\boldsymbol{n}}\right) = 0 \Leftrightarrow \frac{\partial \underline{\boldsymbol{\rho}}}{\partial \underset{\sim}{\xi}} \cdot \frac{\partial^2 \underline{\boldsymbol{n}}}{\partial \underset{\sim}{\xi}^2} = -\underline{\boldsymbol{n}} \cdot \frac{\partial \underline{\boldsymbol{\rho}}_e}{\partial\, \underset{\sim}{\Theta}} + 2\frac{\partial^2 \underline{\boldsymbol{\rho}}}{\partial \underset{\sim}{\xi}^2} \cdot \frac{\partial \underline{\boldsymbol{\rho}}^T}{\partial \underset{\sim}{\xi}} \underset{\approx}{\mathrm{H}}\, \underset{\approx}{\bar{\mathrm{A}}}\,. \qquad [2.89]
$$

Substituting [2.87], [2.88] and [2.89] in [2.86] and consequently in [2.85] gives, after grouping some terms, the final expression:

$$
\boxed{
\begin{aligned}
\underline{\boldsymbol{n}} \cdot \delta\frac{\partial^2 \underline{\boldsymbol{\rho}}_e}{\partial \underset{\sim}{\xi}^2} \quad = &\underline{\boldsymbol{n}} \cdot \delta\frac{\partial^2 \underline{\boldsymbol{\rho}}}{\partial \underset{\sim}{\xi}^2}\left(\underset{\approx}{\mathrm{I}} - 2h_e \underset{\approx}{\mathrm{H}}\, \underset{\approx}{\bar{\mathrm{A}}}\right) - \underset{\approx}{\mathrm{H}}\, \underset{\approx}{\bar{\mathrm{A}}}\left(\underline{\boldsymbol{n}} \cdot \delta\frac{\partial \underline{\boldsymbol{\rho}}}{\partial \underset{\sim}{\xi}}\right)\frac{\partial h_e^T}{\partial \underset{\sim}{\xi}} - \frac{\partial h_e}{\partial \underset{\sim}{\xi}}\left(\underline{\boldsymbol{n}} \cdot \delta\frac{\partial \underline{\boldsymbol{\rho}}^T}{\partial \underset{\sim}{\xi}}\right) \underset{\approx}{\mathrm{H}}\, \underset{\approx}{\bar{\mathrm{A}}} \\
&+ h_e \frac{\partial \underline{\boldsymbol{\rho}}}{\partial \underset{\sim}{\xi}} \cdot \delta\frac{\partial \underline{\boldsymbol{\rho}}^T}{\partial \underset{\sim}{\xi}} \underset{\approx}{\mathrm{H}}^2\, \underset{\approx}{\bar{\mathrm{A}}}^2 + h_e \underset{\approx}{\mathrm{H}}\, \underset{\approx}{\bar{\mathrm{A}}}\, \delta\frac{\partial \underline{\boldsymbol{\rho}}}{\partial \underset{\sim}{\xi}} \cdot \frac{\partial \underline{\boldsymbol{\rho}}^T}{\partial \underset{\sim}{\xi}} \underset{\approx}{\mathrm{H}}\, \underset{\approx}{\bar{\mathrm{A}}} + \\
&+ h_e \left(\underline{\boldsymbol{n}} \cdot \delta\frac{\partial \underline{\boldsymbol{\rho}}^T}{\partial \underset{\sim}{\xi}}\right) \underset{\approx}{\bar{\mathrm{A}}}\left(-\underline{\boldsymbol{n}} \cdot \frac{\partial \underline{\boldsymbol{\rho}}_e}{\partial\, \underset{\sim}{\Theta}} + 2\frac{\partial^2 \underline{\boldsymbol{\rho}}}{\partial \underset{\sim}{\xi}^2} \cdot \frac{\partial \underline{\boldsymbol{\rho}}^T}{\partial \underset{\sim}{\xi}} \underset{\approx}{\mathrm{H}}\, \underset{\approx}{\bar{\mathrm{A}}} + 2\frac{\partial \underline{\boldsymbol{\rho}}}{\partial \underset{\sim}{\xi}} \cdot \frac{\partial^2 \underline{\boldsymbol{\rho}}}{\partial \underset{\sim}{\xi}^2} \underset{\approx}{\mathrm{H}}\, \underset{\approx}{\bar{\mathrm{A}}}\right)
\end{aligned}
} \qquad [2.90]
$$

The dot product of the basis v-vector with the variation of its second derivative can be expressed as:

$$\begin{aligned}\frac{\partial \underset{\sim}{\boldsymbol{\rho}}}{\partial \underset{\sim}{\xi}} \cdot \delta \frac{\partial^2 \underset{\sim}{\boldsymbol{\rho}}_e}{\partial \underset{\sim}{\xi}^2} &= \frac{\partial \underset{\sim}{\boldsymbol{\rho}}}{\partial \underset{\sim}{\xi}} \cdot \left(\delta \frac{\partial^2 \underset{\sim}{\boldsymbol{\rho}}}{\partial \underset{\sim}{\xi}^2} + \delta \frac{\partial \underset{\sim}{\boldsymbol{n}}}{\partial \underset{\sim}{\xi}} \frac{\partial h_e}{\partial \underset{\sim}{\xi}}^T + \frac{\partial h_e}{\partial \underset{\sim}{\xi}} \delta \frac{\partial \underset{\sim}{\boldsymbol{n}}}{\partial \underset{\sim}{\xi}}^T + h_e \delta \frac{\partial^2 \underset{\sim}{\boldsymbol{n}}}{\partial \underset{\sim}{\xi}^2} + \delta \underset{\sim}{\boldsymbol{n}} \frac{\partial^2 h_e}{\partial \underset{\sim}{\xi}^2} \right) = \\ = \frac{\partial \underset{\sim}{\boldsymbol{\rho}}}{\partial \underset{\sim}{\xi}} \cdot \delta \frac{\partial^2 \underset{\sim}{\boldsymbol{\rho}}}{\partial \underset{\sim}{\xi}^2} &+ \frac{\partial \underset{\sim}{\boldsymbol{\rho}}}{\partial \underset{\sim}{\xi}} \cdot \delta \frac{\partial \underset{\sim}{\boldsymbol{n}}}{\partial \underset{\sim}{\xi}} \frac{\partial h_e}{\partial \underset{\sim}{\xi}}^T + \frac{\partial \underset{\sim}{\boldsymbol{\rho}}}{\partial \underset{\sim}{\xi}} \cdot \frac{\partial h_e}{\partial \underset{\sim}{\xi}} \delta \frac{\partial \underset{\sim}{\boldsymbol{n}}}{\partial \underset{\sim}{\xi}}^T + h_e \frac{\partial \underset{\sim}{\boldsymbol{\rho}}}{\partial \underset{\sim}{\xi}} \cdot \delta \frac{\partial^2 \underset{\sim}{\boldsymbol{n}}}{\partial \underset{\sim}{\xi}^2} - \underset{\sim}{\boldsymbol{n}} \cdot \delta \frac{\partial \underset{\sim}{\boldsymbol{\rho}}}{\partial \underset{\sim}{\xi}} \frac{\partial^2 h_e}{\partial \underset{\sim}{\xi}^2}\end{aligned} \quad [2.91]$$

2.6.2.1. *First variations*

Now we can derive all the variations for the enriched geometry. Although all expressions needed have just been derived without approximation of small gap, in order to keep the text more compact, below we present the variations of the enriched geometrical quantities only within the assumption of small gap. According to [2.23] the variation of the normal gap [2.23] using [2.75] is:

$$\delta g_n^e = \underline{\boldsymbol{n}}_e \cdot (\delta \underline{\boldsymbol{r}}_s - \delta \underline{\boldsymbol{\rho}}_e) \rightarrow \boxed{\delta g_n^e = \underline{\boldsymbol{n}}_e \cdot \left(\delta \underline{\boldsymbol{r}}_s - \delta \underline{\boldsymbol{\rho}} + h_e \left(\underline{\boldsymbol{n}} \cdot \delta \frac{\partial \underline{\boldsymbol{\rho}}}{\partial \underset{\sim}{\xi}} \right)^T \underset{\approx}{\bar{\mathrm{A}}} \frac{\partial \underline{\boldsymbol{\rho}}}{\partial \underset{\sim}{\xi}} \right)} \quad [2.92]$$

The approximated variation of the surface parameter [2.26] for the enriched surface is:

$$\delta \underset{\sim}{\xi} = \underset{\approx}{\bar{\mathrm{A}}}_e \frac{\partial \underline{\boldsymbol{\rho}}_e}{\partial \underset{\sim}{\xi}} \cdot (\delta \underline{\boldsymbol{r}}_s - \delta \underline{\boldsymbol{\rho}}_e) \rightarrow \boxed{\delta \underset{\sim}{\xi} = \underset{\approx}{\bar{\mathrm{A}}}_e \frac{\partial \underline{\boldsymbol{\rho}}_e}{\partial \underset{\sim}{\xi}} \cdot \left(\delta \underline{\boldsymbol{r}}_s - \delta \underline{\boldsymbol{\rho}} + h_e \left(\underline{\boldsymbol{n}} \cdot \delta \frac{\partial \underline{\boldsymbol{\rho}}}{\partial \underset{\sim}{\xi}} \right)^T \underset{\approx}{\bar{\mathrm{A}}} \frac{\partial \underline{\boldsymbol{\rho}}}{\partial \underset{\sim}{\xi}} \right)} \quad [2.93]$$

2.6.2.2. *Second variations*

The approximated second variation of the normal gap [2.31] is:

$$\Delta \delta g_n = -\underline{\boldsymbol{n}}_e \cdot \left(\delta \frac{\partial \underline{\boldsymbol{\rho}}_e}{\partial \underset{\sim}{\xi}}^T \Delta \underset{\sim}{\xi} + \Delta \frac{\partial \underline{\boldsymbol{\rho}}_e}{\partial \underset{\sim}{\xi}}^T \delta \underset{\sim}{\xi} \right) - \Delta \underset{\sim}{\xi}^T \underset{\approx}{\mathrm{H}}_e \delta \underset{\sim}{\xi} \quad [2.94]$$

Replacing of $\underline{\boldsymbol{n}}_e$ by [2.76] and carrying [2.80] and [2.83], we get:

$$\begin{aligned}\Delta \delta g_n \quad &= - \left(\mathrm{a}_1 \underline{\boldsymbol{n}} \cdot \delta \frac{\partial \underline{\boldsymbol{\rho}}_e}{\partial \underset{\sim}{\xi}}^T + \underset{\sim}{\mathrm{a}}_2^T \frac{\partial \underline{\boldsymbol{\rho}}}{\partial \underset{\sim}{\xi}} \cdot \delta \frac{\partial \underline{\boldsymbol{\rho}}_e}{\partial \underset{\sim}{\xi}}^T \right) \Delta \underset{\sim}{\xi} - \\ &- \left(\mathrm{a}_1 \underline{\boldsymbol{n}} \cdot \Delta \frac{\partial \underline{\boldsymbol{\rho}}_e}{\partial \underset{\sim}{\xi}}^T + \underset{\sim}{\mathrm{a}}_2^T \frac{\partial \underline{\boldsymbol{\rho}}}{\partial \underset{\sim}{\xi}} \cdot \Delta \frac{\partial \underline{\boldsymbol{\rho}}_e}{\partial \underset{\sim}{\xi}}^T \right) \delta \underset{\sim}{\xi} - \Delta \underset{\sim}{\xi}^T \underset{\approx}{\mathrm{H}}_e \delta \underset{\sim}{\xi}\end{aligned} \quad [2.95]$$

$$\boxed{\Delta\delta g_n = -\mathrm{a}_1 \underline{\boldsymbol{n}} \cdot \left(\delta \frac{\partial \underline{\boldsymbol{\rho}}^T}{\partial \underset{\sim}{\xi}} \underset{\approx}{\mathrm{b}}_2 \Delta \underset{\sim}{\xi} + \Delta \frac{\partial \underline{\boldsymbol{\rho}}^T}{\partial \underset{\sim}{\xi}} \underset{\approx}{\mathrm{b}}_2 \delta \underset{\sim}{\xi} \right) - \underset{\sim}{\mathrm{a}}_2^T [\delta \underset{\approx}{\mathrm{Q}} \Delta \underset{\sim}{\xi} + \Delta \underset{\approx}{\mathrm{Q}} \delta \underset{\sim}{\xi}] - \Delta \underset{\sim}{\xi}^T \underset{\approx}{\mathrm{H}}_e \delta \underset{\sim}{\xi}} \quad [2.96]$$

where a_1, $\underset{\sim}{\mathrm{a}}_2^T$ and $\underset{\approx}{\mathrm{b}}_2$ can be found in [2.77] and $\delta \underset{\approx}{\mathrm{Q}}$ and $\Delta \underset{\approx}{\mathrm{Q}}$ in [2.83].

The expression for the second variation of the surface parameter for the enriched surface can be obtained from [2.34]:

$$\begin{aligned} \Delta\delta \underset{\sim}{\xi} \;=\; & \underset{\approx}{\bar{\mathrm{A}}}_e \left\{ \delta g_n^e \left(\underline{\boldsymbol{n}}_e \cdot \Delta \frac{\partial \underline{\boldsymbol{\rho}}_e}{\partial \underset{\sim}{\xi}} + \underset{\approx}{\mathrm{H}}_e \Delta \underset{\sim}{\xi} \right) + \Delta g_n^e \left(\underline{\boldsymbol{n}}_e \cdot \delta \frac{\partial \underline{\boldsymbol{\rho}}_e}{\partial \underset{\sim}{\xi}} + \underset{\approx}{\mathrm{H}}_e \delta \underset{\sim}{\xi} \right) - \right. \\ & \left. - \frac{\partial \underline{\boldsymbol{\rho}}_e}{\partial \underset{\sim}{\xi}} \cdot \left(\delta \frac{\partial \underline{\boldsymbol{\rho}}_e^T}{\partial \underset{\sim}{\xi}} \Delta \underset{\sim}{\xi} + \Delta \frac{\partial \underline{\boldsymbol{\rho}}_e^T}{\partial \underset{\sim}{\xi}} \delta \underset{\sim}{\xi} \right) - \Delta \underset{\sim}{\xi}^T \left(\frac{\partial \underline{\boldsymbol{\rho}}_e}{\partial \underset{\sim}{\xi}} \cdot \frac{\partial^2 \underline{\boldsymbol{\rho}}_e}{\partial \underset{\sim}{\xi}^2} \right) \delta \underset{\sim}{\xi} \right\} \end{aligned} \quad [2.97]$$

As previously, we replace $\underline{\boldsymbol{n}}_e$ and $\frac{\partial \underline{\boldsymbol{\rho}}_e}{\partial \underset{\sim}{\xi}}$ by [2.76], [2.77] and group terms, next we substitute [2.80] and [2.83] and get:

$$\boxed{\begin{aligned} \Delta\delta \underset{\sim}{\xi} \;=\; & \underset{\approx}{\bar{\mathrm{A}}}_e \left[\mathrm{a}_1 \underset{\approx}{\mathrm{b}}_2 \left(\delta g_n^e \Delta \frac{\partial \underline{\boldsymbol{\rho}}}{\partial \underset{\sim}{\xi}} + \Delta g_n^e \delta \frac{\partial \underline{\boldsymbol{\rho}}}{\partial \underset{\sim}{\xi}} \right) \cdot \underline{\boldsymbol{n}} + \underset{\approx}{\mathrm{H}}_e (\delta g_n^e \Delta \underset{\sim}{\xi} + \Delta g_n^e \delta \underset{\sim}{\xi}) - \right. \\ & - \Delta \underset{\sim}{\xi}^{\intercal} \left(\frac{\partial \underline{\boldsymbol{\rho}}_e}{\partial \underset{\sim}{\xi}} \cdot \frac{\partial^2 \underline{\boldsymbol{\rho}}_e}{\partial \underset{\sim}{\xi}^2} \right) \delta \underset{\sim}{\xi} + [\delta \underset{\approx}{\mathrm{Q}}]^{\intercal} \underset{\sim}{\mathrm{a}}_2 \Delta g_n^e + [\Delta \underset{\approx}{\mathrm{Q}}]^{\intercal} \underset{\sim}{\mathrm{a}}_2 \delta g_n^e - \\ & \left. - \underset{\approx}{\mathrm{b}}_2 \delta \underset{\approx}{\mathrm{Q}} \Delta \underset{\sim}{\xi} + \underset{\approx}{\mathrm{b}}_2 \Delta \underset{\approx}{\mathrm{Q}} \delta \underset{\sim}{\xi} - \underset{\sim}{\mathrm{b}}_1 \underline{\boldsymbol{n}} \cdot \left(\delta \frac{\partial \underline{\boldsymbol{\rho}}^{\intercal}}{\partial \underset{\sim}{\xi}} \underset{\approx}{\mathrm{b}}_2 \Delta \underset{\sim}{\xi} + \Delta \frac{\partial \underline{\boldsymbol{\rho}}^{\intercal}}{\partial \underset{\sim}{\xi}} \underset{\approx}{\mathrm{b}}_2 \delta \underset{\sim}{\xi} \right) \right] \end{aligned}} \quad [2.98]$$

where a_1, $\underset{\sim}{\mathrm{a}}_2^T$, $\underset{\sim}{\mathrm{b}}_1$ and $\underset{\approx}{\mathrm{b}}_2$ have been taken from [2.77] and $\delta \underset{\approx}{\mathrm{Q}}$ and $\Delta \underset{\approx}{\mathrm{Q}}$ from [2.83].

Now it remains to define the enriching functions $h_e(\underset{\sim}{\xi})$ for the master surfaces and substitute them into [2.56] and consequently in the expressions for the variations. During this operation, we have to take into account that the projection procedure has to be changed (see Figure 2.13). Briefly, the new Newton's procedure used for the definition of the projection point has the same form as [2.9], but obviously all quantities related to the master should be replaced by their enriched analogs:

$$\Delta \underset{\sim}{\xi} = \left[\underset{\approx}{\mathrm{A}}_e - (\underline{\boldsymbol{r}}_s - \underline{\boldsymbol{\rho}}_e) \cdot \frac{\partial^2 \underline{\boldsymbol{\rho}}_e}{\partial \underset{\sim}{\xi}^2} \right]^{-1} \cdot \left[(\underline{\boldsymbol{r}}_s - \underline{\boldsymbol{\rho}}_e) \cdot \frac{\partial \underline{\boldsymbol{\rho}}_e}{\partial \underset{\sim}{\xi}} \right] \quad [2.99]$$

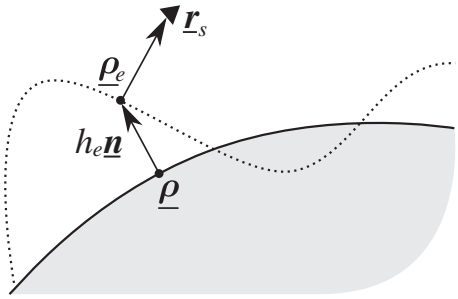

Figure 2.13. *Projection procedure for enriched geometry*

The shadow-projection procedures undergo the same modifications and are not presented here.

Remark 2.4. On enriched geometry

As already mentioned, the enriching function h_e has to be rather smooth C^2 and its value $|h_e|$ must remain smaller than the minimal local curvature radius. Moreover, if we use the normal projection, it is necessary to keep in mind that Newton's method allows us to determine only one projection point (closest to the starting point). So in the case of enrichment of the master surface with a nonlinear function $h_e(\underset{\sim}{\xi})$, Newton's method may be insufficient to find the projection point (see Figure (a)), a more advanced technique should be used, for example a dissection method combined with Newton's method.

Contrary to the normal projection, the shadow-projection is unique if there is no "self-shadow" from the master surface on its own, so we have to pay attention to avoid shadows due to the enrichment (see Figure (b)).

In order to preserve the continuity of the discretized master surface, enriching functions have to be zero at edges of each segment $\underset{\sim}{\xi}_e \in \Gamma_e$: $h_e(\underset{\sim}{\xi}_e) = 0$ (see Figure (c)). It has to be mentioned that there is a possibility of intersection of enriched geometries of adjacent master segments; it also has to be avoided (see Figure (d)).

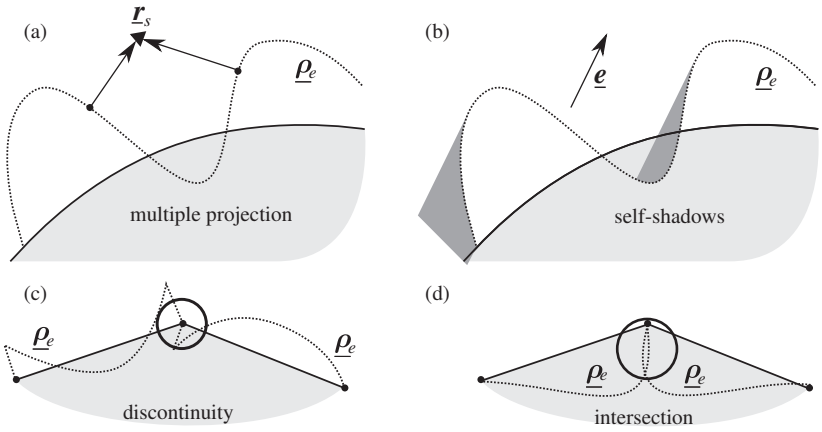

Issues related to the enriching geometry: (a) multiple normal projection within one segment (Newton's method is not sufficient to find the closest point); (b) possible presence of self-shadows on the master surface; (c) discontinuity of enriched master surface and (d) self intersection of enriched master surface.

2.6.3. *Example of enrichment*

Below we derive the expressions needed for implementation of a frictionless contact for the case of a linear 2D element enriched by a function $h_e(\xi)$ (Figure 2.14), where ξ is a segment parameter $\xi \in [0; 1]$.

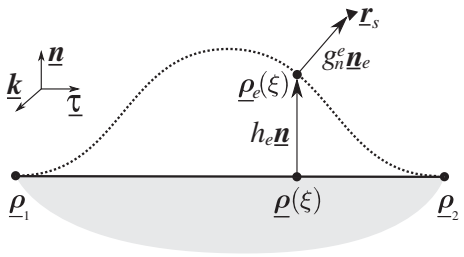

Figure 2.14. *Example of linear master segments enriched by cosine wave*

Master segments are assumed to be linear; if we introduce the following notation:

$$\underline{\boldsymbol{t}} = \frac{1}{l}(\underline{\boldsymbol{\rho}}_2 - \underline{\boldsymbol{\rho}}_1)$$

where $l = \| \underline{\boldsymbol{\rho}}_2 - \underline{\boldsymbol{\rho}}_1 \|$, then

$$\begin{gathered} \underline{\boldsymbol{\rho}}(\xi) = \underline{\boldsymbol{\rho}}_1 + \xi\, l\underline{\boldsymbol{t}}; \quad \frac{\partial \underline{\boldsymbol{\rho}}}{\partial \xi} = l\underline{\boldsymbol{t}}; \\ \underline{\boldsymbol{n}} = \frac{\underline{\boldsymbol{k}} \times \frac{\partial \underline{\boldsymbol{\rho}}}{\partial \xi}}{\| \frac{\partial \underline{\boldsymbol{\rho}}}{\partial \xi} \|} = \underline{\boldsymbol{k}} \times \underline{\boldsymbol{t}} \end{gathered} \qquad [2.100]$$

The unit normal vector $\underline{\boldsymbol{n}}$, defined in such a way, points outward from the solid if the unit vector $\underline{\boldsymbol{k}}$ points outward from the page (to us) and at the same time if master nodes in Figure 2.14 are enumerated from left to right. The enriched master geometry is defined by:

$$\underline{\boldsymbol{\rho}}_e(\xi) = \underline{\boldsymbol{\rho}}(\xi) + h_e(\xi)\underline{\boldsymbol{n}}$$

and consequently, as $\frac{\partial \underline{\boldsymbol{n}}}{\partial \xi} = 0$

$$\frac{\partial \underline{\boldsymbol{\rho}}_e}{\partial \xi} = l\underline{\boldsymbol{t}} + \frac{\partial h_e}{\partial \xi}\underline{\boldsymbol{n}} \;\Rightarrow\; \underline{\boldsymbol{n}}_e = \frac{\underline{\boldsymbol{k}} \times \frac{\partial \underline{\boldsymbol{\rho}}_e}{\partial \xi}}{\| \frac{\partial \underline{\boldsymbol{\rho}}_e}{\partial \xi} \|} = \frac{l\underline{\boldsymbol{n}} - \frac{\partial h_e}{\partial \xi}\underline{\boldsymbol{t}}}{\sqrt{l^2 + \frac{\partial h_e}{\partial \xi}^2}} \qquad [2.101]$$

in notations that have been introduced in the previous section:

$$\frac{\partial \underline{\boldsymbol{\rho}}_e}{\partial \xi} = b_1\underline{\boldsymbol{n}} + b_2 l\underline{\boldsymbol{t}}, \quad b_1 = \frac{\partial h_e}{\partial \xi},\ b_2 = 1 \qquad [2.102]$$

According to [2.92], we get the first variation of the normal gap to the enriched surface:

$$\delta g_n^e = \frac{l\underline{\boldsymbol{n}} - \frac{\partial h_e}{\partial \xi}\underline{\boldsymbol{t}}}{\sqrt{l^2 + \frac{\partial h_e}{\partial \xi}^2}} \cdot (\delta \underline{\boldsymbol{r}}_s - \delta \underline{\boldsymbol{\rho}}) - \frac{h_e \frac{\partial h_e}{\partial \xi}}{l\sqrt{l^2 + \frac{\partial h_e}{\partial \xi}^2}}\underline{\boldsymbol{n}} \cdot \delta \frac{\partial \underline{\boldsymbol{\rho}}}{\partial \xi} \qquad [2.103]$$

In a ready-to-implement form, if $\underline{\boldsymbol{\rho}} = \underline{\boldsymbol{\rho}}^i(t)\phi_i(\xi)$:

$$\delta g_n^e = \frac{1}{\sqrt{l^2 + \frac{\partial h_e}{\partial \xi}^2}} \left(\left(l\underline{\boldsymbol{n}} - \frac{\partial h_e}{\partial \xi}\underline{\boldsymbol{t}} \right) \begin{bmatrix} 1 \\ -\phi_1 \\ -\phi_2 \end{bmatrix}^\intercal - \frac{h_e \frac{\partial h_e}{\partial \xi}}{l} \underline{\boldsymbol{n}} \begin{bmatrix} 0 \\ \frac{\partial \phi_1}{\partial \xi} \\ \frac{\partial \phi_2}{\partial \xi} \end{bmatrix}^\intercal \right) \cdot \begin{bmatrix} \delta \underline{\boldsymbol{r}}_s \\ \delta \underline{\boldsymbol{\rho}}_1 \\ \delta \underline{\boldsymbol{\rho}}_2 \end{bmatrix} \quad [2.104]$$

From [2.93] adapted to the 2D case, the first variation of the surface parameter is:

$$\delta\xi = \frac{1}{l^2}\left(l\underline{\boldsymbol{t}} + \frac{\partial h_e}{\partial \xi}\underline{\boldsymbol{n}} \right) \cdot (\delta \underline{\boldsymbol{r}}_s - \delta \underline{\boldsymbol{\rho}}) + \frac{h_e}{l^2}\underline{\boldsymbol{n}} \cdot \delta \frac{\partial \underline{\boldsymbol{\rho}}}{\partial \xi} \quad [2.105]$$

The second variation of the normal gap [2.96] adapted to 2D case for linear elements has the following form:

$$\Delta\delta g_n^e = \frac{-1}{\sqrt{l^2 + \left(\frac{\partial h_e}{\partial \xi}\right)^2}} \left[l\underline{\boldsymbol{n}} \cdot \left(\delta \frac{\partial \underline{\boldsymbol{\rho}}}{\partial \xi}\Delta\xi + \Delta \frac{\partial \underline{\boldsymbol{\rho}}}{\partial \xi}\delta\xi \right) - \frac{\frac{\partial h_e}{\partial \xi}}{l}(\delta Q \Delta\xi + \Delta Q \delta\xi) \right] - \Delta\xi H_e \delta\xi$$

where from [2.83]:

$$Q = \frac{\partial \underline{\boldsymbol{\rho}}}{\partial \xi} \cdot \delta \frac{\partial \underline{\boldsymbol{\rho}}}{\partial \xi} - \underline{\boldsymbol{n}} \cdot \delta \frac{\partial \underline{\boldsymbol{\rho}}}{\partial \xi} \frac{\partial h_e}{\partial \xi}$$

and from [2.74] we get the expression for H_e:

$$H_e = \frac{l\left(\frac{\partial h_e}{\partial \xi}\right)^2}{\sqrt{l^2 + \left(\frac{\partial h_e}{\partial \xi}\right)^2}}$$

And finally the expression for the second variation of the normal gap for the enriched surface takes the following form:

$$\begin{aligned} \Delta\delta g_n^e = & -\frac{l}{\sqrt{l^2 + \left(\frac{\partial h_e}{\partial \xi}\right)^2}} \underline{\boldsymbol{n}} \cdot \left(\delta \frac{\partial \underline{\boldsymbol{\rho}}}{\partial \xi}\Delta\xi + \Delta \frac{\partial \underline{\boldsymbol{\rho}}}{\partial \xi}\delta\xi \right) - \Delta\xi \frac{l\frac{\partial h_e}{\partial \xi}^2}{\sqrt{l^2 + \left(\frac{\partial h_e}{\partial \xi}\right)^2}}\delta\xi - \\ - & \frac{\frac{\partial h_e}{\partial \xi}}{l\sqrt{l^2 + \left(\frac{\partial h_e}{\partial \xi}\right)^2}} \left(\left[\frac{\partial \underline{\boldsymbol{\rho}}}{\partial \xi} \cdot \delta \frac{\partial \underline{\boldsymbol{\rho}}}{\partial \xi} - \underline{\boldsymbol{n}} \cdot \delta \frac{\partial \underline{\boldsymbol{\rho}}}{\partial \xi} \frac{\partial h_e}{\partial \xi} \right] \Delta\xi + \left[\frac{\partial \underline{\boldsymbol{\rho}}}{\partial \xi} \cdot \Delta \frac{\partial \underline{\boldsymbol{\rho}}}{\partial \xi} - \underline{\boldsymbol{n}} \cdot \Delta \frac{\partial \underline{\boldsymbol{\rho}}}{\partial \xi} \frac{\partial h_e}{\partial \xi} \right] \delta\xi \right) \end{aligned} \quad [2.106]$$

after grouping terms:

$$\Delta\delta g_n^e = \frac{l}{\sqrt{l^2+\left(\frac{\partial h_e}{\partial\xi}\right)^2}}\left[\frac{\left(\left(\frac{\partial h_e}{\partial\xi}\right)^2 - l^2\right)\underline{\boldsymbol{n}} - \frac{\partial h_e}{\partial\xi}\, l\underline{\boldsymbol{t}}}{l^2}\cdot\left(\delta\frac{\partial\underline{\boldsymbol{\rho}}}{\partial\xi}\Delta\xi + \Delta\frac{\partial\underline{\boldsymbol{\rho}}}{\partial\xi}\delta\xi\right) - \Delta\xi\frac{\partial h_e^2}{\partial\xi}\delta\xi\right] \qquad [2.107]$$

To get the ready-to-implement expression, we need to use [2.105] for $\delta\xi$ and $\Delta\xi$.

2.6.4. *Concluding remarks*

The enrichment of the contact geometry by an arbitrary function permits:

1) to take into account a complicated geometry within one contact element;

2) to account for a change of the local geometry due to loading conditions.

As mentioned, if the enrichment is chosen to be localized within NTS contact elements, the choice of the enrichment function is limited: its value must be zero at the edges of the master segments. It implies a strong connection between the discretization and the enrichment. A possible application of this approach is the modeling of periodic structures using a regular mesh (Figure 2.15). Enrichment of thin-walled or beam structure geometries by a constant enriching function seems to be meaningful, since the predominant deformation of such structures does not affect the geometry of the surface [Figures 2.15(a) and (b)]. Moreover, the enrichment technique is the only way to account for the surface topology for shell and beam elements. A possible application is a modeling of contact with grid structures, microcontact with fiber, etc. An anisotropic friction can be simulated implicitly by a special enrichment of the master surface [Figures 2.16(a) and (b)].

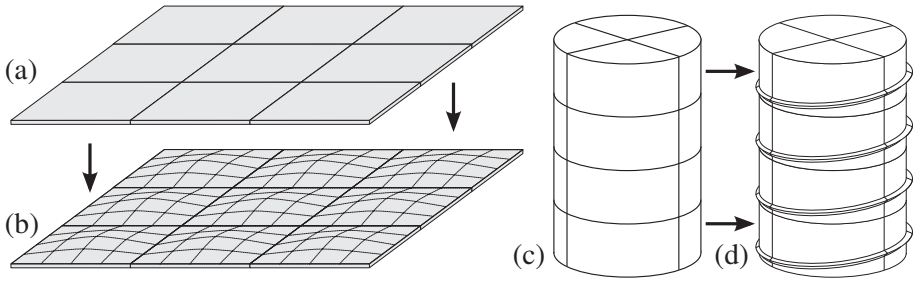

Figure 2.15. *Enriched geometry of the master finite element mesh: (a–b) periodic thin-walled structure, (c–d) mesh of a screw with four turns, represented by enrichment of 16 segments with a screw function* $\underline{\boldsymbol{\rho}}_e$ *of the master surface* $\underline{\boldsymbol{\rho}}$

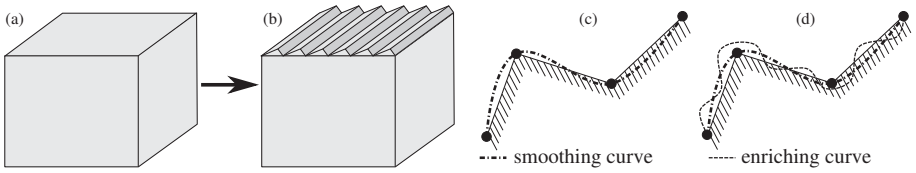

Figure 2.16. *(a–b) an example of enrichment for simulating anisotropic friction; (c–d) enrichment coupled with smoothing procedure*

If we couple the enrichment technique with a global smoothing procedure (Figures 2.16(c) and (d)) (for discussion of the latter, see, for example [PIE 97, WRI 01, KRS 02]), the mentioned shortcoming of the enrichment approach vanishes. Since the master surface is globally smooth, it is no longer required anymore that the enriching function is zero along the edges of the master segments/faces. However, it becomes a real challenge to obtain the needed variations of the geometrical quantities for the resulting enriched surface. On the other hand, this coupling makes it possible to simulate properly the phenomenon of wear and to enrich the master geometry independently on the mesh.

The simulation of wear is possible even in the simplest case, when the enriching function depends only on the number of cycles and the loading at the given cycle. Even though the surface becomes discontinuous, the convergence is ensured because of small rotations and a similar amount of wear at adjacent segments. Rigorously, if we remove the material from elements, the density of elastic energy has to be corrected.

Chapter 3

Contact Detection

Locating the contact points between two surfaces is an important step in the numerical treatment of contact problems. Moreover, this is one of the major computational costs of contact algorithms both in explicit and implicit computations. A fast and accurate detection of contact is not an easy task and has to be considered in detail. Here, we present several classical approaches and suggest some improvements. We will mainly focus on the so-called local contact detection adapted for node-to-segment/surface (NTS) discretization for implicit finite element analysis, but many results are relevant for explicit codes.

First, we introduce some notions and explain different types and strategies of contact detection. Then, we discuss simple algorithms and a more elaborated algorithm both in the case of a known and unknown (e.g. self-contact) master–slave discretizations. We conclude with some comments on parallelization of the discussed algorithms.

3.1. Introduction

Roughly, two steps can be distinguished in the contact algorithm: contact detection and resolution. Resolution implies that penetration between contacting solids has to be eliminated by applying repulsive forces to penetrating elements. Consequently, the detection phase must determine which elements of the discretized solids they are going to penetrate. It is worth mentioning the key difference between contact detection in explicit and implicit resolutions:

– explicit – it is necessary to detect elements that have already penetrated and further apply contact forces;

– implicit – possible penetration has to be known at the beginning of each resolution step in order to include additional degrees of freedom[1] in the problem and to change the residual vector and the stiffness matrix.

In the finite element analysis, contact can occur between discretized deformable bodies or between one discretized deformable body and an analytically defined rigid surface (curve). The penetration can be described in different ways (see Figure 3.1). The definition of the penetration often introduces an asymmetry in the contact problem and the contacting surfaces have to be treated differently, at least locally, in space and time. This procedure is strongly connected with the asymmetric geometrical description of contact and the discretization of the contact interface, i.e. contact detection relates to the discretization method, thus symmetric discretizations (segment-to-segment type) should use symmetric detection and vice versa. We restrict ourself to NTS discretization, so it is natural to define the penetration as the penetration of nodes of one discretized solid (slave) under the segments of the second discretized solid (master) or under an analytical surface. In the following, we will use these classical notions of master and slave for surfaces and for their components (slave nodes of the slave surface, and master segments and master nodes of the master surface).

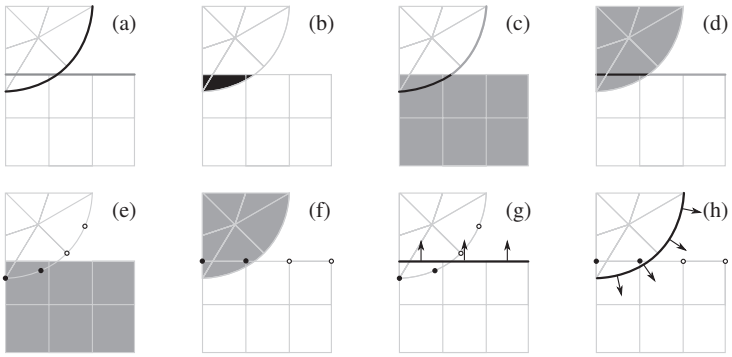

Figure 3.1. *Various definitions of the penetration. Symmetric: (a) segment intersection; (b) volume intersection. Asymmetric: (c, d) segment in volume; (e, f) node in volume; (g, h) node under surface*

Two contact search phases should be distinguished [WRI 06]: spatial search and contact detection. The first notion is used for searching between separate solids coming into contact, that is rather between separate geometries than discretizations.

1 Supplementary degrees of freedom appear in Lagrange multiplier method and the coupled augmented Lagrangian method.

Contact spatial search methods are of great importance in multibody systems and discrete element methods where interaction between more or less-identical particles such as crashed stone, sand and snow is considered to analyze mud flows, opencast mines, avalanches, etc. It is worth mentioning that previously particular attention of the scientific community has focused mostly on this phase of contact search, as local discretization of solids often remained rather moderate and even the simplest all-to-all approach often appeared to be rather efficient and a fast enough technique, especially in the case of a small slip when only one execution of the detection procedure is required.

However, in large deformation and large sliding problems, contact detection was one of the major computational costs, because the contact geometry changes significantly through computation and detection is required almost at each time step. The number of time steps depends on the resolution framework (implicit, explicit) and on the nonlinearity of the problem. Naturally, since the number of time steps is significantly higher in case of explicit calculations, the contact detection has been first considered in detail in the framework of explicit codes [BEN 90]. Many simple and efficient techniques have been proposed. They were inspired by the hidden line algorithm from computer graphics and was based on the bucket sort method. The recent advances in parallel computing make possible extremely large implicit and explicit contact simulations between very finely meshed solids and so it imposes even more severe requirements to the time needed for contact detection. The contact detection algorithms are connected with the contact discretization method and the parallel framework. However, there are not so many publications concerning that phase of the contact algorithm and frequently in moderate size engineering applications, the basic ideas of the bucket sort, proposed 20 years ago, are used. Some more recent techniques can be found in [OLD 94, BRU 02, FUJ 01]. It is worth mentioning that the recently developed mortar-based methods require a specific symmetric detection; a method based on the bounding volume trees has been proposed by B. Yang and T. A. Laursen [YAN 08a, YAN 08b].

The goal of the detection phase in implicit analysis consists of creating "contact elements" – abstract (not structural) elements, which include (in the case of an NTS discretization) a slave node and several master nodes united by a master surface segment[2]; normally this master segment should be the closest master element and the slave node has a normal projection on it. The simplest and straightforward method is the all-to-all detection: all slave nodes are projected on all master segments and if for the current slave node one or several projections exist, the closest master segment is

2 In case of Lagrange multiplier or coupled augmented Lagrangian methods, contact elements contain also some additional degrees of freedom (Lagrange multipliers) – one in case of frictionless contact and two or three in frictional case in 2D and 3D, respectively. To keep track of stick-slip-stick behavior, it is sometimes necessary to store also an internal history variable.

chosen. The growth rate of the method is $O(N_s \times N_m)$, where N_s and N_m are the numbers of slave nodes and master segments, respectively. If the master and slave discretization is unknown *a priori*, the same problem will require four times more time to achieve detection. If we consider a master surface formed by quadrilateral segments[3], then the determination of the projection requires the solution of a nonlinear equation and takes several iterations; however, often only one iteration is required to realize that there is no projection.

The first generally accepted simplification of the detection is to start from the detection of the closest node instead of the closest segment. Although the growth rate remains the same $O(N_s \times N_m)$, where N_m now denotes the number of master nodes, the time needed to achieve such a detection is significantly smaller. After detection of the closest master node, the slave node is projected on the master segments adjacent to the determined master node. For each slave node, the closest master segment is then established if it exists. Many sorting algorithms from spatial search can be used for local detection in this framework, based on the search of the closest node.

So there are two strategies: closest-node-and-adjacent-segment and closest-segment. However, both of them are time consuming and not robust (especially the strategy based on the closest node detection, see remark 3.1). Although detection methods based on the closest node strategy have been used for many years, these methods cannot be easily improved to perform a correct contact detection in all cases. That is why we will not base the detection procedure on this strategy. The rigorous formulation of the closest point given in the previous chapter will be exploited.

Let us imagine a set of spatially distributed compact objects (nodes, segments). The problem is to detect for a given object the closest one from this set. Human vision accomplishes this task easily by analyzing just a few objects. It does not need any analysis of the whole set of objects while the simple detection algorithm does, because it is "blind" and needs to "touch" all the objects one-by-one and compare distances between them (e.g. between their centers of mass). The techniques that have been worked out for contact detection are aimed at reducing the quantity of points to "touch": bucket sort [BEN 90, FUJ 00], the heap sort, the Octree method [WIL 99] and others.

Another improvement to reduce the detection time in the master–slave approach consists of considering only those parts of the contact surfaces, which are situated in a limited zone (bounding box), where contact can occur in the current solution step. This zone can be confined to a bounding box that will be updated during the

3 Second-order master surface in 2D, or any master surface in 3D, except that surface formed from triangles, requires an iterative process to determine the projection point.

computation. It is proposed to determine this detection bounding box as an intersection of bounding boxes spanned on master and slave surfaces. Another improvement, proposed in [BEN 90], consists of a smart update of the closest element: an expensive detection procedure is carried out only in the first time step (for each slave node, the closest master element (node, segment) is detected). For the following computational steps, slaves nodes are checked for proximity only with master elements neighboring to the previously determined. However, this method is not very general and sometimes fails. These improvements are not applicable for contact detection in the case of unknown *a priori* master segment discretization.

As already mentioned, the main difference in detection in explicit and implicit simulations is that for the second case, it is necessary to predict possible contact occurrence and to establish contact elements before penetration occurs. This implies that slave nodes approaching master surfaces have to be detected at a certain distance, the maximal detection distance (MDD), which is an important parameter of the detection procedure. It is good to know that the meaning of the MDD for closest-node and closest-segment-based procedures is quite different and will be discussed later.

Further we give a detailed description, analysis and validation of different contact detection techniques. We start from the development of a robust all-to-all detection technique, which is acceptable for a moderate number of nodes in contact. Two strategies are considered based on the closest node and the rigorous closest point definition. Multi-face contact elements, inspired from [HEE 93] and [BAR 02] are introduced. Some important remarks will be given on the closest-node-based detection and on the relation between the MDD and the mesh size. Further, the bucket sort method is considered in detail, the optimal bucket size is deduced and validated numerically. An extension of the considered methods to contact in case of unknown *a priori* master–slave discretization is discussed. Another contribution of this chapter is an extension of the bucket detection method to parallel framework inspired from the so-called linked cell method widely used in molecular dynamic simulations for short-range interactions [GRI 07]. Some tests of contact detection for very large problems are also presented.

To conclude this introduction, it is worth mentioning that there is a strong correlation between robustness, accuracy of contact detection and the CPU time. This dependence is not always inversely proportional. Sometimes we can sacrifice robustness to keep things simple, a good example is the “closest node” strategy complemented with bucket sort [BEN 90] – a quite simple and rather robust strategy for quadrilateral meshes. However, to preserve both the accuracy of contact detection and the simplicity of the algorithm, we propose a new robust and fast detection algorithm based on the rigorous formulation of the closest point and on the bucket sort.

3.2. All-to-all detection

All-to-all algorithms are easy and fast to implement but long to execute. Their growth rate is $O(N_s \times N_m)$. Their straightforward implementation is not acceptable for large applications, however some simple improvements mentioned in section 3.1 can significantly improve their performance.

3.2.1. *Preliminary phase*

First of all, the key parameter for the contact detection – MDD $d_{\max}$ – has to be introduced. In the case of NTS dection, $d_{\max}$ determines the following: if a slave node is closer to the master surface than $d_{\max}$, then it is supposed that this node can come in contact during the following time step, otherwise not. If we consider a node-to-node detection technique, then the meaning of the MDD is different. If the distance between a slave $\underline{\boldsymbol{r}}_i$ node and a master node $\underline{\boldsymbol{r}}_j$ $d_{ij} = \text{dist}(\underline{\boldsymbol{r}}_i, \underline{\boldsymbol{r}}_j)$[4] is smaller than the MDD, then the corresponding slave node $\underline{\boldsymbol{r}}_i$ and one of the master surfaces containing the mentioned node $\underline{\boldsymbol{r}}_j$ as its vertex are considered to be potentially into contact during the following time step, otherwise not. This difference naturally results in a limitation on the minimal value of the $d_{\max}$ for the closest-node-based detection: MDD has to be greater than one-half of the maximal distance between master nodes attached to one segment:

$$d_{\max} > \frac{1}{2} \max_{\substack{i=1,\ j=1,\ k=j+1}}^{i=N_m,\ j=N_n^i-1,\ k=N_n^i} \text{dist}(\underline{\boldsymbol{r}}_j^i, \underline{\boldsymbol{r}}_k^i) \qquad [3.1]$$

where N_m is a total number of master segments, N_n^i is a total number of master nodes attached to the ith master segment and $\underline{\boldsymbol{r}}_j^i$ is a coordinate of the jth node of the ith master segment. If the condition [3.1] is not fulfilled, then some slave nodes coming into contact with the master surface can be lost (see Figure 3.2)[5]. The value of $d_{\max}$ can be determined automatically according to the discretization of the master or self-contact surface and to the maximal displacement of nodes on contact interface during one time step. The MDD should be kept as small as possible in order to accelerate the detection procedure and to avoid the creation of non-necessary contact elements. For simplicity, it is proposed to keep the MDD unique for the entire contact area. In contrast to closest-node-based detection, the MDD for the closest-point-based procedure has no connection with the master surface

4 Here, the $\text{dist}(\underline{\boldsymbol{r}}_i, \underline{\boldsymbol{r}}_j)$ denotes Euclidean metric in the global reference frame $\text{dist}(\underline{\boldsymbol{r}}_i, \underline{\boldsymbol{r}}_j) = |\underline{\boldsymbol{r}}_i - \underline{\boldsymbol{r}}_j|$.

5 Here and for the sake of further simplicity and clarity, almost all figures represent two-dimensional cases but can be easily extended to three dimensions.

discretization and can be chosen for the all-to-all procedure only according to the maximal displacement of contact nodes. So, the following discussions on the optimal choice of the MDD relate to the all-to-all closest-node-based detection and to all detection strategies in the framework of the bucket sort, which will be considered later.

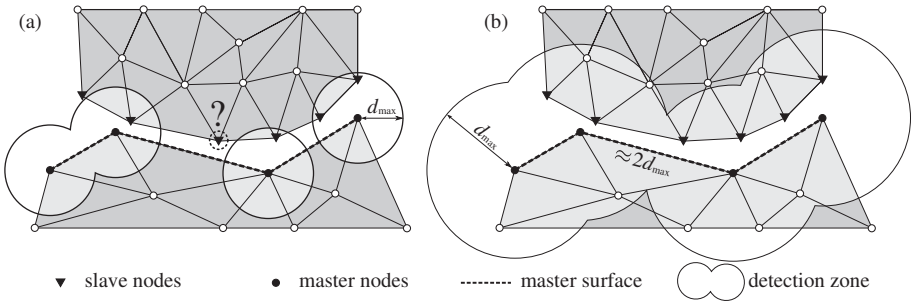

Figure 3.2. *Maximal detection distance $d_{\max}$ for closest-node-based detection strategies: on the left, not correct choice; on the right, correct choice*

For a reasonable number of time steps, in a geometrically or physically nonlinear problem, the MDD can be determined as the dimension of the largest master segment:

$$d_{\max} = \max_{\substack{i=1,\ j=1,\ k=j+1}}^{\substack{i=N_m,\ j=N_n^i-1,\ k=N_n^i}} |r_j^i - r_k^i| \qquad [3.2]$$

Such an estimation is reasonable in case of a regular discretization of the master surface. On the other hand, if the distribution of the master nodes is very heterogeneous, that is a fine surface mesh in one contact region and rough in another, the value of $d_{\max}$ appears to be highly overestimated for certain regions. This fact decreases the efficiency of the method, but in general, for an adequate finite element mesh, the increase in the detection time is not so high. The influence of the MDD on detection time will be discussed later. The possibility of performing an automatic choice of the MDD is of a big practical importance.

In the case of linearly elastic material and frictionless contact, the geometry can change significantly during one time step. So the analysis of the discretization can only provide a lower bound for $d_{\max}$ and that is why its value should be augmented

manually or automatically according to the deformation and/or displacement rate, for example in the following way:

$$d_{\max} = \max \left\{ \max_{i=1,\, j=1,\, k=j+1}^{i=N_m,\, j=N_n^i-1,\, k=N_n^i} |\underline{\boldsymbol{r}}_j^i - \underline{\boldsymbol{r}}_k^i|;\; 2 \max_{i=1}^{N_c} |\Delta \underline{\boldsymbol{r}}_i| \right\} \qquad [3.3]$$

where N_c is a total number of slave and master nodes and $\Delta \underline{\boldsymbol{r}}_i$ is the displacement of the ith node. The factor 2 takes care of possible opposite translations of master and slave nodes. In the case of remeshing or sufficiently large deformations of the master, the detection parameter $d_{\max}$ should be recomputed at each remeshing or at each Nth time step.

To accelerate the procedure before carrying out any detection, the spatial area where contact can take place during the following time step can be limited. It has to contain as few master and slave nodes as possible but obviously it has to include all the nodes potentially coming in contact during the next step. If needed, this area has to be frequently updated. We propose to confine this area by a parallelepiped bounding box defined in the global reference frame.

The determination of the bounding box differs for known *a priori* and unknown master–slave discretizations. In the case of unknown master–slave, the bounding box should include all possible contacting surfaces. But frequently the discretization is known *a priori* even if contact occurs within one body (self-contact). In this case, the construction of an optimal bounding box allows us to exclude from consideration some nodes that cannot come into contact during the next time step (Figure 3.3) and consequently it results in an acceleration of the detection procedure. It is worth mentioning that in the most general case, where any slave node can potentially come into contact with any master segment during the loading, is considered in the discussion. Often, this is not the case and for each slave node the set of possible master segments is limited and partly predefined. But to take this limitation into account, the detection technique should be tuned for each particular case, which is impractical.

First of all, the dimensions of master and slave surfaces are estimated. It is proposed to construct two independent bounding boxes B_s: $\{\underline{\boldsymbol{r}}_s^1, \underline{\boldsymbol{r}}_s^2\}$ and B_m: $\{\underline{\boldsymbol{r}}_m^1, \underline{\boldsymbol{r}}_m^2\}$ containing all slave and master nodes, respectively, where $\underline{\boldsymbol{r}}^1$ and $\underline{\boldsymbol{r}}^2$ are the vectors in the global reference frame of two opposite corners determining the bounding boxes. Note that each bounding box confining master and slave nodes includes also a node-free margin zone, the size of which is the MDD at each side:

$$\begin{aligned} \underline{\boldsymbol{r}}^1 \;:\; r^1_{\{x,y,z\}} &= \min_{i=1}^{N_b} \{\underline{\boldsymbol{e}}_{\{x,y,z\}} \cdot \underline{\boldsymbol{r}}_i\} - d_{\max} \underline{\boldsymbol{e}}_{\{x,y,z\}} \\ \underline{\boldsymbol{r}}^2 \;:\; r^2_{\{x,y,z\}} &= \max_{i=1}^{N_b} \{\underline{\boldsymbol{e}}_{\{x,y,z\}} \cdot \underline{\boldsymbol{r}}_i\} + d_{\max} \underline{\boldsymbol{e}}_{\{x,y,z\}} \end{aligned} \qquad [3.4]$$

where N_b is a number and $\underline{\boldsymbol{r}}_i$ is a vector of nodes to be included in the bounding box and $\underline{\boldsymbol{e}}_{\{x,y,z\}}$ are unit vectors in the global reference frame. The margin of $\pm d_{\max}$ is introduced to avoid any loss of possible contact elements. Some improvements can be introduced in order to reduce the time needed for the construction of the bounding box. The user can predict that if one or several contact surfaces are rigid and do not move, then permanent bounding boxes can be assigned to these surfaces and there is no need to update them. Another possible feature is the prediction by the user that the deformation and displacement of a contact surface is connected to the displacement of certain nodes. It allows us to avoid the verification of all nodes in [3.4]. Since the nodal coordinates are stored in memory in the global reference frame, it is much faster to work directly with these coordinates, so no rotation to the bounding boxes must be applied. The resulting bounding box B: $\{\underline{\boldsymbol{r}}^1, \underline{\boldsymbol{r}}^2\}$ is taken as the intersection of the master and slave bounding boxes $B = B^m \bigcap B^s$. The practice shows that a further contraction of the bounding box does not reduce significantly the detection time. The construction of the bounding box and the verification of the presence of nodes and segments inside the bounding box requires about $2(N_s + N_m)$ operations.

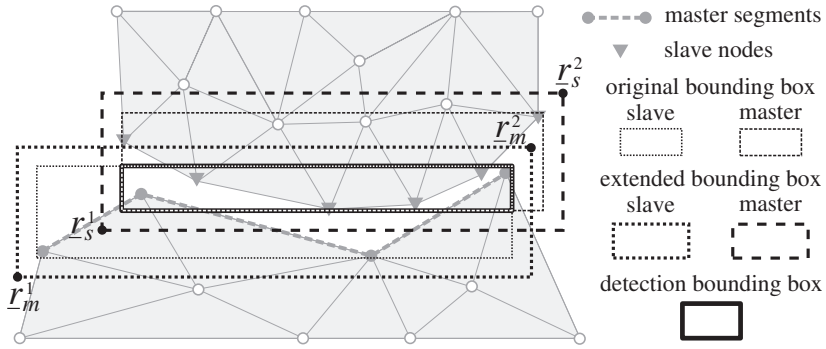

Figure 3.3. *Determination of the bounding box for the contact detection procedure in case of a known master–slave discretization*

3.2.2. *Detection phase*

In order to accelerate the detection procedure, first we can detect for each slave node the closest master node (if there are master nodes closer than MDD). It is then enough to find the projection of the slave node on the master segments having this master node as a vertex. The case where only one projection is found is trivial. It remains to create the corresponding contact element spanned on the slave node and the master surface possessing this projection. If several projections are found, the closest projection is retained to create a contact element. The case where no projection is found has to be considered in detail. There are two possibilities:

1) the slave node is situated in a “blind spot” of the discretized master surface;

2) the slave node does not come into contact but just passes close by to an edge of the master surface.

Let us remind the reader of some facts from the previous chapter. Since the finite element method requires only continuity of the discretization $\left(\Gamma_c \in C^0\right)$, the contacting surface may not be smooth $\left(\Gamma_c \notin C^1\right)$. Each master segment has its “normal projection” zone (Figure 3.4), each point in this zone has at least one normal projection onto the master surface. But often in the junction zone of the master segments (at common edges and nodes), the intersections of the “normal projection” zones do not entirely fill the surrounding space. Some gaps are left, in the form of prisms and pyramids in 3D or of sectors in 2D. This problem exists not only for linear but also for any order master elements. As has been discussed in the previous chapter, the rigorous definition of the closest point does not possess such a problem: if there is no normal projection on the master segments, the closest point is situated on the edges or on the closest master nodes or it does not exist. However, if we are confined to “normal projection” as usual for the NTS discretization, it is necessary to find the closest master segment to establish the contact element. For the sake of generality, we will consider the case when only the normal projection on master segments is checked, which naturally yields to blind spots.

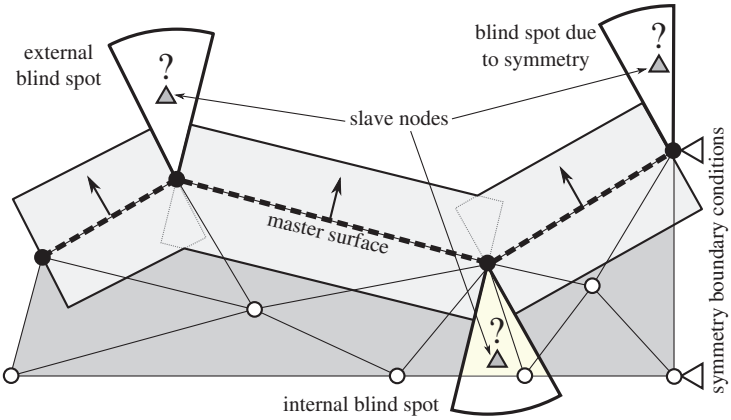

Figure 3.4. *Examples of blind spots: external, internal and due to the symmetry boundary conditions*

Three types of blind spots can be distinguished: internal, external or a blind spot due to boundary conditions (see Figure 3.4). If a slave node in a blind spot is overlooked, different consequences depending on the type of blind spot are possible.

– External blind spot. Slave nodes situated in this kind of spot are not detected before they penetrate under the master surface. After such a penetration, it can be detected during the next time step and brought back onto the surface, but the solution has already been slightly changed. In certain cases, especially in force-driven problems, such a penetration can lead to a failure of the solution algorithm.

– Internal blind spot. Contact is predicted correctly, but if a slave node penetrates just a little under the master surface and appears in its internal blind spot, this node will be lost for the contact detection at least during the next time step. Such little penetrations take place if the penalty method for contact resolution is used or just due to the limited precision of the iterative solution.

– Blind spot due to boundary conditions. This type of blind spot is situated at the boundary and can either be internal or external. It appears due to the presence of symmetric or periodic boundary conditions on the master surface, for example the basic Hertz contact problem with an axisymmetric 2D finite element mesh.

In an explicit formulation, the internal blind spots are the most dangerous, and for an implicit formulation, external blind spots are the most dangerous.

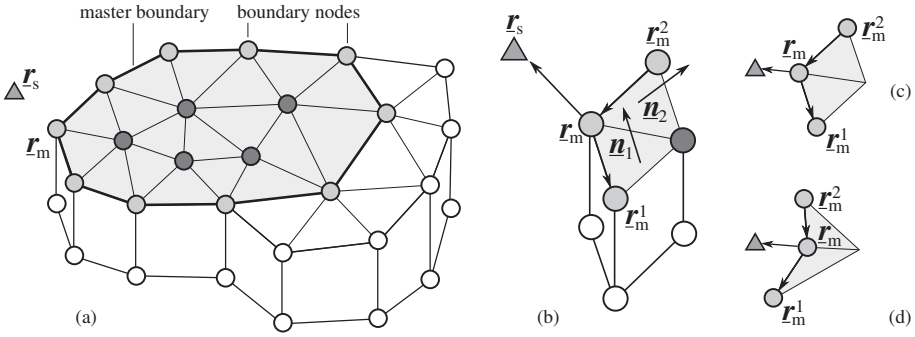

Figure 3.5. *Detection of passing by nodes. (a) master surface and its boundary; (b) zoom on the geometry close to the passing by node; (c) convex master boundary; (d) concave master boundary*

There are different possibilities to avoid the loss of contact in blind spots:

– Artificial smoothing of the master surface for large sliding contact problems [PIE 99, WRI 01, KRS 02], etc. There are no more gaps in the "projection" zones except gaps due to symmetry, that is, there are almost no more blind spots and the problem of passing by nodes does not exist. However, most of these methods have some inherent drawbacks, for example the deformation obtained close to the edge of the active contact zone may be erroneous.

– Master segments can be extended in all directions to cover the gaps in the normal projection zone.

– A "proximal volume" can be constructed by an extrusion of the master surface in the normal direction and in the opposite direction, which fills both projection zones and blind spots. If a slave node is situated in this volume, then it is considered as a node in contact and the master surface is further detected. "Passing by" nodes can be easily detected as they do not appear in the "proximal volume".

The first group of methods in general is too "expensive" if one only uses them for the detection purpose. The methods are not applicable for arbitrary meshes. The second group is good and reliable for linear elements. The third method is also quite time consuming.

We use here a rather rough but quite simple and robust treatment of blind spots. If a detected slave node has no projection and is not a passing by node, then the corresponding contact element is constructed with the closest (see [ZAV 09b]) or randomly chosen master surface attached to the closest master node. For sufficiently small time steps, such an approach is quite reliable. It remains only to determine if the node is passing by or not. One possible technique is represented in Figure 3.5.

First of all, in the preliminary phase, the boundary master nodes surrounding the master contact surface have to be marked. Let us assume that for one of these marked nodes $\underline{\boldsymbol{r}}_m$, the closest slave node $\underline{\boldsymbol{r}}_s$ has been found. If it has no projection onto the master segments attached to the marked master node, two alternatives are possible: either the slave node is situated in a blind spot, or it passes by the master surface. To choose between these two cases, we have to verify if the slave node is located in one of the blind spots attached to the master node, or to check if the slave node is in the local "proximal" volume of the master surface. The second verification seems to be more simple and natural. Note that such a verification is slightly different for locally convex and concave master surface boundaries. The convexity can be known as nodes of each master segment are ordered. The condition of convexity is:

$$(\underline{\boldsymbol{r}}_m - \underline{\boldsymbol{r}}_{m2}) \times (\underline{\boldsymbol{r}}_{m1} - \underline{\boldsymbol{r}}_m) \cdot (\underline{\boldsymbol{n}}_1 + \underline{\boldsymbol{n}}_2) \geq 0 \qquad [3.5]$$

where $\underline{\boldsymbol{n}}_1$ and $\underline{\boldsymbol{n}}_2$ are, respectively, the average normals to the master segments possessing the edges $\{\underline{\boldsymbol{r}}_m, \underline{\boldsymbol{r}}_{m1}\}$ and $\{\underline{\boldsymbol{r}}_m, \underline{\boldsymbol{r}}_{m2}\}$. The criterion of the slave node being in the proximal volume is then:

$$\underline{\boldsymbol{n}}_2 \times (\underline{\boldsymbol{r}}_m - \underline{\boldsymbol{r}}_{m2}) \cdot (\underline{\boldsymbol{r}}_s - \underline{\boldsymbol{r}}_m) \geq 0 \text{ AND } \underline{\boldsymbol{n}}_1 \times (\underline{\boldsymbol{r}}_{m1} - \underline{\boldsymbol{r}}_m) \cdot (\underline{\boldsymbol{r}}_s - \underline{\boldsymbol{r}}_m) \geq 0 \quad [3.6]$$

If this condition is fulfilled, the slave node is taken into account and the contact element is established with the closest master segment. For the concave surface, AND in equation [3.5] should be replaced by OR.

As we can see, considering only normal projections on master segments results in difficulties in detection of slave nodes in blind spots and in the case of passing by nodes. However, these difficulties are small compared to the main drawback of the contact detection based on the closest node, such a detection is not robust and may fail for non-regular meshes (see Figure 3.6 and remark 3.1). So, we propose not to start the detection procedure from searching for the closest master node for each slave. According to the rigorous definition, the closest point can be either on the master segments or master edges or master nodes, so for the purpose of robustness it is recommended to search directly the closest point, that is to check the projection on all master segments, all master edges except edges surrounding the master contact zone and all master nodes. It allows us to avoid problems associated with blind spots and passing by nodes. It increases significantly the robustness of the detection as well.

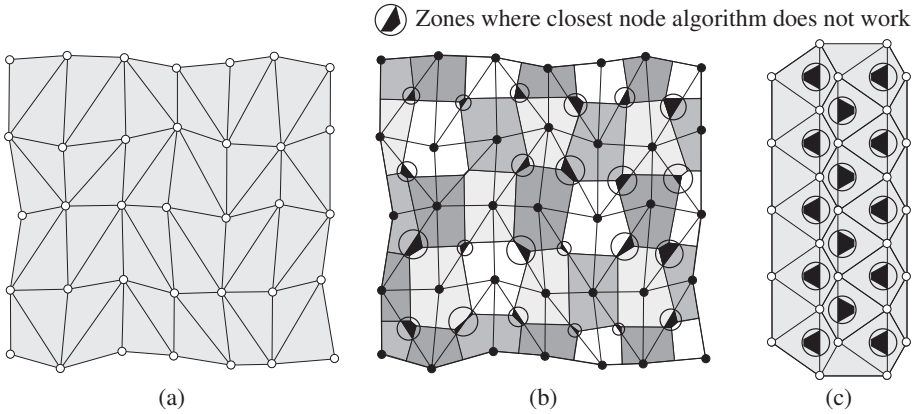

Figure 3.6. *Examples of failure of the contact detection algorithm based on the closest node: (a) flat triangular mesh of master surface; (b) gray scales correspond to the proximity zones of the master nodes; (c, d) if a slave node is situated in a black region, it has its projection on the master segment that is not attached to its closest master node; (e) on this particular mesh configuration, the fraction of "bad" zones is more than 15%*

Remark 3.1. On the contact detection based on the closest node

The detection based on the closest node takes place in two stages:

1) for each slave node, the closest master node is determined;

2) if the master node is close enough, then we suppose that the "normal projection" of the slave node onto the master surface is located on one of the master segments that have the master node as one of their vertices; the projection point is then calculated.

As mentioned in [BEN 90], the fundamental assumption of such an algorithm (the normal projection of the slave node is situated on master segments adjacent to the closest master node) is not always correct. The slave node can penetrate a master segment that is not attached to its closest master node. To demonstrate this, the authors give an example of a highly distorted quadrilateral surface mesh. However, to keep the detection algorithm fast, they accept the risk. There are several arguments in defense of their choice: they are very experienced users, they used regular quadrilateral mesh and a two pass penalty method. These facts reduce the risk almost to zero.*

However, for the general case and one pass resolution algorithms, the situation is more dramatic and the risk to overlook penetrations is high, especially for the triangular surface mesh of the master. Even a flat and quite regular surface mesh consisting of triangles may have many zones where slave nodes can penetrate under master segments that are not attached to the closest master nodes (see Figures 3.6, 3.7 and 3.8). For non-flat meshes, the risk to miss or to create an incorrect contact element is significantly higher. That is why we recommend avoiding contact detection methods based on the closest master node.

---

* *In this case, one node can be both master and slave during one increment.*

3.3. Bucket sort detection

Bucket sort based on the closest node has been proposed by Benson and Hallquist [BEN 90] for DYNA3D [BEN 07]. It has been slightly improved in [FUJ 00] and recently revisited with some improvements and several comments concerning parallelization in [YAS 11b]. Here, we adapt the bucket approach to account for the rigorous definition of the closest point from the previous section. Many details of the algorithm based on the closest node [YAS 11b] remain unchanged. Nevertheless, the detection of the closest point requires now about two to three times more verifications and several times more floating point operations: the slave point is checked against master nodes, edges and elements. On the other hand, it is not necessary to check for passing by nodes and blind spots.

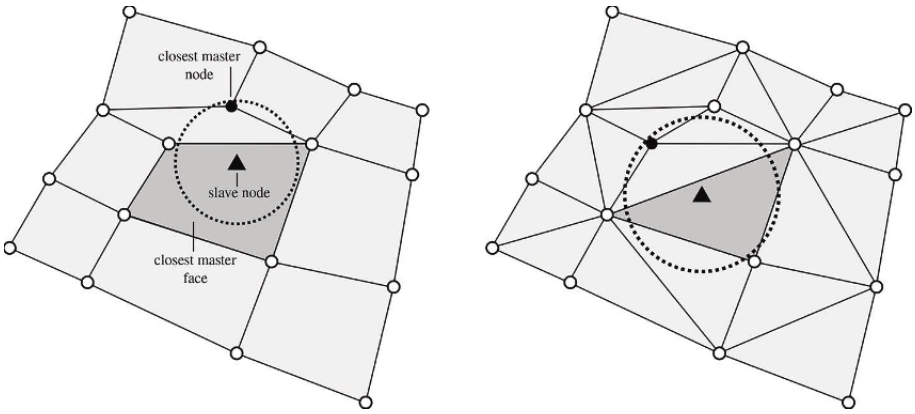

Figure 3.7. *Three-dimensional examples of failure of a detection algorithm based on the closest node search: a flat distorted quadrilateral and triangular master meshes, triangle denotes a slave node for which closest master point is not situated on the master segments having the closest master node as its vertex*

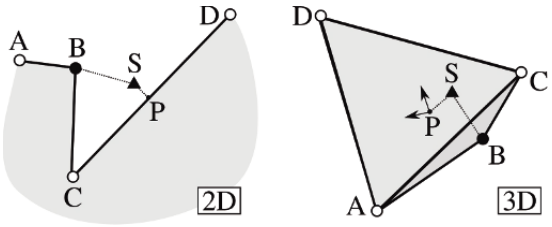

Figure 3.8. *Two-dimensional case: the slave node S has its closest point on the master segment CD not attached to the closest node B; 3D case: the closest point to the slave node S is situated on the segment ACD not attached to the closest node B*

Before discussing particular details, let us derive a short description of the bucket sort detection method. As previously, two phases can be distinguished. In the preliminary phase, the optimal size of the bucket is evaluated, then a potential contact area is determined and split into buckets (cells) by an enumerated regular grid. That allows us to reduce locally the area of the closest point search. Finally, all slave and master components (nodes, edges, segments) situated in the detection area are distributed in the cells of the grid. In the detection phase, for each slave node, we check for the closest master component in the current cell. If needed, we check one or several neighboring cells for possible proximal master components. A contact element is finally created in a special manner.

3.3.1. *Preliminary phase*

First of all, the MDD $d_{\max}$ is chosen equal to the maximal size of the biggest segment of the master surface (N_m operations). The spatial bounding box is then determined as the intersection of the master and slave bounding boxes exactly as described in the previous section ($N_m + N_s$ operations). An internal grid should be constructed in a proper way: it should be regular and the cell size w should be optimum, that is not too large in order to keep the number of slave and master nodes in the cell as small as possible. On the other hand, if we limit the operations to checking only one neighboring layer of cells (nine cells in 2D and 27 in 3D), it can be shown that the cell side must be greater than $w \geq \sqrt{2}d_{\max}$ for linear elements in order not to overlook segments such as AB for slave node S in Figure 3.9. For quadratic elements, the limitation depends on the maximal curvature of the master segments, but the rough estimation $w > \sqrt{2}d_{\max}$ seems to be reliable. If the size of the cell is smaller, more than one layer of neighboring cells has to be checked. It significantly complicates the coding of the algorithm and, moreover, the growth rate of the maximal number of cells to be checked N_c is cubical:

$$\text{if } w = \frac{d_{\max}}{n}, n > 1 \Rightarrow N_c = (3 + 2n)^3 \qquad [3.7]$$

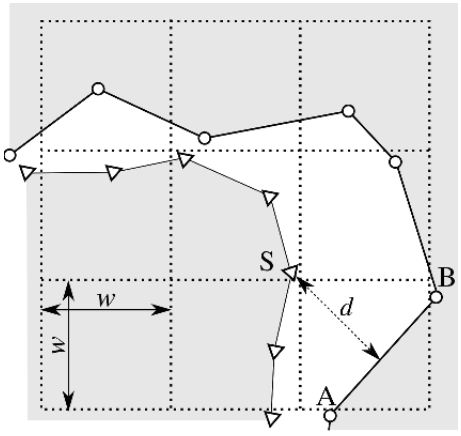

Figure 3.9. *Example of nine buckets (cells) and master–slave solids, triangles – slave nodes, circles – master nodes. distance between slave node S and master segment AB (which is not included in the right bottom bucket) is higher than MDD if cell side $w > \sqrt{2}d_{\max}$: there is no risk to overlook possible contact*

The smaller the cell size, the higher the total number of cells and consequently the smaller the number of contact nodes per cell. On the other hand, the small cell size increases the need to carry out the detection in neighboring cells. It can be shown

analytically by means of probability methods that for the even distribution of master and slave elements both in 2D and 3D cases, the minimal detection time is unique and corresponds to the minimal possible cell size. Such a simple analysis predicts a quadratic growth of the detection time in 2D case and cubic in 3D. However, in real simulations, the distribution of the contact elements is not even and so some numerical tests have been performed in order to investigate the dependence of the detection CPU time t on the cell size w.

3.3.2. *Numerical tests*

For the purpose of the optimal cell size definition, several artificial finite element meshes have been considered. Slave and master surfaces consist of about 10,200 nodes each. Three sets have been considered: proximal meshes with homogeneous (Figure 3.10, left top) and heterogeneous (Figure 3.10, left bottom) node distributions and a convex mesh with a heterogeneous node distribution (Figure 3.10, right). Each set is represented by five different realizations of curved surfaces. By homogeneous node distribution, we mean that the maximal segment dimension does not exceed 200% of the minimal segment dimension. In heterogeneous case, this difference reaches 700%.

Figure 3.10. *Example of finite element meshes used to determine the optimal cell size: proximal meshes with homogeneous (a) and heterogeneous (b) spatial node distribution and convex meshes (c)*

In Figure 3.11, the dependence of the average detection CPU time and the average number of investigated neighboring cells on the normalized cell size $w/d_{\max}$ is represented for different sets. As expected, the detection time for convex meshes is smaller because of the smaller associated bounding boxes. Different discretizations ($256 \times 256, 512 \times 512$) have been tested. In all the cases, the same dependence takes place. According to the analytical estimation and to the test results, the optimal grid size is the minimal one and equal to the MDD amplified by $\sqrt{2}$:

$$w = \sqrt{2} d_{\max} \qquad [3.8]$$

For such a choice, each grid cell contains the minimal number of elements, but on the other hand it is necessary to carry out the detection procedure in many neighboring cells: an average 12–16 cells from 26 surrounding cells in 3D (Figure 3.11).

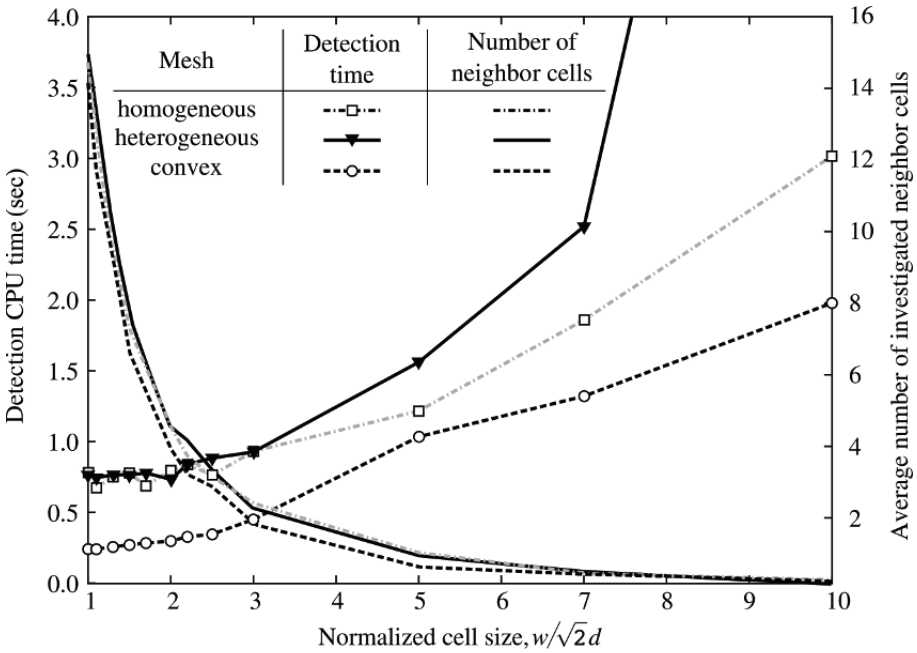

Figure 3.11. *The dependence of the detection time and the average number of neighboring cells investigated during the detection on the normalized cell size*

This investigation allows us to determine automatically the optimal MDD and the size of the detection cell depending on the discretization of the master surface. It makes the algorithm user friendly and in most cases accelerates the computation. However, sometimes it is necessary to keep the MDD significantly smaller than the

biggest master element. Such a situation arises in complex self-contact problems with unknown *a priori* master–slave discretization. In this case, the detection cell size is kept equal to the dimension of the largest master element d multiplied by $\sqrt{2}$ and the MDD is set smaller than d.

When the MDD is determined and the bounding box is constructed, the internal grid has to be established in the bounding box and, further, all slave nodes situated in the bounding box as well as all master components (nodes, edges and segments) have to be distributed in the cells of the grid. Since the optimal cell size $w_{\min} = \sqrt{2}d_{\max}$, the number of cells in each dimension of the grid is defined as:

$$N_{x,y,z} = \max\left\{\left[\frac{r^2_{x,y,z} - r^1_{x,y,z}}{\sqrt{2}d_{\max}}\right];\ 1\right\} \qquad [3.9]$$

where $[x]$ stands for the integer part of x. Such a choice of cell numbers provides the size of the cell Δx, Δy and Δz not smaller than $w_{\min}$ at least in case of $N > 1$:

$$\Delta\{x, y, z\} = \frac{r^2_{x,y,z} - r^1_{x,y,z}}{N_{x,y,z}} \geq \sqrt{2}d_{\max} \qquad [3.10]$$

Each cell of the grid has to be enumerated, the unique integer number $N \in [0;\ N_x \times N_y \times N_z - 1]$ is given to each cell with spatial "coordinates" i_x, i_y and i_z, where $i_{x,y,z} \in [0;\ N_{x,y,z} - 1]$

$$N = i_x + i_y N_x + i_z N_x N_y \qquad [3.11]$$

Now the growth rate of the method can be estimated roughly as $O\left(\frac{N_s N_m}{N_x N_y N_z}\right)$. If the average number of master and slave nodes per cell is supposed to be constant[6] $\varrho = \frac{N}{N_c}$, where $N_c = N_x N_y N_z$ and N is an average number of master and slave nodes, then the growth rate of the method can be rewritten as $O(N)$. However, in practice, the distribution of nodes is not even and the growth rate is higher. Consequently, the clustering of nodes and the non-regularity of the mesh significantly influences the performance of the method.

Slave nodes and master components situated in the bounding box have to be distributed in the cells. For this purpose, several arrays A^s and A^m_n, A^m_e, A^m_s are

6 The number of master nodes per cell can be considered constant as cell size is proportional to the maximal distance between master nodes.

created corresponding to slave nodes, master nodes, edges and segments, respectively. These arrays contain identification numbers (IDs) of components that are contained in each cell: IDs of slave and master nodes, and edge segments. Another possibility is to construct only one array for master components, which will include only master nodes, since edges and segments can be derived from this information; but in this case, it is necessary to avoid identical verifications. For example, element $A^s[i,j]$ keeps the ID of the jth slave node in the ith cell of the grid, $i \in [0; N_x N_y N_z - 1]$, $j \in [0; N_i^s]$, N_i^s being the number of slave nodes in the ith cell. On average, the number of integer (32 bits) elements in an array does not exceed the number of contact nodes and so even for extremely large problems it makes just a minor contribution in memory requirement. However, the arrays can be replaced by linked-list storages as in [FUJ 00].

For each node with coordinates $\underline{\boldsymbol{r}} : \{r_x, r_y, r_z\}$ inside the bounding box, the corresponding cell number is easily determined as:

$$N_{\text{cell}} = \left[\frac{r_x - r_x^1}{\Delta x}\right] + \left[\frac{r_y - r_y^1}{\Delta y}\right] N_x + \left[\frac{r_z - r_z^1}{\Delta z}\right] N_x N_y \qquad [3.12]$$

master segments and edges are supposed to be in the cell if at least one of their nodes is in the cell. So contrary to nodes, master segments and edges can be associated with several different cells.

3.3.3. *Detection phase*

All steps described previously represent the preliminary part of the detection algorithm, which demands in general 7–10% of the total detection time. The next steps of the algorithm correspond to the detection of the closest point and the construction of contact elements. For each grid cell c_i and for each slave node $\underline{\boldsymbol{r}}_{ij}^s$ in this cell, that is for each node with ID $A^s[i,j]$, we look for the closest point on the master components associated with the current cell, that is the closest component among $A_n^m[i], A_e^m[i], A_s^m[i]$ if they are not empty. Let us suppose that among all master components in the cell the distance to the closest point is $d_{ij}^s \leq d_{\max}$. It is obvious that the master components situated in neighboring cells (maximum eight cells in 2D, 26 in 3D) have to be checked as well. Not all the cells are considered, but only those whose boundaries are sufficiently close to the slave node. The criterion of the proximity is the following: if any boundary of the current cell (face, edge or vertex) is closer than the closest master node found previously, that is closer than d_{ij}^s, then the detection procedure has to be carried out in all neighboring cells attached to the boundary one-by-one.

For example, let us consider a vertex of the ith cell $\underline{\boldsymbol{r}}_i^v$. For instance, after checking all master components in the current cell, we find that the closest component is remote at d_{ij}^s from the slave. Then if the considered slave node is closer to the vertex than this distance, that is $\underline{\boldsymbol{r}}_i^v$: $|\underline{\boldsymbol{r}}_{ij}^s - \underline{\boldsymbol{r}}_i^v| < d_{ij}^s$, then all the master components in one of the neighboring cells attached to the vertex $\underline{\boldsymbol{r}}_i^v$ have to be considered and consequently d_{ij}^s has to be decreased or left unchanged if no closer master components are found in these cells. And so on for other cells attached to this corner. In general, the same procedure has to be performed for all eight vertices, 12 edges and six faces of the ith cell. To get a more optimal algorithm, it is better if such an investigation of neighboring cells starts from the closest faces, further edges and finish as the verification with vertices if needed. Note that each verified cell may decrease the d_{ij}^s and consequently can decrease the number of cells to be checked. In such a manner, all possibly proximal slave and master nodes are detected cell-by-cell. The average number of verified neighboring cells for different meshes is represented in Figure 3.11. This number decreases with increasing normalized grid size $1/\sqrt{2}w/d_{\max}$ but as the optimal ratio $w/d_{\max} = \sqrt{2}$, the average number of verified neighboring cells remains quite high, typically 12–16 cells.

3.3.4. *Multi-face contact elements*

In this manner, each slave node in the bounding box is checked and for some of them the closest master component, has been found. Now let us discuss how to create NTS contact elements. Barboteu *et al.* in [BAR 02] proposed to use multi-face NTS contact elements. Even earlier, it has been proposed by Heegaard and Curnier for large-slip contact [HEE 93]. This idea is particularly interesting for accelerating the overall computation time, moreover in some cases it renders a more accurate algorithm. It consists of creating contact elements made of one slave node and several master segments, in order:

– to avoid frequent updating of the contact elements;

– to treat large sliding (more than one master segment) during one increment;

– to avoid random choice between two equally close master segments;

– to create an NTS element even when no normal projection has been found.

If the master–slave discretization is not too dense, then NTS contact elements can contain one slave node and all possible master segments, as done in [ALA 04]. Consequently, the values in the global stiffness matrix must be updated, but not its structure, which decreases significantly the total computational time. However, multi-face contact element should be used carefully due to the risk of infinite loop, if a slave node finds itself in a concave region of the master surface.

If a master component has been detected close enough to a given slave node, several segments attached to this master component are included in the contact element (see Figure 3.12). If a slave node has the closest:

– point on a master segment: the current master segment and several neighboring segments are included in contact element;

– point on a master edge: the master segments adjacent to this edge are included in contact;

– master node: the master segments having this node as one of their vertex are included in contact.

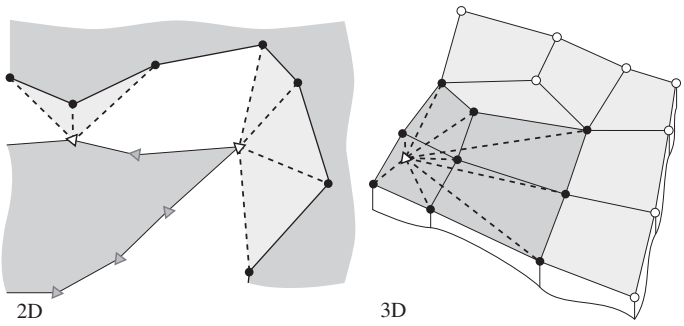

Figure 3.12. *Examples of multi-face contact elements in 2D and 3D, dashed lines connect nodes of multi-face contact elements: triangles – slave nodes; circles – master nodes*

Master segments, nodes and edges in such an element can be either active (slave node passes over segment, edge or node) or passive. Only active components introduce non-zero values to the residual vector and stiffness matrix.

3.3.5. *Improvements*

As proposed in [BEN 90], then used in [PIE 97] and many others, in case of a known master–slave discretization, all slave and master components should be included in the detection procedure only once. Further contact elements that have been already created can be updated in a more efficient manner. If the slave node still has a projection on a master component included in its contact element, this element will not be removed. If not, the detection is performed only in a close vicinity of the former contact element and a new element is created. By close vicinity we mean master components neighboring to the former contact element. Normally, it can be rather easily found as the mesh topology is known. If a slave node has no associated

contact element on the previous time step, it should be included in the detection procedure. Obviously, the slave bounding box is computed only for such inactive slave nodes, and the master bounding box is still based on all master components. This technique appears to be quite efficient and accelerates significantly the detection phase and the matrix reconstruction.

Another technique consists of increasing the number of buckets, but since this number is connected to the discretization of the master surface, the minimal dimension of the buckets is strictly limited. However, there is a way to solve this issue: several artificial nodes can be set on each master segment, which results in an automatic decrease in the limit on the MDD and consequently the number of buckets increases. Two examples are given in Figure 3.13.

3.4. Case of unknown master–slave

There are mechanical problems for which the determination of master and slave surfaces presents a big challenge or may be impossible. Among such problems, there are multibody systems, problems with complicated geometries (e.g. highly porous media like metal foams), large deformation problems with non-regular discretization and self-contact problems.

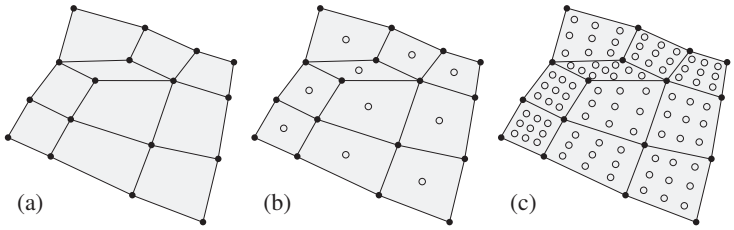

Figure 3.13. *Examples of artificial nodes on the master surface: (a) – original master mesh, (b) – one supplementary node per segment; (c) – 9 supplementary nodes per segment*

This class of contact problems needs a particular contact detection procedure. In the past, the bucket sort has been successfully applied to contact detection and it is widely known as single surface contact algorithm [BEN 90]. Here, a more accurate adaptation of the previously derived formulation for a problem with unknown *a priori* master–slave discretization is proposed. A particular attention is paid to self-contact problems. Some examples will be given in Chapter 6. Such an adaptation demands considerable modifications in all stages of the grid detection procedure. The growth rate of the method is the same as for the case of known *a priori* master–slave discretization. The method is straightforward and adapted for NTS discretization. In

case of a mortar-based formulation, the reader is referred to the recently developed technique proposed in [YAN 08a].

A self-contact is more probable for thin or oblong solids, for which one or two dimensions are much smaller than others, so often shell elements are used to simulate self-contact. But there is a challenge that is illustrated in Figure 3.14. For a thin solid with one- or two-sided contact zones, it is complicated to detect the contact with the reverse side (circles in Figure 3.14) even if in addition to node positions their normal vectors and corresponding surfaces are taken into account. Precisely, an ordinary detection algorithm would suppose that the circles are penetrating under the surface marked with another circle of the same color, consequently associated contact components have to be included in the contact. A possible solution is to determine an MDD smaller than the double minimal thickness of the contacting structure, however very small time steps have to be made. A better solution has been proposed in [BEN 90], where the authors introduce an additional history variable to keep track of the side from which the contact surface has penetrated. This approach allows the MDD to overpass the thickness of the structure. Remark that this problem is more severe if both surfaces can contact each other.

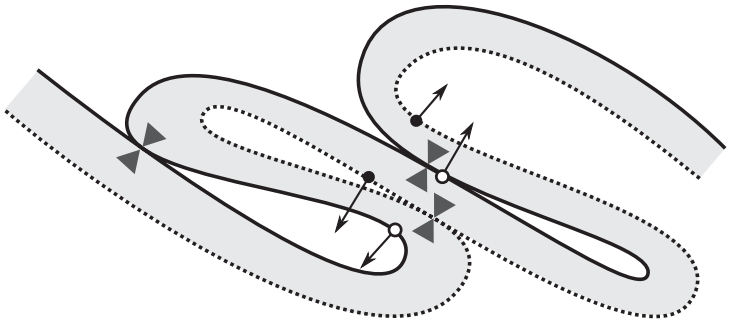

Figure 3.14. *Usual case of self-contact in a thin-walled structure: example demonstrates the inherent problem of self-contact detection: triangles mark a correctly detected contact; circles mark zones that can be recognized as active contact zones*

Let us enumerate the features of the implementation of the detection method in case of unknown *a priori* master–slave discretization. The main modification is that not only nodes, edges and segments have to be considered but also the associated normals to determine potentially contacting elements.

1) The bounding box has to include all contact components; it can be chosen constant, if we know *a priori* a sufficiently small area, from where the contact nodes do not escape.

2) Normals have to be assigned to each contact node and contact edge at the beginning of each time step.

3) Only one array A^c is created and filled with contact components. The process is the same as in the case of simple contact.

4) Since we cannot distinguish master and slave, the detection of the closest point has to be carried out for each contact node – future slave node against all contact components in the cell. To be sure that contact components can contact and are not attached to a common element, the normals associated with the slave node and the closest master component should point toward each other $\underline{\boldsymbol{n}}_i \cdot \underline{\boldsymbol{n}}_j \leq 0$. Obviously some neighboring cells have to be verified as in the case of simple contact.

5) Nodes for which a close enough contact component has been determined should be marked as slaves and should not be included as a slave node for another contact element.

Details for self-contact detection based on the closest node are quite similar and are discussed in [BEN 90] and [YAS 11b]. The detection time is higher than for the contact of the same order with a known *a priori* master–slave discretization, because the preliminary stage requires the assignation of normals to every node and edge. Moreover, as the main detection stage requires significantly more verifications of distance and normal than in master–slave conception, in practice, the difference in detection time between known *a priori* and unknown master–slave depends significantly on the geometry and its evolution.

Remark 3.2. On the definition of the normal vector for contact nodes

Normal at node $\underline{\boldsymbol{n}}$ can be defined in different ways:

– averaged vector of the averaged normals of the adjacent segments:

$$\underline{\boldsymbol{n}} = \frac{1}{N} \sum_{i=1,N} \underline{\boldsymbol{n}}_i$$

where N is the number of adjacent segments and $\underline{\boldsymbol{n}}_i$ is the associated average normal of segment i, normals in the middle of segments or normals in the point where the needed node is situated (Figure 3.15a).

– average between weighted average normals of adjacent segments (Figure 3.15b):

$$\underline{\boldsymbol{n}} = \frac{1}{A} \sum_{i=1,N} \underline{\boldsymbol{n}}_i A_i$$

where A_i is area (length) of the ith adjacent segment, A is the total area (length) of segments $A = \sum_{i=1,N} A_i$ and n_i is the average normal of the ith segment.

– If the surface is smooth, then the associated normal is unique (Figure 3.15c).

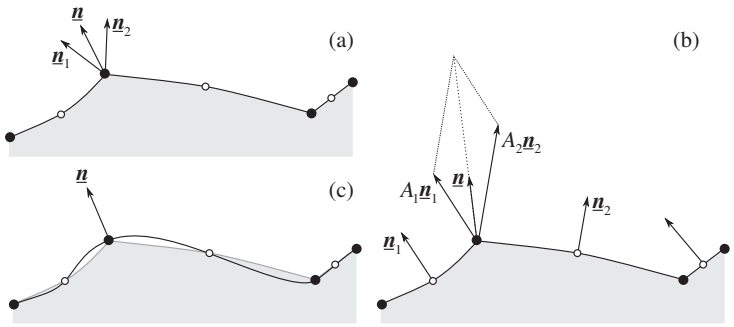

Figure 3.15. *Different possibilities to define the normal at node/edge: (a) average between normals of adjacent segments in the node; (b) average weighted normal; for smoothed surfaces [e.g. with Bézier curve, (c)], the definition of normal is explicit and unique.*

In conclusion, we confirm that the bucket sort method based on a rigorous definition of the closest point can be extended to the case of unknown *a priori* master–slave discretizations. The required detection time is significantly higher but of the same order of magnitude as the time needed for simple contact detection for the same problem. The availability of such a powerful method for self-contact detection extends significantly the capacities of the FEA of contact problems. Some numerical examples will be given in Chapter 6.

3.5. Parallel contact detection

3.5.1. *General presentation*

The sequential treatment of the problems presented above (tire-road, curved contact surfaces, operculum structure) requires either too long a computational time or may be just impossible due to the large amount of memory needed. The use of the parallelization paradigm is then a good way out. Many parallelization techniques are available nowadays, the class of non-overlapping domain decomposition, also called iterative substructuring method, is successfully and widely used in computational mechanics ([FAR 94, TOS 05, GOS 06]). It implies a splitting of an entire finite element mesh into sub-domains that intersect only at their interfaces. Each sub-domain is treated by one or several associated processors, and the global solution is obtained by enforcing displacement continuity and the balance of reactions across sub-domains. The use of these techniques with affordable and powerful parallel computers allows us to solve very large mechanical problems in a reasonable time. In general, the resolution step cannot start before the detection procedure has been finished, so the last one is very important for the efficiency of the parallel computations [BRO 00]. It should not present a bottleneck in the whole process and, if possible, it has to use all the available capacities of parallel computers.

The key point for the contact detection procedure in parallel treatment is the fact that the finite element mesh and possibly the contact surface are divided into some parts associated with different processors and that, in the case of distributed memory, it is not entirely available on a particular processor. Since in principle we need the entire contact surface(s) to perform the detection procedure, this repartition implies data exchanges between sub-domains containing different parts of this surface(s). The amount of data transfer should be kept minimal. This will be our goal in the framework of the contact detection based on the bounding box conception and the bucket sort.

Two strategies for the parallel treatment of contact problems are proposed and analyzed: Single (processor) Detection, Multiple (processor) Resolution (SDMR) and Multiple Detection, Multiple Resolution (MDMR). As it is straightforward from the notations, SDMR carries out the contact detection on a single processor whereas MDMR uses all the available resources for the detection procedure. The last implies a parallelization of the detection procedure, which will be discussed in details and tested.

3.5.2. *Single detection, multiple resolution approach*

Let us consider the SDMR approach. The main idea is that all necessary information is collected by one processor that carries out the contact detection in the way explained above and distributes consequently the created contact elements

among all concerned sub-domains. This method can be efficiently applied to any contact problem and is relatively easy to implement. On the other hand, this method does not use efficiently all available resources, that is except one, all the processors are idle and inactive during the main detection phase; however, all the processors possessing a contact surface are active during the preliminary stage.

At first, the bounding box for the contact detection has to be defined. This task is easily performed in parallel. Each sub-domain $i \in [1; N^c]$ possessing a part of contacting surfaces examines it and derives the corresponding bounding boxes ${}^m\underline{\boldsymbol{r}}_i^1,\ {}^s\underline{\boldsymbol{r}}_i^1,\ {}^m\underline{\boldsymbol{r}}_i^2,\ {}^s\underline{\boldsymbol{r}}_i^2$ and the maximal dimension of the master segment $d_{\max}^i$. After data transfer, the global MDD $d_{\max} = \max\limits_{i=1,N^c}\{d_{\max}^i\}$ and the master and slave bounding boxes are determined:

$$ {}^{m,s}r_{\{x,y,z\}}^1 = \min_{i=1}^{N^c}\{{}^{m,s}r_{i\{x,y,z\}}^1\} - d_{\max},\ {}^{m,s}r_{\{x,y,z\}}^2 = \max_{i=1}^{N^c}\{{}^{m,s}r_{i\{x,y,z\}}^2\} + d_{\max} \qquad [3.13] $$

Finally, the resulting bounding box $\{\underline{\boldsymbol{r}}^1,\ \underline{\boldsymbol{r}}^2\}$ is constructed as the intersection of master and slave bounding boxes, exactly as in the sequential procedure. The data transfer involves at most $3N^c$ operations but the load is not uniformly distributed between processors, because not all of them contain the contact surface and, for those containing a contact zone, the size of the surface may be quite different. Anyway, this operation is quite fast even for huge meshes.

The next step consists of the union of all the necessary parts of the contact surface in one processor-detector. First, the information about the global bounding box is distributed among the sub-domains possessing the contact surface, each of them counts the number of master and slave nodes located in the bounding box, further the sub-domain with the maximal number of master and slave nodes is chosen as detector. Another possibility would be that this choice is made in agreement with the processor network topology, to accelerate the data transfer on the next detection step. At this stage, the data exchange between sub-domains remains negligible.

It remains to transfer all master components and slave nodes from the bounding box (global IDs, hosting sub-domain ID, coordinates, etc.) to the sub-domain detector, to carry out the detection as described in section 3.3 and to attribute the constructed contact elements to the relevant sub-domains. If a contact element is made of a slave node and master nodes from different sub-domains, the interface between them has to be created or updated. Duplicated slave nodes have to be formed as well. This step is the most expensive in the terms of data exchange. The technical part of this operation is also quite complicated, because in general it is not possible to exchange directly mesh quantities: nodes, segments, edges. So, the developer has to design an

appropriate class structure for geometrical objects, which does not contain any global pointers on the finite element mesh, elements, etc.

3.5.3. *Multiple detection, multiple resolution approach*

In MDMR, the preliminary part of a bounding box construction is exactly the same as in SDMR approach. The key difference between MDMR and SDMR appears in the next step. Instead of transferring all necessary information to the detector, the information is distributed between all sub-domains in a special way. As shown above, the grid is constructed in such a way that, for each slave node, only one surrounding layer of neighboring cells has to be checked to find the closest point on the master surface. If self-contact is excluded, we do not care about slave nodes in the neighboring cells. That is why the bounding box with associated buckets can be divided into N non-overlapping parts, each of them consisting of an integer number of buckets. Each part is then extended in all directions (not exceeding the bounding box) by one cell overlapping layer; the extended part is filled only with master components. An example involving two sub-domains is presented in Figure 3.16. It shows the internal cells (non-overlapping with other parts, dark gray) including both master components and slave nodes and external cells (shared with neighboring parts, light gray) including only master segments. Each part is associated with a processor. The nodes and surfaces located in the part (global IDs, hosting sub-domain ID, coordinates, etc.) are collected from different sub-domains and transferred to the relevant sub-domain. The detection can then be carried out independently, that is in parallel for each part. No more data exchange is needed, so that the performance and scalability of the MDMR approach are significantly improved. The advantage of the method is that the total number of operations per processor during the main phase of detection does not increase for a given fraction of contacting nodes per number of processors. It is worth mentioning, that during the main detection phase, the number of operations is not homogeneously distributed between processors: there is still a need for a special algorithm to perform a smart split of the detection buckets, which would take into account the distribution of contact elements into buckets. Actually we use a simple split taking into account that the number of sub-domains is even and that the number of buckets is much smaller than the number of sub-domains. As in many applications, the contact interface is concentrated in a thin flat zone, the 3D bounding box is not split along its smallest side.

The same parallel procedure can be used for self-contact problems. The first difference is that master and slave nodes are not distinguished and hence all contact components have to be included in the overlapping cells. The second difference in treating contact components in internal and external (overlapping) cells is that nodes from the latter cannot be assigned as slave nodes. The described method is very similar to the parallelization of the linked cell method widely used in molecular dynamic simulations for short-range interactions [GRI 07].

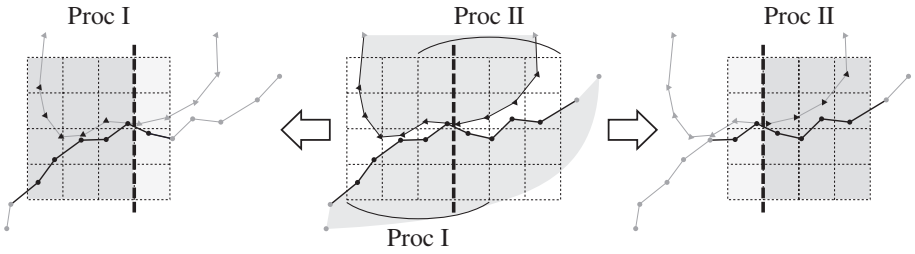

Figure 3.16. *Example of cells partition between two processors: each processor gets one-half of the total number of cells (with slave nodes and master components, represented by triangles and connected circles, respectively) as well as one boundary layer from another half that contain only master segments*

3.5.4. *Scalability test*

The scalability test for the MDMR approach has been performed between two meshes containing more than 66,000 contact nodes each. The results obtained for slightly different surface roughness are represented in Figure 3.17. "Heterogeneous distribution" of active contact zones means that the parts of bounding box associated with different processors possess a significantly different number of potential contact elements. In the considered case, some of the sub-domains may not have contact elements at all. "Homogeneous distribution" means that this number is similar for different parts ($\pm \approx 5\%$). The gain for a given number of processors is defined as the ratio between the reference CPU time for a single processor to the CPU time of the slowest processor. The average gain is calculated as the ratio of the reference CPU time for a single processor to the average CPU time of all processors. The difference between linear gain and the average gain highlights the time devoted to data exchange between sub-domains. The pronounced difference between the gain for heterogeneous and homogeneous active contact zones distributions can be explained by the following observation. If there is no master component in the cell of the slave node and in neighboring cells, the time needed to conclude it is very small. On contrary, if the considered cells are not empty and contain several master components, it takes a much longer time to carry out the closest point detection. Even in these conditions, the gain is quite high and its rate does not decrease with increasing number of detecting processors (for a reasonable ratio of contact nodes to number of processors).

The SDMR and MDMR approaches can be efficiently applied to parallel contact treatment. The second approach requires a larger amount of programming but its performance allows us to neglect the detection time for large and extremely large contact problems.

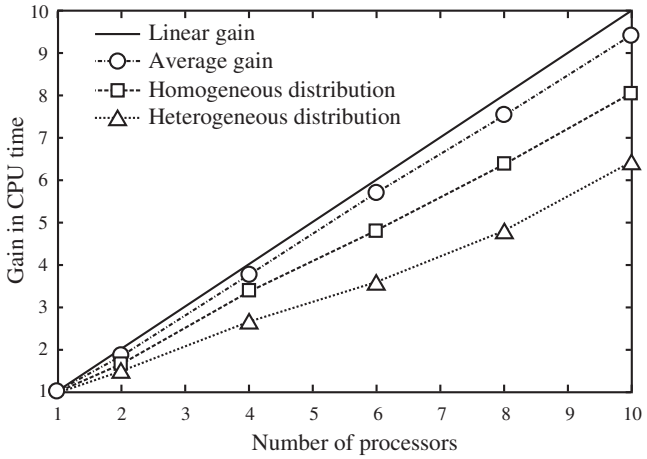

Figure 3.17. *Time gain for the parallel contact detection procedure (average gain depicts the gain averaged by processors' CPU time)*

3.6. Conclusion

A very fast local detection method has been elaborated on the basis of the bucket method and a rigorous definition of the closest point. Sequential and parallel implementations of the method have been discussed in detail for known *a priori* and unknown master–slave discretizations. Many previously proposed detection techniques starting from the historical article of Benson and Hallquist [BEN 90] are based on the closest node detection. Here, we demonstrate that such an approach is not robust. However, the bucket technique can be easily generalized with a rigorous definition of the closest point.

The strong connections between the finite element mesh of the master surface, the MDD and the optimal dimension of the detection cells are established. The analytical estimation and numerous tests demonstrate that the optimal cell size is equal to the MDD multiplied by the square root of 2, and that the MDD can be chosen arbitrary. A reasonable choice for the MDD is the dimension of the biggest master segment if contact geometry changes relatively slowly. A particular attention has been paid to the bounding box construction and to the optimal choice of the neighboring cells to be verified. Techniques based on the closest node strategy and related challenges ("passing by node" and blind spot analysis) have been also discussed. An efficient implementation of the approach on distributed memory parallel computers has been also examined.

The method is very flexible but it is not well adapted for very heterogeneous distributions of the master segment dimensions or for very different mesh densities of

the master and slave surfaces. Contrary to the closest node strategy, the dimension of the biggest master segment is not connected with the MDD but only with cell size. If the master surface has at least one segment whose dimension is 10–100 times larger than the dimension of an average segment, the detection time can be rather high, but always less than in the all-to-all approach.

The validation of the method has been performed on different contact problems in sequential and parallel cases: contact between rough surfaces with different geometries, tire-road contact, self-contact of a snail operculum and on the extremely large contact problem between two rough meshes including more than 1,000,000 segments on the master surface against 1,000,000 slave nodes. For the latter problem, the detection time changes significantly for different geometries from several seconds to 30–40 min in comparison to almost eight days needed for the all-to-all detection technique.

Two parallel strategies for contact detection have been proposed and elaborated: SDMR and MDMR. The last strategy implies the parallelization of the full detection cycle; it can be parallelized in a quite efficient manner, however, for a simple split of the detection zone, the gain depends significantly on the homogeneity of the distribution of the contact elements.

Chapter 4

Formulation of Contact Problems

In this chapter, we give the main notions and derive the governing equations for different classes of contact problems. We start from a simple contact between a deformable solid and a rigid plane, where we formulate frictionless and frictional contact problems. We give an interpretation of contact using partial Dirichlet and Neumann boundary conditions. In the following, we formulate the contact between a deformable solid and an arbitrary rigid smooth surface with and without friction. This section is followed by a general multi-body contact problem, which is formulated using variational equalities for a known contact zone. We obtain weak forms for the general class of contact problems, using penalty, Lagrange multipliers and augmented Lagrangian methods. The advantages and drawbacks of each of them are demonstrated on a simple contact example.

4.1. Contact of a deformable solid with a rigid plane

In this section, we discuss a particular class of contact problems where a deformable solid comes in contact with a rigid solid. These problems may be considered as the simplest in the hierarchy of contact problems. The class of rigid–deformable or unilateral[1] contact includes many important engineering applications. Among them there are indentation testing, metal forming, tire-road interaction, machining and all interaction between solids of significantly different elastic stiffnesses. This class of contact problems sits at the bottom of the complexity hierarchy, because the deformation of only one contacting component is involved and

1 By unilateral contact we understand this as frictionless and frictional contact between a rigid surface and a deformable solid.

all motions, strictly relative in the general case, can be considered as absolute. This consideration simplifies formulation of contact constraints and also accelerates the convergence of numerical schemes. Nevertheless, it requires almost the same set of tools needed to solve general contact problems, because it possesses many mathematical and numerical difficulties associated with them. Here, we formulate a unilateral contact problem in the case of frictionless and frictional contact and discuss numerical methods to solve it. Many notions and methods are directly applicable to contact between deformable solids, and thus will be used in the following chapters. However, if we need to solve a unilateral contact, all needed information is confined to this chapter in the preliminary section where the basic notions were given. We start from the simplest case: contact with a rigid plane. In addition, we extend the formulation to the case of an arbitrary rigid surface. In the following, we employ methods from optimization theory and a method based on dynamically prescribed boundary conditions to solve unilateral contact problems. In conclusion, we present several validation and test problems.

4.1.1. *Unilateral contact with a rigid plane*

We wish to describe the motion of a deformable body coming in contact with a rigid plane (Figure 4.1). Points of the body are identified by vector $\underline{\boldsymbol{X}}$ in the reference configuration Ω^0 and by vector $\underline{\boldsymbol{x}}(\underline{\boldsymbol{X}}, t)$ in the actual configuration Ω at time t. The motion is described relatively to a fixed spatial frame defined by orthonormal basis vectors $\{\underline{\boldsymbol{e}}_x, \underline{\boldsymbol{e}}_y, \underline{\boldsymbol{e}}_z\}$.

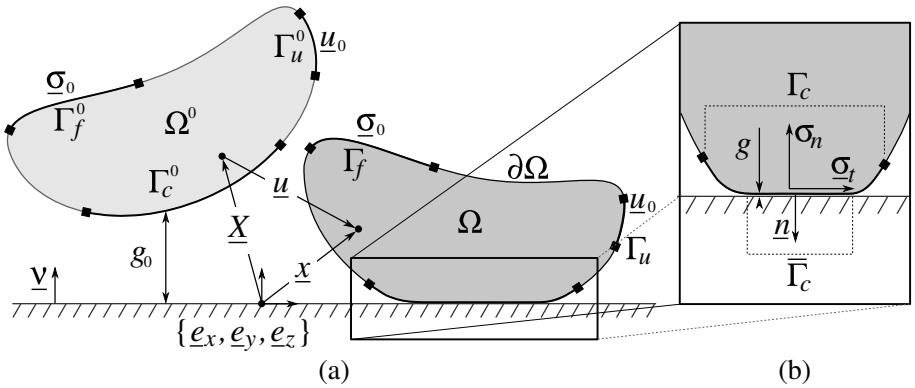

Figure 4.1. *(a) Reference $\underline{\boldsymbol{X}} \in \Omega^0$ and actual $\underline{\boldsymbol{x}} \in \Omega$ configurations of a deformable body in contact with a rigid plane; (b) Zoom on the contact region in actual configuration*

4.1.1.1. *Kinematic constraint*

Let a rigid impenetrable plane be defined by $z = 0$ with unit external normal $\underline{\boldsymbol{\nu}} = \underline{\boldsymbol{e}}_z$; the motion of the body is restricted to the upper half-space $z \geq 0$. Then the following contact constraint on displacements of the body is imposed by:

$$g(\underline{\boldsymbol{x}}) = \underline{\boldsymbol{x}} \cdot \underline{\boldsymbol{\nu}} \geq 0, \qquad [4.1]$$

where $g(\underline{\boldsymbol{x}})$ is a gap between the current point $\underline{\boldsymbol{x}}$ of body's surface and the rigid plane. In other words, points of the body at all time instants cannot appear under the rigid plane. If the displacement of a point is defined as $\underline{\boldsymbol{u}} = \underline{\boldsymbol{x}} - \underline{\boldsymbol{X}}$, then expressing $\underline{\boldsymbol{x}}$ from this equality gives [4.1] in the form:

$$\boxed{g = \underline{\boldsymbol{u}} \cdot \underline{\boldsymbol{\nu}} + g_0 \geq 0}, \qquad [4.2]$$

where $g_0 = \underline{\boldsymbol{X}} \cdot \underline{\boldsymbol{\nu}}$ is an initial gap for point $\underline{\boldsymbol{X}}$. If the body retains its integrity as well as if its deformations are consistent, the non-penetration conditions [4.1] and [4.2] are applied only to surface points $\partial\Omega$, precisely, to the so-called *potential contact zone*[2] denoted Γ_c in the actual configuration. Γ_c can be split into two non-intersecting sets: active $\overline{\Gamma}_c$ (points are in contact) and inactive $\Gamma_c \setminus \overline{\Gamma}_c$ (points are not in contact) contact zones. The active contact zone in the actual configuration is defined by the following equality:

$$\underline{\boldsymbol{x}} \in \overline{\Gamma}_c \text{ if and only if } \underline{\boldsymbol{x}} \cdot \underline{\boldsymbol{\nu}} = 0, \qquad [4.3]$$

and in the reference configuration the contact zone is determined as:

$$\underline{\boldsymbol{X}} \in \overline{\Gamma}_c^{\,0} \text{ if and only if } \underline{\boldsymbol{u}} \cdot \underline{\boldsymbol{\nu}} = -g_0. \qquad [4.4]$$

As follows from the definition, the active contact zone $\overline{\Gamma}_c$ is an unknown *a priori* part of the potential contact zone: $\overline{\Gamma}_c \subset \Gamma_c \subset \partial\Omega$.

2 Definition of the potential contact zone makes sense in numerical treatment, because it reduces the detection and calculation time, at the same time it requires users to know in advance which part of body may come in contact. In most cases, it is not complicated to do.

4.1.1.2. *Static constraint*

In the actual configuration, the stress state is described by the Cauchy stress tensor $\underline{\underline{\boldsymbol{\sigma}}}$ and in the reference configuration by the first Piola–Kirchhoff stress tensor $\underline{\underline{\boldsymbol{P}}}$, which are connected in the following way:

$$\underline{\underline{\boldsymbol{P}}} = J\underline{\underline{\boldsymbol{\sigma}}} \cdot \underline{\underline{\boldsymbol{F}}}^{-\mathrm{T}}, \qquad [4.5]$$

where $\underline{\underline{\boldsymbol{F}}}$ is the non-symmetric deformation gradient tensor:

$$\underline{\underline{\boldsymbol{F}}} = \frac{\partial \underline{\boldsymbol{x}}}{\partial \underline{\boldsymbol{X}}} ,$$

J is the determinant of the deformation gradient (Jacobian), which should be positive in order to prevent self-penetration of points of the body:

$$J = \det \underline{\underline{\boldsymbol{F}}} > 0.$$

As $\det \underline{\underline{\boldsymbol{F}}} > 0$, there exists a finite inverse of the deformation gradient tensor:

$$\underline{\underline{\boldsymbol{F}}}^{-1} = \frac{\partial \underline{\boldsymbol{X}}}{\partial \underline{\boldsymbol{x}}}, \quad \underline{\underline{\boldsymbol{F}}}^{-1} \cdot \underline{\underline{\boldsymbol{F}}} = \underline{\underline{\boldsymbol{I}}} .$$

The Cauchy stress vector on the surface is given by $\underline{\boldsymbol{\sigma}} = \underline{\boldsymbol{n}} \cdot \underline{\underline{\boldsymbol{\sigma}}}$, where $\underline{\boldsymbol{n}}$ is the outward normal on the surface of the body in the actual configuration. In the active contact zone, this normal is opposite to the normal of the rigid plane $\underline{\boldsymbol{n}} = -\underline{\boldsymbol{\nu}}$, so the contact pressure σ_n in the actual configuration can be written as:

$$\sigma_n = \underline{\boldsymbol{\sigma}} \cdot \underline{\boldsymbol{n}} = \underline{\boldsymbol{\nu}} \cdot \underline{\underline{\boldsymbol{\sigma}}} \cdot \underline{\boldsymbol{\nu}}.$$

In the reference configuration, the normal to the surface is $\underline{\boldsymbol{n}}^0$, so the contact pressure can be written in terms of the first Piola–Kirchhoff stress:

$$\sigma_n^0 = \underline{\boldsymbol{P}} \cdot \underline{\boldsymbol{n}}^0 = \underline{\boldsymbol{n}}^0 \cdot \underline{\underline{\boldsymbol{P}}} \cdot \underline{\boldsymbol{n}}^0.$$

Applying the relations between the normal vector $\underline{\boldsymbol{n}} = \underline{\underline{\boldsymbol{F}}}^{-\mathrm{T}} \cdot \underline{\boldsymbol{n}}^0$ or $\underline{\boldsymbol{n}}^0 = \underline{\underline{\boldsymbol{F}}}^{\mathrm{T}} \cdot \underline{\boldsymbol{n}}$ and using equation [4.5] allows us to rewrite the previous equalities as:

$$\sigma_n^0 = J\underline{\boldsymbol{n}} \cdot \underline{\underline{\boldsymbol{F}}} \cdot \underline{\underline{\boldsymbol{\sigma}}} \cdot \underline{\boldsymbol{n}} = J\underline{\boldsymbol{\nu}} \cdot \underline{\underline{\boldsymbol{F}}} \cdot \underline{\underline{\boldsymbol{\sigma}}} \cdot \underline{\boldsymbol{\nu}}.$$

The tangential component of the stress vector is:

$$\underline{\boldsymbol{\sigma}}_t = (\underline{\underline{\boldsymbol{I}}} - \underline{\boldsymbol{n}} \otimes \underline{\boldsymbol{n}}) \cdot \underline{\boldsymbol{\sigma}} = \underline{\boldsymbol{\sigma}} - \sigma_n \underline{\boldsymbol{n}}. \qquad [4.6]$$

To prevent the body from penetrating the plane, a contact pressure arises in the contact zone. If we confine ourself to the description of non-adhesive contact, then the contact pressure should be non-positive (zero in inactive and negative in active contact zones). In the case of frictionless contact we require the tangential component to vanish $\underline{\boldsymbol{\sigma}}_t = 0$, in other words the contact interface does not have any tangential resistance. Finally, for non-adhesive frictionless contact, we require that:

$$\boxed{\sigma_n \leq 0 \text{ at } \Gamma_c} \quad \text{or} \quad \sigma_n^0 \leq 0 \text{ at } {\Gamma_c}^0. \qquad [4.7]$$

However, we have to keep in mind the limitations of this condition. When contact is considered in a gas/liquid environment, this condition is acceptable only if the environmental pressure is negligible compared to arising contact pressures. Another limitation is that this equality is limited to non-adhesive contact.

4.1.1.3. *Hertz–Signorini–Moreau contact conditions*

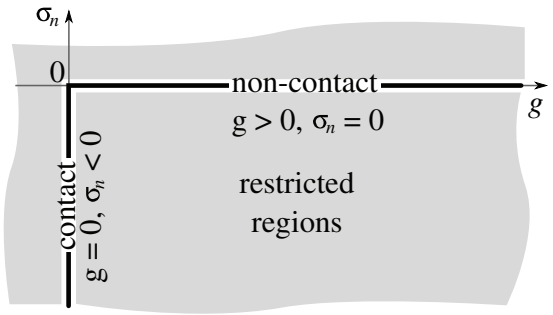

Figure 4.2. *Schematic representation of contact conditions, which depicts regions of permitted and not-permitted combinations of the gap g and the contact pressure σ_n*

In addition to kinematic and static constraints, we state that if a point is in contact, then $\sigma_n \leq 0$ otherwise $\sigma_n = 0$. This leads to the complementary non-penetration–non-adhesion condition:

$$\boxed{g\,\sigma_n = 0}. \qquad [4.8]$$

Conditions [4.1], [4.7] and [4.8] are called Hertz–Signorini–Moreau conditions[3]:

$$\boxed{g \geq 0, \quad \sigma_n \leq 0, \quad \sigma_n g = 0}. \qquad [4.9]$$

Being complemented by a non-frictional condition $\underline{\boldsymbol{\sigma}}_t = 0$ they take the following form:

$$\boxed{g \geq 0, \quad \sigma_n \leq 0, \quad \sigma_n g = 0, \quad \underline{\boldsymbol{\sigma}}_t = 0}. \qquad [4.10]$$

Often these conditions are depicted on a $\{g, \sigma_n\}$ plot as presented in Figure 4.2. However, they should not be interpreted as a function, but just as a visualization of regions that correspond to permitted and not-permitted combinations of the gap and the contact pressure.

These contact conditions together with the related boundary conditions complement the static local balance of momentum and angular momentum ($\underline{\underline{\boldsymbol{\sigma}}} = \underline{\underline{\boldsymbol{\sigma}}}^{\mathsf{T}}$):

$$\boxed{\begin{cases} \nabla \cdot \underline{\underline{\boldsymbol{\sigma}}} + \underline{\boldsymbol{f}}_v = 0 & \text{in } \Omega, \\ \underline{\underline{\boldsymbol{\sigma}}} \cdot \underline{\boldsymbol{n}} = \underline{\boldsymbol{\sigma}}_0 & \text{at } \Gamma_f, \\ \underline{\boldsymbol{u}} = \underline{\boldsymbol{u}}_0 & \text{at } \Gamma_u, \\ g \geq 0, \;\; \sigma_n \leq 0, \quad \sigma_n g = 0, \quad \underline{\boldsymbol{\sigma}}_t = 0 & \text{at } \Gamma_c, \end{cases}} \qquad [4.11]$$

3 These contact conditions are named after three scientists who made a paramount contribution to the mathematical formulation of contact mechanics: *Heinrich Rudolf Hertz* (1857–1894), a German physicist who first formulated and solved the frictionless contact problem between elastic ellipsoidal bodies; *Antonio Signorini* (1888–1963), an Italian mathematical physicist who gave a general and rigorous mathematical formulation of contact constraints, and *Jean Jacques Moreau* (1923), a French mathematician who formulated a non-convex optimization problem based on these conditions and introduced pseudo-potentials in contact mechanics. Often, when the contact problem is considered from the point of view of the optimization theory, these conditions are referred to as Karush–Kuhn–Tucker conditions being in general a first-order condition necessary for a solution in nonlinear programming, they are named after three mathematicians who formulated them: *William Karush* (1917–1997) and *Harold William Kuhn* (1925), both American, and *Albert William Tucker* (1905–1995), a Canadian mathematician.

where $\underline{\boldsymbol{f}}_v$ is a vector of volume forces, $\underline{\boldsymbol{\sigma}}_0$ is a prescribed traction (Neumann boundary conditions) and $\underline{\boldsymbol{u}}_0$ is a prescribed displacement (Dirichlet boundary conditions). That is the starting point for the following investigation. But, first, we will discuss in detail the Hertz–Signorini–Moreau conditions and their interpretation.

4.1.2. *Interpretation of contact conditions*

Idea 4.1. Replacement of contact conditions by Dirichlet-like boundary conditions

Often the contact conditions are interpreted as a special type of Neumann boundary condition (penalty, Lagrange multiplier methods) as a function of displacement, the problem being to find which contact pressure has to be applied in order to fulfill kinematic contact constraint. However, the problem can be inverse: instead of prescribing the pressure at the contact zone, we can impose directly the displacement according to the kinematic constraint, i.e. apply Dirichlet-like boundary conditions depending on the stress-state.

The contact conditions [4.9] can be split into two parts for active $\overline{\Gamma}_c$ and inactive $\Gamma_c \setminus \overline{\Gamma}_c$ contact zones:

$$g \geq 0, \;\; \sigma_n \leq 0, \quad \sigma_n g = 0 \;\; \text{on } \Gamma_c \Leftrightarrow \begin{cases} g = 0, \; \sigma_n < 0 & \text{at } \overline{\Gamma}_c \quad \text{(a)} \\ g > 0, \; \sigma_n = 0 & \text{at } \Gamma_c \setminus \overline{\Gamma}_c. \quad \text{(b)} \end{cases} \qquad [4.12]$$

First, let us interpret conditions [4.12] as a Dirichlet-like boundary condition. According to [4.2] and the definition of the active contact zone [4.4], the first term of [4.12a] can be rewritten as follows:

$$g = 0 \quad \Leftrightarrow \quad \underline{\boldsymbol{\nu}} \cdot \underline{\boldsymbol{u}} = -g^0 \quad \Leftrightarrow \quad \boxed{u_z = -g^0}, \qquad [4.13]$$

the boxed term gathers the partial Dirichlet boundary condition[4]. The condition [4.12b] is equivalent to the free boundary outside the active contact zone, so it is

4 Partial boundary conditions are not very common for boundary value problems in mechanics, and often we require that regions of Neumann and Dirichlet boundary conditions have no intersections. At the same time, this type of boundary conditions is widely employed in numerical treatment, e.g. in a finite element method, to enforce symmetry, mimic test boundary conditions and avoid rigid body motion.

equivalent to a singular Neumann boundary condition $\underline{\boldsymbol{\sigma}} = 0$. Finally, the Hertz–Signorini–Moreau conditions for the case of frictionless contact between a deformable body and a rigid plane can be written as:

$$\begin{cases} \boxed{u_z = -g^0}, \ \underline{\boldsymbol{\sigma}}_t = 0 \ \text{ for } \{ \ \underline{\boldsymbol{x}} \mid \underline{\boldsymbol{x}} \in \Gamma_c \text{ and } \sigma_n(\underline{\boldsymbol{x}}) < 0 \} ; \\ \underline{\boldsymbol{\sigma}} = 0 \ \text{ for } \underline{\boldsymbol{x}} \in \Gamma_c \setminus \overline{\Gamma}_c. \end{cases} \qquad [4.14]$$

The contact conditions have been replaced by the partial Dirichlet boundary conditions (boxed term) on the unknown active contact zone $\overline{\Gamma}_c$, which is determined by negative contact pressure. On the same zone the partial singular Neumann boundary condition $\underline{\boldsymbol{\sigma}}_t = 0$ is prescribed, whereas singular Neumann boundary condition is set on the inactive contact zone. The nonlinearity of the problem consists of determining the active contact zone $\overline{\Gamma}_c$. Note that in numerical treatment the essential component of conditions [4.14] is only the boxed term, the remaining part (singular boundary conditions) is fulfilled automatically.

Note that only one component u_z of the displacement vector $\underline{\boldsymbol{u}}$ is prescribed, and that the other components u_x and u_y are not specified. This is easily interpreted in the finite element method, where the displacement vector in three dimensions (3D) contains three degrees of freedom, each of them can be prescribed independently. Note that the Cartesian, cylindrical or spherical basis in 3D allows us to replace the contact conditions by simple conditions analogous to [4.14] in the case of a rigid plane, cylinder or sphere, respectively. Moreover, the limits of the possible contact zone can be restricted to a specific spatial region of the rigid plane R in the following way:

$$\begin{cases} \boxed{u_z = -g^0}, \ \underline{\boldsymbol{\sigma}}_t = 0 \ \text{ for } \{ \ \underline{\boldsymbol{x}} \mid \underline{\boldsymbol{x}} \in \Gamma_c \cap R(\underline{\boldsymbol{x}}) \text{ and } \sigma_n(\underline{\boldsymbol{x}}) < 0 \} ; \\ \underline{\boldsymbol{\sigma}} = 0 \ \text{ for } \underline{\boldsymbol{x}} \in \Gamma_c \setminus \overline{\Gamma}_c. \end{cases} \qquad [4.15]$$

where $R(\underline{\boldsymbol{x}}) = R(x, y)$ is an arbitrary region or regions fixed in space. Such an interpretation provides us with a rather simple and multipurpose approach for unilateral contact with a flat region. Intuitively, it is easier to prescribe a given displacement than an unknown contact pressure distribution on unknown active contact zones. In the first case, the active contact zone is simply determined by the sign of the contact pressure, and in the second case by a zero value of the normal gap.

Up to now we discussed the cases when the normal to the rigid plane (cylindrical or spherical surface) is parallel to one of the basis vectors in the chosen reference frame. The situation changes drastically for the finite element method, if the latter is not the case. Generalization of the presented approach for an arbitrary rigid surface would lead to the classical Signorini's problem and will be discussed in the following

section. But first, we will give a formulation of frictional conditions for the case of the unilateral contact with a rigid plane.

4.1.3. *Friction*

In real life all contact interfaces are resistant to sliding because of the presence of friction. At the macroscopic scale this resistance reveals itself as follows: a body pressed in contact retains its initial position under a certain tangential load. When the later reaches a critical value the body starts to slide, this sliding or slip is accompanied by energy dissipation. We can distinguish between the frictional resistance and the tangential stress $\underline{\boldsymbol{\sigma}}_t$ that are the same by the absolute value but opposite in direction. Note that hereinafter the developments are done with respect to $\underline{\boldsymbol{\sigma}}_t$.

4.1.3.1. *Tangential stress and frictional resistance*

In general, the tangential stress vector $\underline{\boldsymbol{\sigma}}_t = (\underline{\underline{\boldsymbol{I}}} - \underline{\boldsymbol{n}} \otimes \underline{\boldsymbol{n}}) \cdot \underline{\boldsymbol{\sigma}}$ at the frictional interface can be introduced as a function of many parameters:

$$\underline{\boldsymbol{\sigma}}_t = \underline{\boldsymbol{\sigma}}_t(\sigma_n, \dot{\sigma}_n, \underline{\boldsymbol{v}}_t, d, t, \dots), \qquad [4.16]$$

where $\dot{\sigma}_n$ is the contact pressure rate, $\underline{\boldsymbol{v}}_t$ is the relative sliding velocity[5], d is the slip distance and t is time, dots may stand for history variables, temperature, etc.

For the time being we restrict ourself to the classical non-associated[6] Coulomb's friction law. In this case, the friction law states that the value of the tangential stress depends only on the contact pressure $\underline{\boldsymbol{\sigma}}_t = \sigma_t(\sigma_n)$. So in the case of frictional contact with a rigid plane, a stress vector at the interface contains both normal and tangential components:

$$\underline{\boldsymbol{\sigma}} = \sigma_n \underline{\boldsymbol{n}} + \underline{\boldsymbol{\sigma}}_t(\sigma_n).$$

---

5 This book is limited to the consideration of quasi-static contact problems, so the motion being an inherently dynamic phenomenon is not presented in all developments. Therefore, the motion should be understood as a transition from one equilibrium state to another under changes in boundary conditions and the velocity should be understood as a change in relative position. However, we should not forget that this "motion" is associated with energy dissipation.

6 The term "non-associated" comes from the theory of plasticity and is related, roughly speaking, to a particular projection on the Coulomb's cone. In stress space $\{\sigma_n, \sigma_{t_1}, \sigma_{t_2}\}$ the Coulomb's cone is described by $f = |\underline{\boldsymbol{\sigma}}_t| + \mu\sigma_n = 0$, where μ is a coefficient of friction. This cone determines the surface at which slip is possible, so it can be referred to as a *slip surface*. To find the equilibrium stress state for a given point $\{\sigma_n^*, \sigma_{t_1}^*, \sigma_{t_2}^*\}$, which is situated out of the cone ($f(\sigma_n^*, \sigma_{t_1}^*, \sigma_{t_2}^*) > 0$), we project this point not on the cone but on the circle, i.e. value σ_n^* is retained fixed. That is why this projection and the friction law is called non-associated. A detailed discussion of non-associativity is given in section 4.1.4.

4.1.3.2. *Stick constraint*

At the same time, the relative motion of the point along the rigid plane is confined by the frictional tangential force in the way that the point remains at the initial contact location (its tangential relative velocity vanishes $\underline{\boldsymbol{v}}_t = 0$) if the tangential stress vector is smaller than the critical frictional stress, which in Coulomb's friction law is proportional to the contact pressure with the coefficient of proportionality μ being the coefficient of friction:

$$\boxed{\underline{\boldsymbol{v}}_t = 0 \quad \Leftrightarrow \quad \mu|\sigma_n| - |\underline{\boldsymbol{\sigma}}_t| > 0}. \qquad [4.17]$$

This equation denotes a *stick state*, which is associated with a region where the tangential stress is below its limit value. According to the Newton's third law in equilibrium state, the reaction should be equal in value and opposite in direction to the action, i.e. the stress vector integrated over a small surface of the body $\underline{\boldsymbol{\sigma}} dA$ should be equal by modulus and opposite to the force vector at the rigid plane[7] $d\underline{\boldsymbol{F}}^r$. Up to the limit resistance value $\mu|\sigma_n|$ a motionless equilibrium state is preserved $\underline{\boldsymbol{\sigma}}_t dA + \underline{\boldsymbol{F}}^r = 0, \mu|\sigma_n| - |\underline{\boldsymbol{\sigma}}_t| \geq 0$.

4.1.3.3. *Slip constraint*

In order to preserve the equilibrium in the system under restriction $\mu|\sigma_n| - |\underline{\boldsymbol{\sigma}}_t| \geq 0$, the points of the body enable us to change their relative positions with respect to the rigid surface if, and only if, the following condition is preserved locally $\mu|\sigma_n| - |\underline{\boldsymbol{\sigma}}_t| = 0$. This definition of the *slip state* can be summarized as follows:

$$\boxed{|\underline{\boldsymbol{v}}_t| > 0 \quad \Leftrightarrow \quad \mu|\sigma_n| - |\underline{\boldsymbol{\sigma}}_t| = 0}. \qquad [4.18]$$

It is important to understand that the presence of motion in considering problems is only nominal (see also footnote 5). We consider quasi-static problems in which dynamics is not present, so the motion here should be understood as follows: to reach an equilibrium under modified boundary conditions, some points have to change their relative positions with respect to the rigid surface. However, the change of position under non-zero pressure entails a frictional dissipation of energy that contributes to the balance of energy and virtual work and thus should not be neglected. Note that the dot product of slip velocity and the tangential stress vector should be positive[8]:

$$\underline{\boldsymbol{v}}_t \cdot \underline{\boldsymbol{\sigma}}_t \geq 0. \qquad [4.19]$$

---

7 Note that when talking about equilibrium in unilateral contact, we have to pass from reasoning in stresses to reasoning in forces, as the term *stress* is not appropriate for rigid bodies.

8 The negative work is done by the frictional resistance force that is opposite in direction and thus dissipates the energy.

In the case of Coulomb's friction, the directions of the slip and tangential stress are the same:

$$|\underline{\boldsymbol{v}}_t| > 0\text{: } \frac{\underline{\boldsymbol{v}}_t}{|\underline{\boldsymbol{v}}_t|} = \frac{\underline{\boldsymbol{\sigma}}_t}{|\underline{\boldsymbol{\sigma}}_t|}.$$

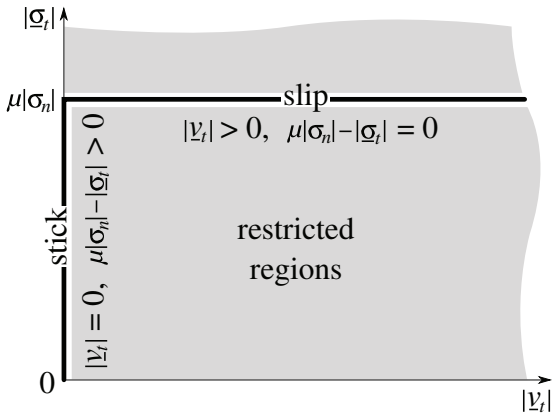

Figure 4.3. *Graphical representation of Coulomb's frictional conditions* [4.20]*: the point corresponding to a given state can be either on the vertical line – stick state* ($\underline{\boldsymbol{v}}_t = 0,\ \mu|\sigma_n| - |\underline{\boldsymbol{\sigma}}_t| > 0$*) or on the horizontal line – slip state* ($|\underline{\boldsymbol{v}}_t| \geq 0,\ \mu|\sigma_n| - |\underline{\boldsymbol{\sigma}}_t| = 0$*); the gray regions correspond to restricted combinations of parameters*

4.1.3.4. *Frictional constraints*

The stick [4.17] and slip [4.18] constraints can be reformulated as Karush–Kuhn–Tucker conditions (see footnote 3) or frictional constraints as follows:

$$\boxed{|\underline{\boldsymbol{v}}_t| \geq 0, \quad \mu|\sigma_n| - |\underline{\boldsymbol{\sigma}}_t| \geq 0, \quad |\underline{\boldsymbol{v}}_t|\,(\,\mu|\sigma_n| - |\underline{\boldsymbol{\sigma}}_t|\,) = 0}, \qquad [4.20]$$

and are classically depicted in $\{|\underline{\boldsymbol{\sigma}}_t|, |\underline{\boldsymbol{v}}_t|\}$ space as in Figure 4.3. Note again that as for Figure 4.2, this figure only indicates permitted and restricted regions for the combination of parameters. Remark also that equation [4.19] does not constitute a part of these conditions, as it comes naturally from the solution of the problem. In 2D problems the sliding velocity and tangential stress are essentially 1D parameters and can be expressed as $\underline{\boldsymbol{v}}_t = v_t\underline{\boldsymbol{t}}$, $\underline{\boldsymbol{\sigma}}_t = \sigma_t\underline{\boldsymbol{t}}$, where $\underline{\boldsymbol{t}}$ is a unit tangential vector orthogonal to normal vector $\underline{\boldsymbol{\nu}}$; in this case, the graphical representation of the frictional conditions (Figure 4.3) can be extended as shown in Figure 4.4.

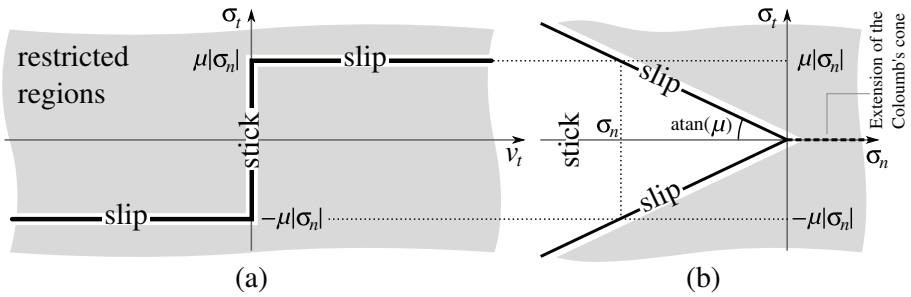

Figure 4.4. *Graphical representation of Coulomb's frictional conditions for 2D contact problem: (a) relation between the relative tangential velocity and the tangential stress, vertical line ($\dot{g}_t = 0,\ |\sigma_t| < \mu|\sigma_n|$) represents stick state, horizontal line ($|\sigma_t| = \mu|\sigma_n|$) – slip state; (b) relation between the contact pressure and the contact tangential stress: the white region ($|\sigma_t| < \mu|\sigma_n|$) and its closure ($|\sigma_t| = \mu|\sigma_n|$) correspond to stick and slip states, respectively; the dashed line depicts an extension of the Coulomb's cone and the gray regions correspond to restricted combinations of parameters*

The graphical representation of frictional conditions in 3D can be found in Figure 4.5. The following notions were introduced:

$$\underline{\boldsymbol{v}}_t = v_{t_1}\underline{\boldsymbol{t}}_1 + v_{t_2}\underline{\boldsymbol{t}}_2, \quad \underline{\boldsymbol{\sigma}}_t = \|\underline{\boldsymbol{\sigma}}_t\|\underline{\boldsymbol{s}} = \sigma_{t_1}\underline{\boldsymbol{t}}_1 + \sigma_{t_2}\underline{\boldsymbol{t}}_2,$$

where $\underline{\boldsymbol{t}}_1$ and $\underline{\boldsymbol{t}}_2$ are orthonormal vectors in the contact plane, which is orthogonal to normal vector $\underline{\boldsymbol{\nu}}$. The cone in axes $\{\sigma_{t_1},\ \sigma_{t_2},\ \sigma_n\}$ in Figure 4.5 is called the Coulomb's cone:

$$C(\sigma_n) = \sqrt{\sigma_{t_1}^2 + \sigma_{t_2}^2} < \mu|\sigma_n|.$$

Any stress state fulfilling frictional conditions corresponds to a unique point either in the interior of the cone:

$\underline{\boldsymbol{\sigma}}_t \in C(\sigma_n)$ stick state;

or on its closure

$\underline{\boldsymbol{\sigma}}_t \in \partial C(\sigma_n)$ slip state.

The zone of positive contact pressure is excluded by the non-adhesion condition (see Hertz–Signorini–Moreau conditions, [4.9]). However, to separate completely normal and frictional constraints, the Coulomb's cone can be extended to the zone of positive contact pressures as represented in Figures 4.4 and 4.5 by a dashed line. Thus the extended frictional conditions take the following form:

$$\boxed{|\underline{\boldsymbol{v}}_t| \geq 0, \quad \mu\langle -\sigma_n\rangle - |\underline{\boldsymbol{\sigma}}_t| \geq 0, \quad |\underline{\boldsymbol{v}}_t|\,(\,\mu\langle -\sigma_n\rangle - |\underline{\boldsymbol{\sigma}}_t|\,) = 0}, \qquad [4.21]$$

where $\langle x\rangle = \max(0, x)$ denotes the Macaulay brackets. Note also that this form of frictional constraints is more compatible with numerical resolution schemes than the first constraint [4.20], as will be shown later.

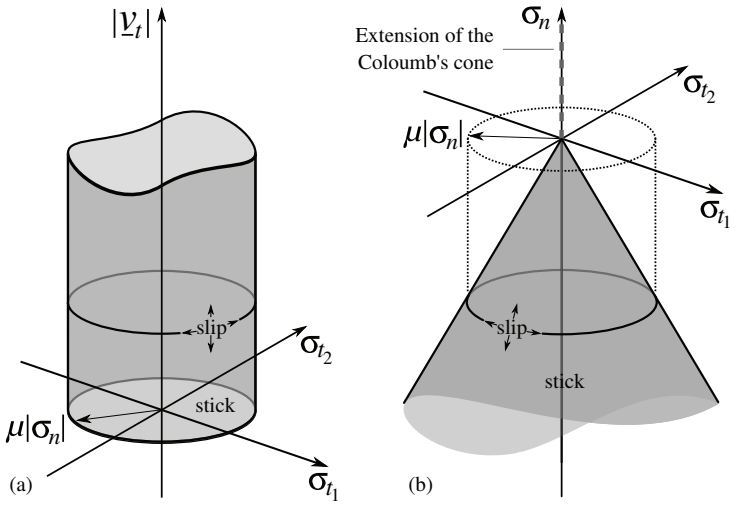

Figure 4.5. *Graphical representation of Coulomb's frictional conditions for 3D contact problem: (a) relation between the absolute value of the tangential velocity and the components of the tangential stress vector: the admissible points are situated either on the in-plane circle, which corresponds to the stick state ($|\underline{\boldsymbol{v}}_t| = 0,\ |\underline{\boldsymbol{\sigma}}_t| < \mu|\sigma_n|$) or on the surface of the semi-infinite cylinder, which corresponds to the slip state ($|\underline{\boldsymbol{v}}_t| \geq 0,\ |\underline{\boldsymbol{\sigma}}_t| = \mu|\sigma_n|$); (b) relation between the contact pressure and the components of the tangential stress vector: interior of the Coulomb's cone (in gray) corresponds to the stick state ($|\underline{\boldsymbol{\sigma}}_t| < \mu|\sigma_n|$), the surface of the cone corresponds to the slip state ($|\underline{\boldsymbol{\sigma}}_t| = \mu|\sigma_n|$), the dashed line is an extension of the Coulomb's cone to positive contact pressures*

4.1.3.5. *Example: slip and stick paths*

Let us consider a point that slides on a rigid plane under a constant contact pressure σ_n. In Figure 4.6 we plot its path in three spaces: stress, velocity and displacement. Along the $[0-1)$ path, the frictional stress remains inside the circle (the section of the Coulomb's cone for a given contact pressure) $\underline{\boldsymbol{\sigma}}_t \in C(\sigma_n)$, so no relative sliding occurs, the point is in the stick state. At position 1, the frictional stress reaches its limit – the boundary of the circle $\underline{\boldsymbol{\sigma}}_t \in \partial C(\sigma_n)$ and stays on it until position 3 is reached. Consequently, the relative sliding velocity follows the path $[1-2-3]$ in the velocity space in such a way that the vector of frictional stress and the tangential velocity are collinear at every moment (see, for example, position 2), this state corresponds to *slip*. The relative displacement $\Delta \underline{\boldsymbol{g}}_t$ is simply the integral of the velocity vector over the sliding time, as seen in Figure 4.6 the point moves from the stick point 1 to another stick position 3 by the curved trajectory $1-2-3$. At position 3, the relative velocity returns to zero, as in the stress space the point dives again inside the circle. Any combination of parameters in the interior of the Coulomb's cone does not lead to a relative tangential displacement and any relative sliding implies that the point is situated at the surface of the Coulomb's cone in stress space. In general, contrary to this example, the normal pressure changes during sliding and consequently the limits of the stick zone in stress space change dynamically. Note that the velocity value has been chosen to be non-trivially curved. It was done to show that the absolute value of the velocity is arbitrary and depends on the internal stress state.

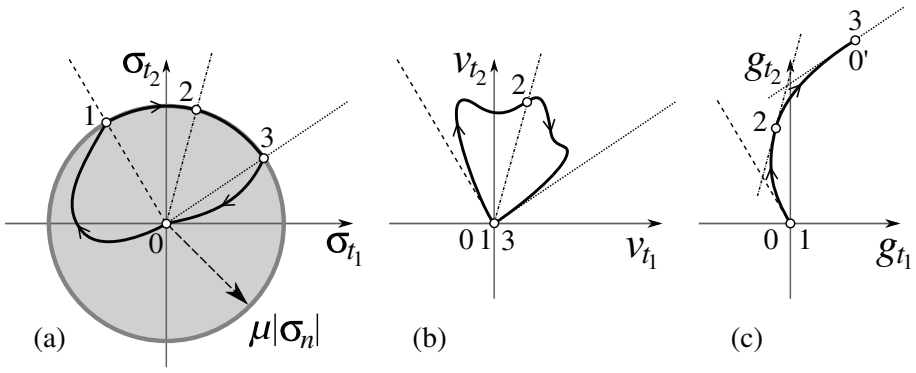

Figure 4.6. *Graphical representation of frictional motion in (a) stress, (b) velocity and (c) displacement spaces: path* $0-1$ *corresponds to stick, path* $1-2-3$ *– to slip and path* $3-0$ *or* $3-0'$ *again to stick*

4.1.4. *An analogy with plastic flow*

The derived formulation of friction is very similar to the formulation of plastic flow [MIC 78, CUR 84]. First, by analogy with the theory of plasticity, we construct a frictional [yield][9] criterion. For Coulomb's friction it takes the form:

$$f(\underline{\boldsymbol{\sigma}}) = |\underline{\boldsymbol{\sigma}}_t| - \mu|\sigma_n| \leq 0 \qquad [4.22]$$

Points that fulfill $f(\underline{\boldsymbol{\sigma}}) = 0$ form a slip [yield] surface. Similar to plasticity, we can formulate the relations between kinematic (slip velocity) and static (stresses) quantities or slip [flow] rules:

$$\underline{\boldsymbol{v}} = \lambda \frac{\partial h(\underline{\boldsymbol{\sigma}})}{\partial \underline{\boldsymbol{\sigma}}} \qquad [4.23a]$$

$$\underline{\boldsymbol{\sigma}} = \frac{\partial d(\underline{\boldsymbol{v}}, \underline{\boldsymbol{\sigma}})}{\partial \underline{\boldsymbol{v}}} \qquad [4.23b]$$

where $h(\underline{\boldsymbol{\sigma}})$ is the slip [plastic] potential, $\lambda > 0$ is an arbitrary positive constant and $d(\underline{\boldsymbol{v}}, \underline{\boldsymbol{\sigma}})$ is a dissipation function. If $h(\underline{\boldsymbol{\sigma}}) = f(\underline{\boldsymbol{\sigma}})$ then we have an associative slip [flow] and the dissipative function takes a simple form $d(\underline{\boldsymbol{v}}, \underline{\boldsymbol{\sigma}}) = \underline{\boldsymbol{v}} \cdot \underline{\boldsymbol{\sigma}}$. However, it is not the case, neither for friction nor for plasticity. It is easy to demonstrate the falsity of the associative slip rule, using [4.23b] with $h(\underline{\boldsymbol{\sigma}}) = f(\underline{\boldsymbol{\sigma}})$ from [4.22], we get:

$$\underline{\boldsymbol{v}} = \lambda \frac{\partial f(\underline{\boldsymbol{\sigma}})}{\partial \underline{\boldsymbol{\sigma}}} = \lambda \left(\frac{\underline{\boldsymbol{\sigma}}_t}{|\underline{\boldsymbol{\sigma}}_t|} - \mu \frac{\sigma_n}{|\sigma_n|} \underline{\boldsymbol{n}} \right),$$

so the velocity vector has a non-zero vertical component, moreover, since in contact $\sigma_n < 0$, $\underline{\boldsymbol{v}} \cdot \underline{\boldsymbol{n}} > 0$ which takes the point out of contact. Thus, to be meaningful, the slip rule should be non-associative. In the case of Coulomb's friction the choice:

$$h(\underline{\boldsymbol{\sigma}}) = |\underline{\boldsymbol{\sigma}}_t|$$

gives a correct slip

$$\underline{\boldsymbol{v}} = \underline{\boldsymbol{v}}_t = \lambda \frac{\underline{\boldsymbol{\sigma}}_t}{|\underline{\boldsymbol{\sigma}}_t|} \quad \text{or} \quad \frac{\underline{\boldsymbol{\sigma}}_t}{|\underline{\boldsymbol{\sigma}}_t|} = \frac{\underline{\boldsymbol{v}}_t}{|\underline{\boldsymbol{v}}_t|}.$$

9 In square brackets, we give associated terms from the theory of plasticity.

It means that any change in stress, such that $f(\underline{\boldsymbol{\sigma}}_t + d\underline{\boldsymbol{\sigma}}_t, \sigma_n) > 0$, results in slip $\underline{\boldsymbol{v}}_t dt$ in the direction of $\underline{\boldsymbol{\sigma}}_t$, but not in the direction of the stress increment $d\underline{\boldsymbol{\sigma}}_t$ (see Figure 4.7, dashed and dash-dotted lines denote directions of $\underline{\boldsymbol{\sigma}}_t$ and $d\underline{\boldsymbol{\sigma}}_t$, respectively). The slip rule is non-associated since there is no irreversible slip in the normal direction (see $\underline{\boldsymbol{v}}_t = \lambda \partial f / \partial \underline{\boldsymbol{\sigma}}$, Figure 4.7(c)). This slip rule is similar to the non-associated Drucker–Prager yield criterion for pressure dependent plastic flow [DE 98]. Also in this reference, authors discuss limit analysis theorem, which was first considered by Drucker [DRU 53] with application to the dry friction, who also gave several obvious cases that show the "misleading similarity" between the frictional slip and stress–strain relationship in elastic-perfectly plastic materials.

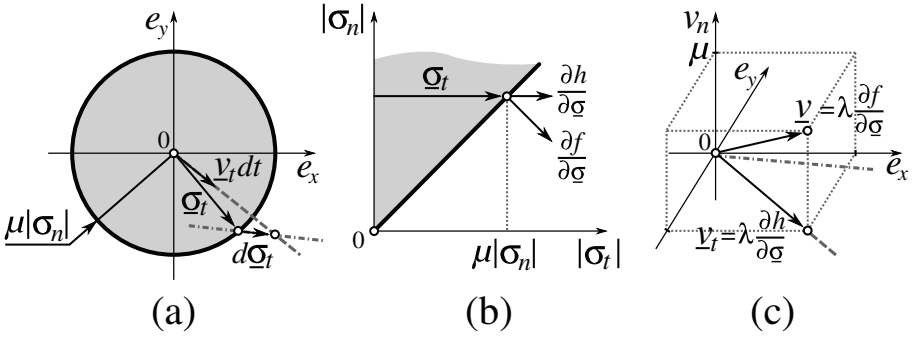

Figure 4.7. *Slip rule in friction: (a) for a point on the slip surface $f(\underline{\boldsymbol{\sigma}}) = 0$, stress increment $\underline{\boldsymbol{\sigma}}_t \to \underline{\boldsymbol{\sigma}}_t + d\underline{\boldsymbol{\sigma}}_t$ results in slip increment $\underline{\boldsymbol{v}}_t dt$ in the direction $\underline{\boldsymbol{\sigma}}_t + d\underline{\boldsymbol{\sigma}}_t$ (dashed line) but not in the direction of the stress increment $d\underline{\boldsymbol{\sigma}}_t$ (dash-dotted line); (b) directions determined by the associated and non-associated slip rules in the stress space and (c) slip direction $\underline{\boldsymbol{v}}_t / |\underline{\boldsymbol{v}}_t|$ according to the associated and non-associated slip rules, remark also dashed and dash-dotted lines corresponding to the directions of the full stress and stress increment, respectively*

4.1.4.1. *Adhesion and slip*

Using the formalism of the non-associated plastic flow and following [CUR 84], we will enhance the friction law. First, we split the relative motion of two solids into a normal and a tangential part:

$$\underline{\boldsymbol{g}} = g_n \underline{\boldsymbol{n}} + \underline{\boldsymbol{g}}_t,$$

next each component is split into adherence [elastic deformation] and slip [plastic deformation] components:

$$\underline{\boldsymbol{g}} = (g_n^a + g_n^s)\, \underline{\boldsymbol{n}} + \left(\underline{\boldsymbol{g}}_t^a + \underline{\boldsymbol{g}}_t^s \right).$$

A physical interpretation of this split is the following. Since all surfaces are rough, under a certain magnification, the contact occurs on a small fraction of the nominal or apparent contact area. The contact is established precisely on the asperities of contacting surfaces (see Figure 4.8(a)). When subjected to a tangential load, the contact interface resists to sliding and asperities deform elastically (Figure 4.8(b)), which result in tangential displacement $g_t^{a_1} > 0$. These deformations are reversible: if the tangential load is removed, the initial position is recovered (Figure 4.8(a)). However, if the external load reaches its critical value $|\underline{\boldsymbol{\sigma}}_t| = \mu|\sigma_n|$, a slip occurs (Figure 4.8(c)) resulting in total slip $g_t = g_t^s + g_t^a$ (see point 3 in Figure 4.8(d)), where g_t^s is the accumulated slip and $g_t^a = \mu|\sigma_n|/E_a$ is a reversible slip due to the elastic deformation of asperities (see point 4 in Figure 4.8(d)), where $E_a[N/m^3]$ is an effective elastic modulus of the interface taking into account the mean separation between rough surfaces (see, [COU 57] for detail). See also section 5.2, which clarifies the numerical technique from computational plasticity that is directly applicable to the numerical treatment of frictional contact with the split of relative movement into adhesive and irreversible parts.

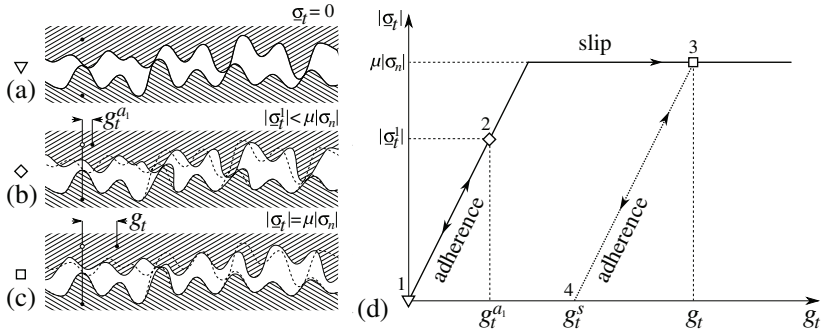

Figure 4.8. *Interpretation of adherence at frictional contact interface: (a) initial stick contact state, $\underline{\boldsymbol{\sigma}}_t = 0$; (b) deformation of contacting asperities below critical load $|\underline{\boldsymbol{\sigma}}_t| < \mu|\sigma_n|$; (c) slip, critical load is reached $|\underline{\boldsymbol{\sigma}}_t| = \mu|\sigma_n|$; and (d) corresponding tangential displacement–stress curve*

4.1.4.2. *Example: rheology of a one-dimensional frictional system*

To compare the effect of deformation that splits into adherence and slip, let us analyze the behavior of a point on a spring (Figure 4.9) subjected to a tangential and normal force f and p, respectively; the coefficient of friction is μ. The rheology of the system is depicted for two cases: Figure 4.10, a pure stick system, for which the relative motion in stick is not permitted and Figure 4.11, for which an adherence slip is possible in stick state. Note first that the initial equilibrium state for $f = 0$ includes a large interval of permitted initial displacements $-p\mu/k \leq u_0 \leq p\mu/k$. Contrary

to most nonlinear systems the initial state does not always depend on the frictional history, but may be a result of bringing a prestressed system into contact. The motion of the system is limited to a region $\mathcal{C}(p, u, f)$ described by (see the gray zones in Figures 4.10 and 4.11):

$$\mathcal{C}(p, u, f)\colon -p\mu/k + f \le u \le p\mu/k + f.$$

Inside the region all points are in stick state, upon the region's closure the points are in slip state, moreover, the direction of slip is given by the relation $\dot{u}/|\dot{u}| = \dot{f}/|\dot{f}|$. The difference between two considering systems is a slip-in-adherence, which if permitted results in a higher force needed to bring a system from stick to slip. It also results in a one-to-one correspondence of force and displacement in the stick region which does not exist for pure stick systems.

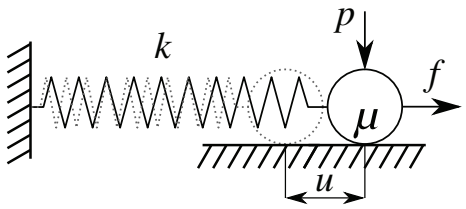

Figure 4.9. *A one-dimensional frictional system under consideration; a block attached to a rigid wall by a spring (stiffness k) and subjected to an external tangential force f and a normal force p, the coefficient of friction is μ*

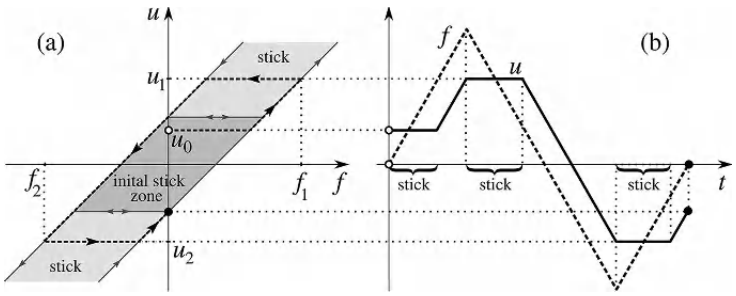

Figure 4.10. *Rheology of a* pure stick *one-dimensional frictional system under varying tangential load: (a) displacement–force space, the dark gray color depicts the zone of initial equilibrium, the gray zone and its closure denote stick and slip, respectively; (b) force and displacement paths of the considering system*

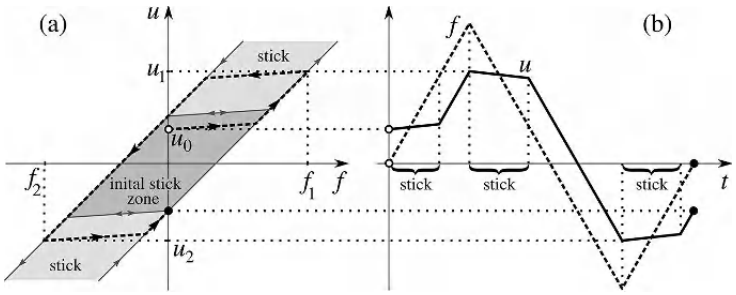

Figure 4.11. *Rheology of a one-dimensional frictional system with a split of displacement into adherence and slip, the system is subjected to a varying tangential load: (a) displacement–force space, the dark gray color depicts the zone of initial equilibrium, the gray zone and its closure denote stick and slip, respectively; (b) force and displacement paths of the considering system*

4.1.5. *Interpretation of frictional conditions*

Idea 4.2. Replacement of frictional contact conditions by Dirichlet–Neumann boundary conditions

In case of unilateral contact with a rigid plane, Hertz–Signorini–Moreau conditions can be replaced by prescribing partial Dirichlet boundary conditions on the unknown a priori active contact zone $\overline{\Gamma}_c$. Similarly, we can interpret frictional constraints. To take the frictional resistance into account, depending on the stress state, we can either complement the Dirichlet-like conditions (contact) to ordinary Dirichlet conditions (stick state) or apply the Dirichlet-like boundary conditions in combination with partial Neumann boundary conditions (frictional slip state).

Let us split the active contact zone $\overline{\Gamma}_c$ into a slip Γ_s and a stick/adherence Γ_a zone (in reference configuration Γ_s^0 and Γ_a^0, respectively), such that $\Gamma_a \cup \Gamma_s = \overline{\Gamma}_c$ and $\Gamma_a \cap \Gamma_s = \emptyset$. Then the frictional conditions can be rewritten as:

$$\begin{cases} g = 0,\ \underline{\boldsymbol{v}}_t = 0,\ \sigma_n < 0,\ |\underline{\boldsymbol{\sigma}}_t| - \mu|\sigma_n| < 0, & \text{in the stick zone } \Gamma_a \quad \text{(a)} \\ g = 0,\ \sigma_n < 0,\ |\underline{\boldsymbol{\sigma}}_t| - \mu|\sigma_n| = 0, & \text{in the slip zone } \Gamma_s \quad \text{(b)} \\ g > 0,\ \sigma_n = 0,\ \underline{\boldsymbol{\sigma}}_t = 0, & \text{in the inactive contact zone } \Gamma_c \setminus \overline{\Gamma}_c. \quad \text{(c)} \end{cases} \qquad [4.24]$$

4.1.5.1. *Interpretation of stick*

Obviously, the first condition [4.24a] for a motionless rigid plane can be replaced by an ordinary Dirichlet boundary condition:

$$\underline{\boldsymbol{u}} = -g_n^0 \underline{\boldsymbol{\nu}} + \underline{\boldsymbol{u}}_t(t^\bullet), \quad \text{if } \underline{\boldsymbol{X}} \in {\Gamma_a}^0, \tag{4.25}$$

where

$$\underline{\boldsymbol{u}}_t(t^\bullet) = \left[\underline{\underline{\boldsymbol{I}}} - \underline{\boldsymbol{\nu}} \otimes \underline{\boldsymbol{\nu}} \right] \cdot (\underline{\boldsymbol{x}}(t^\bullet) - \underline{\boldsymbol{X}}),$$

of which time $t^\bullet$ denotes the moment when the material point switches to stick state either from slip state or from non-contact state, and the term in square brackets is nothing but a projection on the contact plane. The stick state of a point is determined by the stress vector, precisely, the point is supposed to stick if its stress vector is inside the Coulomb's cone:

$$\Gamma_a \colon \underline{\boldsymbol{\sigma}}_t \in C(\sigma_n), \sigma_n < 0.$$

The boundary condition [4.25] is not transparent and it is preferable to prescribe directly the position of the point in the actual configuration, which corresponds to prescribing the boundary conditions in the actual configuration at time $t > t^\bullet$, then equation [4.25] can be rewritten simply as:

$$\underline{\boldsymbol{x}}(t) = \underline{\boldsymbol{x}}(t^\bullet), \text{ if } \underline{\boldsymbol{x}}(t) \in \Gamma_a. \tag{4.26}$$

The interpretation is simple: if a point switches to a stick state it fixes to the position at which this switch has occurred and cannot move before a switch to another state happens.

4.1.5.2. *Interpretation of slip*

The boundary conditions in the slip zone Γ_s [4.24b] correspond to partial Dirichlet boundary conditions for the z component of the displacement (in general, component orthogonal to the rigid surface) and to partial Neumann boundary conditions (external stress vector $\underline{\boldsymbol{\sigma}}_t^e$) in the contact plane $0XY$ (in general, tangential or contact plane), in the actual configuration, which is written as:

$$x_z = 0, \ \underline{\boldsymbol{\sigma}}_t^e = \mu |\sigma_n| \frac{\underline{\boldsymbol{\sigma}}_t}{|\underline{\boldsymbol{\sigma}}_t|}, \quad \text{if } \underline{\boldsymbol{x}}(t) \in \Gamma_s, \tag{4.27}$$

where the slip region is determined according to the stress state on the surface of the Coulomb's cone $\underline{\boldsymbol{\sigma}}_t \in \partial C(\sigma_n)$, *i.e.* $|\underline{\boldsymbol{\sigma}}_t| = \mu|\sigma_n|$.

Without any loss of generality, points are allowed to come into contact only through the stick state and escape from the contact by any state, this can be summarized in the following scheme, where arrows denote switches:

$$\text{non-contact} \quad \rightarrow \quad \text{stick} \quad \rightarrow \quad \begin{bmatrix} \text{non-contact} \\ \text{slip} \quad \rightarrow \quad \begin{bmatrix} \text{non-contact} \\ \text{stick} \end{bmatrix} \end{bmatrix}$$

This assumption allows us to correctly prescribe Neumann boundary conditions for the slip state. Suppose that a material point $\underline{\boldsymbol{X}}$ touches the plane at $\underline{\boldsymbol{x}}(t)$ and changes its state from non-contact to stick. According to equation [4.25], the point fixes to the plane and reaction stresses appear: a contact pressure $\sigma_n < 0$ and a tangential stress $\underline{\boldsymbol{\sigma}}_t$. Two cases are possible: the tangential reaction is either in the Coulomb's cone $\underline{\boldsymbol{\sigma}}_t \in C(\sigma_n) \cup \partial C(\sigma_n)$ or outside of the cone. For the former, the point remains in the stick; for the latter, the point switches to the slip state and a Neumann boundary condition should be applied so that the shear stress vector acts in the direction of the reaction stress vector and its normal is equal to the maximal allowed frictional stress:

$$\underline{\boldsymbol{\sigma}}_t^e = \mu|\sigma_n|\frac{\underline{\boldsymbol{\sigma}}_t}{|\underline{\boldsymbol{\sigma}}_t|}. \qquad [4.28]$$

In this case, the tangential displacement should be set free $\forall\, u_x, u_y$; non-zero slip will occur naturally.

The inactive contact zone $\Gamma_c \setminus \overline{\Gamma}_c$ [4.24c] remains free, only singular Neumann boundary conditions are applied. The source of nonlinearity comes from the presence of unknown stick $\Gamma_a \in \Gamma_c$ and slip $\Gamma_s \in \Gamma_c$ zones ($\Gamma_a \cup \Gamma_s = \overline{\Gamma}_c$). As we assumed that the points always pass through the stick state, this nonlinear problem can be split into two iteratively repeated problems:

– determination of the active contact zone $\overline{\Gamma}_c$;

– determination of the slip zone $\Gamma_s = \overline{\Gamma}_c \setminus \Gamma_a$.

Finally, we get the following set of boundary conditions that replace frictional conditions formulated in [4.20]:

$$\boxed{\begin{cases} \underline{\boldsymbol{x}} = \underline{\boldsymbol{x}}(t^\bullet), & \text{if } \underline{\boldsymbol{x}} \in \Gamma_a \\ x_z = 0,\ \underline{\boldsymbol{\sigma}}_t^e = \mu|\sigma_n|\dfrac{\underline{\boldsymbol{\sigma}}_t}{|\underline{\boldsymbol{\sigma}}_t|}, & \text{if } \underline{\boldsymbol{x}} \in \Gamma_s \end{cases}}. \qquad [4.29]$$

This formulation is simple and its implementation is straightforward in a finite element method, if a dynamical update of the boundary conditions is allowed. As previously discussed, this method is applicable for a rigid surface determined by a constant value of one of the coordinates in the current reference frame:

$$\zeta_i = \text{constant},$$

for example, it can be a sphere in spherical coordinates $r =$ constant, a cylinder in polar coordinates $\rho =$ constant or a plane in Cartesian coordinates $x =$ constant, $y =$ constant or $z =$ constant. Obviously, any region of such surfaces can be chosen. The extension of such an approach for an arbitrary rigid surface will be discussed later.

4.2. Contact of a deformable solid with an arbitrary rigid surface

In this section, we present a theoretical foundation for a contact between a deformable solid and an arbitrary rigid surface, which may be considered as a generalization of the theory discussed in the previous section. The case considered here is often referred to as *unilateral contact* and the problem as frictional or frictionless *Signorini's problem*. The main difference is that now there is no possibility to formulate a unique contact constraint for all points of the solid, as it was done for a rigid plane. The contact constraints become local and their form depends on the actual configuration. A non-self-intersecting, motionless and smooth rigid surface S is described by a vector:

$$\underline{\boldsymbol{r}}(\underset{\sim}{\zeta}) \in S,$$

where $\underset{\sim}{\zeta}$ is a 2D vector of surface coordinates. Each point of the surface has two basis vectors forming s-vectors $\frac{\partial \underline{\boldsymbol{r}}}{\partial \underset{\sim}{\zeta}}$ and $\overline{\frac{\partial \underline{\boldsymbol{r}}}{\partial \underset{\sim}{\zeta}}}$ covariant and contravariant coordinates, respectively:

$$\frac{\partial \underline{\boldsymbol{r}}}{\partial \underset{\sim}{\zeta}} = \underset{\approx}{\mathrm{A}}_{\zeta} \overline{\frac{\partial \underline{\boldsymbol{r}}}{\partial \underset{\sim}{\zeta}}}, \quad \underset{\approx}{\mathrm{A}}_{\zeta} = \frac{\partial \underline{\boldsymbol{r}}}{\partial \underset{\sim}{\zeta}} \cdot \frac{\partial \underline{\boldsymbol{r}}}{\partial \underset{\sim}{\zeta}}^{\mathsf{T}}, \quad \bar{\underset{\approx}{\mathrm{A}}}_{\zeta} = \overline{\frac{\partial \underline{\boldsymbol{r}}}{\partial \underset{\sim}{\zeta}}} \cdot \overline{\frac{\partial \underline{\boldsymbol{r}}}{\partial \underset{\sim}{\zeta}}}^{\mathsf{T}}, \quad \underset{\approx}{\mathrm{A}}_{\zeta}\, \bar{\underset{\approx}{\mathrm{A}}}_{\zeta} = \underset{\approx}{\mathrm{I}},$$

where $\underset{\approx}{\mathrm{A}}_{\zeta}$ is the first fundamental surface tensor (2D), $\bar{\underset{\approx}{\mathrm{A}}}_{\zeta} = \underset{\approx}{\mathrm{A}}_{\zeta}^{-1}$, its inverse, is the first fundamental contravariant surface tensor. For details see Chapter 2. The surface

coordinates are chosen in a way that the external unit normal to the surface is determined by:

$$\underline{\boldsymbol{\nu}} = \frac{\frac{\partial \underline{\boldsymbol{r}}}{\partial \zeta_1} \times \frac{\partial \underline{\boldsymbol{r}}}{\partial \zeta_2}}{\left\| \frac{\partial \underline{\boldsymbol{r}}}{\partial \zeta_1} \times \frac{\partial \underline{\boldsymbol{r}}}{\partial \zeta_2} \right\|}.$$

Initially, the deformable body is situated entirely on the one side of the rigid surface and is not allowed to penetrate on the other side.

The surface of the body $\partial\Omega$ can be described in exactly the same manner. Each point of the surface in the actual configuration is characterized by the vector:

$$\underline{\boldsymbol{\rho}}(t, \underset{\sim}{\xi}) \in \partial\Omega,$$

where $\underset{\sim}{\xi}$ is a 2D vector of surface coordinates. The corresponding pair of covariant basis vectors $\frac{\partial \underline{\boldsymbol{\rho}}}{\partial \underset{\sim}{\xi}}$ is enumerated to get the outward unit normal as:

$$\underline{\boldsymbol{n}} = \frac{\frac{\partial \underline{\boldsymbol{\rho}}}{\partial \xi_1} \times \frac{\partial \underline{\boldsymbol{\rho}}}{\partial \xi_2}}{\left\| \frac{\partial \underline{\boldsymbol{\rho}}}{\partial \xi_1} \times \frac{\partial \underline{\boldsymbol{\rho}}}{\partial \xi_2} \right\|}.$$

The first fundamental covariant surface tensor is $\underset{\approx}{\mathrm{A}}_{\xi} = \frac{\partial \underline{\boldsymbol{\rho}}}{\partial \underset{\sim}{\xi}} \cdot \frac{\partial \underline{\boldsymbol{\rho}}^{\mathsf{T}}}{\partial \underset{\sim}{\xi}}$ and its contravariant form is given by $\underset{\approx}{\bar{\mathrm{A}}}_{\xi} = \underset{\approx}{\mathrm{A}}_{\xi}^{-1}$.

4.2.1. *Non-penetration condition*

The contact between a point $\underline{\boldsymbol{\rho}} \in \Gamma_c \subset \partial\Omega$ and the rigid surface in the point $\underline{\boldsymbol{r}}$ implies two equalities if both surfaces are smooth in the vicinity of the contact point:

$$\begin{cases} \underline{\boldsymbol{\rho}}(t) - \underline{\boldsymbol{r}} = 0 & \text{(a)} \\ \underline{\boldsymbol{n}}(t) + \underline{\boldsymbol{\nu}} = 0. & \text{(b)} \end{cases} \qquad [4.30]$$

If, at least for one of the surfaces, the normal cannot be uniquely determined, then only the first equality holds [4.30a]. For the sake of simplicity here and afterwards, we

will suppose that the contacting surfaces are locally smooth. Then the non-penetration condition can be reformulated in two equivalent forms:

$$\left[\begin{array}{l}(\underline{\boldsymbol{\rho}}(t+\delta t)-\underline{\boldsymbol{\rho}}(t))\cdot\underline{\boldsymbol{n}}(t)\leq 0\\(\underline{\boldsymbol{\rho}}(t+\delta t)-\underline{\boldsymbol{\rho}}(t))\cdot\underline{\boldsymbol{\nu}}\geq 0\end{array}\right. , \qquad [4.31]$$

which imply that in the "near future" ($t+\delta t$, where δt is infinitely small) the point $\underline{\boldsymbol{\rho}}$ either remains on the surface or moves outward it. To get a more compact form, we can divide the inequalities [4.30] by δt, take the limit and get the formulation in velocities:

$$\left[\begin{array}{l}\underline{\dot{\boldsymbol{\rho}}}(t)\cdot\underline{\boldsymbol{n}}(t)\leq 0\\\underline{\dot{\boldsymbol{\rho}}}(t)\cdot\underline{\boldsymbol{\nu}}\geq 0\end{array}\right. . \qquad [4.32]$$

Note that these definitions are valid only for the active contact area.

4.2.1.1. *Gap function*

The inequalities derived above are valid only for the contact state and are local in time. A more consistent description requires a scalar gap function $g(\underline{\boldsymbol{\rho}},S)$ for each point of the deformable surface $\underline{\boldsymbol{\rho}}$. This function is:

– positive, if there is no contact between $\underline{\boldsymbol{\rho}}$ and the surface;

– zero, if the point is in contact;

– negative, if this point penetrates under the surface.

The gap can be defined for points of deformable solid with respect to the rigid surface $g(\underline{\boldsymbol{\rho}}\in\partial\Omega,S)$ or for points of the rigid surface with respect to the deformable surface $g(\underline{\boldsymbol{r}}\in S,\partial\Omega)$. These two descriptions are equivalent but not identical (due to asymmetry of gap definition). The first definition is preferred in terms of convergence of numerical schemes and will be used further in our developments. For non-penetration we require that:

$$g(\underline{\boldsymbol{\rho}},S)\geq 0. \qquad [4.33]$$

In the following, we recall gap functions considered in Chapter 2:

– *normal gap*

$$\boxed{g_n(\underline{\boldsymbol{\rho}},S)=(\underline{\boldsymbol{\rho}}-\underline{\boldsymbol{r}})\cdot\underline{\boldsymbol{\nu}}(\underline{\boldsymbol{r}}),}$$

where $\underline{\boldsymbol{r}} \in S$ is the point on the rigid surface closest to the point $\underline{\boldsymbol{\rho}}$ and $\underline{\boldsymbol{\nu}}$ – the normal at point $\underline{\boldsymbol{r}}$. This definition implies smoothness of the rigid;

– *closest point gap* can be defined as a distance to the closest point with the relevant sign:

$$g_c(\underline{\boldsymbol{\rho}}, S) = \beta \|\underline{\boldsymbol{\rho}} - \underline{\boldsymbol{r}}\|,$$

where $\beta = \pm 1$ determines the sign of the gap; this definition does not require smoothness of the surfaces and is more appropriate for the description of discretized media, however, additional efforts have to be undertaken to determine the sign β.

– *shadow gap* g_s is the signed distance between the point $\underline{\boldsymbol{\rho}}$–and its "shadow projection" on the rigid surface S:

$$\boxed{g_s(\underline{\boldsymbol{\rho}}, S) = (\underline{\boldsymbol{\rho}} - \underline{\boldsymbol{r}}) \cdot \underline{\boldsymbol{e}}(\underline{\boldsymbol{\rho}})},$$

where $\underline{\boldsymbol{e}}$ is a unit vector pointing to the emitter of the light from the given position $\underline{\boldsymbol{\rho}}$.

Note that in general all these gap functions are not identical.

Remark 4.1. On the asymmetry in gap definition

According to [4.30]*, we can rewrite* [4.31] *as:*

$$\left[\begin{array}{l} (\underline{\boldsymbol{\rho}}(t + \delta t) - \underline{\boldsymbol{r}}) \cdot \underline{\boldsymbol{n}}(\underline{\boldsymbol{\rho}}) \leq 0 \\ (\underline{\boldsymbol{\rho}}(t + \delta t) - \underline{\boldsymbol{r}}) \cdot \underline{\boldsymbol{\nu}}(\underline{\boldsymbol{r}}) \geq 0 \end{array} \right. , \qquad [4.34]$$

the second line is equivalent to the definition of the normal gap g_n*. By analogy, we could define the gap according to the first line of* [4.34] *as:*

$$g(\underline{\boldsymbol{\rho}}, S) = (\underline{\boldsymbol{r}} - \underline{\boldsymbol{\rho}}) \cdot \underline{\boldsymbol{n}}(\underline{\boldsymbol{\rho}}),$$

However, this definition is erroneous and may lead to incorrect results. If the gap is defined according to the point $\underline{\boldsymbol{\rho}}$*, then* $\underline{\boldsymbol{r}}$ *is the closest point of the rigid surface to* $\underline{\boldsymbol{\rho}}$*. But as normal* $\underline{\boldsymbol{n}}$ *is defined on the deformable surface, such a definition may give zero or even a negative gap even if there is no contact between* $\underline{\boldsymbol{\rho}}$ *and* $\underline{\boldsymbol{r}}$ *(see Figure 4.12(a))*

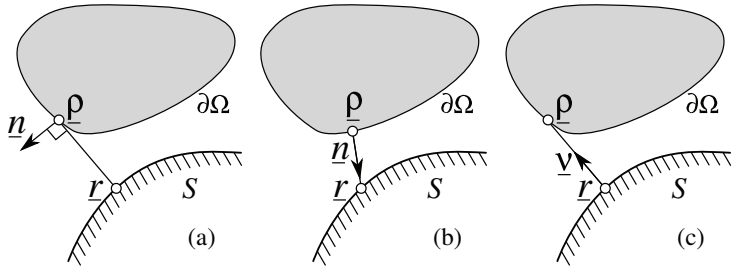

Figure 4.12.

The correct definition for the gap with respect to the surface $\partial\Omega$ has the following form:

$$g(\underline{\boldsymbol{r}}, \partial\Omega) = (\underline{\boldsymbol{r}} - \underline{\boldsymbol{\rho}}) \cdot \underline{\boldsymbol{n}}, \qquad \textit{(Figure 4.12(b))}$$

where $\underline{\boldsymbol{\rho}}$ is the closest point on $\partial\Omega$ to $\underline{\boldsymbol{r}}$. The correct symmetric gap will be given by:

$$g(\underline{\boldsymbol{\rho}}, S) = (\underline{\boldsymbol{\rho}} - \underline{\boldsymbol{r}}) \cdot \underline{\boldsymbol{\nu}}, \qquad \textit{(Figure 4.12(c))}$$

where $\underline{\boldsymbol{r}}$ is the closest point on S to $\underline{\boldsymbol{\rho}}$.

Sometimes it is convenient to introduce a gap vector $\underline{\boldsymbol{g}}(\underline{\boldsymbol{\rho}}, S)$:

– *normal gap vector*

$$\underline{\boldsymbol{g}}_n(\underline{\boldsymbol{\rho}}, S) = \underline{\boldsymbol{\rho}} - \underline{\boldsymbol{r}},$$

where $\underline{\boldsymbol{r}} \in S \in C^1$ is the normal projection of point $\underline{\boldsymbol{\rho}}$ on surface S; $|\underline{\boldsymbol{g}}_n| = |g_n|$;

– *closest point gap vector*

$$\underline{\boldsymbol{g}}_c(\underline{\boldsymbol{\rho}}, S) = \underline{\boldsymbol{\rho}} - \underline{\boldsymbol{r}},$$

where $\underline{\boldsymbol{r}} \in S \in C^0$ is the closest point to the point $\underline{\boldsymbol{\rho}}$; $|\underline{\boldsymbol{g}}_c| = |g_c|$;

– *shadow gap vector*

$$\underline{\boldsymbol{g}}_s(\underline{\boldsymbol{\rho}}, S) = \underline{\boldsymbol{\rho}} - \underline{\boldsymbol{r}},$$

where $\underline{\boldsymbol{r}} = \underline{\boldsymbol{\rho}} - g_s\underline{\boldsymbol{e}}$ is the shadow of the point $\underline{\boldsymbol{\rho}}$ corresponding to the light emitter situated in the direction $\underline{\boldsymbol{e}}$ from the point $\underline{\boldsymbol{\rho}}$; $|\underline{\boldsymbol{g}}_s| = |g_s|$.

Finally, the penetration is restricted by the following inequality formulated for the points of the deformable surface $\underline{\boldsymbol{\rho}} \in \partial\Omega$ respectively to the rigid surface S:

$$\boxed{g(\underline{\boldsymbol{\rho}}, S) \geq 0, \quad \underline{\boldsymbol{\rho}} \in \Gamma_c \subset \partial\Omega}. \qquad [4.35]$$

The set of points for which the gap function is equal to zero is nothing but the active contact zone $\overline{\Gamma}_c$:

$$g(\underline{\boldsymbol{\rho}} \in \overline{\Gamma}_c, S) = 0.$$

4.2.2. *Hertz–Signorini–Moreau's contact conditions*

As discussed previously, due to the restriction on penetration, a reaction stress arises at contacting points $\underline{\boldsymbol{\rho}} \in \overline{\Gamma}_c$. For frictionless contact, the only non-zero term is the normal stress:

$$\begin{aligned} \sigma_n &= \underline{\boldsymbol{n}} \cdot \underline{\underline{\boldsymbol{\sigma}}} \cdot \underline{\boldsymbol{n}}, \\ \underline{\boldsymbol{\sigma}}_t &= \underline{\underline{\boldsymbol{\sigma}}} \cdot \underline{\boldsymbol{n}} - \sigma_n \underline{\boldsymbol{n}} = 0. \end{aligned} \qquad [4.36]$$

If contact holds and surfaces are smooth, according to [4.30b] $\underline{\boldsymbol{n}} = -\underline{\boldsymbol{\nu}}$ and consequently:

$$\boxed{\begin{aligned} \sigma_n &= \underline{\boldsymbol{\nu}} \cdot \underline{\underline{\boldsymbol{\sigma}}} \cdot \underline{\boldsymbol{\nu}} \leq 0, \\ \underline{\boldsymbol{\sigma}}_t &= \underline{\underline{\boldsymbol{\sigma}}} \cdot \underline{\boldsymbol{\nu}} - \sigma_n \underline{\boldsymbol{\nu}} = 0, \end{aligned}} \qquad [4.37]$$

We require a non-positive contact pressure (for non-adhesive contact) and zero tangential stresses for frictionless contact. The complementary condition (switch between non-contact and contact states) holds the same as in the previous section. So the Hertz–Signorini–Moreau contact conditions for frictionless contact become:

$$\boxed{g \geq 0, \quad \sigma_n \leq 0, \quad g\sigma_n = 0, \quad \underline{\boldsymbol{\sigma}}_t = 0}. \qquad [4.38]$$

The boundary value problem retains the same form as in the previous section:

$$\boxed{\begin{cases} \nabla \cdot \underline{\underline{\boldsymbol{\sigma}}} + \underline{\boldsymbol{f}} = 0 \quad \text{in } \Omega \\ \underline{\underline{\boldsymbol{\sigma}}} \cdot \underline{\boldsymbol{\nu}} = \underline{\boldsymbol{\sigma}}_0 \quad \text{at } \Gamma_f \\ \underline{\boldsymbol{u}} = \underline{\boldsymbol{u}}_0 \quad \text{at } \Gamma_u \\ g \geq 0, \;\; \sigma_n \leq 0, \quad \sigma_n g = 0, \;\; \underline{\boldsymbol{\sigma}}_t = 0 \quad \text{at } \Gamma_c \end{cases}} \qquad [4.39]$$

Existence and uniqueness of the solution of this problem has been proven for linear material and small deformations by Kikuchi and Oden [KIK 88]. For further numerical analysis, this problem has to be reformulated in a proper way. It will be done later for the general case of two deformable bodies.

4.2.3. *Interpretation of contact conditions*

Now an attempt to extend the approach considered in the previous section will be undertaken. The ultimate aim is to replace classical contact conditions by boundary conditions imposed on the active contact zone for an arbitrary rigid surface S. To replace the contact conditions by a special type of Dirichlet–Neumann's boundary conditions, we return first to equation [4.31]:

$$\big(\underline{\boldsymbol{\rho}}(t+\delta t) - \underline{\boldsymbol{\rho}}(t)\big) \cdot \underline{\boldsymbol{\nu}} \geq 0,$$

which can be rewritten if we put $\underline{\boldsymbol{\rho}}(t+\delta t) = \underline{\boldsymbol{\rho}}(t) + \delta\underline{\boldsymbol{u}}(t)$

$$\delta\underline{\boldsymbol{u}}(t) \cdot \underline{\boldsymbol{\nu}} \geq 0. \qquad [4.40]$$

The small variation of the displacement $\delta\underline{\boldsymbol{u}}$ may be split in an orthonormal system of coordinates into three vectors:

$$\delta\underline{\boldsymbol{u}} = \delta u_1 \underline{\boldsymbol{e}}_1 + \delta u_2 \underline{\boldsymbol{e}}_2 + \delta u_3 \underline{\boldsymbol{e}}_3.$$

In the active contact zone $\overline{\Gamma}_c$, the inequality [4.40] converts into an equality, which can be rewritten using the previously split form:

$$\delta u_1 \cos(\phi_1) + \delta u_2 \cos(\phi_2) + \delta u_3 \cos(\phi_3) = 0,$$

where $\cos(\phi_i) = \underline{\boldsymbol{e}}_i \cdot \underline{\boldsymbol{\nu}}$. Since the vectors $\underline{\boldsymbol{e}}_i$ are orthonormal, at least one of the three cosine is non-zero. Without any loss of generality let us assume that $\cos(\phi_3) \neq 0$, then we deduce directly:

$$\delta u_3 = -\delta u_1 \frac{\cos(\phi_1)}{\cos(\phi_3)} - \delta u_2 \frac{\cos(\phi_2)}{\cos(\phi_3)}, \qquad [4.41]$$

According to the later equality, one of the three displacement components of the point $\underline{\boldsymbol{\rho}} \in \overline{\Gamma}_c$ depends on two other components.

Another way to link displacement vector components consists of the following: if for $\underline{\boldsymbol{\nu}} \cdot \underline{\boldsymbol{e}}_3 \neq 0$ and in a vicinity of a point $\underline{\boldsymbol{r}}$ the rigid surface can be presented as:

$$\underline{\boldsymbol{r}} \in S : \; r_3 = s(r_1, r_2), \qquad [4.42]$$

where r_i are the coordinates of the point $\underline{\boldsymbol{r}}$ in an orthonormal basis. Then the fact that the point $\underline{\boldsymbol{\rho}} \in \overline{\Gamma}_c$ is in contact implies that:

$$\rho_3 = s(\rho_1, \rho_2) \quad \Leftrightarrow \quad \rho_3(t_0 + \delta t) = s(\rho_1(t_0 + \delta t), \rho_2(t_0 + \delta t)).$$

If we expand the last equality in a Taylor's series, keep the first two terms and subtract $\rho_3(t_0)$ from the left part and $s(\rho_1(t_0), \rho_2(t_0)$ from the right part, then for small δt we get the following relationship between displacement components:

$$\delta u_3 = \frac{\partial s}{\partial \rho_1} \delta u_1 + \frac{\partial s}{\partial \rho_2} \delta u_2, \qquad [4.43]$$

which is equivalent to the relation [4.41]. If the considered rigid surface is flat and orthogonal to the vector $\underline{\boldsymbol{e}}_3$, the following equality holds:

$$s(r_1, r_2) = \text{constant} = r_3,$$

then from [4.43] we directly get the boundary condition that we imposed in the previous section:

$$\delta u_3 = 0.$$

Equations [4.41] and [4.43] are nothing but linearized forms of equation [4.42], which implies that if point $\underline{\boldsymbol{\rho}}$ is in contact, it remains on surface S and its coordinates fulfill the condition:

$$\rho_3 = s(\rho_1, \rho_2) \Leftrightarrow u_3(t_0 + t) = s\left(\rho_1(t_0) + u_1(t_0 + t), \rho_2(t_0) + u_2(t_0 + t)\right) - \rho_3(t_0),$$

$$\boxed{u_3 = s(\rho_1 + u_1, \rho_2 + u_2) - \rho_3, \quad \text{if } \underline{\boldsymbol{\rho}} + \underline{\boldsymbol{u}} \in \overline{\Gamma}_c}. \qquad [4.44]$$

This is the relationship between the components of the displacement for a point being in contact on the surface $S\colon R_3 = s(R_1, R_2)$, where u_i are the displacement components with respect to the configuration at time $t \geq t_0$, where t_0 is the moment when the point comes in contact and ρ_i are the spatial coordinates of this point at time t_0. The active contact zone is determined by a negative contact pressure and a zero tangential stress at point $\underline{\boldsymbol{\rho}}$:

$$\begin{cases} \sigma_n \leq 0 \\ \underline{\boldsymbol{\sigma}}_t = 0 \end{cases}, \quad \text{on } \overline{\Gamma}_c.$$

The second condition is automatically fulfilled if the relations between the components of the displacement are imposed in such a way that the point slides freely along the tangential plane [4.43].

4.2.4. *Frictional conditions and their interpretation*

In the case of a contact with an arbitrary rigid surface, the frictional conditions derived in the previous section hold:

$$|\underline{\boldsymbol{v}}_t| \geq 0, \quad \mu|\sigma_n| - |\underline{\boldsymbol{\sigma}}_t| \geq 0, \quad |\underline{\boldsymbol{v}}_t| \left(\mu|\sigma_n| - |\underline{\boldsymbol{\sigma}}_t|\right) = 0. \qquad [4.45]$$

Contrary to the case of a rigid plane, the local reference frame changes when the point $\underline{\boldsymbol{\rho}}$ slides over the surface S. The stick state implies that the point $\underline{\boldsymbol{\rho}} \in \Gamma_a$ retains its position on the surface and as the surface is assumed to be motionless:

$$\underline{\boldsymbol{\rho}}(t^\bullet + \delta t) = \underline{\boldsymbol{\rho}}(t^\bullet), \quad \underline{\boldsymbol{\rho}} \in \Gamma_a,$$

where $t^\bullet$ is the time when the point switches to the stick state; stick zone Γ_a is determined according to the stress vector $\underline{\boldsymbol{\sigma}}$, which should fulfill stick constraints:

$$\underline{\boldsymbol{\rho}} \in \Gamma_a : \sigma_n < 0, \ |\underline{\boldsymbol{\sigma}}_t| < \mu|\sigma_n|. \qquad [4.46]$$

The stick condition can then be simply replaced by an ordinary Dirichlet boundary condition.

The slip condition requires a slightly deeper analysis. For that, as previously, we suppose that locally $\underline{\boldsymbol{\nu}} \cdot \underline{\boldsymbol{e}}_3 \neq 0$ and that a point coming into contact switches first to the stick state, so that a reaction stress vector $\underline{\boldsymbol{\sigma}}$ arises and if:

$$|\underline{\boldsymbol{\sigma}}_t| \geq \mu |\sigma_n|$$

then this point switches to the slip state. It remains to suppress the corresponding part of Dirichlet's boundary conditions to let the point slip along the rigid surface and to apply an external frictional surface force density in the direction of sliding, as it was described in section 4.1.5. The difficulty with the arbitrarity of the rigid surface consists of the fact that it is hard to split degrees of freedom to impose Dirichlet and Neumann boundary conditions simultaneously. For this purpose, we have to define an independent local basis for each contact point with respect to the rigid surface S, precisely $\{\underline{\boldsymbol{\nu}}, \underline{\boldsymbol{t}}_1, \underline{\boldsymbol{t}}_2\}$, where $\underline{\boldsymbol{\nu}} \cdot \underline{\boldsymbol{t}}_1 = \underline{\boldsymbol{\nu}} \cdot \underline{\boldsymbol{t}}_2 = 0$ and $|\underline{\boldsymbol{\nu}}| = |\underline{\boldsymbol{t}}_1| = |\underline{\boldsymbol{t}}_2| = 1$. With this local construction in hand we can easily impose a consistent local set of boundary conditions combining both Dirichlet (in direction $\underline{\boldsymbol{\nu}}$) and Neumann (in plane $\{\underline{\boldsymbol{t}}_1, \underline{\boldsymbol{t}}_2\}$) boundary conditions, as discussed in section 4.1.5.

4.2.5. *Example: rheology of a one-dimensional frictional system on a sinusoidal rigid substrate*

Let us consider a point attached by springs (stiffness k) to two sliding supports and subjected to external force $\underline{\boldsymbol{f}} = f \underline{\boldsymbol{e}}_x$; the point is in contact with a sinusoidal surface $y = y_0 + A \sin(\omega x + \phi)$; coefficient of friction is μ. Let us first determine the force acting on the point:

$$\underline{\boldsymbol{F}} = (f - kx)\underline{\boldsymbol{e}}_x - [y_0 + A \sin(\omega x + \phi)]\underline{\boldsymbol{e}}_y = F_x \underline{\boldsymbol{e}}_x - F_y \underline{\boldsymbol{e}}_y,$$

then by projecting in the local reference frame the slip condition reads as:

$$|\underline{\boldsymbol{F}} \cdot \underline{\boldsymbol{t}}| = \mu |\underline{\boldsymbol{F}} \cdot \underline{\boldsymbol{n}}|,$$

where $\underline{\boldsymbol{t}}$ and $\underline{\boldsymbol{n}}$ are respectively unit vectors tangential and normal to the surface. If we denote $\underline{\boldsymbol{t}} \cdot \underline{\boldsymbol{e}}_x = \cos(\alpha)$ and $\underline{\boldsymbol{t}} \cdot \underline{\boldsymbol{e}}_y = \sin(\alpha)$, then the slip condition may be rewritten as:

$$| F_x \cos(\alpha) - F_y \sin(\alpha) | \leq \mu | - F_x \sin(\alpha) - F_y \cos(\alpha)|,$$

and by assuming $F_x \cos(\alpha) - F_y \sin(\alpha) > 0$, we obtain:

$$F_x = F_y \frac{\mu + \tan(\alpha)}{1 - \mu \tan(\alpha)},$$

where $\tan(\alpha) = \partial[y_0 + A\sin(\omega x + \phi)]/\partial x = A\omega \cos(\omega x + \phi)$, so two slip curves are given by:

$$f = \begin{cases} kx \pm \dfrac{[y_0 + A\sin(\omega x + \phi)]\,[\mu + A\omega\cos(\omega x + \phi)]}{1 - \mu A\omega \cos(\omega x + \phi)}, & \text{if } y_0 + A\sin(\omega x + \phi) > 0 \\ kx, & \text{else} \end{cases}. \quad [4.47]$$

When in the system $\mu A\omega \to 1$ then the global friction of the system tends to infinity (see the denominator in equation [4.47]), i.e. the slope may become locally too high to split the force f in the local reference frame in a way to overcome the frictional force. To ensure a continuous sliding we have to ensure a one-to-one correspondance between f and x on a slip curve, for this purpose we require a monotonicity of f with respect to x:

$$\frac{\partial f}{\partial x} \geq 0.$$

An interested reader can undertake this effort and derive explicit form for a criticl coefficient of friction for a given set of system parameters. In Figure 4.13(a) several solutions for $A = 0.1, y_0 = 3, k = 1, \phi = 0, \mu = 0.5$ and for $\omega = 1, \approx 1.6$ and 2.5 are depicted. The case of $\omega \approx 1.6$ corresponds to a transition from continuous to discontinuous slip under external load, see Figure 4.13(b). A particular case $\omega = 5.5$, when the stick is possible only in disconnected regions in force–displacement space, is depicted in Figure 4.13(c) and an example of trajectory in force–displacement space is given.

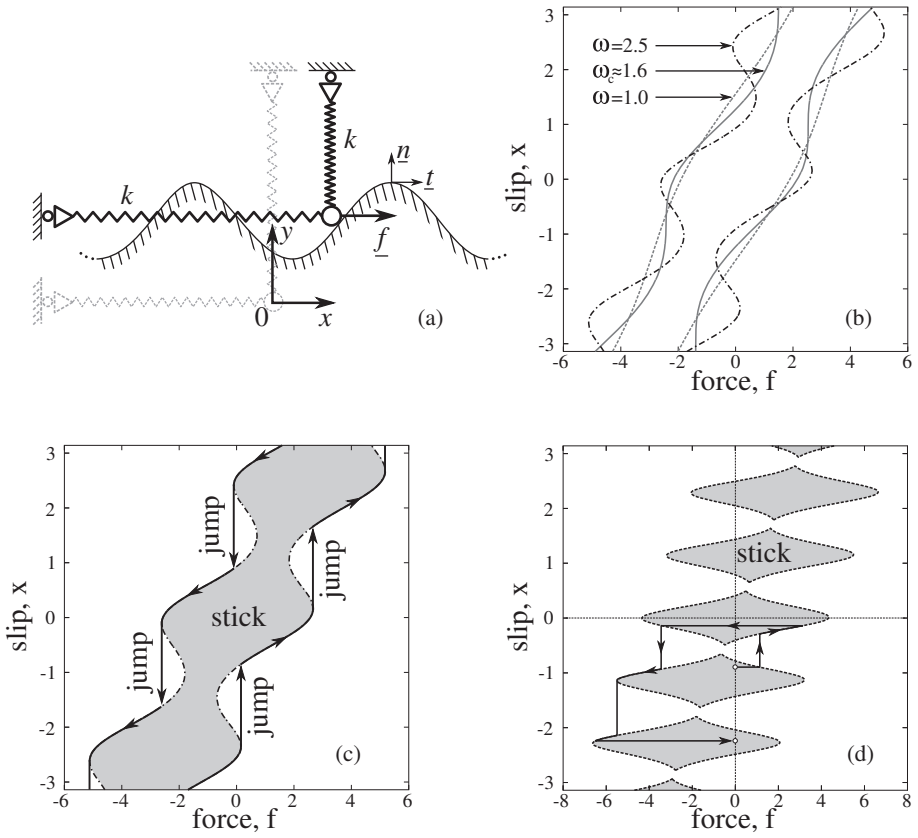

Figure 4.13. *(a) A simple frictional system: a point attached by springs (stiffness k) to two sliding supports is subjected to a force f collinear with $0X$ axis, the point is in contact with a sinusoidal rigid substrate; (b) slip curves of the system for $A = 0.1, y_0 = 3, k = 1$, $\phi = 0, \mu = 0.5$ and $\omega = 1, \approx 1.6$ and 2.5; (c) $\omega = 2.5$, a slip curve and an envelope curve for discontinuous slip of the system; (d) a case of disconnected stick regions and an example of trajectory in force–displacement space*

4.3. Contact between deformable solids

4.3.1. *General formulation and variational inequality*

Up to now we considered a relatively simple case when a deformable body comes in contact with a rigid smooth surface. Here, the formulation will be generalized for the case when the contact interface separates two deformable bodies: it is not important if the contact occurs between parts of one body (contact within a crack,

self-contact) or between several separate bodies; the number of separate contact zones does not change the problem either. So without any loss of generality we confine ourself to the formulation of the problem when contact occurs at a single contact zone between two separate deformable bodies Ω^1 and Ω^2.

As previously shown, the vector $\underline{\boldsymbol{X}} \in \Omega^0$ denotes the position of the material point in the reference configuration and the vector $\underline{\boldsymbol{x}} \in \Omega$ in the actual configuration. To simplify the equations, we introduce the following notations:

– the union of two bodies denotes two open sets $\Omega = \Omega^1 \cup \Omega^2$;

– the union of their closures $\partial\Omega = \partial\Omega^1 \cup \partial\Omega^2$;

– the union of surfaces, where Neumann boundary conditions are applied

$$\partial\Omega \supset \Gamma_f = \Gamma_f^1 \cup \Gamma_f^2;$$

– the union of surfaces, where Dirichlet boundary conditions are applied

$$\partial\Omega \supset \Gamma_u = \Gamma_u^1 \cup \Gamma_u^2;$$

– the potential contact surfaces of two bodies $\Gamma_c^1 \subset \partial\Omega^1$ and $\Gamma_c^2 \subset \partial\Omega^2$.

The static balance of momentum states that for each point $\underline{\boldsymbol{x}} \in \Omega$ at any time the volume is in equilibrium if and only if:

$$\nabla \cdot \underline{\underline{\boldsymbol{\sigma}}} + \underline{\boldsymbol{f}}_v = 0 \quad \text{in } \Omega, \tag{4.48}$$

where $\underline{\underline{\boldsymbol{\sigma}}}$ is the Cauchy stress tensor and $\underline{\boldsymbol{f}}_v$ is the volume force density. If [4.48] is satisfied in each point of the volume Ω then the integral of the dot product of this equation with any arbitrary vector-function $\underline{\boldsymbol{v}}$ (also called test-function or virtual function) over the volume is zero, the converse statement is also true:

$$\nabla \cdot \underline{\underline{\boldsymbol{\sigma}}} + \underline{\boldsymbol{f}}_v = 0 \quad \text{in } \Omega \quad \Leftrightarrow \quad \forall v, \int_\Omega \left[\nabla \cdot \underline{\underline{\boldsymbol{\sigma}}} + \underline{\boldsymbol{f}}_v\right] \cdot \underline{\boldsymbol{v}}\, d\Omega = 0. \tag{4.49}$$

If we require that $\underline{\boldsymbol{v}} \in C^1$, then the first term in the right part of equation [4.49] can be integrated by parts. After using Green's formula, we get:

$$\int_{\partial\Omega} \underline{\boldsymbol{n}} \cdot \underline{\underline{\boldsymbol{\sigma}}} \cdot \underline{\boldsymbol{v}}\, d\Gamma + \int_\Omega \left[\underline{\boldsymbol{f}}_v \cdot \underline{\boldsymbol{v}} - \underline{\underline{\boldsymbol{\sigma}}} \cdot\cdot \nabla \underline{\boldsymbol{v}}\right]\, d\Omega = 0, \tag{4.50}$$

where $\underline{\boldsymbol{n}}$ is an outward unit normal vector at $\partial\Omega$. There is no more terms containing the derivative of the stress tensor. It implies that the requirement on smoothness of the stress vector ($\underline{\underline{\boldsymbol{\sigma}}} \in C^1(\Omega)$) in the differential form [4.48], has now been replaced by a weaker requirement of continuity ($\underline{\underline{\boldsymbol{\sigma}}} \in C^0(\Omega)$). On the other hand, according to [4.50], the test function must be smooth $\underline{\boldsymbol{v}} \in C^1(\Omega)$. Equation [4.50] is called the weak form of the equilibrium equation.

If the abstract test functions $\underline{\boldsymbol{v}} \in C^1(\Omega)$ are replaced by arbitrary test displacements (also called virtual displacements) $\delta\underline{\boldsymbol{u}} = \delta(\underline{\boldsymbol{x}} - \underline{\boldsymbol{X}}) = \delta\underline{\boldsymbol{x}}$, then the weak form [4.50] is nothing but the balance of virtual work:

$$\int_{\partial\Omega} \underline{\boldsymbol{n}} \cdot \underline{\underline{\boldsymbol{\sigma}}} \cdot \delta\underline{\boldsymbol{u}}\, d\Gamma + \int_{\Omega} \left[\underline{\boldsymbol{f}}_v \cdot \delta\underline{\boldsymbol{u}} - \underline{\underline{\boldsymbol{\sigma}}} \cdot\cdot\, \delta\nabla\underline{\boldsymbol{u}} \right] d\Omega = 0. \qquad [4.51]$$

The stress vector $\underline{\boldsymbol{n}} \cdot \underline{\underline{\boldsymbol{\sigma}}}$ entering in the first term in [4.51] is not zero only in the active contact zones ($\overline{\Gamma}_c^1 \in \Gamma_c^1$, $\overline{\Gamma}_c^2 \in \Gamma_c^2$), on the surface where the stress vector is prescribed (Γ_f) and on the surface where the displacement is prescribed (Γ_u). By definition, since displacements are prescribed at Γ_u, $\delta\underline{\boldsymbol{u}} = 0$ at Γ_u, so we get:

$$\int_{\partial\Omega} \underline{\boldsymbol{n}} \cdot \underline{\underline{\boldsymbol{\sigma}}} \cdot \delta\underline{\boldsymbol{u}}\, d\Gamma = \int_{\overline{\Gamma}_c^1} \underline{\boldsymbol{n}} \cdot \underline{\underline{\boldsymbol{\sigma}}} \cdot \delta\underline{\boldsymbol{\rho}}\, d\overline{\Gamma}_c^1 + \int_{\overline{\Gamma}_c^2} \underline{\boldsymbol{\nu}} \cdot \underline{\underline{\boldsymbol{\sigma}}} \cdot \delta\underline{\boldsymbol{r}}\, d\overline{\Gamma}_c^2 + \int_{\Gamma_f} \underline{\boldsymbol{\sigma}}_0 \cdot \delta\underline{\boldsymbol{u}}\, d\Gamma_f, \qquad [4.52]$$

where $\underline{\boldsymbol{\sigma}}_0$ is a prescribed traction (Neumann boundary conditions), $\underline{\boldsymbol{n}}$ is a unit surface normal at $\overline{\Gamma}_c^1$, $\underline{\boldsymbol{\nu}}$ is a unit surface normal at $\overline{\Gamma}_c^2$, $\underline{\boldsymbol{\rho}} = \underline{\boldsymbol{x}}$ at $\overline{\Gamma}_c^1$ and $\underline{\boldsymbol{r}} = \underline{\boldsymbol{x}}$ at $\overline{\Gamma}_c^2$.

In equilibrium state, it follows from Newton's third law that:

$$\underline{\boldsymbol{n}} \cdot \underline{\boldsymbol{\sigma}}\, d\overline{\Gamma}_c^1 = -\underline{\boldsymbol{\nu}} \cdot \underline{\boldsymbol{\sigma}}\, d\overline{\Gamma}_c^1.$$

So the two integrals on the contact surfaces $\overline{\Gamma}_c^1$ and $\overline{\Gamma}_c^2$ can be replaced by one integral over any of the two surfaces, we chose the surface $\overline{\Gamma}_c^1$:

$$\int_{\overline{\Gamma}_c^1} \underline{\boldsymbol{n}} \cdot \underline{\underline{\boldsymbol{\sigma}}} \cdot \delta\underline{\boldsymbol{\rho}}\, d\overline{\Gamma}_c^1 + \int_{\overline{\Gamma}_c^2} \underline{\boldsymbol{\nu}} \cdot \underline{\underline{\boldsymbol{\sigma}}} \cdot \delta\underline{\boldsymbol{r}}\, d\overline{\Gamma}_c^2 = \int_{\overline{\Gamma}_c^1} \underline{\boldsymbol{n}} \cdot \underline{\underline{\boldsymbol{\sigma}}} \cdot \delta(\underline{\boldsymbol{\rho}} - \underline{\boldsymbol{r}})\, d\overline{\Gamma}_c^1, \qquad [4.53]$$

where

$$\underline{\boldsymbol{r}} - \underline{\boldsymbol{\rho}} = \underline{\boldsymbol{g}}(\underline{\boldsymbol{r}}, \overline{\Gamma}_c^1)$$

is a gap vector describing the position of the point $\underline{\boldsymbol{r}}$ relatively to its projection $\underline{\boldsymbol{\rho}}$. So if we want to determine the integrals in [4.53] both in contact and in non-contact states, the vector $\underline{\boldsymbol{\rho}}$ becomes a projection of the slave point $\underline{\boldsymbol{r}}$ on the master surface $\overline{\Gamma}_c^1$, i.e. $\underline{\boldsymbol{\rho}} = \underline{\boldsymbol{\rho}}(t, \underline{\boldsymbol{r}})$. The expression $\delta(\underline{\boldsymbol{r}} - \underline{\boldsymbol{\rho}})$ in the integral implies that the relative motion of the independent point $\underline{\boldsymbol{r}}(t+\delta t)$ is considered relative to the other *independent point* $\underline{\boldsymbol{\rho}}(t+\delta t)$, which *was* the projection of the point $\underline{\boldsymbol{r}}(t)$ in the non-perturbed state at time t.

In case of a shadow projection $\underline{\boldsymbol{g}}_s$ from an infinitely remote emitter (see the previous section and Chapter 2 for details) $\underline{\boldsymbol{r}} = \underline{\boldsymbol{\rho}} + g_s \underline{\boldsymbol{e}}$ and directly:

$$\delta(\underline{\boldsymbol{r}} - \underline{\boldsymbol{\rho}}) = \delta g_s \underline{\boldsymbol{e}} + \frac{\partial \underline{\boldsymbol{\rho}}}{\partial \underset{\sim}{\xi}}^{\mathsf{T}} \delta \underset{\sim}{\xi}, \qquad [4.54]$$

where $\underline{\boldsymbol{e}}$ is a unit vector pointing toward the emitter. In case of a normal gap, $\underline{\boldsymbol{g}}_n$, $\underline{\boldsymbol{r}} = \underline{\boldsymbol{\rho}} + g_n \underline{\boldsymbol{n}}$ and consequently:

$$\delta(\underline{\boldsymbol{r}} - \underline{\boldsymbol{\rho}}) = \delta g_n \underline{\boldsymbol{n}} + g_n \bar{\delta} \underline{\boldsymbol{n}} + \frac{\partial \underline{\boldsymbol{\rho}}}{\partial \underset{\sim}{\xi}}^{\mathsf{T}} \delta \underset{\sim}{\xi}, \qquad [4.55]$$

where $\bar{\delta} \underline{\boldsymbol{n}} = \delta \underline{\boldsymbol{n}} + \frac{\partial \underline{\boldsymbol{n}}}{\partial \underset{\sim}{\xi}}^{\mathsf{T}} \delta \underset{\sim}{\xi}$ is a full variation of the unit normal vector. It is worth noting that $\delta \underset{\sim}{\xi}$ describes a perturbation of the local coordinate of projection of the point $\underline{\boldsymbol{r}}$ on the surface $\overline{\Gamma}_c^1$ and not the displacement of the material point $\underline{\boldsymbol{\rho}}$. The surface stress vector can be split into normal and tangential parts, the latter can be expanded into two components in the contravariant surface basis $\overline{\frac{\partial \underline{\boldsymbol{\rho}}}{\partial \underset{\sim}{\xi}}}$:

$$\underline{\boldsymbol{n}} \cdot \underline{\underline{\boldsymbol{\sigma}}} = \underline{\boldsymbol{n}} \sigma_n + \underline{\boldsymbol{\sigma}}_t = \underline{\boldsymbol{n}} \sigma_n + \underset{\sim}{\sigma}_t^{\mathsf{T}} \overline{\frac{\partial \underline{\boldsymbol{\rho}}}{\partial \underset{\sim}{\xi}}}. \qquad [4.56]$$

Obviously, if the local contravariant basis $\overline{\frac{\partial \underline{\boldsymbol{\rho}}}{\partial \underset{\sim}{\xi}}}$ is not orthonormal, then:

$$\|\underline{\boldsymbol{\sigma}}_t\| \neq \sqrt{\sigma_{t1}^2 + \sigma_{t2}^2},$$

where $\sigma_{ti},\ i = 1, 2$, are components of the v-scalar $\underset{\sim}{\sigma}_t$.

In the contact state, when points $\underline{\boldsymbol{\rho}} = \underline{\boldsymbol{r}}$, the local moment balance is automatically fulfilled, as vectors $\underline{\boldsymbol{\sigma}}_\rho = \underline{\underline{\boldsymbol{\sigma}}} \cdot \underline{\boldsymbol{n}} = -\underline{\underline{\boldsymbol{\sigma}}} \cdot \underline{\boldsymbol{\nu}} = -\underline{\boldsymbol{\sigma}}_r$. When the two points are distant, for a non-zero stress vector, we require that the moment is zero, which is equivalent to the following equality:

$$(\underline{\boldsymbol{r}} - \underline{\boldsymbol{\rho}}) \times \underline{\boldsymbol{\sigma}}_r = 0 \quad \text{or} \quad (\underline{\boldsymbol{\rho}} - \underline{\boldsymbol{r}}) \times \underline{\boldsymbol{\sigma}}_\rho = 0.$$

It requires that when two points are distant, the contact stress vector is collinear with the gap vector:

$$\underline{\boldsymbol{\sigma}} \parallel \underline{\boldsymbol{g}}, \quad \text{if } g \neq 0. \tag{4.57}$$

Substituting [4.54] and [4.56] into the last integral in [4.53] leads to the expression for the contact contribution to the virtual work balance of the system in case of a shadow projection from an infinitely remote emitter:

$$\begin{aligned} \int\limits_{\overline{\Gamma}_c^1} \underline{\boldsymbol{n}} \cdot \underline{\underline{\boldsymbol{\sigma}}} \cdot \delta(\underline{\boldsymbol{\rho}} - \underline{\boldsymbol{r}})\, d\overline{\Gamma}_c^1 &= -\int\limits_{\overline{\Gamma}_c^1} \left(\underline{\boldsymbol{n}}\sigma_n + \underset{\sim}{\sigma}_t^{\mathsf{T}} \frac{\partial \underline{\boldsymbol{\rho}}}{\partial \underline{\underline{\xi}}} \right) \cdot \left(\delta g_s \underline{\boldsymbol{e}} + \frac{\partial \underline{\boldsymbol{\rho}}^{\mathsf{T}}}{\partial \underline{\underline{\xi}}} \underset{\sim}{\delta \xi} \right) d\overline{\Gamma}_c^1 \\ &= \boxed{ -\int\limits_{\overline{\Gamma}_c^1} \left(\sigma_n \delta g_s \underline{\boldsymbol{e}} \cdot \underline{\boldsymbol{n}} + \delta g_s \underset{\sim}{\sigma}_t^{\mathsf{T}} \overline{\frac{\partial \underline{\boldsymbol{\rho}}}{\partial \underline{\underline{\xi}}}} \cdot \underline{\boldsymbol{e}} + \underset{\sim}{\sigma}_t^{\mathsf{T}} \underset{\sim}{\delta \xi} \right) d\overline{\Gamma}_c^1, } \end{aligned} \tag{4.58}$$

where the dot product of contravariant and covariant bases gives the unity tensor (t-scalar) $\overline{\frac{\partial \underline{\boldsymbol{\rho}}}{\partial \underline{\underline{\xi}}}} \cdot \frac{\partial \underline{\boldsymbol{\rho}}^{\mathsf{T}}}{\partial \underline{\underline{\xi}}} = \underset{\approx}{\mathrm{I}}$ and is omitted in the last term. This expression will not be investigated further in this book and suggests further direction of development.

To derive a similar contribution to the virtual work balance in case of the normal projection $g = g_n$, let us first consider the dot product of [4.55] with [4.56]:

$$\begin{aligned} &\left(\underline{\boldsymbol{n}}\sigma_n + \underset{\sim}{\sigma}_t^{\mathsf{T}} \overline{\frac{\partial \underline{\boldsymbol{\rho}}}{\partial \underline{\underline{\xi}}}} \right) \cdot \left(\delta g_n \underline{\boldsymbol{n}} + g_n \delta \underline{\boldsymbol{n}} + \frac{\partial \underline{\boldsymbol{\rho}}^{\mathsf{T}}}{\partial \underline{\underline{\xi}}} \underset{\sim}{\delta \xi} \right) \\ &= \sigma_n \delta g_n + \sigma_n \underbrace{\left[\underline{\boldsymbol{n}} \cdot \frac{\partial \underline{\boldsymbol{\rho}}^{\mathsf{T}}}{\partial \underline{\underline{\xi}}} \right]}_{=0} \underset{\sim}{\delta \xi} + \underset{\sim}{\sigma}_t^{\mathsf{T}} \underbrace{\left[\overline{\frac{\partial \underline{\boldsymbol{\rho}}}{\partial \underline{\underline{\xi}}}} \cdot \underline{\boldsymbol{n}} \right]}_{=0} \delta g_n + \underset{\sim}{\sigma}_t^{\mathsf{T}} \underbrace{\left[\overline{\frac{\partial \underline{\boldsymbol{\rho}}}{\partial \underline{\underline{\xi}}}} \cdot \frac{\partial \underline{\boldsymbol{\rho}}^{\mathsf{T}}}{\partial \underline{\underline{\xi}}} \right]}_{=\underset{\approx}{\mathrm{I}}} \underset{\sim}{\delta \xi} \\ &+ g_n \underbrace{\left(\underline{\boldsymbol{n}}\sigma_n + \underset{\sim}{\sigma}_t^{\mathsf{T}} \overline{\frac{\partial \underline{\boldsymbol{\rho}}}{\partial \underline{\underline{\xi}}}} \right) \cdot \bar{\delta} \underline{\boldsymbol{n}}}_{= g_n \underline{\boldsymbol{\sigma}} \cdot \bar{\delta} \underline{\boldsymbol{n}} = 0, \text{ since } \underline{\boldsymbol{\sigma}} \parallel \underline{\boldsymbol{n}}, \quad \text{if } g_n \neq 0, \text{ see [4.57]}} = \sigma_n \delta g_n + \underset{\sim}{\sigma}_t^{\mathsf{T}} \underset{\sim}{\delta \xi}. \end{aligned} \tag{4.59}$$

Substituting this expression into the last integral in [4.53] gives the expression for the contact contribution to the virtual work in case of the normal projection $g = g_n$:

$$\int\limits_{\overline{\Gamma}_c^1} \underline{\boldsymbol{n}} \cdot \underline{\underline{\boldsymbol{\sigma}}} \cdot \delta(\underline{\boldsymbol{\rho}} - \underline{\boldsymbol{r}})\, d\overline{\Gamma}_c^1 = \boxed{- \int\limits_{\overline{\Gamma}_c^1} \left(\sigma_n \delta g_n + \underset{\sim}{\sigma}_t^{\intercal} \delta \underset{\sim}{\xi} \right)\, d\overline{\Gamma}_c^1.} \qquad [4.60]$$

Finally, the balance of virtual work [4.51] including contact contributions (in the case of the normal projection) and Neumann boundary conditions from [4.52] is:

$$\int\limits_{\Omega} \underline{\underline{\boldsymbol{\sigma}}} \cdot\cdot\, \delta \nabla \underline{\boldsymbol{u}}\, d\Omega + \int\limits_{\overline{\Gamma}_c^1} \left(\sigma_n \delta g_n + \underset{\sim}{\sigma}_t^{\intercal} \delta \underset{\sim}{\xi} \right)\, d\overline{\Gamma}_c^1 = \int\limits_{\Gamma_f} \underline{\boldsymbol{\sigma}}_0 \cdot \delta \underline{\boldsymbol{u}}\, d\Gamma + \int\limits_{\Omega} \underline{\boldsymbol{f}}_v \cdot \delta \underline{\boldsymbol{u}}\, d\Omega. \qquad [4.61]$$

It can be shown that in *actual configuration* the second term, which presents the contribution of the normal contact, is negative. If the condition of non-penetration holds, then point $\underline{\boldsymbol{r}}$ either stays at the surface (sticks or slides over the tangential plane $\delta g_n = 0$) or moves out of the surface, which leads to inequality:

$$\delta g_n = \delta \underline{\boldsymbol{g}}_n \cdot \underline{\boldsymbol{n}} \geq 0.$$

Since the contact pressure is non-positive $\sigma_n \leq 0$ we have $\delta g_n \sigma_n \leq 0$, which becomes in integral form:

$$\int\limits_{\overline{\Gamma}_c^1} \sigma_n \delta g_n\, d\overline{\Gamma}_c^1 \leq 0. \qquad [4.62]$$

Frictional sliding is associated with energy dissipation, i.e. the dot product between force and displacement vectors is negative, so naturally a point slides in the direction opposite to the imposed frictional force. More generally, the angle between the frictional force and the sliding directions is larger than $90°$, i.e:

$$(\underline{\underline{\boldsymbol{I}}} - \underline{\boldsymbol{\nu}} \otimes \underline{\boldsymbol{\nu}}) \cdot \underline{\underline{\boldsymbol{\sigma}}} \cdot \delta \underline{\boldsymbol{g}}_t \leq 0.$$

It follows that the expression in the frictional part of the integral is positive since:

$$\underline{\boldsymbol{\sigma}}_{\tau} = (\underline{\underline{\boldsymbol{I}}} - \underline{\boldsymbol{\nu}} \otimes \underline{\boldsymbol{\nu}}) \cdot \underline{\underline{\boldsymbol{\sigma}}} = -(\underline{\underline{\boldsymbol{I}}} - \underline{\boldsymbol{n}} \otimes \underline{\boldsymbol{n}}) \cdot \underline{\underline{\boldsymbol{\sigma}}} = -\underline{\boldsymbol{\sigma}}_t,$$

i.e.

$$\underset{\sim}{\sigma}_t^{\intercal}\delta\underset{\sim}{\xi} \geq 0.$$

The integral form of this statement is given as:

$$\int_{\overline{\Gamma}_c^1} \underset{\sim}{\sigma}_t^{\intercal}\delta\underset{\sim}{\xi}\, d\overline{\Gamma}_c^1 \geq 0. \qquad [4.63]$$

The virtual work of frictional forces has the same sign as the virtual work of internal forces and it is not conservative, so all this energy dissipates, and cannot be recovered. Since the direction of sliding and penetration and its relations with gap vector are relative, it is important to distinguish master and slave surfaces. Either the stress on the master has to be compared to the gap with respect to the master $g(\underline{\boldsymbol{r}}, \Gamma_c^1)$ (as in the considered case) or stress on the slave has to be compared to the gap with respect to the slave, $g(\underline{\boldsymbol{\rho}}, \Gamma_c^2)$.

According to [4.62], the balance of virtual work [4.61] can be rewritten as a *variational inequality*. The variational inequality has to be complemented by the restrictions on the possible virtual displacement arising from Dirichlet's boundary conditions and non-penetration conditions. Classically, the variational inequality for frictional problem is written following Duvaut and Lions [DUV 71] and Kikuchi and Oden [KIK 88], where the proof of the equivalence between the variational inequalities and the classical formulation can be found. Here we provide a generalized formulation, which does not limit the choice of the frictional law:

$$\boxed{\begin{array}{c} \int_\Omega \underline{\underline{\boldsymbol{\sigma}}} \cdot\cdot\, \delta\nabla\underline{\boldsymbol{u}}\, d\Omega + \int_{\overline{\Gamma}_c^1} \underset{\sim}{\sigma}_t^{\intercal}\delta\underset{\sim}{\xi}\, d\overline{\Gamma}_c^1 \geq \int_{\Gamma_f} \underline{\boldsymbol{\sigma}}_0 \cdot \delta\underline{\boldsymbol{u}}\, d\Gamma + \int_\Omega \underline{\boldsymbol{f}}_v \cdot \delta\underline{\boldsymbol{u}}\, d\Omega, \\ \mathbb{V} = \left\{ \delta\underline{\boldsymbol{u}} \in \mathbb{H}^1(\Omega) \mid \delta\underline{\boldsymbol{u}} = 0 \ \text{ on } \Gamma_u \right\}, \\ \mathbb{K} = \left\{ \delta\underline{\boldsymbol{u}} \in \mathbb{V} \;\middle|\; (\underline{\boldsymbol{r}} + \delta\underline{\boldsymbol{r}} - \underline{\boldsymbol{\rho}} - \delta\underline{\boldsymbol{\rho}}) \cdot \underline{\boldsymbol{n}} \geq -g_{n0} \text{ on } \Gamma_c \right\} \end{array}}. \qquad [4.64]$$

In the case of frictionless contact, the formulation is significantly simpler and is written as:

$$\boxed{\begin{array}{c} \int_\Omega \underline{\underline{\boldsymbol{\sigma}}} \cdot\cdot\, \delta\nabla\underline{\boldsymbol{u}}\, d\Omega \geq \int_{\Gamma_f} \underline{\boldsymbol{\sigma}}_0 \cdot \delta\underline{\boldsymbol{u}}\, d\Gamma + \int_\Omega \underline{\boldsymbol{f}}_v \cdot \delta\underline{\boldsymbol{u}}\, d\Omega, \\ \mathbb{V} = \left\{ \delta\underline{\boldsymbol{u}} \in \mathbb{H}^1(\Omega) \mid \delta\underline{\boldsymbol{u}} = 0 \ \text{ on } \Gamma_u \right\}, \\ \mathbb{K} = \left\{ \delta\underline{\boldsymbol{u}} \in \mathbb{V} \;\middle|\; (\underline{\boldsymbol{r}} + \delta\underline{\boldsymbol{r}} - \underline{\boldsymbol{\rho}} - \delta\underline{\boldsymbol{\rho}}) \cdot \underline{\boldsymbol{n}} \geq -g_{n0} \text{ on } \Gamma_c \right\}, \end{array}}. \qquad [4.65]$$

where $\mathbb{H}^1(\Omega)$ denotes a Hilbert space of the first order, $\delta\underline{\boldsymbol{r}} = \delta\underline{\boldsymbol{u}}$ on $\overline{\Gamma}_c^2$, $\delta\underline{\boldsymbol{\rho}} = \delta\underline{\boldsymbol{u}}$ on $\overline{\Gamma}_c^1$ – contacting material points in actual configuration, $g_{n0} = (\underline{\boldsymbol{X}}_\rho + \underline{\boldsymbol{X}}_r) \cdot \underline{\boldsymbol{n}}$ – initial gap. These variational inequality formulations [4.64] and [4.65] are valid for any material, because the constitutive law does not enter in to equations. However, the presence of the inequality sign differs these expressions from the classical weak form and requires new optimization methods for its numerical treatment. No details are given here, the interested reader is referred to monographs [DUV 76] and [KIK 88], which are dedicated to this approach.

4.3.2. *Remarks on Coulomb's frictional law*

For a detailed analysis of inequalities arising from the formulation of frictional and frictionless cases, the reader is referred to books by Duvaut and Lions [DUV 76] and Kikuchi and Oden [KIK 88], where:

– the equivalence between the variational inequality and the classical formulation of Signorini's problem with Coulomb's friction (following Duvaut and Lions [DUV 71] and [DUV 76]) is determined;

– the existence and uniqueness of the solution is proved for small deformation frictionless contact [KIK 88];

– the finite element problem with unilateral contact with and without friction for small/large deformations, incompressible and elastoplastic materials is treated [KIK 88];

– the questions of convergence of the finite element method are discussed [KIK 88];

– many other developments concerning contact with a rigid foundation are elaborated in the rigorous mathematical framework developed by authors [KIK 88].

Following these works, let us make some remarks considering the frictional problem.

As we can see, no friction law appears in the derived variational inequality for frictional contact [4.64]. If Coulomb's law is assumed:

$$\|\underline{\boldsymbol{\sigma}}_t\| \leq \mu\langle-\sigma_n\rangle, \quad \|\dot{\underline{\boldsymbol{g}}}_t\|\underline{\boldsymbol{\sigma}}_t - \mu\langle-\sigma_n\rangle\dot{\underline{\boldsymbol{g}}}_t = 0, \quad \|\underline{\boldsymbol{s}}\| \,\big\|\, \|\dot{\underline{\boldsymbol{g}}}_t\|\underline{\boldsymbol{\sigma}}_t - \mu\langle-\sigma_n\rangle\dot{\underline{\boldsymbol{g}}}_t \,\big\| = 0,$$

where $\dot{\underline{\boldsymbol{g}}}_t = \frac{\partial \underline{\boldsymbol{\rho}}^{\mathsf{T}}}{\partial \underset{\sim}{\xi}} \dot{\underset{\sim}{\xi}}$ is the relative tangential sliding velocity of the point $\underline{\boldsymbol{r}}$ over $\underline{\boldsymbol{\rho}}$ for $g = 0$. Then, following [DUV 71], the integral related to the contribution of the

frictional forces can be rewritten as:

$$\int_{\overline{\Gamma}_c^1} \underset{\sim}{\sigma}_t^{\intercal}\, \delta\underset{\sim}{\xi}\, d\overline{\Gamma}_c^1 = \int_{\overline{\Gamma}_c^1} \|\underline{\boldsymbol{\sigma}}_t\|\, \|\delta\underline{\boldsymbol{g}}_t\|\, d\overline{\Gamma}_c^1 = \int_{\overline{\Gamma}_c^1} \mu\langle -\sigma_n\rangle\, \|\delta\underline{\boldsymbol{g}}_t\|\, d\overline{\Gamma}_c^1, \qquad [4.66]$$

and the variational inequality for the frictional problem [4.64] becomes:

$$\begin{aligned} \int_\Omega \underline{\underline{\boldsymbol{\sigma}}} \cdot\cdot\, \delta\nabla\underline{\boldsymbol{u}}\, d\Omega + \int_{\overline{\Gamma}_c^1} \mu\langle -\sigma_n\rangle\, \|\delta\underline{\boldsymbol{g}}_t\|\, d\overline{\Gamma}_c^1 &\geq \int_{\Gamma_f} \underline{\boldsymbol{\sigma}}_0 \cdot \delta\underline{\boldsymbol{u}}\, d\Gamma + \int_\Omega \underline{\boldsymbol{f}}_v \cdot \delta\underline{\boldsymbol{u}}\, d\Omega, \\ \mathbb{V} &= \left\{ \delta\underline{\boldsymbol{u}} \in \mathbb{H}^1(\Omega) \;\middle|\; \delta\underline{\boldsymbol{u}} = 0 \;\text{ on } \Gamma_u \right\}, \\ \mathbb{K} &= \left\{ \delta\underline{\boldsymbol{u}} \in \mathbb{V} \;\middle|\; (\underline{\boldsymbol{r}} + \delta\underline{\boldsymbol{r}} - \underline{\boldsymbol{\rho}} - \delta\underline{\boldsymbol{\rho}}) \cdot \underline{\boldsymbol{n}} \geq -g_{n0} \text{ on } \Gamma_c \right\}. \end{aligned} \qquad [4.67]$$

However, the integral [4.66] entering in the variational inequality [4.67] has no meaning, because $\sigma_n = \sigma_n(\underline{\boldsymbol{u}})$ is a contact pressure depending on the solution $\underline{\boldsymbol{u}}$ of the problem with friction. Furthermore, the term [4.66] is non-convex and non-differentiable, consequently the questions of existence and uniqueness of the solution for the problem [4.67] remain open.

> *"...the absence of a complete existence theory for the general problem together with physical evidence of friction have led some investigators to question the validity of the Coulomb friction law."*
>
> N. Kikuchi and J.T. Oden [KIK 88]

To derive some results for the frictional problem, several possible "simplifications" have been proposed: we can either assume *a priori* the known contact pressure or tangential stress or replace Coulomb friction by a regularized law. For the case of a prescribed contact pressure, the existence and uniqueness of the solution is proven under reasonable conditions [DUV 76]. So for the numerical purpose, the iterative procedure can be established using two special cases of known contact pressure and known tangential stress repeated alternately (see [CAM 82]). However, the frictional term remains non-differentiable that presents a problem for the exact numerical treatment of frictional contact. The regularization of the contact term leads to a convex and Gâteaux differentiable integral for which the existence and uniqueness of the solution can be proved. The regularization consists of replacing the absolute value of the virtual displacement in integral [4.66] by a smooth term containing ε:

$$\int_{\overline{\Gamma}_c^1} \mu\langle -\sigma_n\rangle\, \|\delta\underline{\boldsymbol{g}}_t\|\, d\overline{\Gamma}_c^1 \longrightarrow \int_{\overline{\Gamma}_c^1} \mu\langle -\sigma_n\rangle\, R(\delta\underline{\boldsymbol{g}}_t, \varepsilon)\, d\overline{\Gamma}_c^1, \qquad [4.68]$$

such that:

$$R(\delta \underline{\boldsymbol{g}}_t, \varepsilon) \xrightarrow{\varepsilon \to 0} \|\delta \underline{\boldsymbol{g}}_t\|,$$

see [KIK 88] for details. Such a regularization is in a good agreement with experiments on friction between metal surfaces [COU 57] demonstrating that a tangential relative sliding may occur, even for a small tangential stress. This microsliding is governed by the elastoplastic deformation of asperities in contact.

4.4. Variational equality and resolution methods

According to the remarks made in the previous section, the variational inequality is hard to apply for contact with finite sliding and/or rotations. That is why, nowadays, most of the practical studies in contact mechanics are based on the so-called *variational equalities*, which are easy to introduce in a finite element framework and does not require totally new minimization techniques. Here, we derive the framework based on variational equalities constructued for a known active contact zone. Due to the requirement of a known contact zone, such a formulation should be coupled with an active set strategy. An active set denotes such components of the potential contact zone that are in "active" contact at the current solution step. Naturally, the inactive set contains only components of the potential contact surface that are not in contact.

Assuming the known contact zone, it becomes possible to transform the nonlinear optimization problem under constraints into an unconstrained problem and to apply further classical resolution methods. Among the most popular and widely used methods in contact mechanics are those inspired from optimization theory:

– the penalty method (exterior point methods);

– the barrier method (interior point methods);

– direct elimination of constraints;

– the Lagrange multiplier method;

– the perturbed Lagrangian (valid for stick or frictionless slip) method;

– the augmented Lagrangian formulation;

– Nitsche method (weak enforcement of constraints);

– cross-constraint method (see [WRI 06]);

and others, which can be found in [WRI 06] and the multiple references there in. We restrict ourself to three of them: penalty, Lagrange multipliers and augmented Lagrangian methods. All methods have their own advantages and drawbacks, which will be discussed in the following.

4.5. Penalty method

Let us assume that somehow the active contact zones $\overline{\Gamma}_c^1 \in \Gamma_c^1, \overline{\Gamma}_c^2 \in \Gamma_c^2$ are known. Then, the differential formulation of the contact problem can be replaced by a variational equality [4.61] complemented by restrictions on the virtual displacements $\delta\underline{\boldsymbol{u}} \in \mathbb{V}$ and contact constraints:

$$\int_\Omega \underline{\underline{\boldsymbol{\sigma}}} \cdot\cdot\, \delta\nabla\underline{\boldsymbol{u}}\, d\Omega + \int_{\overline{\Gamma}_c^1} \left(\sigma_n \delta g_n + \underset{\sim}{\sigma}_t^{\mathsf{T}} \delta\underset{\sim}{\xi} \right) d\overline{\Gamma}_c^1 = \int_{\Gamma_f} \underline{\boldsymbol{\sigma}}_0 \cdot \delta\underline{\boldsymbol{u}}\, d\Gamma + \int_\Omega \underline{\boldsymbol{f}}_v \cdot \delta\underline{\boldsymbol{u}}\, d\Omega, \qquad [4.69]$$

$$\mathbb{V} = \left\{ \delta\underline{\boldsymbol{u}} \in \mathbb{H}^1(\Omega) \,|\delta\underline{\boldsymbol{u}} = 0 \ \text{ on } \Gamma_u \right\}, \mathbb{K} = \left\{ \delta\underline{\boldsymbol{u}} \in \mathbb{V} \ \middle|\ g(\underline{\boldsymbol{u}}, \delta\underline{\boldsymbol{u}}) \geq 0 \text{ on } \overline{\Gamma}_c \right\}.$$

We have a standard minimization problem under inequality constraints.

4.5.1. *Frictionless case*

The motion of material points $\underline{\boldsymbol{x}} \in \Omega$ is governed by Dirichlet boundary conditions, by non-penetration conditions:

$$g(\underline{\boldsymbol{\rho}}, S) \geq 0,$$

and by stick-slip relations that will be discussed later. First, we confine ourself to the frictionless case. To fulfill the non-penetration conditions, a normal contact pressure $\sigma_n < 0$ arises at the contact interface. Hertz–Signorini–Moreau's conditions summarize this effect:

$$g \geq 0, \ \ \sigma_n \leq 0, \ \ g\sigma_n = 0, \ \ \underline{\boldsymbol{\sigma}}_t = 0. \qquad [4.70]$$

Let us construct the penalty method based on an approximate fulfillment of these conditions. For this, let us suppose that the contact pressure is a continuous function of the penetration:

$$\sigma_n(g) = \epsilon_n\left(\langle -g \rangle\right) = \begin{cases} 0, & g > 0 \\ \epsilon_n(-g), & g \leq 0 \end{cases},$$

where ϵ_n is a non-positive continuous strictly monotonically decreasing function and:

$$\epsilon_n(0) = 0, \quad \epsilon_n(x) \xrightarrow{x\to\infty} -\infty.$$

Then the contact condition is strictly fulfilled for non-negative gaps, however according to the relations between contact pressure and the gap function, real contact appears only for negative gaps, that is only if a penetration takes place:

$$\begin{cases} g \geq 0, \;\; \sigma_n = 0, \;\; g\sigma_n = 0 \\ g < 0, \;\; \sigma_n = \epsilon_n(-g) < 0, \;\; g\sigma_n \neq 0. \end{cases} \qquad [4.71]$$

Logically, the higher the contact stress for small penetration the better Hertz–Signorini–Moreau's conditions are fulfilled. This approximation implies that the contact surface does not restrict penetration but resists to it, the deeper the penetration the higher the resisting reaction. The physical interpretation leads to a representation of the master surface as a series of springs with zero initial length, that can elongate inside the body normally to the master surface. The reaction provided by the springs follows the law $R = \epsilon_n(-U)$, where R is the appearing reaction and U is the elongation of the spring. At the same time, the surface of the master is supposed to be described by non-deformed springs. Because these imaginary springs are jointed to the master surface and transfer the reaction forces to it, it also deforms. The energy accumulated by springs due to their deformation is:

$$W_p = \int_0^{-U} \epsilon_n(U)\, dU = \int_0^{-\langle -g \rangle} \epsilon_n(\langle -g' \rangle)\, dg',$$

which in case of linear penalty method:

$$\epsilon_n(\langle -g \rangle) = -\varepsilon_n \langle -g \rangle, \varepsilon_n \geq 0$$

becomes:

$$W_p = -\int_0^{-\langle -g \rangle} \varepsilon_n \langle -g' \rangle\, dg' = \int_0^{-\langle -g \rangle} \varepsilon_n g'\, dg' = \frac{1}{2}\varepsilon_n \langle -g \rangle^2,$$

which coincides with the energy accumulated by a linear spring of stiffness ε_n due to an elongation or contraction $U = \langle -g \rangle$. Because of its simplicity and mainly due to the smooth contribution (regarding penetration) to the energy of the system, the linear penalty method is one of the most applicable methods for treatment of contact problems both in commercial and scientific finite element codes.

The assumption of dependency of the contact pressure on penetration allows us to represent the frictionless contact integral as the work of the contact pressure σ_n on virtual penetration δg_n, in analogy with the work of a prescribed traction: the contact integral appears to be the virtual work due to the deformation of imaginary springs in the contact interface (Figure 4.14). For normal projection $g_n(\underline{\boldsymbol{r}}, \Gamma_c^1)$, the contact contribution to the balance of virtual work is written as follows:

$$\delta W_c = \int_{\overline{\Gamma}_c^1} \epsilon_n(-g_n)\delta g_n \, d\overline{\Gamma}_c^1 = \int_{\Gamma_c^1} \epsilon_n(\langle -g_n \rangle)\delta g_n \, d\Gamma_c^1, \qquad [4.72]$$

after the choice of the penalty function ϵ_n (with an argument in Macaulay brackets $\langle -g \rangle$), one can integrate the virtual work due to contact not only over the active contact zone but over the full contact zone Γ_c^1, which results in the second equality in [4.72]. For shadow projection from an infinitely remote emitter $g_s(\underline{\boldsymbol{r}}, \Gamma_c^1)$ (see [4.58]), the contact integral has the form:

$$\delta W_c = \int_{\overline{\Gamma}_c^1} \epsilon_n(-g_s)\delta g_s \underline{\boldsymbol{n}} \cdot \underline{\boldsymbol{e}} \, d\overline{\Gamma}_c^1 = \int_{\Gamma_c^1} \epsilon_n(\langle -g_s \rangle)\delta g_s \underline{\boldsymbol{n}} \cdot \underline{\boldsymbol{e}} \, d\Gamma_c^1, \qquad [4.73]$$

where $\underline{\boldsymbol{e}}$ is the unit vector pointing toward the emitter.

The entire weak form for frictionless problems and normal projection writes as:

$$\begin{aligned} &\int_\Omega \underline{\underline{\boldsymbol{\sigma}}} \cdot\cdot \, \delta\nabla\underline{\boldsymbol{u}} \, d\Omega + \int_{\Gamma_c^1} \epsilon_n(\langle -g_n \rangle)\delta g_n \, d\overline{\Gamma}_c^1 = \int_{\Gamma_f} \underline{\boldsymbol{\sigma}}_0 \cdot \delta\underline{\boldsymbol{u}} \, d\Gamma + \int_\Omega \underline{\boldsymbol{f}}_v \cdot \delta\underline{\boldsymbol{u}} \, d\Omega, \\ &\mathbb{V} = \left\{ \delta\underline{\boldsymbol{u}} \in \mathbb{H}^1(\Omega) \mid \delta\underline{\boldsymbol{u}} = 0 \ \text{ on } \Gamma_u \right\}. \end{aligned} \qquad [4.74]$$

If the mechanical problem can be formulated as a minimization of the functional $F(\underline{\boldsymbol{u}})\colon \mathbb{V} \to \mathbb{R}$ under constraints $g(\underline{\boldsymbol{u}}) \geq 0$ and if the penalty functional is $P(\underline{\boldsymbol{u}})\colon \mathbb{V} \to \mathbb{R}_0^+$ then,

> *"The idea behind penalty method is, roughly speaking, to append to F a "penalty functional" P which increases the magnitude accordingly to how severely the constraint is violated."*
>
> N. Kikuchi and J.T. Oden [KIK 88]

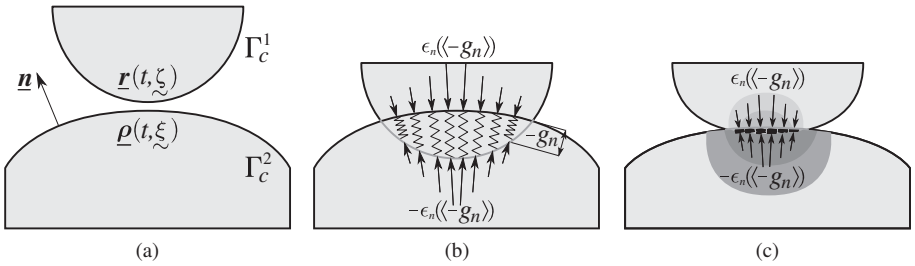

Figure 4.14. *Spring interpretation of the penalty method: (a) undeformed configuration; (b) configuration after penetration $g_n(\xi)$, which in turn results in a contact pressure $\sigma_n(\xi) = \epsilon_n(-g_n(\xi))$ shown with red arrows on the master and in blue on the slave, contact pressure results in decreasing the penetration due to deformation and results in an (c) equilibrium state*

4.5.2. *Example*

Let us demonstrate the idea of the penalty method on a simple example of minimization under constraints. Let the potential energy of the system with one degree of freedom be:

$$F(x) = \frac{1}{2}\,(2)\,(x+1)^2,$$

It corresponds to a mathematical pendulum in statics (see Figure 4.15) where $c = (2)[N/mm]$ is the stiffness of the sprng and $x[mm]$ is the coordinate of the mass point. We require that, at equilibrium, the energy is minimal or that the variation of the energy is zero:

$$\min_x\{F(x)\} \quad \text{or} \quad \delta F(x) = 0.$$

It corresponds to the point $x = -1[mm]$.

$$\delta F(x) = 2(x+1)\delta x = 0 \Leftrightarrow x = -1.$$

Let us introduce a wall that restricts the penetration in the zone $x < 0$; now the problem is reformulated as:

$$\min_{x\geq 0}\{F(x)\}.$$

Note that, strictly speaking, we cannot use the variational formulation $\delta F(x) = 0, x \geq 0$ because in a contact state, $F(x + \delta x)$ is not determined for any δx. The actual position of the mass can be expressed by $x = X + u$, where $X = -1$ is nothing but the equilibrium state without a wall (position in the reference configuration), then the gap can be simply expressed as:

$$g(x) = x \geq 0 \quad \Leftrightarrow \quad u \geq -X \quad \Leftrightarrow \quad u \geq 1.$$

Then, we can rewrite the problem in displacements:

$$\min_{u \geq 1} \{F(u)\}$$

$$F(x) = F(X + u) = (X + u + 1)^2 = u^2 = F(u).$$

In the framework of variational equalities and the penalty method, the constrained minimization problem can be rewritten as a simple minimization problem:

$$\min_{u \geq 1} \{F(u)\} \quad \rightarrow \quad \min_{u} \{F(u) + F_p(u)\},$$

where $F_p(u)$ is the penalty term due to violation of contact constraints:

$$F_p(u) = \int_0^{-\langle -g(X+u)\rangle} \epsilon(\langle -g(X+u)\rangle) dg(X+u),$$

or in case of linear penalty, $\epsilon(\langle -g(X+u)\rangle) = -\varepsilon\langle -g(X+u)\rangle$

$$F_p(u) = -\int_0^{-\langle -g(X+u)\rangle} \varepsilon_n \langle -g(X+u')\rangle \, dg(X+u'),$$

where

$$g(X+u) = X + u, \quad \langle -g(X+u)\rangle = \begin{cases} -X - u, & X + u < 0 \\ 0, & X + u \geq 0 \end{cases}$$

$$F_p(u) = -\int_0^{X+u} \varepsilon_n(-X-u')\, d(X+u') = \frac{1}{2}\varepsilon_n(X+u)^2 = \frac{1}{2}\varepsilon_n(u-1)^2,$$

so we get the following minimization problem:

$$\min_u \{F(u) + F_p(u)\} \quad \Leftrightarrow \quad \min_x \left\{ u^2 + \frac{1}{2}\varepsilon_n(u-1)^2 \right\}.$$

with the solution

$$\min_u \{F(u) + F_p(u)\} \Leftrightarrow \frac{\partial[F(u) + F_p(u)]}{\partial u} = (2+\varepsilon_n)u - \varepsilon_n = 0 \Leftrightarrow u = \frac{\varepsilon_n}{\varepsilon_n + 2}.$$

Because now the energy function F is determined for any displacements, in a more general form, the problem can be rewritten as a variational problem similar to [4.74]:

$$\delta F(u) + \epsilon(\langle -g(X+u)\rangle)\delta g(X+u) = 0,$$

where

$$\delta g(X+u) = \left.\frac{\partial g(X+u)}{\partial u}\right|_{u=0} \delta u = \delta u$$

which in case of linear penalty method $\epsilon_n(x) = -\varepsilon_n x$ also provides:

$$(2u - \varepsilon_n(1-u))\delta u = 0 \quad \Leftrightarrow \quad u = \frac{\varepsilon_n}{\varepsilon_n + 2}.$$

The functional $F(x)$ and $F(x) + F_p(x)$ for linear penalty are presented in Figure 4.16, which shows the energy functionals of unconstrained and constrained problems, respectively. We can see that the functional is smooth and that the solution converges gradually to the solution of the problem $x^* = 0, u^* = 1$ for increasing penalty parameter ε_n.

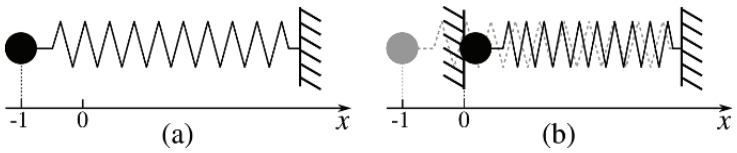

Figure 4.15. *A simple example of contact problem, mathematical pendulum in statics: (a) initial state, (b) deformed state due to the contact with a rigid wall*

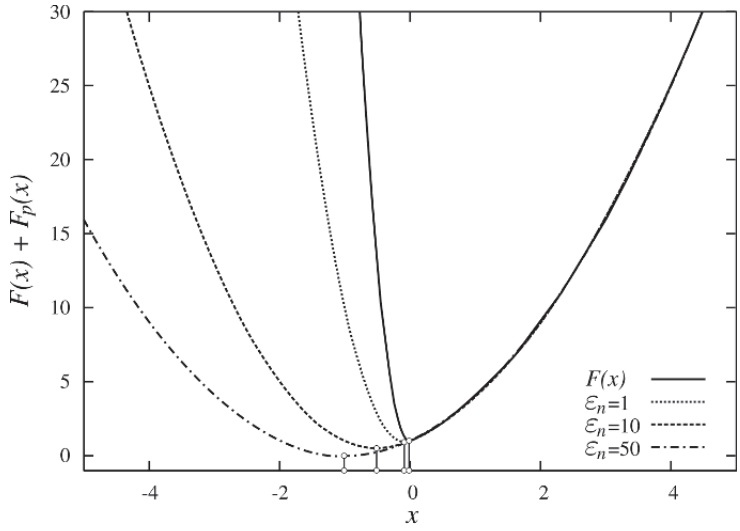

Figure 4.16. *Extended energy functional $F(x) + F_p(x)$ for different values of the penalty ($\varepsilon_n = 1,\ 10,\ 50$) and corresponding solutions for the problem presented in Figure 4.15*

4.5.3. *Nonlinear penalty functions*

The linear penalty method is optimal from a numerical point of view, because it does not introduce additional nonlinearities in the problem. Moreover, its linearization is a feasible task, whereas linearization of any nonlinear penalty function leads to significant computational difficulties. However, as it can be easily shown, the linear penalty function is not optimal from the point of view of the precision. Let us compare linear penalty function with quadratic:

$$\epsilon^q(x) = -\varepsilon_n(x^2 + x), \quad \int \epsilon^q(x)dx = -\varepsilon_n\left(\frac{1}{3}x^3 + \frac{1}{2}x^2\right)$$

and exponential penalty functions:

$$\epsilon^e(x) = -\varepsilon_n x(2+x)e^x, \quad \int \epsilon^e(x)dx = -\varepsilon_n x^2 e^x.$$

As we can see, the contribution of the penalty terms to the energy of the system (integrals) is smooth (value and derivative of the energy due to penalty in $x = 0$ is zero). In Tables 4.1–4.3, a comparison between linear, quadratic and exponential penalty methods is presented for different values of the penalty parameter $\varepsilon_n = 1$, $\varepsilon_n = 10$, $\varepsilon_n = 100$. To compare these methods on a nonlinear problem, we assume that the spring energy is given by $W = \frac{1}{2}cx^4$, with a parameter $c = \frac{1}{2}$. It means that the value of penalty coefficient $\varepsilon_n = 1$ has the same order of magnitude as the stiffness parameter. According to the tables, we see that for a high penalty $\varepsilon_n \sim 100c$ (Table 4.3), the linear method converges much faster than both others and the solutions of the three are quite close. For a moderate penalty $\varepsilon_n \sim 10c$ (Table 4.2), the quadratic penalty function gives a faster convergence than linear and exponential penalty functions. For a small penalty $\varepsilon_n \sim c$ (Table 4.1), the exponential function gives the fastest convergence and a much better solution than the others. It is worth mentioning that, in all cases, quadratic and exponential penalty functions yield a better solution, and that the best precision is obtained with the exponential function in all cases.

Let us also remark, that in 2D and 3D contact problems, the variation of the normal gap function and its second variation are always nonlinear, so even for linear material and a known contact zone, the linear penalty method does not allow us to achieve convergence within one iteration.

	Linear $\epsilon^l(x)$		Quadratic $\epsilon^q(x)$		Exponential $\epsilon^e(x)$	
Iter	Solution u^i	Relative error $\left\lvert\frac{u^i - u^{i-1}}{u^i}\right\rvert$	Solution u^i	Relative error $\left\lvert\frac{u^i - u^{i-1}}{u^i}\right\rvert$	Solution u^i	Relative error $\left\lvert\frac{u^i - u^{i-1}}{u^i}\right\rvert$
1	1.000	1.000	0.667	1.000	0.429	1.000
2	0.692	0.444	0.561	0.189	0.649	0.340
3	0.541	0.279	0.548	0.024	0.657	0.012
4	0.502	0.077	0.548	3.20e-4	0.657	1.81e-5
5	0.500	4.76e-3	0.548	5.67e-8	0.657	4.50e-11
6	0.500	1.71e-5	0.548	1.62e-15	0.657	1.69e-16
7	0.500	2.19e-10	0.548	2.02e-16	0.657	1.69e-16

Table 4.1. *Comparison of different penalty functions, penalty* $\varepsilon_n = 1$*, exact solution* $u^* = 1$

	Linear $\epsilon^l(x)$		Quadratic $\epsilon^q(x)$		Exponential $\epsilon^e(x)$	
Iter	Solution u^i	Relative error $\left\lvert\frac{u^i-u^{i-1}}{u^i}\right\rvert$	Solution u^i	Relative error $\left\lvert\frac{u^i-u^{i-1}}{u^i}\right\rvert$	Solution u^i	Relative error $\left\lvert\frac{u^i-u^{i-1}}{u^i}\right\rvert$
1	1.0	1.0	0.667	1.0	0.429	1.0
2	0.818	0.222	0.815	0.182	0.735	0.417
3	0.798	0.026	0.816	1.7e-3	0.867	0.152
4	0.797	3.0e-4	0.816	2.5e-8	0.884	0.019
5	0.797	3.8e-8	0.816	1.4e-16	0.884	2.38e-4
6	0.797	7.0e-16	0.816	1.4e-16	0.884	3.67e-8
7	0.797	0.0	0.816	1.4e-16	0.884	8.79e-16

Table 4.2. *Comparison of different penalty functions, penalty* $\varepsilon_n = 10$*, exact solution* $u^* = 1$

	Linear $\epsilon^l(x)$		Quadratic $\epsilon^q(x)$		Exponential $\epsilon^e(x)$	
Iter	Solution u^i	Relative error $\left\lvert\frac{u^i-u^{i-1}}{u^i}\right\rvert$	Solution u^i	Relative error $\left\lvert\frac{u^i-u^{i-1}}{u^i}\right\rvert$	Solution u^i	Relative error $\left\lvert\frac{u^i-u^{i-1}}{u^i}\right\rvert$
1	1.000	1.000	0.667	1.000	0.429	1.000
2	0.964	0.037	0.918	0.274	0.746	0.425
3	0.964	1.41e-4	0.967	0.047	0.925	0.193
4	0.964	2.00e-9	0.965	1.61e-3	0.978	0.054
5	0.964	0.0	0.965	1.87e-6	0.982	4.12e-3
6	0.964	0.0	0.965	2.53e-12	0.982	2.25e-5
7	0.964	0.0	0.965	0.0	0.982	6.67e-10

Table 4.3. *Comparison of different penalty functions, penalty* $\varepsilon_n = 100$*, exact solution* $u^* = 1$

4.5.4. *Frictional case*

In the presence of friction, the virtual work due to contact has to be complemented by the frictional term. The classical Coulomb's friction law reads as follows:

$$\|\underline{\boldsymbol{\sigma}}_t\| \leq \mu|\sigma_n|, \quad \underline{\boldsymbol{\sigma}}_t - \mu|\sigma_n|\underline{\boldsymbol{s}} = 0, \quad \|\underline{\boldsymbol{s}}\| \parallel \underline{\boldsymbol{\sigma}}_t - \mu|\sigma_n|\underline{\boldsymbol{s}} \parallel = 0$$

As in the case of the normal contact, this set of conditions can be fulfilled approximately using a penalty function. Let us assume that the tangential stress is

zero except when a tangential sliding $\underline{\boldsymbol{g}}_t$ occurs at the interface, so the tangential stress can be considered as a function of the tangential sliding limited by Coulomb's cone surface:

$$\underline{\boldsymbol{\sigma}}_t = \begin{cases} \epsilon_t(\|\underline{\boldsymbol{g}}_t\|)\underline{\boldsymbol{s}}, & \epsilon_t(\|\underline{\boldsymbol{g}}_t\|) < \mu|\sigma_n| \\ \mu|\sigma_n|\underline{\boldsymbol{s}}, & \epsilon_t(\|\underline{\boldsymbol{g}}_t\|) \geq \mu|\sigma_n|. \end{cases}$$

The penalty function should be positive and monotonically increasing, moreover it should be zero for zero sliding:

$$\epsilon_t(x) \geq 0,\ \epsilon_t(0) = 0,\ \frac{\partial \epsilon_t(x)}{\partial x} \geq 0.$$

Consequently, the contribution to the weak form due to tangential contact in the *stick state* is:

$$\int_{\overline{\Gamma}_c^{1\bullet}} \underline{\boldsymbol{\sigma}}_t \cdot \delta\underline{\boldsymbol{g}}_t \, d\overline{\Gamma}_c^1 = \int_{\overline{\Gamma}_c^{1\bullet}} \epsilon_t(\|\underline{\boldsymbol{g}}_t\|)\underline{\boldsymbol{s}} \cdot \delta\underline{\boldsymbol{g}}_t \, d\overline{\Gamma}_c^1 = \int_{\overline{\Gamma}_c^{1\bullet}} \epsilon_t \left(\left| \frac{\partial \underline{\underline{\boldsymbol{\rho}}}^{\mathsf{T}}}{\partial \underset{\sim}{\xi}} \Delta \underset{\sim}{\xi} \right| \right) \underset{\sim}{\mathrm{s}}^{\mathsf{T}} \delta \underset{\sim}{\xi} \, d\overline{\Gamma}_c^1,$$

where $\overline{\Gamma}_c^{1\bullet}$ denotes the stick contact zone and:

$$\underset{\sim}{\mathrm{s}} = \underline{\boldsymbol{s}} \cdot \overline{\frac{\partial \underline{\underline{\boldsymbol{\rho}}}}{\partial \underset{\sim}{\xi}}}.$$

From the derived expressions, it is clear that their linearization, needed for the implicit treatment of the contact in the framework of the finite element method, is a complicated task. This is why a linear penalty method is used, that gives the following expression for the stick case:

$$\underline{\boldsymbol{\sigma}}_t = \varepsilon_t \Delta \underline{\boldsymbol{g}}_t^{\bullet}, \quad \|\Delta \underline{\boldsymbol{g}}_t^{\bullet}\| < \frac{\mu|\sigma_n|}{\varepsilon_t},$$

where $\Delta \underline{\boldsymbol{g}}_t^{\bullet}$ is a discrepancy from the actual point and the stick point $\underline{\boldsymbol{\rho}}(\underset{\sim}{\xi}^{\bullet})$. The value of this discrepancy is limited by the Coulomb's cone. The integral of the virtual work for the linear penalty can be rewritten as:

$$\begin{aligned} \int_{\overline{\Gamma}_c^{1\bullet}} \underline{\boldsymbol{\sigma}}_t \cdot \delta\underline{\boldsymbol{g}}_t \, d\overline{\Gamma}_c^1 &= \int_{\overline{\Gamma}_c^{1\bullet}} \varepsilon_t \Delta \underline{\boldsymbol{g}}_t^{\bullet} \cdot \delta\underline{\boldsymbol{g}}_t \, d\overline{\Gamma}_c^1 = \int_{\overline{\Gamma}_c^{1\bullet}} \varepsilon_t (\Delta \underset{\sim}{\xi}^{\bullet})^{\mathsf{T}} \overline{\frac{\partial \underline{\underline{\boldsymbol{\rho}}}}{\partial \underset{\sim}{\xi}}} \cdot \frac{\partial \underline{\underline{\boldsymbol{\rho}}}^{T}}{\partial \underset{\sim}{\xi}} \delta \underset{\sim}{\xi} \, d\overline{\Gamma}_c^1 \\ &= \int_{\overline{\Gamma}_c^{1\bullet}} \varepsilon_t (\Delta \underset{\sim}{\xi}^{\bullet})^{\mathsf{T}} \delta \underset{\sim}{\xi} \, d\overline{\Gamma}_c^1, \end{aligned}$$

This integral can be interpreted as the work of the tangential stress vector $\underline{\boldsymbol{\sigma}}_t$ on the virtual relative sliding $\delta\underset{\sim}{\xi}$ in the contact interface. The convective coordinate $\underset{\sim}{\xi}^{\bullet}$ denotes the stick point, to where the slave point $\underline{\boldsymbol{r}}$ returns if the external load is removed. So $\Delta\underset{\sim}{\xi}^{\bullet}$ is an accumulated "slip-in-stick" over solution steps $\Delta\underset{\sim}{\xi}(t) = \underset{\sim}{\xi}(t) - \underset{\sim}{\xi}^{\bullet}$. From a physical point of view, the "slip-in-stick" represents elastic deformations within the contact interface (elastic deformation of asperities) and should vanish when the load is removed. The direct analogy with elasto-plastic deformation is the following: the deformation inside the yield surface results in elastic deformation of the volume element, whereas pushing the yield surface leads to plastic flow. After removing the load, the accumulated plastic deformation remains unchanged and the elastic deformation vanishes. By analogy, the total slip $\underline{\boldsymbol{g}}_t$ can be split into a sum of "slip-in-stick" $\underline{\boldsymbol{g}}_t{}^{\bullet}$ and real slip $\underline{\boldsymbol{g}}_t{}^{*}$:

$$\underline{\boldsymbol{g}}_t = \underline{\boldsymbol{g}}_t{}^{\bullet} + \underline{\boldsymbol{g}}_t{}^{*} \quad \sim \quad \underline{\underline{\boldsymbol{\varepsilon}}} = \underline{\underline{\boldsymbol{\varepsilon}}}^{e} + \underline{\underline{\boldsymbol{\varepsilon}}}^{p}.$$

Note that $\underline{\boldsymbol{g}}_t{}^{\bullet}$ and $\underline{\boldsymbol{g}}_t{}^{*}$ may be not collinear. To determine the slip direction, we need to reformulate this expression in velocities:

$$\dot{\underline{\boldsymbol{g}}}_t = \dot{\underline{\boldsymbol{g}}}_t{}^{\bullet} + \dot{\underline{\boldsymbol{g}}}_t{}^{*} \quad \sim \quad \dot{\underline{\underline{\boldsymbol{\varepsilon}}}} = \dot{\underline{\underline{\boldsymbol{\varepsilon}}}}^{e} + \dot{\underline{\underline{\boldsymbol{\varepsilon}}}}^{p}.$$

Applying the incremental Euler method ($\dot{x} = (x^{i+1} - x^{i})/\Delta t$) to integrate this equation, we get:

$$\underline{\boldsymbol{g}}_t{}^{i+1} = \underline{\boldsymbol{g}}_t{}^{i} + \Delta\underline{\boldsymbol{g}}_t{}^{\bullet\, i} + \Delta\underline{\boldsymbol{g}}_t{}^{*\, i},$$

where

$$\Delta\underline{\boldsymbol{g}}_t{}^{\bullet\, i} = \underline{\boldsymbol{g}}_t{}^{\bullet\, i+1} - \underline{\boldsymbol{g}}_t{}^{\bullet\, i}, \quad \Delta\underline{\boldsymbol{g}}_t{}^{*\, i} = \underline{\boldsymbol{g}}_t{}^{*\, i+1} - \underline{\boldsymbol{g}}_t{}^{*\, i}.$$

So for $\Delta t \to 0$, the frictional conditions can be reformulated as:

$$\|\underline{\boldsymbol{\sigma}}_t\| \le \mu|\sigma_n|, \quad \underline{\boldsymbol{\sigma}}_t - \mu|\sigma_n|\frac{\Delta\underline{\boldsymbol{g}}_t^{*}}{\|\Delta\underline{\boldsymbol{g}}_t^{*}\|} = 0, \quad \|\underline{\boldsymbol{g}}_t^{*}\| \left\| \underline{\boldsymbol{\sigma}}_t - \mu|\sigma_n|\frac{\Delta\underline{\boldsymbol{g}}_t^{*}}{\|\Delta\underline{\boldsymbol{g}}_t^{*}\|} \right\| = 0.$$

This representation is important for the numerical treatment of frictional contact problems by means of penalty method, which will be discussed in details in section 5.2.

As proposed in [WRI 06], in stick state, there is no need to distinguish normal and tangential directions. The slave point has to stick to the master point at which stick occurred and, according to the penalty method, all violations of the stick condition will be penalized by a penalty stress vector $\underline{\underline{\boldsymbol{\sigma}}} \cdot \underline{\boldsymbol{n}}$ in the direction of such a violation $\underline{\boldsymbol{g}} = \underline{\boldsymbol{r}} - \underline{\boldsymbol{\rho}}$, that is:

$$\underline{\underline{\boldsymbol{\sigma}}} \cdot \underline{\boldsymbol{n}} = \epsilon(\|\underline{\boldsymbol{g}}\|) \frac{\underline{\boldsymbol{g}}}{\|\underline{\boldsymbol{g}}\|}, \quad \text{if } g_n \leq 0, \|\underline{\boldsymbol{\sigma}}_t\| < \mu|\sigma_n|, \qquad [4.75]$$

where $\epsilon(x) \geq 0$ is a positive penalty function of the stick constraint violation. Such a formulation can be easily integrated in the weak form by substituting [4.75] in [4.53], which leads to:

$$\int_{\overline{\Gamma}_c^1{}^{\bullet}} \epsilon(\|\underline{\boldsymbol{g}}\|) \frac{\underline{\boldsymbol{g}}}{\|\underline{\boldsymbol{g}}\|} \cdot \delta(\underline{\boldsymbol{\rho}} - \underline{\boldsymbol{r}}) \, d\overline{\Gamma}_c^1,$$

and for a linear penalty function to a simpler form:

$$-\int_{\overline{\Gamma}_c^1{}^{\bullet}} \varepsilon(\underline{\boldsymbol{r}} - \underline{\boldsymbol{\rho}}) \cdot \delta(\underline{\boldsymbol{r}} - \underline{\boldsymbol{\rho}}) \, d\overline{\Gamma}_c^1,$$

such an approach is formally equivalent to the standard linear penalty, if we put $\varepsilon_n = \varepsilon_t = \varepsilon$, but it yields a simpler numerical formulation as shown in [WRI 06].

In slip state, the tangential stress is determined by the contact pressure and the slip direction:

$$\underline{\boldsymbol{\sigma}}_t^* = \mu|\sigma_n| \frac{\dot{\underline{\boldsymbol{g}}}_t}{\|\dot{\underline{\boldsymbol{g}}}_t\|} = \mu|\sigma_n|\underline{\boldsymbol{s}} = \mu|\sigma_n| \underset{\sim}{\mathrm{S}}^{\intercal} \overline{\frac{\partial \underline{\boldsymbol{\rho}}}{\partial \underset{\sim}{\xi}}};$$

the integral due to frictional contact in slip contact zone is formulated as:

$$\int_{\overline{\Gamma}_c^1{}^{*}} \mu|\sigma_n|\underline{\boldsymbol{s}} \cdot \delta\underline{\boldsymbol{g}}_t \, d\overline{\Gamma}_c^1 = \int_{\overline{\Gamma}_c^1{}^{*}} \mu|\sigma_n| \underset{\sim}{\mathrm{S}}^{\intercal} \delta\underset{\sim}{\xi} \, d\overline{\Gamma}_c^1.$$

Because $|\sigma_n| = -\epsilon_n(\langle -g_n \rangle)$, we finally get the following integral due to frictional sliding, which has to be introduced in the weak form:

$$\int_{\overline{\Gamma}_c^{1\,*}} \mu|\sigma_n|\underset{\sim}{\mathrm{s}}^{\intercal}\delta\underset{\sim}{\xi}\, d\overline{\Gamma}_c^1 = \int_{\overline{\Gamma}_c^{1\,*}} -\epsilon_n(\langle -g_n \rangle)\mu\underset{\sim}{\mathrm{s}}^{\intercal}\delta\underset{\sim}{\xi}\, d\overline{\Gamma}_c^1.$$

For linear penalty $|\sigma_n| = \varepsilon_n\langle -g_n \rangle$, the integral takes the following form:

$$\int_{\overline{\Gamma}_c^{1\,*}} \mu|\sigma_n|\underset{\sim}{\mathrm{s}}^{\intercal}\delta\underset{\sim}{\xi}\, d\overline{\Gamma}_c^1 = \int_{\overline{\Gamma}_c^{1\,*}} \varepsilon_n\langle -g_n \rangle\mu\underset{\sim}{\mathrm{s}}^{\intercal}\delta\underset{\sim}{\xi}\, d\overline{\Gamma}_c^1,$$

Finally, the full variational equality – balance of virtual works – for frictional contact (Coulomb's friction) and linear penalty method is:

$$\begin{gathered}\int_\Omega \underline{\underline{\boldsymbol{\sigma}}} \cdot\cdot\, \delta\nabla\underline{\boldsymbol{u}}\, d\Omega - \int_{\overline{\Gamma}_c^{1\,*}} \varepsilon_n\langle -g_n \rangle \left(\delta g_n - \mu\underset{\sim}{\mathrm{s}}^{\intercal}\delta\underset{\sim}{\xi}\right) d\overline{\Gamma}_c^1 - \int_{\Gamma_f} \underline{\boldsymbol{\sigma}}_0 \cdot \delta\underline{\boldsymbol{u}}\, d\Gamma - \int_\Omega \underline{\boldsymbol{f}}_v \cdot \delta\underline{\boldsymbol{u}}\, d\Omega + \\ + \int_{\overline{\Gamma}_c^{1\,\bullet}} -\varepsilon_n\langle -g_n \rangle\delta g_n + \epsilon_t \Delta\underset{\sim}{\xi}^{\bullet\intercal}\delta\underset{\sim}{\xi}\, d\overline{\Gamma}_c^1 = 0, \\ \mathbb{V} = \left\{\delta\underline{\boldsymbol{u}} \in \mathbb{H}^1(\Omega) \mid \delta\underline{\boldsymbol{u}} = 0 \ \text{ on } \Gamma_u\right\},\end{gathered} \qquad [4.76]$$

where $\overline{\Gamma}_c^{1\,*} \in \overline{\Gamma}_c^1$ and $\overline{\Gamma}_c^{1\,\bullet} \in \overline{\Gamma}_c^1$ are respectively the slip and the stick active contact zones on the master. In case of frictionless contact, the variational equality becomes:

$$\begin{gathered}\int_\Omega \underline{\underline{\boldsymbol{\sigma}}} \cdot\cdot\, \delta\nabla\underline{\boldsymbol{u}}\, d\Omega + \int_{\Gamma_c^1} -\varepsilon_n\langle -g_n \rangle\delta g_n\, d\overline{\Gamma}_c^1 - \int_{\Gamma_f} \underline{\boldsymbol{\sigma}}_0 \cdot \delta\underline{\boldsymbol{u}}\, d\Gamma - \int_\Omega \underline{\boldsymbol{f}}_v \cdot \delta\underline{\boldsymbol{u}}\, d\Omega = 0 \\ \mathbb{V} = \left\{\delta\underline{\boldsymbol{u}} \in \mathbb{H}^1(\Omega) \mid \delta\underline{\boldsymbol{u}} = 0 \ \text{ on } \Gamma_u\right\},\end{gathered} \qquad [4.77]$$

4.6. Method of Lagrange multipliers

The method of Lagrange multipliers also allows us to construct variational equalities for contact problems. This method, named after Joseph-Louis Lagrange, is used in optimization theory to find the extremum of a functional subjected to constraints. Briefly, we have to look for an argument $\underline{\boldsymbol{u}}^*$ that minimizes the scalar functional $\Pi(\underline{\boldsymbol{u}})$ under constraints $g(\underline{\boldsymbol{u}}) = 0$:

$$\min_{g(\underline{\boldsymbol{u}})=0} \Pi(\underline{\boldsymbol{u}}).$$

This problem under certain circumstances can be replaced by the search of a stationary point (extremum, precisely saddle point) of a specifically constructed functional $\mathcal{L}(\underline{\boldsymbol{u}}, \lambda)$ called Lagrangian, where λ is an additional unknown (Lagrange multiplier):

$$\min_{g(\underline{\boldsymbol{u}})=0} \Pi(\underline{\boldsymbol{u}}) \quad \rightarrow \quad \nabla\mathcal{L}(\underline{\boldsymbol{u}}, \lambda) = 0. \qquad [4.78]$$

The Lagrangian is constructed in the following manner:

$$\mathcal{L}(\underline{\boldsymbol{u}}, \lambda) = \Pi(\underline{\boldsymbol{u}}) + \lambda g(\underline{\boldsymbol{u}}), \quad \lambda \leq 0,$$

its gradient reads as:

$$\nabla\mathcal{L}(\underline{\boldsymbol{u}}, \lambda) = \begin{bmatrix} \frac{\partial \mathcal{L}}{\partial \underline{\boldsymbol{u}}} \\ \frac{\partial \mathcal{L}}{\partial \lambda} \end{bmatrix} = \begin{bmatrix} \frac{\partial \Pi(\underline{\boldsymbol{u}})}{\partial \underline{\boldsymbol{u}}} & +\lambda \frac{\partial g(\underline{\boldsymbol{u}})}{\partial \underline{\boldsymbol{u}}} \\ & g(\underline{\boldsymbol{u}}) \end{bmatrix} = 0. \qquad [4.79]$$

The lower equation is nothing but the constraint $g(\underline{\boldsymbol{u}}) = 0$. The upper equation implies that the gradient of the functional Π is opposite to the gradient of the constraint with a multiplier λ:

$$\frac{\partial \Pi(\underline{\boldsymbol{u}})}{\partial \underline{\boldsymbol{u}}} = -\lambda \frac{\partial g(\underline{\boldsymbol{u}})}{\partial \underline{\boldsymbol{u}}}.$$

The solution of the minimization problem is a stationary point of the Lagrangian [4.77], but in general not all stationary problems of [4.77] are solutions of the initial minimization problem. The replacement of a one argument functional $\Pi(\underline{\boldsymbol{u}})$ by a two argument functional $\mathcal{L}(\underline{\boldsymbol{u}}, \lambda)$ obviously implies that the number of unknowns is higher for the Lagrangian. From a numerical point of view, the discretized problem will contain $N_{\mathcal{L}}$ more degrees of freedom than the initial problem, where $N_{\mathcal{L}}$ is the number of geometrical constraints.

4.6.1. *Frictionless case*

The method of Lagrange's multipliers can be extended for multiple and continuous constraints formulated as inequalities. Let us remind the Hertz–Signorini–Moreau conditions:

$$g(\underline{\boldsymbol{u}}) \geq 0, \quad \sigma_n \leq 0, \quad \sigma_n g(\underline{\boldsymbol{u}}) = 0 \quad \text{on } \Gamma_c$$

On the active contact zone $\overline{\Gamma}_c$, we require that:

$$\forall \underline{\boldsymbol{u}} \in \overline{\Gamma}_c \ : \ g(\underline{\boldsymbol{u}}) \geq 0.$$

The constrained minimization problem is formulated as:

$$\min_{\underline{\boldsymbol{u}} \in \mathbb{V},\, g(\underline{\boldsymbol{u}}) \geq 0} \{\Pi(\underline{\boldsymbol{u}})\} \ \Leftrightarrow \ \exists \underline{\boldsymbol{u}}^* : \forall \underline{\boldsymbol{u}} \in \mathbb{V}, g(\underline{\boldsymbol{u}}) \geq 0 \text{ on } \overline{\Gamma}_c : \Pi(\underline{\boldsymbol{u}}^*) \leq \Pi(\underline{\boldsymbol{u}}) \quad \text{in } \Omega,$$

where $\Pi(\underline{\boldsymbol{u}})$ is the energy of the mechanical system in Ω; this problem can be replaced by a stationary point problem for the Lagrangian:

$$\nabla \mathcal{L}(\underline{\boldsymbol{u}}, \lambda_n(\underline{\boldsymbol{X}})) = 0 \quad \text{in } \Omega, \tag{4.80}$$

where $\lambda_n(\underline{\boldsymbol{X}}) \leq 0$ on $\overline{\Gamma}_c^{\,0}$ and $\lambda_n(\underline{\boldsymbol{X}}) = 0$ elsewhere, then the Lagrangian is given by:

$$\mathcal{L}(\underline{\boldsymbol{u}}, \lambda_n) = \Pi(\underline{\boldsymbol{u}}) + \int_{\overline{\Gamma}_c^1} \lambda_n(\underline{\boldsymbol{X}}) g(\underline{\boldsymbol{u}})\, d\overline{\Gamma}_c^1. \tag{4.81}$$

The expression $\lambda_n(\underline{\boldsymbol{X}})$, where $\underline{\boldsymbol{X}}$ denotes a material point in the reference configuration, is rarely used and in the following we will also omit the argument. By λ_n, we mean a continuous set of values on the active contact zone (instead of a real number as in the discrete case). The stationary condition in derivative form [4.80] can be replaced by the variation of the Lagrangian:

$$\delta \mathcal{L}(\underline{\boldsymbol{u}}, \lambda_n) = \delta \Pi(\underline{\boldsymbol{u}}) + \int_{\overline{\Gamma}_c} g(\underline{\boldsymbol{u}})\, \delta\lambda_n + \lambda_n\, \delta g(\underline{\boldsymbol{u}})\, d\overline{\Gamma}_c = 0.$$

The variation of the energy of the system $\delta\Pi(\underline{\boldsymbol{u}})$ is equivalent to the variational principle of virtual work, so the last equality can be rewritten in an extended form:

$$\boxed{\begin{array}{c} \int_\Omega \underline{\underline{\boldsymbol{\sigma}}} \cdot\cdot\, \delta\nabla\underline{\boldsymbol{u}}\, d\Omega + \int_{\overline{\Gamma}_c^1} g(\underline{\boldsymbol{u}})\, \delta\lambda_n + \lambda_n\, \delta g(\underline{\boldsymbol{u}})\, d\overline{\Gamma}_c^1 - \int_{\Gamma_f} \underline{\boldsymbol{\sigma}}_0 \cdot \delta\underline{\boldsymbol{u}}\, d\Gamma - \int_\Omega \underline{\boldsymbol{f}}_v \cdot \delta\underline{\boldsymbol{u}}\, d\Omega = 0 \\ \mathbb{V} = \left\{ \delta\underline{\boldsymbol{u}} \in \mathbb{H}^1(\Omega) \ | \ \delta\underline{\boldsymbol{u}} = 0 \ \text{ on } \Gamma_u \right\} \quad \lambda_n \leq 0 \ \text{ on } \Gamma_c^1, \end{array}} \tag{4.82}$$

The constraint $\lambda_n \leq 0$ has still to be fulfilled, that is why the Lagrange multiplier method does not convert a minimization problem with inequality constraints to a fully unconstrained one. For a more rigorous formulation of the Lagrange multiplier method for contact problems, the reader is referred to the book of Kikuchi and Oden [KIK 88]. The integral due to contact for zero gap $g(\underline{\boldsymbol{u}}) = 0$ degenerates to:

$$\int_{\overline{\Gamma}_c^1} \lambda_n \, \delta g(\underline{\boldsymbol{u}}) \, d\overline{\Gamma}_c^1 \quad \rightarrow \quad \int_{\overline{\Gamma}_c} \lambda_n \, \delta g(\underline{\boldsymbol{u}}) \, d\overline{\Gamma}_c^1 \quad \sim \quad \int_{\overline{\Gamma}_c^1} \sigma_n \, \delta g(\underline{\boldsymbol{u}}) \, d\overline{\Gamma}_c^1 .$$

This term is quite similar to the frictionless part of the contact integral in [4.69], where instead of λ_n the contact pressure σ_n appears, both of them should be negative. The Lagrange multiplier λ_n is interpreted as the contact pressure needed to fulfill the contact constraints. By analogy with a potential field $\Pi(\underline{\boldsymbol{r}})$ and the force $\underline{\boldsymbol{F}}$, it generates in point $\underline{\boldsymbol{r}}$ (gradient of the field):

$$\underline{\boldsymbol{F}} = -\frac{\partial \Pi}{\partial \underline{\boldsymbol{r}}},$$

the contact pressure is the gradient of the "energy" $\mathcal{L}(\underline{\boldsymbol{u}}, \lambda_n)$ with respect to the gap function:

$$|\sigma_n| = |\lambda_n| = -\frac{\partial \mathcal{L}}{\partial g}.$$

So we introduced a new unknown, the contact pressure λ_n, which will be obtained as the solution $(\underline{\boldsymbol{u}}^*, {\lambda_n}^*)$, such that:

$$\forall \underline{\boldsymbol{u}} \in \mathbb{V}, \lambda_n \leq 0\text{: } \mathcal{L}(\underline{\boldsymbol{u}}^*, \lambda_n) \leq \mathcal{L}(\underline{\boldsymbol{u}}^*, {\lambda_n}^*) \leq \mathcal{L}(\underline{\boldsymbol{u}}^*, \lambda_n)$$

which can be shortly formulated as a so-called min–max problem or saddle point problem:

$$\min_{\underline{\boldsymbol{u}} \in \mathbb{V}} \max_{\lambda_n \leq 0} \mathcal{L}(\underline{\boldsymbol{u}}, \lambda_n).$$

4.6.2. *Frictional case*

In case of frictional contact, a complementary condition on tangential sliding in case of *stick* is:

$$\underline{\dot{\boldsymbol{g}}}_t(\underline{\boldsymbol{u}}) = 0, \quad \text{if } \|\underline{\boldsymbol{\sigma}}_t\| \leq \mu|\sigma_n|, \quad \text{on } \overline{\Gamma}_c^{1\bullet} \tag{4.83}$$

if by analogy with frictionless contact we replace the tangential stress $\underline{\boldsymbol{\sigma}}_t$ by a Lagrange multiplier vector $\underline{\boldsymbol{\lambda}}_t$ defined on the contact surface, the stick condition can be rewritten in new terms as:

$$\underline{\dot{\boldsymbol{g}}}_t(\underline{\boldsymbol{u}}) = 0, \quad \text{if } \|\underline{\boldsymbol{\lambda}}_t\| \leq \mu|\lambda_n|, \quad \text{on } \overline{\Gamma}_c^{1\bullet}. \tag{4.84}$$

It is worth mentioning that the vector $\underline{\boldsymbol{\lambda}}_t$ lies in the tangential plane $\frac{\partial \underline{\boldsymbol{\rho}}}{\partial \underset{\sim}{\xi}}$ and $\lambda_n \underline{\boldsymbol{n}}$ is orthogonal to this plane. So if the Lagrange multipliers $\lambda_n, \underline{\boldsymbol{\lambda}}_t$ are added as degrees of freedom of the problem, contrary to the ordinary degrees of freedom determined in the global reference frame, they always correspond to the local frame and consequently are invariant to any global rotations. The Lagrangian with the stick term is:

$$\mathcal{L}(\underline{\boldsymbol{u}}, \lambda_n, \underline{\boldsymbol{\lambda}}_t) = \Pi(\underline{\boldsymbol{u}}) + \int_{\overline{\Gamma}_c^{1\bullet}} \lambda_n g(\underline{\boldsymbol{u}}) + \underline{\boldsymbol{\lambda}}_t \cdot \underline{\dot{\boldsymbol{g}}}_t(\underline{\boldsymbol{u}})\, d\overline{\Gamma}_c^1$$

and the corresponding equilibrium of virtual works $\delta\mathcal{L}(\underline{\boldsymbol{u}}, \lambda_n, \underline{\boldsymbol{\lambda}}_t)$ gives:

$$\delta\mathcal{L}(\underline{\boldsymbol{u}}, \lambda_n, \underline{\boldsymbol{\lambda}}_t) = \delta\Pi(\underline{\boldsymbol{u}}) + \int_{\overline{\Gamma}_c^{1\bullet}} g(\underline{\boldsymbol{u}})\delta\lambda_n + \lambda_n \delta g(\underline{\boldsymbol{u}}) + \underline{\dot{\boldsymbol{g}}}_t(\underline{\boldsymbol{u}}) \cdot \delta\underline{\boldsymbol{\lambda}}_t + \underline{\boldsymbol{\lambda}}_t \cdot \delta\underline{\dot{\boldsymbol{g}}}_t(\underline{\boldsymbol{u}})\, d\overline{\Gamma}_c^1.$$

A more straightforward formulation of this functional can be obtained if instead of $\underline{\dot{\boldsymbol{g}}}_t(\underline{\boldsymbol{u}}) = 0$ it is explicitly required that the surface coordinate $\dot{\underset{\sim}{\xi}} = 0$, then:

$$\delta\mathcal{L}(\underline{\boldsymbol{u}}, \lambda_n, \underline{\boldsymbol{\lambda}}_t) = \delta\Pi(\underline{\boldsymbol{u}}) + \int_{\overline{\Gamma}_c^{1\bullet}} g(\underline{\boldsymbol{u}})\delta\lambda_n + \lambda_n \delta g(\underline{\boldsymbol{u}}) + \dot{\underset{\sim}{\xi}}^{\intercal} \delta \underset{\sim}{\lambda}_t + \underset{\sim}{\lambda}_t^{\intercal} \delta \dot{\underset{\sim}{\xi}}\, d\overline{\Gamma}_c^1,$$

where $\underset{\sim}{\lambda}_t^{\intercal} = \underline{\boldsymbol{\lambda}}_t \cdot \overline{\frac{\partial \underline{\boldsymbol{\rho}}}{\partial \underline{\xi}}}^{\intercal}$ or $\underline{\boldsymbol{\lambda}}_t = \underset{\sim}{\lambda}_t^{\intercal} \overline{\frac{\partial \underline{\boldsymbol{\rho}}}{\partial \underline{\xi}}}$. Consequently, the stick criterion can be rewritten in new notations:

$$\sqrt{\underline{\boldsymbol{\lambda}}_t \cdot \underline{\boldsymbol{\lambda}}_t} < \mu|\lambda_n| \quad \Leftrightarrow \quad \sqrt{\underset{\sim}{\lambda}_t^{\intercal} \underset{\approx}{\mathrm{A}} \underset{\sim}{\lambda}_t} < \mu|\lambda_n|.$$

As noted in [WRI 06], in stick state there is no need to distinguish tangential and normal directions so that the two constraints $g = 0$ and $\underline{\dot{\boldsymbol{g}}}_t = 0$ can be replaced by one:

$$\underline{\boldsymbol{g}}(\underline{\boldsymbol{u}}) = \underline{\boldsymbol{r}} - \underline{\boldsymbol{\rho}}(\underline{\boldsymbol{X}}^{\bullet}) = 0,$$

where $\underline{\boldsymbol{X}}^{\bullet}$ denotes the material point at which $\underline{\boldsymbol{r}}$ and $\underline{\boldsymbol{\rho}}$ stick together, the associated spatial Lagrange multiplier vector – $\{\underline{\boldsymbol{\lambda}}\}$ – represents the contact stress vector. The Lagrangian of the energy becomes:

$$\mathcal{L}(\underline{\boldsymbol{u}}, \underline{\boldsymbol{\lambda}}) = \Pi(\underline{\boldsymbol{u}}) + \int_{\overline{\Gamma}_c^1} \underline{\boldsymbol{\lambda}} \cdot \underline{\boldsymbol{g}}(\underline{\boldsymbol{u}})\, d\overline{\Gamma}_c^1.$$

The criterion of stick is:

$$\left\| \underline{\boldsymbol{\lambda}} \cdot (\underline{\underline{\boldsymbol{I}}} - \underline{\boldsymbol{n}} \otimes \underline{\boldsymbol{n}}) \right\| < \mu|\underline{\boldsymbol{\lambda}} \cdot \underline{\boldsymbol{n}}|,$$

where $\underline{\boldsymbol{n}}$ is the unit normal vector on the master surface. Finally, the variation on the Lagrangian takes the following form:

$$\delta\mathcal{L}(\underline{\boldsymbol{u}}, \lambda_n, \underline{\boldsymbol{\lambda}}_t) = \delta\Pi(\underline{\boldsymbol{u}}) + \int_{\overline{\Gamma}_c^{1\bullet}} \underline{\boldsymbol{g}}(\underline{\boldsymbol{u}}) \cdot \delta\underline{\boldsymbol{\lambda}} + \underline{\boldsymbol{\lambda}} \cdot \delta\underline{\boldsymbol{g}}(\underline{\boldsymbol{u}})\, d\overline{\Gamma}_c^1, \qquad [4.85]$$

In case of slip, for Coulomb's friction law, the tangential stress is fully determined by the contact pressure and the sliding direction, that is why there is no more geometrical constraint on the tangential slip and so we do not need the Lagrange multiplier $\underline{\boldsymbol{\lambda}}_t$ that can be expressed through the λ_n:

$$\underline{\boldsymbol{\sigma}}_t = \mu|\sigma_n|\,\underline{\boldsymbol{s}} \quad \Leftrightarrow \quad \underline{\boldsymbol{\sigma}}_t = \mu|\lambda_n| \frac{\dot{\underset{\sim}{\xi}}^{\intercal}}{|\dot{\underset{\sim}{\xi}}^{\intercal} \underset{\approx}{\bar{\mathrm{A}}} \dot{\underset{\sim}{\xi}}|} \overline{\frac{\partial \underline{\boldsymbol{\rho}}}{\partial \underline{\xi}}} = \mu|\lambda_n| \underset{\sim}{\mathrm{s}}^T \overline{\frac{\partial \underline{\boldsymbol{\rho}}}{\partial \underline{\xi}}},$$

and the virtual work balance takes the form:

$$\delta\mathcal{L}(\underline{\boldsymbol{u}},\lambda_n,\underline{\boldsymbol{\lambda}}_t)=\delta\Pi(\underline{\boldsymbol{u}})+\int\limits_{\overline{\Gamma}_c^{1\,*}} g(\underline{\boldsymbol{u}})\delta\lambda_n+\lambda_n\delta g(\underline{\boldsymbol{u}})+\mu|\lambda_n|\underset{\sim}{\mathrm{s}}^{\intercal}\delta\underset{\sim}{\dot{\xi}}\,d\overline{\Gamma}_c^1.$$

Finally, for the active contact zone (union of non-intersecting stick and slip zones $\overline{\Gamma}_c^1=\overline{\Gamma}_c^{1\,\bullet}\cup\overline{\Gamma}_c^{1\,*}$), the variational formulation becomes:

$$\begin{aligned}\delta\mathcal{L}(\underline{\boldsymbol{u}},\lambda_n,\underline{\boldsymbol{\lambda}}_t)=\delta\Pi(\underline{\boldsymbol{u}})+&\int\limits_{\overline{\Gamma}_c^{1\,*}} g(\underline{\boldsymbol{u}})\delta\lambda_n+\lambda_n\delta g(\underline{\boldsymbol{u}})+\mu|\lambda_n|\underset{\sim}{\mathrm{s}}^{\intercal}\delta\underset{\sim}{\dot{\xi}}\,d\overline{\Gamma}_c^1+\\&+\int\limits_{\overline{\Gamma}_c^{1\,\bullet}} g(\underline{\boldsymbol{u}})\delta\lambda_n+\lambda_n\delta g(\underline{\boldsymbol{u}})+\underset{\sim}{\dot{\xi}}^{\intercal}\delta\underset{\sim}{\lambda}_t+\underset{\sim}{\lambda}_t^{\intercal}\delta\underset{\sim}{\dot{\xi}}\,d\overline{\Gamma}_c^1,\\ \mathbb{V}=\left\{\delta\underline{\boldsymbol{u}}\in\mathbb{H}^1(\Omega)\;\middle|\;\delta\underline{\boldsymbol{u}}=0\;\text{ on }\Gamma_u\right\}&\quad\lambda_n\le 0\;\text{ on }\Gamma_c^1.\end{aligned}\qquad[4.86]$$

or if we use [4.85]:

$$\begin{aligned}\delta\mathcal{L}(\underline{\boldsymbol{u}},\lambda_n,\underline{\boldsymbol{\lambda}}_t)=\delta\Pi(\underline{\boldsymbol{u}})+&\int\limits_{\overline{\Gamma}_c^{1\,*}} g(\underline{\boldsymbol{u}})\delta\lambda_n+\lambda_n\delta g(\underline{\boldsymbol{u}})+\mu|\lambda_n|\underset{\sim}{\mathrm{s}}^{\intercal}\delta\underset{\sim}{\dot{\xi}}\,d\overline{\Gamma}_c^1+\\&+\int\limits_{\overline{\Gamma}_c^{1\,\bullet}}\underline{\boldsymbol{g}}(\underline{\boldsymbol{u}})\cdot\delta\underline{\boldsymbol{\lambda}}+\underline{\boldsymbol{\lambda}}\cdot\delta\underline{\boldsymbol{g}}(\underline{\boldsymbol{u}})\,d\overline{\Gamma}_c^1\\ \mathbb{V}=\left\{\delta\underline{\boldsymbol{u}}\in\mathbb{H}^1(\Omega)\;\middle|\;\delta\underline{\boldsymbol{u}}=0\;\text{ on }\Gamma_u\right\}&\quad\lambda_n\le 0\;\text{ on }\Gamma_c^1.\end{aligned}\qquad[4.87]$$

As we can see, one constraint, $\lambda_n\le 0$ is still remaining. To get rid of this constraint, λ_n is often replaced by:

$$\lambda_n\quad\rightarrow\quad\lambda_n-\mathrm{dist}(\lambda_n,\mathbb{R}_-^0)=-\langle-\lambda_n\rangle=\begin{cases}0, & \lambda_n>0\\ \lambda_n, & \lambda_n\le 0\end{cases},$$

where $\langle\bullet\rangle$ are the Macaulay brackets and $\mathrm{dist}(\lambda_n,\mathbb{R}_-^0)$ means the distance from λ_n to the negative half-line, that is:

$$\mathrm{dist}(\lambda_n,\mathbb{R}_-^0)=\begin{cases}\lambda_n, & \lambda_n\notin\mathbb{R}_-^0\\ 0, & \lambda_n\in\mathbb{R}_-^0\end{cases}.$$

4.6.3. *Example*

Let us consider the same example as in the penalty method. The energy functional and the contact constraint are given by:

$$F(x) = \frac{1}{2}(2)(x+1)^2, g(x) = x \geq 0,$$

expressed in displacement $u = x + 1$, it writes as:

$$F(u) = u^2, g(u) = u - 1 \geq 0,$$

The corresponding Lagrangian has the following form:

$$\mathcal{L}(u, \lambda) = u^2 + \lambda(u - 1), \quad \lambda \leq 0$$

or using Macaulay brackets:

$$\mathcal{L}(x, \lambda) = u^2 - \langle -\lambda \rangle (u - 1).$$

The contours of this Lagrangian are represented in Figure 4.17. The saddle point is easy to locate $u = 1,\ \lambda = -4$. The right plot in the figure allows us to demonstrate visually the lack of smoothness on the line $\lambda = 0$ (marked with a black dashed line), which separates contact and non-contact zones.

The variation of the Lagrangian writes:

$$\delta\mathcal{L}(u, \lambda) = \begin{bmatrix} 2u + \lambda \\ u - 1 \end{bmatrix}^{\mathsf{T}} \begin{bmatrix} \delta u \\ \delta\lambda \end{bmatrix} = 0, \quad \lambda \leq 0.$$

As δu and $\delta\lambda$ are arbitrary, for the solution we require that:

$$\begin{cases} 2u + \lambda = 0 \\ u - 1 = 0 \end{cases} \quad \Leftrightarrow \quad \begin{bmatrix} 2 & 1 \\ 1 & 0 \end{bmatrix} \begin{bmatrix} x \\ \lambda \end{bmatrix} + \begin{bmatrix} 0 \\ -1 \end{bmatrix} = 0.$$

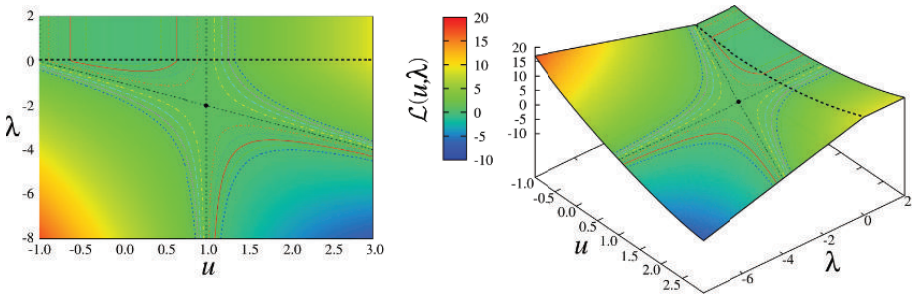

Figure 4.17. *Lagrangian $\mathcal{L}(u, \lambda)$ and several isolines, the saddle point is easy to detect $u = 1,\ \lambda = -2$; on the black dashed line, the Lagrangian lacks of smoothness by λ*

The solution of the last equation is $[u \ \ \lambda]^\intercal = [1 \quad -2]^\intercal$. Because λ is negative, $x = 1$ is the solution, otherwise the second equation has to be excluded from consideration and we simply get equality $2u = 0$.

Let us demonstrate how a numerical solution for the nonlinear problem with a Newton–Raphson's method can be obtained: as in the analysis of the nonlinear penalty method, we suppose that the spring is nonlinear with an energy functional $F(u) = 1/4u^4$, where $u = x + 1$, the contact constraint is $u - 1 \geq 0$. The Lagrangian takes the form:

$$\mathcal{L}(u, \lambda) = \frac{1}{4}u^4 + \lambda(u - 1), \quad \lambda \leq 0$$

or

$$\mathcal{L}(u, \lambda) = \frac{1}{4}u^4 - \langle -\lambda \rangle (u - 1),$$

and its variation gives:

$$\delta\mathcal{L}(u, \lambda) = \begin{bmatrix} u^3 + \lambda \\ u - 1 \end{bmatrix}^\intercal \begin{bmatrix} \delta u \\ \delta\lambda \end{bmatrix} = 0. \qquad [4.88]$$

This system of equations is nonlinear, so we choose the starting point $[u_0, \ \lambda_0]$ and we resort to the help of Newton's method. Thus, we need to linearize the equation [4.88] for a known iteration $[u_i, \ \lambda_i]$ to complete the increments $[\Delta u_i, \ \Delta\lambda_i]$:

$$\delta\mathcal{L}(u_{i+1}, \lambda_{i+1}) = \delta\mathcal{L}(u_i, \lambda_i) + \Big[\Delta\delta\mathcal{L}(u, \lambda)\Big]_{u_i, \lambda_i} \begin{bmatrix} \Delta u_i \\ \Delta\lambda_i \end{bmatrix} = 0, \qquad [4.89]$$

where

$$\delta\mathcal{L}(u_i,\lambda_i)=\begin{bmatrix}u_i^3+\lambda_i\\ u_i-1\end{bmatrix}$$

$$\Big[\Delta\delta\mathcal{L}(u,\lambda)\Big]_{u_i,\lambda_i}=\left[\begin{matrix}\frac{\partial^2\mathcal{L}(u,\lambda)}{\partial u^2} & \frac{\partial^2\mathcal{L}(u,\lambda)}{\partial u\partial\lambda}\\ \frac{\partial^2\mathcal{L}(u,\lambda)}{\partial\lambda\partial u} & \frac{\partial^2\mathcal{L}(u,\lambda)}{\partial\lambda^2}\end{matrix}\right]\Bigg|_{u_i,\lambda_i}=\begin{bmatrix}3u_i^2 & 1\\ 1 & 0\end{bmatrix},$$

Finally, from [4.89]: the expression for the increments is:

$$\begin{bmatrix}\Delta u_i\\ \Delta\lambda_i\end{bmatrix}=-\begin{bmatrix}3u_i^2 & 1\\ 1 & 0\end{bmatrix}^{-1}\begin{bmatrix}u_i^3+\lambda_i\\ u_i-1\end{bmatrix},\qquad\begin{bmatrix}u_{i+1}\\ \lambda_{i+1}\end{bmatrix}=\begin{bmatrix}u_i\\ \lambda_i\end{bmatrix}+\begin{bmatrix}\Delta u_i\\ \Delta\lambda_i\end{bmatrix}. \quad [4.90]$$

For any initial conditions $[u_0,\ \lambda_0]$, this procedure converges to the exact solution in three iterations. However, we should not forget about the restrictions $\lambda\le 0$ and $g\ge 0$. There are several possibilities to fulfill these conditions: note that one of them is of limited use (marked with a star *). Advantages and drawbacks will be discussed below and some examples will be given. The aim is to determine if the constraint is active or not, so we will call these approaches – local active set strategies. In the following, three of them are presented:

1) If on certain iterations the geometrical constraint is inactive $g(u_i)>0$, then the constraint is excluded and the reduced system [4.91] will be solved. If on the k-th iteration $g(u_k)\le 0$, then we turn back to the full system [4.90] and solve it for starting from the initial guess $[u_k,0]$.

2*) If during iterations a positive Lagrange multiplier occurs $\lambda_{i+1}>0$, then a reduced system of equation will be solved:

$$\Delta u_{i+1}=-\frac{u_{i+1}^3}{3u_{i+1}^2},\qquad u_{i+2}=u_{i+1}+\Delta u_{i+1},\ \lambda_{i+2}=0, \quad [4.91]$$

else the full system [4.90] is solved.

3) Both approaches can be combined: on the first iteration, we solve the full system [4.90]. On the following iterations, if $\lambda_i>0$ or $g(u_i)>0$, we solve the reduced system [4.91], else we return to the full system [4.90].

The first active set strategy, based on the check of the violation of the geometrical constraints $g\ge 0$, is frequently used due to its robustness. It provides the correct

solution; however sometimes it can take more iterations to converge. The second strategy is based on the check of the positivity of the Lagrange multiplier, sometimes it leads to a constant switch between two systems [4.90] and [4.91], that is between two functionals:

$$\mathcal{L}(u,\lambda) \quad \leftrightarrow \quad F(u),$$

which results in infinite oscillations if we quickly change the geometrical constraint so that the solution of the problem switches from constrained to unconstrained state. So, this active set strategy (2*) should be avoided. By anticipating things, we remark that when the solution of the problem remains constrained in the following step, the second strategy converges to the correct solution faster than the first strategy. That was the motivation for developing the third strategy – which is based on both constraints. It converges quickly toward the correct solution in all considered cases. However, because on the first iteration the material point follows the contact constraint, a fast removal of contact may create a situation when the initial point for Newton's iterations is too far from equilibrium, so it may cause convergence problems. Finally, we conclude that the first strategy is robust and conditionless, but it is not always fast. The second strategy is of limited use. The third strategy is fast and robust, but its convergence rate strongly depends on the loading of the problem. Note that when two initially separated points come and stay in contact, the three strategies are equivalent. However, in case of unloading, they behave quite differently. Each strategy is characterized by its piecewise-smooth functional, where u denotes the displacement from the reference state of the spring. Each functional is presented graphically in Figures 4.18–4.20. A thick black dashed line separates the domains of different functionals (Lagrangian in the contact and original functional in the non-contact domains).

It is worth mentioning that in implicit finite element codes, it is expensive to remove or add degrees of freedom during iterations, so the equation due to the Lagrange multiplier is not eliminated, as was done in [4.91], but the stiffness matrix and the residual vector of the problem are to be changed:

$$[K] \ : \ \begin{bmatrix} 3u_i^2 & 1 \\ 1 & 0 \end{bmatrix} \quad \rightarrow \quad \begin{bmatrix} 3u_i^2 & 0 \\ 0 & 1 \end{bmatrix}, \qquad [R] \ : \ \begin{bmatrix} u_i^3 + \lambda_i \\ u_i - 1 \end{bmatrix} \quad \rightarrow \quad \begin{bmatrix} u_i^3 \\ 0 \end{bmatrix}$$

Two functionals $F(u)$ and $\mathcal{L}(u,\lambda)$ for different active set strategies occupy different domains:

1) Active set strategy 1 (Figure 4.18):

$$\boxed{g(u) > 0 : \ F(u) \quad g(u) \leq 0 : \ \mathcal{L}(u,\lambda)}.$$

2*) Active set strategy 2 (Figure 4.19):

$$\boxed{\lambda > 0: \ F(u) \quad \lambda \leq 0: \ \mathcal{L}(u, \lambda)}.$$

3) Active set strategy 3 (Figure 4.20):

$$\boxed{g(u) > 0 \ \text{ and } \lambda > 0: \ F(u) \quad g(u) \leq 0 \ \text{ or } \lambda \leq 0: \ \mathcal{L}(u, \lambda)}.$$

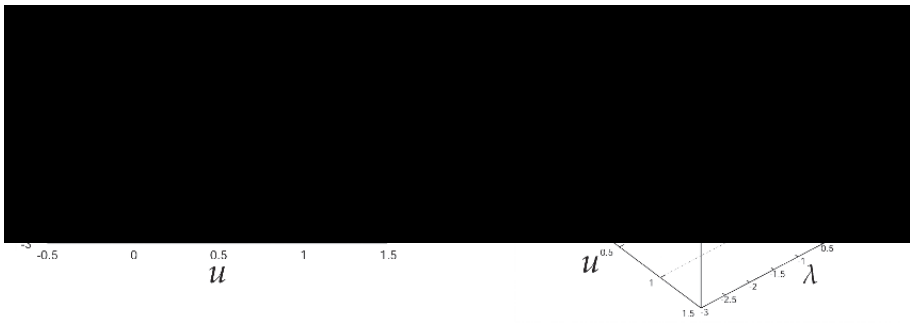

Figure 4.18. *Energy functional for the active set strategy 1*

Figure 4.19. *Energy functional for the active set strategy 2*

To demonstrate these three strategies, let us consider the same configuration of a mass on a nonlinear spring, but for the start point we choose the previously archived solution $[u = 1, \lambda = -1]$ – stressed spring due to the presence of the wall at $x = 0$. The displacement u will be related to this configuration, so $u = x$. We remember that the spring is free of stresses if the coordinate of the mass is $x = -1$. Two cases are considered:

– case I – the rigid wall is moved from position $x = 0$ to $x = -0.9$, see Table 4.4;

– case II – the rigid wall is moved from position $x = 0$ to $x = -1.1$, see Table 4.5.

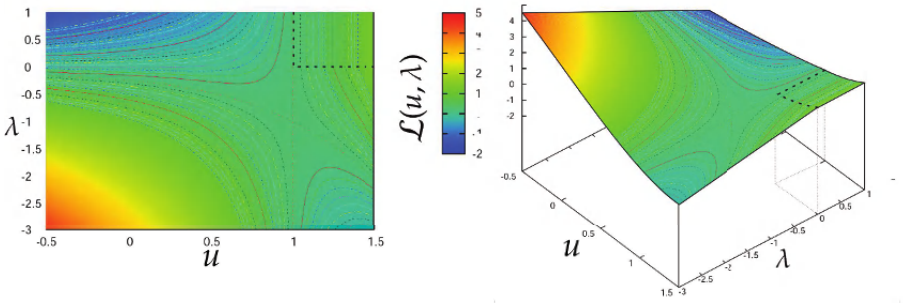

Figure 4.20. *Energy functional for the active set strategy 3*

As the tangent matrix is zero on the solution point, the convergence rate of the Newton–Raphson method is only linear. The solution due to the second active set strategy in the case of full unloading (case II) oscillates, and finally after iteration 20, we get an infinite loop between $[-1.05,\ 0.00]$ and $[-1.075,\ 4e-4]$. The third strategy converges in all the cases faster than others, however, as has been mentioned, the number of iterations in this case strongly depends on how far the constraint has been moved. Roughly speaking, the difference between the first and third strategies depends on the concrete situation, namely, on how the solution is closer to the final state with enforced contact or to the reference state with contact.

	Strategy ASS 1		Strategy ASS 2		Strategy ASS 3	
Iter, i	u_i	λ_i	u_i	λ_i	u_i	λ_i
1	−0.333	0.0	−0.900	1.70	−0.900	1.70
2	−0.556	0.0	−0.933	0.0	−0.933	0.0
3	−0.704	0.0	−0.933	−1.70	−0.933	−1.70
4	−0.802	0.0	−0.900	−7.4e-4	−0.900	−7.4e-4
5	−0.868	0.0	−0.900	−1.0e-3	−0.900	−1.0e-3
6	−0.912	0.0	**−0.900**	**−1.0e-3**	**−0.900**	**−1.0e-3**
7	−1.800	1.70	-	-	-	-
8	−0.900	−1.30	-	-	-	-
9	−0.900	−1.0e-3	-	-	-	-
10	**−0.900**	**−1.0e-3**	-	-	-	-

Table 4.4. *Case I. Comparison of different active set strategies (ASS) in case of partial unloading, exact solution* $u^* = -0.9,\ \lambda^* = -1e-3$ *(converged iteration put in* ***bold****)*

	Strategy ASS 1		Strategy ASS 2		Strategy ASS 3	
Iter, i	u_i	λ_i	u_i	λ_i	u_i	λ_i
1	−0.333	0.0	−1.100	2.30	−1.100	2.3
2	−0.556	0.0	−1.067	0.0	−1.067	0.0
3	−0.704	0.0	−1.067	−2.30	−1.044	0.0
4	−0.803	0.0	−1.100	7.4e-4	−1.030	0.0
5	−0.868	0.0	−1.067	0.0	−1.020	0.0
6	−0.912	0.0	−1.067	2.6e-4	−1.013	0.0
7	−0.941	0.0	−1.044	0.0	−1.009	0.0
8	−0.961	0.0	−1.078	4.8e-4	−1.008	0.0
9	−0.974	0.0	−1.051	0.0	−1.004	0.0
10	−0.983	0.0	−1.074	3.9e-4	−1.002	0.0

Table 4.5. ***Case II.*** *Comparison of different active set strategies (ASS) in case of full unloading, exact solution* $u^* = -1.0,\ \lambda^* = 0.0$

4.7. Augmented Lagrangian Method

4.7.1. *Introduction*

Another approach for the problem of minimization under constraints has been proposed in 1969 independently by Hestenes [HES 69] and by Powell [POW 69]. Originally, the method got the name "the multiplier method of Hestenes and Powell" or "method of multipliers". This method consists of a special combination of the penalty and Lagrange multiplier methods, it converges to the solution for a finite "penalty" coefficient and provides an unconstrained minimization problem with a smooth functional, which is a great advantage from a numerical point of view.

Let us shortly outline the idea. Let $F(x)$ be the functional to minimize under constraint $g(x) = 0$, in case of use of penalty or Lagrange multiplier methods the functional to minimize (or maxi-minimize) changes respectively as:

$$F_p(x) = F(x) + \frac{1}{2}\varepsilon g(x)^2; \qquad \mathcal{L}(x,\lambda) = F(x) + \lambda g(x).$$

For a given $\lambda = \lambda_i$, the Lagrangian can be considered as a function of one argument x:

$$\mathcal{L}(x,\lambda_i) = F(x) + \lambda_i g(x).$$

The application of the penalty method to this functional leads to:

$$\mathcal{L}^a(x,\lambda_i) = \mathcal{L}(x,\lambda_i) + \frac{1}{2}\varepsilon g(x)^2 = F(x) + \lambda_i g(x) + \frac{1}{2}\varepsilon g(x)^2.$$

If $[x_*, \lambda_*]^\intercal$ is a solution of $\min_x \max_\lambda \mathcal{L}(x,\lambda)$, then it can be shown that it is also the solution of the $\min_x \max_\lambda \mathcal{L}^a(x,\lambda)$. The original formulation was strictly iterative and supposed an independent update of λ_i at each iteration. In contact mechanics, this approach is also known as Uzawa's algorithm [ARR 58a] (named after *Hirofumi Uzawa*, Japanese economist). Let $[x_i, \lambda_i]^\intercal$ be the result of the current iteration, then the linearization procedure of Newton's method provides us with the following expression for the solution increment:

$$\begin{gathered}\mathcal{L}^a(x_i + \Delta x_i, \lambda_i) \approx \mathcal{L}^a(x_i,\lambda_i) + \left.\frac{\partial \mathcal{L}^a(x,\lambda_i)}{\partial x}\right|_{x_i} \Delta x_i = 0 \\ \left[F(x_i) + \lambda_i g(x_i) + \frac{1}{2}\varepsilon g(x_i)^2\right] + \left[\frac{\partial F(x)}{\partial x} + \boxed{[\,\lambda_i + \varepsilon g(x)\,]}\frac{\partial g(x)}{\partial x}\right]\Bigg|_{x_i} \Delta x_i = 0.\end{gathered} \qquad [4.92]$$

So according to the last equality, we evaluate the increment Δx_i, further we need to update λ. Hestenes draws our attention to the boxed term in [4.92], which suggests the updating procedure:

$$\lambda_{i+1} = \lambda_i + \varepsilon_i g(x_i), \quad \Delta\lambda_i = \varepsilon_i g(x_i),$$

where $0 < \varepsilon_i \leq \varepsilon$, which implies that if $g(x_i) < 0$ then the Lagrange multiplier λ should be decreased: as λ can be considered as a force, so it will push x_i closer to the solution and vice versa: if $g(x_i) > 0$, the Lagrange multiplier should be increased to pull x_i to the solution. If $g(x_i)$ gradually tends to zero, λ_i converges to the solution λ_*. Also, the authors propose to choose $\varepsilon_i = \gamma\varepsilon$, where γ is positive and smaller than 1, or to choose ε_i in order to approach the constraint from one side (a kind of monotonic convergence):

$$g(x_i)g(x_{i+1}) > 0$$

In all cases, the rate of convergence of this method, where primal x and dual λ variables are updated independently, is linear [POW 69]. In addition, this method has been generalized in 1973 by Rockafellar [ROC 73b, ROC 73a] for inequality

constraints, the author formulated a new unconstrained functional for the minimization of $F(x)$ subjected to the constraint $g(x) \geq 0$[10]:

$$\mathcal{L}^a(x, \lambda_i) = F(x) - \frac{1}{2\varepsilon}\left(\lambda_i^2 - \langle -(\,\lambda_i + \varepsilon g(x)\,)\rangle^2\right). \qquad [4.93]$$

In an expanded form, it rewrites as:

$$\mathcal{L}^a(x, \lambda_i) = \begin{cases} F(x) + \lambda_i g(x) + \frac{1}{2}\varepsilon g(x)^2, & \lambda_i + \varepsilon g(x) \leq 0 \\ F(x) - \frac{1}{2\varepsilon}\lambda_i^2, & \lambda_i + \varepsilon g(x) > 0. \end{cases} \qquad [4.94]$$

Note that the Lagrange multiplier λ is not restricted to be non-positive as in case of optimization under inequality constraints by the Lagrange multiplier method.

The variation of [4.121] with respect to x results in the following condition:

$$\delta\mathcal{L}^a(x, \lambda_i) = \delta F(x) - \langle -(\,\lambda_i + \varepsilon g(x_i)\,)\rangle \frac{\partial g(x)}{\partial x}\delta x = 0, \qquad [4.95]$$

from where, Rockafellar deduced:

$$\lambda_{i+1} = -\langle -(\,\lambda_i + \varepsilon g(x_i)\,)\rangle \leq 0$$

or

$$\lambda_{i+1} = \lambda_i + \varepsilon\frac{\partial\mathcal{L}^a(x, \lambda)}{\partial\lambda} = \lambda_i - \varepsilon\frac{1}{\varepsilon}(\lambda_i + \langle -(\,\lambda_i + \varepsilon g(x)\,)\rangle)$$

in an extended form:

$$\lambda_{i+1} = \begin{cases} \lambda_i + \varepsilon g(x), & \lambda_i + \varepsilon g(x) \leq 0 \\ 0, & \lambda_i + \varepsilon g(x) > 0. \end{cases}$$

10 In the following section, we follow Rockafellar [ROC 73b], except for the sign of the constraint, to make the formulation adapted for contact problems within the previously introduced notations.

Another possible interpretation of the update procedure can be derived if we reasonably assume that the Lagrangian multiplier should be a "force" due to a change of the potential $\mathcal{L}^a(x,\lambda)$ related to the change of the constraint $g(x)$, so we get directly the expression for the update procedure:

$$\lambda_{i+1} = \frac{\mathcal{L}^a(x,\lambda)}{g(x)} = -\frac{1}{\varepsilon}\langle -(\,\lambda_i + \varepsilon g(x)\,)\rangle\varepsilon = \begin{cases} \lambda_i + \varepsilon g(x), & \lambda_i + \varepsilon g(x) \leq 0 \\ 0, & \lambda_i + \varepsilon g(x) > 0. \end{cases}$$

However, the linear instead of quadratic convergence rate is quite a high price to pay for the unconstrained minimization even if a non-infinite penalty coefficient leads to the exact solution and even if no additional unknowns[11] are introduced in the global convergence cycle. The advantage of the method is that the functional $\mathcal{L}^a(x,.)$ is smooth so that a standard Newton's technique is applicable. Moreover, there is no need to control the non-positivity of the Lagrange multipliers.

In 1970, Fletcher [FLE 70] had developed a technique where both variables were adjusted simultaneously. It follows quite naturally from previous developments. Instead of the functional $\mathcal{L}^a(x,\lambda_i)$ where λ_i is fixed, the author proposed to consider a full functional where both primal x and dual variables λ are equivalent, $\mathcal{L}^a(x,\lambda)$. Then we obtain the min–max problem, where solution $[x_*,\lambda_*]$ minimizes the functional by x and maximizes by λ.

$$\min_x \max_\lambda \mathcal{L}^a(x,\lambda).$$

In the case of the lack of a strictly convex functional $F(x)$, we reformulate the problem as a variational problem:

$$\delta\mathcal{L}^a(x,\lambda) = \frac{\partial\mathcal{L}^a}{\partial x}\delta x + \frac{\partial\mathcal{L}^a}{\partial\lambda}\delta\lambda = 0, \qquad [4.96]$$

The associated numerical iterative scheme can then be easily deduced, but another problem is generated: the new functional $\mathcal{L}^a(x,\lambda)$ is not sufficiently smooth and so a generalization of the iterative scheme, often Newton's method, is required, which would ensure the convergence. A generalized Newton method (GNM) has been proposed by Alart and Curnier for non-smooth potential present in contact mechanics (first for the penalty method [CUR 88], then for the augmented Lagrangian method [ALA 88, ALA 91]. Some generalizations can be found in [ALA 97]).

11 Additional unknowns are nested in local update procedure.

An application of the augmented Lagrangian method to frictionless contact problems can be found in Glowinski and Le Tallec [GLO 89] and also in a report of Wriggers, Simo and Taylor [MID 85]. The first application of the augmented Lagrangian method with Uzawa algorithm to frictional problems has been reported by Simo and Laursen in [SIM 92]. The first successful attempt to apply the coupled augmented Lagrangian method to large displacement frictional contact problems has been undertaken by Alart [ALA 88] and Alart and Curnier [ALA 91]. The augmented Lagrangian approach has been elaborated by developing the perturbation approach to convex minimization as proposed in [ROC 70] and first applied by Fortin [FOR 76] to viscoplastic flow problems (similar to frictional contact problems). Further developments can be found in [HEE 93, PIE 97, PIE 99]. For the following developments of the augmented Lagrangian method for nonlinear constraints the reader is referred, for example, to Powell's survey paper [POW 78] and for an extended theory of optimization, to the related books [LUE 03, BER 03, BON 06].

To conclude the introductory part of this section, I would like to cite Dimitri Bertsekas' statement on the augmented Lagrangian method

> *"The original proposal of an Augmented Lagrangian method by Hestenes (1969) and Powell (1969) may be viewed as a significant milestone in the recent history of the constrained optimization area. Augmented Lagrangian methods are not only practically important in their own right, but have also served as the starting point for a chain of research developments centering around the use of penalty functions, Lagrange multiplier iterations, and Newton's method for solving the system of necessary optimality conditions."*
>
> Dimitri P. Bertsekas [BER 81]

4.7.2. *Application to contact problems*

4.7.2.1. *Contact conditions in subdifferential formalism*

A very detailed description of the application of the augmented Lagrangian method has been given in the PhD thesis of Pietrzak [PIE 97] and in the related article [PIE 99]. All developments are based on the formalism applied in contributions of Alart and Curnier [ALA 91] and Heegaard and Curnier [HEE 93], which in turn followed Moreau's works on convex analysis, the references can be found in the cited articles. Following the cited authors, we first introduce an indicator function–the indicator function of the positive half line $x \geq 0$:

$$\psi^+(x)\text{: } \forall x \in \mathbb{R} \rightarrow \psi^+(x) \in \mathbb{R}_0^+ \cup \infty,$$

$$\psi^+(x) = \begin{cases} \infty, & x < 0 \\ 0, & x \geq 0. \end{cases}$$

Following [HEE 93], a simple interpretation of the indicator function can be given using a piecewise linear function $\tilde{\psi}^+(x,r),\ r \geq 0$:

$$\tilde{\psi}^+(x,r) = \begin{cases} -rx, & x < 0 \\ 0, & x \geq 0. \end{cases}$$

Then, the indicator function is a limit of the function $\tilde{\psi}^+(x,r)$ if r tends to infinity:

$$\tilde{\psi}^+(x,r) \xrightarrow{r\to\infty} \approx \psi^+(x).$$

The functions $\psi^+(x)$ and $\tilde{\psi}^+(x,r)$ are non-differentiable in $x = 0$, however the last function has left- and right-sided derivatives. Now we can give a short formulation of the *sub-differential* of a function. For a simple locally convex function $f(x)$: $\mathbb{R} \to \mathbb{R}$, the sub-differential in the point x^* is a set of all real numbers contained between left- and right-sided derivatives. This set is denoted $\partial f(x^*)$. If the function is concave in a vicinity of the point x^*, then the sub-differential is confined between right- and left-sided derivatives. The sub-differential of the function $\psi^+(0)$ is such that:

$$\partial\psi^+(0) = (-\infty, 0] \quad \sim \quad \partial\psi^+(0) = \left.\frac{d\tilde{\psi}^+(x,r)}{dx}\right|_{x=0-}, \forall\, 0 \leq r < \infty.$$

Any element of the sub-differential is called the *subgradient*:

$$s \in \partial\psi^+(0).$$

If, at a given point, there is only one subgradient, then the function is at least once differentiable at this point.

$$\partial\psi^+(x) = \begin{cases} \emptyset, & x < 0 \\ (-\infty, 0], & x = 0 \\ 0, & x > 0. \end{cases}$$

A slightly extended discussion of sub-differentials and sub-gradients in the framework of non-smooth optimization will be given in the following chapter, see section 5.1.4, where some useful references are also given.

The Hertz–Signorini–Moreau condition for normal contact can be rewritten as a so-called *sub-differential inclusion*:

$$\boxed{\sigma_n \in \partial\psi^+(g_n)}.$$

It means that for a positive argument $g_n > 0$, the contact pressure can take only a zero value, and for $g_n = 0$, it can take any negative value. Indeed, contact pressure is non-positive, for negative normal gap the sub-differential is undefined, so the normal gap is non-negative and the complementary condition is also fulfilled:

$$\sigma_n \in (-\infty, 0], \quad g_n \in [0, \infty), \quad g_n\sigma_n = 0.$$

Introducing a conjugate indicator function – indicator of the negative half-line $x \leq 0$"

$$\psi^-(x) \ : \ \forall x \in \mathbb{R} \to \psi^-(x) \in \mathbb{R}_0^- \cup \{-\infty\},$$

$$\psi^-(x) = \begin{cases} 0, & x \leq 0 \\ -\infty, & x > 0. \end{cases}$$

allows us to reformulate the normal contact conditions as another sub-differential inclusion:

$$\boxed{g_n \in \partial\psi^-(\sigma_n)}.$$

Now let us introduce a disk $C(R)$ of radius R centered at the origin:

$$C_R = \left\{ \ \underline{\boldsymbol{x}} \ \middle| \ \|\underline{\boldsymbol{x}}\| \leq R \ \right\}.$$

The corresponding scalar indicator function of the vector argument is given by:

$$\psi_R(\underline{\boldsymbol{x}}) \ : \ \mathbb{T}_1^2 \to \mathbb{R}_0^+ \cup \infty,$$

$$\psi_R(\underline{\boldsymbol{x}}) = \begin{cases} 0, & \underline{\boldsymbol{x}} \in C_R \\ \infty, & \underline{\boldsymbol{x}} \notin C_R. \end{cases}$$

We can extend the interpretation given in [HEE 93] for a 2D cases:

$$\tilde{\psi}_R(\underline{\boldsymbol{x}}, r) = \begin{cases} 0, & \underline{\boldsymbol{x}} \in C_R \\ r(\|\underline{\boldsymbol{x}}\| - R), & \underline{\boldsymbol{x}} \notin C_R \end{cases}, \ r \geq 0.$$

The sub-differential of the disk indicator function can be interpreted as:

$$\partial\psi_R(\underline{\boldsymbol{x}}') = \left.\frac{d\tilde{\psi}_R(\underline{\boldsymbol{x}}, r)}{d\underline{\boldsymbol{x}}}\right|_{\underline{\boldsymbol{x}}=\underline{\boldsymbol{x}}'+}, \forall r \geq 0 = \begin{cases} r\dfrac{\underline{\boldsymbol{x}}}{\|\underline{\boldsymbol{x}}\|}, & \underline{\boldsymbol{x}} \notin C_R \setminus \partial C_R \\ 0, & \underline{\boldsymbol{x}} \in C_R \setminus \partial C_R \end{cases}, \forall r \geq 0,$$

where $\partial C_R = \left\{ \ \underline{\boldsymbol{x}} \ \middle| \ \|\underline{\boldsymbol{x}}\| = R \ \right\}$ is a closure of the disk C_R. The conditions arising from the Coulomb's friction law can be reformulated as a sub-differential inclusion:

$$\boxed{\underline{\dot{\boldsymbol{g}}}_t \in \partial\psi_{\mu|\sigma_n|}(\underline{\boldsymbol{\sigma}}_t)}. \qquad [4.97]$$

This formulation is equivalent to the classic Coulomb's friction law. Indeed, if the tangential contact stress is inside the Coulomb's disk $\|\underline{\boldsymbol{\sigma}}_t\| \in C_{\mu|\sigma_n|} \setminus \partial C_{\mu|\sigma_n|}$, there is no tangential sliding $\underline{\dot{\boldsymbol{g}}}_t = 0$. The closure of the Coulomb's disk $\partial C_{\mu|\sigma_n|}$ is called the *slip surface*. When the tangential contact stress reaches the slip surface of the disk, sliding occurs in the direction of the applied tangential stress and the velocity of sliding takes any non-negative value: $\underline{\dot{\boldsymbol{g}}}_t = r\dfrac{\underline{\boldsymbol{\sigma}}_t}{\|\underline{\boldsymbol{\sigma}}_t\|}, \ \forall r \geq 0.$

The conjugate function or Legendre–Fenchel conjugate of the disk indicator function $\psi_{\mu|\sigma_n|}$ is constructed as a norm function:

$$\psi^*_{\mu|\sigma_n|}(\underline{\dot{\boldsymbol{g}}}_t) = \mu|\sigma_n|\|\underline{\dot{\boldsymbol{g}}}_t\|,$$

which designates a convex cone. Then, the sub-differential of the conjugate function is given by:

$$\partial\psi^*_{\mu|\sigma_n|}(\underline{\dot{\boldsymbol{g}}}_t) = \begin{cases} \mu|\sigma_n|\dfrac{\underline{\dot{\boldsymbol{g}}}_t}{\|\underline{\dot{\boldsymbol{g}}}_t\|}, & \underline{\dot{\boldsymbol{g}}}_t \neq 0; \\ \underline{\boldsymbol{\sigma}}_t, & \underline{\dot{\boldsymbol{g}}}_t = 0, \end{cases}$$

where $\|\underline{\boldsymbol{\sigma}}_t\| \leq \mu|\sigma_n|$. Finally, using sub-differential notations, we can express the tangential contact stress vector as a sub-differential inclusion:

$$\boxed{\underline{\boldsymbol{\sigma}}_t \in \partial\psi^*_{\mu|\sigma_n|}\left(\underline{\dot{\boldsymbol{g}}}_t\right)},$$

which corresponds to the classically formulated frictional conditions.

Finally, for a frictional contact problem in the interface, we have two possible sets of sub-differential inclusions, for kinematic arguments:

$$\boxed{\sigma_n \in \partial\psi^+(g_n), \quad \underline{\boldsymbol{\sigma}}_t \in \partial\psi_{\mu|\sigma_n|}\left(\underline{\dot{\boldsymbol{g}}}_t\right),} \qquad [4.98]$$

and for static arguments:

$$\boxed{g_n \in \partial\psi^-(\sigma_n), \quad \underline{\dot{\boldsymbol{g}}}_t \in \partial\psi^*_{\mu|\sigma_n|}\left(\underline{\boldsymbol{\sigma}}_t\right).} \qquad [4.99]$$

Note that the convex disc $C_{\mu|\sigma_n|}$ is a function of the unknown contact pressure, consequently Alart and Curnier [ALA 91] proposed to call the indicator function $\psi_{\mu|\sigma_n|}$ and its conjugate $\psi^*_{\mu|\sigma_n|}$ *quasi-potentials* to "stress the dependence of the convex set on the pressure". Note also, that if the gap is open $g_n > 0 \quad \Rightarrow \quad \sigma_n = 0$ then the tangential contact stress is also zero $\underline{\boldsymbol{\sigma}}_t = 0$ and the sub-differential $\partial\psi_{\mu|\sigma_n|}(\underline{\boldsymbol{\sigma}}_t)$ degenerates in $\partial\psi_0(0) \ni \forall\underset{\sim}{\boldsymbol{x}}$, which means that tangential sliding is not restricted. In the incremental quasi-static analysis, the tangential relative sliding velocity is replaced by increments:

$$\underline{\dot{\boldsymbol{g}}}_t \quad \rightarrow \quad \underline{\boldsymbol{g}}_t{}^{i+1} - \underline{\boldsymbol{g}}_t{}^{i} = \Delta\underline{\boldsymbol{g}}_t{}^{i} = \underline{\dot{\boldsymbol{g}}}_t(t^{i+1} - t^i) \quad \Rightarrow \quad \underline{\dot{\boldsymbol{g}}}_t = \Delta\underline{\boldsymbol{g}}_t \,/\, (t^{i+1} - t^i).$$

As previously, the increment of the tangential relative sliding will be denoted simply by $\underline{\boldsymbol{g}}_t$ and time will be omitted without any loss of generality:

$$\underline{\dot{\boldsymbol{g}}}_t \quad \rightarrow \quad \Delta\underline{\boldsymbol{g}}_t \,/\, (t^{i+1} - t^i) \quad \rightarrow \quad \underline{\boldsymbol{g}}_t.$$

In the introduced framework of sub-differential inclusions, the variational problem can be formally formulated as follows:

$$\min\left\{\Pi^s(\underline{\boldsymbol{u}}) + \Pi^c(\underline{\boldsymbol{u}})\right\}, \qquad [4.100]$$

where $\Pi^s(\underline{\boldsymbol{u}})$ is a smooth potential energy of the system of contacting elastic bodies or its incremental homologue in plasticity and:

$$\Pi^c(\underline{\boldsymbol{u}}) = \int_{\overline{\Gamma}_c^1} \left[\psi^+(g_n) + \psi^*_{\mu|\sigma_n|}(\underline{\dot{\boldsymbol{g}}}_t) \right] d\overline{\Gamma}_c^1 \qquad [4.101]$$

is a non-differentiable energy of the frictional contact interaction. However, such a formulation is non-applicable in the numerical treatment of contact problems because of the non-differentiability. That is the principal motivation for the augmented Lagrangian method, however the smoothing effect is not the only advantage of the method. The augmented Lagrangian method converts the constrained minimization problem into a fully unconstrained problem, contrary to the Lagrange multiplier method that requires the fulfillment of the constraint related to the Lagrange multiplier $\lambda \leq 0$.

The regularization of the quasi-potentials entering in the contact functional [4.101] by the augmented Lagrangian method is presented in detail in [PIE 97] (see Chapter 5). The reader is referred to this volume for the detailed transformation of the quasi-potentials into smooth potentials – augmented Lagrangians l_n and l_t related to normal and frictional contact, respectively:

$$\psi^+(g_n) \;\rightarrow\; l_n(g_n, \lambda_n, \{\varepsilon_n\}), \quad \psi^*_{\mu|\sigma_n|}(\underline{\dot{\boldsymbol{g}}}_t) \;\rightarrow\; l_t(\underline{\dot{\boldsymbol{g}}}_t, \underline{\boldsymbol{\lambda}}_t, \sigma_n + \varepsilon_n g_n, \{\varepsilon_t\}),$$

where λ_n and $\underline{\boldsymbol{\lambda}}_t$ are Lagrange multipliers representing the contact pressure and the tangential contact stress vector, respectively, ε_n and ε_t are regularization or penalty coefficients for normal and tangential contact, respectively and σ_n is the contact pressure at solution $\underline{\boldsymbol{u}}^*$. Penalty coefficients are supposed to be constant. They are not considered as arguments of the augmented Lagrangians, so they are written in braces and further will be omitted. At solution it also holds:

$$\sigma_n = \sigma_n + \varepsilon_n g_n(\underline{\boldsymbol{u}}^*).$$

The augmented Lagrangian functional is constructed from [4.128] and the regularized form of [4.129]:

$$\begin{aligned}\mathcal{L}^a(&\underline{\boldsymbol{u}}, \lambda_n, \underline{\boldsymbol{\lambda}}_t, \sigma_n + \varepsilon_n g_n, \{\varepsilon_n, \varepsilon_t\}) \\ &= \Pi^s(\underline{\boldsymbol{u}}) + \int_{\Gamma_c^1} l_n(g_n, \lambda_n, \{\varepsilon_n\}) + l_t(\underline{\boldsymbol{g}}_t, \underline{\boldsymbol{\lambda}}_t, \sigma_n + \varepsilon_n g_n, \{\varepsilon_t\})\, d\Gamma_c^1. \end{aligned} \qquad [4.102]$$

The closed forms for l_n and l_t are given in the following section.

4.7.2.2. *Formulation of the virtual work principle*

Here, we give a formulation of the augmented Lagrangian functionals l_n and l_t, which can be directly inserted as integrand in the weak form. The regularized integrand due to the non-penetration–non-adhesion condition for the geometrical constraint $g_n \geq 0$, Lagrange multiplier λ_n (representing contact pressure) and penalty parameter ε_n is written as:

$$l_n(g_n, \lambda_n) = \begin{cases} \lambda_n g_n + \dfrac{\varepsilon_n}{2} g_n^2, & \lambda_n + \varepsilon_n g_n \leq 0, \ \textit{contact} \\ -\frac{1}{2\varepsilon_n} {\lambda_n}^2, & \lambda_n + \varepsilon_n g_n > 0, \ \textit{non-contact} \end{cases}$$

Using Macaulay brackets, a more compact form is given as:

$$l_n(g_n, \lambda_n) = -\frac{1}{2\varepsilon_n} \left({\lambda_n}^2 - \langle -(\lambda_n + \varepsilon_n g_n) \rangle^2 \right).$$

If following [PIE 97], the augmented Lagrange multiplier is denoted by a hat:

$$\hat{\lambda}_n = \lambda_n + \varepsilon_n g_n$$

then the formulation can be shortened as:

$$\boxed{l_n(g_n, \lambda_n) = -\frac{1}{2\varepsilon_n} \left({\lambda_n}^2 - \langle -\hat{\lambda}_n \rangle^2 \right).} \qquad [4.103]$$

The expanded form with hat notations takes the following form:

$$l_n(g_n, \lambda_n) = \begin{cases} g_n \hat{\lambda}_n - \dfrac{\varepsilon_n}{2} g_n^2, & \hat{\lambda}_n \leq 0, \ \textit{contact} \\ -\dfrac{1}{2\varepsilon_n} {\lambda_n}^2, & \hat{\lambda}_n > 0, \ \textit{non-contact.} \end{cases} \qquad [4.104]$$

The regularized integrand due to Coulomb's friction law for the incremental tangential relative displacement $\underline{\boldsymbol{g}}_t$, the corresponding Lagrange multiplier $\underline{\boldsymbol{\lambda}}_t$ (representing tangential contact stress vector) and the penalty parameter ε_t is written as:

$$l_t(\underline{\boldsymbol{g}}_t, \underline{\boldsymbol{\lambda}}_t, \hat{\sigma}_n) = \begin{cases} \left\{ \begin{array}{ll} \underline{\boldsymbol{\lambda}}_t \cdot \underline{\boldsymbol{g}}_t + \dfrac{\varepsilon_t}{2} \underline{\boldsymbol{g}}_t \cdot \underline{\boldsymbol{g}}_t, & \|\underline{\hat{\boldsymbol{\lambda}}}_t\| \leq -\mu \hat{\sigma}_n, \\ -\dfrac{1}{2\varepsilon_t} \left(\underline{\boldsymbol{\lambda}}_t \cdot \underline{\boldsymbol{\lambda}}_t + 2\mu \hat{\sigma}_n \left\| \underline{\hat{\boldsymbol{\lambda}}}_t \right\| + \mu^2 \hat{\sigma}_n^2 \right), & \|\underline{\hat{\boldsymbol{\lambda}}}_t\| > -\mu \hat{\sigma}_n, \end{array} \right\}, \hat{\sigma}_n \leq 0 \\ -\dfrac{1}{2\varepsilon_t} \underline{\boldsymbol{\lambda}}_t \cdot \underline{\boldsymbol{\lambda}}_t, & \hat{\sigma}_n > 0 \end{cases} \qquad [4.105]$$

where $\hat{\sigma}_n$ is a regularized contact pressure at solution:

$$\hat{\sigma}_n = \sigma_n + \varepsilon_n g_n,$$

and $\hat{\underline{\boldsymbol{\lambda}}}_t$ denotes the augmented Lagrange multiplier:

$$\hat{\underline{\boldsymbol{\lambda}}}_t = \underline{\boldsymbol{\lambda}}_t + \varepsilon_t \underline{\boldsymbol{g}}_t.$$

Note that the tangential regularized functional l_t is extended to the non-contact domain $\hat{\sigma}_n > 0$. Making use of Macaulay brackets provides a shorter form of the regularized functional l_t:

$$\boxed{l_t(\underline{\boldsymbol{g}}_t, \underline{\boldsymbol{\lambda}}_t, \hat{\sigma}_n) = -\frac{1}{2\varepsilon_t}\left(\underline{\boldsymbol{\lambda}}_t \cdot \underline{\boldsymbol{\lambda}}_t - \|\hat{\underline{\boldsymbol{\lambda}}}_t\|^2 + \langle \|\hat{\underline{\boldsymbol{\lambda}}}_t\| - \mu\langle -\hat{\sigma}_n\rangle\rangle^2\right)}. \qquad [4.106]$$

The integration of expressions [4.103] and [4.106] over the master surface leads to the following contribution of the contact conditions to the energy of the system:

$$\begin{aligned} W^c &= \int\limits_{\Gamma_c^1} l_n(g_n, \lambda_n) + l_t(\underline{\boldsymbol{g}}_t, \underline{\boldsymbol{\lambda}}_t, \hat{\sigma}_n)\, d\overline{\Gamma}_c^1 \\ &= \int\limits_{\Gamma_c^1} -\tfrac{1}{2\varepsilon_n}\left(\lambda_n{}^2 - \langle -\hat{\lambda}_n\rangle^2\right) - \frac{1}{2\varepsilon_t}\left(\underline{\boldsymbol{\lambda}}_t \cdot \underline{\boldsymbol{\lambda}}_t - \|\hat{\underline{\boldsymbol{\lambda}}}_t\|^2 + \langle \|\hat{\underline{\boldsymbol{\lambda}}}_t\| - \mu\langle -\hat{\sigma}_n\rangle\rangle^2\right) d\overline{\Gamma}_c^1. \end{aligned} \qquad [4.107]$$

For frictionless contact, the augmented functional l_t should be omitted. Variation of the integral W^c leads to:

$$\begin{aligned} \delta W^c &= \int\limits_{\Gamma_c^1} \delta l_n(g_n, \lambda_n) + \delta l_t(\underline{\boldsymbol{g}}_t, \underline{\boldsymbol{\lambda}}_t, \hat{\sigma}_n)\, d\overline{\Gamma}_c^1 \\ &= \int\limits_{\Gamma_c^1} \frac{\partial l_n}{\partial g_n}\delta g_n + \frac{\partial l_n}{\partial \lambda_n}\delta\lambda_n + \frac{\partial l_t}{\partial \underline{\boldsymbol{g}}_t} \cdot \delta\underline{\boldsymbol{g}}_t + \frac{\partial l_t}{\partial \underline{\boldsymbol{\lambda}}_t} \cdot \delta\underline{\boldsymbol{\lambda}}_t\, d\overline{\Gamma}_c^1. \end{aligned} \qquad [4.108]$$

Note that the contact pressure $\hat{\sigma}_n$ is not subjected to the variation even if it contains the geometrical quantity $\hat{\sigma}_n = \sigma_n + \varepsilon_n g_n$. This is due to the fact that the contact pressure is assumed to be the known contact pressure at solution, so its variation is zero. Because there are three possible contact statuses (stick, slip and non-contact), it is convenient to split the contact zone into three non-intersecting zones:

$$\Gamma_c^1 = \Gamma_c^{1*} \cup \Gamma_c^{1\bullet} \cup \Gamma_c^1 \setminus \overline{\Gamma}_c^1,$$

where Γ_c^{1*} is a slip zone, $\Gamma_c^{1\bullet}$ is a stick zone, $\overline{\Gamma}_c^1$ is an active contact zone and consequently, $\Gamma_c^1 \setminus \overline{\Gamma}_c^1$ is a non-contact zone.

To simplify the derivations further, four simple derivatives are given here:

$$\frac{\partial \hat{\lambda}_n}{\partial g_n} = \varepsilon_n, \quad \frac{\partial \hat{\lambda}_n}{\partial \lambda_n} = 1, \quad \frac{\partial \hat{\underline{\boldsymbol{\lambda}}}_t}{\partial \underline{\boldsymbol{g}}_t} = \varepsilon_t \underline{\underline{\boldsymbol{I}}}, \quad \frac{\partial \hat{\underline{\boldsymbol{\lambda}}}_t}{\partial \underline{\boldsymbol{\lambda}}_t} = \underline{\underline{\boldsymbol{I}}}.$$

Here and afterwards, it is more convenient to write all the derivatives in a classical way using [4.104] and [4.105], instead of short expressions with Macaulay brackets [4.103] and [4.106]:

$$\frac{\partial l_n(g_n, \lambda_n)}{\partial g_n} = \begin{cases} \hat{\lambda}_n, & \hat{\lambda}_n \leq 0, \ \textit{contact} \\ 0, & \hat{\lambda}_n > 0, \ \textit{non-contact}, \end{cases} \tag{4.109}$$

$$\frac{\partial l_n(g_n, \lambda_n)}{\partial \lambda_n} = \begin{cases} g_n, & \hat{\lambda}_n \leq 0, \ \textit{contact} \\ -\dfrac{1}{\varepsilon_n}\lambda_n, & \hat{\lambda}_n > 0, \ \textit{non-contact}, \end{cases} \tag{4.110}$$

$$\frac{\partial l_t(\underline{\boldsymbol{g}}_t, \underline{\boldsymbol{\lambda}}_t)}{\partial \underline{\boldsymbol{g}}_t} = \begin{cases} \begin{cases} \hat{\underline{\boldsymbol{\lambda}}}_t, & \|\hat{\underline{\boldsymbol{\lambda}}}_t\| \leq -\mu\hat{\sigma}_n \quad \textit{stick} \\ -\mu\hat{\sigma}_n \dfrac{\hat{\underline{\boldsymbol{\lambda}}}_t}{\|\hat{\underline{\boldsymbol{\lambda}}}_t\|}, & \|\hat{\underline{\boldsymbol{\lambda}}}_t\| > -\mu\hat{\sigma}_n, \quad \textit{slip} \end{cases}, & \hat{\sigma}_n \leq 0 \\ 0, & \hat{\sigma}_n > 0, \end{cases} \tag{4.111}$$

$$\frac{\partial l_t(\underline{\boldsymbol{g}}_t, \underline{\boldsymbol{\lambda}}_t)}{\partial \underline{\boldsymbol{\lambda}}_t} = \begin{cases} \begin{cases} \underline{\boldsymbol{g}}_t, & \|\hat{\underline{\boldsymbol{\lambda}}}_t\| \leq -\mu\hat{\sigma}_n \quad \textit{stick} \\ -\dfrac{1}{\varepsilon_t}\left(\underline{\boldsymbol{\lambda}}_t + \mu\hat{\sigma}_n \dfrac{\hat{\underline{\boldsymbol{\lambda}}}_t}{\|\hat{\underline{\boldsymbol{\lambda}}}_t\|}\right), & \|\hat{\underline{\boldsymbol{\lambda}}}_t\| > -\mu\hat{\sigma}_n, \quad \textit{slip} \end{cases}, & \hat{\sigma}_n \leq 0 \\ -\dfrac{1}{\varepsilon_t}\underline{\boldsymbol{\lambda}}_t, & \hat{\sigma}_n > 0. \end{cases} \tag{4.112}$$

After grouping all the derivatives [4.109]-[4.112], the contact contribution to the virtual work [4.108] takes the following form in case of frictional contact:

$$\delta W^c = \begin{cases} \int\limits_{\Gamma_c^{1\bullet}} \hat{\lambda}_n \delta g_n + g_n \delta\lambda_n + \hat{\underline{\boldsymbol{\lambda}}}_t \cdot \delta\underline{\boldsymbol{g}}_t + \underline{\boldsymbol{g}}_t \cdot \delta\underline{\boldsymbol{\lambda}}_t \, d\Gamma_c^1, & \|\hat{\underline{\boldsymbol{\lambda}}}_t\| \leq -\mu\hat{\sigma}_n, \ \textit{stick} \\ \int\limits_{\Gamma_c^{1*}} \hat{\lambda}_n \delta g_n + g_n \delta\lambda_n - \mu\hat{\sigma}_n \dfrac{\hat{\underline{\boldsymbol{\lambda}}}_t}{\|\hat{\underline{\boldsymbol{\lambda}}}_t\|} \cdot \delta\underline{\boldsymbol{g}}_t - \dfrac{1}{\varepsilon_t}\left(\underline{\boldsymbol{\lambda}}_t + \mu\hat{\sigma}_n \dfrac{\hat{\underline{\boldsymbol{\lambda}}}_t}{\|\hat{\underline{\boldsymbol{\lambda}}}_t\|}\right) \cdot \delta\underline{\boldsymbol{\lambda}}_t \, d\Gamma_c^1, & \|\hat{\underline{\boldsymbol{\lambda}}}_t\| > -\mu\hat{\sigma}_n, \ \textit{slip} \\ \int\limits_{\Gamma_c^1 \setminus \overline{\Gamma}_c^1} -\dfrac{1}{\varepsilon_n}\lambda_n \delta\lambda_n - \dfrac{1}{\varepsilon_t}\underline{\boldsymbol{\lambda}}_t \cdot \delta\underline{\boldsymbol{\lambda}}_t \, d\Gamma_c^1, & \hat{\sigma}_n > 0, \ \textit{non-contact} \end{cases} \tag{4.113}$$

and a much simpler form in case of frictionless contact:

$$\delta W^c = \begin{cases} \int\limits_{\overline{\Gamma}_c^1} \hat{\lambda}_n \delta g_n + g_n \delta \lambda_n \, d\overline{\Gamma}_c^1, & \hat{\sigma}_n \leq 0 \quad \textit{contact} \\ \int\limits_{\Gamma_c^1 \setminus \overline{\Gamma}_c^1} -\dfrac{1}{\varepsilon_n} \lambda_n \delta \lambda_n \, d\overline{\Gamma}_c^1, & \hat{\sigma}_n > 0 \quad \textit{non-contact.} \end{cases} \qquad [4.114]$$

After incorporating the contact integral into the equation of the virtual work balance, the following expression is obtained for the frictional contact:

$$\begin{gathered} \delta \mathcal{L}^a(\underline{\boldsymbol{u}}, \lambda_n, \underline{\boldsymbol{\lambda}}_t, \hat{\sigma}_n) = \int\limits_\Omega \underline{\underline{\boldsymbol{\sigma}}} \cdot\cdot \, \delta \nabla \underline{\boldsymbol{u}} \, d\Omega - \int\limits_{\Gamma_f} \underline{\boldsymbol{\sigma}}_0 \cdot \delta \underline{\boldsymbol{u}} \, d\Gamma - \int\limits_\Omega \underline{\boldsymbol{f}}_v \cdot \delta \underline{\boldsymbol{u}} \, d\Omega + \\ + \int\limits_{\Gamma_c^{1\bullet}} \hat{\lambda}_n \delta g_n + g_n \delta \lambda_n + \hat{\underline{\boldsymbol{\lambda}}}_t \cdot \delta \underline{\boldsymbol{g}}_t + \underline{\boldsymbol{g}}_t \cdot \delta \underline{\boldsymbol{\lambda}}_t \, d\Gamma_c^1 + \\ + \int\limits_{\Gamma_c^{1*}} \hat{\lambda}_n \delta g_n + g_n \delta \lambda_n - \mu \hat{\sigma}_n \frac{\hat{\underline{\boldsymbol{\lambda}}}_t}{\|\hat{\underline{\boldsymbol{\lambda}}}_t\|} \cdot \delta \underline{\boldsymbol{g}}_t - \frac{1}{\varepsilon_t} \left(\underline{\boldsymbol{\lambda}}_t + \mu \hat{\sigma}_n \frac{\hat{\underline{\boldsymbol{\lambda}}}_t}{\|\hat{\underline{\boldsymbol{\lambda}}}_t\|} \right) \cdot \delta \underline{\boldsymbol{\lambda}}_t \, d\Gamma_c^1 + \\ + \int\limits_{\Gamma_c^1 \setminus \overline{\Gamma}_c^1} -\frac{1}{\varepsilon_n} \lambda_n \delta \lambda_n - \frac{1}{\varepsilon_t} \underline{\boldsymbol{\lambda}}_t \cdot \delta \underline{\boldsymbol{\lambda}}_t \, d\Gamma_c^1 = 0, \\ \mathbb{V} = \left\{ \delta \underline{\boldsymbol{u}} \in \mathbb{H}^1(\Omega) \mid \delta \underline{\boldsymbol{u}} = 0 \ \text{ on } \Gamma_u \right\}, \end{gathered} \qquad [4.115]$$

and for frictionless contact:

$$\begin{gathered} \delta \mathcal{L}^a(\underline{\boldsymbol{u}}, \lambda_n, \underline{\boldsymbol{\lambda}}_t, \hat{\sigma}_n) = \int\limits_\Omega \underline{\underline{\boldsymbol{\sigma}}} \cdot\cdot \, \delta \nabla \underline{\boldsymbol{u}} \, d\Omega - \int\limits_{\Gamma_f} \underline{\boldsymbol{\sigma}}_0 \cdot \delta \underline{\boldsymbol{u}} \, d\Gamma - \int\limits_\Omega \underline{\boldsymbol{f}}_v \cdot \delta \underline{\boldsymbol{u}} \, d\Omega + \\ + \int\limits_{\overline{\Gamma}_c^1} \hat{\lambda}_n \delta g_n + g_n \delta \lambda_n \, d\Gamma_c^1 + \int\limits_{\Gamma_c^1 \setminus \overline{\Gamma}_c^1} -\frac{1}{\varepsilon_n} \lambda_n \delta \lambda_n \, d\Gamma_c^1 = 0, \\ \mathbb{V} = \left\{ \delta \underline{\boldsymbol{u}} \in \mathbb{H}^1(\Omega) \mid \delta \underline{\boldsymbol{u}} = 0 \ \text{ on } \Gamma_u \right\}, \end{gathered} \qquad [4.116]$$

4.7.3. *Example*

Let us illustrate how the augmented Lagrangian work in the simple case of one primal unknown. For this purpose, we return to the example considered in the previous sections (Figure 4.15): a mass (point) on a spring subjected to a constraint

due to the contact with a rigid wall $g(u) = u - 1 \geq 0$. The spring is considered to be nonlinear with a potential $F(u) = 1/2cu^4$, as previously mentioned. In the following computations, we put $c = \frac{1}{2}$, but we will keep this constant in derivatives to make the example more meaningful from the numerical point of view. The augmented Lagrangian takes the form:

$$\mathcal{L}^a(u, \lambda_n) = \begin{cases} \frac{1}{2}cu^4 + \lambda_n(u-1) + \frac{1}{2}\varepsilon_n(u-1)^2, & \lambda_n + \varepsilon_n(u-1) \leq 0 \\ \frac{1}{2}cu^4 - \frac{1}{2\varepsilon_n}\lambda_n^2, & \lambda_n + \varepsilon_n(u-1) > 0. \end{cases}$$

The graphical representation of the functional $\mathcal{L}^a$ in the neighborhood of the solution point $[1; -1]$ for different penalties $\varepsilon_n = 0.5;\ 1;\ 5;\ 10$ can be found in Figure 4.21; visually, it is obvious that the functional is rather smooth: isolines cross smoothly the line (white thick dashed line) dividing contact and non-contact zones $\lambda_n + \varepsilon_n(u-1) = 0$, this line is almost undetectable. The solution corresponds to the saddle point that retains its position independently on the penalty parameter, but higher stiffness leads to a higher concentration of isolines in the direction of the primal variable x. It is also interesting to visualize gradients (Figure 4.22) of the augmented Lagrangian $\nabla_x \mathcal{L}^a(x, \lambda_n)$ and $\nabla_{\lambda_n} \mathcal{L}^a(x, \lambda_n)$, which loose the smoothness across the contact–non-contact interface $\lambda_n + \varepsilon_n(u-1) = 0$.

The variation of the augmented Lagrangian is, for the considered case:

$$\delta\mathcal{L}^a(u, \lambda_n) = \begin{cases} \begin{bmatrix} 2cu^3 + \lambda_n + \varepsilon_n(u-1) \\ u - 1 \end{bmatrix}^{\mathsf{T}} \begin{bmatrix} \delta u \\ \delta\lambda_n \end{bmatrix} = 0, & \lambda_n + \varepsilon_n(u-1) \leq 0 \\ \begin{bmatrix} 2cu^3 \\ -\frac{1}{\varepsilon_n}\lambda_n \end{bmatrix}^{\mathsf{T}} \begin{bmatrix} \delta u \\ \delta\lambda_n \end{bmatrix} = 0, & \lambda_n + \varepsilon_n(u-1) > 0, \end{cases} \quad [4.117]$$

and the second variation needed for the linearization of [4.117] is as follows:

$$\Delta\delta\mathcal{L}^a(u, \lambda_n) = \begin{cases} \begin{bmatrix} \delta u \\ \delta\lambda_n \end{bmatrix}^{\mathsf{T}} \begin{bmatrix} 6cu^2 + \varepsilon_n & 1 \\ 1 & 0 \end{bmatrix} \begin{bmatrix} \delta u \\ \delta\lambda_n \end{bmatrix}, & \lambda_n + \varepsilon_n(u-1) \leq 0 \\ \begin{bmatrix} \delta u \\ \delta\lambda_n \end{bmatrix}^{\mathsf{T}} \begin{bmatrix} 6cu^2 & 0 \\ 0 & -\frac{1}{\varepsilon_n} \end{bmatrix} \begin{bmatrix} \delta u \\ \delta\lambda_n \end{bmatrix}, & \lambda_n + \varepsilon_n(u-1) > 0. \end{cases} \quad [4.118]$$

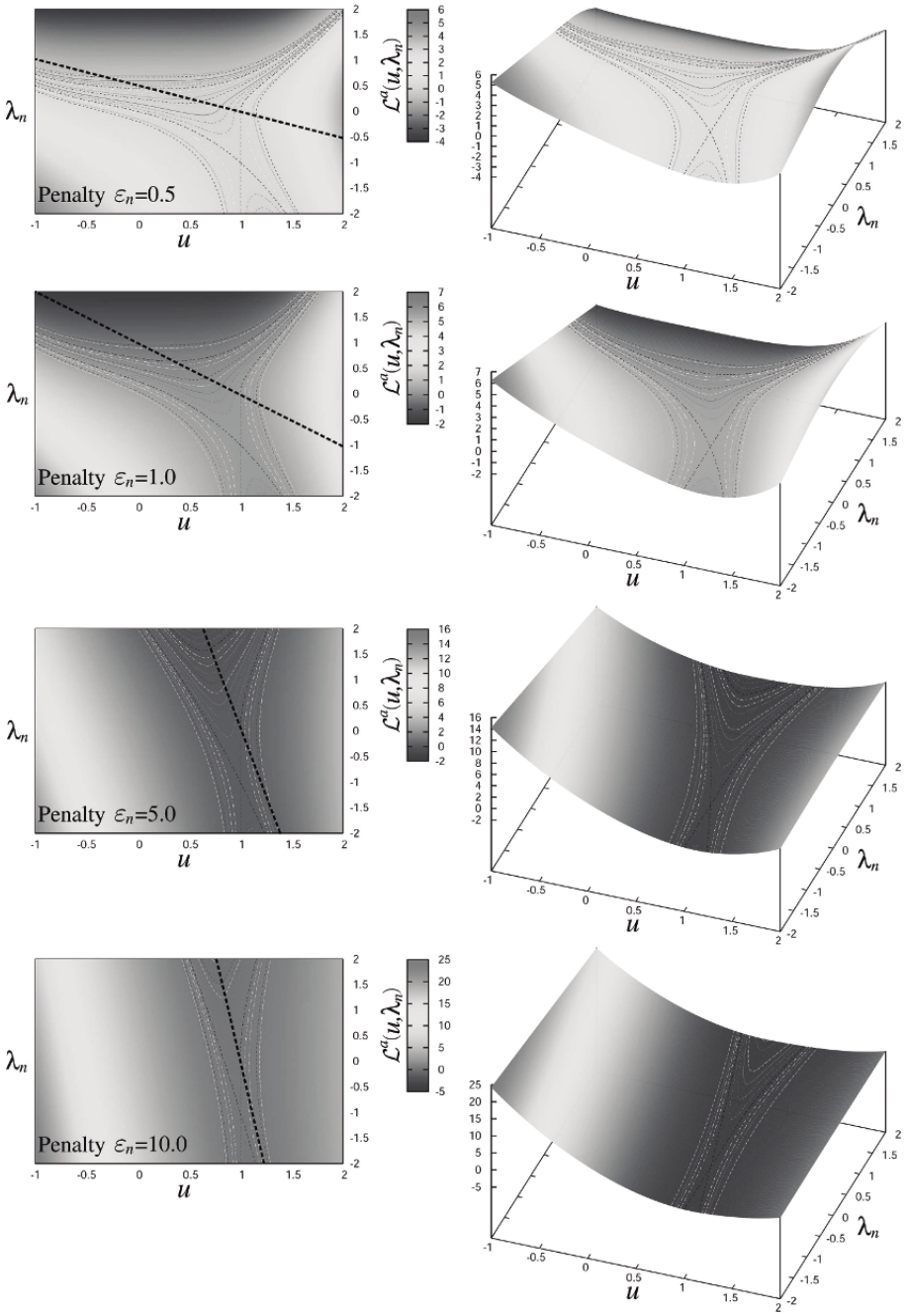

Figure 4.21. *Augmented Lagrangian for a nonlinear spring compressed by a rigid wall, plotted for different penalty parameters:* $\varepsilon_n = 0.5;\ 1;\ 5;\ 10$

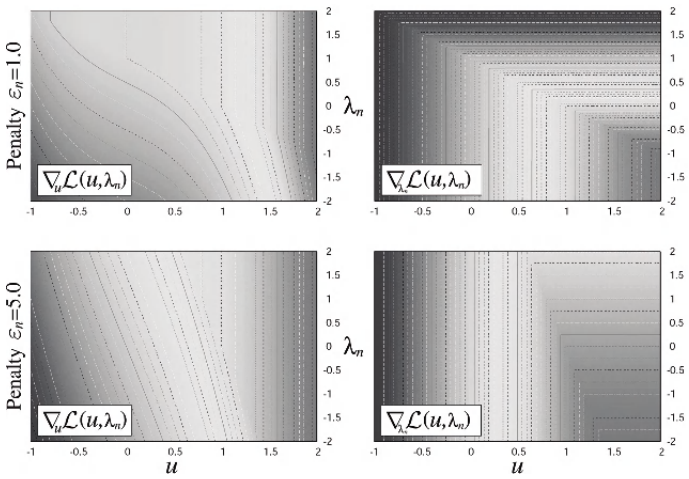

Figure 4.22. *Gradients $\nabla_x \mathcal{L}^a(x, \lambda_n)$ and $\nabla_{\lambda_n} \mathcal{L}^a(x, \lambda_n)$ of the augmented Lagrangian for a nonlinear spring compressed by a rigid wall are plotted for different penalty parameters: $\varepsilon_n = 0.5;\ 5$*

We can note that the first variation of $\mathcal{L}^a$ [4.118] (the balance of virtual work), is continuous for any values of u and λ, but its derivative [4.118] is not continuous. It motivates the usage of the generalized Newton's method. Note that, for linear material, the $\{11\}$ component of the matrix in [4.118] has a form similar to $c + \varepsilon_n$, however in the finite element method, the size of the finite element will be present. This observation leads to an appropriate choice of the penalty parameter of the order of the stiffness ($\varepsilon_n \sim c$). If the $\{11\}$ component of the matrix in [4.118] has the form $c\,\phi(u) + \varepsilon_n\,\psi(u)$, which is the case for nonlinear material and nonlinear constraints, and if u tends to the solution u^* in the way that function $\psi(u*) \rightarrow 0$, then it is reasonable to increase the penalty coefficient during iterations in order to improve the convergence of the augmented Lagrangian without danger of ill-conditioning of the matrix. Different techniques for the penalty update have been proposed (see, for example, [BUS 09]).

Let us demonstrate the convergence of the augmented Lagrangian method on a simple example of loading and unloading of the spring–mass system considered in the previous section. The convergence for different constant penalty coefficients and for the updated technique is compared in Table 4.6. In case of loading, the free spring deforms due to the contact with a rigid wall, the augmented Lagrangian method converges in three iterations (as the Lagrange multiplier method), that is at the second iteration the exact solution is obtained. Let us consider the case when from the obtained loaded state $x = 0$, $\lambda = -1$, we move the wall at $x_w = -0.9$, so the

spring remains compressed. The system of equation respectively to the deformed state becomes:

$$\begin{cases} [R] = \begin{bmatrix} 2c(u^i+1)^3 + \lambda_n^i + \varepsilon_n(u^i - x_w) \\ u^i - x_w \end{bmatrix}^\intercal, \\ [K] = \begin{bmatrix} 6c(u^i+1)^2 & 1 \\ 1 & 0 \end{bmatrix}, \end{cases} \quad \textit{contact} \quad \lambda_n^{i-1} + \varepsilon_n(u^{i-1} - x_w) \leq 0$$

$$\begin{cases} [R] = \begin{bmatrix} 2c(u^i+1)^3 \\ -\dfrac{\lambda_n^i}{\varepsilon_n} \end{bmatrix}^\intercal, \\ [K] = \begin{bmatrix} 6c(u^i+1)^2 & 0 \\ 0 & -\frac{1}{\varepsilon_n} \end{bmatrix} \end{cases} \quad \textit{non-contact} \quad \lambda_n^{i-1} + \varepsilon_n(u^{i-1} - x_w) > 0 \qquad . \quad [4.119]$$

At each iteration, we evaluate the solution increment in the following manner:

$$\begin{bmatrix} \Delta u^i \\ \Delta \lambda_n^i \end{bmatrix} = -[K]^{-1}[R].$$

In case of non-contact, the eigenvalues of the tangent matrix are $\lambda_{\max} = 6c(u^i+1)^2$ and $\lambda_{\min} = -\dfrac{1}{\varepsilon_n}$ and the condition number is:

$$\text{Cond}(K) = \frac{|\lambda_{\min}|}{|\lambda_{\min}|} = 6c(u^i+1)^2\varepsilon_n \ \sim \ c\varepsilon_n.$$

For a high penalty coefficient ε_n and a high stiffness coefficient c, the condition number of the tangent matrix becomes very high which is crucial for the precision of the solution and its convergence. That is the price of the fully unconstrained smooth energy functional. So even if formally the coupled augmented Lagrangian derives the precise solution, it suffers from numerical errors and its convergence is hindered. This is one of the main motivations to update the primal and dual variables separately by means of the Uzawa's algorithm. In case of simultaneous resolution, the penalty coefficients should be chosen reasonably small, at least, in case of non-contact. This is especially true for the frictional problems, for which a high penalty coefficient may lead to cycling over the solution. For more details on the condition numbers and the convergence of Newton's scheme, the reader is referred to section 5.1.

Two different convergences can be observed, which depend on the penalty parameter ε_n (see Figure 4.23). If $\lambda_n^0 + \varepsilon_n(u^0 - x_w) \leq 0$, we start from the "contact" type cycle, that is if $\varepsilon_n \leq \varepsilon_n* = -\frac{{\lambda_n}^0}{u^0 - x_w}$, otherwise this is a no-contact cycle. Sometimes, it is advantageous to start from a "contact" type cycle, so that for contact pressure $\sigma_n \leftarrow \lambda_n$ should be transferred from one converged increment to the following increment. In Table 4.6, for example, we make a start from ${\lambda_n}^0 = -1$,

which was the solution of the spring problem when it came into contact with a rigid wall. It is also interesting to compare the simultaneous (coupled) resolution of the problem for primal and dual variables with Uzawa's algorithm (nested resolution) (last four columns in Table 4.6). The last column converges significantly more slowly than the coupled algorithm in the contact domain. Note that the initial guess of being in the contact domain (Uzawa for $\varepsilon_n \leq \varepsilon_n*$) only disturbs the solution and increases the number of necessary iterations. The linear convergence rate becomes clear when we study the relative error (not given in the table). In the case of full unloading $x_w = -1.1$, there are no spurious modes, and the algorithm converges properly to the minimum of the unconstrained functional both for Uzawa and coupled algorithms.

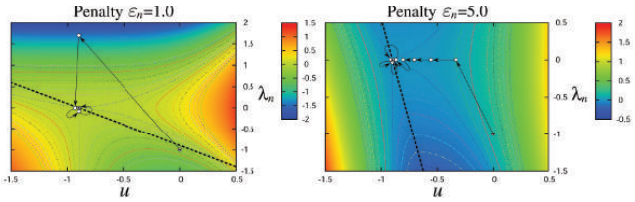

Figure 4.23. *Two different types of convergence of the augmented Lagrangian method in a case of partial unloading: the convergence path depends on the initial position of the point – inside contact domain or inside non-contact domain, which in turn depends upon the penalty coefficient*

	Coupled resolution				Nested resolution (Uzawa)			
	Penalty $\varepsilon_n \leq \varepsilon_n*$		Penalty $\varepsilon_n > \varepsilon_n*$		Penalty $\varepsilon_n \leq \varepsilon_n*$		Penalty $\varepsilon_n > \varepsilon_n*$	
Iter, i	u_i	λ_i	u_i	λ_i	u_i	λ_i	u_i	λ_i
0	0.0	-1.0	0.0	-1.0	0.0	-1.0	0.0	-1.0
1	-0.90	1.7	-0.333	0.0	-0.225	-0.325	-0.333	0.0
2	-0.93	0.0	-0.556	0.0	-0.483	0.0	-0.556	0.0
3	-0.90	-0.087	-0.704	0.0	-0.656	0.0	-0.704	0.0
4	-0.90	$-1e$-3	-0.802	0.0	-0.770	0.0	-0.802	0.0
5	-0.90	$-1e$-3	-0.868	0.0	-0.847	0.0	-0.868	0.0
6	-0.90	$-1e$-3	-0.913	0.0	-0.898	0.0	-0.912	0.0
7	-0.90	$-1e$-3	-0.90	-0.03	-0.932	0.0	-0.900	$-9.54e$-4
8	-0.90	$-1e$-3	-0.90	$-1e$-3	-0.901	$-7.48e$-4	-0.900	$-9.99e$-4
9	-0.90	$-1e$-3	-0.90	$-1e$-3	-0.900	-9.92-4	-0.900	$-9.99e$-4
10	-0.90	$-1e$-3	-0.90	$-1e$-3	-0.900	$-9.99e$-4	-0.900	$-1e$-3
11	-0.90	$-1e$-3	-0.90	$-1e$-3	-0.900	$-9.99e$-4	-0.900	$-1e$-3
12	-0.90	$-1e$-3	-0.90	$-1e$-3	-0.900	$-1e$-3	-0.900	$-1e$-3

Table 4.6. *Augmented Lagrangian convergence in case of partial unloading*

Chapter 5

Numerical Procedures

This chapter deals with the numerical aspects of contact mechanics. The classical *Newton's method* is presented. Some remarks on its applicability to contact problems are made, then the multidimensional version of the method is stated and the main characteristics of the resulting system of linear equations are briefly discussed. Further, we give a detailed description of the *return mapping algorithm*, which is often used for the integration of frictional conditions together with the penalty method (PM). Next, the finite element method (FEM) formalism is briefly introduced by using the new notations of s-structures. After setting up this numerical framework, the closed-form expressions for the implementation of PM. Lagrange multiplier method (LMM) and coupled augmented Lagrangian method (ALM) in a finite element code are given. Finally, some technical details are presented.

5.1. Newton's method

Generally for a locally convex and smooth function, the solution of the nonlinear problem can be approximated by a well-known Newton method or, also called Newton–Raphson procedure, which replaces a nonlinear problem by a series of linear problems. If the starting point is sufficiently close to the solution (here, it implies, for example, small changes of boundary conditions), the Newton–Raphson method provides a quadratic rate of convergence if the conditions of convexity and smoothness are fulfilled. However, as has been shown in Chapter 4, it is not always possible to fulfill these conditions: the virtual work functional is not smooth. Here, a short discussion of the Newton–Raphson method is given and its extension to the class of non-differentiable problems arising from contact mechanics are given.

5.1.1. *One-dimensional Newton's method*

The main idea of Newton's method can be easily captured on a one-dimensional (1D) example. Let the solution x of an equation depend on an external parameter f, then any equation can be written in the following form:

$$R(x, f) = 0$$

where R is a scalar function of two scalar arguments x and f. To fulfill this equation, a change of f should result in a change of x. A straightforward analogy with the mechanical system in statics containing one degree of freedom (dof) is, for example, the displacement x of the mass m attached to a spring with a linear stiffness k, under a gravity force $f = mg$. If the system is conservative, then the solution corresponds to the minimum of its energy:

$$W(x, g) = \frac{1}{2}cx^2 + mgx \rightarrow \frac{\partial W}{\partial x} = cx + mg = 0 \quad \sim \quad R(x, g) = cx + mg = 0$$

Let us consider a time-discretized model, that is the external parameter f changes incrementally $f_0, f_1, f_2, \ldots$, and we seek the values of the argument $x_0, x_1, x_2, \ldots$, which fulfill $R(x_i, f_i) = 0$ at least with a given precision $|R(x_i, f_i)| \leq \varepsilon$. We suppose that the starting point x_0 is known from the initial conditions or from a previously solved increment x_i:

$$R(x_i, f_i) = 0$$

For the following increment, the external parameter f becomes f_{i+1}. The aim is to find x_{i+1}. If the problem is nonlinear, an iterative scheme should be used. The first terms of the Taylor series of $R(x, f)$ centered at the previous iteration x^j are:

$$\begin{aligned} R(x^j + \Delta x^j, f_{i+1}) &= 0 \;\Rightarrow\; R(x^j + \Delta x^j, f_{i+1}) \\ &= R(x^j, f_{i+1}) + \left.\frac{\partial R}{\partial x}\right|_{x^j} \Delta x^j + r_1(x^j) = 0 \end{aligned} \qquad [5.1]$$

If higher order terms $r_1(x^j)$ are negligibly small and if a non-zero derivative $\left.\frac{\partial R}{\partial x}\right|_{x^j} \neq 0$ exists, then the increment $\Delta \underline{\boldsymbol{u}}^i$ can be written as:

$$\Delta x^j \approx -\left.\frac{\partial R}{\partial x}\right|^{-1}_{x^j} R(x^j, f_{i+1}), \quad x^{j+1} = x^j + \Delta x^j \qquad [5.2]$$

Further, we put $x^{j+1} = x^j + \Delta x^j$ and check if the new result is sufficiently close to zero $|R(x^{j+1}, f_{i+1}| \leq \varepsilon$, if not we repeat [5.1], where Taylor series is centered at x^{j+1}.

According to equation [5.1], we should require smoothness of the function $R(x, .)$ at least in points x^j. Since these points are arbitrary, we require that:

$$R(x) \in C^1(x) \qquad [5.3]$$

It is also important that a small change in f leads to a small change in R, in other words:

$$\exists\, K\colon 0 < K < \infty\colon \forall f^1, f^2\colon \left|R(x, f^2) - R(x, f^1)\right| \leq K \left\| f^2 - f^1 \right\| \qquad [5.4]$$

the smaller the parameter K, the slower function R changes with f, that is $R(., f)$ is a Lipschitz continuous function $R(., f) \in L^K$. As we can notice, the higher derivatives of R do appear explicitly in the derived equations, however, since we neglected all terms contained in $r_1(x^j)$, we suppose that they are negligibly small. Let us demonstrate that this residual $r_1(x^j)$ plays an important role. Let us rewrite the residual in Lagrange form:

$$r_1(x^j) = \frac{1}{2} \left.\frac{\partial^2 R}{\partial x^2}\right|_{\xi^j} (x^* - x^j)^2$$

where $\xi^j = x^* + \theta(x^j - x^*)$, $0 < \theta < 1$ and x^* is the exact solution. The expansion of the function R is:

$$R(x^*, f_{i+1}) = R(x^j, f_{i+1}) + \left.\frac{\partial R}{\partial x}\right|_{x^j} (x^* - x^j) + \frac{1}{2} \left.\frac{\partial^2 R}{\partial x^2}\right|_{\xi^j} (x^* - x^j)^2 = 0$$

Dividing by $\frac{\partial R}{\partial x} \neq 0$ and grouping the terms gives:

$$\left(\left.\frac{\partial R}{\partial x}\right|_{x^j}^{-1} R(x^j, f_{i+1}) - x^j \right) + x^* = -\frac{1}{2} \left.\frac{\partial R}{\partial x}\right|_{x^j}^{-1} \left.\frac{\partial^2 R}{\partial x^2}\right|_{\xi^j} (x^* - x^j)^2$$

According to [5.2], the first brackets are nothing but $-x^{j+1}$, so if the distance to the solution is denoted as $x^* - x^j = \varepsilon_j$, the equality can be rewritten as:

$$\varepsilon_{j+1} = -\frac{1}{2}\left.\frac{\partial R}{\partial x}\right|_{x^j}^{-1}\left.\frac{\partial^2 R}{\partial x^2}\right|_{\xi^j}\varepsilon_j^2$$

from where some corollaries can be deduced:

– if everywhere $\frac{\partial^2 R}{\partial x^2} = 0$, then, $\varepsilon_{j+1} = 0$, the function R is linear and the algorithm converges in one iteration;

– if $\exists C, L\ :\ 0 < \{C, L\} < \infty$ such that

$$\frac{1}{2}\left|\left.\frac{\partial^2 R}{\partial x^2}\right|_{\xi^j}\right| \leq C < \infty \quad \text{and} \quad \left|\left.\frac{\partial R}{\partial x}\right|_{x^j}^{-1}\right| \leq L < \infty$$

at least locally, then

$$|\varepsilon_{j+1}| \leq CL|\varepsilon_j|^2,$$

if $CL|\varepsilon_j| < 1$ ε_j then x^j converges to the solution x^*, and if the starting point x^0 is sufficiently close to the solution x^*, that is $CL|\varepsilon_0| < 1$ then the convergence is quadratic;

– if we add to the previously formulated conditions, the following condition

$$\begin{gathered}\text{sign}\left[\left.\frac{\partial^2 R}{\partial x^2}\right|_{\xi^j}\right] = \text{const},\ \text{sign}\left[\left.\frac{\partial R}{\partial x}\right|_{x^j}^{-1}\right] = \text{const},\\ \text{sign}[\varepsilon_0] = \text{sign}[x^0 - x^*] = \text{sign}\left[\left.\frac{\partial^2 R}{\partial x^2}\right|_{\xi^j}\right]\end{gathered} \qquad [5.5]$$

that is $R(x, .)$, is strictly monotonic and if the convexity does not change. Moreover, if the first point x_0 is to the right of the solution for the convex and to the left for concave the function, then x^j converges quadratically and monotonically to the solution;

– it follows, for example, that if:

$$\left.\frac{\partial R}{\partial x}\right|_{x^j} \xrightarrow{x^j \to x^*} 0 \quad \text{or} \quad \left|\left.\frac{\partial^2 R}{\partial x^2}\right|_{x^j}\right| \xrightarrow{x^j \to x^*} \infty$$

then the convergence, which it presents, is not quadratic (as in examples considered in Chapter 4).

This short reminder allows us to proceed with analysis of Newton's method for special cases. Let us note that the rigorous statement of Newton's method on convergence in a n-dimensional space is given by the Kantorovich theorem [KAN 48], where among other conditions the Lipschitz continuity of the first derivative is required:

$$\left\| \frac{\partial \boldsymbol{R}(x,.)}{\partial \boldsymbol{x}} - \frac{\partial \boldsymbol{R}(y,.)}{\partial \boldsymbol{y}} \right\| \leq L \| \boldsymbol{x} - \boldsymbol{y} \|$$

where bold symbols mean $\boldsymbol{a} \in \mathbb{R}^n$. Continuing with the results of this section, we will shortly consider the application of Newton's method for the case of non-differentiable functions, which is essentially the case in computational treatment of contact problems. But first let us show how Newton's method works in a multidimensional space.

5.1.2. *Multidimensional Newton's method*

In the discretized case, if the problem can be stated as:

$$\boldsymbol{R}(\boldsymbol{u}, \boldsymbol{f}) = 0,$$

where $\boldsymbol{R} \in \mathbb{R}^n$ is a vector function of vector arguments $\boldsymbol{u} = [u^1, u^2, \ldots, u^n]^T \in \mathbb{R}^n$ and $\boldsymbol{f} = [f^1, f^2, \ldots, f^m]^T \in \mathbb{R}^m$, the equation for the solution increment in the framework of Newton's method is written as:

$$\Delta \boldsymbol{u}^i = -\boldsymbol{K}(\boldsymbol{u}^i)^{-1} \boldsymbol{R}(\boldsymbol{u}^i, \boldsymbol{f}_{k+1}), \qquad \boldsymbol{u}^{i+1} = \boldsymbol{u}^i + \Delta \boldsymbol{u}^i$$

where the upper index i, as before, denotes the iteration number and the lower index the solution step or increment number. The matrix $\boldsymbol{K}$ in the FEM is called the *tangent stiffness matrix* for elastic problems or the *tangent matrix* for nonlinear problems. In optimization theory it is called the *Hessian* (second-order derivative of the objective function to be minimized), named after Ludwig Otto Hesse (1811–1874), a German mathematician or the *Jacobian* (named after Carl Gustav Jacob Jacobi (1804–1851), German mathematician) of the vector R:

$$\boldsymbol{K}(\boldsymbol{u}^{\boldsymbol{i}}) = \left. \frac{\partial\, R(\boldsymbol{u}, \boldsymbol{f})}{\partial \boldsymbol{u}} \right|_{\boldsymbol{u}^i}$$

The inverse of this matrix exists if and only if its determinant is not zero, which is equivalent to the condition that the spectrum of the matrix $\sigma(\boldsymbol{K})$ does not contain any zero eigenvalue:

$$\det \boldsymbol{K}(\boldsymbol{u^i}) \neq 0 \;\Leftrightarrow\; \forall \lambda_i \in \sigma\left(\boldsymbol{K}(\boldsymbol{u^i})\right) : \lambda_i \neq 0$$

If the matrix is not Lipschitz continuous, that is

$$\nexists\, K : 0 < K < \infty : \forall \lambda_i \in \sigma(\boldsymbol{K}),\ \forall \boldsymbol{u}_1, \boldsymbol{u}_2 :\ \ |\lambda_i(\boldsymbol{u}_1) - \lambda_i(\boldsymbol{u}_2)| \leq K \| \boldsymbol{u}_1 - \boldsymbol{u}_2 \|$$

then the assumptions of the Kantorovich theorem are not fulfilled and the convergence of the Newton–Raphson method may experience some problems. This case will be considered in the next section.

Another important characteristic of the tangent matrix is its condition number Cond$[K]$:

$$\text{Cond}(\boldsymbol{K}) = \frac{\lambda_{max}}{\lambda_{min}},$$

where λ_{max} and λ_{min} are, respectively, the maximal and the minimal *by moduli* eigenvalues of the matrix $[K]$. In numerical analysis, the solution $\boldsymbol{u}_{*n}$ is different from the exact solution $\boldsymbol{u}_*$, first due to the finite precision required by the user, ε, for instance like this $\|\boldsymbol{u}_{i+1} - \boldsymbol{u}_i\| \leq \varepsilon$, and second due to the finite number of digits in computer data types. The higher the condition number of the matrix, the lower the number of correctly evaluated digits in the solution. The number of lost digits N in the accuracy can be calculated according to the simple formula:

$$N = \log_{10} \text{Cond}(\boldsymbol{K})$$

So ill-conditioning of the matrix (high condition number) results in loss of accuracy and may also result even in divergence of the iterative schemes. For that reason, the so-called preconditioners should be used, which replace the problem $\boldsymbol{K}\boldsymbol{u} = \boldsymbol{f}$ with solution $\boldsymbol{u}_*$ by a problem $\tilde{\boldsymbol{K}}[u] = \tilde{\boldsymbol{f}}$ such that the solution remains the same but $\text{Cond}(\tilde{\boldsymbol{K}}) < \text{Cond}(\boldsymbol{K})$. In this context, it becomes evident that, if the PM increases the condition number of the stiffness matrix proportionally to the penalty coefficient, then a high penalty coefficient results in ill-conditioning of the matrix. It is also true for the ALM.

It is worth mentioning that the procedure of the stiffness matrix calculation is a major contribution to the computational time in the implicit FEM. That is the main motivation for the group of so-called quasi-Newton's methods, for which the stiffness matrix is approximated according to some rules (see, e.g. [BON 06]): DFP (Davidon–Fletcher–Powell formula), BFGS (Broyden–Fletcher–Goldfarb–Shanno method), Broyden method, etc. Another approach is to inverse the stiffness matrix only once at the zeroth iteration and calculate all solution increments with this matrix, which can be also updated as:

$$\Delta \boldsymbol{u}^i = -\boldsymbol{K}(\boldsymbol{u}^0)^{-1}\boldsymbol{R}(\boldsymbol{u}^i, \boldsymbol{f}_{k+1})$$

These methods allows us to avoid problems that appear if R is not strictly monotonic, that is possible zero determinant of the stiffness matrix. The convergence rate of such methods is slower, but each iteration is faster. There are many techniques based on Newton's method and resulting in faster convergence in physical and/or numerical sense, see [FLE 77, BON 06, BER 03]. Another class of methods often used in finite element codes is the method of conjugate gradient methods, however we will not consider them.

5.1.3. *Application to non-differentiable functions*

Let us return to conditions formulated for the 1D case, that is non-zero and Lipschitz continuous first derivative $L(\mathbb{U}) \ni \frac{\partial \boldsymbol{R}(\boldsymbol{u},.)}{\partial \boldsymbol{u}} \neq 0$ and Lipschitz continuity by parameter $R(., \boldsymbol{f}) \in L(\mathbb{F})$, where $\mathbb{U}$ and $\mathbb{F}$ are allowable sets for the argument $\boldsymbol{u}$ and the parameter $\boldsymbol{f}$, respectively. The condition for the parameter holds for contact problems: any small change of boundary conditions results in a smooth change in energy of the system and consequently in continuous change of its variation. However, due to geometrical restrictions on the displacement field we cannot require that function $\boldsymbol{R}(\boldsymbol{u}, .)$ (variation of the energy) would be everywhere smooth. It leads to a relatively new domain in optimization theory – non-smooth or non-differentiable optimization. According to the derived equations and the simple examples considered in Chapter 4, we know that the function $\boldsymbol{R}(\boldsymbol{u}, .)$ resulting from the virtual work principle is piecewise-smooth and so there is a set of points, also called "kinks" $\boldsymbol{u}^s \in \mathbb{V}^s \subset \mathbb{V}$, for which there is no unique but several one-sided derivatives.

$$\forall \boldsymbol{u}^s \in \mathbb{V}^s \ : \ \exists \bigcup_i \left\{ \left. \frac{\partial \boldsymbol{R}}{\partial \boldsymbol{u}} \right|_{\boldsymbol{u}^s} \right\}_i \neq \emptyset$$

However, the measure of such a set is zero in the whole space $\mathbb{V} \ni \boldsymbol{u}$

$$M\left(\mathbb{V}^s\right) = 0, \ M\left(\mathbb{V}\right) > 0$$

It means that in practice the probability during iterations $\boldsymbol{u} \in \mathbb{V}^s$ is zero, however often such points (kinks) appear to be solutions of minimization problems, it is also true in our case. It is clear that in the vicinity of such points the derivative is no longer Lipschitz continuous:

$$\nexists\, K\colon 0<K<\infty\colon \forall \boldsymbol{u}^1, \boldsymbol{u}^2\ \forall i,j\colon \left\| \left\{ \left.\frac{\partial \boldsymbol{R}}{\partial \boldsymbol{u}}\right|_{\boldsymbol{u}^1} \right\}_i - \left\{ \left.\frac{\partial \boldsymbol{R}}{\partial \boldsymbol{u}}\right|_{\boldsymbol{u}^2} \right\}_j \right\| \leq K \|\boldsymbol{u}^1 - \boldsymbol{u}^2\|$$

So, a complementary convergence analysis is required, since Kantorovich theorem [KAN 48] (statement of multidimensional convergence of Newton's method) requires a Lipschitz continuity of this derivative.

5.1.4. *Subdifferentials and subgradients*

In non-smooth optimization, the gradient is generalized to the class of non-differentiable functions in the following way, in the kink point a non-empty convex set is introduced as follows:

$$\boldsymbol{\partial} f(\boldsymbol{x}) = \left\{ \boldsymbol{s} \;\middle|\; \boldsymbol{s} \in \mathbb{R}^n,\ \forall \boldsymbol{y} \in \mathbb{R}^n\colon f(\boldsymbol{y}) \geq f(\boldsymbol{x}) + \boldsymbol{s}\cdot(\boldsymbol{y}-\boldsymbol{x}) \right\}$$

where by a dot we mean the scalar product of vectors in $\mathbb{R}^n$. Another more straightforward definition can be given in terms of directional derivatives, where the direction is defined by a vector $\boldsymbol{d} \in \mathbb{R}^n$:

$$\boldsymbol{\partial} f(\boldsymbol{x}) = \left\{ \boldsymbol{s} \;\middle|\; \boldsymbol{s} \in \mathbb{R}^n,\ \forall \boldsymbol{d} \in \mathbb{R}^n\colon \boldsymbol{s}\cdot\boldsymbol{d} \leq \lim_{\alpha\to 0} \frac{f(\boldsymbol{x}+\alpha\boldsymbol{d}) - f(\boldsymbol{x})}{\alpha} \right\}$$

This set is called a convex *subdifferential* of the function f at point x^k and each component of the subdifferential of f at x is called a *subgradient*.

In my opinion, it would even be preferable to use the definition given below and graphically illustrated by the 1D case in Figure 5.1. Let us imagine that the kink point $\boldsymbol{x}^k$ is surrounded by an hypersphere $\mathfrak{H} \in \mathbb{R}^{n+1}$:

$$\boldsymbol{x}, f \in \mathfrak{H}\colon \left(f(\boldsymbol{x}) - f(\boldsymbol{x}^k)\right)^2 + (\boldsymbol{x}-\boldsymbol{x}^k)\cdot(\boldsymbol{x}-\boldsymbol{x}^k) = R^2$$

where R is the radius of the hypersphere $\mathfrak{H}$ (Figure 5.1(b)). Then, if $f(x)$ is locally convex in the vicinity of the kink point, we can confine ourself to the lower half of the hypersphere $\mathfrak{H}_-$:

$$\boldsymbol{x}, f \in \mathfrak{H}_-: f_{\mathfrak{H}}(\boldsymbol{x}) = f(\boldsymbol{x}^k) - \sqrt{R^2 - (\boldsymbol{x} - \boldsymbol{x}^k) \cdot (\boldsymbol{x} - \boldsymbol{x}^k)} < f(\boldsymbol{x}^k)$$

The gradient of such a function $f_{\mathfrak{H}}(\boldsymbol{x})$ at all points of the lower hypersphere in all directions always exists and takes all values $(-\infty,\ \infty)$:

$$\nabla f_{\mathfrak{H}}(\boldsymbol{x}) \cdot \boldsymbol{d} = \frac{(\boldsymbol{x} - \boldsymbol{x}^k) \cdot \boldsymbol{d}}{\sqrt{R^2 - (\boldsymbol{x} - \boldsymbol{x}^k) \cdot (\boldsymbol{x} - \boldsymbol{x}^k)}} \in (-\infty,\ \infty) \text{ for all } \boldsymbol{x} \in \mathfrak{H}$$

Now we can tighten this lower hypersphere into a point $R \to 0$, then $f_{\mathfrak{H}}(x) \to f(x^k)$ but all gradients do not vanish but appear to be "condensed" in the kink point if we replace:

$$\boldsymbol{x} - \boldsymbol{x}^k = \alpha R \boldsymbol{e}'$$

where $\boldsymbol{e}'$ – is a vector filled with 1 and $\alpha \in (-1;\ 1)$. Then, for any $R \geq 0$

$$\nabla f_{\mathfrak{H}}(\boldsymbol{x}, \alpha) \cdot \boldsymbol{d} = \frac{\alpha \boldsymbol{e}' \cdot \boldsymbol{d}}{\sqrt{1 - \alpha^2}} \in (-\infty,\ \infty)\ \forall \alpha \in (-1;\ 1)$$

Let us denote by $\boldsymbol{e}_j = [0,\ \ldots\ 0,\ \underbrace{1}_{j},\ 0,\ \ldots\ , 0]^T$. This hypersphere point is put in the kink point and, further, we can define the positive and negative subdifferential components j such that if:

$$\boldsymbol{\partial} f_j^+ = \nabla f_{\mathfrak{H}}(\boldsymbol{x}, \alpha) \cdot \boldsymbol{e}_j,\ \forall \alpha: 0 \leq \alpha \leq \alpha_j^+$$

$$\boldsymbol{\partial} f_j^- = \nabla f_{\mathfrak{H}}(\boldsymbol{x}, \alpha) \cdot \boldsymbol{e}_j,\ \forall \alpha: \alpha_j^- \leq \alpha < 0$$

where $\partial f / \partial x_j^+$ and $\partial f / \partial x_j^- i$ define positive and negative one-sided derivative by the argument x_j, respectively, (Figure 5.1(b)), and

$$\alpha_j^+ \ :\ \nabla f_{\mathfrak{H}}(\boldsymbol{x}, \alpha_j^+) \cdot \boldsymbol{e}_j = \frac{\partial f}{\partial x_j^+}, \quad \alpha_j^- \ :\ -\nabla f_{\mathfrak{H}}(\boldsymbol{x}, \alpha_j^-) \cdot \boldsymbol{e}_j = \frac{\partial f}{\partial x_j^-}$$

The subdifferential is then defined as the union of positive and negative subdifferentials:

$$\boldsymbol{\partial} f = \boldsymbol{\partial} f^- \cup \boldsymbol{\partial} f^+$$

or in a more compact form (Figure 5.1(c))

$$\boldsymbol{\partial} f = \nabla f_{\mathfrak{H}}(\boldsymbol{x}, \boldsymbol{\alpha}),\ \forall \boldsymbol{\alpha}^- \leq \boldsymbol{\alpha} \leq \boldsymbol{\alpha}^+$$

where through condition $\boldsymbol{\alpha}^- \leq \boldsymbol{\alpha} \leq \boldsymbol{\alpha}^+$ we mean that $\forall j\ \alpha_j^- \leq \alpha_j \leq \alpha_j^+$. In other words, the subdifferential is defined as a set of derivatives of the hypersphere limited by one-sided derivatives of the function f: $\partial f/\partial x_j^-$ and $\partial f/\partial x_j^+$, obviously if $\partial f/\partial x_j^- = \partial f/\partial x_j^+$, then $\boldsymbol{\partial} f_j = \partial f/\partial x_j$. Such a definition is quite long but hopefully it provides a more intuitive and tangible visualization of the subdifferential notion. Moreover, in my opinion, it is easy to deal with a very small and smooth sphere than with simply a singular kink point. In case of a locally concave function f, the subdifferential defined on a hypersphere is easy to generalize. For this purpose, instead of the lower hemisphere, we should consider the upper hemisphere of the hypersphere $f_{\mathfrak{H}}$. The generalization is also straightforward in case of a concave–convex function f.

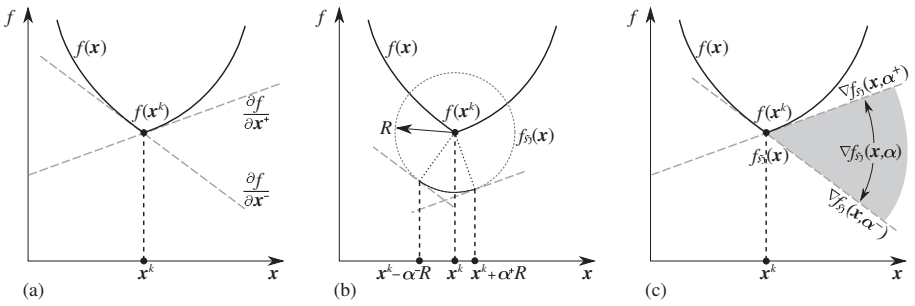

Figure 5.1. *Graphical representation of a subdifferential based on hypersphere notion: (a) kink point x_k of the non-smooth function $f(x)$ and two one-sided derivatives: left-sided $\frac{\partial f}{\partial x^-}\big|_{x^k}$ and right-sided $\frac{\partial f}{\partial x^+}\big|_{x^k}$; (b) a hypersphere $f_{\mathfrak{H}}(x^k)$ of finite radius R and limits on α: $\alpha^- = \frac{\partial f}{\partial x^-}\big|_{x^k}$, $\alpha^+ = \frac{\partial f}{\partial x^+}\big|_{x^k}$; and (c) subdifferential $\partial f = \nabla f_{\mathfrak{H}}(x, \alpha),\ \forall \alpha^- \leq \alpha \leq \alpha^+$*

A more sophisticated description of subdifferentials applied to contact mechanics can be found in the works of Alart and Curnier [ALA 91, HEE 93], Heegaard and

Curnier [ALA 97]. A general subdifferential theory can be found, for example, in [ROC 70].

Idea 5.1. Application of hyperspheres to normal projection procedure

The idea of the subdifferential and particularly of hypersphere can be directly applied to the definition of the normal projection of a slave node on the piecewise-smooth master surface. For this purpose, each master node $\underline{\boldsymbol{\rho}}^i$ *is replaced by a 3D sphere:*

$$S(\underline{\boldsymbol{\rho}}^i, R)\colon (\underline{\boldsymbol{\rho}} - \underline{\boldsymbol{\rho}}^i) \cdot (\underline{\boldsymbol{\rho}} - \underline{\boldsymbol{\rho}}^i) - R^2 = 0$$

and each edge curve $\underline{\boldsymbol{\rho}}^j(\zeta)$ *by a channel surface*[1] *(see figure below):*

$$C(\underline{\boldsymbol{\rho}}^j(\zeta), R)\colon (\underline{\boldsymbol{\rho}}(\zeta) - \underline{\boldsymbol{\rho}}^j(\zeta)) \cdot (\underline{\boldsymbol{\rho}}(\zeta) - \underline{\boldsymbol{\rho}}^j(\zeta)) - R^2 = 0$$

Further, we set $R \to 0$ *and* $S(\underline{\boldsymbol{\rho}}^i, R) \to S(\underline{\boldsymbol{\rho}}^i, 0)$, $C(\underline{\boldsymbol{\rho}}^j(\zeta), R) \to C(\underline{\boldsymbol{\rho}}^j(\zeta), 0)$. *The derivative* $\frac{\partial \underline{\boldsymbol{\rho}}}{\partial \underset{\sim}{\xi}}$ *always exists on the master surface, but on edges and on nodes the derivative is not unique.*

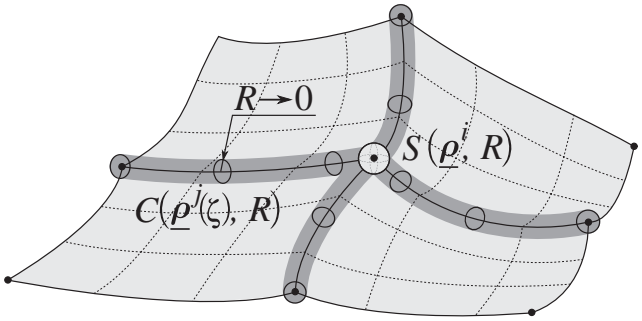

Figure. Improvement of the master surface with zero radius spheres on nodes and zero radius channel surfaces on edges in order to provide an everywhere differentiable surface

1 A channel or canal surface is a surface formed as the envelope of a family of spheres whose centers lie on a space curve (Wikipedia: http://en.wikipedia.org/wiki/Channel_surface)

5.1.5. *Generalized Newton method*

Even if the probability to meet a kink point (point where no classical derivative exists) during the iteration process is zero, the convergence of the Newton scheme is not anymore ensured by Kantorovich theorem. This is linked to the fact that the solution of the contact problem is itself a kink point. If the convergence is not monotonic, the probability of convergence decreases. Moreover, for non-smooth functional, it is sometimes not possible to fulfill the condition of minimum $\nabla f(x) = 0$ or even $\|\nabla f(x)\| \leq \varepsilon$. A simple example is a nonlinearity arising in Coulomb's friction law $f(x) = |x|$. The derivative of this function is resembling the sign function that takes the values -1 and 1 and so $\nexists |\nabla f(x)| < \varepsilon < 1$. There are other problems relevant to this kind of non-smoothness: 1) evaluation of gradients may give different results on different computers because of round off errors and 2) gradients of such functions approximated by a perturbation method may not belong to subdifferential derivative.

Since the late 1980s Alart [ALA 88], Alart and Curnier [ALA 91], Curnier and Alart [CUR 88] and Heegaard and Curnier [HEE 93] investigated an application of Newton's method to non-smooth problems arising in contact mechanics. Authors worked out a generalized Newton method (GNM) and investigated its convergence properties for coupled ALM [ALA 97]. Among obtained results there are:

– a good convergence observed for frictionless contact in case of small and large slip;

– conditions on convergence of the GNM for frictionless contact, however as asserted by the authors the conditions appear to be too strict and are not fulfilled in real problems;

– the maximal number of iterations for the convergence is estimated by 2^{n-1}, where n is number of dofs subjected to contact-type conditions, moreover, at least one local status (e.g. non-contact – contact) changes without ever a switch to the previous status;

– the absence of simple infinite cycling of the GNM around solution for frictionless problem, however this remains the main cause of divergence in the case of frictional contact;

– a very important result is the upper estimation for penalty coefficient in ALM applied to frictional problems, which avoids infinite cycling:

$$0 < \varepsilon_t < 2\lambda_{\min}(K)$$

where ε_t is the penalty factor related to tangential slip and K is a stiffness matrix corresponding to the problem without contact; here, the introduction of two penalty parameters, for normal ε_n and tangential ε_t contact, becomes justified.

Following the cited authors let us derive the main principles. First of all, the nonlinear vector equation $\boldsymbol{R}(\boldsymbol{x}, \boldsymbol{\lambda}) = 0$ arising from application of the ALM to contact problems is split into a differentiable structural part $\boldsymbol{R}^d(x)$ (due to virtual work of contact-free system) and a non-differentiable contact part $\boldsymbol{R}^n(\boldsymbol{x}, \boldsymbol{\lambda})$ (virtual work due to contact) parts:

$$\boldsymbol{R}(\boldsymbol{x}, \boldsymbol{\lambda}) = \boldsymbol{R}^d(x) + \boldsymbol{R}^n(\boldsymbol{x}, \boldsymbol{\lambda}) = 0$$

Further, the GNM is stated as:

$$\begin{bmatrix} \Delta \boldsymbol{x}^{i+1} \\ \\ \Delta \boldsymbol{\lambda}^{i+1} \end{bmatrix} = \begin{bmatrix} \frac{\partial \boldsymbol{R}^d(\boldsymbol{x})}{\partial \boldsymbol{x}} + \nabla_{\boldsymbol{x}} \boldsymbol{R}^n(\boldsymbol{x}, \boldsymbol{\lambda}) \\ \\ \nabla_{\boldsymbol{\lambda}} \boldsymbol{R}^n(\boldsymbol{x}, \boldsymbol{\lambda}) \end{bmatrix} \Bigg|^{-1}_{\boldsymbol{x}^i, \boldsymbol{\lambda}^i} \begin{bmatrix} \\ \boldsymbol{R}^d(x^i) + \boldsymbol{R}^n(\boldsymbol{x}^i, \boldsymbol{\lambda}^i) \\ \\ \end{bmatrix}$$

where $i, i+1$ denotes iteration numbers. The subgradients $\nabla_{\boldsymbol{x}} \boldsymbol{R}^n$ and $\nabla_{\boldsymbol{\lambda}} \boldsymbol{R}^n$ are components of the generalized Jacobians (here also, Hessians) $\partial_{\boldsymbol{\lambda}} R^n$ and $\partial_{\boldsymbol{\lambda}} R^n$ for primal and dual variables, respectively:

$$\nabla_{\boldsymbol{x}} \boldsymbol{R}^n(\boldsymbol{x}, \boldsymbol{\lambda}) \in \partial_{\boldsymbol{\lambda}} R^n(\boldsymbol{x}, \boldsymbol{\lambda}), \quad \nabla_{\boldsymbol{\lambda}} \boldsymbol{R}^n(\boldsymbol{x}, \boldsymbol{\lambda}) \in \partial_{\boldsymbol{\lambda}} R^n(\boldsymbol{x}, \boldsymbol{\lambda})$$

In other words, these notions are a generalization of the subdifferentials to the class of vector functions $\boldsymbol{f}(\boldsymbol{x})$ of vector argument $\boldsymbol{x}$: each i-th line of the generalized Jacobian is the subdifferential of the scalar component $f_i(\boldsymbol{x})$:

$$\partial \boldsymbol{f}(\boldsymbol{x}) = \begin{bmatrix} \partial f_1(\boldsymbol{x}) & \dots & \partial f_i(\boldsymbol{x}) & \dots & \partial f_n(\boldsymbol{x}) \end{bmatrix}^T$$

The condition providing the convergence of the ALM for the frictional problem has been formulated as "sufficient stability conjecture" in [ALA 91] and investigated in more details in [ALA 97]:

$$0 < \varepsilon_t < 2\lambda_{\min} \left(\nabla_{\boldsymbol{x}} \boldsymbol{R}^n(\boldsymbol{x}, \boldsymbol{\lambda}) \right)$$

A more sophisticated study of this condition can be found in theorem 6 in [ALA 97]. Let us give a short demonstration of the analysis performed by the author. Let us consider a scalar non-convex and non-differentiable function $f(x)$ (Figure 5.2). If this function is such that close to the solution its maximal derivative is $\sup |x - x^*| < \varepsilon f' = a$, to the right from the solution $x > x^*$ there are points where

the smallest derivative $f'(x) = b < a$ and to the left $\inf_{x<x^*}(f'(x)) = c < a$, then there is a risk that Newton's method does not converge, that is start to cycle over two branches (Figure 5.2(a)). Moreover, if the left branch is convex and the right branch is concave, each iteration will move away from the solution. A similar function arises from frictional contact problems, even the simplest one with one dof and prescribed contact pressure. However, Newton's method does not always diverge (Figure 5.2(b)). The question is then to check what is the condition on a, b, c that ensures the convergence of the method. P. Alart proved that Newton method or GNM converge if the maximal derivative of the function $f(x)$ is not bigger than twice the minimal derivative of the function $f(x)$ at least in a vicinity of possible iterations of the Newton's method ($\mathbb{N}(x)$):

$$\sup f'(x) < 2 \inf f'(x), x \in \mathbb{N}(x)$$

In case of a non-differentiable function, the ordinary derivatives f' are replaced by subdifferentials $\partial f'$:

$$\sup \partial f(x) < 2 \inf \partial f(x), x \in \mathbb{N}(x)$$

Further, the author generalizes this result to the n-dimensional case by comparing with convergence conditions of Uzawa's algorithm.

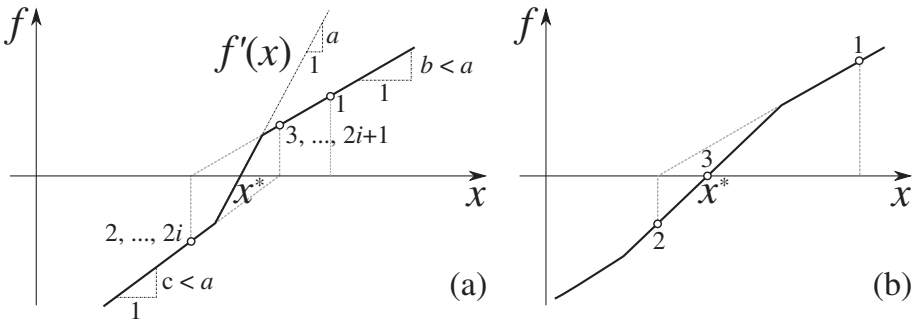

Figure 5.2. *Non-convex non-differentiable function $f(x)$ for which Newton's method or GNM may not converge: (a) methods do not converge if the starting point is located on the left or the right branch with a smaller slope, that the slope close to the solution point x^* and (b) methods always converge*

The one-dimensional convergence problem can be reformulated as a geometrical problem (Figure 5.3) as follows: Newton's method converges if for a, b, c, which were

introduced previously, and for three straight lines:

$$L_1\colon y = bx + d, \quad L_2\colon y = cx + e, \quad L_3\colon y = ax + g, \quad a > b,\ a > c$$

there is no horizontal line $L_c\colon y = h$, such that part of L_3 enclosed between L_1 and L_2 lies entirely in quadrangle $ABCD$, where $A = (x_A, h)$ is the intersection of L_1 and L_c, $D = (x_D, h)$ is the intersection of L_2 and L_c and $B = L_2(x_A),\ C = L_1(x_B)$.

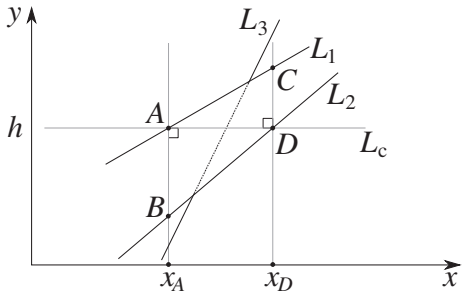

Figure 5.3. *Geometrical problem arising from convergence conditions of Newton's method*

5.2. Return mapping algorithm

The return mapping algorithm (in a 1D case) or radial return mapping algorithm originally proposed in [WIL 64] is a well-known scheme employed in computational elastoplasticity [SIM 98]. Since there is a direct analogy between plasticity and friction as stated in section 4.1.3, this method can be successfully applied to the local resolution of frictional conditions. The idea of this method in words few: elastic problem is solved, for a given strain increment, and a trial stress is evaluated. If the new stress is situated inside the yield surface, then this is the solution. Otherwise the slip rate increment is changed to return to the yield surface and the stress is updated. The application of the return mapping algorithm for frictional contact integration for the PM can be found in [GIA 89, WRI 90, SIM 92][2] and for the ALM with Uzawa's algorithm in [SIM 92]. For the sake of completeness, the return mapping algorithm is presented below.

2 Note that there is a small misprint in equation [3.13] in [SIM 92], where the penalty return mapping algorithm is stated, and the correct equation is given below.

The contribution of the contact to virtual work principle was stated in Chapter 4 as:

$$I_c(\underline{\boldsymbol{u}}, \delta\underline{\boldsymbol{u}}) = \int_{\overline{\Gamma}_c^{1\,*}} \sigma_n \left(\delta g_n - \mu \underline{\boldsymbol{s}} \cdot \delta \underline{\boldsymbol{g}}_t\right) d\overline{\Gamma}_c^1 + \int_{\overline{\Gamma}_c^{1\,\bullet}} \left(\sigma_n \delta g_n + \underline{\boldsymbol{\sigma}}_t \cdot \delta \underline{\boldsymbol{g}}_t\right) d\overline{\Gamma}_c^1 \quad [5.6]$$

where $\overline{\Gamma}_c^{1\,*}$ and $\overline{\Gamma}_c^{1\,\bullet}$ are slip and stick zones in active contact zones, respectively, σ_n is the contact pressure, $\underline{\boldsymbol{\sigma}}_t$ is the tangential contact stress vector, δg_n is the variation of the normal gap, $\delta \underline{\boldsymbol{g}}_t$ and is the variation of the tangential relative sliding. For a linear PM, contact pressure and tangential stress vector $\sigma_n, \underline{\boldsymbol{\sigma}}_t$ are linear functions of the normal gap and of the relative sliding $g_n, \Delta \underline{\boldsymbol{g}}_t$:

$$\sigma_n = -\varepsilon_n \langle -g_n \rangle, \quad \underline{\boldsymbol{\sigma}}_t = \begin{cases} \varepsilon_t \|\Delta \underline{\boldsymbol{g}}_t\| \, \underline{\boldsymbol{s}}, & \varepsilon_t \|\Delta \underline{\boldsymbol{g}}_t\| \leq \mu |\sigma_n| \\ \mu |\sigma_n| \, \underline{\boldsymbol{s}}, & \varepsilon_t \|\Delta \underline{\boldsymbol{g}}_t\| > \mu |\sigma_n| \end{cases}$$

where $\varepsilon_n, \varepsilon_t > 0$ is the penalty parameters and is $\underline{\boldsymbol{s}}$ the slip direction. Substituting contact pressure and tangential stress vector into equation. [5.6], we get:

$$I_c(\underline{\boldsymbol{u}}, \delta\underline{\boldsymbol{u}}) = -\int_{\overline{\Gamma}_c^{1\,*}} \varepsilon_n \langle -g_n \rangle \left(\delta g_n - \mu \underline{\boldsymbol{s}} \cdot \delta \underline{\boldsymbol{g}}_t\right) d\overline{\Gamma}_c^1 - \int_{\overline{\Gamma}_c^{1\,\bullet}} \left(\varepsilon_n \langle -g_n \rangle \delta g_n - \varepsilon_t \|\Delta \underline{\boldsymbol{g}}_t\| \, \underline{\boldsymbol{s}} \cdot \delta \underline{\boldsymbol{g}}_t\right) d\overline{\Gamma}_c^1$$

The constitutive equation for friction were given in [4.20] as:

$$\|\underline{\boldsymbol{\sigma}}_t\| \leq \mu |\sigma_n|, \quad \|\dot{\underline{\boldsymbol{g}}}_t\| \underline{\boldsymbol{\sigma}}_t - \mu |\sigma_n| \dot{\underline{\boldsymbol{g}}}_t = 0, \quad \|\underline{\boldsymbol{s}}\| \, \| \, \|\dot{\underline{\boldsymbol{g}}}_t\| \underline{\boldsymbol{\sigma}}_t - \mu |\sigma_n| \dot{\underline{\boldsymbol{g}}}_t \, \| = 0 \quad [5.7]$$

They can be reformulated in terms of elasto-plasticity: the slip surface $f(\sigma_n, \underline{\boldsymbol{\sigma}}_t)$ is given by:

$$f(\sigma_n, \underline{\boldsymbol{\sigma}}_t) = \|\underline{\boldsymbol{\sigma}}_t\| - \mu |\sigma_n| \leq 0$$

The slip rule is:

$$\dot{\underline{\boldsymbol{g}}}_t = \dot{\gamma} \frac{\partial f}{\partial \underline{\boldsymbol{\sigma}}_t}$$

where $\dot{\gamma}$ is a slip rate and $\partial f/\partial \underline{\boldsymbol{\sigma}}_t$ determines the normal to the slip surface and also the slip direction, which for Coulomb's friction is a radial unit vector.

$$\frac{\partial f}{\partial \underline{\boldsymbol{\sigma}}_t} = \frac{\underline{\boldsymbol{\sigma}}_t}{\|\underline{\boldsymbol{\sigma}}_t\|} = \underline{\boldsymbol{s}}_t$$

The numerical resolution of the contact problems is incremental, so let us suppose that on the i-th increment we know the solution $\underline{\boldsymbol{u}}^i$ and all corresponding quantities $\sigma_n^i, \underline{\boldsymbol{\sigma}}_t^i$. On the first iteration of the next increment, we suppose that the entire active contact zone switches to stick:

$$I_c(\underline{\boldsymbol{u}}^{i+1}, \delta\underline{\boldsymbol{u}}) = \int_{\overline{\Gamma}_c^{1\bullet}} \left(\sigma_n^{i+1}\delta g_n + \underline{\boldsymbol{\sigma}}_t^{i+1} \cdot \delta\underline{\boldsymbol{g}}_t\right) d\overline{\Gamma}_c^1$$

where

$$\sigma_n^{i+1} = -\varepsilon_n\langle -g_n(\underline{\boldsymbol{u}}^{i+1})\rangle.$$

Further, by analogy with plasticity, we determine the trial stick tangential stress vector:

$$\underline{\boldsymbol{\sigma}}_t^{i+1}{}_{\text{trial}} = \underline{\boldsymbol{\sigma}}_t^i + \varepsilon_t\left(\underline{\boldsymbol{g}}_t{}^{i+1} - \underline{\boldsymbol{g}}_t{}^i\right) = \underline{\boldsymbol{\sigma}}_t^i + \varepsilon_t\Delta\underline{\boldsymbol{g}}_t{}^i$$

A graphical interpretation of the return mapping algorithm is presented in Figures 5.4 and 5.5 for two-dimensional and in Figure 5.6 for three-dimensional cases. Now, we check if this stress vector does not exceed the permissible stress, that is it not outside of the Coulomb's slip surface for the new contact pressure σ_n^{i+1}:

$$f_{\text{trial}}^{i+1} = \|\underline{\boldsymbol{\sigma}}_t^{i+1}{}_{\text{trial}}\| - \mu|\sigma_n^{i+1}|$$

If $f_{\text{trial}}^{i+1} \leq 0$, the trial tangential stress is a correct stress:

$$\underline{\boldsymbol{\sigma}}_t^{i+1} = \underline{\boldsymbol{\sigma}}_t^{i+1}{}_{\text{trial}}, \quad \text{if } f_{\text{trial}}^{i+1} \leq 0$$

otherwise if $f_{\text{trial}}^{i+1} > 0$, the current point switches to slip state and a tangential stress is put:

$$\underline{\boldsymbol{\sigma}}_t^{i+1} = \underline{\boldsymbol{\sigma}}_t^{i+1}{}_{\text{trial}} - \varepsilon_t\Delta\gamma^i\underline{\boldsymbol{s}}_t^i, \quad \text{if } f_{\text{trial}}^{i+1} > 0$$

where $\underline{\boldsymbol{s}}_t^i$ is the slip direction determined by the trial stress and $\Delta\gamma$ is the slip increment, determining the slip distance:

$$\underline{\boldsymbol{s}}_t^i = \frac{\underline{\boldsymbol{\sigma}}_t^{i+1}{}_{\text{trial}}}{\|\underline{\boldsymbol{\sigma}}_t^{i+1}{}_{\text{trial}}\|}$$

$$\Delta\gamma^i = \frac{f_{\text{trial}}^{i+1}}{\varepsilon_t}$$

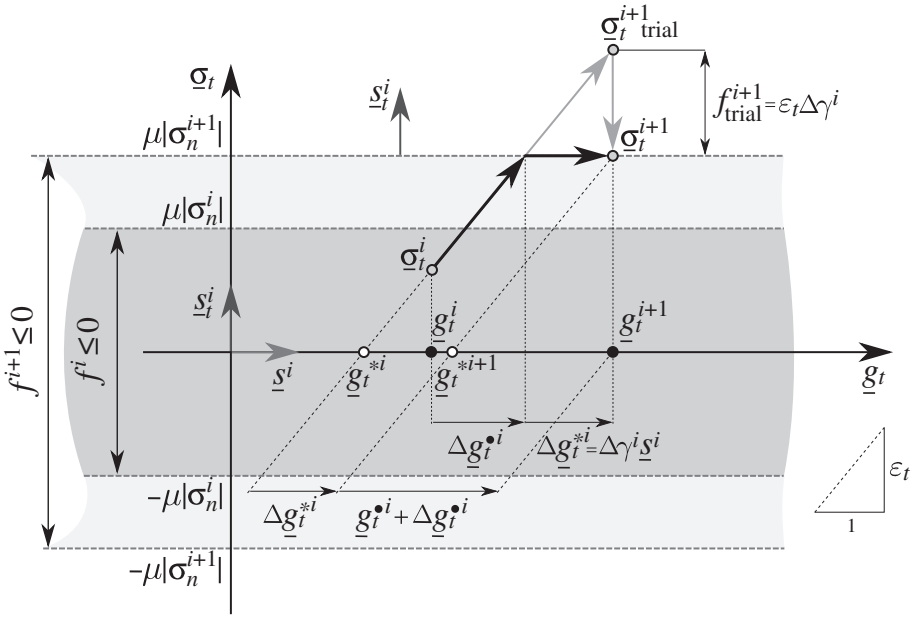

Figure 5.4. *Representation of the return mapping algorithm applied to a 2D contact problem. A sequential set of step points is represented by red contoured circles: initial state* $\{\underline{\boldsymbol{g}}_t{}^i,\ \underline{\boldsymbol{\sigma}}_t^i\}$, *trial step* $\{\underline{\boldsymbol{g}}_t{}^{i+1},\ \underline{\boldsymbol{\sigma}}_t^{i+1}{}_{trial}\}$, *return mapping on the slip surface gives the solution point* $\{\underline{\boldsymbol{g}}_t{}^{i+1},\ \underline{\boldsymbol{\sigma}}_t^{i+1}{}_{trial} - \varepsilon_t\Delta\gamma\,\underline{\boldsymbol{s}}_t^i\}$; *the initial center of stick or previously accumulated slip is* $\underline{\boldsymbol{g}}_t{}^{*i}$, *and "slip-in-stick" on the* i*th increment is given by* $\underline{\boldsymbol{g}}_t{}^{\bullet i} = \underline{\boldsymbol{g}}_t{}^i - \underline{\boldsymbol{g}}_t{}^{*i}$, *the total slip during increment is* $\underline{\boldsymbol{g}}_t{}^{i+1} - \underline{\boldsymbol{g}}_t{}^i$, *which is the sum of "slip-in-stick" increment* $\Delta\underline{\boldsymbol{g}}_t{}^{\bullet i}$ *and real slip, accumulated during increment,* $\Delta\underline{\boldsymbol{g}}_t{}^{*i}$, *final solution vector* $\underline{\boldsymbol{g}}_t{}^{i+1}$ *consists of accumulated slip* $\underline{\boldsymbol{g}}_t{}^{*i+1} = \underline{\boldsymbol{g}}_t{}^{*i} + \Delta\underline{\boldsymbol{g}}_t{}^{*i}$ *and actual "slip-in-stick"* $\underline{\boldsymbol{g}}_t{}^{\bullet i+1} = \underline{\boldsymbol{g}}_t{}^{\bullet i} + \Delta\underline{\boldsymbol{g}}_t{}^{\bullet i}$

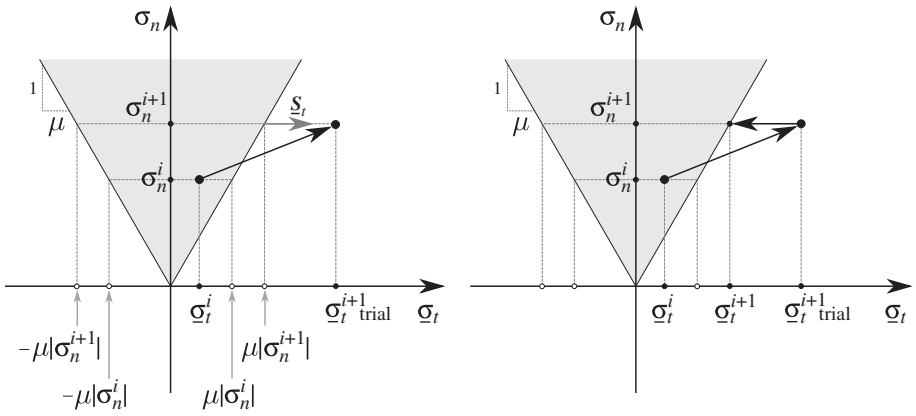

Figure 5.5. *Representation of the return mapping algorithm for a 2D problem in stress space. A sequential set of step points is represented by black circles: initial state* $\{\underline{\boldsymbol{\sigma}}_t^i,\ \sigma_n^i\}$*, trial step* $\{\underline{\boldsymbol{\sigma}}_t^{i+1}{}_{trial},\ \sigma_n^{i+1}\}$ *and non-associated return mapping gives the solution state* $\{\underline{\boldsymbol{\sigma}}_t^{i+1},\ \sigma_n^{i+1}\}$

Both results $\forall f_{\text{trial}}^{i+1}$, can be stated in one formula using Macaulay brackets

$$\boxed{\underline{\boldsymbol{\sigma}}_t^{i+1} = \underline{\boldsymbol{\sigma}}_t^{i+1}{}_{\text{trial}} - \varepsilon_t \langle \Delta\gamma^i \rangle \underline{\boldsymbol{s}}_t^i} \qquad [5.8]$$

Note that in the two-dimensional case, the sliding vector $\underline{\boldsymbol{s}}^i$ and the stress unit vector $\underline{\boldsymbol{s}}_t^i$ turn simply into $\text{sign}(\underline{\boldsymbol{g}}_t)$ and $\text{sign}(\underline{\boldsymbol{\sigma}}_t)$, respectively, obviously $\text{sign}(\underline{\boldsymbol{g}}_t) = \text{sign}(\underline{\boldsymbol{\sigma}}_t)$.

As discussed in Chapter 4, the total slip can be split into a sum of "slip-in-stick" $\underline{\boldsymbol{g}}_t{}^\bullet$ and real slip $\underline{\boldsymbol{g}}_t{}^*$:

$$\underline{\boldsymbol{g}}_t = \underline{\boldsymbol{g}}_t{}^\bullet + \underline{\boldsymbol{g}}_t{}^*$$

This split becomes more clear in the incremental procedure. Let us briefly demonstrate by simple algebraic calculations and geometrical schemes the meaning of such a split in the frame of the return mapping algorithm. On each increment the relative sliding vector splits into an accumulated slip over the previous increments $\underline{\boldsymbol{g}}_t{}^{*i}$ and the total "slip-in-stick" relatively to this point $\underline{\boldsymbol{g}}_t{}^{\bullet i}$:

$$\underline{\boldsymbol{g}}_t{}^i = \underline{\boldsymbol{g}}_t{}^{\bullet i} + \underline{\boldsymbol{g}}_t{}^{* i}, \quad \underline{\boldsymbol{g}}_t{}^{i+1} = \underline{\boldsymbol{g}}_t{}^{\bullet i+1} + \underline{\boldsymbol{g}}_t{}^{* i+1} \qquad [5.9]$$

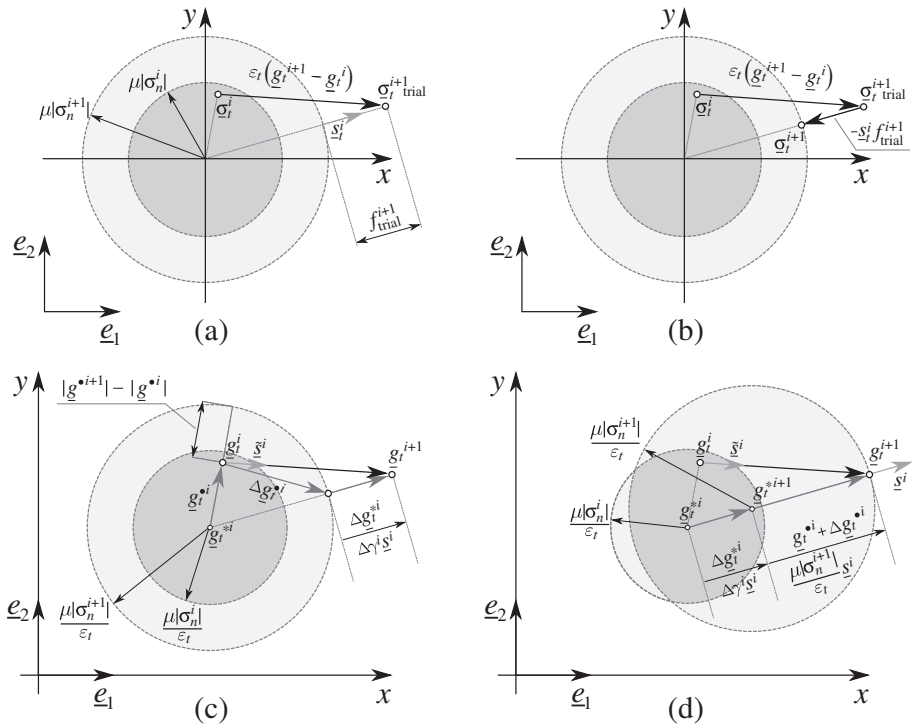

Figure 5.6. *Representation of the return mapping algorithm for three-dimensional contact problem,* $\{\underline{\boldsymbol{e}}_1, \underline{\boldsymbol{e}}_2\}$ *orthonormal basis with coordinates* $\{x, y\}$*; (a) and (b) represent stress state in contact interface, (c) and (d) represent displacements in contact interface; sequential set of step points is represented by contoured circles for stress (a,b) and for displacement (c,d): initial state* $\left\{\underline{\boldsymbol{g}}_t{}^i,\ \underline{\boldsymbol{\sigma}}_t^i\right\}$*, trial step* $\left\{\underline{\boldsymbol{g}}_t{}^{i+1},\ \underline{\boldsymbol{\sigma}}_t^{i+1}{}_{trial}\right\}$*, return mapping or radial return mapping on the slip surface* ***(b.)*** *gives the solution point for stress and moving of slip circle in direction* $\underline{\boldsymbol{s}}^i$ *by value of real slip* $\Delta\gamma^i$ *gives the solution state for displacements* ***(d.)*** $\left\{\underline{\boldsymbol{g}}_t{}^{i+1},\ \underline{\boldsymbol{\sigma}}_t^{i+1}{}_{trial} - \varepsilon_t \Delta\gamma\, \underline{\boldsymbol{s}}_t^i\right\}$*; increment of position vector* $\Delta\underline{\boldsymbol{g}}_t{}^i = \|\underline{\boldsymbol{g}}_t{}^{i+1} - \underline{\boldsymbol{g}}_t{}^i\|\, \tilde{\underline{\boldsymbol{s}}}^i$ *can be presented as the sum of differently oriented vectors* $\Delta\underline{\boldsymbol{g}}_t{}^{*i}$ *and* $\Delta\underline{\boldsymbol{g}}_t{}^{\bullet i}$ *corresponding to an increment of real slip and an increment of "slip-in-stick", respectively; however, as discussed above, it is more natural to consider a displacement increment starting from stick point* $\underline{\boldsymbol{g}}_t{}^{*i}$ *on the* i*th increment, then* $\underline{\boldsymbol{g}}_t{}^{*i} + \Delta\underline{\boldsymbol{g}}_t{}^i = \Delta\underline{\boldsymbol{g}}_t{}^{*i} + \underline{\boldsymbol{g}}_t{}^{\bullet i} + \Delta\underline{\boldsymbol{g}}_t{}^{\bullet i}$*, where* $\Delta\underline{\boldsymbol{g}}_t{}^{*i} = \Delta\gamma^i \underline{\boldsymbol{s}}^i$ *– real slip increment and actual "slip-in-stick" is presented by* $\underline{\boldsymbol{g}}_t{}^{\bullet i} + \Delta\underline{\boldsymbol{g}}_t{}^{\bullet i} = \frac{\mu|\sigma_n^{i+1}|}{\varepsilon_t}\underline{\boldsymbol{s}}^i$*, for Coulomb's friction* $\underline{\boldsymbol{s}}^i = \underline{\boldsymbol{s}}_t^i \neq \tilde{\underline{\boldsymbol{s}}}^i$

Further, the position vector on the increment $i+1$ can be expressed as the sum of the vectors on the previous increment of slip-in-stick $\Delta\underline{\boldsymbol{g}}_t{}^{\bullet i}$ and of slip increments $\Delta\underline{\boldsymbol{g}}_t{}^{* i}$:

$$\underline{\boldsymbol{g}}_t{}^{i+1} = \underline{\boldsymbol{g}}_t{}^{i} + \Delta\underline{\boldsymbol{g}}_t{}^{* i} + \Delta\underline{\boldsymbol{g}}_t{}^{\bullet i}, \quad \text{or simply} \quad \Delta\underline{\boldsymbol{g}}_t{}^{i} = \Delta\underline{\boldsymbol{g}}_t{}^{* i} + \Delta\underline{\boldsymbol{g}}_t{}^{\bullet i} \quad [5.10]$$

where

$$\Delta\underline{\boldsymbol{g}}_t{}^{\bullet i} = \underline{\boldsymbol{g}}_t{}^{\bullet i+1} - \underline{\boldsymbol{g}}_t{}^{\bullet i}, \quad \Delta\underline{\boldsymbol{g}}_t{}^{* i} = \underline{\boldsymbol{g}}_t{}^{* i+1} - \underline{\boldsymbol{g}}_t{}^{* i}, \quad \Delta\underline{\boldsymbol{g}}_t{}^{i} = \underline{\boldsymbol{g}}_t{}^{i+1} - \underline{\boldsymbol{g}}_t{}^{i}$$

In other words, it follows from equation [5.10] that $\underline{\boldsymbol{g}}_t{}^{i} + \Delta\underline{\boldsymbol{g}}_t{}^{* i}$ is the new position of stick, where the point will return if external load vanishes. However, equation [5.10] is not easy to interpret, because slip occurs relatively to the point of previous stick $\underline{\boldsymbol{g}}_t{}^{* i}$ and the direction of the total sliding increment $\underline{\tilde{\boldsymbol{s}}}^{i}$ does not make sense:

$$\underline{\tilde{\boldsymbol{s}}}^{i} = \frac{\Delta\underline{\boldsymbol{g}}_t{}^{i}}{\|\Delta\underline{\boldsymbol{g}}_t{}^{i}\|}$$

Since this is the direction of the sum of "slip-in-stick" and slip vectors, but not of an occurred slip. All directions, in general, are different[3], that is:

$$\Delta\underline{\boldsymbol{g}}_t{}^{* i} \not\parallel \Delta\underline{\boldsymbol{g}}_t{}^{\bullet i} \not\parallel \Delta\underline{\boldsymbol{g}}_t{}^{i} = \underline{\tilde{\boldsymbol{s}}}^{i}\, \|\Delta\underline{\boldsymbol{g}}_t{}^{i}\|$$

On the other hand, if $\underline{\boldsymbol{g}}_t{}^{i}$ is split into "slip-in-stick" and accumulated slip parts, then equation [5.10] can be rewritten as:

$$\underline{\boldsymbol{g}}_t{}^{i+1} = \underline{\boldsymbol{g}}_t{}^{* i} + \Delta\underline{\boldsymbol{g}}_t{}^{* i} + \underline{\boldsymbol{g}}_t{}^{\bullet i} + \Delta\underline{\boldsymbol{g}}_t{}^{\bullet i} \quad [5.11]$$

where

$$\left\{\underline{\boldsymbol{g}}_t{}^{\bullet i} + \Delta\underline{\boldsymbol{g}}_t{}^{\bullet i}\right\} \;\parallel\; \Delta\underline{\boldsymbol{g}}_t{}^{* i} \;\parallel\; \left\{\underline{\boldsymbol{g}}_t{}^{i+1} - \underline{\boldsymbol{g}}_t{}^{* i}\right\}$$

3 All these arguments are related to three-dimensional contact. In 2D problems, where all vectors at the interface can be interpreted simply as signed real numbers $\text{sign}(\underline{\tilde{\boldsymbol{s}}}^{i}) = \text{sign}(\underline{\boldsymbol{s}}^{i}) = \text{sign}(\underline{\boldsymbol{s}}_t^{i})$, the present discussion is not relevant.

that is all these vectors can be rewritten as products of norms and sliding vector $\underline{\boldsymbol{s}}^i$:

$$\begin{aligned}
&\underline{\boldsymbol{g}}_t{}^{\bullet i} + \Delta\underline{\boldsymbol{g}}_t{}^{\bullet i} = \| \underline{\boldsymbol{g}}_t{}^{\bullet i} + \Delta\underline{\boldsymbol{g}}_t{}^{\bullet i} \| \underline{\boldsymbol{s}}^i \\
&\underline{\boldsymbol{g}}_t{}^{i+1} - \underline{\boldsymbol{g}}_t{}^{*i} = \| \underline{\boldsymbol{g}}_t{}^{i+1} - \underline{\boldsymbol{g}}_t{}^{*i} \| \underline{\boldsymbol{s}}^i \\
&\Delta\underline{\boldsymbol{g}}_t{}^{*i} = \| \Delta\underline{\boldsymbol{g}}_t{}^{*i} \| \underline{\boldsymbol{s}} = \Delta\gamma\, \underline{\boldsymbol{s}}^i
\end{aligned} \qquad [5.12]$$

Equation [5.11] can be stated in an algebraic form:

$$\boxed{\Delta\gamma = \| \underline{\boldsymbol{g}}_t{}^{i+1} - \underline{\boldsymbol{g}}_t{}^{*i} \| - \| \underline{\boldsymbol{g}}_t{}^{\bullet i} + \Delta\underline{\boldsymbol{g}}_t{}^{\bullet i} \|}$$

In other words, slip increment is the difference between total slip from the point of the previous stick $\| \underline{\boldsymbol{g}}_t{}^{i+1} - \underline{\boldsymbol{g}}_t{}^{*i} \|$ and final "slip-in-stick" $\| \underline{\boldsymbol{g}}_t{}^{\bullet i} + \Delta\underline{\boldsymbol{g}}_t{}^{\bullet i} \|$.

Note that independently on the direction of the increment of tangential stress $\underline{\boldsymbol{\sigma}}_t^{i+1} - \underline{\boldsymbol{\sigma}}_t^i$ or tangential slip $\underline{\boldsymbol{g}}_t{}^{i+1} - \underline{\boldsymbol{g}}_t{}^i$, the slip is supposed to occur in the direction of the resultant trial stress $\underline{\boldsymbol{\sigma}}_t^{i+1}{}_{\text{trial}}$. For an anisotropic friction law, the slip direction depends upon the choice of the model: associated and non-associated slip can be distinguished (see [MIC 78]).

Remark that in a large deformation – large sliding problems, a rigorous definition must be used for the relative sliding velocity expressed through the convective coordinates $\underset{\sim}{\xi}$, as discussed in section 2.2.6:

$$\dot{\underline{\boldsymbol{g}}}_t = \frac{\partial \underline{\boldsymbol{\rho}}}{\partial \underset{\sim}{\xi}} \circ \dot{\underset{\sim}{\xi}}$$

where $\dot{\underline{\boldsymbol{g}}}_t$ denotes Lie's derivative of the relative tangential displacement vector. For a detailed analysis of such a formulation, the reader is referred to works by Laursen and Simo [LAU 93], Laursen [LAU 94] and recent articles by Konyukhov and Schweizerhof [KON 05, KON 06b, KON 07a].

5.3. Finite element method

In this section, the main notions of the FEM will be given: mesh, elements, nodes, basis functions. Non-structural contact elements will be introduced and the evaluation of contact integrals will be discussed.

5.3.1. *Introduction*

The FEM is a powerful and widely used method for the numerical resolution of boundary value problems:

$$\mathfrak{F}\left(f(\underline{\boldsymbol{u}})\right) = 0 \quad + \quad \text{boundary and initial conditions}$$

where $\mathfrak{F}(f)$ is a combination of differential operators applied to a tensor function $f(\underline{\boldsymbol{u}})$ of vector argument $\underline{\boldsymbol{u}}$ (in structural mechanical problem). The method is applicable for arbitrary geometries as well as for linear and nonlinear constitutive equations. The idea is to replace a continuous problem (i.e. infinitely dimensional) by a finite dimensional problem. The method belongs to the class of Bubnov–Galerkin methods, that is the solution of the problem $\underline{\boldsymbol{u}}^*$ is approximated by a decomposition over a finite number of basis function $\phi_i(\underline{\boldsymbol{X}}_i),\ i = 1, N$:

$$\underline{\boldsymbol{u}}^*(t, \underline{\boldsymbol{X}}) \approx \underline{\boldsymbol{u}}^h(t, \underline{\boldsymbol{X}}) = \sum_{i=1}^{N} \underline{\boldsymbol{u}}_i^h(t)\, \phi_i(\underline{\boldsymbol{X}}) \qquad [5.13]$$

where t is the time, $\underline{\boldsymbol{X}}$ denotes a material point vector in reference configuration, and $\underline{\boldsymbol{u}}_i^h(t)$ is a coefficient at the i-th basis function. For structural problems, this coefficient is a vector. The basis functions can be chosen in such a way that $\underline{\boldsymbol{u}}_i^h(t)\, \phi_i(\underline{\boldsymbol{X}}_i) = \underline{\boldsymbol{u}}_i^h(t)$ is the solution value at the ith *node* – material point $\underline{\boldsymbol{X}}_i$. It implies that the ith basis function is one in the associated node i and zero in all other nodes $j \neq i$.

$$\phi_i(\underline{\boldsymbol{X}}_j) = \delta_i^j$$

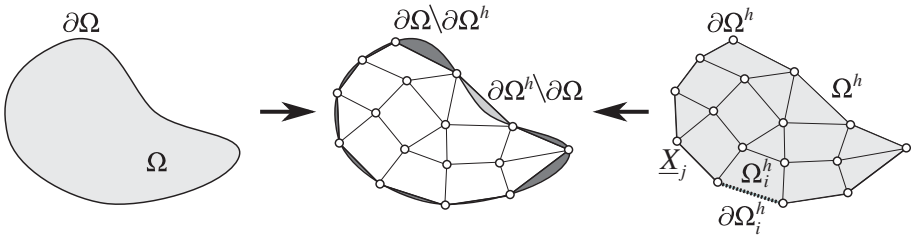

Figure 5.7. *Continuous body Ω and its discretized representation – finite element mesh Ω^h consisting of nodes $\underline{\boldsymbol{X}}_j$ and elements Ω_i^h. Surface of the body $\partial\Omega$, approximated by surface $\partial\Omega^h = \bigcup_i \partial\Omega_i^h$*

The considered volume Ω – body – at which differential equation $\mathfrak{F}(f(\underline{\boldsymbol{u}}))$ is prescribed is split into *finite elements* $\Omega_i^h,\ i = 1, N^e$ spanned onto *nodes* $\underline{\boldsymbol{X}}^j$, which all together form a *finite element mesh* – a discretized representation of the body $\Omega^h = \bigcup_{i=1,N^e} \Omega_i^h \sim \Omega$ (Figure 5.7). If the body Ω is continuous and non-self-intersecting, then for *almost* all points of the body $\underline{\boldsymbol{X}}$ there is a discrete form:

$$\underline{\boldsymbol{X}} = \sum_{j=1}^{M} \underline{\boldsymbol{X}}_j \psi_j(\underline{\boldsymbol{X}}) \qquad [5.14]$$

where $\psi_j(\underline{\boldsymbol{X}})$ is another set of basis functions describing the geometry and N^n number of such functions and number of nodes. Note that for a finite number of basis functions, some of the points of the continuous body Ω have no homologue in the discretized geometry and vice versa, that is in general:

$$\Omega \setminus \Omega^h \neq \emptyset, \quad \Omega^h \setminus \Omega \neq \emptyset$$

This difference appears only close to the boundary, which is essential for accurately imposing boundary conditions and especially for contact treatment: in general, the real surface of the body is different from the surface of the finite element mesh:

$$\partial\Omega \neq \partial\Omega^h = \bigcup_{i=1,N^s} \partial\Omega_i^h$$

Another observation: in general, the geometrical basis functions (shape functions) are compact, that is zero outside the element (see Figures 5.8, 5.9), for example, for element i spanned on N_i^n nodes, the shape functions $\phi_i^j(\underline{\boldsymbol{X}}),\ j = 1, N_i^n$ are defined as:

$$\phi_i^j(\underline{\boldsymbol{X}}) = 0,\ \underline{\boldsymbol{x}} \notin \Omega_i^h \quad \text{and} \quad \phi_i^j(\underline{\boldsymbol{X}}_k) = \delta_k^j,\ \underline{\boldsymbol{X}}_k \in \Omega_i^h$$

Shape functions are normally infinitely differentiable $\phi_i \in C^\infty$, but since they are compact on the element, on the interface between elements any smooth function approximated by shape functions is, in general, not differentiable, that is:

$$\nabla\phi_i^j(\underline{\boldsymbol{X}}_j) \neq \nabla\phi_k^j(\underline{\boldsymbol{X}}_j)$$

where $\underline{\boldsymbol{X}}_i$ is a common node of elements i and k.

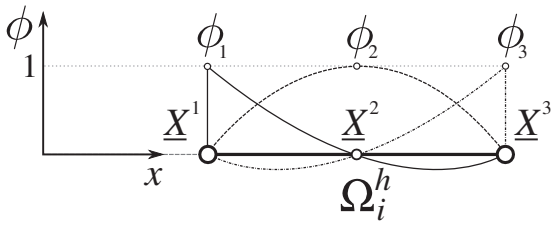

Figure 5.8. *Example of compact shape functions $\phi_i(\underline{\boldsymbol{X}})$ for the 1D 3-node quadratic element Ω_i^h*

Often the set of geometrical basis functions $\psi_j(\underline{\boldsymbol{X}})$ is chosen the same as the set of basis functions approximating the solution $\phi_i(\underline{\boldsymbol{X}})$ (isoparametric approximation of the problem). Further, all basis functions will be called shape functions and denoted with ϕ:

$$\underline{\boldsymbol{X}} = \sum_{i=1}^{N} \underline{\boldsymbol{X}}_i \phi_i(\underline{\boldsymbol{X}})$$

An isoparametric choice of the basis functions is rather natural for structural problems, if we seek for the field of displacement vectors, then the actual configuration of *almost* each point can be presented as:

$$\underline{\boldsymbol{x}} = \underline{\boldsymbol{X}} + \underline{\boldsymbol{u}} = \sum_{i=1}^{N} (\, \underline{\boldsymbol{X}}_i + \underline{\boldsymbol{u}}_i \,) \phi_i(\underline{\boldsymbol{X}})$$

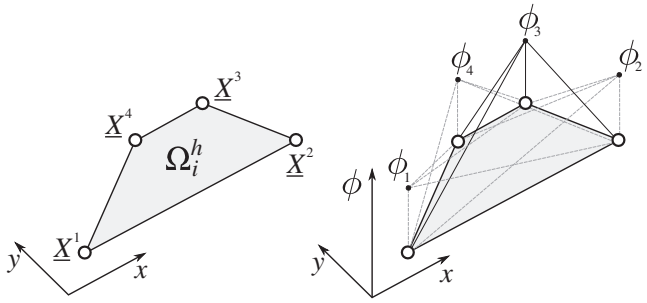

Figure 5.9. *Example of compact shape functions $\phi_i(\underline{\boldsymbol{X}})$ for 2D 4-node linear element Ω_i^h*

The index h often stands to demonstrate that the current decomposition by basis functions is finite dimensional, and h represents a maximal size of *finite elements*

into which geometry is split, then the solution of the discretized problem tends to the precise solution if the maximal size of the finite elements h tends to zero, or equal if the number of basis functions N tends to infinity:

$$\underline{\boldsymbol{u}}^h \xrightarrow{h\to 0} \underline{\boldsymbol{u}}^*$$

Since, further, we will deal only with discretized quantities, the h index will be omitted.

It is often convenient to determine the shape functions independently of the reference coordinates $\underline{\boldsymbol{X}} \in \Omega$. For this purpose, for each type of element, a standard simple reference configuration – the parent space $\widetilde{\Omega}$ – is defined (Figure 5.10) and then the approximation of the geometry/solution within the i-th finite element can be reformulated as:

$$\forall \underline{\boldsymbol{X}} \in \Omega_i, \quad \xi, \eta \in \widetilde{\Omega}_i, \quad \underline{\boldsymbol{u}}(t, \underline{\boldsymbol{X}}) = \sum_{j=1, N_i^n} \underline{\boldsymbol{u}}_j^i(t) \phi_j^i(\xi, \eta)$$

where $\underline{\boldsymbol{u}}_j^i$ is the j-th node of the i-th element and ϕ_j^i is the j-th shape function of the i-th element and $\{\xi, \eta\}$ are *convective* coordinates of the point $\underline{\boldsymbol{X}}$ in the parent space $\widetilde{\Omega}^i$. For contact problems, it is particularly important to consider the mapping from the parent configuration to the actual configuration for the contact surface Γ_c – a part of the body $\partial\Omega = \cup_i \partial\Omega_i$. The closure of 2D simply connected bodies is a curve and of 3D bodies is a surface, so the dimension of the topology is one less compared to the dimension of the problem. In Chapter 2, we considered the mapping from a 2D parent space into a 3D vector space (3D tensor space of first order):

$$\mathbb{R}^2 \ni \{\xi, \eta\} \quad \rightarrow \quad \underline{\boldsymbol{\rho}}(\xi, \eta) \in \mathbb{T}_1^3$$

and also the mapping from 1D parent space to a 2D vector space:

$$\mathbb{R} \ni \{\zeta\} \quad \rightarrow \quad \underline{\boldsymbol{\rho}}(\zeta) \in \mathbb{T}_1^2$$

In Chapter 2, we made use of the s-structures (Appendix A1.6). In the new formalism, instead of $\mathbb{R}^2$ parent space, it is considered as a 2D v-scalar space ${}^2_1\mathbb{S}^3_0$ over scalars of 3D space or simply as a 2D vector space $\mathbb{T}_1^2$. The mapping we need (Figure 5.11) becomes then:

$${}^2_1\mathbb{S}^3_0 \ni \underset{\sim}{\xi} \quad \rightarrow \quad \underline{\boldsymbol{\rho}}(\underset{\sim}{\xi}) \in \mathbb{T}_1^3$$

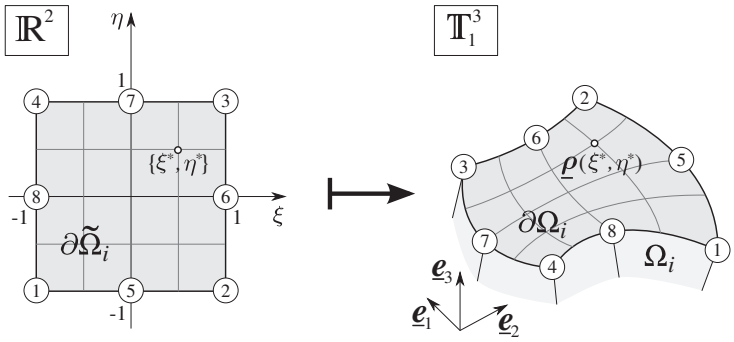

Figure 5.10. *Surface segment of element: mapping from 2D reference space* $\mathbb{R}^2 \ni \{\xi,\eta\}$ *to 3D vector space* $\underline{\boldsymbol{\rho}}(\xi,\eta) \in \mathbb{T}^3_1$

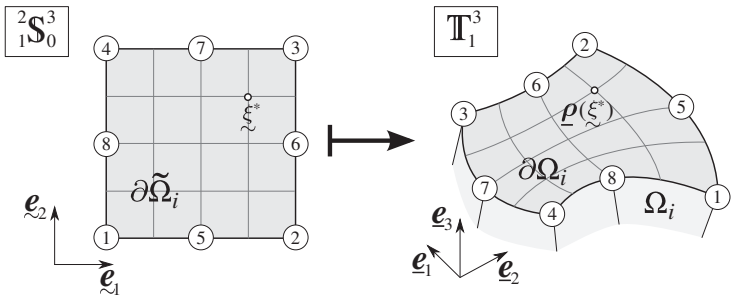

Figure 5.11. *Surface segment of element: mapping from 2D v-scalar space* $^2_1\mathbb{S}^3_0$ *to 3D vector space* $\mathbb{T}^3_1$

Moreover, the set of shape functions $\phi^i_j(\underset{\sim}{\xi}),\ j=1,N^n_i$ can be replaced by another v-scalar of dimension N^n_i:

$$\phi^i_j(\underset{\sim}{\xi}) \quad \sim \quad \underset{\sim}{\phi}^i(\underset{\sim}{\xi}) \in {}^{N^n_i}_1\mathbb{S}^3_0$$

and on the other hand, the set of nodal vectors $\underline{\boldsymbol{u}}^i_j,\ j=1,N^n_i$ can be replaced by a v-vector:

$$\underline{\boldsymbol{u}}^i_j \quad \sim \quad \underset{\sim}{\underline{\boldsymbol{u}}}^i \in {}^{N^n_i}_1\mathbb{S}^3_1$$

Then the finite element approximation of a vector field $\underline{\boldsymbol{u}}$ within the surface of the i-th element can be written as:

$$\boxed{\forall \underline{\boldsymbol{X}} \in \partial\Omega_i, \quad \underset{\sim}{\xi}(\underline{\boldsymbol{X}}) \in \partial\widetilde{\Omega}_i, \quad \underline{\boldsymbol{u}}(t,\underline{\boldsymbol{X}}) = \underset{\sim}{\underline{\boldsymbol{u}}}^i(t) \circ \underset{\sim}{\phi}^i(\underset{\sim}{\xi})}$$

Note that the dimensions of $\underset{\sim}{\xi} \in {}^2_1\mathbb{S}^3_0$ and $\underset{\sim}{\phi}^i \in {}^{N^n_i}_1\mathbb{S}^3_0$, $\underset{\sim}{\underline{\boldsymbol{u}}}^i \in {}^{N^n_i}_1\mathbb{S}^3_1$ are different.

5.3.2. *Contact elements*

When two separated surfaces Γ_c^1 and Γ_c^2 come in contact from a continuum mechanics point of view, they form a continuous contact interface. Through this zone, contact stresses are transferred from one body to another according to a constitutive law due to the physical, mechanical and chemical phenomena occurring in the contact interface. From a numerical point of view, each contacting surface is represented by a number of nodes and surfaces or line segments – these components are not connected, so do not interact. In Chapter 4, contact surfaces and related contact stresses have been incorporated in the integral weak form – balance of virtual works – that implies that work of contact stresses has to be integrated for given virtual displacements within the contact interface. Due to the balance of forces in the contact interface, the integration can be performed over any of its sides.

The side over which the integrals will be evaluated is a master surface Γ_c^2. In the FEM, it is presented as a set of master segments:

$$\Gamma_c^2 = \bigcup_{i=1}^{M} \partial\Omega_i$$

Another side of the contact interface is the slave surface, which in the node-to-segment (NTS) approach is presented by nodes:

$$\Gamma_c^1 = \bigcup_{i=1}^{S} \underline{\boldsymbol{x}}_i$$

As discussed in Chapter 3, for all slave nodes, one or several master components are determined. For the sake of simplicity, let us suppose that for all contact nodes, sufficiently close to the master surface, there exists the closest master segment. Then, the integral of the virtual work over the master surface, can be split into a sum of M integrals over the master segments $\partial\Omega^i,\ i = 1, M$. One slave node is attached at least to each segment, $\underline{\boldsymbol{x}}_j^i,\ j = 1, N^i$, where N^i is a number of slave nodes attached to the segment i:

$$\int_{\Gamma_c^2} F(g_n, \dot{\underline{\boldsymbol{g}}}_t, \sigma_n, \underline{\boldsymbol{\sigma}}_t, \delta g_n, \delta \underline{\boldsymbol{g}}_t, \delta\sigma_n, \delta\underline{\boldsymbol{\sigma}}_t)\, d\Gamma_c^2 = \sum_{i=1}^{M} \int_{\partial\Omega_i} \sum_{j=1}^{N^i} F\big(\{g_n\}_j^i, \{\dot{\underline{\boldsymbol{g}}}_t\}_j^i, \{\sigma_n\}_j^i, \{\underline{\boldsymbol{\sigma}}_t\}_j^i, \{\delta g_n\}_j^i, \{\delta \underline{\boldsymbol{g}}_t\}_j^i, \{\delta\sigma_n\}_j^i, \{\delta\underline{\boldsymbol{\sigma}}_t\}_j^i\big)\, d\partial\Omega_i \qquad [5.15]$$

where F is a scalar function of the relative surface motion $g_n, \dot{\underline{\boldsymbol{g}}}_t$ and of the arising contact stresses in normal and tangential directions $\sigma_n, \underline{\boldsymbol{\sigma}}_t$. Indices $\{.\}_j^i$ denote quantities related to the i-th master segment and the j-th master node interaction,

whereas indices $\{.\}_i$ represent the contribution of the master segment quantities. The scalar function F depends on the choice of the resolution method (see Chapter 4). Note that $\sum_{i=1,M} N_j^i = S-$number of slave nodes. It implies that in active contact the number of slave nodes should be not smaller that the number of master segments.

The combination of the j-th slave node $\underline{\boldsymbol{r}}_s$ associated with the i-th master segment $\underline{\boldsymbol{\rho}} \in \partial\Omega^i$ presents the geometrical part of the *contact element*, which (depending on resolution method) can be complemented by a virtual node to store Lagrange multipliers – the contact stresses (Figures 5.11, 5.13, 5.14). Since by definition a slave node can belong to only one contact element, the last can be denoted by one index i – Ω_i^c.

Let us consider the contribution of one contact element to the virtual work of the system:

$$\begin{aligned}\delta W_i^c \quad = \quad & \int_{\partial\Omega_i} F\big(\{g_n\}_j^i, \{\underline{\dot{\boldsymbol{g}}}_t\}_j^i, \{\sigma_n\}_j^i, \\ & \{\underline{\boldsymbol{\sigma}}_t\}_j^i, \{\delta g_n\}_j^i, \{\delta \underline{\boldsymbol{g}}_t\}_j^i, \{\delta\sigma_n\}_j^i, \{\delta\underline{\boldsymbol{\sigma}}_t\}_j^i\big)\, d\partial\Omega_i\end{aligned} \qquad [5.16]$$

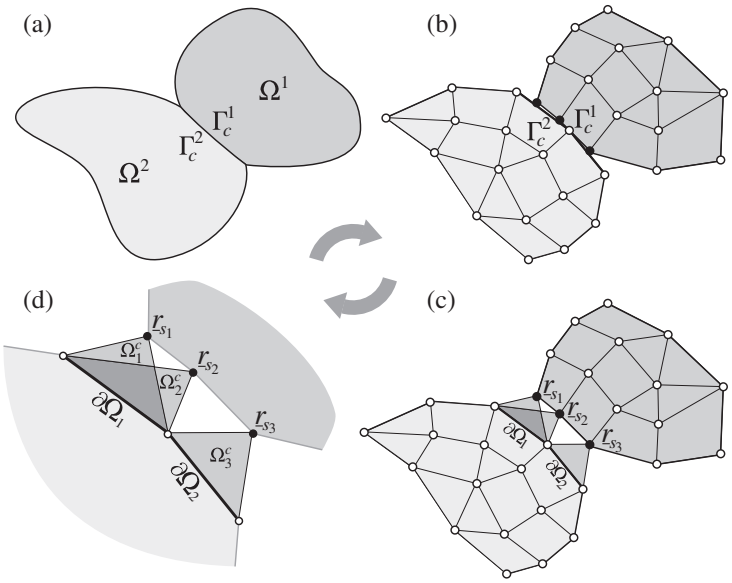

Figure 5.12. *Construction of contact elements: (a) continuous geometry two bodies Ω_1 and Ω_2 are in contact, active contact surfaces are Γ_c^1 (slave surface) and Γ_c^2 (master surface) (b) a discretized representation of bodies and contact interface, (c) three contact elements spanned on three slave nodes $\underline{\boldsymbol{r}}_{s1},\ \underline{\boldsymbol{r}}_{s2},\ \underline{\boldsymbol{r}}_{s3}$ and two master segments $\partial\Omega_1,\ \partial\Omega_2$ and (d) zoom on three constructed contact elements $\Omega_1^c,\ \Omega_2^c,\ \Omega_3^c$*

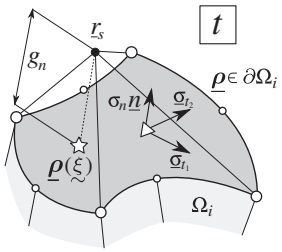

Figure 5.13. *Three-dimensional contact element based on a quadratic master surface. The complementary node for Lagrange multipliers is marked with a triangle. The projection of the slave node (black circle) is marked by a star*

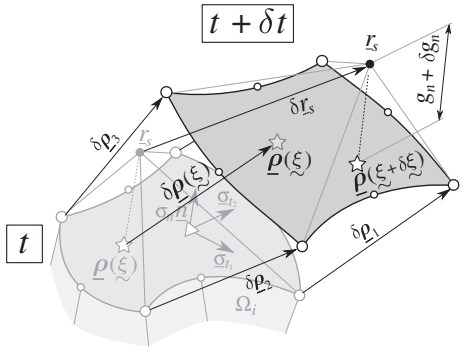

Figure 5.14. *Three-dimensional contact element of Figure 5.13 presented at two consecutive time steps t (transparent) and $t + \delta t$. Variational vectors are depicted as well as the variation of the main geometrical quantities: the convective surface parameter and the normal gap*

The function F is a linear function of the variations $\{\delta g_n\}^i_j$, $\{\delta \underline{\boldsymbol{g}}_t\}^i_j$, $\{\delta \sigma_n\}^i_j$, $\{\delta \underline{\boldsymbol{\sigma}}_t\}^i_j$, which can be presented as follows (in the following layouts, indices will be omitted):

$$F = F_{g_n}\delta g_n + \underline{\boldsymbol{F}}_{\underline{\boldsymbol{v}}_t} \cdot \delta \underline{\boldsymbol{g}}_t + F_{\sigma_n}\delta\sigma_n + \underline{\boldsymbol{F}}_{\underline{\boldsymbol{\sigma}}_t} \cdot \delta \underline{\boldsymbol{\sigma}}_t = [F_{g_n},\ \underline{\boldsymbol{F}}_{\underline{\boldsymbol{v}}_t},\ F_{\sigma_n},\ \underline{\boldsymbol{F}}_{\underline{\boldsymbol{\sigma}}_t}] \cdot \begin{bmatrix} \delta g_n \\ \delta \underline{\boldsymbol{g}}_t \\ \delta\sigma_n \\ \delta \underline{\boldsymbol{\sigma}}_t \end{bmatrix} \quad [5.17]$$

on the other hand

$$g_n = g_n(\underline{\boldsymbol{r}}_s, \underline{\boldsymbol{\rho}}), \quad \underline{\boldsymbol{g}}_t = \underline{\boldsymbol{g}}_t(\underline{\boldsymbol{r}}_s, \underline{\boldsymbol{\rho}}), \quad \underline{\boldsymbol{r}}_s = \underline{\boldsymbol{x}}^i_j,\ \underline{\boldsymbol{\rho}} \in \partial\Omega^i$$

representing $\underline{\boldsymbol{\rho}}$ by nodal values $\underline{\boldsymbol{\rho}}^i$ and shape functions $\phi_i(\underset{\sim}{\xi})$, $\underset{\sim}{\xi} \in \partial\widetilde{\Omega}^i$

$$\begin{bmatrix} \underline{\boldsymbol{r}}_s(t) \\ \underline{\boldsymbol{\rho}}(t, \underset{\sim}{\xi}) = \underline{\boldsymbol{\rho}}^i(t) \cdot \phi_i(\underset{\sim}{\xi}) \end{bmatrix} \quad \Rightarrow \quad \begin{bmatrix} \delta\underline{\boldsymbol{r}}_s(t) \\ \delta\underline{\boldsymbol{\rho}}(t, \underset{\sim}{\xi}) = \delta\underline{\boldsymbol{\rho}}^i(t) \cdot \phi_i(\underset{\sim}{\xi}) \end{bmatrix}$$

The variations of the geometrical quantities can be presented, as it was done in section 2.5:

$$\delta g_n = [\nabla_{\underline{\boldsymbol{r}}} g_n,\ \nabla_{\underline{\boldsymbol{\rho}}} g_n] \cdot \begin{bmatrix} \delta\underline{\boldsymbol{r}}_s \\ \delta\underline{\boldsymbol{\rho}}^i \end{bmatrix}^T, \quad \delta\underline{\boldsymbol{g}}_t = [\nabla_{\underline{\boldsymbol{r}}}\underline{\boldsymbol{g}}_t,\ \nabla_{\underline{\boldsymbol{\rho}}}\underline{\boldsymbol{g}}_t] \cdot \begin{bmatrix} \delta\underline{\boldsymbol{r}}_s \\ \delta\underline{\boldsymbol{\rho}}^i \end{bmatrix}^T$$

In a general case, contact stresses are also split over dual shape functions $\psi_i(\underset{\sim}{\xi})$, that is:

$$\sigma_n(t, \underset{\sim}{\xi}) = \sigma_n^i(t)\psi_i(\underset{\sim}{\xi}), \quad \underline{\boldsymbol{\sigma}}_t(t, \underset{\sim}{\xi}) = \underline{\boldsymbol{\sigma}}_t^i(t)\psi_i(\underset{\sim}{\xi})$$

5.3.3. *Discretization of the contact interface*

Both shape functions for geometry $\phi_i(\underset{\sim}{\xi})$ and for contact stresses $\psi_i(\underset{\sim}{\xi})$ have to be chosen such that Babuška-Brezzi conditions (BB-conditions, also called inf-sup conditions) are fulfilled. It does not present any difficulties for small deformations and small sliding when contacting surface have matching nodes (*node-to-node (NTN) discretization*). For nonconforming meshes, the *mortar method* (based on Lagrange multipliers) and *Nitsche method* (purely displacement based) are commonly used approaches, which provide a stable discretization. Mortar approach was first applied in the framework of the domain decomposition methods to "glue" the solution on the interface of non-matching meshes corresponding to different subdomains. For an extensive mathematical description, the reader is referred to the book by Wohlmuth [WOH 01] and references there in. For application to contact problems, see [BEL 98]. Further development originates from works due to McDevitt and Laursen [MCD 00], Puso [PUS 04] and Puso and Laursen [PUS 03]. More recently, we retain contributions for 2D frictionless [FIS 05] and frictional contact [YAN 05, FIS 06] and for 3D frictional contact [YAN 08b]. However, such a discretization requires the establishment of a segment-to-segment discretization as proposed by Simo, Wriggers and Taylor [SIM 85], see also [ZAV 98, WRI 06], which is a particularly complicated task for arbitrary contacting meshes in 3D contact problems. Another idea – *the contact domain method* – proposed recently by Oliver, *et al.* [OLI 09] and Hartmann

et al. [HAR 09] consists of replacing the integral over the surface by an integral over the interior of the contact interface. A 3D version has been proposed by the authors in [OLI 10]. However, a 3D version requires the triangulation of the volume between two arbitrary contacting surfaces, which is not always possible.

Here, we consider a simple but rather robust, widely used and multipurpose NTS *discretization*, so there is no freedom in the choice of the discretization for the contact stresses: the contact stress within master segments is restricted to a constant value, that is $\psi_i(\underset{\sim}{\xi}) = 1$ and $\sigma_n(t, \underset{\sim}{\xi}) = \sigma_n(t)$, $\underline{\boldsymbol{\sigma}}_t(t, \underset{\sim}{\xi}) = \underline{\boldsymbol{\sigma}}_t(t)$. Note that this discretization does not fulfill the BB-conditions and so can exhibit locking, moreover, as is well known, NTS discretization fails the patch test – contact interface for nonconforming meshes cannot transfer uniform pressure, see Taylor and Papadopoulos [TAY 91]. On the other hand, in the same article, the authors demonstrated that in case of the LMM and a sufficient number of slave nodes, the "two-pass" NTS approach is able to transfer correctly the uniform pressure, that is passes the patch test. Recently, Zavarise and De Lorenzis [ZAV 09a] proposed a modified NTS discretization passing the patch test for the PM.

5.3.4. *Virtual work for discretized contact interface*

According to all the aforementioned, the integrand of one contact element can be written as:

$$F = [\underline{\boldsymbol{F}}_{\underline{\boldsymbol{r}}_s} \quad \underset{\sim}{\underline{\boldsymbol{F}}}_{\underline{\boldsymbol{\rho}}} \quad F_{\sigma_n} \quad \underline{\boldsymbol{F}}_{\underline{\boldsymbol{\sigma}}_t}] \cdot \begin{bmatrix} \delta\underline{\boldsymbol{r}}_s \\ \delta\underline{\boldsymbol{\rho}} \\ \delta\sigma_n \\ \delta\underline{\boldsymbol{\sigma}}_t \end{bmatrix} \quad \sim \quad F = \begin{bmatrix} \underset{\sim}{\underline{\boldsymbol{F}}}_x \\ \\ \underset{\sim}{\underline{\mathrm{F}}}_\lambda \end{bmatrix}^T \overset{\circ}{\cdot} \begin{bmatrix} \delta\underset{\sim}{\underline{\boldsymbol{x}}} \\ \\ \delta\underset{\sim}{\lambda} \end{bmatrix} \qquad [5.18]$$

where $\underset{\sim}{\underline{\boldsymbol{x}}}$ is a v-vector containing the actual vectors of all geometrical nodes of the contact element.

$$\left\{ {}^{M+1}_{1}\mathbb{S}^{D}_{1} \right\} \ni \underset{\sim}{\underline{\boldsymbol{x}}} \sim \begin{bmatrix} \underline{\boldsymbol{r}}_s & \underline{\boldsymbol{\rho}}_1 & \underline{\boldsymbol{\rho}}_2 & \cdots & \underline{\boldsymbol{\rho}}_M \end{bmatrix}^T$$

where M is the number of master nodes and D is a dimension of the contact problem. Any point on the master surface is then determined by:

$$\partial\Omega \ni \underline{\boldsymbol{\rho}} = \underset{\sim}{\phi}(0, \underset{\sim}{\xi}) \circ \underset{\sim}{\underline{\boldsymbol{x}}} \qquad [5.19]$$

where $\underset{\sim}{\phi}(\underset{\sim}{\xi})$ is a v-scalar of the contact element shape functions constructed as:

$$\left\{ {}^{M+1}_{1}\mathbb{S}^{3}_{0} \right\} \ni \underset{\sim}{\phi}(\zeta, \underset{\sim}{\xi}) \sim \begin{bmatrix} \zeta & \phi_1(\underset{\sim}{\xi}) & \phi_2(\underset{\sim}{\xi}) & \dots & \phi_M(\underset{\sim}{\xi}) \end{bmatrix}^T$$

Then, for example:

$$g_n \underline{\boldsymbol{n}} = -\underset{\sim}{\phi}(-1, \underset{\sim}{\xi}_\pi) \circ \underline{\underline{\boldsymbol{x}}}$$

where $\underset{\sim}{\xi}_\pi$ is a normal projection point of the slave node on the master surface. Further, $\underset{\sim}{\lambda}$ is a v-scalar containing Lagrange multipliers (contact stresses): the normal contact pressure and the contravariant coordinates of the tangential contact stress vector in the local surface basis are:

$$\left\{ {}^{D}_{0}\mathbb{S}^{D}_{0} \right\} \ni \underset{\sim}{\lambda} \sim \begin{bmatrix} \sigma_n & \underset{\sim}{\sigma}_t \end{bmatrix}^T = \begin{bmatrix} \lambda_n & \underset{\sim}{\lambda}_t \end{bmatrix}^T, \quad \underset{\sim}{\lambda}_t \circ \overline{\frac{\partial \underline{\boldsymbol{\rho}}}{\partial \underset{\sim}{\xi}}} = \underline{\boldsymbol{\sigma}}_t$$

Due to the large number of s-structures of different dimensions:

$$\underset{\sim}{\xi}, \underset{\sim}{\lambda}_t, \underset{\sim}{\sigma}_t \in \left\{ {}^{D-1}_{0}\mathbb{S}^{D}_{0} \right\}, \quad \underset{\sim}{\lambda}, \underset{\sim}{\mathrm{F}}_\lambda \in \left\{ {}^{D}_{0}\mathbb{S}^{D}_{0} \right\}, \quad \underline{\underline{\boldsymbol{x}}}, \underline{\underline{\boldsymbol{F}}}_x \in \left\{ {}^{M+1}_{1}\mathbb{S}^{D}_{1} \right\}$$

all computations should be carried out carefully. The remaining terms $\underset{\sim}{\mathrm{F}}_\lambda$ and $\underline{\underline{\boldsymbol{F}}}_x$ in [5.18] are v-vector and v-scalar corresponding to forces acting on the virtual geometrical displacements $\delta\underline{\underline{\boldsymbol{x}}}$ and "forces" acting on the virtual Lagrange multiplier stresses (contact stresses), respectively. Finally, in new notations, from [5.16], the integral contribution of the i-th contact element to the total virtual work becomes:

$$\boxed{\delta W_i^c = \int\limits_{\partial\Omega_i} \begin{bmatrix} \underline{\underline{\boldsymbol{F}}}_x & \underset{\sim}{\mathrm{F}}_\lambda \end{bmatrix} \overset{\cdot}{\circ} \begin{bmatrix} \delta\underline{\underline{\boldsymbol{x}}} \\ \delta\underset{\sim}{\lambda} \end{bmatrix} d\partial\Omega_i = \begin{bmatrix} \int\limits_{\partial\Omega_i} \underline{\underline{\boldsymbol{F}}}_x \, d\partial\Omega_i & \int\limits_{\partial\Omega_i} \underset{\sim}{\mathrm{F}}_\lambda \, d\partial\Omega_i \end{bmatrix} \overset{\cdot}{\circ} \begin{bmatrix} \delta\underline{\underline{\boldsymbol{x}}} \\ \delta\underset{\sim}{\lambda} \end{bmatrix}}$$

[5.20]

Let us demonstrate that in terms of the FEM the left term in [5.20] is a kind of residual vector and the right term is a kind of vector of dofs. For that, we consider a spatial basis $\underline{\underline{\boldsymbol{e}}}$:

$$\underline{\underline{\boldsymbol{e}}} \sim \begin{bmatrix} \underline{\boldsymbol{e}}_1 & \dots & \underline{\boldsymbol{e}}_D \end{bmatrix}$$

Then, the dot product of $\underset{\sim}{\underline{\boldsymbol{e}}}$ components $\underline{\boldsymbol{e}}_k, k = 1, D$ with v-vectors from [5.20] provides the components of the scalar residual vector:

$$\begin{aligned}
&\int_{\partial\Omega_i} \left(\underset{\sim}{\boldsymbol{F}}_x \cdot \underline{\boldsymbol{e}}_k \right) d\partial\Omega_i = \underset{\sim}{\mathrm{R}}_x^k \sim [R_x^i]_{k+j\times D} \in \mathbb{R}^{(M+1)\times D}, j \in [1, M+1] \\
&\delta\underset{\sim}{\underline{\boldsymbol{x}}} \cdot \underline{\boldsymbol{e}}_k \sim \delta[x^i]_{k+j\times D} \in \mathbb{R}^{(M+1)\times D}, j \in [1, M+1] \\
&\int_{\partial\Omega_i} \underset{\sim}{\mathrm{F}}_\lambda \, d\partial\Omega_i = \underset{\sim}{\mathrm{R}}_\lambda \sim [R_\lambda^i] \in \mathbb{R}^D, \quad \delta\underset{\sim}{\lambda} \sim \delta[\lambda^i] \in \mathbb{R}^D
\end{aligned} \qquad [5.21]$$

and the full residual vector $[R^i]$ of the i-th contact element and vector of its unknown $[x^i]$ take the form:

$$\mathbb{R}^{M+D+1} \ni \; [R^i] = \begin{bmatrix} R_x^i \\ R_\lambda^i \end{bmatrix}, \quad \mathbb{R}^{M+D+1} \ni \; [x^i] = \begin{bmatrix} \delta x^i \\ \delta\lambda^i \end{bmatrix}$$

This expression is given simply to have a link with classical notations of the FEM.

We recap that the form of $\underset{\sim}{\boldsymbol{F}}_x$ and $\underset{\sim}{\mathrm{F}}_\lambda$ depends on the resolution method and will be given in the following parts. Now let us assemble all contributions to the virtual work balance equation. Here, we will focus on the contact elements and so the contribution of all structural finite elements will not be derived in closed form. All necessary routines can be found in books on FEM for solid mechanics: Zienkiewicz and Taylor [ZIE 00a, ZIE 00b], Chrisfield [CRI 00a, CRI 00b], Bathe [BAT 96], Belytschko *et al.* [BEL 08] and others. Let us denote by δW_j^s the contribution to the virtual work of the j-th structural element. To enforce equilibrium conditions, we require the total virtual work on solution path to be zero:

$$\sum_{j=1}^{N^e} \delta W_j^s + \sum_{i=1}^{S} \delta W_i^c = 0 \qquad [5.22]$$

N^e is the total number of structural elements and S is the number of contact elements and at the same time the number of slave nodes included in the contact elements. This equation can be presented as a set of $\approx N^n + S$ vector equations, where N^n is a number of free nodes. The sign $\approx$ expresses that Dirichlet boundary conditions can be imposed on any components of a displacement vector, so that the number of algebraic equations in [5.22] is equal to the number of free dofs N^{dof} plus the number of contact elements multiplied by the dimension of the problem SD. If LMM or coupled ALM

is used, in case of use of PM or augmented Lagrangian with Uzawa's algorithm, the number of equations in [5.22] reduces to N^{dof}:

$$\sum_{j=1}^{N^e} \delta W_j^s + \sum_{i=1}^{S} \delta W_i^c = 0 \quad \sim \quad \begin{bmatrix} R_x^s + R_x^c & R_\lambda \end{bmatrix} \delta \begin{bmatrix} x \\ \lambda \end{bmatrix} = 0 \qquad [5.23]$$

where R_x^s is a dense[4] residual vector related to structural elements, R^s a sparse residual vector related to the contact elements, R_i^s may be non-zero if the i-th dof belongs to one node of the contact elements. $x, R_x^c, R^s, x \in \mathbb{R}^{N^{\text{dof}}}$ and $\lambda, R_\lambda^c \in \mathbb{R}^{SD}$. Since virtual displacements and virtual Lagrange multipliers are arbitrary, equation [5.23] can be satisfied only if:

$$\begin{bmatrix} R_x^s + R_x^c \\ R_\lambda^c \end{bmatrix} = 0 \qquad [5.24]$$

This is a set of $N^{\text{dof}} + SD$ nonlinear algebraic equations; the nonlinearity is preserved, even though in the structural part the condition $R_x^s = 0$ is a set of linear algebraic equations, the contact problem is still nonlinear. Therefore, a solution technique for nonlinear equations has to be applied, for example Newton's method discussed in section 5.1. Hence, the linearization of this system of equations is required.

5.3.5. *Linearization of equations*

Newton's method and its generalization for non-smooth problems have been discussed in section 5.1. In this section, this method will be applied for a system of nonlinear algebraic equation [5.23] derived in the previous section. We assume that the solution $\{u_k, \lambda_k\}$ for given boundary conditions f_k at time step t_k is given either as an initial condition or as the solution of the k-th increment.

$$\begin{bmatrix} R_x^s(x_k, f_k) + R_x^c(x_k, \lambda_k) \\ R_\lambda^c(x_k, \lambda_k) \end{bmatrix} \approx 0 \qquad [5.25]$$

At time step t_{k+1}, a change of boundary conditions $f_{k+1} = f_k + \Delta f_k$ makes the system lose its equilibrium state. So, we establish an iterative procedure $0, 1, 2, \ldots, i$ and we wish that the sequence $\{u^i, \lambda^i\}$ converges to the solution $\{u_{k+1}, \lambda_{k+1}\}$,

4 Here, dense vector is used in the sense that all components may be non-zero.

which returns the system to equilibrium for the new given boundary conditions f_{k+1}. According to Newton's method, the iteration increment is given by:

$$\begin{bmatrix} \Delta x^i \\ \Delta \lambda^i \end{bmatrix} = - \begin{bmatrix} \frac{\partial R_x^s}{\partial x} + \frac{\partial R_x^c}{\partial x} & \frac{\partial R_\lambda^c}{\partial x} \\ \frac{\partial R_x^c}{\partial \lambda} & \frac{\partial R_\lambda^c}{\partial \lambda} \end{bmatrix} \Bigg|^{-1}_{\{x^i, \lambda^i, f_{n+1}\}} \begin{bmatrix} R_x^s(x^i, f_{k+1}) + R_x^c(x^i, \lambda^i) \\ R_\lambda^c(x^i, \lambda^i) \end{bmatrix} \quad [5.26]$$

and the corresponding update rule is given by:

$$x^{i+1} = x^i + \Delta x^i, \quad \lambda^{i+1} = \lambda^i + \Delta \lambda^i$$

The structural tangent matrix is denoted by $\frac{\partial R_x^s}{\partial x} = K^s$ and we are particularly interested in this remaining terms that can be called *tangent contact matrix*.

$$\begin{bmatrix} K^s & 0 \\ 0 & 0 \end{bmatrix} + \boxed{\begin{bmatrix} \frac{\partial R_x^c}{\partial x} & \frac{\partial R_\lambda^c}{\partial x} \\ \frac{\partial R_x^c}{\partial \lambda} & \frac{\partial R_\lambda^c}{\partial \lambda} \end{bmatrix}} = \begin{bmatrix} K^s + K_{xx}^c & K_{\lambda x}^c \\ K_{x\lambda}^c & K_{\lambda\lambda}^c \end{bmatrix}$$

The full tangent contact matrix is an assembly of contact element stiffness:

$$\begin{bmatrix} K_{xx}^c & K_{\lambda x}^c \\ K_{x\lambda}^c & K_{\lambda\lambda}^c \end{bmatrix} = \bigcup_{i=1}^{S} \begin{bmatrix} K_{xx}^{ci} & K_{\lambda x}^{ci} \\ K_{x\lambda}^{ci} & K_{\lambda\lambda}^{ci} \end{bmatrix}$$

Returning to [5.20], we can express all the terms of the elementary tangent contact matrix through derivatives of v-vector $\underset{\sim}{\underset{\sim}{\boldsymbol{F}}}_x$ and v-scalar $\underset{\sim}{\mathrm{F}}_\lambda$, so:

$$\begin{bmatrix} K_{xx}^{ci} & K_{\lambda x}^{ci} \\ K_{x\lambda}^{ci} & K_{\lambda\lambda}^{ci} \end{bmatrix} \sim \begin{bmatrix} \int\limits_{\partial\Omega_i} \left[\frac{\partial \underset{\sim}{\underset{\sim}{\boldsymbol{F}}}_x}{\partial \underset{\sim}{\underset{\sim}{\boldsymbol{x}}}} \right] d\partial\Omega_i & \int\limits_{\partial\Omega_i} \left[\frac{\partial \underset{\sim}{\mathrm{F}}_\lambda}{\partial \underset{\sim}{\underset{\sim}{\boldsymbol{x}}}} \right] d\partial\Omega_i \\ \int\limits_{\partial\Omega_i} \left[\frac{\partial \underset{\sim}{\underset{\sim}{\boldsymbol{F}}}_x}{\partial \underset{\sim}{\lambda}} \right] d\partial\Omega_i & \int\limits_{\partial\Omega_i} \left[\frac{\partial \underset{\sim}{\mathrm{F}}_\lambda}{\partial \underset{\sim}{\lambda}} \right] d\partial\Omega_i \end{bmatrix}$$

So, to integrate contact into the resolution, it remains only to precise the form of the functions:

$$\underset{\sim}{\underset{\sim}{\boldsymbol{F}}}_x, \ \underset{\sim}{\mathrm{F}}_\lambda$$

and to evaluate their derivatives

$$\frac{\partial \underset{\sim}{\boldsymbol{F}}_x}{\partial \underset{\sim}{\boldsymbol{x}}}, \frac{\partial \underset{\sim}{\mathrm{F}}_\lambda}{\partial \underset{\sim}{\boldsymbol{x}}}, \frac{\partial \underset{\sim}{\boldsymbol{F}}_x}{\partial \underset{\sim}{\lambda}}, \frac{\partial \underset{\sim}{\mathrm{F}}_\lambda}{\partial \underset{\sim}{\lambda}}$$

5.3.6. *Example*

Here, we give an example of the tangent matrix construction for a mechanical problem with contact. Let us consider two structural elements Ω_1 and Ω_2 (Figure 5.15), which come in contact. A constant pressure is imposed on the upper segment between nodes 1 and 3. Nodes 6 and 7 are fixed so they are not included in the computations. The tangent stiffness matrix for such a configuration has the form presented in Figure 5.15(a). The detection procedure determines that the slave node 2 may come in contact with the master segment between nodes 4 and 5. So the contact element $2-4-5$ with a complementary node 8 for the Lagrange multipliers is constructed and added to the global tangent stiffness matrix (Figure 5.15(b)).

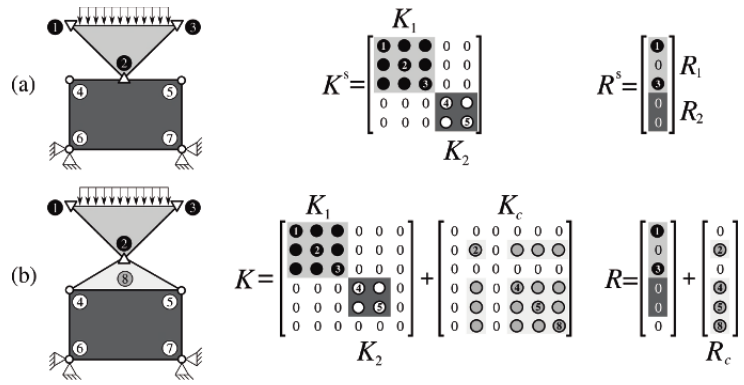

Figure 5.15. *Example of tangent matrix: (a) structural matrix K^s for two elements Ω_1 and Ω_2 and given boundary conditions and (b) contribution of the contact element (spanned on slave node 2 and master segment 4–5 with a complementary node 8 for Lagrange multipliers) to the tangent matrix*

5.4. Residual vectors and tangent matrices for contact elements

Residual vectors and tangent contact matrices for different resolution methods will be derived in this section. All necessary integrals have been formulated in Chapter 4 and all geometry-related variations have been derived in Chapter 2. Here, it remains to give closed forms for:

$$\underset{\sim}{\boldsymbol{R}}^c{}_x, \underset{\sim}{\boldsymbol{R}}^c{}_\lambda \quad \text{and} \quad \underset{\approx}{\boldsymbol{K}}^c{}_{xx}, \underset{\approx}{\boldsymbol{K}}^c{}_{\lambda x}, \underset{\approx}{\boldsymbol{K}}^c{}_{x\lambda}, \underset{\approx}{\boldsymbol{K}}^c{}_{\lambda\lambda}$$

These vectors and matrices will be given for arbitrary discretization forms for PM (linear penalty) and coupled ALM.

5.4.1. *Penalty method: frictionless case*

5.4.1.1. *Residual vector*

The virtual work due to frictionless contact was given in [4.77] for continuous problems. In the finite element framework, the contribution of the i-th NTS contact element for the linear PM can be written as:

$$\delta W_i^c = \int_{\partial\Omega_i} -\varepsilon_n \langle -g_n \rangle \delta g_n \, d\partial\Omega_i \qquad [5.27]$$

According to [2.43], the variation of the normal gap can be presented as $\delta g_n = [\nabla g_n]^T \cdot \delta[\underline{\boldsymbol{x}}]$ or in s-structure notations:

$$\delta g_n = \underset{\sim}{\underline{\boldsymbol{G}}}(\underset{\sim}{\xi}_\pi) \overset{\circ}{\cdot} \delta \underset{\sim}{\underline{\boldsymbol{x}}}$$

where $\underset{\sim}{\xi}_\pi$ is the projection of the slave node on the master surface and $\underset{\sim}{\underline{\boldsymbol{G}}}$ is a v-vector of first variation of the normal gap δg_n given in [2.43]. So, equation [5.27] takes the form:

$$\begin{aligned} \delta W_i^c &= \int_{\partial\Omega_i} -\varepsilon_n \langle -g_n \rangle \underset{\sim}{\underline{\boldsymbol{G}}}(\underset{\sim}{\xi}_\pi) \overset{\circ}{\cdot} \delta \underset{\sim}{\underline{\boldsymbol{x}}} \, d\partial\Omega_i \\ &= \left[\int_{\partial\Omega_i} \underset{\sim}{\underline{\boldsymbol{F}}}_x \, d\partial\Omega_i \right] \overset{\circ}{\cdot} \delta \underset{\sim}{\underline{\boldsymbol{x}}} = [R_x^c]^T [\delta x^i] \end{aligned} \qquad [5.28]$$

Consequently, $\underset{\sim}{\underline{\boldsymbol{F}}}_x$ is given as:

$$\underset{\sim}{\underline{\boldsymbol{F}}}_x = -\varepsilon_n \langle -g_n \rangle \underset{\sim}{\underline{\boldsymbol{G}}}(\underset{\sim}{\xi}_\pi)$$

The integral of $\underset{\sim}{\underline{\boldsymbol{F}}}_x$ over the master surface $\partial\Omega_i$ can be simply evaluated, since the integrand does not depend on the surface parameter $\underset{\sim}{\xi}$:

$$\int_{\partial\Omega_i} \underset{\sim}{\underline{\boldsymbol{F}}}_x \, d\partial\Omega_i = -\int_{\partial\Omega_i} \varepsilon_n \langle -g_n \rangle \, d\partial\Omega_i \, \underset{\sim}{\underline{\boldsymbol{G}}}(\underset{\sim}{\xi}_\pi) = P_n \, \underset{\sim}{\underline{\boldsymbol{G}}}(\underset{\sim}{\xi}_\pi) \qquad [5.29]$$

where the first term is nothing but a normal contact force P_n calculated on the i-th iteration configuration.

$$P_n = \underset{\sim}{\boldsymbol{F}} \cdot \underline{\boldsymbol{n}} = \int_{\partial\Omega_i} -\varepsilon_n \langle -g_n \rangle \, d\partial\Omega_i$$

Finally, the residual v-vector is given by:

$$\boxed{\underset{\sim}{\boldsymbol{R}}^c_x = P_n \underset{\sim}{\boldsymbol{G}}(\underset{\sim}{\xi}_\pi)}$$

5.4.1.2. *Tangent contact matrix*

To evaluate the elemental tangent contact matrix, it is necessary to take a partial derivative of the v-vector $\underset{\sim}{\boldsymbol{F}}_x$:

$$\frac{\partial \underset{\sim}{\boldsymbol{F}}_x}{\partial \underset{\sim}{\boldsymbol{x}}} = \begin{cases} \varepsilon_n \frac{\partial g_n}{\partial \underset{\sim}{\boldsymbol{x}}} \overset{\boxtimes}{\otimes} \underset{\sim}{\boldsymbol{G}} + \varepsilon_n g_n \underset{\approx}{\boldsymbol{H}}, & g_n < 0 \\ 0, & g_n \geq 0 \end{cases}$$

where all geometry-related s-structures come from connections between the variation of the geometrical quantities and the nodal coordinate vectors.

$$\delta g_n = \frac{\partial g_n}{\partial \underset{\sim}{\boldsymbol{x}}} \cdot \delta \underset{\sim}{\boldsymbol{x}} = \underset{\sim}{\boldsymbol{G}} \cdot \delta \underset{\sim}{\boldsymbol{x}} \text{ and } \Delta\delta g_n = \Delta \underset{\sim}{\boldsymbol{x}} \cdot \frac{\partial^2 g_n}{\partial \underset{\sim}{\boldsymbol{x}}^2} \cdot \delta \underset{\sim}{\boldsymbol{x}} = \Delta \underset{\sim}{\boldsymbol{x}} \cdot \underset{\approx}{\boldsymbol{H}} \cdot \delta \underset{\sim}{\boldsymbol{x}}$$

These s-structures have been derived in section 2.5. In general form, we get:

$$\frac{\partial \underset{\sim}{\boldsymbol{F}}_x}{\partial \underset{\sim}{\boldsymbol{x}}} = \begin{cases} \varepsilon_n \underset{\sim}{\boldsymbol{G}} \overset{\boxtimes}{\otimes} \underset{\sim}{\boldsymbol{G}} + \varepsilon_n g_n \underset{\approx}{\boldsymbol{H}}, & g_n < 0 \\ 0, & g_n \geq 0 \end{cases}$$

Integrating over the master surface gives:

$$\int_{\partial\Omega_i} \frac{\partial \underset{\sim}{\boldsymbol{F}}_x}{\partial \underset{\sim}{\boldsymbol{x}}} \, d\partial\Omega_i = \varepsilon_n \underset{\sim}{\boldsymbol{G}} \overset{\boxtimes}{\otimes} \underset{\sim}{\boldsymbol{G}} \partial\Omega_i + P_n \underset{\approx}{\boldsymbol{H}}$$

This expression can be interpreted as a tangent contact t-tensor $\underset{\approx}{\underline{\underline{\boldsymbol{K}}}}^c_{xx}$:

$$\boxed{\underset{\approx}{\underline{\underline{\boldsymbol{K}}}}^c_{xx} = \varepsilon_n \underset{\sim}{\underline{\boldsymbol{G}}} \otimes \underset{\sim}{\underline{\boldsymbol{G}}}\, \partial\Omega_i + P_n \underset{\approx}{\underline{\underline{\boldsymbol{H}}}}, \quad g_n < 0}$$

or in a slightly different form:

$$\boxed{\underset{\approx}{\underline{\underline{\boldsymbol{K}}}}^c_{xx} = \varepsilon_n \partial\Omega_i \left[\underset{\sim}{\underline{\boldsymbol{G}}} \otimes \underset{\sim}{\underline{\boldsymbol{G}}} - \langle -g_n \rangle \underset{\approx}{\underline{\underline{\boldsymbol{H}}}} \right], \quad g_n < 0}$$

5.4.2. *Penalty method: frictional case*

In case of frictional contact, we have to distinguish stick and slip states, since residual vector and stiffness matrix are different in each case. The virtual work due to frictional contact was given in expanded form [4.77] for continuous problem. In the finite element framework, contribution of the i-th NTS contact element for linear PM can be written as:

$$\delta W_i^c = \begin{cases} \int\limits_{\partial\Omega_i} -\varepsilon_n \langle -g_n \rangle \left(\delta g_n - \mu \underline{\boldsymbol{s}} \cdot \delta \underline{\boldsymbol{g}}_t \right) d\partial\Omega_i, & \textit{slip} \\ \int\limits_{\partial\Omega_i} \varepsilon_n \langle -g_n \rangle \delta g_n + \varepsilon_t \underline{\boldsymbol{g}}_t^{\bullet} \cdot \delta \underline{\boldsymbol{g}}_t \, d\partial\Omega_i, & \textit{stick} \end{cases} \qquad [5.30]$$

from [2.43] and [2.46], we get:

$$\delta g_n = [\nabla g_n]^T \cdot \delta[\underline{\boldsymbol{x}}], \;\; \delta \underline{\boldsymbol{g}}_t = \frac{\partial \underline{\boldsymbol{\rho}}}{\partial \xi_1} \delta\xi^1 + \frac{\partial \underline{\boldsymbol{\rho}}}{\partial \xi_2} \delta\xi^2 = \left\{ \frac{\partial \underline{\boldsymbol{\rho}}}{\partial \xi_1} \left[\nabla \xi^1\right]^T + \frac{\partial \underline{\boldsymbol{\rho}}}{\partial \xi_2} \left[\nabla \xi^2\right]^T \right\} \cdot \delta[\underline{\boldsymbol{x}}]$$

In s-structure notations, these formulae can be rewritten as:

$$\delta g_n = \underset{\sim}{\underline{\boldsymbol{G}}}(\underset{\sim}{\xi}_\pi) \cdot \delta \underset{\sim}{\underline{\boldsymbol{x}}}, \qquad \delta \underline{\boldsymbol{g}}_t = \frac{\partial \underline{\boldsymbol{\rho}}}{\partial \underset{\sim}{\xi}} \circ \delta \underset{\sim}{\xi} = \frac{\partial \underline{\boldsymbol{\rho}}}{\partial \underset{\sim}{\xi}} \circ \underset{\approx}{\underline{\underline{\boldsymbol{T}}}} \cdot \delta \underset{\sim}{\underline{\boldsymbol{x}}}$$

where $\underset{\approx}{\underline{\underline{\boldsymbol{T}}}}$ is a v-v-vector (two v-vectors gathered together in a v-structure). In these notations, the integral in [5.31] takes the form:

$$\delta W_i^c = \begin{cases} \left[\int\limits_{\partial\Omega_i} -\varepsilon_n \langle -g_n \rangle \left(\underset{\sim}{\underline{\boldsymbol{G}}}(\underset{\sim}{\xi}_\pi) - \mu \underline{\boldsymbol{s}} \cdot \left(\frac{\partial \underline{\boldsymbol{\rho}}}{\partial \underset{\sim}{\xi}} \circ \underset{\approx}{\underline{\underline{\boldsymbol{T}}}} \right) \Big|_{\underset{\sim}{\xi}_\pi} \right) d\partial\Omega_i \right] \cdot \delta \underset{\sim}{\underline{\boldsymbol{x}}}, & \textit{slip} \\ \left[\int\limits_{\partial\Omega_i} -\varepsilon_n \langle -g_n \rangle \underset{\sim}{\underline{\boldsymbol{G}}}(\underset{\sim}{\xi}_\pi) + \varepsilon_t \underline{\boldsymbol{g}}_t^{\bullet} \cdot \left(\frac{\partial \underline{\boldsymbol{\rho}}}{\partial \underset{\sim}{\xi}} \circ \underset{\approx}{\underline{\underline{\boldsymbol{T}}}} \right) \Big|_{\underset{\sim}{\xi}^{\bullet}} d\partial\Omega_i \right] \cdot \delta \underset{\sim}{\underline{\boldsymbol{x}}}, & \textit{stick} \end{cases} \qquad [5.31]$$

Note that the term $\frac{\partial \underline{\boldsymbol{\rho}}}{\partial \underset{\sim}{\xi}} \underline{\underline{\boldsymbol{T}}}$ is evaluated at different points: in case of stick at point $\underset{\sim}{\xi}^{\bullet}$ and in case of slip at the current projection point $\underset{\sim}{\xi}_{\pi}$ (see also remark 9.2 in [WRI 06]). This difference can be explained schematically if we assume that in the contact interface there are rigid bars hinged to the master segment by a nonlinear circular spring (Figure 5.16). The slave node, penetrating under the surface at $|g_n|$, is assumed to be in contact with this bar, so the tangential movement of the slave produces a rotation of the bar (angle ϕ) such as:

$$|\underline{\boldsymbol{g}}_t| = |g_n| \tan \phi$$

A resulting force $\underline{\boldsymbol{F}}_t$

$$F_t = \varepsilon_t |\underline{\boldsymbol{g}}_t| = \varepsilon_t |g_n| \tan \phi$$

acts on the slave node and on the hinge of the bar. If the external force is removed, then the slave node unloads the bar and returns to the stick position. According to Coulomb's law, the tangential resistance is limited by the normal force multiplied by the friction coefficient:

$$F_t = \mu F_n = \mu \varepsilon_n |g_n| \;\Leftrightarrow\; F_t = \varepsilon_t |g_n| \tan \phi^* = \mu \varepsilon_n |g_n| \;\Rightarrow\; \phi^* = \arctan\left(\frac{\mu \varepsilon_n}{\varepsilon_t}\right)$$

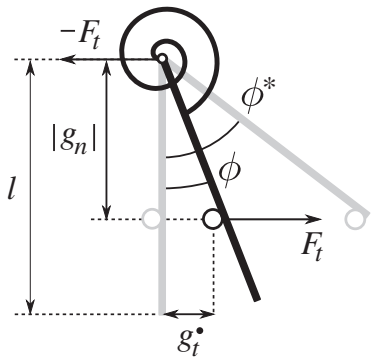

Figure 5.16. *Rigid bar hinged by a spring to the master segment and its interaction with a slave node*

This critical angle ϕ^* determines the length of the bar:

$$l = \frac{g_n}{\cos \phi^*} = \frac{g_n \sqrt{\mu^2 \varepsilon_n^2 + \varepsilon_t^2}}{\varepsilon_t}$$

When the critical angle is reached, the slave node jumps from the current bar to the next bar (see Figure 5.17), which results in a new distribution of forces in the master slave interface. Formally, this interpretation is valid only for the stick state. Remark the fact that slave node penetrates under the master surface and slides over stick point results in appearance of a momentum.

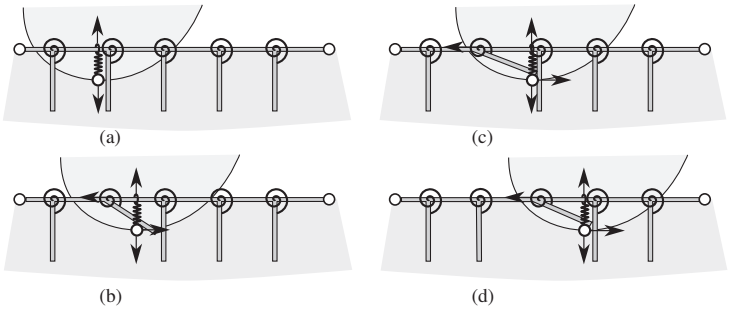

Figure 5.17. *Representation of tangential interaction of the slave node with a master, as interaction with a set of rigid bars hinged to the master segment by a spring: (a, b and c) stick state and (d) slip state*

5.4.2.1. *Residual vector*

Since in the integral [5.31] the integrands do not depend on the convective coordinate $\underset{\sim}{\xi}$, the evaluation of the residual v-vector is straightforward:

$$\underset{\sim}{\boldsymbol{R}}{}^{c}_{x} = \begin{cases} P_n \left(\underset{\sim}{\boldsymbol{G}}(\underset{\sim}{\xi}_{\pi}) - \mu \underline{\boldsymbol{s}} \cdot \left(\frac{\partial \underline{\boldsymbol{\rho}}}{\partial \underset{\sim}{\xi}} \circ \underset{\approx}{\boldsymbol{T}} \right) \Big|_{\underset{\sim}{\xi}_{\pi}} \right), & \textit{slip} \\ P_n \underset{\sim}{\boldsymbol{G}}(\underset{\sim}{\xi}_{\pi}) + \underline{\boldsymbol{F}}_t \cdot \left(\frac{\partial \underline{\boldsymbol{\rho}}}{\partial \underset{\sim}{\xi}} \circ \underset{\approx}{\boldsymbol{T}} \right) \Big|_{\underset{\sim}{\xi}^{\bullet}}, & \textit{stick} \end{cases} \qquad [5.32]$$

where normal and tangential contact forces are $P_n = \int\limits_{\partial\Omega_i} -\varepsilon_n \langle -g_n \rangle \, d\partial\Omega_i$ and $F_t = \int\limits_{\partial\Omega_i} \varepsilon_t \underline{\boldsymbol{g}}_t^{\bullet} \, d\partial\Omega_i$, respectively.

Making use of the return mapping algorithm (see section 5.2) leads to the following scheme. We make a start from the evaluation of the contact pressure for a given displacement field:

$$\sigma_n^{k+1} = -\varepsilon_n \langle -g_n^{k+1} \rangle \quad \Rightarrow \quad P_n^{k+1} = -\varepsilon_n \langle -g_n^{k+1} \rangle \partial\Omega_i \qquad [5.33]$$

(let us remind that the lower index i denotes the i-th contact element and the upper indices $k, k+1$ denote solution increments). Further, the trial tangential contact force in stick is calculated as:

$$\underline{\boldsymbol{F}}_t^{\text{trial}} = \underline{\boldsymbol{F}}_t^k + \int_{\partial\Omega_i} \varepsilon_t \overline{\frac{\partial \underline{\boldsymbol{\rho}}}{\partial \underset{\sim}{\xi}}}^{k+1} \circ (\bar{\underset{\sim}{\xi}}^{k+1} - \bar{\underset{\sim}{\xi}}^{k})\, d\partial\Omega_i = \varepsilon_t \partial\Omega_i (\bar{\underset{\sim}{\xi}}^{k+1} - \bar{\underset{\sim}{\xi}}^{\bullet\, k}) \circ \overline{\frac{\partial \underline{\boldsymbol{\rho}}}{\partial \underset{\sim}{\xi}}}^{k+1} \quad [5.34]$$

where $\bar{\underset{\sim}{\xi}}^{\bullet\, k}$ is the convective covariant coordinate of the stick point for k-th increment. Further, we check if this trial force is inside the Coulomb's cone:

$$\|\underline{\boldsymbol{F}}_t^{\text{trial}}\| \leq \mu |P_n^{k+1}|$$

If not, then the trial force has to be corrected. According to equation [5.8], the tangential contact force can be written as:

$$\underline{\boldsymbol{F}}_t^{k+1} = \underline{\boldsymbol{F}}_t^{\text{trial}} - \int_{\partial\Omega_i} \varepsilon_t \langle \Delta\gamma^k \rangle \underline{\boldsymbol{s}}_t^k \, d\partial\Omega_i$$

where

$$\underline{\boldsymbol{s}}_t^k = \frac{\underline{\boldsymbol{F}}_t^{\text{trial}}}{\|\underline{\boldsymbol{F}}_t^{\text{trial}}\|} \quad [5.35]$$

$$\langle \Delta\gamma^k \rangle = \frac{\langle \|\underline{\boldsymbol{\sigma}}_t^{\text{trial}}\| - \mu |\sigma_n^{k+1}| \rangle}{\varepsilon_t}$$

The integral of the slip $\Delta\gamma^k$ is:

$$\int_{\partial\Omega_i} \langle \Delta\gamma^k \rangle \, d\partial\Omega_i = \frac{\langle \|F_t^{\text{trial}}\| - \mu |P_n^{k+1}| \rangle}{\varepsilon_t}$$

The stick point is updated according to the simple rule:

$$\bar{\underset{\sim}{\xi}}^{\bullet\, \{k+1\}} = \bar{\underset{\sim}{\xi}}^{\bullet\, k} + \Delta\gamma^k \underset{\sim}{\mathrm{s}}_t^k$$

where $\underset{\sim}{s}_t^k$ is the v-scalar of covariant coordinates of the sliding vector.

$$\underset{\sim}{s}_t^k = \underline{\boldsymbol{s}}_t^k \cdot \frac{\partial \underline{\boldsymbol{\rho}}}{\partial \underset{\sim}{\xi}}$$

Finally, we get the following return mapping scheme:

$$\begin{cases} \underline{\boldsymbol{F}}_t^{k+1} = \underline{\boldsymbol{F}}_t^{\text{trial}}, \ \underset{\sim}{\bar{\xi}}^{\bullet\,\{k+1\}} = \underset{\sim}{\bar{\xi}}^{\bullet\,k}, \ \|\underline{\boldsymbol{F}}_t^{k+1}\| \leq \mu |P_n^{k+1}|, \ \textit{stick} \\ \underline{\boldsymbol{F}}_t^{k+1} = \mu |P_n^{k+1}| \underline{\boldsymbol{s}}_t^k, \ \underset{\sim}{\bar{\xi}}^{\bullet\,\{k+1\}} = \underset{\sim}{\bar{\xi}}^{\bullet\,k} + \Delta\gamma^k \underset{\sim}{s}_t^k, \ \|\underline{\boldsymbol{F}}_t^{k+1}\| > \mu |P_n^{i+1}|, \ \textit{slip} \end{cases} \quad [5.36]$$

Expressing the tangential force for stick in the contravariant basis gives the following expressions (it seems to be more advantageous for the following linearization to retain vector form for tangential slip $\underline{\boldsymbol{s}}_t^k$):

$$\begin{cases} \underline{\boldsymbol{F}}_t^{k+1} = \left(\underline{\boldsymbol{F}}_t^{\text{trial}} \cdot \frac{\partial \underline{\boldsymbol{\rho}}^{k+1}}{\partial \underset{\sim}{\xi}} \right) \circ \overline{\frac{\partial \underline{\boldsymbol{\rho}}}{\partial \underset{\sim}{\xi}}}^{k+1} = \underset{\sim}{\mathrm{F}}_t^{\text{trial}} \circ \overline{\frac{\partial \underline{\boldsymbol{\rho}}}{\partial \underset{\sim}{\xi}}}^{k+1}, \quad \textit{stick} \\ \underline{\boldsymbol{F}}_t^{k+1} = \mu |P_n^{k+1}| \underline{\boldsymbol{s}}_t^k, \quad \textit{slip} \end{cases} \quad [5.37]$$

According to the definition of the updated normal contact force [5.33] and the trial tangential contact force [5.34], we get:

$$\begin{cases} \underline{\boldsymbol{F}}_t^{k+1} = \varepsilon_t \partial\Omega_i (\underset{\sim}{\bar{\xi}}^{k+1} - \underset{\sim}{\bar{\xi}}^{\bullet\,k}) \circ \overline{\frac{\partial \underline{\boldsymbol{\rho}}}{\partial \underset{\sim}{\xi}}}^{k+1}, \quad \textit{stick} \\ \underline{\boldsymbol{F}}_t^{k+1} = \mu \varepsilon_n \partial\Omega_i \langle -g_n^{k+1} \rangle \underline{\boldsymbol{s}}_t^k, \quad \textit{slip} \end{cases} \quad [5.38]$$

For the following linearization, we derive here the variation of the sliding unit vector $\underline{\boldsymbol{s}}_t^k$; from its definition [5.35] we get:

$$\underline{\boldsymbol{s}}_t^k = \frac{\underline{\boldsymbol{F}}_t^{\text{trial}}}{\|\underline{\boldsymbol{F}}_t^{\text{trial}}\|} = \frac{\underline{\boldsymbol{F}}_t^{\text{trial}}}{\sqrt{\underline{\boldsymbol{F}}_t^{\text{trial}} \cdot \underline{\boldsymbol{F}}_t^{\text{trial}}}} \quad \Rightarrow \quad \Delta \underline{\boldsymbol{s}}_t^k = \left(\underline{\underline{\boldsymbol{I}}} - \underline{\boldsymbol{s}}_t^k \otimes \underline{\boldsymbol{s}}_t^k \right) \cdot \frac{\Delta \underline{\boldsymbol{F}}_t^{\text{trial}}}{\|\underline{\boldsymbol{F}}_t^{\text{trial}}\|} \quad [5.39]$$

If the unity tensor is presented as:

$$\underline{\underline{\boldsymbol{I}}} = \underline{\boldsymbol{n}} \otimes \underline{\boldsymbol{n}} + \underline{\tilde{\boldsymbol{s}}}^k \otimes \underline{\tilde{\boldsymbol{s}}}^k + \underline{\boldsymbol{s}}_t^k \otimes \underline{\boldsymbol{s}}_t^k$$

where $\tilde{\underline{\boldsymbol{s}}}^k$ is an in-plane unit vector orthogonal to the sliding direction, since we have to take a dot product of the slip vector variation with in-plane basis vectors (see [5.32]), we can neglect the normal components $\underline{\boldsymbol{n}} \otimes \underline{\boldsymbol{n}}$, then the expression [5.39] can be rewritten as:

$$\Delta \underline{\boldsymbol{s}}_t^k = \tilde{\underline{\boldsymbol{s}}}^k \otimes \tilde{\underline{\boldsymbol{s}}}^k \cdot \frac{\Delta \underline{\boldsymbol{F}}_t^{\text{trial}}}{\|\underline{\boldsymbol{F}}_t^{\text{trial}}\|} \qquad [5.40]$$

where the variation of the tangential trial force follows from [5.34]:

$$\Delta \underline{\boldsymbol{F}}_t^{\text{trial}} = \varepsilon_t \partial\Omega_i \Delta \underset{\sim}{\bar{\xi}}^{k+1} \circ \overline{\frac{\partial \underline{\boldsymbol{\rho}}}{\partial \underset{\sim}{\xi}}}^{k+1} + \varepsilon_t \partial\Omega_i (\underset{\sim}{\bar{\xi}}^{k+1} - \underset{\sim}{\bar{\xi}}^{\bullet\, k}) \circ \Delta \overline{\frac{\partial \underline{\boldsymbol{\rho}}}{\partial \underset{\sim}{\xi}}}^{k+1} \qquad [5.41]$$

If we represent the unit vector $\tilde{\underline{\boldsymbol{s}}}^k$ in the covariant basis:

$$\tilde{\underline{\boldsymbol{s}}}^k = \left(\tilde{\underline{\boldsymbol{s}}}^k \cdot \overline{\frac{\partial \underline{\boldsymbol{\rho}}}{\partial \underset{\sim}{\xi}}}^{k+1} \right) \circ \frac{\partial \underline{\boldsymbol{\rho}}}{\partial \underset{\sim}{\xi}}^{k+1} = \underset{\sim}{\tilde{\mathrm{s}}}^k \circ \frac{\partial \underline{\boldsymbol{\rho}}}{\partial \underset{\sim}{\xi}}^{k+1}$$

the variation of the sliding vector takes a simpler form:

$$\Delta \underline{\boldsymbol{s}}_t^k = \frac{\varepsilon_t \partial\Omega_i}{\|\underline{\boldsymbol{F}}_t^{\text{trial}}\|} \underset{\sim}{\tilde{\mathrm{s}}}^k \circ \left[\Delta \underset{\sim}{\bar{\xi}}^{k+1} + \frac{\partial \underline{\boldsymbol{\rho}}}{\partial \underset{\sim}{\xi}}^{k+1} \overset{\boxtimes}{\cdot} \Delta \overline{\frac{\partial \underline{\boldsymbol{\rho}}}{\partial \underset{\sim}{\xi}}}^{k+1} \circ (\underset{\sim}{\bar{\xi}}^{k+1} - \underset{\sim}{\bar{\xi}}^{\bullet\, k}) \right] \underset{\sim}{\tilde{\mathrm{s}}}^k \circ \frac{\partial \underline{\boldsymbol{\rho}}}{\partial \underset{\sim}{\xi}}^{k+1} \qquad [5.42]$$

As it is hard to evaluate the variation of the contravariant basis, we express it through the variation of the covariant basis vectors:

$$\frac{\partial \underline{\boldsymbol{\rho}}}{\partial \underset{\sim}{\xi}} \overset{\boxtimes}{\cdot} \overline{\frac{\partial \underline{\boldsymbol{\rho}}}{\partial \underset{\sim}{\xi}}} = \underset{\approx}{\mathrm{I}} \;\Rightarrow\; \Delta \frac{\partial \underline{\boldsymbol{\rho}}}{\partial \underset{\sim}{\xi}} \overset{\boxtimes}{\cdot} \overline{\frac{\partial \underline{\boldsymbol{\rho}}}{\partial \underset{\sim}{\xi}}} + \frac{\partial \underline{\boldsymbol{\rho}}}{\partial \underset{\sim}{\xi}} \overset{\boxtimes}{\cdot} \Delta \overline{\frac{\partial \underline{\boldsymbol{\rho}}}{\partial \underset{\sim}{\xi}}} = 0 \;\Leftrightarrow\; \frac{\partial \underline{\boldsymbol{\rho}}}{\partial \underset{\sim}{\xi}} \overset{\boxtimes}{\cdot} \Delta \overline{\frac{\partial \underline{\boldsymbol{\rho}}}{\partial \underset{\sim}{\xi}}} = -\Delta \frac{\partial \underline{\boldsymbol{\rho}}}{\partial \underset{\sim}{\xi}} \overset{\boxtimes}{\cdot} \overline{\frac{\partial \underline{\boldsymbol{\rho}}}{\partial \underset{\sim}{\xi}}}$$

Omitting increment indices in the expression [5.42], we finally get:

$$\boxed{\Delta \underline{\boldsymbol{s}}_t = \frac{\varepsilon_t \partial\Omega_i}{\|\underline{\boldsymbol{F}}_t^{\text{trial}}\|} \underset{\sim}{\tilde{\mathrm{s}}} \circ \left[\Delta \underset{\sim}{\bar{\xi}} - \Delta \frac{\partial \underline{\boldsymbol{\rho}}}{\partial \underset{\sim}{\xi}} \overset{\boxtimes}{\cdot} \overline{\frac{\partial \underline{\boldsymbol{\rho}}}{\partial \underset{\sim}{\xi}}} \circ (\underset{\sim}{\bar{\xi}} - \underset{\sim}{\bar{\xi}}^{\bullet}) \right] \underset{\sim}{\tilde{\mathrm{s}}} \circ \frac{\partial \underline{\boldsymbol{\rho}}}{\partial \underset{\sim}{\xi}}} \qquad [5.43]$$

5.4.2.2. *Tangent contact matrix*

To evaluate the elementary tangent contact matrix, it is necessary to take a partial derivative of the residual v-vector $\underset{\sim}{\underline{\boldsymbol{R}}}^{c}{}_{x}$ from [5.32], however, it is more convenient to start from the variation of the virtual work $\Delta\delta W_i^c$:

$$\Delta\delta W_i^c = \Delta P_n \delta g_n + P_n \Delta\delta g_n + \Delta\underline{\boldsymbol{F}}_t \cdot \delta\underline{\boldsymbol{g}}_t + \underline{\boldsymbol{F}}_t \cdot \Delta\delta\underline{\boldsymbol{g}}_t \qquad [5.44]$$

Since the normal contact force P_n is a function of the normal gap g_n, its derivative is evaluated as follows:

$$P_n = \int_{\partial\Omega^i} -\varepsilon_n \langle -g_n \rangle \, d\partial\Omega^i \quad \Rightarrow \quad \Delta P_n = \begin{cases} \int\limits_{\partial\Omega^i} \varepsilon_n \underset{\sim}{\boldsymbol{G}} \cdot \delta\underset{\sim}{\boldsymbol{x}} \, d\partial\Omega^i, & g_n < 0; \\ 0, & g_n \geq 0 \end{cases}$$

and by replacing the integral:

$$\Delta P_n = \delta\underset{\sim}{\boldsymbol{x}} \overset{\circ}{\cdot} \left[\varepsilon_n \partial\Omega^i \underset{\sim}{\boldsymbol{G}} \right], \quad g_n < 0$$

Substituting of the last expression into [5.44] and considering the first two terms gives:

$$\boxed{\Delta P_n \delta g_n + P_n \Delta\delta g_n = \delta\underset{\sim}{\boldsymbol{x}} \overset{\circ}{\cdot} \left[\varepsilon_n \partial\Omega^i \left(\underset{\sim}{\boldsymbol{G}} \overset{\boxtimes}{\otimes} \underset{\sim}{\boldsymbol{G}} - \langle -g_n \rangle \underset{\approx}{\underline{\underline{\boldsymbol{H}}}} \right) \right] \overset{\circ}{\cdot} \Delta\underset{\sim}{\boldsymbol{x}}} \qquad [5.45]$$

Instead of the variation of the tangential force, a dot product with the tangential sliding should be considered, slip and stick have to also be distinguished.

$$\Delta(\underline{\boldsymbol{F}}_t \cdot \delta\underline{\boldsymbol{g}}_t)$$

where

$$\delta\underline{\boldsymbol{g}}_t = \frac{\partial\underline{\boldsymbol{\rho}}}{\partial\underset{\sim}{\xi}} \circ \delta\underset{\sim}{\xi}$$

According to [5.38] (increment indices are omitted), we get:

$$\begin{cases} \underline{\boldsymbol{F}}_t \cdot \delta \underline{\boldsymbol{g}}_t = \varepsilon_t \partial\Omega_i (\underset{\sim}{\xi} - \underset{\sim}{\xi}^{\bullet}) \circ \delta \underset{\sim}{\xi}, \quad \textit{stick} \\ \underline{\boldsymbol{F}}_t \cdot \delta \underline{\boldsymbol{g}}_t = \mu\varepsilon_n \partial\Omega_i \langle -g_n \rangle \underline{\boldsymbol{s}}_t \cdot \underline{\frac{\partial \boldsymbol{\rho}}{\partial \xi}} \circ \delta \underset{\sim}{\xi}, \quad \textit{slip} \end{cases} \tag{5.46}$$

The variation of these expressions results in the following:

$$\Delta(\underline{\boldsymbol{F}}_t \cdot \delta \underline{\boldsymbol{g}}_t) = \varepsilon_t \partial\Omega_i \Delta \underset{\sim}{\xi} \circ \delta \underset{\sim}{\xi} + \varepsilon_t \partial\Omega_i (\underset{\sim}{\xi} - \underset{\sim}{\xi}^{\bullet}) \circ \Delta\delta \underset{\sim}{\xi}, \quad \textbf{\textit{stick}} \tag{5.47}$$

$$\begin{aligned} \Delta(\underline{\boldsymbol{F}}_t \cdot \delta \underline{\boldsymbol{g}}_t) &= -\mu\varepsilon_n \partial\Omega_i \Delta g_n \underline{\boldsymbol{s}}_t \cdot \underline{\frac{\partial \boldsymbol{\rho}}{\partial \xi}} \circ \delta \underset{\sim}{\xi} + \mu\varepsilon_n \partial\Omega_i \langle -g_n \rangle \Delta \underline{\boldsymbol{s}}_t \cdot \underline{\frac{\partial \boldsymbol{\rho}}{\partial \xi}} \circ \delta \underset{\sim}{\xi} \\ &+ \mu\varepsilon_n \partial\Omega_i \langle -g_n \rangle \underline{\boldsymbol{s}}_t \cdot \Delta \underline{\frac{\partial \boldsymbol{\rho}}{\partial \xi}} \circ \delta \underset{\sim}{\xi} + \mu\varepsilon_n \partial\Omega_i \langle -g_n \rangle \underline{\boldsymbol{s}}_t \cdot \underline{\frac{\partial \boldsymbol{\rho}}{\partial \xi}} \circ \Delta\delta \underset{\sim}{\xi}, \quad \textbf{\textit{slip}}, \; g_n < 0 \end{aligned} \tag{5.48}$$

The expression for the stick appears directly in a convenient form, whereas for the slip additional computations are needed. Carrying [5.34], the first right-hand term in [5.48] becomes:

$$-\mu\varepsilon_n \partial\Omega_i \Delta g_n \underline{\boldsymbol{s}}_t \cdot \underline{\frac{\partial \boldsymbol{\rho}}{\partial \xi}} \circ \delta \underset{\sim}{\xi} = -\frac{\mu\varepsilon_n \varepsilon_t \partial\Omega_i^2}{\|\underline{\boldsymbol{F}}_t^{\text{trial}}\|} \Delta g_n (\underset{\sim}{\xi} - \underset{\sim}{\xi}^{\bullet}) \circ \delta \underset{\sim}{\xi} \tag{5.49}$$

Using [5.43] allows to expand the second term in [5.48]:

$$\begin{aligned} &\mu\varepsilon_n \partial\Omega_i \langle -g_n \rangle \Delta \underline{\boldsymbol{s}}_t \cdot \underline{\frac{\partial \boldsymbol{\rho}}{\partial \xi}} \circ \delta \underset{\sim}{\xi} \\ &= \langle -g_n \rangle \frac{\mu\varepsilon_n \varepsilon_t \partial\Omega_i^2}{\|\underline{\boldsymbol{F}}_t^{\text{trial}}\|} \underset{\sim}{\tilde{\mathrm{s}}} \circ \left[\Delta \underset{\sim}{\xi} - \Delta \underline{\frac{\partial \boldsymbol{\rho}}{\partial \xi}} \boxtimes \overline{\underline{\frac{\partial \boldsymbol{\rho}}{\partial \xi}}} \circ (\underset{\sim}{\xi} - \underset{\sim}{\xi}^{\bullet}) \right] \underset{\sim}{\tilde{\mathrm{s}}} \circ \underset{\approx}{\mathrm{A}} \circ \delta \underset{\sim}{\xi} \end{aligned} \tag{5.50}$$

Expansion of the third term in [5.48] follows directly from substituting [5.34] for the unit sliding vector:

$$\mu\varepsilon_n \partial\Omega_i \langle -g_n \rangle \underline{\boldsymbol{s}}_t \cdot \Delta \underline{\frac{\partial \boldsymbol{\rho}}{\partial \xi}} \circ \delta \underset{\sim}{\xi} = \langle -g_n \rangle \frac{\mu\varepsilon_n \varepsilon_t \partial\Omega_i^2}{\|\underline{\boldsymbol{F}}_t^{\text{trial}}\|} (\underset{\sim}{\xi} - \underset{\sim}{\xi}^{\bullet}) \circ \overline{\underline{\frac{\partial \boldsymbol{\rho}}{\partial \xi}}} \boxtimes \Delta \underline{\frac{\partial \boldsymbol{\rho}}{\partial \xi}} \circ \delta \underset{\sim}{\xi} \tag{5.51}$$

The same procedure for the last term in [5.48] yields:

$$\mu\varepsilon_n\partial\Omega_i\langle -g_n\rangle\underline{\boldsymbol{s}}_t\cdot\frac{\partial\underline{\boldsymbol{\rho}}}{\partial\underset{\sim}{\xi}}\circ\Delta\delta\underset{\sim}{\xi}=\langle -g_n\rangle\frac{\mu\varepsilon_n\varepsilon_t\partial\Omega_i^2}{\|\underline{\boldsymbol{F}}_t^{\text{trial}}\|}(\underset{\sim}{\xi}-\underset{\sim}{\xi}^{\bullet})\circ\Delta\delta\underset{\sim}{\xi} \qquad [5.52]$$

The variation of the basis vectors can be expressed directly through the variation of the nodal coordinate vectors if we make use of [5.19].

$$\underline{\boldsymbol{\rho}}=\underset{\sim}{\phi}(0,\underset{\sim}{\xi})\circ\underset{\approx}{\boldsymbol{x}}\quad\Rightarrow\quad\Delta\frac{\partial\underline{\boldsymbol{\rho}}}{\partial\underset{\sim}{\xi}}=\frac{\partial\underset{\sim}{\phi}(0,\underset{\sim}{\xi})}{\partial\underset{\sim}{\xi}}\circ\Delta\underset{\approx}{\boldsymbol{x}} \qquad [5.53]$$

Together with [5.53], we use the following expressions:

$$\delta g_n=\underset{\sim}{\boldsymbol{G}}\overset{\circ}{\cdot}\delta\underset{\approx}{\boldsymbol{x}},\quad\delta\underset{\sim}{\xi}=\underset{\approx}{\boldsymbol{T}}\overset{\circ}{\cdot}\delta\underset{\approx}{\boldsymbol{x}},\quad\Delta\underset{\sim}{\xi}=\underset{\approx}{\boldsymbol{T}}\overset{\circ}{\cdot}\Delta\underset{\approx}{\boldsymbol{x}},\quad\Delta\delta\underset{\sim}{\xi}=\Delta\underset{\approx}{\boldsymbol{x}}\overset{\circ}{\cdot}\underset{\approx\approx}{\underset{=}{\boldsymbol{S}}}\overset{\circ}{\cdot}\delta\underset{\approx}{\boldsymbol{x}} \qquad [5.54]$$

where $\underset{\approx\approx}{\underset{=}{\boldsymbol{S}}}$ is a v-t-tensor (precisely two t-tensors gathered in v-vector) connecting nodal variation vectors with the second variation of the convective coordinate v-scalar.

$$\Delta\delta\underset{\sim}{\xi}=\Delta\underset{\approx}{\boldsymbol{x}}\overset{\circ}{\cdot}\underset{\approx\approx}{\underset{=}{\boldsymbol{S}}}\overset{\circ}{\cdot}\delta\underset{\approx}{\boldsymbol{x}}$$

all expressions for $\underset{\sim}{\boldsymbol{G}}$, $\underset{\approx}{\boldsymbol{T}}$, $\underset{\approx}{\underset{=}{\boldsymbol{H}}}$ and $\underset{\sim}{\underset{\approx\approx}{\underset{=}{\boldsymbol{S}}}}$ can be found in section 2.5 in equations [2.43], [2.46], [2.49] and [2.54], respectively. Careful grouping of terms in [5.49]–[5.52] and the substituting of [5.53] and [5.54] leads to the following expression for the variation of the tangential part for stick and slip.

5.4.2.2.1. Stick

$$\boxed{\Delta(\underline{\boldsymbol{F}}_t\cdot\delta\underline{\boldsymbol{g}}_t)=\Delta\underset{\approx}{\boldsymbol{x}}\overset{\circ}{\cdot}\left[\varepsilon_t\partial\Omega_i\left(\underset{\approx}{\boldsymbol{T}}\overset{\circ}{\underset{\otimes}{\boxtimes}}\underset{\approx}{\boldsymbol{T}}+(\underset{\sim}{\xi}-\underset{\sim}{\xi}^{\bullet})\circ\underset{\approx\approx}{\underset{=}{\boldsymbol{S}}}\right)\right]\overset{\circ}{\cdot}\delta\underset{\approx}{\boldsymbol{x}}} \qquad [5.55]$$

5.4.2.2.2. Slip

$$\Delta(\underline{\boldsymbol{F}}_t \cdot \delta\underline{\boldsymbol{g}}_t) = \Delta\underset{\sim}{\boldsymbol{x}} \overset{\circ}{\cdot} \left[\frac{\mu\varepsilon_n\varepsilon_t\partial\Omega_i^2}{\|\underline{\boldsymbol{F}}_t^{\text{trial}}\|} \left\{ -\underset{\sim}{\boldsymbol{G}} \overset{\boxtimes}{\otimes} \underset{\approx}{\boldsymbol{T}} \circ (\underset{\sim}{\xi} - \underset{\sim}{\xi}^{\bullet}) + \right.\right.$$
$$+ \langle -g_n \rangle \left(\underset{\sim}{\tilde{\mathrm{s}}} \circ \underset{\approx}{\boldsymbol{T}} \overset{\boxtimes}{\otimes} \underset{\approx}{\boldsymbol{T}} \circ \underset{\approx}{\mathrm{A}} \circ \underset{\sim}{\tilde{\mathrm{s}}} - \underset{\sim}{\tilde{\mathrm{s}}} \circ \frac{\partial\phi}{\partial\underset{\sim}{\xi}} \boxtimes \overline{\frac{\partial\underline{\boldsymbol{\rho}}}{\partial\underset{\sim}{\xi}}} \overset{\circ}{\otimes} (\underset{\sim}{\xi} - \underset{\sim}{\xi}^{\bullet}) \underset{\sim}{\tilde{\mathrm{s}}} \circ \underset{\approx}{\mathrm{A}} \circ \underset{\approx}{\boldsymbol{T}} + \right.$$
$$\left.\left.\left. + \ (\underset{\sim}{\xi} - \underset{\sim}{\xi}^{\bullet}) \circ \overline{\frac{\partial\underline{\boldsymbol{\rho}}}{\partial\underset{\sim}{\xi}}} \boxtimes \frac{\partial\phi}{\partial\underset{\sim}{\xi}} \circ \underset{\approx}{\boldsymbol{T}} + (\underset{\sim}{\xi} - \underset{\sim}{\xi}^{\bullet}) \circ \underset{\approx\approx}{\boldsymbol{S}} \right) \right\} \right] \overset{\circ}{\cdot} \delta\underset{\sim}{\boldsymbol{x}}$$

[5.56]

Grouping of [5.45] with [5.55] or [5.56] and getting rid of nodal variations gives the tangential contact t-tensor for stick and slip states, respectively.

$$\underset{\approx\approx}{\boldsymbol{K}}{}^{c\ \text{stick}}_{xx} = \varepsilon_n\partial\Omega^i \left(\underset{\sim}{\boldsymbol{G}} \overset{\boxtimes}{\otimes} \underset{\sim}{\boldsymbol{G}} - \langle -g_n \rangle \underset{\approx\approx}{\boldsymbol{H}} \right) + \varepsilon_t\partial\Omega_i \left(\underset{\approx}{\boldsymbol{T}} \overset{\circ}{\boxtimes}_{\otimes} \underset{\approx}{\boldsymbol{T}} + (\underset{\sim}{\xi} - \underset{\sim}{\xi}^{\bullet}) \circ \underset{\approx\approx}{\boldsymbol{S}} \right)$$

[5.57]

and

$$\underset{\approx\approx}{\boldsymbol{K}}{}^{c\ \text{slip}}_{xx} = \varepsilon_n\partial\Omega^i \left(\underset{\sim}{\boldsymbol{G}} \overset{\boxtimes}{\otimes} \underset{\sim}{\boldsymbol{G}} - \langle -g_n \rangle \underset{\approx\approx}{\boldsymbol{H}} \right) + \frac{\mu\varepsilon_n\varepsilon_t\partial\Omega_i^2}{\|\underline{\boldsymbol{F}}_t^{\text{trial}}\|} \left\{ -\underset{\sim}{\boldsymbol{G}} \overset{\boxtimes}{\otimes} \underset{\approx}{\boldsymbol{T}} \circ (\underset{\sim}{\xi} - \underset{\sim}{\xi}^{\bullet}) \right.$$
$$+ \langle -g_n \rangle \left(\underset{\sim}{\tilde{\mathrm{s}}} \circ \underset{\approx}{\boldsymbol{T}} \overset{\boxtimes}{\otimes} \underset{\approx}{\boldsymbol{T}} \circ \underset{\approx}{\mathrm{A}} \circ \underset{\sim}{\tilde{\mathrm{s}}} - \underset{\sim}{\tilde{\mathrm{s}}} \circ \frac{\partial\phi}{\partial\underset{\sim}{\xi}} \boxtimes \overline{\frac{\partial\underline{\boldsymbol{\rho}}}{\partial\underset{\sim}{\xi}}} \overset{\circ}{\otimes} (\underset{\sim}{\xi} - \underset{\sim}{\xi}^{\bullet}) \underset{\sim}{\tilde{\mathrm{s}}} \circ \underset{\approx}{\mathrm{A}} \circ \underset{\approx}{\boldsymbol{T}} + \right.$$
$$\left.\left. + \ (\underset{\sim}{\xi} - \underset{\sim}{\xi}^{\bullet}) \circ \overline{\frac{\partial\underline{\boldsymbol{\rho}}}{\partial\underset{\sim}{\xi}}} \boxtimes \frac{\partial\phi}{\partial\underset{\sim}{\xi}} \circ \underset{\approx}{\boldsymbol{T}} + (\underset{\sim}{\xi} - \underset{\sim}{\xi}^{\bullet}) \circ \underset{\approx\approx}{\boldsymbol{S}} \right) \right\}$$

[5.58]

5.4.3. *Augmented Lagrangian method: frictionless case*

5.4.3.1. *Residual vector*

Virtual work due to frictionless contact was given in [4.116] for continuous problems. The significant difference of the coupled ALM from LMM and PM is that all constructed contact elements contribute to the virtual work of the system independently if the gap between slave node and master segment is open or closed, that is contact element is inactive or active. This fact ensures the smoothness of the energy potential and the continuity of the virtual work. However, as was shown on a simple example in section 4.7.3, the inactive contact elements increase significantly the condition number of the tangent matrix of the system. That is why the less useless contact elements have been formed during the detection step, the better it is for the resolution step. So a careful detection procedure is highly recommended, especially for the ALM.

Remark that the difference between frictional (containing several complementary dofs for Lagrange multipliers) and frictionless (containing only one complementary dof) contact elements should be made at the stage of their creation to accelerate the solution.

Below the contribution to the virtual energy of the i-th NTS contact element is given for contact and non-contact status, respectively.

$$\delta W_i^c = \begin{cases} \int\limits_{\partial\Omega_i} \hat{\lambda}_n \delta g_n + g_n \delta\lambda_n \, d\partial\Omega_i, & \hat{\lambda}_n \leq 0 \\ \int\limits_{\partial\Omega_i} -\frac{1}{\varepsilon_n}\lambda_n \delta\lambda_n \, d\partial\Omega_i, & \hat{\lambda}_n > 0 \end{cases} \qquad [5.59]$$

We can recap that the hat denotes the augmented Lagrange multipliers:

$$\hat{\lambda}_n = \lambda_n + \varepsilon_n g_n$$

As discussed previously, the variation of the normal gap δg_n is replaced by the following double dot product:

$$\delta g_n = \underset{\sim}{\boldsymbol{G}} \overset{\circ}{:} \delta \underset{\sim}{\boldsymbol{x}} \qquad [5.60]$$

By grouping terms in matrices and replacing the integral by master segment area, we get:

$$\delta W_i^c = \begin{cases} \begin{bmatrix} \hat{\lambda}_n \underset{\sim}{\boldsymbol{G}} \partial\Omega_i \\ g_n \partial\Omega_i \end{bmatrix}^T \overset{\circ}{\cdot} \begin{bmatrix} \delta \underset{\sim}{\boldsymbol{x}} \\ \delta\lambda_n \end{bmatrix}, & \hat{\lambda}_n \leq 0 \\ \begin{bmatrix} 0 \\ -\frac{\partial\Omega_i}{\varepsilon_n}\lambda_n \end{bmatrix}^T \overset{\circ}{\cdot} \begin{bmatrix} \delta \underset{\sim}{\boldsymbol{x}} \\ \delta\lambda_n \end{bmatrix}, & \hat{\lambda}_n > 0 \end{cases}$$

The residual v-vector for the primal variables (nodal displacement vectors) and the scalar residual component for the only dual variable takes then the forms:

$$\begin{cases} \begin{bmatrix} \hat{\lambda}_n \underset{\sim}{\boldsymbol{G}} \partial\Omega_i \\ g_n \partial\Omega_i \end{bmatrix}^T, & \hat{\lambda}_n \leq 0, \ \textit{contact} \\ \begin{bmatrix} 0 \\ -\frac{\partial\Omega_i}{\varepsilon_n}\lambda_n \end{bmatrix}^T, & \hat{\lambda}_n > 0, \quad \textit{non-contact} \end{cases} \qquad [5.61]$$

5.4.3.2. *Tangent contact matrix*

To get the elementary tangent contact matrix, we take a variation of the virtual work of the i-th contact element [5.59]

$$\Delta\delta W_i^c = \begin{cases} \int\limits_{\partial\Omega_i} \Delta\hat{\lambda}_n \delta g_n + \hat{\lambda}_n \Delta\delta g_n + \Delta g_n \delta\lambda_n \, d\partial\Omega_i, & \hat{\lambda}_n \leq 0 \\ \int\limits_{\partial\Omega_i} -\frac{1}{\varepsilon_n}\Delta\lambda_n \delta\lambda_n \, d\partial\Omega_i, & \hat{\lambda}_n > 0 \end{cases} \qquad [5.62]$$

As Lagrange multiplier is an independent variable, its second variations vanishes. Expanding the variation of the augmented Lagrange multiplier:

$$\Delta\hat{\lambda}_n = \Delta\lambda_n + \varepsilon_n \Delta g_n$$

and using the expression for the variation of the normal gap [5.60], we can extract the tangent matrix from the resulting expression:

$$\Delta\delta W_i^c = \begin{cases} \begin{bmatrix} \Delta \underset{\sim}{\boldsymbol{x}} \\ \Delta\lambda_n \end{bmatrix}^T \overset{\circ}{\cdot} \begin{bmatrix} \varepsilon_n \partial\Omega_i \underset{\sim}{\boldsymbol{G}} \overset{\boxtimes}{\otimes} \underset{\sim}{\boldsymbol{G}} + \hat{\lambda}_n \underset{\approx}{\underset{=}{\boldsymbol{H}}} & \partial\Omega_i \underset{\sim}{\boldsymbol{G}} \\ \partial\Omega_i \underset{\sim}{\boldsymbol{G}} & 0 \end{bmatrix} \overset{\circ}{\cdot} \begin{bmatrix} \delta \underset{\sim}{\boldsymbol{x}} \\ \delta\lambda_n \end{bmatrix}, & \hat{\lambda}_n \leq 0 \\ \begin{bmatrix} \Delta \underset{\sim}{\boldsymbol{x}} \\ \Delta\lambda_n \end{bmatrix}^T \overset{\circ}{\cdot} \begin{bmatrix} 0 & 0 \\ 0 & -\frac{\partial\Omega_i}{\varepsilon_n} \end{bmatrix} \overset{\circ}{\cdot} \begin{bmatrix} \delta \underset{\sim}{\boldsymbol{x}} \\ \delta\lambda_n \end{bmatrix}, & \hat{\lambda}_n > 0 \end{cases} \qquad [5.63]$$

where $\underset{\approx}{\underset{=}{\boldsymbol{H}}}$ is a t-tensor connecting nodal variation vectors with the second variation of the normal gap.

$$\Delta\delta g_n = \Delta\underset{\sim}{\boldsymbol{x}} \overset{\circ}{\cdot} \underset{\approx}{\underset{=}{\boldsymbol{H}}} \overset{\circ}{\cdot} \delta\underset{\sim}{\boldsymbol{x}}$$

All needed expressions $\underset{\sim}{\boldsymbol{G}}$ and $\underset{\approx}{\underset{=}{\boldsymbol{H}}}$ for arbitrary discretization can be found in section 2.5. The resulting elemental tangent contact matrices for contact and non-contact statuses are given below. These matrices are symmetric.

$$K^c{}_{\text{contact}} = \begin{bmatrix} \varepsilon_n \partial\Omega_i \underset{\sim}{\boldsymbol{G}} \overset{\boxtimes}{\otimes} \underset{\sim}{\boldsymbol{G}} + \hat{\lambda}_n \underset{\approx}{\underset{=}{\boldsymbol{H}}} & \partial\Omega_i \underset{\sim}{\boldsymbol{G}} \\ \partial\Omega_i \underset{\sim}{\boldsymbol{G}} & 0 \end{bmatrix}, \quad \hat{\lambda}_n \leq 0, \quad \textit{contact} \qquad [5.64]$$

$$K^c{}_{\text{non-contact}} = \begin{bmatrix} 0 & 0 \\ 0 & -\frac{\partial\Omega_i}{\varepsilon_n} \end{bmatrix}, \quad \hat{\lambda}_n > 0, \quad \textit{non-contact} \qquad [5.65]$$

The structure of these matrices can be depicted by blocks:

$$K^c = \begin{bmatrix} \begin{bmatrix} & \nabla_x\nabla_x & \\ & & \end{bmatrix}_{\{N\times N\}} & \begin{bmatrix} \nabla_{\lambda_n}\nabla_x \\ \end{bmatrix}_{\{N\times 1\}} \\ \begin{bmatrix} & \nabla_x\nabla_{\lambda_n} & \end{bmatrix}_{\{1\times N\}} & \begin{bmatrix} \nabla_{\lambda_n}\nabla_{\lambda_n} \end{bmatrix}_{\{1\times 1\}} \end{bmatrix} (l_n + l_t) \qquad [5.66]$$

where $n \times m$ in each block designates the number of "strings" n and the number of "columns" m, where in s-structure representation $N = D(M+1)$ and in scalar representation $N = D(M+1)$: D is the dimension of the problem and M is the number of nodes on the master segment and $M+1$ is a total number of geometrical nodes of the contact element.

5.4.4. *Augmented Lagrangian method: frictional case*

5.4.4.1. *Residual vector*

The balance of virtual work for frictional contact coming from the variation of the augmented Lagrangian functional was stated in [4.115]. The contribution of the

frictional contact interface extracted from [4.115] being split into three integrals over slip, stick and non-contact zones is stated below.

$$\begin{aligned}\delta W^c &= \int_{\Gamma_c^{1*}} \hat{\lambda}_n \delta g_n + g_n \delta \lambda_n - \mu \hat{\sigma}_n \frac{\hat{\underline{\boldsymbol{\lambda}}}_t}{\|\hat{\underline{\boldsymbol{\lambda}}}_t\|} \cdot \delta \underline{\boldsymbol{g}}_t - \frac{1}{\varepsilon_t} \left(\underline{\boldsymbol{\lambda}}_t + \mu \hat{\sigma}_n \frac{\hat{\underline{\boldsymbol{\lambda}}}_t}{\|\hat{\underline{\boldsymbol{\lambda}}}_t\|} \right) \cdot \delta \underline{\boldsymbol{\lambda}}_t \, d\Gamma_c^1 \\ &+ \int_{\Gamma_c^{1\bullet}} \hat{\lambda}_n \delta g_n + g_n \delta \lambda_n + \hat{\underline{\boldsymbol{\lambda}}}_t \cdot \delta \underline{\boldsymbol{g}}_t + \underline{\boldsymbol{g}}_t \cdot \delta \underline{\boldsymbol{\lambda}}_t \, d\Gamma_c^1 \\ &+ \int_{\Gamma_c^1 \setminus \overline{\Gamma}_c^1} -\frac{1}{\varepsilon_n} \lambda_n \delta \lambda_n - \frac{1}{\varepsilon_t} \underline{\boldsymbol{\lambda}}_t \cdot \delta \underline{\boldsymbol{\lambda}}_t \, d\Gamma_c^1 \end{aligned} \qquad [5.67]$$

A given contact element can be in one of three states: slip, stick or non-contact. Depending on the status, its contribution to the virtual work of the system is given by one of the three possible integrals stated below.

$$\delta W_i^c = \begin{cases} \int_{\partial\Omega_i} \hat{\lambda}_n \delta g_n + g_n \delta \lambda_n - \mu \hat{\sigma}_n \frac{\hat{\underline{\boldsymbol{\lambda}}}_t}{\|\hat{\underline{\boldsymbol{\lambda}}}_t\|} \cdot \delta \underline{\boldsymbol{g}}_t - \frac{1}{\varepsilon_t} \left(\underline{\boldsymbol{\lambda}}_t + \mu \hat{\sigma}_n \frac{\hat{\underline{\boldsymbol{\lambda}}}_t}{\|\hat{\underline{\boldsymbol{\lambda}}}_t\|} \right) \cdot \delta \underline{\boldsymbol{\lambda}}_t \, d\partial\Omega_i, & \underbrace{\|\hat{\underline{\boldsymbol{\lambda}}}_t\| > -\mu \hat{\sigma}_n}_{\textit{slip}} \\ \int_{\partial\Omega_i} \hat{\lambda}_n \delta g_n + g_n \delta \lambda_n + \hat{\underline{\boldsymbol{\lambda}}}_t \cdot \delta \underline{\boldsymbol{g}}_t + \underline{\boldsymbol{g}}_t \cdot \delta \underline{\boldsymbol{\lambda}}_t \, d\partial\Omega_i, & \underbrace{\|\hat{\underline{\boldsymbol{\lambda}}}_t\| \leq -\mu \hat{\sigma}_n}_{\textit{stick}} \\ \int_{\partial\Omega_i} -\frac{1}{\varepsilon_n} \lambda_n \delta \lambda_n - \frac{1}{\varepsilon_t} \underline{\boldsymbol{\lambda}}_t \cdot \delta \underline{\boldsymbol{\lambda}}_t \, d\partial\Omega_i, & \underbrace{\hat{\sigma}_n > 0}_{\textit{non-contact}} \end{cases} \qquad [5.68]$$

To extract the residual s-structures, we make use of the relations between the variation of the nodal coordinate vectors of the contact element and the corresponding variations of the geometrical quantities: see [5.60] and:

$$\delta \underline{\boldsymbol{g}}_t = \frac{\partial \underline{\boldsymbol{\rho}}}{\partial \underset{\sim}{\xi}} \circ \delta \underset{\sim}{\xi} = \frac{\partial \underline{\boldsymbol{\rho}}}{\partial \underset{\sim}{\xi}} \circ \underline{\underline{\boldsymbol{T}}} \overset{\circ}{\cdot} \delta \underline{\underline{\boldsymbol{x}}} \qquad [5.69]$$

Further, let us replace the sliding direction by $\hat{\underline{\boldsymbol{s}}}$:

$$\hat{\underline{\boldsymbol{s}}} = \frac{\hat{\underline{\boldsymbol{\lambda}}}_t}{\|\hat{\underline{\boldsymbol{\lambda}}}_t\|} \qquad [5.70]$$

This sliding can be presented in the contravariant basis as well as the augmented Lagrange multiplier vector corresponding to the tangential contact stress.

$$\hat{\underline{\boldsymbol{s}}} = \left(\hat{\underline{\boldsymbol{s}}} \cdot \frac{\partial \underline{\boldsymbol{\rho}}}{\partial \underset{\sim}{\xi}}\right) \circ \overline{\frac{\partial \underline{\boldsymbol{\rho}}}{\partial \underset{\sim}{\xi}}} = \hat{\underset{\sim}{\bar{s}}} \circ \overline{\frac{\partial \underline{\boldsymbol{\rho}}}{\partial \underset{\sim}{\xi}}}, \quad \hat{\underline{\boldsymbol{\lambda}}}_t = \left(\hat{\underline{\boldsymbol{\lambda}}}_t \cdot \frac{\partial \underline{\boldsymbol{\rho}}}{\partial \underset{\sim}{\xi}}\right) \circ \overline{\frac{\partial \underline{\boldsymbol{\rho}}}{\partial \underset{\sim}{\xi}}} = \hat{\underset{\sim}{\lambda}}_t \circ \overline{\frac{\partial \underline{\boldsymbol{\rho}}}{\partial \underset{\sim}{\xi}}} \quad [5.71]$$

Regardless possible confusions, the Lagrange multiplier $\underline{\boldsymbol{\lambda}}_t$ should be presented in the contravariant basis and its variation in the covariant basis:

$$\underline{\boldsymbol{\lambda}}_t = \left(\underline{\boldsymbol{\lambda}}_t \cdot \frac{\partial \underline{\boldsymbol{\rho}}}{\partial \underset{\sim}{\xi}}\right) \circ \overline{\frac{\partial \underline{\boldsymbol{\rho}}}{\partial \underset{\sim}{\xi}}} = \bar{\underset{\sim}{\lambda}}_t \circ \overline{\frac{\partial \underline{\boldsymbol{\rho}}}{\partial \underset{\sim}{\xi}}}, \quad \delta \underline{\boldsymbol{\lambda}}_t = \underset{\sim}{\lambda}_t \circ \frac{\partial \underline{\boldsymbol{\rho}}}{\partial \underset{\sim}{\xi}} \quad [5.72]$$

and finally the incremental change of the tangential relative sliding vector is also given in the contravariant basis:

$$\underline{\boldsymbol{g}}_t \sim \underline{\dot{\boldsymbol{g}}}_t (t^{i+1} - t^i) \quad \Rightarrow \quad \underline{\boldsymbol{g}}_t = (\bar{\underset{\sim}{\xi}}^{\,i+1} - \bar{\underset{\sim}{\xi}}^{\,i}) \circ \overline{\frac{\partial \underline{\boldsymbol{\rho}}}{\partial \underset{\sim}{\xi}}} \quad [5.73]$$

Note that this vector should be zero in stick state. Note also that this vector appears in the split of the augmented Lagrange multiplier $\hat{\underline{\boldsymbol{\lambda}}}_t$. After substituting all these expressions into [5.4.4.1] and replacing the integral by the area of the master segment $\partial\Omega_i$, we get:

$$\delta W^c_{i\ \text{slip}} = \begin{bmatrix} \left(\hat{\lambda}_n \underset{\sim}{\boldsymbol{G}} - \mu \hat{\sigma}_n \hat{\underset{\sim}{\bar{s}}} \circ \underset{\approx}{\boldsymbol{T}}\right) \partial\Omega_i \\ g_n \partial\Omega_i \\ -\frac{\partial\Omega_i}{\varepsilon_t} \left(\bar{\underset{\sim}{\lambda}}_t + \mu \hat{\sigma}_n \hat{\underset{\sim}{\bar{s}}}\right) \end{bmatrix}^T \overset{\circ}{\cdot} \begin{bmatrix} \delta \underset{\sim}{\boldsymbol{x}} \\ \delta \lambda_n \\ \delta \underset{\sim}{\lambda}_t \end{bmatrix}, \quad \|\hat{\underline{\boldsymbol{\lambda}}}_t\| \geq \hat{\sigma}_n, \hat{\sigma}_n \leq 0, \ \textit{slip}$$

$$\delta W^c_{i\ \text{stick}} = \begin{bmatrix} \left(\hat{\lambda}_n \underset{\sim}{\boldsymbol{G}} + \hat{\underset{\sim}{\lambda}}_t \circ \underset{\approx}{\boldsymbol{T}}\right) \partial\Omega_i \\ g_n \partial\Omega_i \\ (\bar{\underset{\sim}{\xi}}^{\,i+1} - \bar{\underset{\sim}{\xi}}^{\,i}) \partial\Omega_i \end{bmatrix}^T \overset{\circ}{\cdot} \begin{bmatrix} \delta \underset{\sim}{\boldsymbol{x}} \\ \delta \lambda_n \\ \delta \underset{\sim}{\lambda}_t \end{bmatrix}, \quad \|\hat{\underline{\boldsymbol{\lambda}}}_t\| < \hat{\sigma}_n, \hat{\sigma}_n \leq 0, \ \textit{stick}$$

$$\delta W^c_{i\ \text{non-contact}} = \begin{bmatrix} 0 \\ -\frac{\partial\Omega_i \lambda_n}{\varepsilon_n} \\ -\frac{\partial\Omega_i \underset{\sim}{\bar{\lambda}}_t}{\varepsilon_t} \end{bmatrix}^T \circ \begin{bmatrix} \delta \underset{\approx}{\boldsymbol{x}} \\ \delta\lambda_n \\ \delta \underset{\sim}{\lambda}_t \end{bmatrix}, \quad \|\hat{\underline{\boldsymbol{\lambda}}}_t\| < \hat{\sigma}_n, \hat{\sigma}_n \leq 0, \ \textit{stick}$$

The left hand matrices in these expressions represent the residual vectors for slip, stick and non-contact, respectively.

5.4.4.2. *Tangent contact matrix*

To derive the tangent contact matrix, we start from the variation of the virtual work contributions arising from one contact element [5.4.4.1]. Slip, stick and non-contact states will be considered separately. As Lagrange multipliers are independent variables, their second variations vanish. It is worth mentioning that the augmented contact pressure $\hat{\sigma}_n = \sigma_n + \varepsilon_n g_n$, previously assumed known, now becomes the unknown variable and is replaced by the augmented Lagrange multiplier $\hat{\lambda}_n = \lambda_n + \varepsilon_n g_n$.

5.4.4.2.1. Slip state

$$\begin{aligned} \Delta\delta W^c_{i\ \text{slip}} &= \int_{\partial\Omega_i} \Delta\hat{\lambda}_n \delta g_n + \hat{\lambda}_n \Delta\delta g_n + \Delta g_n \delta\lambda_n - \mu\Delta\hat{\lambda}_n \underline{\hat{\boldsymbol{s}}} \cdot \delta\underline{\boldsymbol{g}}_t \\ &- \mu\hat{\lambda}_n \frac{\Delta\hat{\underline{\boldsymbol{\lambda}}}_t}{\|\hat{\underline{\boldsymbol{\lambda}}}_t\|} \cdot \left(\underline{\underline{\boldsymbol{I}}} - \underline{\hat{\boldsymbol{s}}} \otimes \underline{\hat{\boldsymbol{s}}} \right) \cdot \delta\underline{\boldsymbol{g}}_t \mu\hat{\lambda}_n \underset{\sim}{\hat{\underline{\underline{s}}}} \circ \Delta\delta \underset{\sim}{\xi} - \frac{1}{\varepsilon_t} \Delta\underline{\boldsymbol{\lambda}}_t \cdot \delta\underline{\boldsymbol{\lambda}}_t \quad [5.74] \\ &- \frac{\mu\hat{\lambda}_n}{\varepsilon_t} \frac{\Delta\hat{\underline{\boldsymbol{\lambda}}}_t}{\|\hat{\underline{\boldsymbol{\lambda}}}_t\|} \cdot \left(\underline{\underline{\boldsymbol{I}}} - \underline{\hat{\boldsymbol{s}}} \otimes \underline{\hat{\boldsymbol{s}}} \right) \cdot \delta\underline{\boldsymbol{\lambda}}_t - \frac{1}{\varepsilon_t} \mu\Delta\hat{\lambda}_n \underline{\hat{\boldsymbol{s}}} \cdot \delta\underline{\boldsymbol{\lambda}}_t \, d\partial\Omega_i \end{aligned}$$

Let us get rid of dot products replacing them by s-dot products by means of the expressions derived in [5.69]–[5.73]:

$$\underline{\hat{\boldsymbol{s}}} \cdot \delta\underline{\boldsymbol{g}}_t = \underset{\sim}{\hat{\underline{\underline{s}}}} \circ \delta\underset{\sim}{\xi}, \quad \frac{\Delta\hat{\underline{\boldsymbol{\lambda}}}_t}{\|\hat{\underline{\boldsymbol{\lambda}}}_t\|} \cdot \left(\underline{\underline{\boldsymbol{I}}} - \underline{\hat{\boldsymbol{s}}} \otimes \underline{\hat{\boldsymbol{s}}} \right) \cdot \delta\underline{\boldsymbol{g}}_t = \frac{\Delta\,\hat{\underset{\sim}{\lambda}}_t}{\|\hat{\underline{\boldsymbol{\lambda}}}_t\|} \circ \left(\underset{\approx}{\mathrm{A}} - \underset{\sim}{\hat{\underline{\underline{s}}}} \boxtimes \underset{\sim}{\hat{\underline{\underline{s}}}} \right) \circ \delta\underset{\sim}{\xi}$$

$$\begin{aligned} \Delta\underline{\boldsymbol{\lambda}}_t \cdot \delta\underline{\boldsymbol{\lambda}}_t &= \Delta\underset{\sim}{\lambda}_t \circ \underset{\approx}{\mathrm{A}} \circ \delta\underset{\sim}{\lambda}_t, \ \frac{\Delta\hat{\underline{\boldsymbol{\lambda}}}_t}{\|\hat{\underline{\boldsymbol{\lambda}}}_t\|} \cdot \left(\underline{\underline{\boldsymbol{I}}} - \underline{\hat{\boldsymbol{s}}} \boxtimes \underline{\hat{\boldsymbol{s}}} \right) \cdot \delta\underline{\boldsymbol{\lambda}}_t \\ &= \frac{\Delta\,\hat{\underset{\sim}{\lambda}}_t}{\|\hat{\underline{\boldsymbol{\lambda}}}_t\|} \circ \left(\underset{\approx}{\mathrm{A}} - \underline{\hat{\boldsymbol{s}}} \boxtimes \underline{\hat{\boldsymbol{s}}} \right) \circ \delta\underset{\sim}{\lambda}_t \end{aligned}$$

$$\underline{\hat{\boldsymbol{s}}} \cdot \delta\underline{\boldsymbol{\lambda}}_t = \underset{\sim}{\hat{\underline{\underline{s}}}} \circ \delta\underset{\sim}{\lambda}_t$$

Expanding of the augmented Lagrange multipliers under the variation sign:

$$\delta\hat{\lambda}_n = \delta\lambda_n + \varepsilon_n \delta g_n, \quad \delta\hat{\underline{\boldsymbol{\lambda}}}_t = \delta\underline{\boldsymbol{\lambda}}_t + \varepsilon_t \delta\underline{\boldsymbol{g}}_t \quad \Leftrightarrow \quad \delta\hat{\underset{\sim}{\lambda}}_t = \delta\underset{\sim}{\lambda}_t + \varepsilon_t \delta\underset{\sim}{\xi}$$

Now, we state the variation of the elemental virtual work in the expanded form:

$$\begin{aligned}
\Delta\delta W^c_{i\ \text{slip}} = \int_{\partial\Omega_i} & \Delta\lambda_n \delta g_n + \varepsilon_n \Delta g_n \delta g_n + \hat{\lambda}_n \Delta\delta g_n + \Delta g_n \delta\lambda_n - \mu\Delta\lambda_n \hat{\underset{\sim}{\mathrm{s}}} \circ \delta\underset{\sim}{\xi} \\
& - \mu\varepsilon_n \Delta g_n \hat{\underset{\sim}{\mathrm{s}}} \circ \delta\underset{\sim}{\xi} - \mu\hat{\lambda}_n \frac{\Delta\underset{\sim}{\lambda}_t}{\|\hat{\underline{\boldsymbol{\lambda}}}_t\|} \circ \left(\underset{\approx}{\mathrm{A}} - \hat{\underset{\sim}{\mathrm{s}}} \boxtimes \hat{\underset{\sim}{\mathrm{s}}} \right) \circ \delta\underset{\sim}{\xi} \\
& - \mu\hat{\lambda}_n \varepsilon_t \frac{\Delta\underset{\sim}{\xi}}{\|\hat{\underline{\boldsymbol{\lambda}}}_t\|} \circ \left(\underset{\approx}{\mathrm{A}} - \hat{\underset{\sim}{\mathrm{s}}} \boxtimes \hat{\underset{\sim}{\mathrm{s}}} \right) \circ \delta\underset{\sim}{\xi} - \mu\hat{\lambda}_n \hat{\underset{\sim}{\mathrm{s}}} \circ \Delta\delta\underset{\sim}{\xi} \\
& - \frac{1}{\varepsilon_t} \Delta\underset{\sim}{\lambda}_t \circ \underset{\approx}{\mathrm{A}} \circ \delta\underset{\sim}{\lambda}_t - \frac{\mu\hat{\lambda}_n}{\varepsilon_t} \frac{\Delta\underset{\sim}{\lambda}_t}{\|\hat{\underline{\boldsymbol{\lambda}}}_t\|} \circ \left(\underset{\approx}{\mathrm{A}} - \hat{\underset{\sim}{\mathrm{s}}} \boxtimes \hat{\underset{\sim}{\mathrm{s}}} \right) \circ \delta\underset{\sim}{\lambda}_t \\
& - \mu\hat{\lambda}_n \frac{\Delta\underset{\sim}{\xi}}{\|\hat{\underline{\boldsymbol{\lambda}}}_t\|} \circ \left(\underset{\approx}{\mathrm{A}} - \hat{\underset{\sim}{\mathrm{s}}} \boxtimes \hat{\underset{\sim}{\mathrm{s}}} \right) \circ \delta\underset{\sim}{\lambda}_t - \\
& - \frac{1}{\varepsilon_t} \mu\Delta\lambda_n \hat{\underset{\sim}{\mathrm{s}}} \circ \delta\underset{\sim}{\lambda}_t - \mu\Delta g_n \hat{\underset{\sim}{\mathrm{s}}} \circ \delta\underset{\sim}{\lambda}_t \, d\partial\Omega_i
\end{aligned} \qquad [5.75]$$

Finally, the geometrical variations are expressed through the variations of the nodal coordinate vectors and the integral is replaced simply by the area of the master segment, which results in a "matrix":

$$\Delta\delta W^c_{i\ \text{slip}} = \begin{bmatrix} \Delta\underset{\sim}{\boldsymbol{x}} \\ \Delta\lambda_n \\ \Delta\underset{\sim}{\lambda}_t \end{bmatrix}^T \overset{\circ}{\cdot} \begin{bmatrix} \underset{\approx}{\boldsymbol{K}}_{xx} & \underset{\sim}{\boldsymbol{K}}_{x\lambda_n} & \underset{\approx}{\boldsymbol{K}}_{x\lambda_t} \\ \underset{\sim}{\boldsymbol{K}}_{\lambda_n x} & K_{\lambda_n\lambda_n} & \underset{\sim}{\mathrm{K}}_{\lambda_n\lambda_t} \\ \underset{\approx}{\boldsymbol{K}}_{\lambda_t x} & \underset{\sim}{\mathrm{K}}_{\lambda_t\lambda_n} & \underset{\approx}{\mathrm{K}}_{\lambda_t\lambda_t} \end{bmatrix} \overset{\circ}{\cdot} \begin{bmatrix} \Delta\underset{\sim}{\boldsymbol{x}} \\ \Delta\lambda_n \\ \Delta\underset{\sim}{\lambda}_t \end{bmatrix} \qquad [5.76]$$

The components of this "matrix" are stated below. Terms in braces denote unsymmetrical components of the matrix:

$$
\begin{aligned}
&\underset{\approx}{\underset{=}{\boldsymbol{K}}}_{xx} = \partial\Omega_i \left(\varepsilon_n \underset{\sim}{\boldsymbol{G}} \underset{\otimes}{\boxtimes} \underset{\sim}{\boldsymbol{G}} + \hat{\lambda}_n \underset{\approx}{\underset{=}{\boldsymbol{H}}} - \left\{ \varepsilon_n \mu \underset{\sim}{\boldsymbol{G}} \underset{\otimes}{\boxtimes} \hat{\underset{\sim}{\mathrm{s}}} \circ \underset{\approx}{\boldsymbol{T}} \right\} \right) - \\
&\quad - \frac{\mu \hat{\lambda}_n \varepsilon_t \partial\Omega_i}{\|\hat{\underset{\sim}{\boldsymbol{\lambda}}}_t\|} \underset{\approx}{\boldsymbol{T}} \circ \left(\underset{\approx}{\mathrm{A}} - \hat{\underset{\sim}{\mathrm{s}}} \boxtimes \hat{\underset{\sim}{\mathrm{s}}} \right) \circ \underset{\approx}{\boldsymbol{T}} - \mu \hat{\lambda}_n \partial\Omega_i \hat{\underset{\sim}{\mathrm{s}}} \circ \underset{\approx}{\underset{=}{\boldsymbol{S}}} \\
&\underset{\sim}{\boldsymbol{K}}_{x\lambda_n} = \partial\Omega_i \underset{\sim}{\boldsymbol{G}} \\
&\underset{\approx}{\boldsymbol{K}}_{x\lambda_t} = -\frac{\mu \hat{\lambda}_n \partial\Omega_i}{\|\hat{\underset{\sim}{\boldsymbol{\lambda}}}_t\|} \underset{\approx}{\boldsymbol{T}} \circ \left(\underset{\approx}{\mathrm{A}} - \hat{\underset{\sim}{\mathrm{s}}} \boxtimes \hat{\underset{\sim}{\mathrm{s}}} \right) - \left\{ \mu \partial\Omega_i \underset{\sim}{\boldsymbol{G}} \boxtimes \hat{\underset{\sim}{\mathrm{s}}} \right\} \\
&\underset{\sim}{\boldsymbol{K}}_{\lambda_n x} = \partial\Omega_i \underset{\sim}{\boldsymbol{G}} - \left\{ \partial\Omega_i \mu \hat{\underset{\sim}{\mathrm{s}}} \circ \underset{\approx}{\boldsymbol{T}} \right\} \\
&K_{\lambda_n \lambda_n} = 0 \\
&\underset{\sim}{\mathrm{K}}_{\lambda_n \lambda_t} = - \left\{ \frac{\mu \partial\Omega_i}{\varepsilon_t} \hat{\underset{\sim}{\mathrm{s}}} \right\} \\
&\underset{\approx}{\boldsymbol{K}}_{\lambda_t x} = -\frac{\mu \hat{\lambda}_n \partial\Omega_i}{\|\hat{\underset{\sim}{\boldsymbol{\lambda}}}_t\|} \circ \left(\underset{\approx}{\mathrm{A}} - \hat{\underset{\sim}{\mathrm{s}}} \boxtimes \hat{\underset{\sim}{\mathrm{s}}} \right) \circ \underset{\approx}{\boldsymbol{T}} \\
&\underset{\sim}{\mathrm{K}}_{\lambda_t \lambda_n} = 0 \\
&\underset{\approx}{\mathrm{K}}_{\lambda_t \lambda_t} = -\frac{\partial\Omega_i}{\varepsilon_t} \underset{\approx}{\mathrm{A}} - \frac{\mu \hat{\lambda}_n \partial\Omega_i}{\varepsilon_t \|\hat{\underset{\sim}{\boldsymbol{\lambda}}}_t\|} \left(\underset{\approx}{\mathrm{A}} - \hat{\underset{\sim}{\mathrm{s}}} \boxtimes \hat{\underset{\sim}{\mathrm{s}}} \right)
\end{aligned}
\qquad [5.77]
$$

All s-structures arising from variations of the geometrical quantities, namely $\underset{\sim}{\boldsymbol{G}}$, $\underset{\approx}{\boldsymbol{T}}$, $\underset{\approx}{\underset{=}{\boldsymbol{H}}}$ and $\underset{\approx}{\underset{=}{\boldsymbol{S}}}$, can be found in section 2.5.

5.4.4.2.2. Stick state

In the case of stick, the elemental tangent contact matrix has a more simple form. As discussed previously, we start from the variation of the contact element contribution (5.4.4.1, *stick*) to the virtual work of the system:

$$
\begin{aligned}
\Delta\delta W^c_{i\ \text{stick}} &= \int_{\partial\Omega_i} \Delta\lambda_n \delta g_n + \varepsilon_n \Delta g_n \delta g_n + \hat{\lambda}_n \Delta\delta g_n + \Delta g_n \delta\lambda_n \\
&+ \Delta \underset{\sim}{\lambda}_t \circ \underset{\approx}{\mathrm{A}} \circ \delta\underset{\sim}{\xi} + \varepsilon_t \Delta \underset{\sim}{\xi} \circ \underset{\approx}{\mathrm{A}} \circ \delta\underset{\sim}{\xi} + \hat{\underset{\sim}{\lambda}}_t \circ \Delta\delta \underset{\sim}{\xi} \\
&+ \Delta \underset{\sim}{\xi} \circ \underset{\approx}{\mathrm{A}} \circ \delta \hat{\underset{\sim}{\lambda}}_t \, d\partial\Omega_i
\end{aligned}
\qquad [5.78]
$$

The replacement of the geometrical variations by dot products of s-structures with variation of the nodal coordinate vectors and replacement of the integral by the area of the master segment leads to the following structure:

$$\Delta\delta W^c_{i\ \text{stick}} = \begin{bmatrix} \Delta\underset{\sim}{\boldsymbol{x}} \\ \Delta\lambda_n \\ \Delta\underset{\sim}{\lambda}_t \end{bmatrix}^T \overset{\circ}{\cdot} \begin{bmatrix} \underset{\approx}{\underset{=}{\boldsymbol{K}}}_{xx} & \underset{\sim}{\boldsymbol{K}}_{x\lambda_n} & \underset{\approx}{\boldsymbol{K}}_{x\lambda_t} \\ \underset{\sim}{\boldsymbol{K}}_{\lambda_n x} & K_{\lambda_n\lambda_n} & \underset{\sim}{\mathrm{K}}_{\lambda_n\lambda_t} \\ \underset{\approx}{\boldsymbol{K}}_{\lambda_t x} & \underset{\sim}{\mathrm{K}}_{\lambda_t\lambda_n} & \underset{\approx}{\mathrm{K}}_{\lambda_t\lambda_t} \end{bmatrix} \overset{\circ}{\cdot} \begin{bmatrix} \Delta\underset{\sim}{\boldsymbol{x}} \\ \Delta\lambda_n \\ \Delta\underset{\sim}{\lambda}_t \end{bmatrix} \qquad [5.79]$$

The components of this *symmetric* "matrix" are stated below.

$$\begin{aligned} &\underset{\approx}{\underset{=}{\boldsymbol{K}}}_{xx} = \partial\Omega_i \left(\varepsilon_n \underset{\sim}{\boldsymbol{G}} \overset{\boxtimes}{\otimes} \underset{\sim}{\boldsymbol{G}} + \varepsilon_t \underset{\approx}{\boldsymbol{T}} \circ \underset{\approx}{\mathrm{A}} \circ \underset{\approx}{\boldsymbol{T}} + \partial\Omega_i \hat{\lambda}_n \underset{\approx}{\underset{=}{\boldsymbol{H}}} + \hat{\underset{\sim}{\lambda}}_t \circ \underset{\approx}{\underset{=}{\boldsymbol{S}}} \right) \\ &\underset{\sim}{\boldsymbol{K}}_{x\lambda_n} = \underset{\sim}{\boldsymbol{K}}_{\lambda_n x} = \partial\Omega_i \underset{\sim}{\boldsymbol{G}} \\ &\underset{\approx}{\boldsymbol{K}}_{x\lambda_t} = \underset{\approx}{\boldsymbol{K}}_{\lambda_t x} = \partial\Omega_i \underset{\approx}{\mathrm{A}} \circ \underset{\approx}{\boldsymbol{T}} \\ &K_{\lambda_n\lambda_n} = 0,\ \underset{\sim}{\mathrm{K}}_{\lambda_n\lambda_t} = \underset{\sim}{\mathrm{K}}_{\lambda_t\lambda_n} = 0,\ \underset{\approx}{\boldsymbol{K}}_{\lambda_t x} = 0,\ \underset{\approx}{\mathrm{K}}_{\lambda_t\lambda_t} = 0 \end{aligned} \qquad [5.80]$$

See section 2.5 for expressions of $\underset{\sim}{\boldsymbol{G}}$, $\underset{\approx}{\boldsymbol{T}}$, $\underset{\approx}{\underset{=}{\boldsymbol{H}}}$ and $\underset{\approx}{\underset{=}{\boldsymbol{S}}}$.

5.4.4.2.3. Non-contact state

In the case of non-contact, the tangent contact "matrix" can be stated immediately:

$$K^c_{i\ \text{non-contact}} = \begin{bmatrix} 0 & 0 & 0 \\ 0 & -\dfrac{\partial\Omega_i}{\varepsilon_n} & 0 \\ 0 & 0 & -\dfrac{\partial\Omega_i}{\varepsilon_t}\underset{\sim}{\mathrm{I}} \end{bmatrix} \qquad [5.81]$$

Obviously, this "matrix" is symmetric.

The structure of the derived matrices for frictional case can be depicted by blocks:

$$K^c = \begin{bmatrix} \begin{bmatrix} \nabla_x \nabla_x \\ \end{bmatrix}_{\{N \times N\}} & \begin{bmatrix} \nabla_{\lambda_n} \nabla_x \\ \end{bmatrix}_{\{N \times 1\}} & \begin{bmatrix} \nabla_{\lambda_t} \nabla_x \\ \end{bmatrix}_{\{N \times D\}} \\ \begin{bmatrix} \nabla_x \nabla_{\lambda_n} \\ \end{bmatrix}_{\{1 \times N\}} & \begin{bmatrix} \nabla_{\lambda_n} \nabla_{\lambda_n} \\ \end{bmatrix}_{\{1 \times 1\}} & \begin{bmatrix} \nabla_{\lambda_n} \nabla_{\lambda_t} \\ \end{bmatrix}_{\{1 \times D\}} \\ \begin{bmatrix} \nabla_x \nabla_{\lambda_t} \\ \end{bmatrix}_{\{D \times N\}} & \begin{bmatrix} \nabla_{\lambda_n} \nabla_{\lambda_t} \\ \end{bmatrix}_{\{D \times 1\}} & \begin{bmatrix} \nabla_{\lambda_t} \nabla_{\lambda_t} \\ \end{bmatrix}_{\{D \times D\}} \end{bmatrix} (l_n + l_t) \quad [5.82]$$

where $\{n \times m\}$ in each block designates the number of "strings" n and the number of "columns" m, where in s-structure representation $N = D(M+1)$ and in scalar representation $N = D(M+1)$. D is the dimension of the problem and M is a number of nodes on the master segment and $M+1$ is a total number of geometrical nodes of the contact element.

Remark 5.1. On the residual vector and the tangent matrix for the multi-face contact elements

If we use multi-face contact elements proposed by [HEE 93, BAR 02] and mentioned in section 3.3.4, then the structure of the residual vector and the tangent matrix are slightly different. Among N^m master segments of the i-th contact element, there is one active segment $\partial\Omega_i^a$ on the current iteration:

$$\partial\Omega_i^a \in \bigcup_{j=1}^{N^m} \partial\Omega_i^j$$

All master nodes of the contact element can be split into active nodes (denoted by an upper index a), which are attached to the active and passive master segment (all other nodes denoted by an upper index p). Active master nodes should be complemented by the slave node. Then, the v-vector of the nodal coordinate vectors of the contact element can be written as:

$$\underset{\sim}{\boldsymbol{x}} \sim [\underset{\sim}{\boldsymbol{x}}^a \quad \underset{\sim}{\boldsymbol{x}}^p]^T$$

The residual contact vector and tangent contact matrix take the following forms:

$$R_i^c \sim \begin{bmatrix} \begin{bmatrix} R^c_{x^a} \\ 0 \\ R^c_{\lambda_n} \\ R^c_{\lambda_t} \end{bmatrix} \end{bmatrix}, \quad K_i^c \sim \begin{bmatrix} \begin{bmatrix} K_{x^a x^a} & 0 & K_{x^a \lambda_n} & K_{x^a \lambda_t} \\ 0 & 0 & 0 & 0 \\ K_{\lambda_n x^a} & 0 & K_{\lambda_n \lambda_n} & K_{\lambda_n \lambda_t} \\ K_{\lambda_t x^a} & 0 & K_{\lambda_t \lambda_n} & K_{\lambda_t \lambda_t} \end{bmatrix} \end{bmatrix}$$

In case of smoothing of the master surface (e.g. see, [PIE 97, WRI 01], more references can be found in [WRI 06]), the structure of the residual vectors and tangent matrices does not change, the only difference is that the v-vector of nodal coordinate vectors will consists of all the nodes of the contact element. To make use of the smoothed master surface, it remains only to construct a new set of shape functions $\underset{\sim}{\phi}$*, corresponding to a smoothed master surface spanned on all master nodes, further this v-scalar of shape functions should be substituted into the expressions of* $\underset{\sim}{\boldsymbol{G}}$, $\underset{\approx}{\boldsymbol{T}}$, $\underset{\approx\approx}{\boldsymbol{H}}$ *and* $\underset{\approx\approx\sim}{\boldsymbol{S}}$ *from Section 2.5. No additional computational efforts are needed.*

5.5. Method of partial Dirichlet–Neumann boundary conditions

Here, we give a brief explanation of the technique described in sections 4.1.2, 4.1.5, 4.2.3 and 4.2.4 in the framework of the FEM. The main idea is to replace the geometrical constraints due to normal and frictional contact by *partial Dirichlet–Neumann* (PDN) boundary conditions. Furthermore, we will refer to this method as the PDN method. This technique is very advantageous in comparison to the standard methods described in the previous sections of this chapter (PM, LMM and ALM), because there is no need to evaluate the residual vectors and the tangent matrices. Here, we confine ourself to the contact between a deformable body and a rigid surface. In this case, the rigid surface can be described by a smooth function and there is no need for contact detection or contact elements. This method can be extended to the case of two-body contact [WRI 06]. Moreover, coupled with a LMM, it is equivalent to a *mortar method*, but contrary to LMM and ALM, which increase the number of unknowns in the system, the PDN method reduces the number of unknowns. Moreover, the PDN method is trivial to integrate in a parallelized finite element code.

5.5.1. *Description of the numerical technique*

Standard methods are based on a search for the contact stress vectors ensuring the fulfillment of geometrical inequality constraints and equilibrium of the bodies – this approach leads to an inequality variational problem that has a limited use. If inequality constraints are replaced by equality constraints, that is active contact zone

is assumed to be known, then the standard weak form can be constructed and implemented in a finite element code, as shown previously in this chapter. In any case, the problem consists of determining unknown contact stresses. The advantage of the PDN method is that, instead of seeking for contact stress vectors, the geometrical inequality constraints are imposed directly as partial Dirichlet boundary conditions and consequently the contact stress arises directly as a reaction. It remains for us to determine the active contact zone, this task will be discussed in the following section.

Four different classes of deformable-rigid contact can be distinguished:

1) frictionless contact with a rigid plane[5];

2) frictional contact with a rigid plane;

3) frictionless contact with an arbitrary rigid surface (Signorini's problem);

4) frictional contact with an arbitrary rigid surface.

To solve the first two classes (1, 2), the finite element code should include the possibility of a dynamical update of boundary conditions. In addition to this feature, solving of remaining classes (3, 4) needs to make use of the so-called multi-point constraints (MPCs). Furthermore, we will consider only the last classes of Signorini problem since they include the rigid plane as a subcase.

Briefly, the MPC implies that a chosen dof – "slave" dof u^s – is replaced by a linear combination of "master" dofs $u_i^m,\ i = 1, M$:

$$u^s = \alpha^i u_i^m + \beta$$

where α^i and β are scalar coefficients. To replace the Hertz–Signorini–Moreau conditions in case of an arbitrary rigid surface, the MPC is used in such a way that one dof of the contacting node – slave dof – is expressed through the other dofs of the same contacting node (two in 3D, one in 2D):

$$u^s = \underset{\sim}{\alpha} \circ \underset{\sim}{\mathrm{u}}^m + \beta$$

where $\underset{\sim}{\mathrm{u}}^m$ is a v-scalar of master dofs, $\underset{\sim}{\alpha}$ is a v-scalar of the scalar coefficients and β is also a scalar coefficient. The slave dof can be chosen arbitrarily for each contacting node, however it is required that locally the coefficients

$$\underset{\sim}{\alpha} < \infty$$

5 Here, by a plane we mean any surface at which any coordinate of the problem's reference frame takes a constant value, that is a plane in Cartesian coordinates, a cylinder in cylindrical coordinates or a sphere in spherical coordinates.

According to section 4.2.3, this condition is equivalent to the requirement that $\underline{\boldsymbol{e}}^s \cdot \underline{\boldsymbol{n}} \neq 0$, where $\underline{\boldsymbol{e}}^s$ is a unit vector, along which the coordinate of the slave dof is measured, and $\underline{\boldsymbol{n}}$ is a normal to the rigid surface at projection point.

5.5.2. *Frictionless case*

As was discussed in detail in the cited sections, the Hertz–Signorini–Moreau conditions can be replaced by MPC boundary conditions, which allow sliding of the contacting node only in the tangential plane. After introducing some notations, a general algorithm will be given. Let $\underline{\boldsymbol{x}}^i$ be a coordinate vector of a contacting node on the i-th iteration and $\underline{\boldsymbol{x}}^0$ the coordinate vector of this node at the previous increment, then the incremental displacement vector is given by:

$$\underline{\boldsymbol{u}}^i = \underline{\boldsymbol{x}}^i - \underline{\boldsymbol{x}}^0$$

The increment of the dofs is given by splitting of the vector $\underline{\boldsymbol{u}}$ into the reference frame basis:

$$u^i_j = \underline{\boldsymbol{u}}^i \cdot \underline{\boldsymbol{e}}_j$$

where $\underline{\boldsymbol{e}}_j$ is a set of basis vectors (normally in the finite element code an orthonormal set of basis vectors is used, so we will not distinguish basis and dual basis). The rigid surface in general can be described by a vector $\underline{\boldsymbol{\rho}}(\underset{\sim}{\xi}) = \rho_j(\underset{\sim}{\xi})\underline{\boldsymbol{e}}_j$ with a normal $\underline{\boldsymbol{n}}$ pointing to the permitted area of body motion. Without any loss of generality, let us suppose that locally it exists as a function f such that:

$$z = f(x, y)$$

where x, y, z are coordinates of the surface points in the chosen coordinate system

$$x = \underline{\boldsymbol{\rho}} \cdot \underline{\boldsymbol{e}}_1, \quad y = \underline{\boldsymbol{\rho}} \cdot \underline{\boldsymbol{e}}_2, \quad z = \underline{\boldsymbol{\rho}} \cdot \underline{\boldsymbol{e}}_3$$

Then, the geometrical constraint can be rewritten in the classical form:

$$x^i_3 \geq f(x^i_1, x^i_2) \quad \Leftrightarrow \quad u^i_3 \geq f(x^0_1 + u^i_1, x^0_2 + u^i_2) - x^0_3$$

The tangential plane at the given point $\{x^*, y^*\}$ is determined by the following equality:

$$P \ : \ z = \left.\frac{\partial f}{\partial x}\right|_{\{x^*, y^*\}} (x - x^*) + \left.\frac{\partial f}{\partial y}\right|_{\{x^*, y^*\}} (y - y^*) + f(x^*, y^*)$$

after introducing the following notations:

$$a = \left.\frac{\partial f}{\partial x}\right|_{\{x^*,y^*\}}, \quad b = \left.\frac{\partial f}{\partial y}\right|_{\{x^*,y^*\}}, \quad c = f(x^*, y^*)$$

the equation for the tangential plane can be rewritten as:

$$P\text{: } z = a(x - x^*) + b(y - y^*) + c$$

and the MPC to be imposed is given as:

$$u_3 = au_1 + bu_2 + c - x_3^0$$

where x_3^0 is a z coordinate of the node at the beginning of the increment (see Figure 5.18). Further, it is necessary to check that there is no tension forces in the created contact interface. The reaction force $\underline{\boldsymbol{R}}$ appearing in the nodes, where the MPC boundary conditions have been imposed, has to be checked:

$$\underline{\boldsymbol{R}} \cdot \underline{\boldsymbol{n}} \geq 0$$

the normal contact force should precisely point in the same direction as the normal to the rigid surface, otherwise the imposed MPC at adhering node should be removed (see Figure 5.19). The full algorithm is stated in the box below.

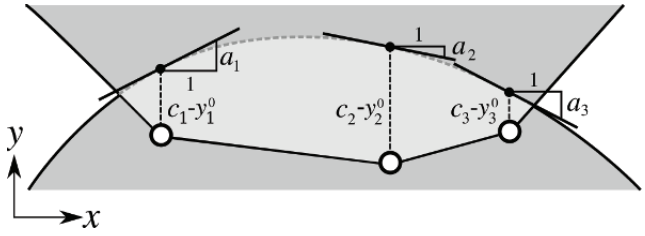

Figure 5.18. *MPC boundary conditions* $y = ax + x - y^0$

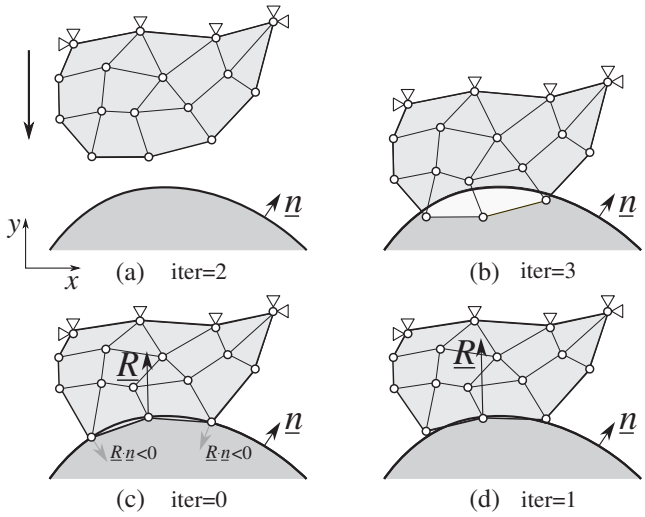

Figure 5.19. *Illustration of the iterative process of MPC update procedure: (a) initial configuration, (b) first iteration, three MPC boundary conditions are imposed at penetrated nodes, (c) after solution some nodes adhere to the surface and MPC at these nodes are removed and (d) final solution*

PDN algorithm for frictionless contact

- Iterations $(\mathtt{i}=0;\ \mathtt{i}<\mathtt{i}_{\max};\ \mathtt{i}++)$
  1. Loop over possible contacting nodes j
     - IF penetration $(\mathtt{x}_3^{\mathtt{i}} < \mathtt{f}(\mathtt{x}_1^{\mathtt{i}}, \mathtt{x}_2^{\mathtt{i}}))$ THEN
       - impose MPC boundary condition
         $\mathtt{u}_3^{\mathtt{i}+1} = \mathtt{a}^{\mathtt{i}}\mathtt{u}_1^{\mathtt{i}+1} + \mathtt{b}^{\mathtt{i}}\mathtt{u}_2^{\mathtt{i}+2} + \mathtt{c}^{\mathtt{i}} - \mathtt{x}_3^{\mathtt{i}}$
  2. Solve $\mathtt{i} \to \mathtt{i}+1$
  3. Check convergence: loop over possible contacting nodes j
     - IF penetration $\left(\mathtt{x}_3^{\mathtt{i}+1} < \mathtt{f}(\mathtt{x}_1^{\mathtt{i}+1}, \mathtt{x}_2^{\mathtt{i}+1})\right)$ THEN
       - impose MPC boundary condition
         $\mathtt{u}_3^{\mathtt{i}+2} = \mathtt{a}^{\mathtt{i}+1}\mathtt{u}_1^{\mathtt{i}+2} + \mathtt{b}^{\mathtt{i}+1}\mathtt{u}_2^{\mathtt{i}+2} + \mathtt{c}^{\mathtt{i}+1} - \mathtt{x}_3^{\mathtt{i}+1}$
     - IF adhesion $\underline{\mathtt{R}}^{\mathtt{i}+1} \cdot \underline{\mathtt{n}}^{\mathtt{i}+1} < 0$ THEN
       - remove MPC
     - IF penetration or adhesion
       - GOTO 1
     - ELSE finish

5.5.2.1. *Active set search*

For simple geometries of contacting body and rigid plane: for example, a sphere on a plane or a sphere on a sphere, for a reasonable time step this algorithm converges in one iteration. However, for certain geometries and/or boundary conditions the cycling between contact and non-contact states is possible. This is why we propose a simple algorithm that provides a fast determination of the active contact zone and ensures the absence of the cycling.

In case of undesirable adhesion, the proposed technique suppresses the imposed MPC boundary conditions gradually. The idea consists of sorting of all nodes in the contact interface by their statuses (normal contact, adhesion and non-contact) and further analysis of the contact topology. Below the algorithm is explained in detail.

Contacting surface consists of a set of segments:

$$\Gamma_c = \bigcup_i \Gamma_{ci}$$

Each segment has several nodes:

$$\underline{\boldsymbol{x}}_j^i \in \Gamma_{ci}$$

After the solution step (step 3 in the box above) to each node in the contact interface, the corresponding status α_j^i is assigned: normal contact $\alpha_j^i < 0$, adhesion $\alpha_j^i > 0$ or non-contact $\alpha_j^i = 0$. If there are penetrations of nodes then new MPC boundary conditions are imposed. If there is an adhesion the detections algorithm is executed: it checks all contact segment Γ_{ci}, which contain at least one node in adhesion, $\alpha_j^i > 0$, if all other nodes of this segment are in adhesion or in normal contact:

$$\alpha_j^i \alpha_k^i > 0 \text{ or } \alpha_j^i \alpha_k^i < 0, \quad k = 1, N^i, k \neq j$$

the algorithm goes to the next contact segment, otherwise if there is at least one node with non-contact status:

$$\exists k \ : \ \alpha_j^i \alpha_k^i = 0$$

or if the adhering node is situated on the edge of the contact zone, then the MPC boundary conditions are removed on the given contact segment i. In other words, it means that the algorithm unsticks nodes layer by layer starting from the edge of the adhesion zone (see Figure 5.20).

The proposed technique is adapted for globally convex geometry of contacting interfaces and in a more complicated situation the full topology of contact, non-contact and adhesion zones should be analyzed. Since this technique depends on the number of nodes in contact interface, it is not directly applicable to large problems. An adaptation is required: instead of detaching node-by-node we should detach entire groups of nodes determined according to the topology. This is especially crucial for frictional contact, where all nodes may slip.

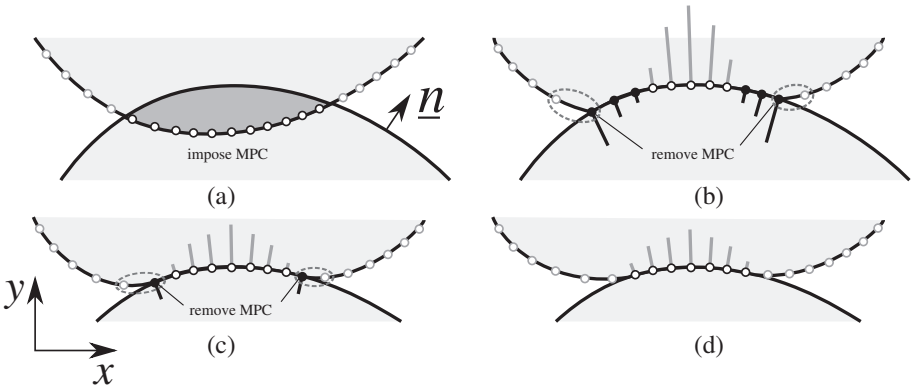

Figure 5.20. *Active set strategy based on the gradual suppression of the MPC boundary conditions starting from the edges of the contact zone: (a) MPC boundary conditions are imposed at all penetrated nodes, (b) arising reactions in blue normal contact in red adhesion, MPC is removed at adhering nodes on the edges of the contact zone, (c) still some nodes adhere and MPC is removed at edge nodes and (d) converged solution*

5.5.3. *Frictional case*

The frictional case has been discussed in detail for the case of contact with a rigid plane orthogonal to one of the basis vectors in section 4.1.5. The idea consists of replacing the stick conditions by full Dirichlet boundary conditions, that is if a node $\underline{\boldsymbol{x}}$ penetrates the rigid plane, it should be returned to the penetration point $\underline{\boldsymbol{x}}^{\bullet}$ and stuck to this point by imposing:

$$\underline{\boldsymbol{u}} = \underline{\boldsymbol{x}}^{\bullet} - \underline{\boldsymbol{x}}$$

Further, the reaction $\underline{\boldsymbol{R}}$ arising at the node should be split into the normal $\underline{\boldsymbol{R}}_n$ and tangential $\underline{\boldsymbol{R}}_t$ parts, and the non-adhesion condition:

$$\underline{\boldsymbol{R}}_n \cdot \underline{\boldsymbol{n}} \geq 0$$

should be checked as well as the stick–slip condition:

$$\begin{cases} \underline{\boldsymbol{R}}_t \in C_f(\underline{\boldsymbol{R}}_n, \underline{\boldsymbol{R}}_t, \dots), & \textit{stick} \\ \underline{\boldsymbol{R}}_t \notin C_f(\underline{\boldsymbol{R}}_n, \underline{\boldsymbol{R}}_t, \dots), & \textit{slip} \end{cases}$$

where $C_f(\underline{\boldsymbol{R}}_n, \underline{\boldsymbol{R}}_t, \dots)$ denotes the stick zone. In the case of Coulomb's friction law, the stick–slip conditions take the following form:

$$\begin{cases} \|\underline{\boldsymbol{R}}_t\| \leq \mu \|\underline{\boldsymbol{R}}_n\|, & \textit{stick} \\ \|\underline{\boldsymbol{R}}_t\| > \mu \|\underline{\boldsymbol{R}}_n\|, & \textit{slip} \end{cases}$$

In case of slip, the full Dirichlet boundary condition has to be replaced by an MPC boundary condition (in case of arbitrary surface) or by a partial Dirichlet boundary condition in the direction orthogonal to the rigid plane (in the case discussed in section 4.1.5). Moreover, in the tangent plane, the external force $\underline{\boldsymbol{F}}^e$ should be applied to the sliding node in the opposite direction to the arisen tangential reaction $\underline{\boldsymbol{R}}_t$, and the magnitude of the applied load is evaluated according to:

$$\underline{\boldsymbol{F}}^e = -\mu \|\underline{\boldsymbol{R}}_n\| \frac{\underline{\boldsymbol{R}}_t}{\|\underline{\boldsymbol{R}}_t\|}$$

Elaboration of this scheme to an arbitrary rigid surface has not been yet achieved.

5.5.4. *Remarks*

Many engineering contact problems can be approximated by a contact between a deformable body and rigid surface: metal forming and metal processing, a tire-road contact, polymer-metal water seals, indentation tests and, in general, any contact occurring between materials with significantly different stiffnesses. The PDN method seems to be very useful for the mentioned problems: first, because of its simplicity and second due to its stability and accurate fulfillment of the geometrical constraints. It is worth mentioning that the method is applied both for linear and higher order discretization[6] of the finite element mesh in the contact interface. The practice demonstrates that the most challenging part is the determination of the active contact zone. Further investigation is still required on the subject. The PDN method can be also efficiently used in case of possible contact through the planes of symmetry, that is, it can be considered as a "symmetry contact boundary condition", see examples in Chapter 6.

5.6. Technical details

This section contains short descriptions on different contact-related features and improvements that have been incorporated in the finite element code *ZéBuLoN* (Zset) [BES 97].

---

6 The method is applicable to second-order discretizations in 2D case; in 3D case, additional developments are required.

5.6.1. *Rigid master surface*

Sometimes, it is useful to approximate one of the contacting surfaces by a rigid surface. Frequently the master is chosen to be rigid, since that provides a better convergence of the numerical scheme. For that purpose, it is convenient to organize one-directional transfer of contact stresses, that is contact stress arise only on the slave surface due to violation of geometrical constraints but are not transferred through the contact interface to the master surface.

From a technical point of view, such an approximation leads to much simpler forms of the geometrical variations $\underset{\sim}{\boldsymbol{G}}$, $\underset{\approx}{\boldsymbol{T}}$, $\underset{\equiv}{\boldsymbol{H}}$ and $\underset{\approx\sim}{\underset{\equiv}{\boldsymbol{S}}}$ and consequently to simpler forms of the residual vector and tangent matrix. As the reader may remember that these s-structures connect the variations of geometrical quantities with variations of nodal coordinate vectors of the contact element.

$$\delta g_n = \underset{\sim}{\boldsymbol{G}} \cdot \delta \underset{\sim}{\boldsymbol{x}}, \quad \delta \underset{\sim}{\xi} = \underset{\approx}{\boldsymbol{T}} \cdot \delta \underset{\sim}{\boldsymbol{x}}, \quad \Delta\delta g_n = \Delta \underset{\sim}{\boldsymbol{x}} \cdot \underset{\equiv}{\boldsymbol{H}} \cdot \delta \underset{\sim}{\boldsymbol{x}}, \quad \Delta\delta \underset{\sim}{\xi} = \Delta \underset{\sim}{\boldsymbol{x}} \cdot \underset{\approx\sim}{\underset{\equiv}{\boldsymbol{S}}} \cdot \delta \underset{\sim}{\boldsymbol{x}}$$

To obtain a simplified discretization, we simply have to put all variations of the master nodes to zero, that is if $\underset{\sim}{\boldsymbol{x}}$ is a v-vector of contact element nodal coordinate vectors:

$$\underset{\sim}{\boldsymbol{x}} \sim \begin{bmatrix} \underline{\boldsymbol{r}}_s & \underline{\boldsymbol{\rho}}^1 & \cdots & \underline{\boldsymbol{\rho}}^M \end{bmatrix}$$

where $\underline{\boldsymbol{r}}_s$ and $\underline{\boldsymbol{\rho}}^i$ are coordinate vectors of the slave and master nodes, respectively. Then, the v-vector of variations has the following form:

$$\underset{\sim}{\boldsymbol{x}} \sim \begin{bmatrix} \delta\underline{\boldsymbol{r}}_s & 0 & \ldots & 0 \end{bmatrix}$$

It allows us to reduce the order of geometrical s-structures:

$$\underset{\sim}{\boldsymbol{G}} \to \underline{\boldsymbol{G}}, \quad \underset{\approx}{\boldsymbol{T}} \to \underline{\underline{\boldsymbol{T}}}, \quad \underset{\equiv}{\boldsymbol{H}} \to \underline{\underline{\underline{\boldsymbol{H}}}}, \quad \underset{\approx\sim}{\underset{\equiv}{\boldsymbol{S}}} \to \underline{\underline{\underline{\underline{\boldsymbol{S}}}}}$$

$$\delta g_n = \underline{\boldsymbol{G}} \cdot \delta \underline{\boldsymbol{r}}_s, \quad \delta \underset{\sim}{\xi} = \underline{\underline{\boldsymbol{T}}} \cdot \delta \underline{\boldsymbol{r}}_s, \quad \Delta\delta g_n = \Delta \underline{\boldsymbol{r}}_s \cdot \underline{\underline{\underline{\boldsymbol{H}}}} \cdot \delta \underline{\boldsymbol{r}}_s, \quad \Delta\delta \underset{\sim}{\xi} = \Delta \underline{\boldsymbol{r}}_s \cdot \underline{\underline{\underline{\underline{\boldsymbol{S}}}}} \cdot \delta \underline{\boldsymbol{r}}_s$$

To obtain simplified expressions for the variations of the geometrical quantities, we can simply put the corresponding shape functions to zero:

$$\phi_i = 0$$

in [2.43] and [2.46], and

$$\left[\Phi_i'\right] = 0, \quad \left[\Phi_{ij}''\right] = 0, \quad \left[\Phi_{ijk}'''\right] = 0$$

in [2.49] and [2.54]. Or directly put

$$\delta\underline{\boldsymbol{\rho}} = 0, \quad \delta\frac{\partial\underline{\boldsymbol{\rho}}}{\partial\underset{\sim}{\xi}} = 0, \quad \Delta\frac{\partial\underline{\boldsymbol{\rho}}}{\partial\underset{\sim}{\xi}} = 0, \quad \delta\frac{\partial^2\underline{\boldsymbol{\rho}}}{\partial\underset{\sim}{\xi}^2} = 0, \quad \Delta\frac{\partial^2\underline{\boldsymbol{\rho}}}{\partial\underset{\sim}{\xi}^2} = 0$$

in continuous form of the geometrical variations of the normal gap [2.23], surface parameter [2.24], second variations of the normal gap [2.31] and surface parameter [2.33]. These settings results in simple expressions given below:

– *Variation of the normal gap*

$$\delta g_n = \underline{\boldsymbol{n}} \cdot \delta\underline{\boldsymbol{r}}_s \quad \Rightarrow \quad \underline{\boldsymbol{G}} = \underline{\boldsymbol{n}}$$

– *Variation of the surface parameter* (convective coordinate)

$$\delta\underset{\sim}{\xi} = \left(\underset{\approx}{\mathrm{A}} - g_n\underset{\approx}{\mathrm{H}}\right)^{-1} \circ \frac{\partial\underline{\boldsymbol{\rho}}}{\partial\underset{\sim}{\xi}} \cdot \delta\underline{\boldsymbol{r}}_s \quad \Rightarrow \quad \underset{\sim}{\boldsymbol{T}} = \left(\underset{\approx}{\mathrm{A}} - g_n\underset{\approx}{\mathrm{H}}\right)^{-1} \circ \frac{\partial\underline{\boldsymbol{\rho}}}{\partial\underset{\sim}{\xi}}$$

– *Second variation of the normal gap*

$$\Delta\delta g_n = \Delta\underline{\boldsymbol{r}}_s \cdot \left[-\underset{\sim}{\boldsymbol{T}} \circ \underset{\approx}{\mathrm{H}} \circ \underset{\sim}{\boldsymbol{T}} + g_n\underset{\sim}{\boldsymbol{T}} \circ \underset{\approx}{\mathrm{H}} \circ \bar{\underset{\approx}{\mathrm{A}}} \circ \underset{\approx}{\mathrm{H}} \circ \underset{\sim}{\boldsymbol{T}}\right] \cdot \delta\underline{\boldsymbol{r}}_s$$

$$\underline{\underline{\boldsymbol{H}}} = -\underset{\sim}{\boldsymbol{T}} \circ \underset{\approx}{\mathrm{H}} \circ \underset{\sim}{\boldsymbol{T}} + g_n\underset{\sim}{\boldsymbol{T}} \circ \underset{\approx}{\mathrm{H}} \circ \bar{\underset{\approx}{\mathrm{A}}} \circ \underset{\approx}{\mathrm{H}} \circ \underset{\sim}{\boldsymbol{T}}$$

– *Second variation of the surface parameter*

$$\begin{aligned}\Delta\delta\underset{\sim}{\xi} \;=\; \Delta\underline{\boldsymbol{r}}_s \cdot \Bigg[& \left(g_n\underset{\approx}{\mathrm{H}} - \underset{\approx}{\mathrm{A}}\right)^{-1} \circ \left\{\underset{\sim}{\boldsymbol{T}} \circ \left(\frac{\partial\underline{\boldsymbol{\rho}}}{\partial\underset{\sim}{\xi}} \boxtimes \frac{\partial^2\underline{\boldsymbol{\rho}}}{\partial\underset{\sim}{\xi}^2} + g_n\underline{\boldsymbol{n}} \cdot \frac{\partial^3\underline{\boldsymbol{\rho}}}{\partial\underset{\sim}{\xi}^3}\right) \circ \underset{\sim}{\boldsymbol{T}}\right. \\ & - \underline{\boldsymbol{n}} \otimes \underset{\sim}{\boldsymbol{T}} \circ \underset{\approx}{\mathrm{H}} - \underset{\approx}{\mathrm{H}} \circ \underset{\sim}{\boldsymbol{T}} \otimes \underline{\boldsymbol{n}} \\ & + \left. g_n\underset{\sim}{\boldsymbol{T}} \circ \left(\frac{\partial^2\underline{\boldsymbol{\rho}}}{\partial\underset{\sim}{\xi}^2} \boxtimes \frac{\partial\underline{\boldsymbol{\rho}}}{\partial\underset{\sim}{\xi}} \circ \bar{\underset{\approx}{\mathrm{A}}} \circ \underset{\approx}{\mathrm{H}} + \underset{\approx}{\mathrm{H}} \circ \bar{\underset{\approx}{\mathrm{A}}} \circ \frac{\partial\underline{\boldsymbol{\rho}}}{\partial\underset{\sim}{\xi}} \boxtimes \frac{\partial^2\underline{\boldsymbol{\rho}}}{\partial\underset{\sim}{\xi}^2}\right) \circ \underset{\sim}{\boldsymbol{T}}\right\}\Bigg] \cdot \delta\underline{\boldsymbol{r}}_s\end{aligned} \qquad [5.83]$$

These variations are relatively simple and can be easily integrated in any finite element code as a special case for rigid master surfaces.

5.6.2. *Multi-face contact elements and smoothing techniques*

Multi-face contact elements have been discussed in section 3.3.4 and some remarks concerning the residual vector and tangent matrix are made in section 5.4.4.2. Here,

a brief discussion of the multi-face contact element will be given in the framework of the finite element analysis (FEA).

A standard contact element consists of one slave node and one master segment. What happens when the slave node during the iterative process slides out of the master segment? It has no more projection on the master segment, but excluding this slave node from the solution would result in a penetration. So a possible way out is to create a new contact element, but this procedure is quite time consuming, because it requires an update of the tangential stiffness matrix and its re-factorization. There are two possibilities:

1) extend the parent domain of the master segment (see 5.21, *a*);

2) extend the standard contact element by adding the adjacent master segments, that is create a *multi-face* contact element in advance, before starting the iterative solution procedure.

The first possibility results in continuous sliding of the slave node along the extension of the current master segment before the equilibrium is reached. Such a sliding results either in penetration if the surface is locally concave or in opening of the gap in case of convex surface. These drawbacks are negligible if the sliding increment is small in comparison to the size of master segment, otherwise the solution becomes unrealistic. In this case, the use of multi-face elements is highly desirable: when the slave node passes from one master segment to another, the residual vector and tangent matrix are reformulated, respectively, to the new active master segment and the corresponding master nodes (see Figure 5.21(b)). Note also that in a frictional case the described situation results in the loss of the sliding path tracking, that is the relative sliding increment cannot be approximated by:

$$\Delta \underline{\boldsymbol{g}}_t = \frac{\partial \underline{\boldsymbol{\rho}}}{\partial \underset{\sim}{\xi}} \circ \Delta \underset{\sim}{\xi}$$

and hence some special techniques are required, see for example [KON 07a] and [WRI 06]. Another drawback is the presence of possible oscillations in the neighborhood of concave angles – constant switching between two adjacent segments. Such oscillations are also possible within the first approach but in this case the oscillations take place from one increment to another and the local convergence is often achieved (see Fig. 5.22). In other words, to avoid this undesirable effect the NTN, node-to-edge and node-to-vertex elements should be available in the finite element code, however it does not always solve the problem, another approach is required.

An extension of the multi-face contact elements leads to an even more advantageous treatment of the problem: instead of distinguishing between active and

inactive master segments, we can construct a C^1-smooth surface based on all master nodes included in the multi-face contact element (see Figure 5.23). One of the first successful applications of the smoothing procedures to large sliding contact problems can be found in [PIE 97] and [PIE 99], where authors use Bézier curves and Splines to smooth a structured surface mesh consisting of regular quadrilateral segments. However, in case of arbitrary surface mesh, the construction of a C^1-smooth surface is not evident and presents an up to date research topic in computational contact mechanics; many details, examples and references on this topic can be found in the books of Wriggers [WRI 06] and Laursen [LAU 02]). Hermitian, Spline and Bézier polynomials as well as Gregory patches are used for smoothing the master surface in 2D and 3D contact problems.

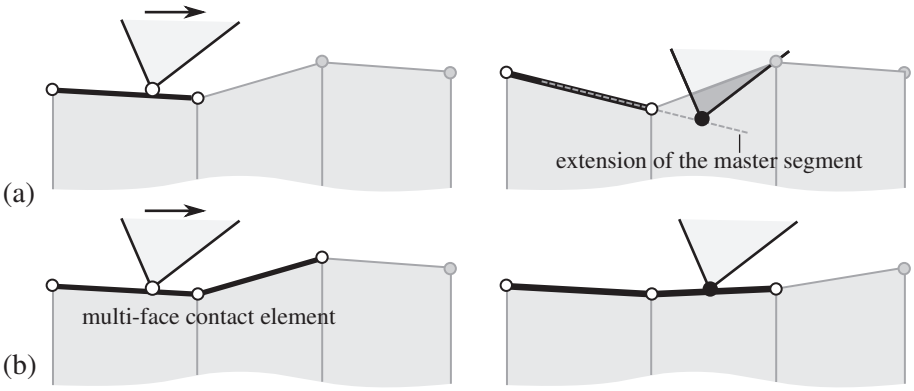

Figure 5.21. *Example of 2D large sliding contact: (a) extension of the master segment and (b) multi-face contact element*

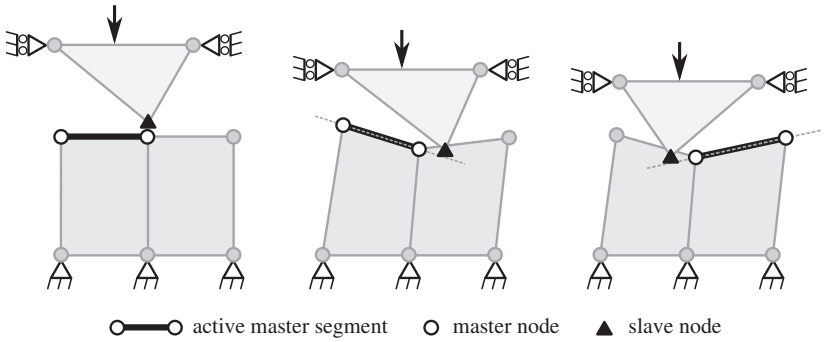

Figure 5.22. *Example of frictionless oscillations in a neighborhood of the concave vertex*

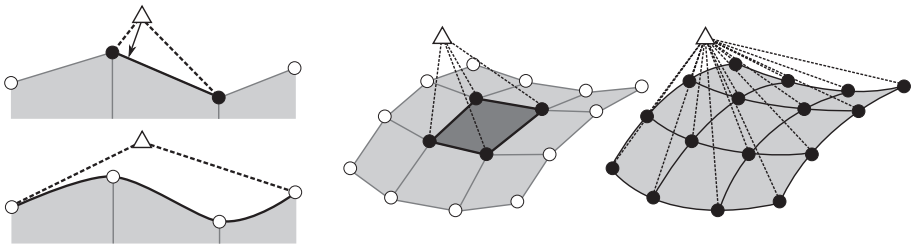

Figure 5.23. *Examples of master surface smoothing by a cubic Bézier (a) curve and (b) surface*

5.6.3. *Heterogeneous friction*

Contact modeling of heterogeneous materials (composites, alloys with an explicit representation of the microstructure) leads to a problem with heterogeneous friction. For engineering aspects of the problem, see [DIC 06a, DIC 06b, DIC 08]. The computational aspects of this type of problem are briefly discussed below. Two types of friction heterogeneity can be distinguished:

– friction properties are determined by domains (e.g. composite material, polycrystalline surface, Figure 5.24);

– friction properties change smoothly along the contact interface (e.g. due to temperature distribution).

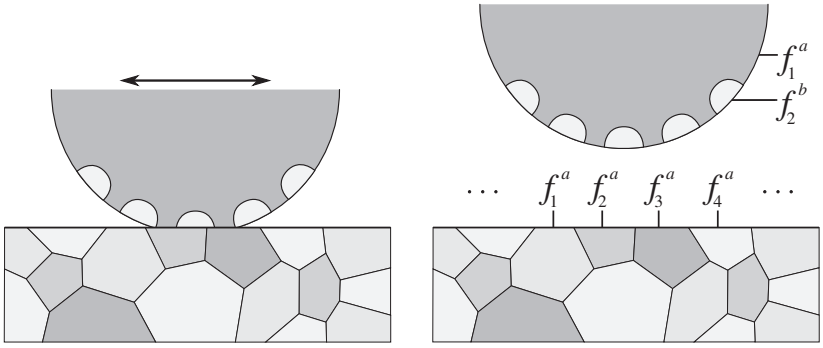

Figure 5.24. *Example of heterogeneous friction between a composite and polycrystalline structure*

A rigorous treatment of the friction change within one master segment leads to a quite complicated linearization of the virtual work, however it seems to be always possible to assume a constant friction within one contact element.

Note that the friction is an interface phenomenon, that is both contacting surfaces determine the friction properties. For example, in the case of contact between two bi-phase composites f_1^1, f_2^1 and f_1^2, f_2^2, four local coefficients of friction (in the case of Coulomb's friction law) have to be defined if self-contact is excluded:

$$\mu_1 = \mu_1(f_1^1, f_1^2),\ \mu_2 = \mu_2(f_1^1, f_2^2),\ \mu_3 = \mu_3(f_2^1, f_1^2),\ \mu_4 = \mu_4(f_2^1, f_2^2)$$

Treatment of such problems requires a proper definition of the friction coefficient for each contact element. A standard NTS contact element consists of one slave node and master segment, so to each slave node and master segment friction IDs f_i^s and f_j^m should be assigned and a corresponding rule for friction coefficients:

$$\mu_{ij} = \mu_{ij}(f_i^s, f_j^m)$$

Another possibility leading to a symmetric treatment of contacting surfaces consists of assignment of friction IDs to both slave and master nodes: $f_i^s, f_{j_1}^m,\ f_{j_2}^m,\ \ldots,\ f_{j_M}^m$ and a corresponding rule, for example, as proposed below:

$$\mu_{ij} = \frac{1}{M}\sum_{k=1}^{M} \alpha_k \mu_{ij}(f_i^s, f_{j_k}^m), \quad \sum_{k=1}^{M} \alpha_k = 1$$

Such an approach is valid both for normal and self-contact and includes the previous possibility as a subcase for properly chosen α_k coefficients.

5.6.4. *Short remarks*

Below some short remarks concerning the code organization are listed:

– It is often advantageous to organize the code in a way that *independent contact zones* can be treated separately but within a common contact framework; it leads to an efficient organization of the contact detection procedure (as described in Chapter 3) and also to a smart update of the tangent matrix.

– The components of contact elements may change from one increment to another, however sometimes it is advantageous to *keep the values of Lagrange multipliers* from the previous time step and use them as an initial guess. It is easy to save these values directly for each slave node as well as the sliding path; the initial guess is especially important in the case of the use of Uzawa's algorithm.

– Regardless all advantages of the ALM, its convergence strongly depends on the choice and *update of the penalty parameters* ε_n and ε_t related to normal and tangential contact, respectively. We did not elaborate any consistent and theoretically based updating technique, but some general rules can be deduced. From remarks given in section 5.1, according to the investigations of Alart [ALA 97] and Alart and Curnier [ALA 91] on the convergence of the augmented Lagrangian in

frictional contact it follows that if a frictional cycling occurs, then the tangential penalty parameter should be decreased:

$$\text{stick-slip cycling} \quad \Rightarrow \quad \varepsilon_t^{i+1} = \alpha_t \varepsilon_t^i, \quad 0 < \alpha_t < 1$$

On the other hand, if a slave node looses the contact, then high penalty coefficients ε_n and ε_t may result in a poor conditioning of the tangent matrix, so both of them should be decreased:

$$\text{non-contact} \quad \Rightarrow \quad \varepsilon_n^{i+1} = \beta_n \varepsilon_n^i, \quad \varepsilon_t^{i+1} = \beta_t \varepsilon_t^i, \quad 0 < \beta,\, \beta_t < 1$$

And finally, if the contact status of the contact element remain constant (slip or stick), then the penalty parameters should be increased in order to enforce the fulfillment of geometrical constraints.

$$\text{stick or slip} \quad \Rightarrow \quad \varepsilon_n^{i+1} = \gamma_n \varepsilon_n^i, \quad \varepsilon_t^{i+1} = \gamma_t \varepsilon_t^i, \quad \gamma_n,\, \gamma_t > 1$$

A more elaborated update scheme may also take into account the values of normal gap, tangential sliding and of the corresponding Lagrange multipliers. An example of phenomenological update scheme can be found in [BUS 09].

– An finite element problem, containing, for example, two initially separated bodies, has a tangent matrix (sparse matrix) with a block structure and the minimal thickness of the bandwidth of each block is ensured by a smart numbering of nodes and dofs. If contact occurs between these bodies the *optimality of the sparse structure* may be lost, that is the bandwidth can be significantly enlarged. Hence, the storage of the sparse matrix becomes non-optimal and requirements on the needed memory space can reach the amount needed for storage of the full matrix. There are at least two solutions:

- renumbering of nodes after construction of contact elements at each change of mesh topology;

- one preliminary renumbering of nodes in the way that all possible mesh graphs (due to presence of contact element) retain a narrow bandwidth.

– According to our experience, the *user friendliness* of the FEA code is very important, namely, the FEA tool should check automatically the *orientation* of the master surface and change it if needed, also it should choose *automatically* the optimal "maximal detection distance" parameter and the detection cell size, the latter two are possible in the framework of the bucket sort detection algorithm (see Chapter 3).

– In the case of complex geometry, large deformations and/or self-contact, it is complicated or even impossible to know the master-slave discretization *a priori*. This is why Benson and Hallquist [BEN 90] introduced the *single contact surface*. From

the programing point of view, such a surface is nothing but a master surface. It is necessary simply to adapt the detection algorithm, as described in Chapter 3, the rest of the code remains unchanged. It is worth mentioning also that, in case of simple buckling simulations, the contact may occur only after a certain amount of time. In order to accelerate the solution, the contact detection procedure should not be executed before that time.

– *Parallel treatment* of contact problems requires a special detection technique. From the programing point of view, it is easy to construct a single contact detection procedure that takes as arguments master and slave surfaces. Furthermore in the parallel framework, it remains only to join all the parts of the slave and master surfaces from different subdomains and to pass them to the detection procedure. This approach was called single detection, multiple resolution (SDMR). If there are several independent contact zones, then the SDMR detection procedure can be carried out independently for each zone at different processors. The same detection procedure is valid for multiple detection multiple resolution (MDMR) technique, in this case each processor does not receive the entire master and slave surfaces, but their close parts, which should be simply passed to the detection procedure (for details, see Chapter 3).

Chapter 6

Numerical Examples

In this chapter, we present some examples and validation tests. Penalty, augmented Lagrangian method (ALM) and partial Dirichlet–Neumann (PDN) method are used. Two- and three-dimensional frictional and frictionless contact problems are considered in small and large deformations for linear and nonlinear material models. The more contact elements the problem contains, the more complicated is its numerical treatment, so in order to demonstrate the performance of the contact implementation in the finite element code (ZéBuLoN) we use quite fine discretizations, even when a coarser mesh would provide a reliable estimation of the solution. Full input data are given for many considered problems.

6.1. Two dimensional problems

6.1.1. *Indentation by a rigid flat punch*

Indentation of an elastic half-space by a rigid axisymmetric flat punch is considered in the presence of finite friction. The analytical solution can be found, for example, in [SPE 75]. An attempt at a numerical solution within the finite element method and the ALM was undertaken in [PIE 97, PIE 99]; however, the numerical solution appears to be significantly different than the analytical solution. This error can be explained by the coarse mesh used by the authors. Here, a more precise numerical solution is given, but the discrepancy between the numerical and analytical solutions still exists.

A rigid flat axisymmetric punch of radius a is indented into an elastic half-space by a force P (see Figure 6.1). The Coulomb's friction law with the coefficient of

friction μ is considered. The frictionless contact pressure distribution is described by the following function (see, e.g. [JOH 94]):

$$\sigma_n(\rho) = \frac{P}{\sqrt{a^2 - \rho^2}}$$

where ρ is a distance from the axis of symmetry. Note that due to this equation, the mesh convergence cannot be obtained for this problem because of the singularity on the edge of the flat punch $\rho = a$. However, a rather good numerical estimation can be given.

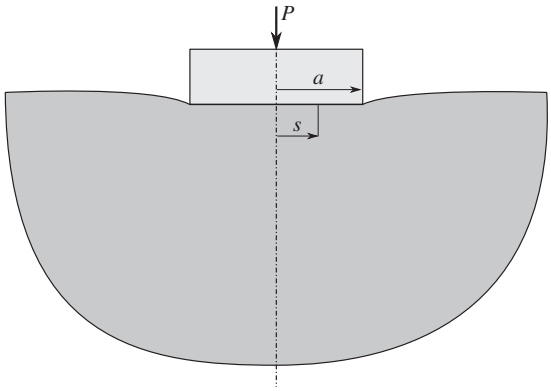

Figure 6.1. *Indentation of an elastic half-space by a rigid axisymmetric flat punch: a = radius on the punch, s = radius of the stick zone*

The problem is solved with an axisymmetric mesh. All relevant data are listed in the box below, all quantities are given in force units (f.u.) and length units (l.u.), which consequently will be omitted. The finite element mesh of the half-space consists of a half circle fixed along the radial perimeter $R = 9a$. The indenter (master) is constructed in such a way that its nodes coincide with the nodes on the opposite contact surface of the half-space (slave). Such a construction of the finite element mesh allows us to avoid the inherent problem of the node to segment discretization – inability to transfer a uniform pressure through the contact interface for an arbitrary discretization. Three finite element meshes were used with 41, 201 and 401 nodes on the active slave surface. The meshes contain 4,183, 60,533 and 95,872 nodes, respectively.

⊞ **Data:**

– Linearly elastic material, small deformations:

Young's modulus $E = 1,000$ [f.u./l.u.^{2}];

Poisson's ration $\nu = 0$.

– Boundary conditions and geometry:

Punch radius $a = 1$ [l.u.];

Pressure on the indenter $p = 1.61$ [f.u./l.u.^{2}];

Friction coefficient $\mu = 0.2063,\ 0.2986,\ 0.4013$.

– Solution conditions:

Method: Augmented Lagrangian;

Penalty coefficients $\varepsilon_n = \varepsilon_t = 100$ [f.u./l.u.^{2}];

Increment 1.

– Finite element mesh:

Linear full integration quadrilateral axisymmetric elements (four nodes and four integration points).

In [SPE 75], the author gives semi-analytical estimations of the friction coefficients μ for different stick regions s/a and different Poisson's ratios ν. His estimations are presented for $\nu = 0$ in Table 6.1. Here, the problem is inverse and for the given friction coefficient, the stick region is measured, the results for different finite element meshes are shown in Table 6.2. The convergence is quite slow and the correct values of the stick zone taken from [SPE 75] have not been reached. Contour plots of shear stress σ_{12}, stress σ_{22}, von Mises stress σ_v and horizontal displacement u_1 distributions are represented in Figure 6.2. The stress distribution (extrapolation from Gauss points to nodes) in the contact interface is plotted in Figure 6.3.

μ	0.2063	0.2986	0.4013	0.4862
s/a	0.24	0.5	0.7	0.8

Table 6.1. *Semi-analytical estimations (from [SPE 75]) for the friction coefficient ensuring stick zone of radius c for $\nu = 0$*

Friction μ	0.2063	0.2986	0.4013
FE mesh N_s	stick zone s/a		
41	0.300	0.550	0.750
201	0.260	0.534	0.735
401	0.255	0.520	0.717
exact	0.240	0.50	0.700

Table 6.2. *Finite element estimation of the stick region radii for given friction coefficients ($\nu = 0$), convergence by mesh*

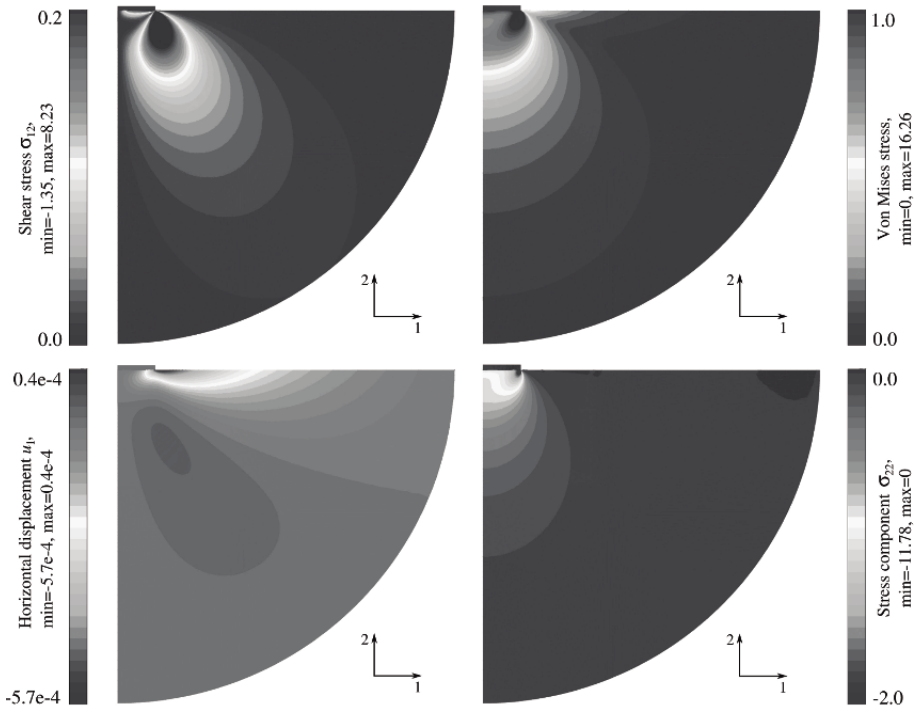

Figure 6.2. *Contour plots of shear stress σ_{12}, von Mises stress σ_v, horizontal displacement u_1 and stress component σ_{22} for $\mu = 0.2063$*

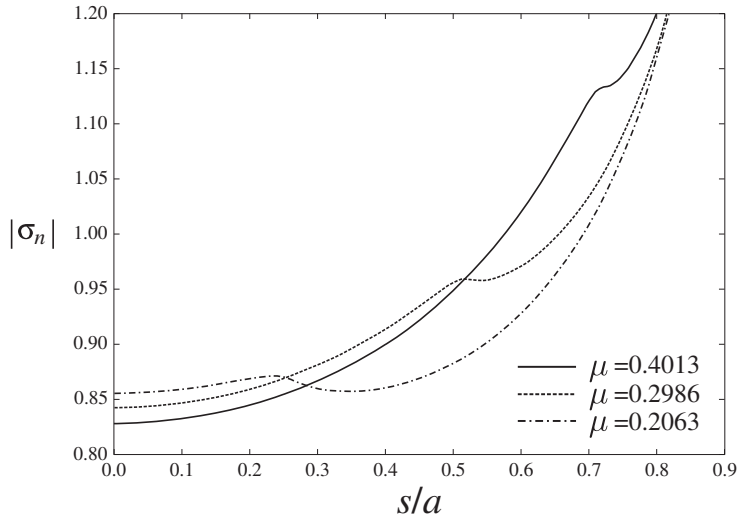

Figure 6.3. *Distribution of the contact pressure for different coefficients of friction*

6.1.2. *Elastic disk embedded in an elastic bored plane*

The geometry presents a thin elastic infinite plane with a hole of almost the same radius as a thin elastic disk, embedded in the hole. A concentrated force is applied in the middle of the disk, the value of the force is chosen such that the contact occurs at one-third (120^o) of the interface between the hole and the disk (Figure 6.4). Coulomb's friction law is assumed at the interface. Again due to the inability of the node-to-segment (NTS) discretization to transfer correctly the contact pressure through an arbitrary discretization, we use a finite element mesh with matching nodes on contacting interfaces (see Figure 6.5). As we can see in the middle of the embedded disk, we introduce a circular hole in the center, where the concentrated force is applied to a node on the axis of symmetry and multipoint constraints (MPC) are applied to all other nodes of this hole to retain its circular form. A solution for this problem was found by Klang [KLA 79] and numerical treatments can be found in [ALA 91, PIE 97, PIE 99]. The concentrated load is applied in several increments. As proposed in [ALA 91] and the force value changes quadratically with increments:

$$F_i = F_{\max} \frac{t_i^2}{t_{\max}^2}$$

where $F_{\max}$ is the load and $t_i \in [0; t_{\max}]$ is the incremental time with $t_i = i\, t_{\max}/n$, where n is a number of increments and $t_{\max}$ is the total solution time. The remaining data are given in the box below.

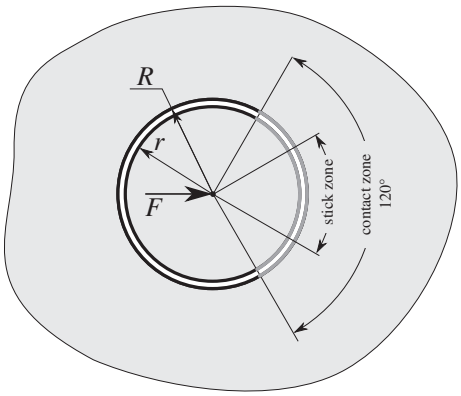

Figure 6.4. *Setting of the problem: a thin elastic disk embedded in a thin elastic infinite plane with a circular hole*

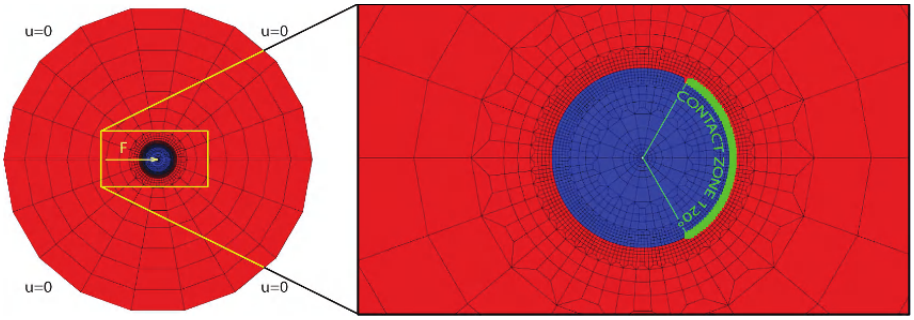

Figure 6.5. *Finite element mesh (2,502 nodes, 54 active slave nodes in the interface) and zoom on the contact region*

⊞ **Data:**

– Linear elastic material, small deformations:

Young's modulus $E = 2.1e7$ [f.u./l.u.^{2}];

Poisson's ration $\nu = 0.3$.

– Boundary conditions and geometry:

Plane stress;

Disk external radius $r = 5.999$;

Disk internal radius $r = 0.1$;

Hole radius $R = 6$;

Space external radius $R = 60$;

Concentrated force $F = 9375t^2/t_0^2$;

Friction coefficient $\mu = 0.4$.

– Solution conditions:

Method: Augmented Lagrangian;

Penalty coefficients $\varepsilon_n = \varepsilon_t = 500$ [f.u./l.u.^{2}];

Increment $1, 5, 10, 25, 50, 100$.

– Finite element mesh:

Linear full integration quadrilateral axisymmetric elements (four nodes and four integration points); 2,502 nodes, 54 active slave nodes in the interface.

The experience shows that the shear contact stress distribution in the slip zone and the limit of the stick zone ($-40^o < \alpha_s < 40^o$) as well as the contact zone width $-60^o < \alpha_s < 60^o$ are easily achieved in at least two increments. However, the shear stress distribution in the stick zone appears to be strongly dependent on the mesh density and on the number of increments. The correct shear stress distribution in the stick zone for the considered finite element mesh is achieved only when the load is applied in more than approximately 50 increments. That is a good example demonstrating the path dependence of friction even for small deformations and small slidings. The distribution of, the shear stress in the contact zone for different number of increments is represented in Figure 6.6. Our experience demonstrated that the precision of the mesh node positioning at the interface must be very accurate: for example, the negligible, at first glance, relative error $5 \times 10^{-3}\%$ in node positioning with respect to the size of element leads to severe oscillations of the solution at the interface; the precision of $5 \times 10^{-7}\%$ in node positioning yields a smooth result. The difference between the analytical solution and the numerical results is probably due to the inability to capture correctly the stress field due to a concentrated force.

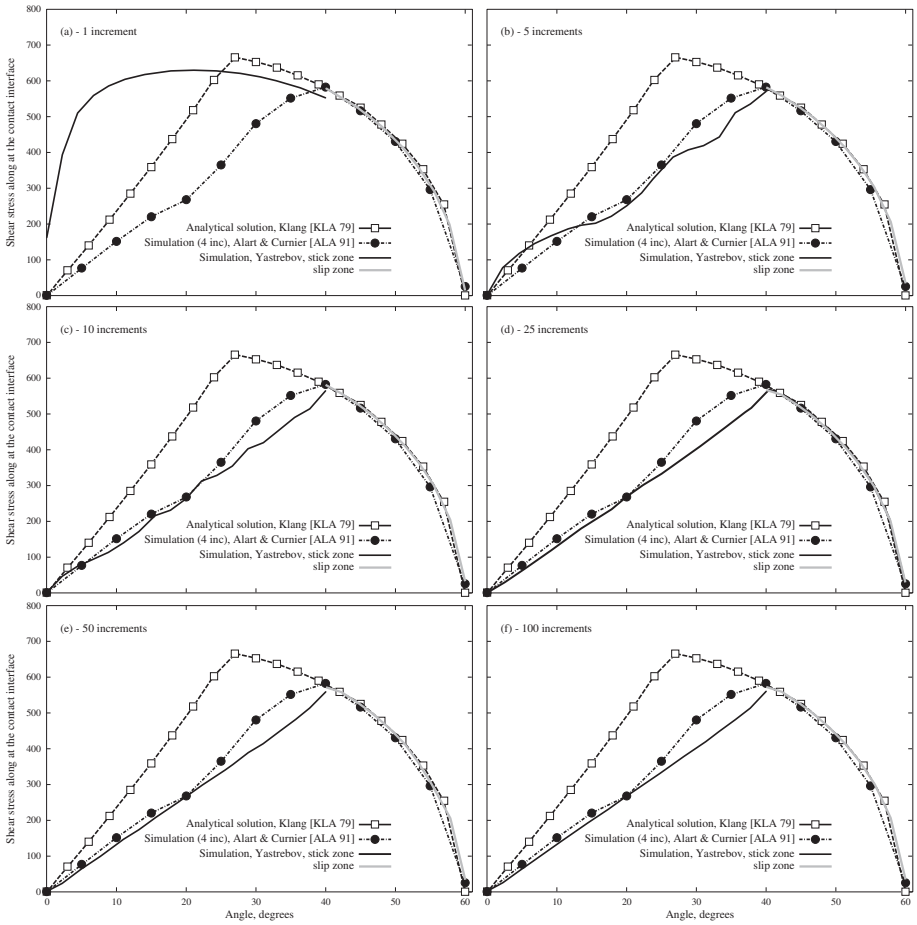

Figure 6.6. *Shear stress distribution in the contact interface for different number of increments are compared with analytical results and numerical results from [ALA 91]*

6.1.3. *Indentation of an elastic rectangle by a circular indenter*

This short example illustrated the PDN method performance for a non-flat rigid surface in contact with a deformable body. The geometry of the problem is depicted in Figure 6.7. All data are given in the box below. The von Mises stress distributions in Gauss points and nodal reactions in the interface due to MPC boundary conditions, arising from application of the PDN method, are represented in Figure 6.8 for linear and quadratic meshes.

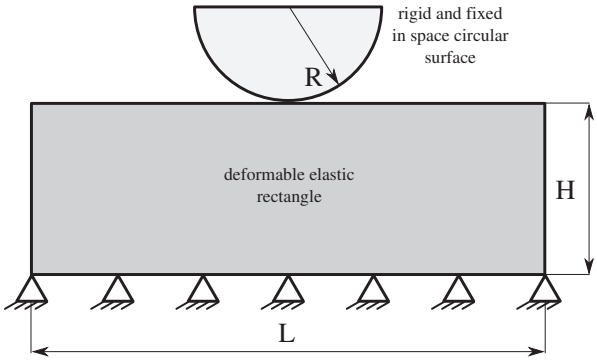

Figure 6.7. *Scheme of the problem: indentation of an elastic rectangle by a rigid circle*

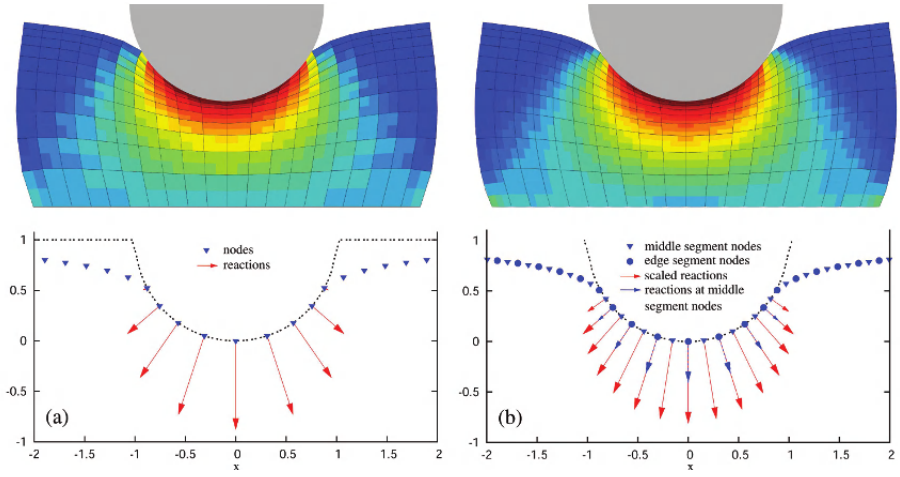

Figure 6.8. *Von Mises stress distribution and nodal reactions for (a) linear and (b) quadratic meshes*

⊞ **Data:**

– Linearly elastic material, small deformations:

Young's modulus $E = 210$;

Poisson's ration $\nu = 0.3$.

– Boundary conditions and geometry:

Indenter radius $R = 1$;

Rectangle $L = 4, H = 2$;

Friction coefficient $\mu = 0$;

Bottom of the block is fixed and moved toward the indenter $u_x = 0, u_y = 1$.

– Solution conditions:

Method: PDN;

Increment 10.

– Finite element mesh:

Linear and quadratic full integration quadrilateral plane-strain elements (four nodes, four integration points for linear and eight nodes, nine integration points); 200 elements.

6.1.4. *Axisymmetric deep cup drawing*

The metal forming process is one of the important engineering applications of the computational contact mechanics and many examples can be found in scientific literature. Here, we consider an axisymmetric deep cup drawing problem, stated in [ROU 09], see Figure 6.9. This problem engenders many nonlinearities: large deformations within the updated Lagrangian framework, frictional contact and nonlinear material model (elasto-visco-plastic with exponential hardening). All parameters of the problem are stated in the box below. The problem is mixed force-displacement driven: the holding pressure p is applied linearly within the first 100 time units, and the die is gradually moved down up to $t = 335$, then removed. To stabilize the solution, a soft spring (700 times softer than the material of the sheet) is attached to the edge of the sheet, as shown in Figure 6.9.

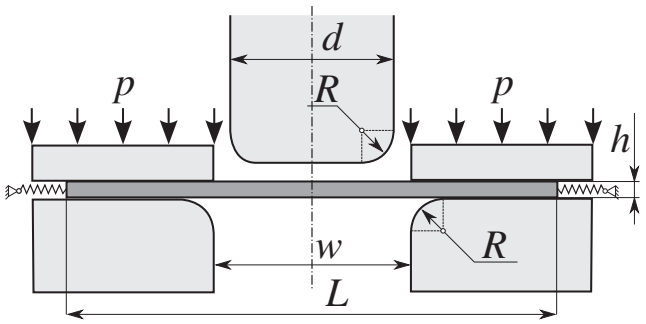

Figure 6.9. *Geometrical setting of the deep cup drawing problem: rounded cylindrical die and metal sheet fixed within the tool*

On average, on each time step 1,000 contact elements are created and 400 of them are active. On average, convergence on each time step is achieved within 10–15 iterations. The distribution of accumulated plastic strain for different time steps is represented in Figure 6.11. The force-displacement curve is represented in Figure 6.12. Note that even in the presence of viscosity, the reaction force oscillates (see the inset in Figure 6.12). This is due to the fact that at this stage the sheet slides along the surface of the holder, which is not smooth. That is why in the case of large sliding, it is more advantageous to use either smoothing of the master surface or determine the holder and the punch as analytical surfaces, or use the PDN method described in previous chapters.

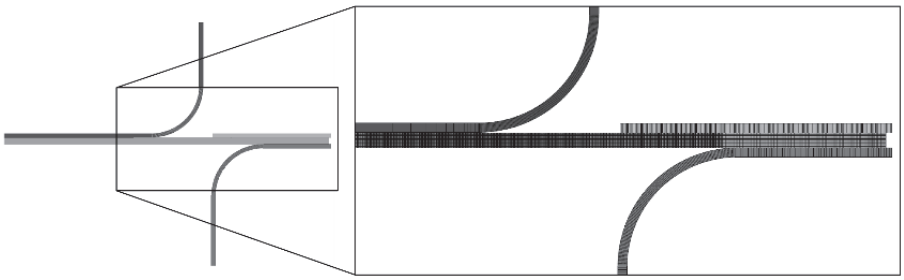

Figure 6.10. *Finite element mesh for the axisymmetric deep cup drawing problem*

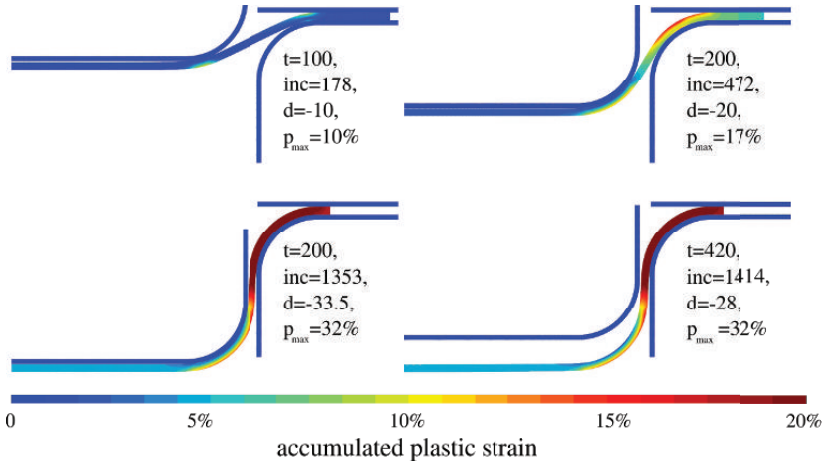

Figure 6.11. *Distribution of accumulated plastic strain (in Gauss points) on different time steps*

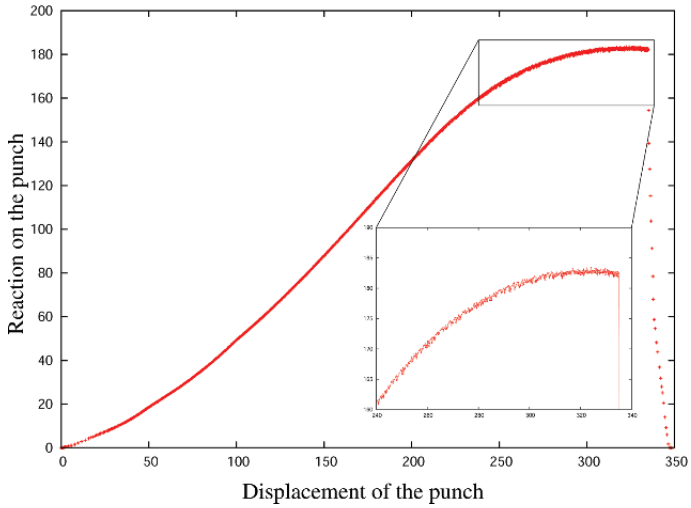

Figure 6.12. *Evolution of the reaction on the punch with time, time* $= 10\times$ *vertical displacement of the punch up to* $t = 335$*; in the inset zoom on the region, where the oscillations of the reaction on the punch become significant*

⊞ **Data:**

– Finite deformation elastoplasticity (updated Lagrangian):

Young's modulus $E = 69$;

Poisson's ration $\nu = 0.33$;

Yield criterion: von Mises $R_0 = 0.22$.

Norton creep power law:

$$\dot{\lambda} = \langle f/K \rangle^n, \ K = 0.5, \ n = 7$$

Isotropic power hardening law:

$$R = R_0 + K(e_0 + p)^n, \ K = 0.99, \ e_0 = 7e^{-4}, \ n = 7$$

– Boundary conditions and geometry:

Applied pressure $p = 1.86e{-}2$;

Die is gradually moved down $u_z = -33.5t/t_l$, and removed $u_z = -33.5 + 5.5\frac{t-t_l}{t_f-t_l}$;

Die diameter $d = 97.46$;

Rounding radius $R = 12.7$;

Die opening $w = 101.48$;

Sheet thickness $h = 1.6$;

Sheet diameter $L = 158.76$;

Friction coefficient $\mu = 0.1$.

– Solution conditions:

Method: Augmented Lagrangian;

Penalty coefficients $\varepsilon_n = \varepsilon_t = 200$;

Increment $1,414$;

Full solution time: loading $t_l = [0, 335]$ and unloading $t_f = [335, 420]$.

– Finite element mesh:

Linear full integration quadrilateral axisymmetric elements (four nodes, four integration points for linear and eight nodes, nine integration points); 6,063 elements (Figure 6.10).

6.1.5. *Shallow ironing*

The example shown in this section consists of sliding of a deformable indenter along a deformable rectangle. The geometrical setting of the problem as well as the finite element mesh are presented in Figure 6.13. This example has been proposed and solved in [FIS 06] with the mortar-based method using moving friction cone (see [WRI 06]), and resolved with contact domain method in [HAR 09]. Here, the problem is solved using the ALM and NTS discretization. Our results are compared with results of the cited authors in Figure 6.14. Contrary to [FIS 06], here, and in [HAR 09] linear elements are used, but the total number of degrees of freedom is approximately preserved.

⊞ **Data:**

– Neo-Hookean material, large deformations:

Indenter: Young's modulus $E^* = 68.96$, Poisson's ratio $\nu^* = 0.32$.

Rectangle: Young's modulus $E = 6.896$, Poisson's ratio $\nu = 0.32$.

– Boundary conditions and geometry:

Displacement on the indenter

$$u_y = t,\ t = [0;1],\ u_y = 1,\ t > 1$$

$$u_x = 0,\ t = [0;1],\ u_x = 10\,(t-1),\ t = [1;2]$$

is prescribed on the top surface.

The rectangle is fixed in all directions on the lower edge:

Geometry: $d_1 = 0.2$, $d_2 = 1.2$, $d_3 = 10.6$;

$r = 0.75$, $h_1 = 0.95$, $h_2 = 1.2$, $a_1 = 0.3$, $a_2 = 0.2$;

Friction coefficient $\mu = 0.3$.

– Solution conditions:

Method: Augmented Lagrangian;

Penalty coefficients $\varepsilon_n = \varepsilon_t = 0.5$;

Increments: 10 for $t \in [0;1]$ and 500 for $t \in [1;2]$.

– Finite element mesh:

A total of 3,672 linear full integration quadrilateral plane strain elements (four nodes, four integration points).

The surface of the rectangle is set as slave and the surfaces of the indenter are considered as masters. Note that both the lower and front surface of the indenter come in contact as depicted in Figure 6.13. A two-dimensional plane strain, displacement driven problem is considered; the indenter is pushed down by $u_y = 1$ in 10 increments then to the right by $u_x = 10$ within 500 increments; the rectangle is 10 times softer than the indenter. A zoom on the contact topology in the vicinity of indenter's corner is given in Figure 6.15 for several consecutive increments. This behavior explains the oscillations in the tangential reaction (Figure 6.14). The distribution of shear stress for several increments is represented in Figure 6.16. All input data are summarized in the box above.

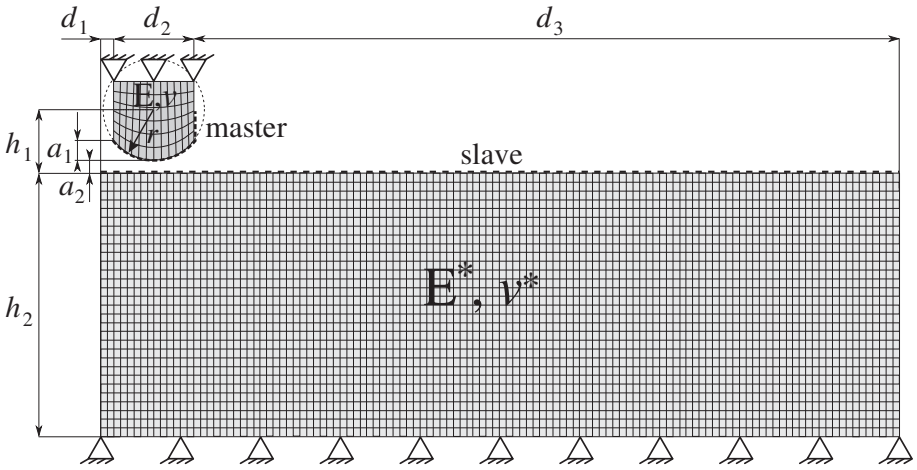

Figure 6.13. *Geometrical setting of the problem and finite element mesh*

6.1.6. *Axisymmetric post-buckling of a thin-walled cylinder*

This axisymmetric problem combines large plastic deformations, buckling, Signorini contact and self-contact phenomena. A force-driven elastoplastic cylinder is forced toward a rigid fixture, where, after some deformations, it gets stuck, and further a series of buckles occur; besides the contact between the cylinder and parts of the fixture, neighboring bends also come in contact. Since the master-slave discretization is not known *a priori*, the single surface algorithm (proposed in [BEN 90] and discussed in Chapter 3) has to be employed. The original numerical solution of this problem was given in [LAU 92]; here, we use the same penalty method, but a finer finite element mesh. All details of the problem setting are given in the box below; geometry and a part of the finite element mesh are given in Figure 6.17. Four independent contact zones can be distinguished as: self-contact within interior and exterior surfaces of the cylinder and Signorini contact between interior and exterior parts of the fixture and the corresponding surfaces of the cylinder.

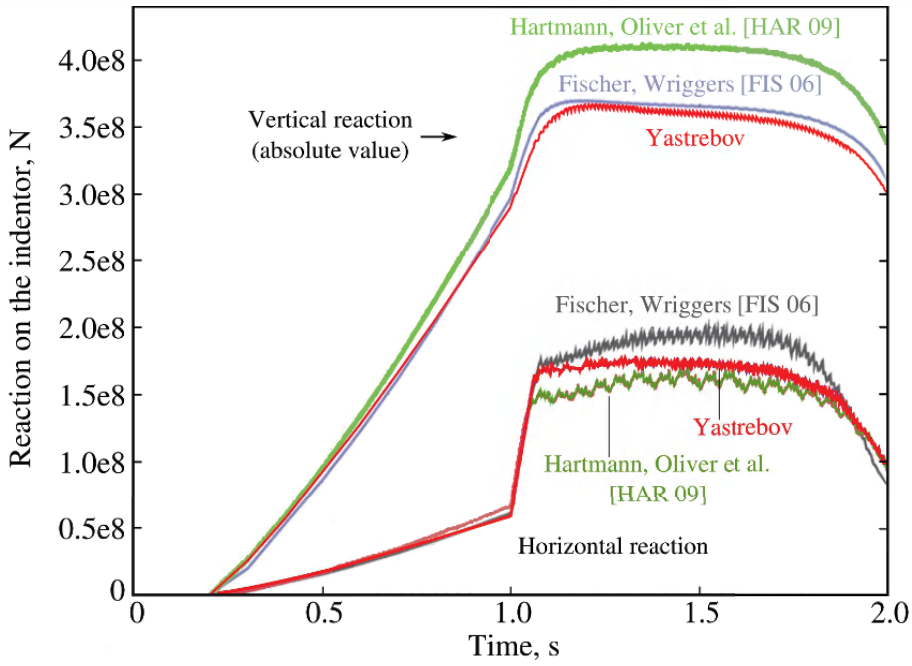

Figure 6.14. *Results of the finite element simulation: comparison of vertical and horizontal reactions on the indenter, data of [FIS 06, HAR 09] and our results*

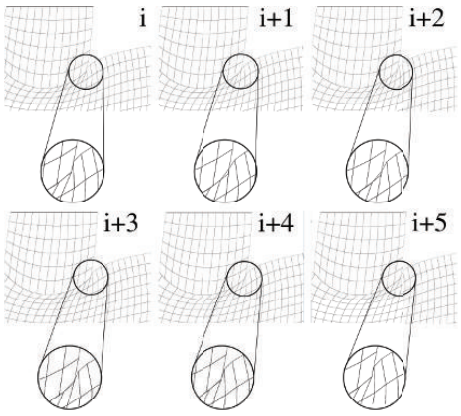

Figure 6.15. *Zoom on the contact zone in the neighborhood of the indenter's angle; six consecutive increments*

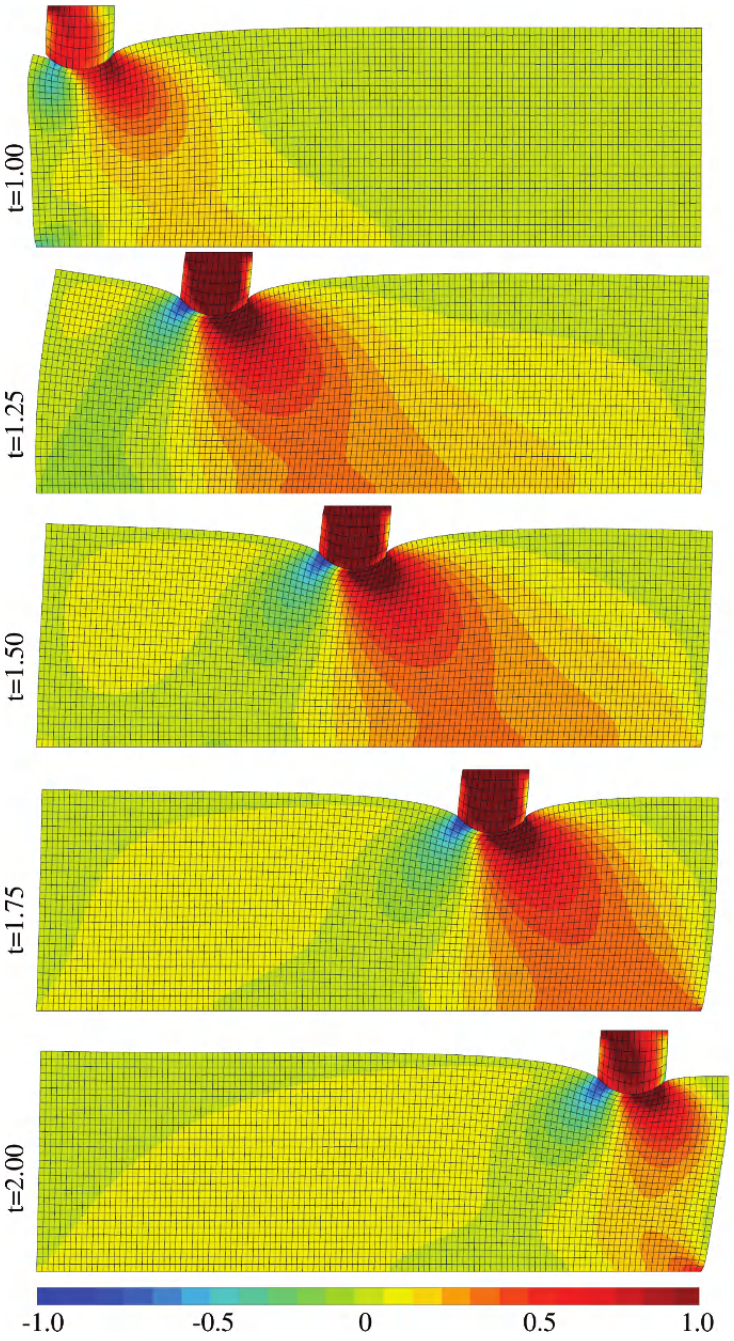

Figure 6.16. *Contour plot of shear stress at time* $t = 1,\ 1.25,\ 1.5,\ 1.75, 2.0$

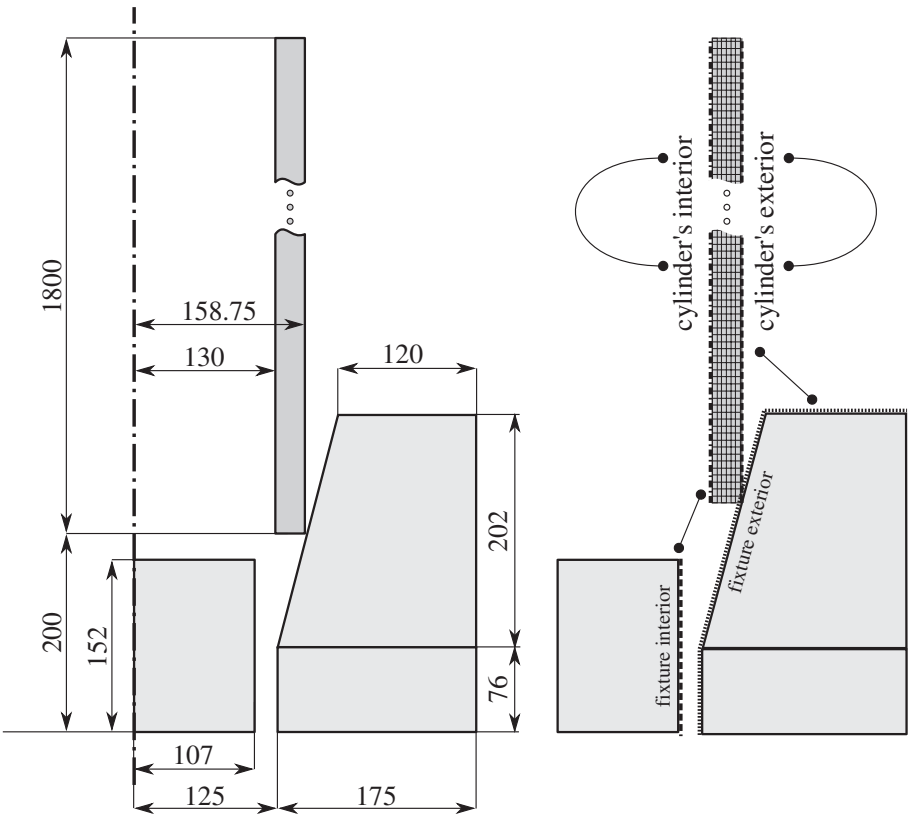

Figure 6.17. *Geometrical setting of the problem and finite element mesh*

An updated Lagrangian formulation is used. The loading conditions are very severe. The accumulated plastic deformation in the interior of the bends reaches 190%. In post-buckling regime, the contact topology changes significantly during the formation of each new bend. Because of the redistribution of momentum, self-contact between already formed bends vanishes on a part of the surface. Figure 6.18 depicts the accumulated plastic strain and post-buckling shapes on different time steps. It is interesting to note that the penalty parameter influences significantly the post-buckling behavior. The number of contact elements in the final stage of the post-buckling deformation reaches 90 elements. PDN method, instead of penalty, is used to enforce the non-penetration conditions on the interior surface of the fixture. The contact is assumed frictionless.

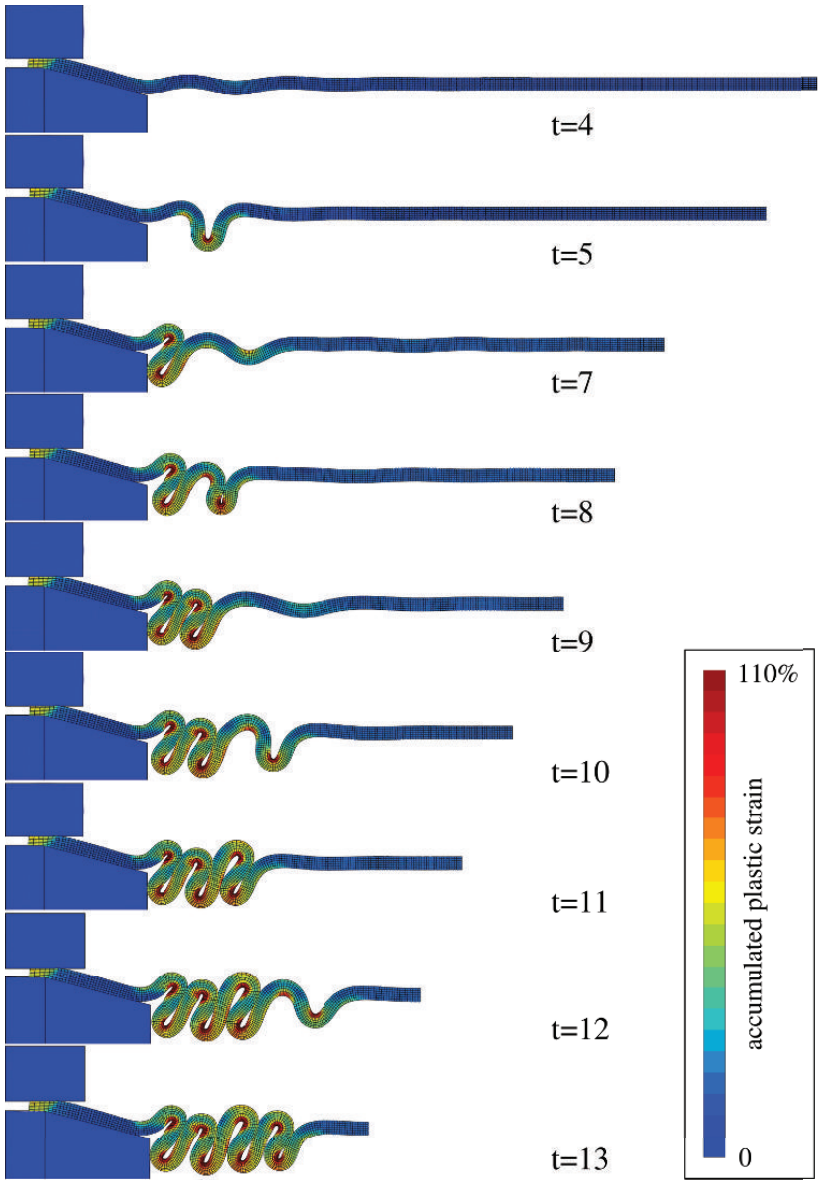

Figure 6.18. *Accumulated plastic strain (Gauss points) at different time steps and corresponding geometry; scale bar is limited by 110% of accumulated plastic strain, however the maximal extrapolated value reaches 194%, maximal value at Gauss points is 181%; penalty value* $\varepsilon_n = 5 \times 10^4$

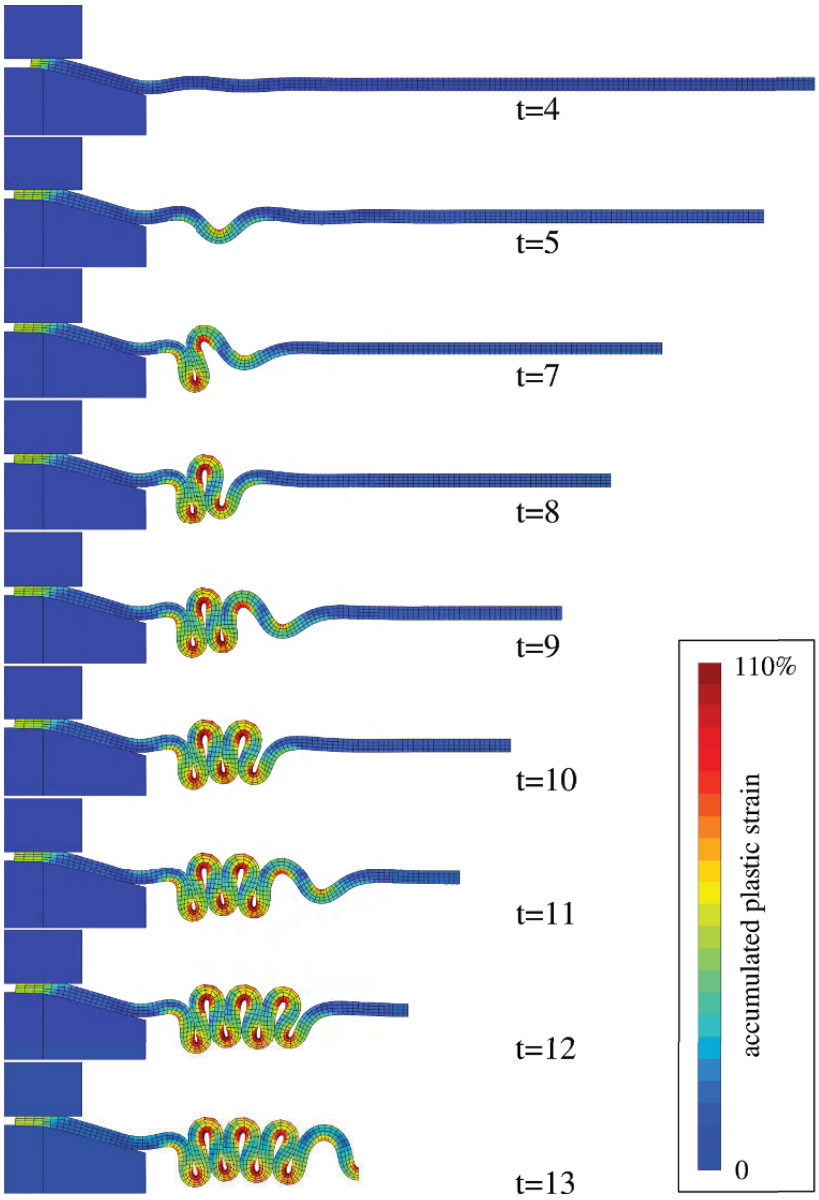

Figure 6.19. *Another post-buckling behavior (penalty value $\varepsilon_n = 1 \times 10^5$): accumulated plastic strain (Gauss points) at different time steps and corresponding geometry; scale bar is limited by 110% of accumulated plastic strain, however the maximal extrapolated value reaches 156%, maximal value at Gauss points is 148%*

⊞ **Data:**

– Finite deformation elastoplasticity (updated Lagrangian):

Young's modulus $E = 210$, Poisson's ratio $\nu = 0.3$;

Von Mises yield strength $R_0 = 0.7$.

Nonlinear isotropic hardening:

$$R = R_0 + Q(1 - e^{-bp}), Q = 10, b = 10.$$

– Boundary conditions and geometry:

Displacement on the top of the cylinder $u_y = -100\,t,\ t \in [0; 13]$.

Friction coefficient $\mu = 0$.

– Solution conditions:

Methods: PDN, penalty;

Penalty coefficients $\varepsilon_n = 5 \times 10^4$ for self-contact, $\varepsilon_n = 1 \times 10^5$ for contact with fixture.

Time $t \in [0; 13]$ increments $N = 15,\ t \in [0; 1.5],\ N = 240,\ t \in [1.5; 10],\ N = 80,\ t \in [10; 13]$.

– Finite element mesh:

Linear full integration quadrilateral plane strain elements (four nodes, four integration points); 2,117 nodes, 1,803 elements.

A totally different post-buckling behavior (see Figure 6.19) is obtained in the simulation with two times higher penalty coefficient ($\varepsilon_n = 10^5$ instead of $\varepsilon_n = 5 \times 10^4$) and a slightly more coarse finite element mesh (765 nodes and 603 elements). No contact occurs between the cylinder and the horizontal surface of the fixture. This example emphasizes that the penalty method should be used very carefully for such error-depending simulation as buckling. It is possible that assuming a non-zero friction in the self-contact interface would lead to a more stable solution.

6.2. Three-dimensional problems

6.2.1. *Accordion post-buckling folding of a thin-walled tube*

This problem is similar to the axisymmetric post-buckling behavior considered in the previous section. One-quarter of an elastoplastic thin walled tube, fixed on both edges, is compressed beyond the critical load, so that it starts to buckle first in axisymmetric mode, then in accordion mode. The problems considered in the two last sections are encountered in crashwortiness research; during post-buckling folding of metal thin walled structures, large amounts of energy due to an impact are consumed. Such structures are thus used for improvement of vehicles safety.

The axisymmetry of the problem is disturbed by small errors due to numerical precision, that is why classical axisymmetric post-buckling changes quickly to an accordion mode. Note that the numerical treatment of this problem is impossible without using symmetric contact boundary conditions[1], which prevent the forming bends from penetration beyond the planes of symmetry, so the penalty method is combined with the PDN method. The geometrical set up and the finite element mesh of the problem are presented in Figure 6.20. All necessary data are listed in the box below.

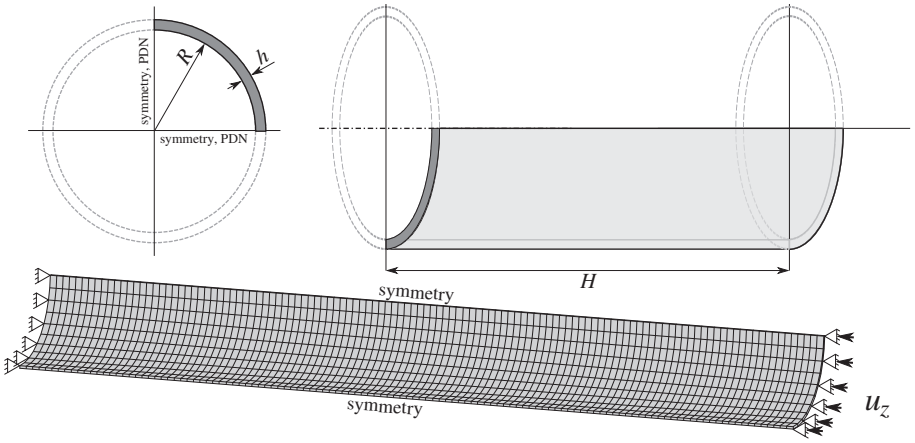

Figure 6.20. *Geometric setting of the problem, boundary conditions and finite element mesh*

1 Symmetric contact boundary conditions are prescribed using the PDN method.

⊞ **Data:**

– Finite deformation elastoplasticity [WEB 90] (updated Lagrangian):

Young's modulus $E = 69$, Poisson's ration $\nu = 0.33$;

Von Mises yield strength $R_0 = 0.25$;

Isotropic hardening constant $Q = 1.5$.

– Boundary conditions and geometry:

Inner radius $R = 14.5$;

Tube thickness $h = 0.5$;

Tube height $H = 150$;

Displacement on the top of the cylinder:

$$u_y = -7\,t,\ t \in [0;10],\ u_y = -70 - 3\,(t-10),\ t \in [10;15]$$

$$u_y = -85 - 13\,(t-15),\ t \in [15;16]$$

Friction coefficient $\mu = 0$.

– Solution conditions:

Methods: PDN, penalty (with updating coefficients);

Initial penalty coefficients $\varepsilon_n^0 = 10^2$, tolerable penetration $g_n = 0.01$;

Time $t \in [0;16]$; increments $N = 100,\ t \in [0;4]$;

$$N = 1,500,\ t \in [4;15],\ N = 300,\ t \in [15;16].$$

– Finite element mesh:

Linear full integration brick elements (eight nodes, eight integration points); 2,662 nodes, 1,200 elements.

Figure 6.21 depicts post-buckling geometry and the corresponding accumulated plastic strain at several time steps, the minimal accumulated plastic strain reaches 7% and the maximal 73% at final time. The reaction-displacement curve is represented in Figure 6.22.

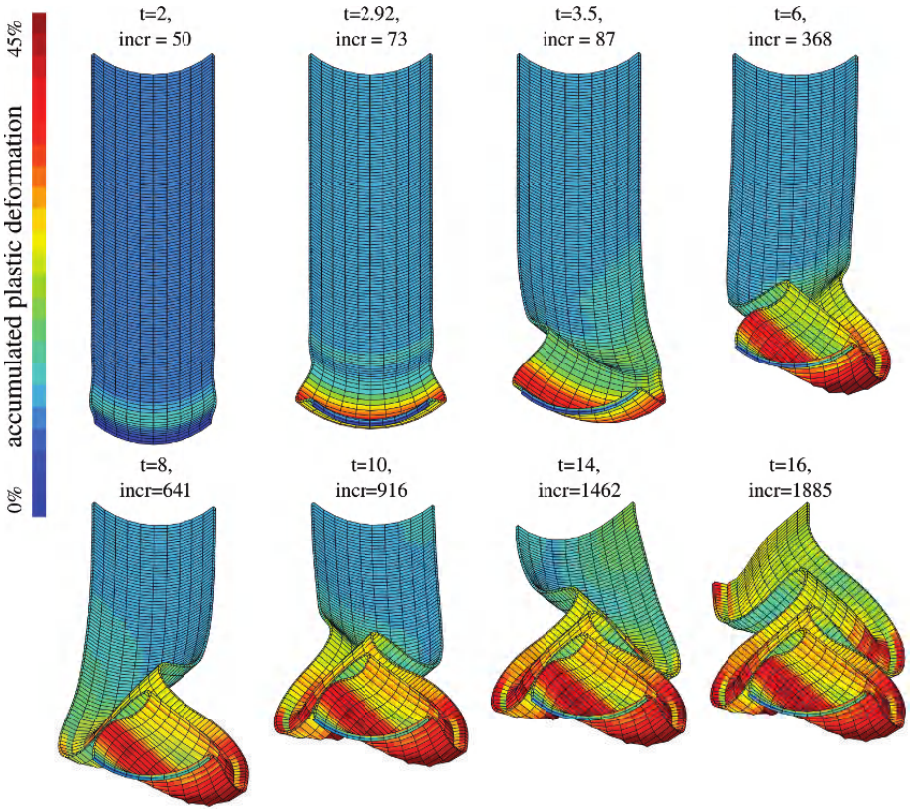

Figure 6.21. *Post-buckling geometry and corresponding accumulated plastic strain*

6.2.2. *Hydrostatic extrusion of a square plate through a circular hole*

This problem deals with an artificial hydrostatic extrusion process: a thin square plate is loaded by a hydrostatic pressure from one side. On the other side, the motion of the plate is limited by a rigid foundation with a hole. Elastic and elastoplastic material models, small and large deformations and different configurations are considered. We do not relate this simulation with any particular industrial problem, it presents simply a demonstration of the PDN method performance in case of large three-dimensional contact problems between a deformable body and a flat rigid foundation with an edge, see Figure 6.23. Two finite element meshes (coarse – 900 linear element and fine – 13,946 linear elements) are presented in Figure 6.24.

Note that the problem is not axisymmetric, but there is a symmetry of the eighth order. However, to demonstrate the performance of the algorithm a quarter of the problem is considered. Regardless a high hydrostatic pressure, a detachment in the

contact zone close to the hole can be observed. Because of this detachment, the determination of the active contact zone takes up to 11 iterations for the fine mesh. The problem with the coarse mesh has been solved for an elastic and elastoplastic material models within small deformations, ratio of the plate side to the diameter of the hole is 5/2. A fine mesh is associated with a problem for a linear material but formulated in large deformations and linear material; to highlight the lack of axisymmetry, the ratio of the plate side to the diameter of the hole is chosen 3/2. All input data are found in the box below.

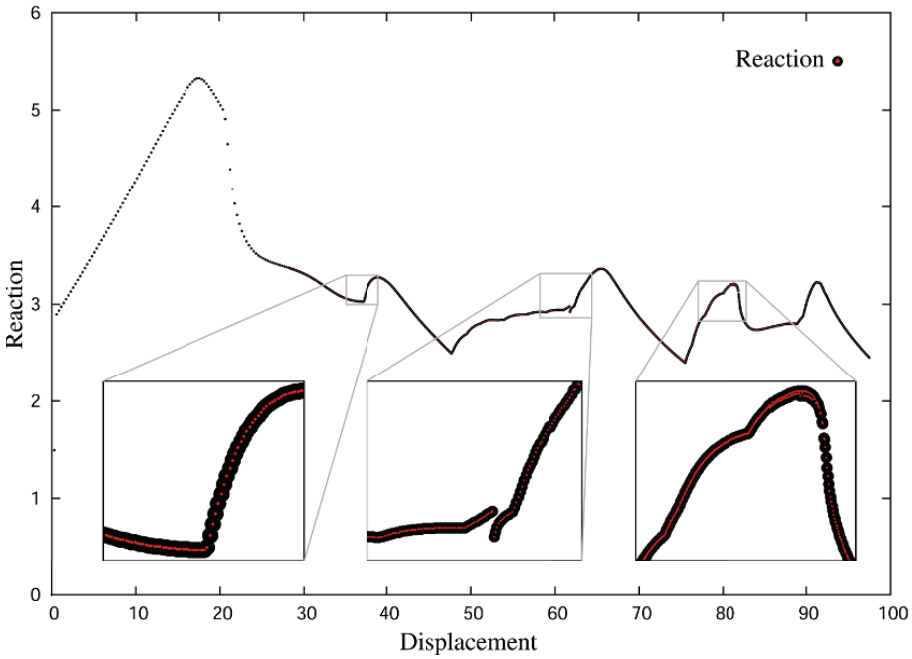

Figure 6.22. *Reaction on the top of the folding cylinder*

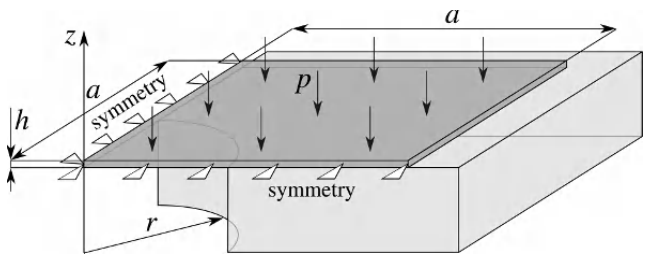

Figure 6.23. *Geometrical setting of the problem*

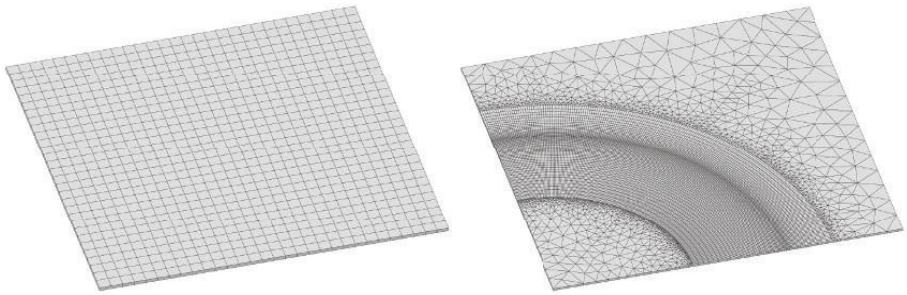

Figure 6.24. *Finite element meshes: coarse and fine*

⊞ **Data:**

– Finite deformation elasticity (updated Lagrangian) for fine mesh; small deformation elasticity and elastoplasticity for coarse mesh.

Young's modulus $E = 210$, Poisson's ration $\nu = 0.3$;

Von Mises yield strength $R_0 = 0.25$.

Nonlinear isotropic hardening:

$$R = R_0 + Q(1 - e^{-bp}), Q = 10, b = 10$$

– Boundary conditions and geometry:

Hole radius $r = 10$;

Plate thickness $h = 0.1$;

Plate half-side $a = 25$ (coarse mesh), $a = 15$ (fine mesh);

Hydrostatic pressure $p = 0.0125$ (coarse mesh), $p = 0.0008$ (fine mesh);

Friction coefficient $\mu = 0$..

– Solution conditions:

Methods: PDN;

Time $t \in [0; 1]$; increments $N = 1$ (coarse mesh), $N = 12$ (fine mesh).

– Finite element mesh:

Coarse mesh – linear full integration brick elements (eight nodes, eight integration points); 1,922 nodes, 900 elements.

Fine mesh – linear full integration brick (eight nodes, eight integration points) and prismatic elements (six nodes, six integration points); 25,350 nodes, 13,946 elements.

The comparison of the deformed shape and the vertical displacement in the detachment zone are presented in Figure 6.25. The maximal vertical displacement of the middle point is about -3 for the case of elastoplastic material model. It is about 30% lower for the elastic material, that is -2.15. Detachment (positive vertical displacement) is quite similar in both cases. The displacements in the radial plane are represented in Figure 6.26 for coarse meshes; besides the quantitative difference, a qualitative difference can be observed in the detachment zone. Note that for the given configuration (ratio of the plate side to the diameter of the hole is 5/2), the entire lower surface of the sheet is expanding due to the applied hydrostatic pressure. Von Mises stress distribution and accumulated plastic strains are plotted on the non-scaled deformed geometry in Figure 6.27. The maximal value of the accumulated plastic strain is situated on the edge of the contact zone and does not overpass 2.4%.

A qualitatively different result has been obtained for the fine mesh, and a central region of radial expansion is followed by a contraction region, see Figures 6.28 and 6.29. Also for the fine mesh, the vertical displacement both in extrusion and detachment zones appears to be axisymmetric, see Figure 6.29. Slight oscillations appear in the stress distribution due to numerical errors. Since the edges of the circular hole are sharp and the detachment effect takes place, the contact zone in the vicinity of the hole edge is given by several nodes with radial coordinate $r = 10$, then $r = 10 - \varepsilon$ are not in contact and $r = 10 + \varepsilon$ are normally in the detachment region.

Figure 6.25. *Vertical displacement on the lower surface of the deforming plate: (a) elastoplastic material and (b) elastic material models; scale of displacement is 500%*

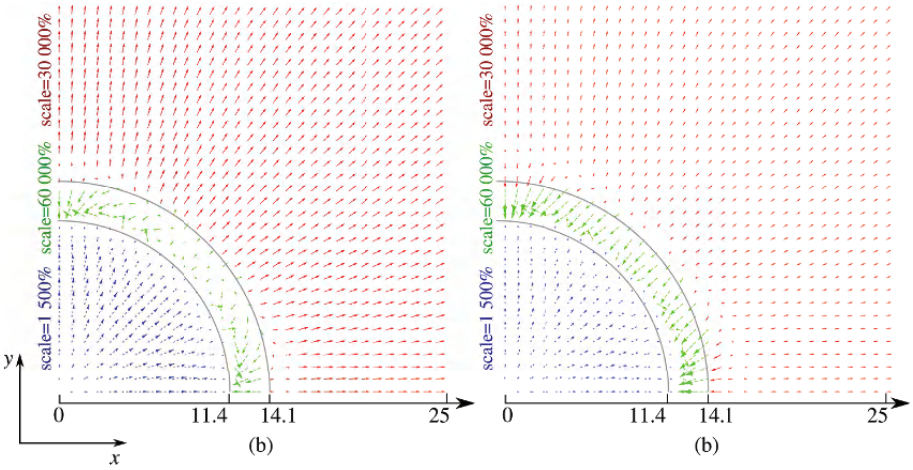

Figure 6.26. *Displacement on the lower surface of the deforming plate in the horizontal plane OXY, different scales are chosen for different zones: (a) elastoplastic and (b) elastic material models*

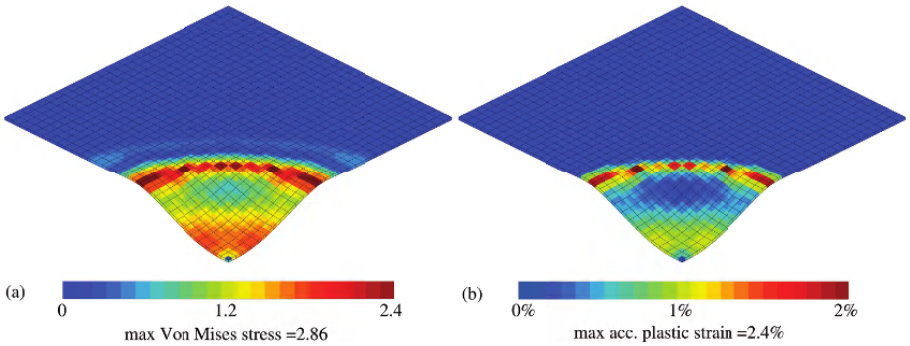

Figure 6.27. *Distribution of von Mises stress at Gauss points for the elastoplastic material (a), accumulated plastic strain (b); scale 100%*

6.2.3. *Frictional sliding of a cube on a rigid plane*

A frictional sliding of a deformable block on a rigid plane demonstrates the difference between local and global (measured) coefficients of friction. The geometry and the finite element mesh are presented in Figure 6.30. A deformable cube is moved towards a rigid plane and further is moved along the plane, three coefficients of friction are considered: $\mu = 0.2,\ 0.5,\ 0.8$; for the latter, a detachment of a part of

a cube takes place in the sliding motion. Rigorously this problem is not well posed, because of sharp angles resulting in infinite stresses; a given finite element discretization can be considered as a regularization of the problem. The mesh of the cube contains 1,000 equal linear brick elements. All data are given in the box below.

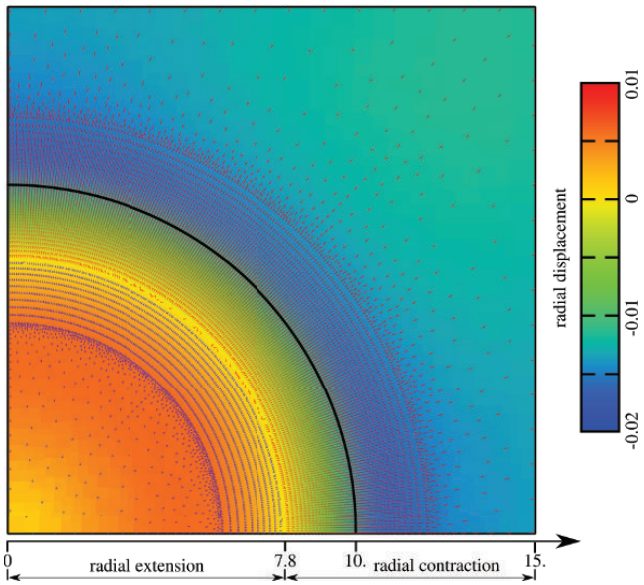

Figure 6.28. *In plane displacements on the lower surface of the deforming plate in case of finite elastic deformations and fine mesh, zones of radial extension and contraction can be distinguished*

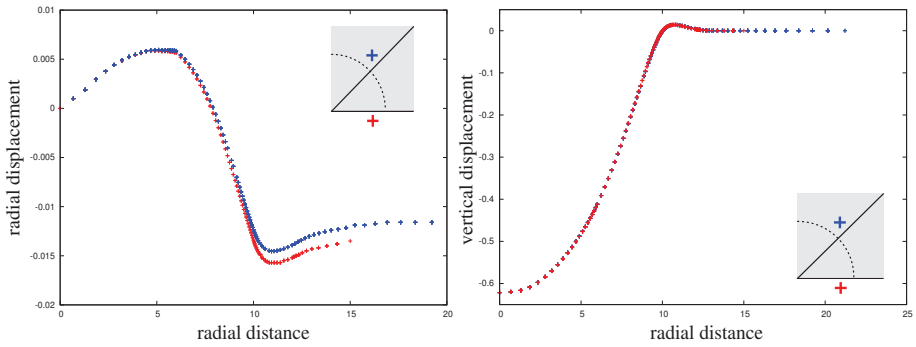

Figure 6.29. *Radial and vertical displacements along two axes of symmetry*

⊞ **Data:**

– Small deformation elasticity:

Young's modulus $E = 210$, Poisson's ratio $\nu = 0.3$.

– Boundary conditions and geometry:

Cube side $a = 1$;

Friction coefficient $\mu = 0.2,\ 0.5,\ 0.8$;

Vertical displacement on the top of cube $u_z = -0.05\,t,\ t \in [0;1],\ u_z = -0.05,\ t > 1$;

Horizontal displacement on the top of cube $u_x = 0,\ t \in [0;1],\ u_x = 1/6\,(t-1),\ t \in [1;3]$.

– Solution conditions:

Methods: PDN.

Time $t \in [0;3]$, increments:
$\mu = 0.2$: $t \in [0;1.2], N = 12, t \in [1.2;3], N = 36$
$\mu = 0.5$: $t \in [0;3], N = 30$
$\mu = 0.8$: $t \in [0;2], N = 20, t \in [2;3], N = 20$

– Finite element mesh:

Linear full integration quadrilateral plane strain elements (four nodes, four integration points); 2,117 nodes, 1,803 elements.

Deformed geometries and the corresponding shear stress σ_{xz} distributions are assembled in Figure 6.31 for the three considered friction coefficients $\mu = 0.2,\ 0.5,\ 0.8$ and three time points $t = 1,\ 2,\ 3$. The case of friction $\mu = 0.8$ is qualitatively different from the two other, since detachment occurs in the contact zone. As a result, there is some stress redistribution in the contact interface and a change of the sliding velocity. Contrary to expectations, due to this detachment, the box with a higher friction $\mu = 0.8$ slides further than the box with a lower friction $\mu = 0.5$. The total vertical reaction scaled by the friction coefficient $\mu|P|$ and the tangential reaction $|T_x|$ is plotted in Figure 6.32. Remark that in slip state the absolute value of the tangential reaction is not equal to the absolute value of the contact pressure multiplied by a friction coefficient $\mu|P| \neq |T_x|$, but:

$$\mu|P| > |T_x|$$

This is due to the fact that the shear stress in the direction orthogonal to sliding σ_{zy} is not zero. Nevertheless, the problem remains symmetric, respectively, to the XOZ

plane passing through the middle of the cube, so the integral of σ_{zy} over the contact interface is zero. To make it evident, nodal tangential reactions in the contact zone are represented in Figure 6.33. The difference between the global coefficient of friction $\bar{\mu}$ and the predefined local cofficient μ remains low. Relative error $(\mu - \bar{\mu})/\mu$ is 3% for $\mu = 0.2$, 2% for $\mu = 0.5$ and only 1.1% for $\mu = 0.8$.

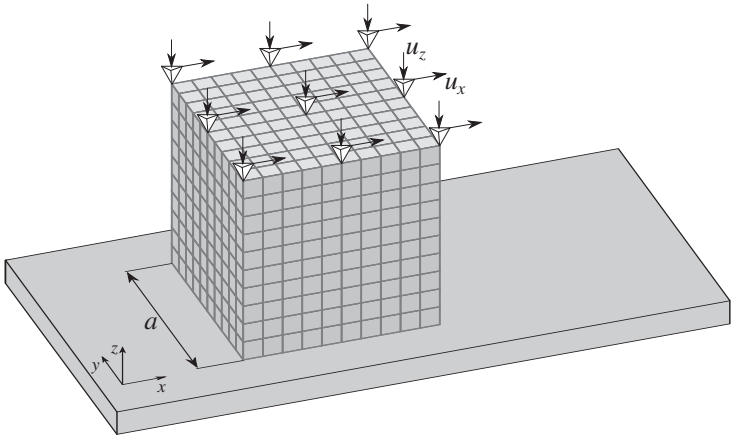

Figure 6.30. *Geometrical setting of the sliding cube problem: finite element mesh and boundary conditions*

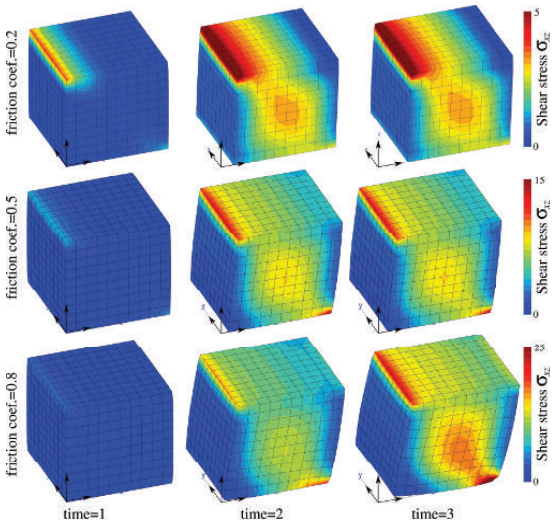

Figure 6.31. *Contour plots of shear stress σ_{xz} for different friction coefficients and time moments*

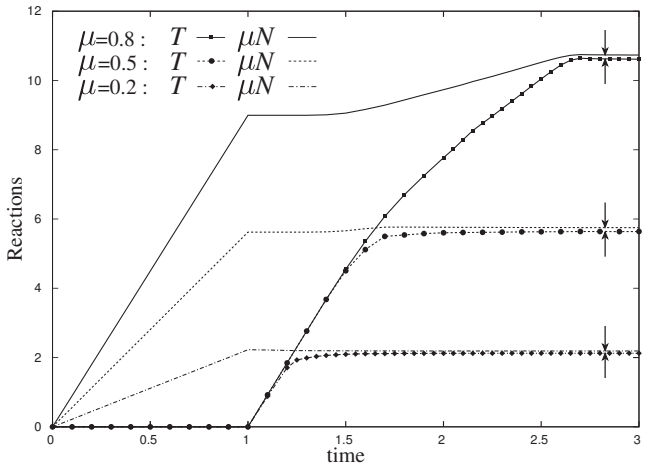

Figure 6.32. *Evolution of the scaled normal reaction $\mu|P|$ and tangential reaction $|T_x|$*

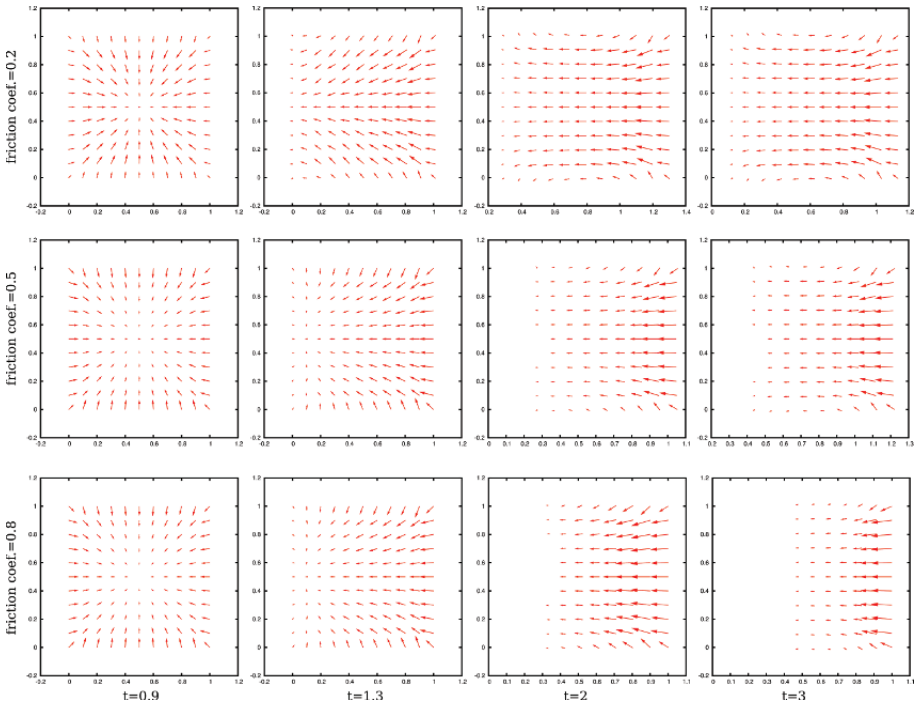

Figure 6.33. *Tangential reactions on the bottom of the cube for different friction coefficients and time moments $t = 0.9,\ 1.3,\ 2.0,\ 3.0$; different scales are used for different plots*

Appendix 1

Vectors, Tensors and s-Structures

"... in mathematics you don't understand things.
You just get used to them."

John von Neumann

Here, the vector-tensor formalism used throughout this book is briefly presented. All computations have been carried out using a rigorous vector–tensor apparatus and the associated notations – the direct "tensor language". In my honest opinion, the formalism used – the direct (component-free) tensor language – is an elegant and intuitive tool that can be easily used in mechanics; moreover, it allows us to decrease significantly the probability of errors and/or misprints in comparison to index notations. In spite of all the aforementioned, sometimes a rigorous proof can be more easily obtained in the coordinate form of a tensor with respect to a given basis. So here almost all operations will be duplicated in index notations.

Generally, in literature, bold symbols or explicit indices are used both for vectors and tensors; sometimes the "array" and "matrix" notations are used. The notations used here are intentionally different and may look unusual. Vectors are underlined by one line, tensors of second and higher orders by two lines. It is due to this fact that we will distinguish two different vector spaces and their elements. This task is hard to accomplish using standard notations.

The first systematic exposition of the tensor language was given by Josiah Willard Gibbs [GIB 84] and improved and extended in [GIB 60]. We follow the course of lectures given by Pavel A. Zhilin at the Saint Petersburg State Polytechnical University [ZHI 01]. The originality of our description of the tensor language consists in the

introduction of new constructions – s-structures, which results in fruitful extension of the tensor language and its application in mathematics and physics.

A1.1. Fundamentals

– A vector $\underline{\boldsymbol{a}}$ of dimension n is an element of the vectorial oriented space:

$$\underline{\boldsymbol{a}} \in {\mathbb{T}_1}^n$$

and should be associated with an oriented segment in this space, but not with a set of n real numbers, which depend upon the choice of the basis. This is the main difference between the direct (component-free) tensor language and the component form.

– A special construction:

$$\mathbb{T}_2^n = {\mathbb{T}_1}^n \otimes {\mathbb{T}_1}^n$$

– the tensor product of two vector spaces – will be called the second-order tensor space and its elements second-order tensors:

$$\underline{\underline{\boldsymbol{a}}} \in \mathbb{T}_2^n$$

The simplest element of this tensor space is a diad [GIB 84] – an ordered pair of vectors:

$$\underline{\boldsymbol{a}} \otimes \underline{\boldsymbol{b}}.$$

Every diad is a second-order tensor but not every second-order tensor is a diad. Any second-order tensor is a formal sum of a finite number of diads:

$$\underline{\underline{\boldsymbol{a}}} = \underline{\boldsymbol{a}} \otimes \underline{\boldsymbol{b}} + \underline{\boldsymbol{c}} \otimes \underline{\boldsymbol{d}} + \cdots + \underline{\boldsymbol{m}} \otimes \underline{\boldsymbol{n}}$$

– In the same manner, higher order tensor spaces can be introduced:

$$\mathbb{T}_m^n = \underbrace{{\mathbb{T}_1}^n \otimes {\mathbb{T}_1}^n \otimes \cdots \otimes {\mathbb{T}_1}^n}_{\text{m times}}$$

For example, the third-order tensor is a formal finite sum of triads:

$${}^3\underline{\underline{\boldsymbol{a}}} = \underline{\boldsymbol{a}} \otimes \underline{\boldsymbol{b}} \otimes \underline{\boldsymbol{c}} + \underline{\boldsymbol{d}} \otimes \underline{\boldsymbol{e}} \otimes \underline{\boldsymbol{f}} + \cdots + \underline{\boldsymbol{m}} \otimes \underline{\boldsymbol{n}} \otimes \underline{\boldsymbol{o}}.$$

In the following, the notation of tensor spaces without upper index $\mathbb{T}_m$ will define vectors and tensors in the three-dimensional (3D) space.

– To move to component notations, the oriented vector space ${\mathbb{T}_1}^n$ has to be complemented by a basis B; every vector can be associated with a unique set of coordinates in the basis $\mathcal{B}$ and vice versa, that is spaces ${\mathbb{T}_1}^n$ and $\mathbb{R}^n$ are bijective. By basis we mean a material point in space, with associated linearly independent axes, and a clock[1] – *reference frame* – and established coordinate system.

– Scalars can be considered as zero-order tensors; a scalar is determined by one real number which does not depend on the choice of the coordinate system. So coordinates of a vector cannot be considered a scalar. Scalars may depend on the reference frame (kinetic energy) or not (temperature, internal energy, etc.)

– For the sake of generality, here and below the expressions in the direct tensor language are followed by the corresponding expressions in component form in dark gray. Each vector is associated with n real numbers – its components in the given coordinate system in the reference frame. In this section, for simplicity, the coordinate system is supposed to be orthonormal. The basis unit vectors of the system are $\underline{\boldsymbol{e}}_1, \underline{\boldsymbol{e}}_2, \ldots, \underline{\boldsymbol{e}}_n$ such as $\underline{\boldsymbol{e}}_i \cdot \underline{\boldsymbol{e}}_j = \delta_i^j$, where "$\cdot$" denotes the dot product (defined below), and δ_i^j is Kronecker delta:

$$\delta_i^j = \begin{cases} 1, & \text{if } i = j \\ 0, & \text{if } i \neq j \end{cases}$$

For such a choice, any vector can be split as follows:

$$\underline{\boldsymbol{a}} = a^1 \underline{\boldsymbol{e}}_1 + a^2 \underline{\boldsymbol{e}}_3 + \cdots + a^n \underline{\boldsymbol{e}}_n = a^i \underline{\boldsymbol{e}}_i,$$

where $a^i = \underline{\boldsymbol{a}} \cdot \underline{\boldsymbol{e}}_i$ are the components of the vector. So each vector for a fixed coordinate system has a one-to-one correspondence with n real numbers:

$$\underline{\boldsymbol{a}} \leftrightarrow a^i, \; i = 1, n$$

The Einstein summation from 1 to n by identical upper-lower indices is used, e.g. $a^i b_i = \sum_{i=1}^{n} a^i b_i$. In details, the basis and all related questions will be considered in the following section.

– Each vector is characterized by a direction and by a length – the vector's norm

$$\| \; \| : {\mathbb{T}_1}^n \to \mathbb{R}_0^+ : \| \underline{\boldsymbol{a}} \| \geq 0.$$

1 Clock is not necessary for the tensor formalism, but for physics for which this formalism is used, the clock is necessary.

Let $\| \ \|$ be the Euclidean norm, so in component form:

$$\|\underline{\boldsymbol{a}}\| = \sqrt{\underline{\boldsymbol{a}}^2} = \sqrt{\underline{\boldsymbol{a}} \cdot \underline{\boldsymbol{a}}}; \quad \|\underline{a}\| = \sqrt{a_i a_i}$$

– Two types of vectors are distinguished: straight vectors and spin-vectors (denoted by $*$, e.g. $\underline{\boldsymbol{a}}_*$). The first ones intuitively describe forward motions (translation), while the second ones characterize proper rotations. There is a correspondence between straight vectors and spin-vectors: this correspondence is uniquely defined if the reference frame is oriented (left-hand or right-hand oriented). A straight vector is called *polar* if it does not change its direction when the orientation of the reference frame changes. An *axial vector* is a straight vector which changes its direction to the opposite if the orientation is changed. Tensors of any order can be polar or axial. The type of tensor is determined by the sensitivity to orientation change: axial tensors are multiplied by -1, polar remain the same, if the orientation changes (independently from left-hand oriented to right-hand or vice versa). Axial tensors of zero order are called pseudoscalar.

– *Vectors summation*

Contrary to mathematics, in physics, vector summation is not abstract and is determined by the well-known triangle or parallelogram rules. The result of the summation is a vector.

- Commutativity: $\underline{\boldsymbol{a}} + \underline{\boldsymbol{b}} = \underline{\boldsymbol{b}} + \underline{\boldsymbol{a}}; \quad a_i + b_i = b_i + a_i$
- Associativity: $(\underline{\boldsymbol{a}} + \underline{\boldsymbol{b}}) + \underline{\boldsymbol{c}} = \underline{\boldsymbol{a}} + (\underline{\boldsymbol{b}} + \underline{\boldsymbol{c}}); \quad (a_i + b_i) + c_i = b_i + (a_i + c_i)$
- Zero vector 0: $\underline{\boldsymbol{a}} + 0 = 0 + \underline{\boldsymbol{a}} = \underline{\boldsymbol{a}}; \quad a_i + 0 = 0 + a_i = a_i$

– *Product of a vector and a scalar*

The product of a vector $\underline{\boldsymbol{a}}$ and a scalar $\alpha \in \mathbb{R}$ is a vector $\underline{\boldsymbol{b}}$:

$$\underline{\boldsymbol{b}} = \alpha \underline{\boldsymbol{a}}; \quad b_i = \alpha a_i,$$

such as $\|\underline{\boldsymbol{b}}\| = |\alpha| \, \|\underline{\boldsymbol{a}}\|$ and if $\alpha > 0$, then vectors $\underline{\boldsymbol{a}}$ and $\underline{\boldsymbol{b}}$ are similarly directed. If $\alpha < 0$ – oppositely directed.

$$\alpha(\underline{\boldsymbol{a}} + \underline{\boldsymbol{b}}) = \alpha \underline{\boldsymbol{a}} + \alpha \underline{\boldsymbol{b}}; \quad \alpha(a_i + b_i) = \alpha a_i + \alpha b_i$$

$$(\alpha + \beta)\underline{\boldsymbol{a}} = \alpha \underline{\boldsymbol{a}} + \beta \underline{\boldsymbol{a}}; \quad (\alpha + \beta) a_i = \alpha a_i + \beta a_i$$

– *Scalar product or dot product of vectors*

The dot product of two vectors is a scalar:

$$\{\cdot\} : \mathbb{T}_1 \times \mathbb{T}_1 \to \mathbb{R}$$

$$\alpha = \underline{\boldsymbol{a}} \cdot \underline{\boldsymbol{b}} = \|\underline{\boldsymbol{a}}\| \, \|\underline{\boldsymbol{b}}\| \, cos(\phi); \quad \alpha = a_i b^i = a^i b_i,$$

where ϕ is the angle between vectors.

- Commutativity: $\underline{\boldsymbol{a}} \cdot \underline{\boldsymbol{b}} = \underline{\boldsymbol{b}} \cdot \underline{\boldsymbol{a}}; \quad a_i b^i = b^i a_i$

- Distributivity: $\underline{\boldsymbol{a}} \cdot (\underline{\boldsymbol{b}} + \underline{\boldsymbol{c}}) = \underline{\boldsymbol{a}} \cdot \underline{\boldsymbol{b}} + \underline{\boldsymbol{a}} \cdot \underline{\boldsymbol{c}}; \quad a_i(b^i + c^i) = a_i b^i + a_i c^i$

– *Orthogonality*

Vectors are orthogonal if their dot product is zero:

$$\underline{\boldsymbol{a}} \perp \underline{\boldsymbol{b}} \;\Leftrightarrow\; \underline{\boldsymbol{a}} \cdot \underline{\boldsymbol{b}} = 0; \quad a_i b^i = 0$$

– *Unit vector*

The unit vector of a nonzero vector $\underline{\boldsymbol{a}}$ is the vector $\underline{\hat{\boldsymbol{a}}}$ such that:

$$\underline{\hat{\boldsymbol{a}}} = \frac{\underline{\boldsymbol{a}}}{\|\underline{\boldsymbol{a}}\|}; \quad \hat{a}_i = \frac{a_i}{\|\underline{\boldsymbol{a}}\|}$$

– *Projections*

Projection of the vector $\underline{\boldsymbol{a}}$ on the vector $\underline{\boldsymbol{b}}$ is a vector $\underline{\boldsymbol{p}}$ such as:

$$\underline{\boldsymbol{p}} = (\underline{\boldsymbol{a}} \cdot \underline{\hat{\boldsymbol{b}}})\underline{\hat{\boldsymbol{b}}}; \quad p_i = a_j \hat{b}^j \hat{b}_i.$$

By projection we often mean a scalar p:

$$p = \underline{\boldsymbol{a}} \cdot \underline{\hat{\boldsymbol{b}}}; \quad p = a_i \hat{b}^i$$

The projection of the vector $\underline{\boldsymbol{a}}$ on the plane with normal $\underline{\boldsymbol{b}}$ is a vector $\underline{\boldsymbol{p}}$ such that:

$$\underline{\boldsymbol{p}} = (\underline{\underline{\boldsymbol{I}}} - \underline{\hat{\boldsymbol{b}}} \otimes \underline{\hat{\boldsymbol{b}}}) \cdot \underline{\boldsymbol{a}}; \quad p_i = (\delta_i^j - \hat{b}_i \hat{b}^j) a_j.$$

– *Vector product or cross product*

The vector product can be introduced only in oriented reference frames, contrary to previously defined operations which are valid also for non-orientation reference frames. Moreover, the vector product is meaningful only in 3D spaces $\mathbb{T}_1 = {\mathbb{T}_1}^3$. So if there is a vector product in equation, spaces are implicitly supposed to be $\mathbb{T}_n^3$. The vector product of two vectors $\underline{\boldsymbol{a}}$ and $\underline{\boldsymbol{b}}$ is a vector:

$$\underline{\boldsymbol{c}} = \underline{\boldsymbol{a}} \times \underline{\boldsymbol{b}}; \quad c_i = \det \begin{bmatrix} \delta_1^i & \delta_2^i & \delta_3^i \\ a_1 & a_2 & a_3 \\ b_1 & b_2 & b_3 \end{bmatrix}$$

such that

$$\underline{\boldsymbol{c}} \cdot \underline{\boldsymbol{a}} = 0;\ \underline{\boldsymbol{c}} \cdot \underline{\boldsymbol{b}} = 0; \|\underline{\boldsymbol{c}}\| = \|\underline{\boldsymbol{a}}\|\,\|\underline{\boldsymbol{b}}\|\,sin(\phi)$$

$$c_i a^i = 0; c_i b^i = 0;\ \|\underline{\boldsymbol{c}}\| = \|\underline{\boldsymbol{a}}\|\,\|\underline{\boldsymbol{b}}\|\,sin(\phi)$$

Two vectors fulfill these conditions: $\underline{\boldsymbol{c}}$ and $-\underline{\boldsymbol{c}}$. To determine the direction of the vector $\underline{\boldsymbol{c}}$, we use a spin-vector $\underline{\boldsymbol{c}}_*$, whose axis is parallel to the vector $\underline{\boldsymbol{c}}$ and whose rotation is oriented from vector $\underline{\boldsymbol{a}}$ to $\underline{\boldsymbol{b}}$ through the minimal angle. If the minimal angle is 0 or 2π, then by definition $\|\underline{\boldsymbol{c}}\| = 0$, so the orientation is meaningless. Finally, the vector $\underline{\boldsymbol{c}}$ or $-\underline{\boldsymbol{c}}$ is associated with the spin-vector $\underline{\boldsymbol{c}}_*$, respectively, to the orientation of the reference frame. For two polar vectors $\underline{\boldsymbol{a}}$ and $\underline{\boldsymbol{b}}$, vector $\underline{\boldsymbol{c}}$ is axial. As can be demonstrated [ZHI 01], vector product of two polar vectors $\underline{\boldsymbol{a}}$, $\underline{\boldsymbol{b}}$ is more meaningful for the spin-vector $\underline{\boldsymbol{c}}_*$ than for the axial-vector $\underline{\boldsymbol{c}}$, since the spin-vector remains valid for mirror symmetries.

$$\underline{\boldsymbol{c}} = \underline{\boldsymbol{a}} \times \underline{\boldsymbol{b}} = -\underline{\boldsymbol{b}} \times \underline{\boldsymbol{a}};\quad c^i = \det \begin{bmatrix} \delta_1^i & \delta_2^i & \delta_3^i \\ a_1 & a_2 & a_3 \\ b_1 & b_2 & b_3 \end{bmatrix} = -\det \begin{bmatrix} \delta_1^i & \delta_2^i & \delta_3^i \\ b_1 & b_2 & b_3 \\ a_1 & a_2 & a_3 \end{bmatrix}$$

$$\underline{\boldsymbol{a}} \times (\underline{\boldsymbol{b}} + \underline{\boldsymbol{c}}) = \underline{\boldsymbol{a}} \times \underline{\boldsymbol{b}} + \underline{\boldsymbol{a}} \times \underline{\boldsymbol{c}};$$

$$\det \begin{bmatrix} \delta_1^i & \delta_2^i & \delta_3^i \\ a_1 & a_2 & a_3 \\ b_1 + c_1 & b_2 + c_2 & b_3 + c_3 \end{bmatrix} = \det \begin{bmatrix} \delta_1^i & \delta_2^i & \delta_3^i \\ a_1 & a_2 & a_3 \\ b_1 & b_2 & b_3 \end{bmatrix} + \det \begin{bmatrix} \delta_1^i & \delta_2^i & \delta_3^i \\ a_1 & a_2 & a_3 \\ c_1 & c_2 & c_3 \end{bmatrix}$$

– *Three vector products*

The mixed product of vectors:

$$\beta = \underline{\boldsymbol{a}} \cdot (\underline{\boldsymbol{b}} \times \underline{\boldsymbol{c}}) = \underline{\boldsymbol{c}} \cdot (\underline{\boldsymbol{a}} \times \underline{\boldsymbol{b}}) = \underline{\boldsymbol{b}} \cdot (\underline{\boldsymbol{c}} \times \underline{\boldsymbol{a}})$$

$$\beta = \det \begin{bmatrix} a_1 & a_2 & a_3 \\ b_1 & b_2 & b_3 \\ c_1 & c_2 & c_3 \end{bmatrix} = \cdots = \ldots$$

The double vector product of vectors:

$$\underline{\boldsymbol{d}} = \underline{\boldsymbol{a}} \times (\underline{\boldsymbol{b}} \times \underline{\boldsymbol{c}}) = \underline{\boldsymbol{b}}(\underline{\boldsymbol{a}} \cdot \underline{\boldsymbol{c}}) - \underline{\boldsymbol{c}}(\underline{\boldsymbol{a}} \cdot \underline{\boldsymbol{b}})$$

$$d_i = \det \begin{bmatrix} \delta_{1i} & \delta_{2i} & \delta_{3i} \\ a_1 & a_2 & a_3 \\ \det \begin{bmatrix} b_2 & b_3 \\ c_2 & c_3 \end{bmatrix} & -\det \begin{bmatrix} b_1 & b_3 \\ c_1 & c_3 \end{bmatrix} & \det \begin{bmatrix} b_1 & b_2 \\ c_1 & c_2 \end{bmatrix} \end{bmatrix} = b_i a_j c_j - c_i a_j b_j.$$

Note that brackets which point the order of operations, i.e. which vector product should be evaluated first, are mandatory since:

$$\underline{\boldsymbol{a}} \times (\underline{\boldsymbol{b}} \times \underline{\boldsymbol{c}}) \neq (\underline{\boldsymbol{a}} \times \underline{\boldsymbol{b}}) \times \underline{\boldsymbol{c}}$$

A1.2. Vector space basis

A basis is any set of linearly independent vectors $\underline{\boldsymbol{e}}_i,\ i = 1, n$. Vectors $\underline{\boldsymbol{e}}_i$ are linearly independent if and only if:

$$\underline{\boldsymbol{e}}_i \alpha^i = 0 \ \Leftrightarrow \ \alpha^i = 0$$

It can be shown that in 3D this condition is equivalent to the condition:

$$\underline{\boldsymbol{e}}_1 \cdot (\underline{\boldsymbol{e}}_2 \times \underline{\boldsymbol{e}}_3) \neq 0$$

Any vector $\underline{\boldsymbol{a}} \in \mathbb{T}_1{}^n$ can be presented as:

$$\underline{\boldsymbol{a}} = \alpha^i \underline{\boldsymbol{e}}_i,$$

where α^i are the coordinates of the vector $\underline{\boldsymbol{a}}$ in the basis $\underline{\boldsymbol{e}}_i$. For two arbitrary bases:

$$\underline{\boldsymbol{a}} \cdot \underline{\boldsymbol{b}} = a^i \underline{\boldsymbol{e}}_i \cdot b^j \underline{\boldsymbol{e}}_j = a^i b^j \underline{\boldsymbol{e}}_i \cdot \underline{\boldsymbol{e}}_j.$$

The dual basis $\underline{\boldsymbol{e}}^i$ is constructed such that:

$$\underline{\boldsymbol{e}}_i \cdot \underline{\boldsymbol{e}}^j = \delta_i^j$$

Naturally vectors of the dual basis are linearly independent. If vectors of the basis $\underline{\boldsymbol{e}}_i$ are normalized, i.e. $\|\underline{\boldsymbol{e}}_i\| = 1$, then the norms of the vectors of the dual basis are not smaller than one:

$$\|\underline{\boldsymbol{e}}^i\| \geq 0, \ \text{ since } \underline{\boldsymbol{e}}_i \cdot \underline{\boldsymbol{e}}^i = \underbrace{\|\underline{\boldsymbol{e}}_i\|}_{=1} \|\underline{\boldsymbol{e}}^i\| \cos(\phi) = 1 \ \Rightarrow \ \|\underline{\boldsymbol{e}}^i\| = \frac{1}{\cos(\phi)},$$

where ϕ is the angle between vectors $\underline{\boldsymbol{e}}_i$ and $\underline{\boldsymbol{e}}^i$.

Now the summation by upper and lower repeated indices becomes more clear. Coordinates a^i of the vector $\underline{\boldsymbol{a}}$ in the basis $\underline{\boldsymbol{e}}_i$ are determined by the dot product of $\underline{\boldsymbol{a}}$ with the corresponding coordinate of the dual basis and vice versa:

$$a^i = \underline{\boldsymbol{a}} \cdot \underline{\boldsymbol{e}}^i; \quad a_i = \underline{\boldsymbol{a}} \cdot \underline{\boldsymbol{e}}_i,$$

where a_i are the coordinates of the vector $\underline{\boldsymbol{a}}$ in the basis $\underline{\boldsymbol{e}}^i$. If the basis $\underline{\boldsymbol{e}}_i$ is orthonormal, then the dual basis is identical to it:

$$\underline{\boldsymbol{e}}_i \cdot \underline{\boldsymbol{e}}_j = \delta_i^j \quad \Leftrightarrow \quad \underline{\boldsymbol{e}}_i = \underline{\boldsymbol{e}}^i.$$

and the coordinates of vectors in both bases are equal $a^i = a_i$. Objects with an upper and lower index will be called, respectively, contravariant and covariant objects. A more detailed explanation and definition is given below.

It is recommended to read the end of this section check briefly the S-structure notations introduced in section A1.6. S-structures are special constructions under the space of tensors of all ranks, which have been introduced in to simplify the formalism and to avoid the indices. In the following, where it will be possible, instead of index notations, s-structure notations will be used:

$$\begin{array}{cccccc} \underline{\boldsymbol{e}}_i & \longrightarrow & \underset{\sim}{\boldsymbol{e}}, & \underline{\boldsymbol{e}}^i & \longrightarrow & \underset{\sim}{\bar{\boldsymbol{e}}} \\ a_i & \longrightarrow & \underset{\sim}{\mathrm{a}}, & a^i & \longrightarrow & \underset{\sim}{\bar{\mathrm{a}}} \end{array}$$

Using this notations, we introduce a special t-scalar $\underset{\approx}{\mathrm{A}}$ called the first fundamental matrix or metric matrix, which is symmetric due to commutativity of the scalar product:

$$\underset{\approx}{\mathrm{A}} = \underset{\sim}{\boldsymbol{e}} \cdot \underset{\sim}{\boldsymbol{e}} = \underset{\approx}{\mathrm{A}}^{\intercal}; \quad A_{ij} = \underline{\boldsymbol{e}}_i \cdot \underline{\boldsymbol{e}}_j = A_{ji}$$

The term "matrix" is used to follow the tradition. It is important to remark that this object is not formally an object of tensor space $\underset{\approx}{\mathrm{A}} \in \mathbb{T}_2^n$, since elements of the tensor space are invariant objects and this object is a double covariant. However in coordinate

form the metric matrix seems very similar to a tensor and is called the metric tensor. From the previous definition, it follows directly that:

$$\underset{\sim}{\boldsymbol{e}} = \underset{\approx}{\mathrm{A}}\,\underset{\sim}{\bar{\boldsymbol{e}}}; \quad \underline{\boldsymbol{e}}_i = (\underline{\boldsymbol{e}}_i \cdot \underline{\boldsymbol{e}}_j)\underline{\boldsymbol{e}}^j$$

In the same manner, the t-scalar $\underset{\approx}{\bar{\mathrm{A}}}$ – metric matrix for the dual basis is determined; it is also symmetric:

$$\underset{\approx}{\bar{\mathrm{A}}} = \underset{\sim}{\bar{\boldsymbol{e}}} \cdot \underset{\sim}{\bar{\boldsymbol{e}}} = \underset{\approx}{\bar{\mathrm{A}}}^{\intercal}; \quad A^{ij} = \underline{\boldsymbol{e}}^i \cdot \underline{\boldsymbol{e}}^j = A^{ji}$$

$$\underset{\sim}{\bar{\boldsymbol{e}}} = \underset{\approx}{\bar{\mathrm{A}}}\,\underset{\sim}{\boldsymbol{e}}; \quad \underline{\boldsymbol{e}}^i = (\underline{\boldsymbol{e}}^i \cdot \underline{\boldsymbol{e}}^j)\underline{\boldsymbol{e}}_j$$

Considering the dot product of two bases:

$$\underset{\approx}{\mathrm{I}} = \underset{\sim}{\bar{\boldsymbol{e}}} \cdot \underset{\sim}{\boldsymbol{e}} = \underset{\approx}{\bar{\mathrm{A}}}\,\underset{\sim}{\boldsymbol{e}} \cdot \underset{\sim}{\bar{\boldsymbol{e}}}\,\underset{\approx}{\mathrm{A}} = \underset{\approx}{\bar{\mathrm{A}}}\,\underset{\approx}{\mathrm{I}}\,\underset{\approx}{\mathrm{A}}; \quad \delta^i_j = \underline{\boldsymbol{e}}^i \cdot \underline{\boldsymbol{e}}_j = A^{ij}\underline{\boldsymbol{e}}_j \cdot \underline{\boldsymbol{e}}^k A_{lk} = A^{ij}\delta^k_j A_{lk}$$

Directly due to the symmetry of fundamental t-scalars:

$$\underset{\approx}{\bar{\mathrm{A}}}\,\underset{\approx}{\mathrm{A}} = \underset{\approx}{\mathrm{I}}, \ \underset{\approx}{\bar{\mathrm{A}}} = \underset{\approx}{\mathrm{A}}^{-1}; \quad A^{ij}A_{jk} = \delta^i_k, \ A^{ij} = \frac{\text{cofactor}\,(A_{ij})}{\det A_{ij}},$$

where by $\text{cofactor}\,(A_{ij})$ we mean the determinant of matrix $\tilde{A}_{ij}$ with suppressed ith line and jth column and multiplied by $(-1)^{i+j}$. It follows directly:

$$\det \underset{\approx}{\bar{\mathrm{A}}} = \frac{1}{\det \underset{\approx}{\mathrm{A}}}$$

Following the derived formulas, any vector $\underline{\boldsymbol{a}}$ can be easily written in both bases:

$$\underline{\boldsymbol{a}} = \underset{\sim}{\mathrm{a}}\,\underset{\sim}{\bar{\boldsymbol{e}}} = \underset{\sim}{\bar{\mathrm{a}}}\,\underset{\sim}{\boldsymbol{e}}; \quad \underline{\boldsymbol{a}} = a^i\underline{\boldsymbol{e}}_i = a_i\underline{\boldsymbol{e}}^i$$

where $\underset{\sim}{\mathrm{a}}$ and $\underset{\sim}{\bar{\mathrm{a}}}$ are the v-scalars of coordinates of the vector $\underline{\boldsymbol{a}}$ in the basis $\underset{\sim}{\bar{\boldsymbol{e}}}$ and $\underset{\sim}{\boldsymbol{e}}$, respectively:

$$\underset{\sim}{\mathrm{a}} = \underset{\approx}{\mathrm{A}}\,\underset{\sim}{\bar{\mathrm{a}}}, \ \underset{\sim}{\bar{\mathrm{a}}} = \underset{\approx}{\bar{\mathrm{A}}}\,\underset{\sim}{\mathrm{a}}; \quad a_i = A_{ij}a^j, \ a^i = A^{ij}a_j$$

A1.2.1. *Transformation matrices, covariant and contravariant objects*

The choice of the basis is arbitrary. Vectors do not depend on this choice, so for any basis the following equality holds:

$$\underline{\boldsymbol{a}} = \underset{\sim}{\bar{\mathrm{a}}}\underset{\sim}{\underline{\boldsymbol{e}}} = \underset{\sim}{\mathrm{a}}\underset{\sim}{\bar{\underline{\boldsymbol{e}}}} = \underset{\sim}{\bar{\mathrm{a}}}'\underset{\sim}{\underline{\boldsymbol{e}}}' = \underset{\sim}{\mathrm{a}}'\underset{\sim}{\bar{\underline{\boldsymbol{e}}}}'$$

where $\underset{\sim}{\underline{\boldsymbol{e}}}'$ and $\underset{\sim}{\bar{\underline{\boldsymbol{e}}}}'$ are the new basis and its dual basis, respectively. As for the dual basis, the transformation t-scalar can be constructed to determine coordinates of vectors in the new basis from known coordinates in the initial basis and vice versa. Vectors of the new basis are expressed by the vectors of the initial basis as follows:

$$\underset{\sim}{\underline{\boldsymbol{e}}}' = (\underset{\sim}{\underline{\boldsymbol{e}}}' \cdot \underset{\sim}{\bar{\underline{\boldsymbol{e}}}})\underset{\sim}{\underline{\boldsymbol{e}}}; \quad \underline{\boldsymbol{e}}_{i'} = (\underline{\boldsymbol{e}}_{i'} \cdot \underline{\boldsymbol{e}}^{j})\underline{\boldsymbol{e}}_{j}$$

the transition t-scalar $\underset{\approx}{\mathrm{P}}$, traditionally referred as the pushforward transformation matrix, is then constructed as follows:

$$\underset{\approx}{\mathrm{P}} = \underset{\sim}{\underline{\boldsymbol{e}}}' \cdot \underset{\sim}{\bar{\underline{\boldsymbol{e}}}}; \quad P^{j}_{i'} = \underline{\boldsymbol{e}}_{i'} \cdot \underline{\boldsymbol{e}}^{j}$$

For backward transition, the t-scalar $\underset{\approx}{\mathrm{P}}'$ – pullback transformation matrix – is given by:

$$\underset{\approx}{\mathrm{P}}' = \underset{\sim}{\bar{\underline{\boldsymbol{e}}}}' \cdot \underset{\sim}{\underline{\boldsymbol{e}}}; \quad P^{i'}_{j} = \underline{\boldsymbol{e}}^{i'} \cdot \underline{\boldsymbol{e}}_{j}$$

Note that these transformation matrices in general are not symmetric, so indices are ordered:

$$\underset{\approx}{\mathrm{P}} \neq \underset{\approx}{\mathrm{P}}^{\intercal}; \quad \underset{\approx}{\mathrm{P}}' \neq \underset{\approx}{\mathrm{P}}'^{\intercal}$$

It is easy to show that the t-scalars $\underset{\approx}{\mathrm{P}}^{\intercal}$ and $\underset{\approx}{\mathrm{P}}'$ are inversely proportional:

$$\underset{\approx}{\mathrm{P}}^{\intercal}\underset{\approx}{\mathrm{P}}' = \underset{\approx}{\mathrm{I}}, \ \underset{\approx}{\mathrm{P}}' = \underset{\approx}{\mathrm{P}}^{-T}; \quad P^{j}_{i'}P^{i'}_{k} = \delta^{j}_{k}, \ P^{j}_{i'} = \frac{\text{cofactor}\left(P^{i'}_{k}\right)}{\det P^{i'}_{k}}$$

We clearly see that the initial basis and the new basis are related by the forward transition $\underset{\approx}{\mathrm{P}}$; the corresponding dual bases are related by the backward transition $\underset{\approx}{\mathrm{P}}'$:

$$\underset{\sim}{\boldsymbol{e}}' = \underset{\approx}{\mathrm{P}}\,\underset{\sim}{\boldsymbol{e}}$$

$$\underset{\sim}{\bar{\boldsymbol{e}}}' = \underset{\approx}{\mathrm{P}}'\,\underset{\sim}{\bar{\boldsymbol{e}}}$$

One of the key notions of the theory is the definition of the covariant and contravariant objects.

If an object $\underset{\sim}{\mathrm{c}}$ of order n depends on the basis choice, then this object is called

– *n-order covariant* if it follows the same transformation as the initial basis:

$$\underset{\sim}{\mathrm{c}}' = \overbrace{\underset{\approx}{\mathrm{P}}\,\underset{\approx}{\mathrm{P}}\dots\underset{\approx}{\mathrm{P}}}^{n\text{ times}}\,\underset{\sim}{\mathrm{c}};\quad c_{\alpha'\beta'\dots\gamma'} = \overbrace{P^{i}_{\alpha'}P^{j}_{\beta'}\dots P^{n}_{\gamma'}}^{n\text{ times}}\,c_{ij\dots n}$$

– *n-order contravariant* if it follows the same transformation as the dual basis:

$$\underset{\sim}{\bar{\mathrm{c}}}' = \overbrace{\underset{\approx}{\mathrm{P}}'\,\underset{\approx}{\mathrm{P}}'\dots\underset{\approx}{\mathrm{P}}'}^{n\text{ times}}\,\underset{\sim}{\bar{\mathrm{c}}};\quad c^{\alpha'\beta'\dots\gamma'} = \overbrace{P^{\alpha'}_{i}P^{\beta'}_{j}\dots P^{\gamma'}_{n}}^{n\text{ times}}\,c^{ij\dots n}$$

– *p-order covariant, q-order contravariant*, $p+q=n$ if it changes p times according to the transformation of the initial basis and q times according to the transformation of the dual basis:

$$\underset{\sim}{\mathrm{c}}' = \overbrace{\underset{\approx}{\mathrm{P}}\,\underset{\approx}{\mathrm{P}}\dots\underset{\approx}{\mathrm{P}}}^{p\text{ times}}\overbrace{\underset{\approx}{\mathrm{P}}'\,\underset{\approx}{\mathrm{P}}'\dots\underset{\approx}{\mathrm{P}}'}^{q\text{ times}}\,\underset{\sim}{\bar{\mathrm{c}}};\quad c^{\varepsilon'\xi'\dots\zeta'}_{\alpha'\beta'\dots\gamma'} = \overbrace{P^{i}_{\alpha'}P^{j}_{\beta'}\dots P^{k}_{\gamma'}}^{p\text{ times}}\overbrace{P^{\varepsilon'}_{l}P^{\xi'}_{m}\dots P^{\zeta'}_{n}}^{q\text{ times}}\,c^{lm\dots n}_{ij\dots k}$$

An object of the first order c which does not follow covariant or contravariant transformation rules is called a non-tensorial object and the position of the index is not important. In such cases, the index is often put in brackets $c_{(i)}$. If an object is m-order covariant and m-order contravariant, then the object is invariant with respect to the change of basis. This is the case for a vector, which consists of covariant coordinates and contravariant basis vector or contravariant coordinates and covariant basis vectors. Since tensors of higher ranks are constructed by means of tensor products of vectors, a tensor of rank m is m-order covariant and m-order contravariant, so it is also invariant in any basis change. The Kronecker delta

$\delta_i^j = \underline{\boldsymbol{e}}_i \cdot \underline{\boldsymbol{e}}^j$ is a first-order covariant and first-order contravariant object, so is also invariant, and can be considered as the coordinates of the second-order unity tensor. Another example is the metric matrix $\underset{\approx}{\mathrm{A}}$ which is a second order covariant; the metric matrix of the dual basis $\underset{\approx}{\bar{\mathrm{A}}}$ is a second-order contravariant and naturally their product $\underset{\approx}{\mathrm{A}}\,\underset{\approx}{\bar{\mathrm{A}}} = \underset{\approx}{\mathrm{I}}$ is an invariant object.

A1.2.2. *Gradient operator or Hamilton's operator*

Let $\underset{\sim}{\underline{\boldsymbol{e}}}$ be a moving coordinate system in the reference frame, then the vector $\underline{\boldsymbol{r}}$ of each point, fixed in the frame of reference, is determined as:

$$\underline{\boldsymbol{r}} = \underline{\boldsymbol{r}}(\underset{\sim}{\bar{\mathrm{y}}}, t),$$

where $\underset{\sim}{\bar{\mathrm{y}}} = \underset{\sim}{\bar{\mathrm{y}}}(t)$ are the coordinates of $\underline{\boldsymbol{r}}$ in the basis $\underset{\approx}{\underline{\boldsymbol{e}}}$ at time t, i.e.:

$$\underline{\boldsymbol{r}} = \underset{\sim}{\bar{\mathrm{y}}}\,\underset{\approx}{\underline{\boldsymbol{e}}}$$

and

$$\dot{\underline{\boldsymbol{r}}} = \frac{\partial \underline{\boldsymbol{r}}}{\partial \underset{\sim}{\bar{\mathrm{y}}}}\,\dot{\underset{\sim}{\bar{\mathrm{y}}}} + \frac{\partial \underline{\boldsymbol{r}}}{\partial t} = 0.$$

For an observer in the moving coordinate system $\underset{\sim}{\underline{\boldsymbol{e}}}$, a change of point $\underline{\boldsymbol{r}}$ leads to a change of coordinates $\underset{\sim}{\bar{\mathrm{y}}}$. Logically there exist changes of $\underline{\boldsymbol{r}}$ in which only one coordinate changes, for example y^i. So for a smooth function $\underline{\boldsymbol{r}}(\underset{\sim}{\bar{\mathrm{y}}})$ at a given time, there exists one curve in space determined by the vector $\underline{\boldsymbol{r}}(y^1, \ldots, y^i, \ldots, y^n)$ where all $y^j = \text{const}$ and only y^i changes. The tangent vector for such a curve is determined by:

$$\underline{\boldsymbol{r}}_i = \frac{\partial \underline{\boldsymbol{r}}}{\partial y^i}$$

A set of such tangent vectors is a covariant v-vector:

$$\underset{\sim}{\mathrm{D}}\,\underline{\boldsymbol{r}} = \frac{\partial}{\partial \underset{\sim}{\bar{\mathrm{y}}}}\underline{\boldsymbol{r}},$$

where $\underset{\sim}{\mathrm{D}}$ is a covariant operator:

$$\underset{\sim}{\mathrm{D}} = \frac{\partial}{\partial \underset{\sim}{\bar{\mathrm{y}}}}$$

The dual local basis can be constructed in a standard manner:

$$\overline{\frac{\partial \underline{\boldsymbol{r}}}{\partial \underset{\sim}{\bar{\mathrm{y}}}}} = \underset{\approx}{\bar{\mathrm{A}}} \frac{\partial \underline{\boldsymbol{r}}}{\partial \underset{\sim}{\bar{\mathrm{y}}}},$$

where $\underset{\approx}{\bar{\mathrm{A}}} = \underset{\approx}{\mathrm{A}}^{-1}$ and

$$\underset{\approx}{\mathrm{A}} = \frac{\partial \underline{\boldsymbol{r}}}{\partial \underset{\sim}{\bar{\mathrm{y}}}} \cdot \frac{\partial \underline{\boldsymbol{r}}}{\partial \underset{\sim}{\bar{\mathrm{y}}}}$$

Covariant or contravariant sets of such tangent vectors can be chosen as a basis. Since the basis depends on the points in the reference frame, such a basis is called local. It can be shown that the basis constructed in such a way is covariant. It is worth mentioning that in [KAG 47], these sets of vectors were interpreted as first rank tensors with vector components – an interpretation of v-vectors.

Finally, the well-known gradient operator (invariant differential operator) is written as:

$$\nabla = \overline{\frac{\partial \underline{\boldsymbol{r}}}{\partial \underset{\sim}{\bar{\mathrm{y}}}}} \circ \underset{\sim}{\mathrm{D}}$$

The gradient vector is an objective operator, which does not depend on the choice of the coordinate system, since it is first-order covariant with respect to covariant operator $\underset{\sim}{\mathrm{D}}$ and first-order contravariant with respect to $\overline{\frac{\partial \underline{\boldsymbol{r}}}{\partial \underset{\sim}{\bar{\mathrm{y}}}}}$. Another example of an objective operator is the full time derivative $\frac{d}{dt}$. An example of a non-objective operator is the partial time derivative $\frac{\partial}{\partial t}$. The two following statements can be easily proved:

$$\nabla \frac{d}{dt} = \frac{d}{dt} \nabla, \quad \nabla \frac{\partial}{\partial t} \neq \frac{\partial}{\partial t} \nabla$$

The gradient operator is very important for mechanical and physical theories. For a scalar field $s(\underline{\boldsymbol{r}}) = s(\underline{\boldsymbol{r}}(\underset{\sim}{\bar{\mathrm{y}}}))$, the influence of the gradient operator is uniquely defined by:

$$\mathrm{grad}(s) = \nabla s = \overline{\frac{\partial \underline{\boldsymbol{r}}}{\partial \underset{\sim}{\bar{\mathrm{y}}}}} \circ \frac{\partial s}{\partial \underset{\sim}{\bar{\mathrm{y}}}}$$

The gradient notation "grad" is equivalent to the tensor product of the gradient operator and the field; in the case of a scalar field, the tensor product is meaningless and so omitted. The gradient vector can act differently on tensor fields of first- and higher orders $\underline{\underline{\boldsymbol{T}}}(\underline{\boldsymbol{r}}) = \underline{\underline{\boldsymbol{T}}}(\underline{\boldsymbol{r}}(\underset{\sim}{\bar{\mathrm{y}}}))$. The side (left-hand or right-hand) and intermediate operators are important. Gradient of a tensor field:

$$\mathrm{grad}\left(\underline{\underline{\boldsymbol{T}}}\right) = \nabla \otimes \underline{\underline{\boldsymbol{T}}} = \overline{\frac{\partial \underline{\boldsymbol{r}}}{\partial \underset{\sim}{\bar{\mathrm{y}}}}} \circ\otimes \frac{\partial \underline{\underline{\boldsymbol{T}}}}{\partial \underset{\sim}{\bar{\mathrm{y}}}} \neq \underline{\underline{\boldsymbol{T}}} \otimes \nabla$$

The tensor product notation is often skipped.

Divergence of a tensor field:

$$\mathrm{div}\left(\underline{\underline{\boldsymbol{T}}}\right) = \nabla \cdot \underline{\underline{\boldsymbol{T}}} = \overline{\frac{\partial \underline{\boldsymbol{r}}}{\partial \underset{\sim}{\bar{\mathrm{y}}}}} \circ\cdot \frac{\partial \underline{\underline{\boldsymbol{T}}}}{\partial \underset{\sim}{\bar{\mathrm{y}}}}$$

Remark that the following equality is correct only for vectors and symmetric second-order tensors:

$$\nabla \cdot \underline{\underline{\boldsymbol{T}}} = \underline{\underline{\boldsymbol{T}}} \cdot \nabla$$

The rotor of a tensor field:

$$\mathrm{rot}\left(\underline{\underline{\boldsymbol{T}}}\right) = \nabla \times \underline{\underline{\boldsymbol{T}}} = \overline{\frac{\partial \underline{\boldsymbol{r}}}{\partial \underset{\sim}{\bar{\mathrm{y}}}}} \circ\times \frac{\partial \underline{\underline{\boldsymbol{T}}}}{\partial \underset{\sim}{\bar{\mathrm{y}}}}$$

$$\nabla \times \underline{\boldsymbol{t}} = -\underline{\boldsymbol{t}} \times \nabla$$

Div and rot are alternative notations for the scalar and vector products of the gradient operator with a tensor field.

Another important operator in physics and mechanics is the Laplace operator or Laplacian Δ, which is defined as:

$$\Delta = \nabla \cdot \nabla = \nabla^2$$

It should not be confused with $\nabla \otimes \nabla \neq \Delta$.

Some examples:

– balance of momentum in the deformable body;

$$\nabla \cdot \underline{\underline{\boldsymbol{\sigma}}} + \underline{\boldsymbol{f}}_v = 0$$

– Cauchy's strain tensor;

$$\underline{\underline{\boldsymbol{\varepsilon}}} = \frac{1}{2}\left(\nabla \otimes \underline{\boldsymbol{u}} + \underline{\boldsymbol{u}} \otimes \nabla\right)$$

– compatibility of (small) deformations;

$$\nabla \times \left(\nabla \times \underline{\underline{\boldsymbol{\varepsilon}}}\right) = 0$$

– compatibility of (finite) deformations;

$$\nabla \times \underline{\underline{\boldsymbol{F}}} = 0$$

– Maxwell's equations.

$$\nabla \cdot \underline{\boldsymbol{E}} = \frac{\rho}{\varepsilon_0}$$

$$\nabla \cdot \underline{\boldsymbol{B}} = 0$$

$$\nabla \times \underline{\boldsymbol{E}} = -\frac{\partial \underline{\boldsymbol{B}}}{\partial t}$$

$$\nabla \times \underline{\boldsymbol{B}} = \mu_0 \underline{\boldsymbol{J}} + \mu_0 \varepsilon_0 \frac{\partial \underline{\boldsymbol{E}}}{\partial t}$$

A1.3. Sub-basis, vector function of v-scalar argument

Let us consider a vector function $\underline{\boldsymbol{\rho}}$ of v-scalar argument $\underset{\sim}{\xi}$ such that:

$$\underline{\boldsymbol{\rho}}(\underset{\sim}{\xi}) : \mathbb{R}^m \to \mathbb{T}_1{}^n,\ m \leq n$$

If for each $\underset{\sim}{\xi}$ there exists only one element $\underline{\boldsymbol{\rho}}(\underset{\sim}{\xi}) \in {\mathbb{T}_1}^n$, where ${\mathbb{T}_1}^n$ is a vector space with a reference frame, then the image of the space $\mathbb{R}^m$ in ${\mathbb{T}_1}^n$ is a set of points. If $\underline{\boldsymbol{\rho}}(\underset{\sim}{\xi}) = \underline{\boldsymbol{\rho}}(t, \underset{\sim}{\xi})$, then this set of points changes in time. For instance, in the 3D space at given time, the image $\mathbf{Im}R^m$ in the space is:

– a point, if $m = 0$;

– a curve, if $m = 1$;

– a surface, if $m = 2$;

– a volume if $m = 3$.

At each time at point $\underline{\boldsymbol{\rho}}(t, \underset{\sim}{\xi})$ a local sub-basis $\underset{\approx}{\underline{\boldsymbol{e}}}$ can be established if the function $\underline{\boldsymbol{\rho}}(t, \xi) \in C^1(\underset{\sim}{\xi})$ is sufficiently smooth versus its second argument $\underset{\sim}{\xi}$:

$$\underset{\approx}{\underline{\boldsymbol{e}}} = \frac{\partial \underline{\boldsymbol{\rho}}}{\partial \underset{\sim}{\xi}}$$

For the given time t^0 and point $\underset{\sim}{\xi}^0$, this basis determines a local subspace ${\mathbb{T}_1}^m$ of the full space ${\mathbb{T}_1}^m \subset {\mathbb{T}_1}^n$:

– a straight line, tangential to the curve at $\underline{\boldsymbol{\rho}}(t^0, \underset{\sim}{\xi}^0)$, if $m = 1$;

– a tangential plane of the surface at $\underline{\boldsymbol{\rho}}(t^0, \underset{\sim}{\xi}^0)$ if $m = 2$;

– a full space, if $m = 3$.

If needed, the basis $\underset{\sim}{\underline{\boldsymbol{e}}}$ can be complemented by vectors orthogonal to the subspace ${\mathbb{T}_1}^n \ni \underline{\boldsymbol{e}}_i \perp \mathbb{T}_1$. Moreover, in the particular case of 3D space $n = 3$ and $m = 2$, the third basis vector can be constructed as the vector product of the basis vectors $\underset{\sim}{\underline{\boldsymbol{e}}}$:

$$\underline{\boldsymbol{e}}_3 = \underline{\boldsymbol{e}}_1 \times \underline{\boldsymbol{e}}_2.$$

However, if we are interested only in the object described by the function $\underline{\boldsymbol{\rho}}(t, \underset{\sim}{\xi})$, there is no need for such a completion.

The metric matrix associated with the object $\underline{\boldsymbol{\rho}}(t, \underset{\sim}{\xi})$ is nothing but:

$$\underset{\approx}{\mathrm{A}} = \frac{\partial \underline{\boldsymbol{\rho}}}{\partial \underset{\sim}{\xi}} \cdot \frac{\partial \underline{\boldsymbol{\rho}}}{\partial \underset{\sim}{\xi}} = \underset{\approx}{\mathrm{A}}^{\mathsf{T}},$$

and consequently the dual basis is:

$$\underset{\sim}{\bar{\boldsymbol{e}}} = \overline{\frac{\partial \underline{\boldsymbol{\rho}}}{\partial \underset{\sim}{\xi}}} = \underset{\approx}{\bar{\mathrm{A}}} \frac{\partial \underline{\boldsymbol{\rho}}}{\partial \underset{\sim}{\xi}},$$

where $\underset{\approx}{\bar{\mathrm{A}}} = \underset{\approx}{\mathrm{A}}^{-1} = \overline{\frac{\partial \underline{\boldsymbol{\rho}}}{\partial \underset{\sim}{\xi}}} \cdot \overline{\frac{\partial \underline{\boldsymbol{\rho}}}{\partial \underset{\sim}{\xi}}} = \underset{\approx}{\bar{\mathrm{A}}}^{\mathsf{T}}$.

A corresponding sub-gradient operator is constructed like in the previous section, (to avoid any confusions the order of the operator is marked):

$$\nabla^{m} = \underset{\sim}{\bar{\boldsymbol{e}}} \circ \frac{\partial}{\partial \underset{\sim}{\xi}} = \overline{\frac{\partial \underline{\boldsymbol{\rho}}}{\partial \underset{\sim}{\xi}}} \circ \frac{\partial}{\partial \underset{\sim}{\xi}}$$

Such a sub-gradient operator is used in the theory of deformable rods ($m = 1$) and shells ($m = 2$).

As one can note, the metric matrix associated with an object in an n-dimensional space has a dimension $m \times m$ instead of $n \times n$. It is a normal situation in differential geometry. But the classical rule of summations by indices cannot be used anymore, since the classical summation by indices is defined according to the dimension of the full space, i.e. from 1 to n. One possible solution used in the literature is to introduce a reduced summation from 1 to m; this summation will be performed only within, for example, small Greek indices or capital letter indices like

$$\underline{\boldsymbol{e}}^{\alpha} = \frac{\partial \underline{\boldsymbol{\rho}}}{\partial \xi^{\alpha}} = A^{\alpha\beta} \frac{\partial \underline{\boldsymbol{\rho}}}{\partial \xi_{\beta}}; \quad \underline{\boldsymbol{e}}^{P} = \frac{\partial \underline{\boldsymbol{\rho}}}{\partial \xi^{P}} = A^{PQ} \frac{\partial \underline{\boldsymbol{\rho}}}{\partial \xi_{Q}}$$

Let us demonstrate the difference between an intuitive form constructed with the direct tensor language and a half-index form based on Greek letters. For quantities related to the surface, both of them are equivalent, but as in practice the probability of error is lower if we use the first formalism (this example is taken from Chapter 2:)

$$\begin{aligned}
\Delta\delta\underset{\sim}{\xi} \quad &= (g_n \underset{\approx}{\mathrm{H}} - \underset{\approx}{\mathrm{A}})^{-1} \left\{ \frac{\partial \underline{\boldsymbol{\rho}}}{\partial \underset{\sim}{\xi}} \cdot \left(\delta \frac{\partial \underline{\boldsymbol{\rho}}}{\partial \underset{\sim}{\xi}}^{\mathsf{T}} \Delta\underset{\sim}{\xi} + \Delta \frac{\partial \underline{\boldsymbol{\rho}}}{\partial \underset{\sim}{\xi}} \delta\underset{\sim}{\xi} \right) + \Delta\underset{\sim}{\xi} \left(\frac{\partial \underline{\boldsymbol{\rho}}}{\partial \underset{\sim}{\xi}} \cdot \frac{\partial^2 \underline{\boldsymbol{\rho}}}{\partial \underset{\sim}{\xi}^2} \right) \delta\underset{\sim}{\xi} - \right. \\
&- g_n \underline{\boldsymbol{n}} \cdot \left(\delta \frac{\partial^2 \underline{\boldsymbol{\rho}}}{\partial \underset{\sim}{\xi}^2} \Delta\underset{\sim}{\xi} + \Delta \frac{\partial^2 \underline{\boldsymbol{\rho}}}{\partial \underset{\sim}{\xi}^2} \delta\underset{\sim}{\xi} \right) - g_n \Delta\underset{\sim}{\xi} \left(\underline{\boldsymbol{n}} \cdot \frac{\partial^3 \underline{\boldsymbol{\rho}}}{\partial \underset{\sim}{\xi}^3} \right) \delta\underset{\sim}{\xi} + \\
&+ \left[g_n \left(\delta \frac{\partial \underline{\boldsymbol{\rho}}}{\partial \underset{\sim}{\xi}} + \frac{\partial^2 \underline{\boldsymbol{\rho}}}{\partial \underset{\sim}{\xi}^2} \delta\underset{\sim}{\xi} \right) \cdot \frac{\partial \underline{\boldsymbol{\rho}}}{\partial \underset{\sim}{\xi}} \underset{\approx}{\bar{\mathrm{A}}} - \delta g_n \underset{\approx}{\mathrm{I}} \right] \left(\underline{\boldsymbol{n}} \cdot \Delta \frac{\partial \underline{\boldsymbol{\rho}}}{\partial \underset{\sim}{\xi}} + \underset{\approx}{\mathrm{H}} \Delta\underset{\sim}{\xi} \right) + \\
&+ \left. \left[g_n \left(\Delta \frac{\partial \underline{\boldsymbol{\rho}}}{\partial \underset{\sim}{\xi}} + \frac{\partial^2 \underline{\boldsymbol{\rho}}}{\partial \underset{\sim}{\xi}^2} \Delta\underset{\sim}{\xi} \right) \cdot \frac{\partial \underline{\boldsymbol{\rho}}}{\partial \underset{\sim}{\xi}} \underset{\approx}{\bar{\mathrm{A}}} - \Delta g_n \underset{\approx}{\mathrm{I}} \right] \left(\underline{\boldsymbol{n}} \cdot \delta \frac{\partial \underline{\boldsymbol{\rho}}}{\partial \underset{\sim}{\xi}} + \underset{\approx}{\mathrm{H}} \delta\underset{\sim}{\xi} \right) \right\} \qquad \text{[A1.1]}
\end{aligned}$$

$$\begin{aligned}\Delta\delta\xi^{\alpha} &= C^{\alpha\beta}\left\{\frac{\partial\rho_i}{\partial\xi_\beta}\left(\delta\frac{\partial\rho^i}{\partial\xi_\gamma}\Delta\xi^{\gamma}+\Delta\frac{\partial\rho^i}{\partial\xi_\gamma}\delta\xi^{\gamma}\right)+\Delta\xi^{\beta}\frac{\partial\rho_i}{\partial\xi_\beta}\frac{\partial^2\rho^i}{\partial\xi_\gamma\partial\xi_\eta}\delta\xi^{\eta}-\right.\\ &-g_n n_i\left(\delta\frac{\partial^2\rho^i}{\partial\xi_\beta\partial\xi_\gamma}\Delta\xi^{\gamma}+\Delta\frac{\partial^2\rho^i}{\partial\xi_\beta\partial\xi_\gamma}\delta\xi^{\gamma}\right)-g_n\Delta\xi^{\gamma}\left(n_i\frac{\partial^3\rho^i}{\partial\xi_\gamma\partial\xi_\beta\partial\xi_\kappa}\right)\delta\xi^{\kappa}+\\ &+\left[g_n\left(\delta\frac{\partial\rho_i}{\partial\xi_\beta}+\frac{\partial^2\rho_i}{\partial\xi_\beta\partial\xi_\gamma}\delta\xi^{\gamma}\right)\frac{\partial\rho^i}{\partial\xi_\eta}A^{\eta\kappa}-\delta g_n\delta^{\kappa}_{\beta}\right]\left(n_i\Delta\frac{\partial\rho^i}{\partial\xi_\kappa}+H_{\kappa\tau}\Delta\xi^{\tau}\right)+\\ &\left.+\left[g_n\left(\Delta\frac{\partial\rho_i}{\partial\xi_\beta}+\frac{\partial^2\rho_i}{\partial\xi_\beta\partial\xi_\gamma}\Delta\xi^{\gamma}\right)\frac{\partial\rho^i}{\partial\xi_\eta}A^{\eta\kappa}-\delta g_n\Delta^{\kappa}_{\beta}\right]\left(n_i\delta\frac{\partial\rho^i}{\partial\xi_\kappa}+H_{\kappa\tau}\delta\xi^{\tau}\right)\right\},\end{aligned} \quad [A1.2]$$

where $C^{\alpha\beta}=(g_nH_{\alpha\beta}-A_{\alpha\beta})^{-1}$, here $\alpha,\beta,\ldots,\kappa\in 1,2$ and $i\in 1,2,3$.

A1.4. Tensors

Scalars and vectors are not sufficient for physical and mechanical theories. More complicated structures, higher order tensors, are required. Second-order tensors seem to be much more abstract and hardly imaginary objects than vectors and scalars. However, a second-order tensor is not a purely mathematical construction. In mechanics, it appeared first as a mathematical formalization of intuitive associations not connected with coordinate systems.

The first second-order tensors (tensor of inertia of a rigid body and rotation tensor) have been introduced by Leonhard Euler in 1758. The term "tensor" was proposed by W. Voigt only in 1900. In 1788, Joseph-Louis Lagrange introduced the second-order tensor of small deformations. In 1822, Augustin-Louis Cauchy introduced a second-order tensor to characterize the stress state – the stress tensor $\underline{\underline{\boldsymbol{\sigma}}}$ – and gave a consistent mathematical framework for the tensor space. Tensors became unavoidable objects for the description of deformable continua. Ever since, this stress tensor is called Cauchy's stress tensor.

– Definition
The second-order tensor space is defined as *tensor* product of first-order tensor spaces (vector spaces).

$$\mathbb{T}_2^n=\mathbb{T}_1{}^n\otimes\mathbb{T}_1{}^n$$

Note that the direct product of such spaces $\mathbb{T}_1{}^n\times\mathbb{T}_1{}^n$ does not lead to a tensor space; such a space is not even a linear space. Although, tensors are "physical" in 3D space ($n=3$), for the sake of generality, the formalism will be derived for an arbitrary n-dimensional space, except some particularities related, for example, to vector product.

Any element of the constructed space – second-order tensor $\underline{\underline{\boldsymbol{A}}} \in \mathbb{T}_2^n$ – can be written as a *formal* sum of the tensor products of vectors:

$$\underline{\underline{\boldsymbol{A}}} = \underline{\boldsymbol{a}} \otimes \underline{\boldsymbol{b}} \;\; \oplus \;\; \underline{\boldsymbol{c}} \otimes \underline{\boldsymbol{d}} \;\; \oplus \;\; \ldots \;\; \oplus \;\; \underline{\boldsymbol{e}} \otimes \underline{\boldsymbol{f}}$$

Note that a tensor product of vectors $\underline{\boldsymbol{a}} \otimes \underline{\boldsymbol{b}}$ is an ordered combination of two vectors called *diads*:

$$\underline{\boldsymbol{a}} \otimes \underline{\boldsymbol{b}} \neq \underline{\boldsymbol{b}} \otimes \underline{\boldsymbol{a}}.$$

The maximum number of independent diads forming the tensor is equal to the dimension of the space n. For diads we require that:

$$\alpha(\,\underline{\boldsymbol{a}} \otimes \underline{\boldsymbol{b}}\,) = (\alpha \underline{\boldsymbol{a}}\,) \otimes \underline{\boldsymbol{b}} = \underline{\boldsymbol{a}} \otimes (\alpha \underline{\boldsymbol{b}}\,) = \alpha \underline{\boldsymbol{a}} \otimes \underline{\boldsymbol{b}}$$

Following this axiom, a *zero diad* is determined if α is put to zero:

$$0\underline{\boldsymbol{a}} \otimes \underline{\boldsymbol{b}} = \underline{\boldsymbol{0}} \otimes \underline{\boldsymbol{b}} = \underline{\boldsymbol{a}} \otimes \underline{\boldsymbol{0}}$$

$$(\alpha + \beta)\underline{\boldsymbol{a}} \otimes \underline{\boldsymbol{b}} = \alpha \underline{\boldsymbol{a}} \otimes \underline{\boldsymbol{b}} + \beta \underline{\boldsymbol{a}} \otimes \underline{\boldsymbol{b}}$$

If $\alpha = 1, \beta = 0$, then

$$(1 + 0)\underline{\boldsymbol{a}} \otimes \underline{\boldsymbol{b}} = \underline{\boldsymbol{a}} \otimes \underline{\boldsymbol{b}} + \underline{\boldsymbol{0}} \otimes \underline{\boldsymbol{b}} = \underline{\boldsymbol{a}} \otimes \underline{\boldsymbol{b}}$$

So a zero diad is a zero element of the diad space and can be denoted by 0.

$$\underline{\boldsymbol{a}} \otimes (\underline{\boldsymbol{b}} + \underline{\boldsymbol{c}}) = \underline{\boldsymbol{a}} \otimes \underline{\boldsymbol{b}} + \underline{\boldsymbol{a}} \otimes \underline{\boldsymbol{c}}$$

$$(\underline{\boldsymbol{a}} + \underline{\boldsymbol{b}}) \otimes \underline{\boldsymbol{c}} = \underline{\boldsymbol{a}} \otimes \underline{\boldsymbol{c}} + \underline{\boldsymbol{b}} \otimes \underline{\boldsymbol{c}}$$

The formal sums of diads $\oplus$ will be replaced by usual symbol $+$, which should be understood as a sign of union like in complex numbers $x + \mathrm{i}y$.

– *Composition/union of tensors*

The sum of diads is not ordered and any their combination defines the same tensor

$$\begin{aligned} \underline{\underline{\boldsymbol{A}}} &= \underline{\boldsymbol{a}} \otimes \underline{\boldsymbol{b}} + \underline{\boldsymbol{c}} \otimes \underline{\boldsymbol{d}} + \cdots + \underline{\boldsymbol{e}} \otimes \underline{\boldsymbol{f}} = \\ &= \underline{\boldsymbol{c}} \otimes \underline{\boldsymbol{d}} + \underline{\boldsymbol{a}} \otimes \underline{\boldsymbol{b}} + \cdots + \underline{\boldsymbol{e}} \otimes \underline{\boldsymbol{f}} = \\ &= \cdots = \underline{\boldsymbol{c}} \otimes \underline{\boldsymbol{d}} + \underline{\boldsymbol{e}} \otimes \underline{\boldsymbol{f}} + \cdots + \underline{\boldsymbol{a}} \otimes \underline{\boldsymbol{b}} \end{aligned} \qquad [A1.3]$$

The product with a scalar results in:

$$\alpha \underline{\underline{\boldsymbol{A}}} = (\alpha \underline{\boldsymbol{a}}) \otimes \underline{\boldsymbol{b}} + (\alpha \underline{\boldsymbol{c}}) \otimes \underline{\boldsymbol{d}} + \cdots + (\alpha \underline{\boldsymbol{e}}) \otimes \underline{\boldsymbol{f}}$$

$$(\alpha + \beta)\underline{\underline{\boldsymbol{A}}} = \alpha \underline{\underline{\boldsymbol{A}}} + \beta \underline{\underline{\boldsymbol{A}}}$$

Composition, sum or union of tensors is a tensor from the same space:

$$\underline{\underline{\boldsymbol{A}}} + \underline{\underline{\boldsymbol{B}}} = \underline{\underline{\boldsymbol{C}}}$$

As it can be easily shown, tensors are invariant objects, i.e. they do not depend on the choice of basis. The second-order tensor space is shown to be linear.

– *Coordinates of tensors*

In coordinate form, any second-order tensor for a given basis and a dual basis can be written in four ways:

$$\underline{\underline{\boldsymbol{A}}} = A^{*j}_{i*} \underline{\boldsymbol{e}}^i \otimes \underline{\boldsymbol{e}}_j = A^{i*}_{*j} \underline{\boldsymbol{e}}_i \otimes \underline{\boldsymbol{e}}^j = A_{ij} \underline{\boldsymbol{e}}^i \otimes caj = A^{ij} \underline{\boldsymbol{e}}_i \otimes \underline{\boldsymbol{e}}_j$$

To avoid any confusions of components' order, the use of stars is mandatory for mixed coordinates (co-covariant and co-contravariant), the same for higher order tensors:

$$^3\underline{\underline{\boldsymbol{A}}} = A^{*j*}_{i*k} \underline{\boldsymbol{e}}^i \otimes \underline{\boldsymbol{e}}_j \otimes \underline{\boldsymbol{e}}^k$$

By analogy with the s-structure formalism, in the basis $\underset{\sim}{\underline{\boldsymbol{e}}}$ and its dual $\underset{\sim}{\underline{\bar{\boldsymbol{e}}}}$, a tensor can be written also in four ways:

$$\underline{\underline{\boldsymbol{B}}} = \underset{\approx}{\bar{\bar{\mathrm{B}}}} \circ\circ \underline{\underline{\underset{\sim}{\boldsymbol{E}}}} = \underset{\approx}{\mathrm{B}} \circ\circ \underline{\underline{\underset{\sim}{\bar{\boldsymbol{E}}}}} = \underset{\approx}{\bar{\mathrm{B}}} \circ\circ \underline{\underline{\underset{\sim}{\bar{\boldsymbol{E}}}}} = \underset{\approx}{\bar{\mathrm{B}}}^{\mathsf{T}} \circ\circ \underline{\underline{\underset{\sim}{\bar{\boldsymbol{E}}}}}$$

where t-tensor $\underline{\underline{\underset{\sim}{\boldsymbol{E}}}}$ contains tensor product of basis vectors and t-scalar $\underset{\approx}{\mathrm{B}}$ contains coordinates of tensor in this basis:

$$\underline{\underline{\underset{\sim}{\boldsymbol{E}}}} = \underset{\sim}{\boldsymbol{e}} \otimes \underset{\sim}{\boldsymbol{e}};\ \ \underline{\underline{\underset{\sim}{\bar{\boldsymbol{E}}}}} = \underset{\sim}{\bar{\boldsymbol{e}}} \otimes \underset{\sim}{\bar{\boldsymbol{e}}};\ \ \underline{\underline{\underset{\sim}{\bar{\boldsymbol{E}}}}} = \underset{\sim}{\boldsymbol{e}} \otimes \underset{\sim}{\bar{\boldsymbol{e}}}\ \ \ \underline{\underline{\underset{\sim}{\bar{\boldsymbol{E}}}}}^{\mathsf{T}} = \underset{\sim}{\bar{\boldsymbol{e}}} \otimes \underset{\sim}{\boldsymbol{e}}$$

All possible coordinates of tensors are connected by the fundamental metric matrices $\underset{\approx}{\mathrm{A}}$ and $\underset{\approx}{\bar{\mathrm{A}}}$. To avoid any confusion, in a component form, these matrices will be put in square bracket $[A_{ij}],\ [A^{ij}]$:

$$B^{ij} = [A^{ik}] B^{*j}_{k*} = [A^{jk}] B^{i*}_{*k} = [A^{ik}][A^{jl}] B_{kl}$$

The change of basis is defined as the pushforward and the pullback transformations:

$$\underset{\sim}{\underline{\boldsymbol{e}}}' = \underset{\approx}{\mathrm{P}}\,\underset{\sim}{\underline{\boldsymbol{e}}}; \qquad \underset{\sim}{\bar{\underline{\boldsymbol{e}}}}' = \underset{\approx}{\mathrm{P}}'\,\underset{\sim}{\bar{\underline{\boldsymbol{e}}}}$$

in component form:

$$\underline{\boldsymbol{e}}_{i'} = [P^{j}_{i'}]\underline{\boldsymbol{e}}_{j}; \qquad \underline{\boldsymbol{e}}^{i'} = [P^{i'}_{j}]\underline{\boldsymbol{e}}^{j},$$

square brackets imply that components $[P^{j}_{i'}]$ do not represent tensors. Using the transformation matrices, the coordinates of tensors can be defined in the new basis $\underset{\sim}{\underline{\boldsymbol{e}}}'$ or its dual $\underset{\sim}{\bar{\underline{\boldsymbol{e}}}}'$, if coordinates in the basis $\underset{\sim}{\underline{\boldsymbol{e}}}$ or $\underset{\sim}{\bar{\underline{\boldsymbol{e}}}}$ are known.

$$\underline{\underline{\boldsymbol{B}}} = B^{i'j'}\,\underline{\boldsymbol{e}}_{i'} \otimes \underline{\boldsymbol{e}}_{j'} = B^{kl}\underline{\boldsymbol{e}}_{k} \otimes \underline{\boldsymbol{e}}_{l} = B^{kl}[P^{i'}_{k}][P^{j'}_{l}]\underline{\boldsymbol{e}}_{i'} \otimes \underline{\boldsymbol{e}}_{j'}$$

So the four pushforward transformation formulas for tensor coordinates are:

$$B^{i'j'} = [P^{i'}_{k}]\; B^{kl}\; [P^{i'}_{l}]; \qquad B_{i'j'} = [P^{k}_{i'}]\; B_{kl}\; [P^{l}_{j'}]$$

$$B^{i'*}_{*j'} = [P^{i'}_{k}]\; B^{*l}_{k*}\; [P^{l}_{j'}]; \qquad B^{*j'}_{i'*} = [P^{k}_{i'}]\; B^{k*}_{*l}\; [P^{j'}_{l}]$$

The pullback transformations can be obtained by the simple substitution of indices without prime by indices with prime and vice versa. In s-structure notations, this set of transformations can be written as follows:

$$\underset{\approx}{\bar{\bar{\mathrm{B}}}}' = \underset{\approx}{\mathrm{P}}' \circ \underset{\approx}{\bar{\bar{\mathrm{B}}}} \circ \underset{\approx}{\mathrm{P}}'^{\mathsf{T}}; \quad \underset{\approx}{\mathrm{B}}' = \underset{\approx}{\mathrm{P}} \circ \underset{\approx}{\mathrm{B}} \circ \underset{\approx}{\mathrm{P}}^{\mathsf{T}};$$

$$\underset{\approx}{\bar{\mathrm{B}}}' = \underset{\approx}{\mathrm{P}} \circ \underset{\approx}{\bar{\mathrm{B}}} \circ \underset{\approx}{\mathrm{P}}'^{\mathsf{T}}; \quad \underset{\approx}{\bar{\mathrm{B}}}^{T\prime} = \underset{\approx}{\mathrm{P}} \circ \underset{\approx}{\bar{\bar{\mathrm{B}}}}^{\mathsf{T}} \circ \underset{\approx}{\mathrm{P}}'^{\mathsf{T}}$$

– *Transposition*

Let $\underline{\underline{\boldsymbol{A}}} = \sum_{i} \underline{\underline{\boldsymbol{D}}}_{i}$, where $\underline{\underline{\boldsymbol{D}}}_{i}$ are diads. The transposition for diads $\underline{\underline{\boldsymbol{D}}} = \underline{\boldsymbol{a}} \otimes \underline{\boldsymbol{b}}$ is defined as follows:

$$\underline{\underline{\boldsymbol{D}}}^{\mathsf{T}} = (\underline{\boldsymbol{a}} \otimes \underline{\boldsymbol{b}})^{\mathsf{T}} = \underline{\boldsymbol{b}} \otimes \underline{\boldsymbol{a}}$$

Transposition of tensor:

$$\underline{\underline{\boldsymbol{A}}}^{\mathsf{T}} = \sum_{i} \underline{\underline{\boldsymbol{D}}}^{\mathsf{T}}_{i}; \quad A^{*j\,\mathsf{T}}_{i*} = A^{j*}_{*i}, \quad A^{\mathsf{T}}_{ij} = A_{ji}, \ \ldots$$

A tensor is called *symmetric* if:

$$\underline{\underline{\boldsymbol{A}}}^{\intercal} = \underline{\underline{\boldsymbol{A}}}$$

A tensor is called *antisymmetric* if:

$$\underline{\underline{\boldsymbol{A}}}^{\intercal} = -\underline{\underline{\boldsymbol{A}}}$$

Any tensor can be split into a sum of symmetric and antisymmetric tensors:

$$\underline{\underline{\boldsymbol{B}}} = \underline{\underline{\boldsymbol{B}}}^{S} + \underline{\underline{\boldsymbol{B}}}^{A}, \quad \underline{\underline{\boldsymbol{B}}}^{\intercal} = \underline{\underline{\boldsymbol{B}}}^{S} - \underline{\underline{\boldsymbol{B}}}^{A}$$

so the symmetric and antisymmetric parts of a tensor are defined as follows:

$$\underline{\underline{\boldsymbol{B}}}^{S} = \frac{1}{2}\left(\underline{\underline{\boldsymbol{B}}} + \underline{\underline{\boldsymbol{B}}}^{\intercal}\right), \quad \underline{\underline{\boldsymbol{B}}}^{A} = \frac{1}{2}\left(\underline{\underline{\boldsymbol{B}}} - \underline{\underline{\boldsymbol{B}}}^{\intercal}\right)$$

The inverse and transposed second-order tensor often denoted as

$$\underline{\underline{\boldsymbol{A}}}^{-T}$$

– *Dot product*

- The inner product (contraction) of second-order tensors gives a second-order tensor:

$$\{\cdot\} : \mathbb{T}_2^n \times \mathbb{T}_2^n \to \mathbb{T}_2^n$$

$$\underline{\underline{\boldsymbol{A}}} = \underline{\underline{\boldsymbol{B}}} \cdot \underline{\underline{\boldsymbol{C}}} = (\underline{\underline{\boldsymbol{C}}}^{\intercal} \cdot \underline{\underline{\boldsymbol{B}}}^{\intercal})^{\intercal}; \quad A^{*j}_{i*} = B^{*k}_{i*} C^{*j}_{k*}$$

- The double inner product (double contraction) of second-order tensors gives a scalar:

$$\{:\} : \mathbb{T}_2^n \times \mathbb{T}_2^n \to \mathbb{R}$$

$$\underline{\underline{\boldsymbol{A}}} : \underline{\underline{\boldsymbol{B}}} = \underline{\underline{\boldsymbol{B}}} : \underline{\underline{\boldsymbol{A}}} = \alpha; \quad A^{*j}_{i*} B^{i*}_{*j} = \alpha$$

- The double scalar product of second-order tensors gives a scalar (in general different from the double inner product):

$$\{\cdot\cdot\} : \mathbb{T}_2^n \times \mathbb{T}_2^n \to \mathbb{R}$$

$$\underline{\underline{\boldsymbol{A}}} \cdot\cdot \underline{\underline{\boldsymbol{B}}} = \underline{\underline{\boldsymbol{A}}} : \underline{\underline{\boldsymbol{B}}}^{\intercal} = \underline{\underline{\boldsymbol{B}}} \cdot\cdot \underline{\underline{\boldsymbol{A}}}^{\intercal} = \alpha; \quad A^j_i B^j_i = B^i_j A^i_j = \alpha$$

The difference between the double inner product and the double scalar product consists of the following: if $\underline{\underline{\boldsymbol{A}}} \cdot\cdot \underline{\underline{\boldsymbol{A}}} = 0$, then $\underline{\underline{\boldsymbol{A}}} = 0$. For double inner product, the equality $\underline{\underline{\boldsymbol{A}}} : \underline{\underline{\boldsymbol{A}}}^{\mathsf{T}} = 0$ does not mean that $\underline{\underline{\boldsymbol{A}}} = 0$. By definition, the double inner product and the double scalar product coincide if at least one of the tensors (in operation) is symmetric. A general rule for the scalar product of qth order is:

$$\mathbb{T}^n_m \underbrace{\cdot \cdots \cdot}_{\text{q times}} \mathbb{T}^n_l \to \mathbb{T}^n_{l+m-2q}.$$

It is obvious that $l + m \geq 2q$ as well as $l \geq q$ and $m \geq q$.

– *Operations with vectors*

- Left and right scalar products of a vector and second-order tensor are defined as:

$$\{\cdot\} : \mathbb{T}^n_2 \times \mathbb{T}_1{}^n \to \mathbb{T}_1{}^n; \quad \{\cdot\} : \mathbb{T}_1{}^n \times \mathbb{T}^n_2 \to \mathbb{T}_1{}^n$$

$$\underline{\boldsymbol{a}} \cdot \underline{\underline{\boldsymbol{B}}} = \underline{\boldsymbol{c}} \neq \underline{\boldsymbol{d}} = \underline{\underline{\boldsymbol{B}}} \cdot \underline{\boldsymbol{a}}; \quad c^j = a^i B^{j*}_{i*} \neq d^j = B^{*i}_{j*} a_i$$

$$\underline{\boldsymbol{a}} \cdot \underline{\underline{\boldsymbol{B}}} = \underline{\underline{\boldsymbol{B}}}^{\mathsf{T}} \cdot \underline{\boldsymbol{a}}$$

- Left and right vector products of a vector and second-order tensor are defined in 3D space:

$$\{\times\} : \mathbb{T}_2 \times \mathbb{T}_1 \to \mathbb{T}_2; \quad \{\times\} : \mathbb{T}_1 \times \mathbb{T}_2 \to \mathbb{T}_2$$

$$\underline{\boldsymbol{a}} \times \underline{\underline{\boldsymbol{B}}} = \underline{\underline{\boldsymbol{C}}} \neq \underline{\underline{\boldsymbol{D}}} = \underline{\underline{\boldsymbol{B}}} \times \underline{\boldsymbol{a}}$$

$$\underline{\boldsymbol{a}} \times \underline{\underline{\boldsymbol{B}}} = -\left(\underline{\underline{\boldsymbol{B}}}^{\mathsf{T}} \times \underline{\boldsymbol{a}}\right)^{\mathsf{T}}$$

- If the space of third-order tensors is defined $\mathbb{T}^n_3 = \mathbb{T}_1{}^n \otimes \mathbb{T}_1{}^n \otimes \mathbb{T}_1{}^n$, then left and right tensor products of a vector and a second-order tensor are defined by:

$$\{\otimes\} : \mathbb{T}^n_2 \times \mathbb{T}_1{}^n \to \mathbb{T}^n_3; \quad \{\otimes\} : \mathbb{T}_1{}^n \times \mathbb{T}^n_2 \to \mathbb{T}^n_3$$

$$\underline{\underline{\boldsymbol{B}}} \otimes \underline{\boldsymbol{a}} = {}^3\underline{\underline{\boldsymbol{C}}} \neq {}^3\underline{\underline{\boldsymbol{D}}} = \underline{\boldsymbol{a}} \otimes \underline{\underline{\boldsymbol{B}}}; \quad C^{*j*}_{i*k} = B^{*j}_{i*} a_k$$

– *Trace of a second-order tensor: scalar and vector invariants*

- *Trace* "tr", or the first invariant of a tensor, is a quantity that is important for mechanics; it also may be denoted as I or I_1. If a second-order tensor is written as a sum of diads $\underline{\underline{\boldsymbol{A}}} = \underline{\boldsymbol{a}} \otimes \underline{\boldsymbol{b}} + \cdots + \underline{\boldsymbol{c}} \otimes \underline{\boldsymbol{d}}$, then:

$$I(\underline{\underline{\boldsymbol{A}}}) = \mathrm{tr}\underline{\underline{\boldsymbol{A}}} = \underline{\boldsymbol{a}} \cdot \underline{\boldsymbol{b}} + \cdots + \underline{\boldsymbol{c}} \cdot \underline{\boldsymbol{d}}; \quad I(A^{j*}_{*i}) = A^{i*}_{*i}$$

$$\mathrm{tr}\left(\underline{\underline{\boldsymbol{A}}} + \underline{\underline{\boldsymbol{B}}}\right) = \mathrm{tr}\underline{\underline{\boldsymbol{A}}} + \mathrm{tr}\underline{\underline{\boldsymbol{B}}}$$

$$\mathrm{tr}\underline{\underline{\boldsymbol{A}}} = \mathrm{tr}\underline{\underline{\boldsymbol{A}}}^{\mathsf{T}}$$

$$\mathrm{tr}(\underline{\underline{\boldsymbol{A}}} \cdot \underline{\underline{\boldsymbol{B}}}) = \mathrm{tr}(\underline{\underline{\boldsymbol{B}}} \cdot \underline{\underline{\boldsymbol{A}}}) = \underline{\underline{\boldsymbol{A}}} : \underline{\underline{\boldsymbol{B}}}$$

$$\mathrm{tr}(\underline{\underline{\boldsymbol{A}}} \cdot \underline{\underline{\boldsymbol{B}}}) = \mathrm{tr}(\underline{\underline{\boldsymbol{A}}}^{\mathsf{T}} \cdot \underline{\underline{\boldsymbol{B}}}^{\mathsf{T}})$$

$$\mathrm{tr}\underline{\underline{\boldsymbol{B}}} = \mathrm{tr}\underline{\underline{\boldsymbol{B}}}^{S}, \quad \mathrm{tr}\underline{\underline{\boldsymbol{B}}}^{A} = 0$$

$$\mathrm{tr}\left(\underline{\underline{\boldsymbol{B}}} \cdot \underline{\underline{\boldsymbol{C}}}^{S}\right) = \mathrm{tr}\left(\underline{\underline{\boldsymbol{B}}}^{S} \cdot \underline{\underline{\boldsymbol{C}}}^{S}\right)$$

- A *vector invariant* of any second-order tensor $\underline{\underline{\boldsymbol{B}}} = \underline{\boldsymbol{a}} \otimes \underline{\boldsymbol{b}} + \cdots + \underline{\boldsymbol{c}} \otimes \underline{\boldsymbol{d}} \in \mathbb{T}$ is a vector $\underline{\underline{\boldsymbol{B}}}_{\times}$ such that:

$$\underline{\underline{\boldsymbol{B}}}_{\times} = \underline{\boldsymbol{a}} \times \underline{\boldsymbol{b}} + \cdots + \underline{\boldsymbol{c}} \times \underline{\boldsymbol{d}}; \quad B^{i}_{\times} = B^{i*}_{*j}\underline{\boldsymbol{e}}_i \times \underline{\boldsymbol{e}}^j$$

$$(\underline{\underline{\boldsymbol{A}}} + \underline{\underline{\boldsymbol{B}}})_{\times} = \underline{\underline{\boldsymbol{A}}}_{\times} + \underline{\underline{\boldsymbol{B}}}_{\times}$$

$$\underline{\underline{\boldsymbol{B}}}_{\times} = 0 \Leftrightarrow \underline{\underline{\boldsymbol{B}}} = \underline{\underline{\boldsymbol{B}}}^{S}$$

Any antisymmetric tensor can be written as:

$$\underline{\underline{\boldsymbol{B}}}^{A} = \underline{\boldsymbol{\omega}} \times \underline{\underline{\boldsymbol{I}}} = \underline{\underline{\boldsymbol{I}}} \times \underline{\boldsymbol{\omega}}, \quad \underline{\boldsymbol{\omega}} = -\frac{1}{2}\underline{\underline{\boldsymbol{B}}}^{A}_{\times}$$

- Note the following useful formulas:

$$\underline{\boldsymbol{a}} \times \underline{\underline{\boldsymbol{I}}} \times \underline{\boldsymbol{b}} = \underline{\boldsymbol{b}} \times \underline{\boldsymbol{a}} - (\underline{\boldsymbol{a}} \cdot \underline{\boldsymbol{b}})\underline{\underline{\boldsymbol{I}}}$$

$$\left(\underline{\boldsymbol{a}} \times \underline{\underline{\boldsymbol{I}}}\right)_{\times} = -2\underline{\boldsymbol{a}}$$

$$\underline{\boldsymbol{a}} \times \underline{\boldsymbol{b}} = (\underline{\boldsymbol{a}} \times \underline{\underline{\boldsymbol{I}}}) \cdot \underline{\boldsymbol{b}}$$

$$\underline{\boldsymbol{a}} \times \underline{\underline{\boldsymbol{I}}} = \underline{\underline{\boldsymbol{I}}} \times \underline{\boldsymbol{a}}$$

– *Invariants of second-order tensors*

Besides the trace or first invariant I_1, two other invariants can be defined for the second-order tensors. These three invariants are called principal invariants of the tensor:

$$I_1 = \mathrm{tr}\underline{\underline{\boldsymbol{A}}}$$

$$I_2 = \frac{1}{2}\left[\,[\mathrm{tr}\underline{\underline{\boldsymbol{A}}}]^2 - \mathrm{tr}[\underline{\underline{\boldsymbol{A}}}^2]\,\right]$$

$$I_3 = \det \underline{\underline{\boldsymbol{A}}} = \frac{1}{6}(\mathrm{tr}\underline{\underline{\boldsymbol{A}}})^3 - \frac{1}{2}\mathrm{tr}\underline{\underline{\boldsymbol{A}}}\mathrm{tr}(\underline{\underline{\boldsymbol{A}}}^2) + \frac{1}{3}\mathrm{tr}(\underline{\underline{\boldsymbol{A}}}^3)$$

The determinant of a tensor will be introduced later in section A1.5.

– *Unit second-order tensor*

The unit second-order tensor (denoted $\underline{\underline{\boldsymbol{I}}}$) such that:

$$\underline{\boldsymbol{a}} = \underline{\underline{\boldsymbol{I}}} \cdot \underline{\boldsymbol{a}} = \underline{\boldsymbol{a}} \cdot \underline{\underline{\boldsymbol{I}}}; \quad I_i^j = \delta_i^j; \;\; a_i = \delta_i^j a_j$$

consequently

$$\underline{\underline{\boldsymbol{A}}} = \underline{\underline{\boldsymbol{I}}} \cdot \underline{\underline{\boldsymbol{A}}} = \underline{\underline{\boldsymbol{A}}} \cdot \underline{\underline{\boldsymbol{I}}}$$

The unit second-order tensor in any basis may be written as:

$$\underline{\underline{\boldsymbol{I}}} = \underset{\sim}{\boldsymbol{e}} \cdot \otimes \underset{\sim}{\bar{\boldsymbol{e}}} = \underset{\sim}{\bar{\boldsymbol{e}}} \cdot \otimes \underset{\sim}{\boldsymbol{e}} = \underline{\boldsymbol{e}}_i \otimes \underline{\boldsymbol{e}}^i = \underline{\boldsymbol{e}}^i \otimes \underline{\boldsymbol{e}}_i$$

– *Projection tensors*

A tensor $\underline{\underline{\boldsymbol{P}}}$ is called a projection if:

$$\underline{\underline{\boldsymbol{P}}} = \underline{\underline{\boldsymbol{P}}}^{\mathsf{T}}, \;\; \underline{\underline{\boldsymbol{P}}} \cdot \underline{\underline{\boldsymbol{P}}} = \underline{\underline{\boldsymbol{P}}}$$

For example,

$$\underline{\boldsymbol{n}} \otimes \underline{\boldsymbol{n}}$$

projects any vector on the direction $\underline{\boldsymbol{n}}$; and tensor:

$$\underline{\underline{\boldsymbol{I}}} - \underline{\boldsymbol{n}} \otimes \underline{\boldsymbol{n}}$$

projects any vector on the space orthogonal to the vector $\underline{\boldsymbol{n}}$.

– *Spherical and deviatoric tensors*

A tensor $\underline{\underline{\boldsymbol{B}}}$ is called *spherical* if it can be written as:

$$\underline{\underline{\boldsymbol{B}}} = \alpha \underline{\underline{\boldsymbol{I}}}, \ \alpha \in \mathbb{R}$$

The *spherical part* of n-dimensional tensor $\underline{\underline{\boldsymbol{C}}}$ is by definition:

$$\frac{1}{n} \mathrm{tr} \underline{\underline{\boldsymbol{C}}} \, \underline{\underline{\boldsymbol{I}}} = \frac{1}{n} \mathrm{tr} \underline{\underline{\boldsymbol{C}}}^S \, \underline{\underline{\boldsymbol{I}}}$$

Any symmetric tensor $\underline{\underline{\boldsymbol{C}}} = \underline{\underline{\boldsymbol{C}}}^\intercal$ for which $\mathrm{tr}\underline{\underline{\boldsymbol{C}}} = 0$ is called *deviatoric tensor*. Note that for $\underline{\underline{\boldsymbol{C}}}^\intercal = -\underline{\underline{\boldsymbol{C}}} \ \Rightarrow \ \mathrm{tr}\underline{\underline{\boldsymbol{C}}} = 0$, but the inverse statement is not true. Any symmetric tensor $\underline{\underline{\boldsymbol{B}}} = \underline{\underline{\boldsymbol{B}}}^\intercal$ can be written as the sum of its spherical part and its deviatoric part:

$$\underline{\underline{\boldsymbol{B}}} = \frac{1}{n} \mathrm{tr} \underline{\underline{\boldsymbol{B}}} \, \underline{\underline{\boldsymbol{I}}} + \underline{\underline{\boldsymbol{B}}}^d$$

Any tensor $\underline{\underline{\boldsymbol{B}}} = \underline{\underline{\boldsymbol{B}}}^S + \underline{\underline{\boldsymbol{B}}}^A$ can be split into spherical and deviatoric part plus its antisymmetric part:

$$\underline{\underline{\boldsymbol{B}}} = \frac{1}{n} \mathrm{tr} \underline{\underline{\boldsymbol{B}}} \, \underline{\underline{\boldsymbol{I}}} + \underline{\underline{\boldsymbol{B}}}^d + \underline{\underline{\boldsymbol{B}}}^A$$

In most mechanical and physical theories, $n = 3$.

A1.5. Tensor as a linear operator on vector space

It can be shown that any linear vector operator on vector space, i.e. an operator which transforms one vector into another:

$$\underline{\boldsymbol{f}} : \mathbb{T}_1 \to \mathbb{T}_1 \qquad \underline{\boldsymbol{y}} = \underline{\boldsymbol{f}}(\underline{\boldsymbol{x}})$$

can be written as a right scalar product of a second-order tensor with the argument:

$$\underline{\boldsymbol{y}} = \underline{\underline{\boldsymbol{B}}} \cdot \underline{\boldsymbol{x}}$$

By definition, tensors fulfill the requirements of linearity:

$$\underline{\underline{\boldsymbol{B}}} \cdot (\alpha \underline{\boldsymbol{a}} + \beta \underline{\boldsymbol{b}}) = \alpha \underline{\underline{\boldsymbol{B}}} \cdot \underline{\boldsymbol{a}} + \beta \underline{\underline{\boldsymbol{B}}} \cdot \underline{\boldsymbol{b}}$$

Let us write the conditions for an operator to be isomorphic, i.e. that it transforms uniquely the space $\mathbb{T}_1$ in itself and that a unique inverse transformation exists. For an arbitrary tensor operator $\underline{\underline{\boldsymbol{B}}} \in \mathbb{T}_2$, the kernel is all vector space, but the image is, rigorously, a subset of this space

$$\mathrm{Im}\underline{\underline{\boldsymbol{B}}} = \mathbb{T}_1, \quad \mathrm{Ker}\underline{\underline{\boldsymbol{B}}} \subset \mathbb{T}_1$$

Let us derive the condition $\mathrm{Ker}\underline{\underline{\boldsymbol{B}}} = \mathbb{T}_1$. If $\underline{\underline{\boldsymbol{B}}}$ transforms three linearly independent vectors into three independent vectors, then $\mathrm{Ker}\underline{\underline{\boldsymbol{B}}} = \mathbb{T}_1$. Let us consider three linearly independent vectors $\underline{\boldsymbol{a}}$, $\underline{\boldsymbol{b}}$, $\underline{\boldsymbol{c}}$, they are independent if and only if:

$$(\underline{\boldsymbol{a}} \times \underline{\boldsymbol{b}}) \cdot \underline{\boldsymbol{c}} \neq 0$$

Their images:

$$\underline{\boldsymbol{a}}' = \underline{\underline{\boldsymbol{B}}} \cdot \underline{\boldsymbol{a}}, \quad \underline{\boldsymbol{b}}' = \underline{\underline{\boldsymbol{B}}} \cdot \underline{\boldsymbol{b}}, \quad \underline{\boldsymbol{c}}' = \underline{\underline{\boldsymbol{B}}} \cdot \underline{\boldsymbol{c}}$$

are linearly independent if and only if

$$(\underline{\boldsymbol{a}}' \times \underline{\boldsymbol{b}}') \cdot \underline{\boldsymbol{c}}' \neq 0$$

The *determinant of the tensor* $\det \underline{\underline{\boldsymbol{B}}}$ is introduced as follows:

$$\det \underline{\underline{\boldsymbol{B}}} = \frac{(\underline{\boldsymbol{a}}' \times \underline{\boldsymbol{b}}') \cdot \underline{\boldsymbol{c}}'}{(\underline{\boldsymbol{a}} \times \underline{\boldsymbol{b}}) \cdot \underline{\boldsymbol{c}}} \qquad \text{[A1.4]}$$

Such a definition of the determinant makes it invariant, i.e. independent of the choice of the basis. It is easy to show that:

$$\det \underline{\underline{\boldsymbol{B}}} = \det[\underline{\underline{\mathrm{A}}}] \det[\bar{\underline{\underline{\mathrm{B}}}}] = \frac{1}{\det[\underline{\underline{\mathrm{A}}}]} \det[\underline{\underline{\mathrm{B}}}] = \det[\bar{\underline{\underline{\mathrm{B}}}}] = \det[\bar{\underline{\underline{\mathrm{B}}}}^{\mathsf{T}}]$$

$$\det \underline{\underline{\boldsymbol{B}}} = \det[A_{ij}] \det B^{ij} = \frac{1}{\det[A_{ij}]} \det B_{ij} = \det B^{i*}_{*j} = \det B^{*i}_{j*},$$

where $\underset{\approx}{\mathrm{A}}$ or $[A_{ij}]$ is the covariant fundamental metric matrix and

$$\underset{\approx}{\bar{\bar{\mathrm{B}}}}, B^{ij}; \quad \underset{\approx}{\bar{\mathrm{B}}}, B^{i*}_{*j}; \quad \underset{\approx}{\bar{\mathrm{B}}}^{\mathsf{T}}, B^{*i}_{j*}; \quad \underset{\approx}{\mathrm{B}}, B_{ij}$$

are the contravariant, contra-covariant, co-contravariant and covariant coordinates of the tensor $\underline{\underline{\boldsymbol{B}}}$.

It is worth noting that a tensor cannot be defined as the set of the matrix of its covariant or contravariant coordinates and the associated transformation rule:

$$B^{i'j'} = [P^{i'}_{k}]\, B^{kl}\, [P^{i'}_{l}]; \qquad B_{i'j'} = [P^{k}_{i'}]\, B_{kl}\, [P^{l}_{j'}]$$

because the determinant of these matrices changes with a basis change:

$$\det B^{i'j'} = \det[P^{i'}_{k}]^2 \det B^{kl},$$

since $\det[P^{i'}_{k}]^2 \neq 1$

$$\det B^{i'j'} \neq \det B^{kl}$$

A tensor is an invariant object and its determinant $\det \underline{\underline{\boldsymbol{B}}}$ should also be invariant. The determinant of a tensor is invariant if it is defined as in [A1.4] or as the determinant of the matrix of co-contravariant or co-covariant coordinates.

It is easy to show that:

$$\det \underset{\approx}{\mathrm{I}} = 1\,; \quad \det \underline{\underline{\boldsymbol{A}}} = \det \underline{\underline{\boldsymbol{A}}}^{\mathsf{T}}\,; \quad \det[\underline{\underline{\boldsymbol{A}}} \cdot \underline{\underline{\boldsymbol{B}}}] = \det \underline{\underline{\boldsymbol{A}}} \det \underline{\underline{\boldsymbol{B}}}$$

Now it is possible to introduce the *inverse tensor* $\underline{\underline{\boldsymbol{B}}}^{-1}$ such that:

$$\underline{\underline{\boldsymbol{B}}}^{-1} \cdot \underline{\underline{\boldsymbol{B}}} = \underline{\underline{\boldsymbol{B}}} \cdot \underline{\underline{\boldsymbol{B}}}^{-1} = \underline{\underline{\boldsymbol{I}}} \;\Rightarrow\; \det \underline{\underline{\boldsymbol{B}}} \det \underline{\underline{\boldsymbol{B}}}^{-1} = 1 \;\Rightarrow\; \det \underline{\underline{\boldsymbol{B}}}^{-1} = \frac{1}{\det \underline{\underline{\boldsymbol{B}}}}$$

The inverse tensor of $\underline{\underline{\boldsymbol{B}}}$ exists if and only if $\det \underline{\underline{\boldsymbol{B}}} \neq 0$.

Similar to the linear vector operator on the space of vectors, a linear tensor operator on the space of tensors can be introduced.

$$\underline{\underline{\boldsymbol{T}}} : \mathbb{T} \to \mathbb{T}$$

Such a linear operator can be interpreted as a fourth-order tensor ${}^{4}\underline{\underline{\boldsymbol{C}}}$. Good examples are the Young–Cauchy elasticity tensor and its inverse are linear bijective operators which state that stress tensor is a linear function of strain tensor and vice versa.

A1.6. S-structures

In practice, in physical and mechanical theories, among widely used "spaces on spaces" there are the following constructions: complex numbers, vectors, tensors of higher orders and matrices. Sometimes there is a need to consider more complex structures, such as: basis (set of vectors), stress–strain state (set of stress and strain tensors), metric matrix (set of scalars), etc. To determine elements of such sets, we make use of indices: $\underline{\boldsymbol{e}}_i$ – ith basis vector, A_{ij} – element of the metric matrix and so on. As practice demonstrates, sometimes it is more convenient to consider such sets not as sets of elements but as "one-piece" elements of "higher" spaces and to work directly with them. To "work" means perform some operations on these elements in order to obtain some results. For example, it seems very natural to determine bases $\underline{\boldsymbol{e}}_i\,,\ \underline{\boldsymbol{e}}^i\,,\ i = 1, m$ as vectors of vectors $\underset{\sim}{\underline{\boldsymbol{e}}}\,, \underset{\sim}{\bar{\underline{\boldsymbol{e}}}}$ and to introduce operations to get the metric matrix not in component form $A_{ij} = \underline{\boldsymbol{e}}_i \cdot \underline{\boldsymbol{e}}_j$, but directly $\underset{\approx}{\mathrm{A}} = \underset{\sim}{\underline{\boldsymbol{e}}} \overset{\boxtimes}{\cdot} \underset{\sim}{\underline{\boldsymbol{e}}}$.

From an abstract mathematical point of view, a space defined on the elements of another space – also called exterior algebra – has been used for long time. A good example, similar to one type of s-structures, is a multivector – element of exterior algebra on a vector space, which consists of linear combinations of k-vectors also called blades: bivectors $\underline{\boldsymbol{a}} \wedge \underline{\boldsymbol{b}}$, trivectors $(\underline{\boldsymbol{a}} \wedge \underline{\boldsymbol{b}}) \wedge \underline{\boldsymbol{c}}$. Operator $\wedge$ is called the wedge operator and somehow is similar in our notations of a tensor product. A generalization of this algebra complemented by relations to exterior algebras is called the Clifford algebra [LOU 01], named after William Kingdon Clifford (1845–1879).

A similar idea of structure of structures appears in programming languages as the "container" class which contain elements of another class. Such a container can be used simply to keep some information. To make better use of such containers, a set of operations should be defined: comparison of element, summation, subtraction, multiplication by scalar, etc. The operation result can be of the same class as the container or of another class. In such a way, the following structures are introduced in

the programming code: complex numbers, vectors, tensors and matrices with related operations. It is also natural for programming languages to use sets of such structures: array of vectors, matrix of tensors, etc. However, to make use of it, a consistent set of operations has to be defined as well as a suitable application.

A considerable part of this book is devoted to the description of surface-point interaction in the framework of classical differential geometry. First, all computations have been performed using index notations. Both points and surfaces are determined in the 3D space $n = 3$, all points $\underline{\boldsymbol{r}}(x^i)$, $i = 1, 2, 3$ are determined by coordinates x^i in 3D basis $\underline{\boldsymbol{e}}_i$. However, a local coordinate system can be established on the surface ξ_α and so it can be parameterized by a vector $\underline{\boldsymbol{\rho}}(\xi_\alpha)$. To avoid any confusion, we are forced to determine new indices $\alpha = 1, 2$. So we have to work with different dimensions: 3D space and two-dimensional (2D) surface. In three dimensions, we use the established formalism of direct tensor language and in two dimensions Greek indices. Why not to say that ξ_1, ξ_2 are covariant coordinates of a 2D vector? In order not to mix up a 3D and 2D vector, the latter will be underlined by a wave $\underset{\sim}{\xi}$.

We are now facing the need to evaluate the full variation of the vector $\underline{\boldsymbol{\rho}}(\underset{\sim}{\xi})$; in index form, it is straightforward:

$$\bar{\delta}\underline{\boldsymbol{\rho}} = \delta\underline{\boldsymbol{\rho}} + \frac{\partial \underline{\boldsymbol{\rho}}}{\partial \xi_\alpha}\delta\xi_\alpha$$

With our new notations of 2D vectors, it is less trivial:

$$\bar{\delta}\underline{\boldsymbol{\rho}} = \delta\underline{\boldsymbol{\rho}} + \frac{\partial \underline{\boldsymbol{\rho}}}{\partial \underset{\sim}{\xi}} \; ? \; \delta\underset{\sim}{\xi}$$

What is the relation between the two last terms? The first component is nothing but a set of two 3D vectors and the second component is a 2D vector; their product should be a 3D vector. So we need to define a product operation between a 2D vector and a set of 3D vectors in a way that it gives a 3D vector. Moreover, this operation should be commutative and the notation should differ from 3D notations. We propose:

$$\underline{\boldsymbol{a}} = \frac{\partial \underline{\boldsymbol{\rho}}}{\partial \underset{\sim}{\xi}} \circ \delta\bar{\underset{\sim}{\xi}} = \delta\bar{\underset{\sim}{\xi}} \circ \frac{\partial \underline{\boldsymbol{\rho}}}{\partial \underset{\sim}{\xi}}$$

It is not so hard to introduce such a product. The situation becomes more complicated when we need to evaluate the surface (induced) metric matrix:

$$A_{\alpha\beta} = \frac{\partial \underline{\boldsymbol{\rho}}}{\partial \xi_\alpha} \cdot \frac{\partial \underline{\boldsymbol{\rho}}}{\partial \xi_\beta}$$

In new notations, we get:

$$\frac{\partial \underline{\underline{\boldsymbol{\rho}}}}{\partial \underset{\sim}{\xi}} \, ? \, \frac{\partial \underline{\underline{\boldsymbol{\rho}}}}{\partial \underset{\sim}{\xi}} =?$$

On the left-hand side of the latter expression, we have an operation between a pair of sets of two 3D vectors. The right-hand side should be a 2×2 symmetric matrix $A_{\alpha\beta}$. In the vector space, there is only one operation which converts two vectors into a scalar: the dot product, so the left-hand part should contain a 3D dot product. On the other hand, the two structures on the left-hand side can be considered as 2D vectors. In a vector space, there is only one operation which converts two vectors into a higher order tensor – the tensor product. Finally, it can be seen that between structures on the left-hand side we have to get two operations, respectively, to 2D and 3D vectors and in the right part a kind of 2D tensor. By analogy with 3D notations, 2D tensors will be underlined by two waves. The s-tensor product "$\boxtimes$" for 2D structure is combined with the dot product "$\cdot$" for 3D structures, so finally we obtain the following definition for the induced metric matrix:

$$\frac{\partial \underline{\underline{\boldsymbol{\rho}}}}{\partial \underset{\sim}{\xi}} \underset{\cdot}{\boxtimes} \frac{\partial \underline{\underline{\boldsymbol{\rho}}}}{\partial \underset{\sim}{\xi}} = \underset{\approx}{\mathrm{A}}$$

Here and later, the upper operation (here $\boxtimes$) relates to 2D structure and the lower operation (here $\cdot$) relates to 3D.

The initial attempt to introduce s-structure over 2D and 3D vector spaces was inspired from this example. After some trials to elaborate a more general form of s-structures, we realized that the use of such structures is much more rich both in mathematical and physical senses. Due to the complicated nature of mixed spaces, the setting of a consistent s-structure "language" is not a trivial task. It is not yet fully elaborated, neither fully exploited. Below, we make an attempt to derive a consistent framework for the space of generalized s-structures with related operations. The full formalism of diad-operations, like in $\frac{\partial \underline{\underline{\boldsymbol{\rho}}}}{\partial \underset{\sim}{\xi}} \underset{\cdot}{\boxtimes} \frac{\partial \underline{\underline{\boldsymbol{\rho}}}}{\partial \underset{\sim}{\xi}}$, will be derived as well as its simplified form based on transpose operations, which is valid for several limited cases.

A1.6.1. *Formal definition, notations and types*

The s-structure formalism consists of the introduction of ordered sets of tensors. The "S" in the name refers to "set" or "super" (higher structure). S-structure can be

interpreted as k order "tensor" on the m-dimensional space of l order tensors of dimension n; all s-structures are elements of S-spaces:

$$ {}^{m}_{k}\mathbb{S}^{n}_{l} = \underbrace{{}^{m}_{1}\mathbb{S}^{n}_{l} \bigotimes \cdots \bigotimes {}^{m}_{1}\mathbb{S}^{n}_{l}}_{\text{k times}} $$

The sign $\otimes$ means that elements are ordered; however, contrary to objects of spaces $\mathbb{T}^{n}_{p}$, S-space elements are not mandatorily invariant, i.e. they do not change according to the standard rules with change of the basis, that is why "tensor" is put in quotes. To avoid any confusion, instead of the previously used notation of tensor spaces, a new one will be used for corresponding s-structures $\tilde{\mathbb{T}}^{n}_{p}$. By definition:

$$ {}^{1}_{0}\mathbb{S}^{1}_{0} = \mathbb{R}, \quad {}^{m}_{1}\mathbb{S}^{n}_{0} = \tilde{\mathbb{T}}^{m}_{1}, \quad {}^{1}_{0}\mathbb{S}^{n}_{1} = \mathbb{T}^{n}_{1}, \quad {}^{m}_{2}\mathbb{S}^{1}_{0} = \tilde{\mathbb{T}}^{m}_{2}, \quad {}^{1}_{0}\mathbb{S}^{n}_{2} = \mathbb{T}^{n}_{2} $$

It is worth noting that s-structures are introduced in such a way that:

$$ {}^{n}_{k}\mathbb{S}^{n}_{k} \neq \mathbb{T}^{n}_{k+k}, \quad {}^{n}_{k}\mathbb{S}^{n}_{k} \neq \tilde{\mathbb{T}}^{n}_{k+k} $$

For instance, it is easy to show that ${}^{n}_{1}\mathbb{S}^{n}_{1} \neq \mathbb{T}^{n}_{2}$, if we consider the derivative of the simple vector $\underline{\boldsymbol{r}}(\underset{\sim}{\mathrm{p}})$ over v-scalar of its contravariant coordinates $\underset{\sim}{\mathrm{p}}$ in basis $\underset{\approx}{\bar{\boldsymbol{e}}}$, $m = n$:

$$ \frac{\partial \underline{\boldsymbol{r}}}{\partial \underset{\sim}{\mathrm{p}}} \in {}^{n}_{1}\mathbb{S}^{n}_{1}, \quad {}^{n}_{1}\mathbb{S}^{n}_{1} \neq \mathbb{T}^{n}_{2}, \quad {}^{n}_{1}\mathbb{S}^{n}_{1} \neq \tilde{\mathbb{T}}^{n}_{2}. $$

This expression is neither an ordinary tensor nor an s-tensor, but a v-vector – an element of ${}^{n}_{1}\mathbb{S}^{n}_{1}$ space. Other definitions are possible but they may destroy the invariance of the vectors.

Let us suppose that a zero-order s-structure is equal to a tensor space over which it is constructed:

$$ {}^{m}_{0}\mathbb{S}^{n}_{l} \equiv \mathbb{T}^{n}_{l} $$

Following this equivalence, we could consider an s-space is a super structure over an s-space of zero order.

An s-structure of order k is a generalization of a first order s-structure. It would be convenient to define the space ${}^{m}_{1}\mathbb{S}^{n}_{l}$ and the related operations. Elements of this space, are considered as generalized vectors. They are underlined by a single wave and will be called v-elements or v-tensors, since these "vectors" are defined over a tensor space. However, since the nature of these elements can be different, depending on the order l of the tensor space over which they are constructed, it would be more convenient to distinguish three types of v-tensors (see below). All the newly introduced operations will be similar to vector operations.

– *V-scalars*

V-scalars are elements of a linear space ${}^{m}_{1}\mathbb{S}^{n}_{0} = \tilde{\mathbb{T}}^{m}_{1}$; note that the dimension of the internal space n, as will be shown later, makes sense and has to be retained. V-scalars and all s-structures are defined through a basis in s-space of dimension m. The subspace or tensor space basis (of dimension n) should not be mixed up with the basis in the s-space. Invariance of such s-elements will be discussed later. As the invariance of s-structures is not always ensured, we put a tilde over the notation of this vector space $\tilde{\mathbb{T}}^{m}_{1}$. So it is better to consider these structures as ordered set of scalars or simply as a matrix $1 \times m$. But contrary to matrix algebra, the operation of transposition will not be introduced[2]. If needed, the dimension m will be mentioned as the left top index ${}^{m}\underset{\sim}{\mathrm{b}}$. Even if $m = n$, i.e. vectors and v-scalars are both defined in an n-dimensional space; they remain elements of different spaces $\underset{\sim}{\mathrm{a}} \in \tilde{\mathbb{T}}^{n}_{1}$, $\underline{\boldsymbol{b}} \in \mathbb{T}^{n}_{1}$ and no invariant operations can be defined between them. In such a case, they are considered as vectors of completely different reference frames (see the difference between reference frame and coordinate system in section A1.1). Physically, we would say that v-scalars and vectors are elements of physical spaces associated with different observers. These spaces are different, see Figure A1.1. However, it does not make sense if there is no connection between those two spaces; further we will consider interdependent spaces.

Some examples of v-scalar:

– A vector of dimension m, $\underset{\sim}{\mathrm{b}}$, invariant for any choice of the s-space basis.

– A set of vector coordinates $\underset{\sim}{\mathrm{a}}$ in any basis of dimension m; in this sense, the dimension of s-space should be limited to $m \leq n$; here, this v-scalar is invariant, respectively, to the change of the s-space basis, but covariant or contravariant, respectively, to the n space basis.

– Values of shape functions for 3D finite element as a function of local coordinate ${}^{3}\underset{\sim}{\mathrm{a}}$, which is a set of three coordinates: $\underset{\sim}{\phi}({}^{3}\underset{\sim}{\mathrm{a}})$, here m is equal to the number of shape functions.

---

2 Transposition of v-scalars will appear in reduced form of s-structures, which can be used as an apparatus of a limited use. The aim is to avoid cumbersome two-level operations appearing in a consistent description of s-structures as well as to represent not invariant structures. See section A1.7.

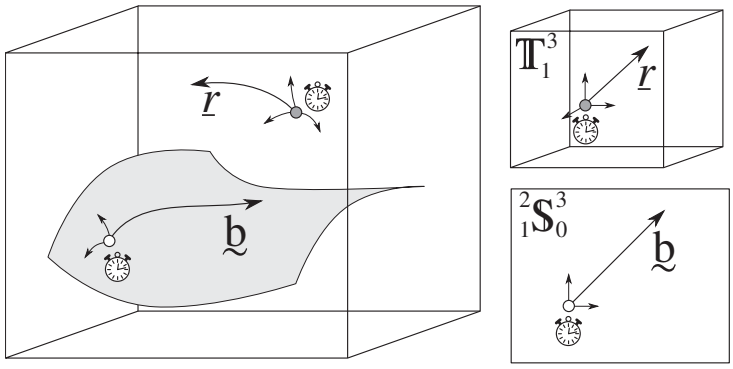

Figure A1.1. *A physical space for an observer A and two reference frames (two other observers) corresponding to space $\mathbb{T}_1^3$ and to two-dimensional $m = 2$ v-scalar space $^2_0\mathbb{S}^3_0$, respectively. Corresponding vector and v-scalar are represented both in the physical space, as observer A can see them, and in their frames of reference on the right*

– *V-vectors*

V-vectors are elements of a linear space $^m_1\mathbb{S}^n_1 = \tilde{\mathbb{T}}^m_1$ seen as ordered sets of invariant vectors. V-vectors are vectors of dimension m. In the given basis in s-space, components of such vectors are vectors. As this structure is invariant with respect to the vector space, it cannot be invariant with respect to the s-space. Some examples of v-vectors:

– A set of vectors of covariant basis $^n\underset{\sim}{\underline{\boldsymbol{e}}}'$ is a v-vector of dimension n over vector space n.

– A set of vectors of contravariant sub-basis $^m\underset{\sim}{\bar{\underline{\boldsymbol{e}}}}'$ is a v-vector of dimension m over the vector space n.

– A set of node vectors of a 3D finite element $^m\underset{\sim}{\underline{\boldsymbol{r}}}$, where m is the number of elements, each vector $\underline{\boldsymbol{r}}$ is a 3D vector $r \in \mathbb{T}_1$.

– *V-tensors*

They are a generalization of v-scalars and v-vectors for higher order tensor ranks. Further elements of linear space $\underset{\sim}{\underline{\underline{\boldsymbol{A}}}} \in {}^m_1\mathbb{S}^n_l$ will be called v-tensors of order l. By "v-tensors", we will simply understand v-tensors of order 2, $\underset{\sim}{\underline{\underline{\boldsymbol{B}}}} \in {}^m_1\mathbb{S}^n_2$.

The generalization of a v-structure is a t-structure ("t" for tensor). A t-structure of order k is defined as the tensor product of k v-spaces. Here, we confine the consideration to second-order t-structures, $k = 2$:

$$ {}^{m}_{2}\mathbb{S}^{n}_{l} = {}^{m}_{1}\mathbb{S}^{n}_{l} \bigotimes {}^{m}_{1}\mathbb{S}^{n}_{l} $$

In this sense, this s-space is a generalization of the tensor concept in a space of tensors, consequently all operations to be introduced will be similar to tensor operations. By analogy with tensor theory notations, elements of such s-spaces will be underlined by two waves. We will distinguish:

– *T-scalars* elements of space ${}^{m}_{2}\mathbb{S}^{n}_{0}$;

– *T-vectors* elements of space ${}^{m}_{2}\mathbb{S}^{n}_{1}$;

– *T-tensors* elements of space ${}^{m}_{2}\mathbb{S}^{n}_{l}$.

Now we need to determine internal operations in all s-spaces and external operations connecting all s-spaces.

A1.6.2. *Simple operations*

A1.6.2.1. *V-scalars*

The most simple elements of s-spaces are v-scalars. All operations are similar to ordinary vector. Let $\underset{\sim}{\mathrm{a}}, \underset{\sim}{\mathrm{b}}, \underset{\sim}{\mathrm{c}} \in \tilde{\mathbb{T}}^{m}_{1}$ and $\alpha, \beta \in \mathbb{R}$. A typical list is:

A1.6.2.1.1. Internal operations

Of type $\tilde{\mathbb{T}}^{m}_{1} \times \tilde{\mathbb{T}}^{m}_{1} \to \tilde{\mathbb{T}}^{m}_{1}$, $\tilde{\mathbb{T}}^{m}_{1} \times \mathbb{R} \to \tilde{\mathbb{T}}^{m}_{1}$.

– $\underset{\sim}{\mathrm{c}} = \underset{\sim}{\mathrm{a}} + \underset{\sim}{\mathrm{b}} = \underset{\sim}{\mathrm{b}} + \underset{\sim}{\mathrm{a}}$; $\quad c^i = a^i + b^i = b^i + a^i$;

– $(\underset{\sim}{\mathrm{a}} + \underset{\sim}{\mathrm{b}}) + \underset{\sim}{\mathrm{c}} = \underset{\sim}{\mathrm{a}} + (\underset{\sim}{\mathrm{b}} + \underset{\sim}{\mathrm{c}})$; $\quad (a^i + b^i) + c^i = a^i + (b^i + c^i)$;

– $\alpha \underset{\sim}{\mathrm{a}} = \underset{\sim}{\mathrm{a}} \alpha = \underset{\sim}{\mathrm{b}}$; $\quad \alpha a^i = a^i \alpha = b^i$;

– $(\alpha + \beta)\underset{\sim}{\mathrm{a}} = \alpha \underset{\sim}{\mathrm{a}} + \beta \underset{\sim}{\mathrm{a}}$; $\quad (\alpha + \beta)a^i = \alpha a^i + \beta a^i$;

– For $\alpha = 0, \beta = 1$, $(0 + 1)\underset{\sim}{\mathrm{a}} = 0\underset{\sim}{\mathrm{a}} + \underset{\sim}{\mathrm{a}} = \underset{\sim}{\mathrm{a}}$, so zero element $0 = \underset{\sim}{0} = 0\underset{\sim}{\mathrm{a}}$.

A1.6.2.1.2. External operations

Of type $\tilde{\mathbb{T}}^{m}_{1} \times \tilde{\mathbb{T}}^{m}_{1} \to \mathbb{R}$

– Scalar or dot product on s-space will be called s-dot product $\underset{\sim}{\mathrm{a}} \circ \underset{\sim}{\mathrm{b}} = \underset{\sim}{\mathrm{b}} \circ \underset{\sim}{\mathrm{a}} = \alpha$; $a_i \underset{\sim}{\mathrm{e}}^i \circ \underset{\sim}{\mathrm{e}}_j b^j = a^i b_j \delta_i^j = a^i b_i = \alpha$;

– Orthogonal v-scalars $\underset{\sim}{\mathrm{a}} \circ \underset{\sim}{\mathrm{b}} = \underset{\sim}{\mathrm{b}} \circ \underset{\sim}{\mathrm{a}} = 0$; $a_i \underset{\sim}{\mathrm{e}}^i \cdot \underset{\sim}{\mathrm{e}}_j b^j = a^i b_i = 0$;

– Norm $\forall \underset{\sim}{\mathrm{a}}\ \exists \|\underset{\sim}{\mathrm{a}}\| \geq 0$: $\|\underset{\sim}{\mathrm{a}}\| = 0 \Leftrightarrow \underset{\sim}{\mathrm{a}} = 0$,
$\|\underset{\sim}{\mathrm{a}}\| = \sqrt{\underset{\sim}{\mathrm{a}} \circ \underset{\sim}{\mathrm{a}}} \geq 0$, $\forall \underset{\sim}{\mathrm{a}} + \underset{\sim}{\mathrm{b}} = \underset{\sim}{\mathrm{c}} : \|\underset{\sim}{\mathrm{a}}\| + \|\underset{\sim}{\mathrm{b}}\| \geq \|\underset{\sim}{\mathrm{c}}\|$;

– Unit v-scalar: if $\|\underset{\sim}{\mathrm{a}}\| \neq 0 \Rightarrow \exists! \hat{\underset{\sim}{\mathrm{a}}} = \frac{\underset{\sim}{\mathrm{a}}}{\|\underset{\sim}{\mathrm{a}}\|}$.

A1.6.2.1.3. External operations

Of type $\tilde{\mathbb{T}}_1^m \times \tilde{\mathbb{T}}_1^m \to \tilde{\mathbb{T}}_2^m$.

Let $\underset{\approx}{\mathrm{C}}, \underset{\approx}{\mathrm{D}} \in \tilde{\mathbb{T}}_2^m$:

– s-Tensor product $\underset{\sim}{\mathrm{a}} \boxtimes \underset{\sim}{\mathrm{b}} = \underset{\approx}{\mathrm{C}} \neq \underset{\approx}{\mathrm{D}} = \underset{\sim}{\mathrm{b}} \boxtimes \underset{\sim}{\mathrm{a}}$ $a_i \underset{\sim}{\mathrm{e}}^i \boxtimes \underset{\sim}{\mathrm{e}}_j b^j \neq b_j \underset{\sim}{\mathrm{e}}^j \boxtimes \underset{\sim}{\mathrm{e}}_i a^i$.

A1.6.2.2. *v-Vectors*

All internal operations are formally similar to v-scalars. Let $\underset{\sim}{\boldsymbol{a}}, \underset{\sim}{\boldsymbol{b}}, \underset{\sim}{\boldsymbol{c}} \in {}_1^m\mathbb{S}_1^n$, $\underset{\sim}{\mathrm{e}}, \underset{\sim}{\mathrm{f}}, \underset{\sim}{\mathrm{g}} \in \tilde{\mathbb{T}}_1^m$ and $\alpha, \beta \in \mathbb{R}$.

A1.6.2.2.1. Internal operations

Of type ${}_1^m\mathbb{S}_1^n \times {}_1^m\mathbb{S}_1^n \to {}_1^m\mathbb{S}_1^n$ and ${}_1^m\mathbb{S}_1^n \times \mathbb{R} \to {}_1^m\mathbb{S}_1^n$

– $\underset{\sim}{\boldsymbol{c}} = \underset{\sim}{\boldsymbol{a}} + \underset{\sim}{\boldsymbol{b}} = \underset{\sim}{\boldsymbol{b}} + \underset{\sim}{\boldsymbol{a}}$; $\underset{\sim}{\boldsymbol{c}}^{(i)} = \underset{\sim}{\boldsymbol{a}}^{(i)} + \underset{\sim}{\boldsymbol{b}}^{(i)} = \underset{\sim}{\boldsymbol{b}}^{(i)} + \underset{\sim}{\boldsymbol{a}}^{(i)}$, all indices are put in brackets as vectors are invariant in vector space $\mathbb{T}_1^n$; but in s-space, they are either covariant or contravariant coordinates of points in space ${}_1^m\mathbb{S}_1^n$, so the position of the index tells it, here, for example, that these vectors are considered to be contravariant coordinates of v-vector in s-space.

– $(\underset{\sim}{\boldsymbol{a}} + \underset{\sim}{\boldsymbol{b}}) + \underset{\sim}{\boldsymbol{c}} = \underset{\sim}{\boldsymbol{a}} + (\underset{\sim}{\boldsymbol{b}} + \underset{\sim}{\boldsymbol{c}})$; $(\underset{\sim}{\boldsymbol{a}}^{(i)} + \underset{\sim}{\boldsymbol{b}}^{(i)}) + \underset{\sim}{\boldsymbol{c}}^{(i)} = \underset{\sim}{\boldsymbol{a}}^{(i)} + (\underset{\sim}{\boldsymbol{b}}^{(i)} + \underset{\sim}{\boldsymbol{c}}^{(i)})$;

– $\alpha \underset{\sim}{\boldsymbol{a}} = \underset{\sim}{\boldsymbol{a}} \alpha = \underset{\sim}{\boldsymbol{b}}$; $\alpha \underset{\sim}{\boldsymbol{a}}^{(i)} = \underset{\sim}{\boldsymbol{a}}^{(i)} \alpha = \underset{\sim}{\boldsymbol{b}}^{(i)}$;

– $(\alpha + \beta)\underset{\sim}{\boldsymbol{a}} = \alpha \underset{\sim}{\boldsymbol{a}} + \beta \underset{\sim}{\boldsymbol{a}}$; $(\alpha + \beta)\underset{\sim}{\boldsymbol{a}}^{(i)} = \alpha \underset{\sim}{\boldsymbol{a}}^{(i)} + \beta \underset{\sim}{\boldsymbol{a}}^{(i)}$;

– For $\alpha = 0, \beta = 1$, $(0 + 1)\underset{\sim}{\boldsymbol{a}} = 0\underset{\sim}{\boldsymbol{a}} + \underset{\sim}{\boldsymbol{a}} = \underset{\sim}{\boldsymbol{a}}$, so zero element $0 = \underset{\sim}{\mathbf{0}} = 0\underset{\sim}{\boldsymbol{a}}$.

A1.6.3. *Invariant s-structures*

A1.6.3.1. *Invariant v-scalars*

To make the s-structure language consistent, we need to prove that s-structures do not depend upon the change of basis. For v-scalars, it is trivial, they are invariant by definition, as vectors. Let us derive the operations that allow us to determine the coordinates of a v-scalar in all bases.

Statement: *the v-scalar* $\underset{\sim}{\mathrm{a}}$ *does not depend on the change of basis*. Let us introduce a basis of m v-scalars $\underset{\sim}{\mathrm{e}}_i$, such that all these v-scalars are linearly independent, that is:

$$\underset{\sim}{\mathrm{e}}_i \alpha^i = 0 \quad \Leftrightarrow \quad \alpha^i = 0$$

Then we construct a dual basis $\underset{\sim}{\mathrm{e}}^i$, following the standard scheme:

$$\underset{\sim}{\mathrm{e}}_i \circ \underset{\sim}{\mathrm{e}}^j = \delta_i^j$$

So now we can write a v-scalar $\underset{\sim}{\mathrm{a}}$ in these two bases:

$$\underset{\sim}{\mathrm{a}} = a^i \underset{\sim}{\mathrm{e}}_i = a_i \underset{\sim}{\mathrm{e}}^i \qquad \text{[A1.5]}$$

Then the s-dot product with $\underset{\sim}{\mathrm{e}}_i$ of the last equality gives:

$$a^i \underset{\sim}{\mathrm{e}}_i \circ \underset{\sim}{\mathrm{e}}_j = a_i \underset{\sim}{\mathrm{e}}^i \circ \underset{\sim}{\mathrm{e}}_j$$

By definition of the dual basis $\underset{\sim}{\mathrm{e}}^i \circ \underset{\sim}{\mathrm{e}}_j = \delta_j^i$ and we get:

$$a^i [S_{ij}] = a_j,$$

where $[S_{ij}] = \underset{\sim}{\mathrm{e}}_i \circ \underset{\sim}{\mathrm{e}}_j$ is the fundamental metric matrix. The same operations are performed with the dual basis: we evaluate the s-dot product of [A1.5] with vectors of the dual basis and get:

$$a^i = \underset{\sim}{\mathrm{e}}^i \circ \underset{\sim}{\mathrm{e}}^j a_j = [S^{ij}] a_j$$

If $\underset{\sim}{\mathrm{e}}_i$ are linearly independent, then $\det[S^{ij}] \neq 0$ and

$$[S^{ij}][S_{jk}] = \delta^i_k$$

Following the process used for vectors, the pushforward and pullback transformation of coordinates can be derived. Introducing a new basis $\underset{\sim}{\mathrm{e}}_{i'}$ and its dual basis $\underset{\sim}{\mathrm{e}}^{i'}$:

$$\underset{\sim}{\mathrm{a}} = a^{i'}\,\underset{\sim}{\mathrm{e}}_{i'} = a^i\,\underset{\sim}{\mathrm{e}}_i$$

The dot product of this expression with the new dual basis vectors gives:

$$a^{j\prime} = a^i\,\underset{\sim}{\mathrm{e}}^{j'} \circ \underset{\sim}{\mathrm{e}}_i$$

where

$$\underset{\sim}{\mathrm{e}}^{j'} \circ \underset{\sim}{\mathrm{e}}_i = [P^{j'}_i]$$

is the pushforward transformation matrix. In the same way:

$$\underset{\sim}{\mathrm{a}} = a_{i'}\,\underset{\sim}{\mathrm{e}}^{i'} = a_i\,\underset{\sim}{\mathrm{e}}^{i} \quad \Rightarrow \quad a_{j'} = a_i\,\underset{\sim}{\mathrm{e}}_{j'} \circ \underset{\sim}{\mathrm{e}}^{i}$$

$$\underset{\sim}{\mathrm{e}}_{j'} \circ \underset{\sim}{\mathrm{e}}^{i} = [P^i_{j'}]$$

is the pullback transformation matrix. Finally:

$$\underset{\sim}{\mathrm{e}}^{j'} = [P^{j'}_i]\,\underset{\sim}{\mathrm{e}}^{i} \qquad \underset{\sim}{\mathrm{e}}_{j'} = [P^i_{j'}]\,\underset{\sim}{\mathrm{e}}_i$$

$$a^{j'} = [P^{j'}_i]a^i \qquad a_{j'} = [P^i_{j'}]a_i$$

and

$$[P^k_{i'}][P^{j'}_k] = \delta^{j'}_{i'}$$

A1.6.3.2. *V-vectors*

The next question is: are v-vectors invariant or not? Yes and no, they are invariant in a certain sense, precisely each component of a v-vector is invariant with respect to the vector space, by definition of a vector, at the same time the set of these vectors is invariant in s-space. But a v-vector is not invariant, respectively, to both spaces simultaneously. Further we will call an element of an s-structure invariant if its components are invariant in tensor space (i.e. follow the transformation rules) and if the whole structure is invariant in the s-space, that is it follows the transformation rules defined in the s-space.

Let a v-vector $\underset{\sim}{\underline{\boldsymbol{a}}}$ be invariant in s-space, then:

$$\underset{\sim}{\underline{\boldsymbol{a}}} = \underline{\boldsymbol{a}}^{(i)} \underset{\sim}{\mathrm{e}}_i = \underline{\boldsymbol{a}}_{(i)} \underset{\sim}{\mathrm{e}}^j$$

from this expression and the previous paragraph it follows:

$$\begin{aligned} &\underline{\boldsymbol{a}}^{(j)} = [S^{ji}]\underline{\boldsymbol{a}}_{(i)} \qquad \underline{\boldsymbol{a}}_{(j)} = [S_{ji}]\underline{\boldsymbol{a}}^{(i)} \\ &\underline{\boldsymbol{a}}^{(j')} = [P_i^{j'}]\underline{\boldsymbol{a}}^{(i)} \qquad \underline{\boldsymbol{a}}_{(j')} = [P_{j'}^{i}]\underline{\boldsymbol{a}}_{(i)} \end{aligned} \qquad \text{[A1.6]}$$

As expected, vectors $\underline{\boldsymbol{a}}^{(i)}$ change in vector space with a changing basis in s-space.

A1.6.3.3. *Remark on induced metric and local basis*

To describe a surface in a 3D space, we use the induced metric t-scalar $\underset{\approx}{\mathrm{A}}$ and another t-scalar $\underset{\approx}{\mathrm{H}}$. These structures are defined as follows:

$$\underset{\approx}{\mathrm{A}} = \frac{\partial \underline{\boldsymbol{\rho}}}{\partial \underset{\sim}{\xi}} \boxtimes \frac{\partial \underline{\boldsymbol{\rho}}}{\partial \underset{\sim}{\xi}}, \qquad \underset{\approx}{\mathrm{H}} = \underline{\boldsymbol{n}} \cdot \frac{\partial^2 \underline{\boldsymbol{\rho}}}{\partial \underset{\sim}{\xi}^2}$$

None of these structures are invariant in the aforementioned sense, because the components of v-vector $\frac{\partial \underline{\boldsymbol{\rho}}}{\partial \underset{\sim}{\xi}}$ determining the local basis do not follow the rule:

$$\frac{\partial \underline{\boldsymbol{\rho}}}{\partial \xi^i} = S^{ij} \frac{\partial \underline{\boldsymbol{\rho}}}{\partial \xi_j}$$

The latter statement is true only if $A^{ij} = S^{ij}$, which is not the case in general. That is why the whole developed theory of invariant s-structures remains for the moment a "thing-in-itself" and is applicable for considering problems only if the basis in s-space is fixed, which is the case for the parent space in the finite element method formalism. However, the range of possible application is not limited by the considered situation.

A1.6.4. *Scalar products of v-vectors*

A1.6.4.1. *Scalar product of v-vector and vector*

The first product operation that will be introduced is the scalar product between a v-vector and a vector. This operation associates one v-scalar to each pair of a v-vector and a vector:

$$ {}^{m}_{1}\mathbb{S}^{n}_{1} \times \mathbb{T}^{n}_{1} \rightarrow {}^{m}_{1}\mathbb{S}^{n}_{0} $$

Let $\underset{\sim}{\mathrm{c}} \in {}^{m}_{1}\mathbb{S}^{n}_{0}, \underset{\approx}{\boldsymbol{a}} \in {}^{m}_{1}\mathbb{S}^{n}_{1}, \underline{\boldsymbol{b}} \in \mathbb{T}1n$, then:

$$ \underset{\sim}{\mathrm{c}} = \underset{\approx}{\boldsymbol{a}} \cdot \underline{\boldsymbol{b}} = \underline{\boldsymbol{b}} \cdot \underset{\approx}{\boldsymbol{a}} $$

This operation is easy to introduce:

$$ c^i \underset{\sim}{\mathrm{e}}_i = (\underline{\boldsymbol{a}}^{(i)} \cdot \underline{\boldsymbol{b}}) \underset{\sim}{\mathrm{e}}_i = (\underline{\boldsymbol{b}} \cdot \underline{\boldsymbol{a}}^{(i)}) \underset{\sim}{\mathrm{e}}_i $$

Let us demonstrate that the resulting s-scalar is bi-invariant, that is it does not depend on the choice of the basis, neither in vector space nor in s-space. Since vectors $\underline{\boldsymbol{a}}^{(i)}$ and $\underline{\boldsymbol{b}}$ do not depend on the choice of the basis in the vector space, it remains to show that:

$$ c^i \underset{\sim}{\mathrm{e}}_i = (\underline{\boldsymbol{a}}^{(i)} \cdot \underline{\boldsymbol{b}}) \underset{\sim}{\mathrm{e}}_i = (\underline{\boldsymbol{a}}_{(i)} \cdot \underline{\boldsymbol{b}}) \underset{\sim}{\mathrm{e}}^i $$

According to [A1.6], the latter equalities can be transformed into:

$$ ([S^{ij}]\underline{\boldsymbol{a}}_{(j)} \cdot \underline{\boldsymbol{b}})[S_{ik}] \underset{\sim}{\mathrm{e}}^k = (\underline{\boldsymbol{a}}_{(k)} \cdot \underline{\boldsymbol{b}}) \underset{\sim}{\mathrm{e}}^k $$

since $[S^{ij}][S_{ik}] = \delta^j_k$, the bi-invariance of such a v-scalar $\underset{\sim}{\mathrm{c}}$ has been demonstrated.

A1.6.4.2. *Scalar product of v-vector and v-scalar*

By analogy we define the scalar product operation between a v-vector and a v-scalar. For each such pair, this operation associates one vector:

$$ {}^{m}_{1}\mathbb{S}^{n}_{1} \times {}^{m}_{1}\mathbb{S}^{n}_{0} \to \mathbb{T}^{n}_{1} $$

Let $\underset{\sim}{\underline{\boldsymbol{a}}} \in {}^{m}_{1}\mathbb{S}^{n}_{1}$, $\underset{\sim}{\mathrm{b}} \in {}^{m}_{1}\mathbb{S}^{n}_{0}$, $\underline{\boldsymbol{c}} \in \mathbb{T}1n$, then:

$$ \underline{\boldsymbol{c}} = \underset{\sim}{\underline{\boldsymbol{a}}} \circ \underset{\sim}{\mathrm{b}} = \underset{\sim}{\mathrm{b}} \circ \underset{\sim}{\underline{\boldsymbol{a}}} $$

In component form:

$$ c^{i}\underline{\boldsymbol{e}}_{i} = \underline{\boldsymbol{a}}^{(i)}(\underset{\sim}{\mathrm{e}}_{i} \circ \underset{\sim}{\mathrm{b}}) = \underline{\boldsymbol{a}}^{(i)}(\underset{\sim}{\mathrm{b}} \circ \underset{\sim}{\mathrm{e}}_{i}) $$

To show that $\underline{\boldsymbol{c}}$ is bi-invariant with respect to a basis change in s-space and vector space, it remains to show that:

$$ c^{i}\underline{\boldsymbol{e}}_{i} = \underline{\boldsymbol{a}}^{(i)}(\underset{\sim}{\mathrm{e}}_{i} \circ \underset{\sim}{\mathrm{b}}) = \underline{\boldsymbol{a}}_{(i)}(\underset{\sim}{\mathrm{e}}^{i} \circ \underset{\sim}{\mathrm{b}}) $$

By analogy with the previous paragraph, according to [A1.6], the last equalities can be transformed into:

$$ [S^{ij}]\underline{\boldsymbol{a}}_{(j)}([S_{ik}]\underset{\sim}{\mathrm{e}}^{k} \circ \underset{\sim}{\mathrm{b}}) = \underline{\boldsymbol{a}}_{(k)}(\underset{\sim}{\mathrm{e}}^{k} \circ \underset{\sim}{\mathrm{b}}) $$

since $[S^{ij}][S_{ik}] = \delta^{j}_{k}$, the bi-invariance of this vector $\underline{\boldsymbol{c}}$ is demonstrated.

A1.6.4.3. *Double scalar product*

Let us show that there is a scalar product operation such that for each pair of v-vectors, it associates a unique real number. This operation will be called a full scalar product or double scalar product:

$$ {}^{m}_{1}\mathbb{S}^{n}_{1} \times {}^{m}_{1}\mathbb{S}^{n}_{1} \to \mathbb{R} $$

The requirement of obtaining a unique scalar implies that such an operation does not depend on basis change both in vector space and s-space. Let $\underset{\sim}{\underline{\boldsymbol{a}}}, \underset{\sim}{\underline{\boldsymbol{b}}} \in {}^{m}_{1}\mathbb{S}^{n}_{1}, \alpha \in \mathbb{R}$ for any value of m and n:

$$< \underset{\sim}{\underline{\boldsymbol{a}}}, \underset{\sim}{\underline{\boldsymbol{b}}} >= \underset{\sim}{\underline{\boldsymbol{a}}} \overset{\circ}{\cdot} \underset{\sim}{\underline{\boldsymbol{b}}} = \alpha$$

This operation can be introduced as follows:

$$\alpha = \underline{\boldsymbol{a}}^{(i)} \cdot \underline{\boldsymbol{b}}_{(i)} = \underline{\boldsymbol{a}}^{(i)} \cdot \underline{\boldsymbol{b}}_{(j)} \delta^{j}_{i}$$

which is equal to

$$\alpha = \underline{\boldsymbol{a}}^{(i)} \cdot \underline{\boldsymbol{b}}_{(j)} \underset{\sim}{\mathrm{e}}_{i} \circ \underset{\sim}{\mathrm{e}}^{j} = [\underline{\boldsymbol{a}}^{(i)} \underset{\sim}{\mathrm{e}}_{i}] \overset{\circ}{\cdot} [\underline{\boldsymbol{b}}_{(j)} \underset{\sim}{\mathrm{e}}^{j}]$$

Let us demonstrate that the SS-product, introduced in such a way, is bi-invariant. For this purpose, let us write the v-vector in the s-space basis:

$$\underset{\sim}{\underline{\boldsymbol{a}}} = \underline{\boldsymbol{a}}^{(i)} \underset{\sim}{\mathrm{e}}_{i} = \underline{\boldsymbol{a}}_{(i)} \underset{\sim}{\mathrm{e}}^{i} \qquad \underset{\sim}{\underline{\boldsymbol{b}}} = \underline{\boldsymbol{b}}^{(j)} \underset{\sim}{\mathrm{e}}_{i} = \underline{\boldsymbol{b}}_{(j)} \underset{\sim}{\mathrm{e}}^{i}$$

Due to the invariance in the s-space, it is necessary and sufficient that:

$$\underline{\boldsymbol{a}}^{(i)} \underset{\sim}{\mathrm{e}}_{i} \overset{\circ}{\cdot} \underline{\boldsymbol{b}}^{(j)} \underset{\sim}{\mathrm{e}}_{j} = \underline{\boldsymbol{a}}^{(i)} \underset{\sim}{\mathrm{e}}_{i} \overset{\circ}{\cdot} \underline{\boldsymbol{b}}_{(j)} \underset{\sim}{\mathrm{e}}^{j} = \underline{\boldsymbol{a}}_{(i)} \underset{\sim}{\mathrm{e}}^{i} \overset{\circ}{\cdot} \underline{\boldsymbol{b}}^{(j)} \underset{\sim}{\mathrm{e}}_{j} = \underline{\boldsymbol{a}}_{(i)} \underset{\sim}{\mathrm{e}}^{i} \overset{\circ}{\cdot} \underline{\boldsymbol{b}}_{(j)} \underset{\sim}{\mathrm{e}}^{j}$$

Carrying $\underset{\sim}{\mathrm{e}}_{i} \circ \underset{\sim}{\mathrm{e}}_{j} = [S_{ij}]$ and $\underset{\sim}{\mathrm{e}}^{i} \circ \underset{\sim}{\mathrm{e}}^{j} = [S^{ij}]$ we get:

$$\underline{\boldsymbol{a}}^{(i)} \cdot \underline{\boldsymbol{b}}^{(j)} [S_{ij}] = \underline{\boldsymbol{a}}^{(i)} \cdot \underline{\boldsymbol{b}}_{(i)} = \underline{\boldsymbol{a}}_{(i)} \cdot \underline{\boldsymbol{b}}^{(i)} = \underline{\boldsymbol{a}}_{(i)} \cdot \underline{\boldsymbol{b}}_{(j)} [S^{ij}]$$

According to [A1.6] and the symmetry of the fundamental metric matrices:

$$[S_{ij}][S^{jk}] \underline{\boldsymbol{a}}^{(j)} \cdot \underline{\boldsymbol{b}}_{(k)} = \underline{\boldsymbol{a}}^{(i)} \cdot \underline{\boldsymbol{b}}_{(i)} = [S_{ij}][S^{ik}] \underline{\boldsymbol{a}}^{(j)} \cdot \underline{\boldsymbol{b}}_{(k)} = [S_{ik}][S^{ij}] \underline{\boldsymbol{a}}^{(k)} \cdot \underline{\boldsymbol{b}}_{(j)}$$

Since $[S_{ij}][S^{jk}] = \delta^{k}_{i}$ and $[S^{ij}] = [S^{ji}]$, the equality is proven. So the SS-product is a bi-invariant operation.

A1.6.4.4. *Scalar product or dot product*

Let us introduce another important bi-invariant operation, which to each pair of ordered v-vectors associates a unique t-scalar. T-scalars being invariant by definition in s-space, let us introduce the operation where the resulting t-scalar is invariant to the change of basis in vector space:

$$\{\cdot\}: {}^{m}_{1}\mathbb{S}^{n}_{1} \times {}^{m}_{1}\mathbb{S}^{n}_{1} \rightarrow {}^{m}_{2}\mathbb{S}^{n}_{0}$$

Let $\underset{\approx}{\underline{\boldsymbol{a}}}, \underset{\approx}{\underline{\boldsymbol{b}}} \in {}^{m}_{1}\mathbb{S}^{n}_{1}$, $\underset{\approx}{\mathrm{C}} \in {}^{m}_{2}\mathbb{S}^{n}_{0}$

$$[\underset{\approx}{\underline{\boldsymbol{a}}}, \underset{\approx}{\underline{\boldsymbol{b}}}] = \underset{\approx}{\underline{\boldsymbol{a}}} \cdot \underset{\approx}{\underline{\boldsymbol{b}}} = \underset{\approx}{\mathrm{C}}$$

It is worth mentioning that n and m can take any value and that the resulting t-scalar may be not symmetric:

$$\underset{\approx}{\underline{\boldsymbol{a}}} \cdot \underset{\approx}{\underline{\boldsymbol{b}}} \neq \underset{\approx}{\underline{\boldsymbol{b}}} \cdot \underset{\approx}{\underline{\boldsymbol{a}}}$$

This operation can be introduced in the following way:

$$\underset{\approx}{\mathrm{C}} = C^{i*}_{*j} \underset{\sim}{\mathrm{e}}_i \boxtimes \underset{\sim}{\mathrm{e}}^j = \left(\underline{\boldsymbol{a}}^{(i)} \cdot \underline{\boldsymbol{b}}_{(j)}\right) \underset{\sim}{\mathrm{e}}_i \boxtimes \underset{\sim}{\mathrm{e}}^j = \left(\underline{\boldsymbol{a}}^{(i)} \underset{\sim}{\mathrm{e}}_i\right) \cdot \left(\underline{\boldsymbol{b}}^{(j)} \underset{\sim}{\mathrm{e}}_j\right)$$

The following condition is requested to ensure the invariance of t-scalar $\underset{\approx}{\mathrm{C}}$:

$$C^{i*}_{*j} \underset{\sim}{\mathrm{e}}_i \boxtimes \underset{\sim}{\mathrm{e}}^j = C^{ij} \underset{\sim}{\mathrm{e}}_i \boxtimes \underset{\sim}{\mathrm{e}}_j = C_{ij} \underset{\sim}{\mathrm{e}}^i \boxtimes \underset{\sim}{\mathrm{e}}^j = C^{*j}_{i*} \underset{\sim}{\mathrm{e}}^i \boxtimes \underset{\sim}{\mathrm{e}}_j$$

which, according to the relations between the basis and the dual basis, is equal to:

$$C^{i*}_{*j} \underset{\sim}{\mathrm{e}}_i \boxtimes \underset{\sim}{\mathrm{e}}^j = C^{ij} \underset{\sim}{\mathrm{e}}_i \boxtimes \underset{\sim}{\mathrm{e}}^k [S_{jk}] = C_{ij} [S^{ik}] \underset{\sim}{\mathrm{e}}_k \boxtimes \underset{\sim}{\mathrm{e}}^j = C^{*j}_{i*} [S^{ik}] \underset{\sim}{\mathrm{e}}_k \boxtimes \underset{\sim}{\mathrm{e}}^l [S_{jl}]$$

which, in turn, is equivalent to:

$$C^{i*}_{*j} = C^{ik}[S_{kj}] = C_{kj}[S^{ki}] = C^{*l}_{k*}[S^{ki}][S_{lj}] \qquad \text{[A1.7]}$$

where the coefficients C are different scalar products of v-vector components. By definition, they are determined as follows:

$$C^{i*}_{*j} = \underline{\boldsymbol{a}}^{(i)} \cdot \underline{\boldsymbol{b}}_{(j)} \qquad C^{ik} = \underline{\boldsymbol{a}}^{(i)} \cdot \underline{\boldsymbol{b}}^{(k)}$$

$$C_{kj} = \underline{\boldsymbol{a}}_{(k)} \cdot \underline{\boldsymbol{b}}_{(j)} \qquad C^{*l}_{k*} = \underline{\boldsymbol{a}}_{(k)} \cdot \underline{\boldsymbol{b}}^{(l)}$$

which according to [A1.6] can be rewritten as:

$$C^{i*}_{*j} = \underline{\boldsymbol{a}}^{(i)} \cdot \underline{\boldsymbol{b}}_{(j)} \qquad C^{ik} = \underline{\boldsymbol{a}}^{(i)} \cdot \underline{\boldsymbol{b}}_{(m)}[S^{km}]$$

$$C_{kj} = [S_{km}]\underline{\boldsymbol{a}}^{(m)} \cdot \underline{\boldsymbol{b}}_{(j)} \qquad C^{*l}_{k*} = [S_{km}]\underline{\boldsymbol{a}}^{(m)} \cdot \underline{\boldsymbol{b}}_{(n)}[S^{ln}]$$

Substituting these expressions in [A1.7] gives:

$$\begin{aligned} \underline{\boldsymbol{a}}^{(i)} \cdot \underline{\boldsymbol{b}}_{(j)} &= \underline{\boldsymbol{a}}^{(i)} \cdot \underline{\boldsymbol{b}}_{(m)}[S^{km}][S_{kj}] = \\ &= [S_{km}]\underline{\boldsymbol{a}}^{(m)} \cdot \underline{\boldsymbol{b}}_{(j)}[S^{ki}] = [S_{km}]\underline{\boldsymbol{a}}^{(m)} \cdot \underline{\boldsymbol{b}}_{(m)}[S^{lm}][S^{ki}][S_{lj}] \end{aligned} \qquad [A1.8]$$

These three equalities are true as $[S^{km}][S_{kj}] = \delta^m_j$, so the bi-invariance of this scalar product has been proven. This operation associates only one t-scalar with each ordered pair of v-vectors. This t-scalar is invariant in the s-space.

A1.6.4.5. *S-scalar product or s-dot product*

By analogy, another bi-variant scalar operation associates a unique tensor for each ordered pair of v-vectors:

$$\{\circ\}: {}^{m}_{1}\mathbb{S}^{n}_{1} \times {}^{m}_{1}\mathbb{S}^{n}_{1} \rightarrow {}^{m}_{0}\mathbb{S}^{n}_{2}$$

Let $\underset{\sim}{\underline{\boldsymbol{a}}}, \underset{\sim}{\underline{\boldsymbol{b}}} \in {}^{m}_{1}\mathbb{S}^{n}_{1}$, $\underset{\approx}{\underline{\mathrm{C}}} \in {}^{m}_{2}\mathbb{S}^{n}_{0}$

$$\{\underset{\sim}{\underline{\boldsymbol{a}}}, \underset{\sim}{\underline{\boldsymbol{b}}}\} = \underset{\sim}{\underline{\boldsymbol{a}}} \circ \underset{\sim}{\underline{\boldsymbol{b}}} = \underset{=}{\underline{\boldsymbol{C}}}$$

It is defined in the following way:

$$\underset{\sim}{\underline{\boldsymbol{a}}} \circ \underset{\sim}{\underline{\boldsymbol{b}}} = \underline{\boldsymbol{a}}^{(i)} \underline{\boldsymbol{e}}_i \circ \underline{\boldsymbol{b}}^{(j)} \underline{\boldsymbol{e}}_j = \underline{\boldsymbol{a}}^{(i)} \otimes \underline{\boldsymbol{b}}^{(j)} \underline{\boldsymbol{e}}_i \circ \underline{\boldsymbol{e}}_j$$

As previously constructed, this operation is introduced for any n, m and in general:

$$\underset{\sim}{\underline{\boldsymbol{a}}} \circ \underset{\sim}{\underline{\boldsymbol{b}}} \neq \underset{\sim}{\underline{\boldsymbol{b}}} \circ \underset{\sim}{\underline{\boldsymbol{a}}}$$

Again, it can be shown that this operation is bi-invariant and the resulting tensor is invariant in tensor space.

A1.6.5. *Inverse v-vector*

A v-vector $\underset{\sim}{\underline{\boldsymbol{B}}} \in {}^{m}_{1}\mathbb{S}^{n}_{1}$ v-vector will be called inverse of a v-vector $\underset{\sim}{\underline{\boldsymbol{A}}} \in {}^{m}_{1}\mathbb{S}^{n}_{1}$, respectively, to the s-space, if the following conditions are fulfilled:

$$\underset{\sim}{\underline{\boldsymbol{A}}} \cdot \underset{\sim}{\underline{\boldsymbol{B}}} = \underset{\approx}{\mathrm{I}} \in {}^{m}_{2}\mathbb{S}^{n}_{0}$$

According to its definition, a unit t-scalar in any basis can be presented as $\underset{\approx}{\mathrm{I}} = \underset{\sim}{\mathrm{e}}_i \boxtimes \underset{\sim}{\mathrm{e}}^i$. Then,

$$\underset{\sim}{\mathrm{e}}_i \boxtimes \underset{\sim}{\mathrm{e}}^i = \underset{\sim}{\underline{\boldsymbol{A}}} \cdot \underset{\sim}{\underline{\boldsymbol{B}}} = \underline{\boldsymbol{A}}^{(i)} \underset{\sim}{\mathrm{e}}_i \cdot \underline{\boldsymbol{B}}_{(j)} \underset{\sim}{\mathrm{e}}^j = [\underline{\boldsymbol{A}}^{(i)} \cdot \underline{\boldsymbol{B}}_{(j)}] \underset{\sim}{\mathrm{e}}_i \boxtimes \underset{\sim}{\mathrm{e}}^j$$

In order to fulfill this equality, we should require that:

$$\underline{\boldsymbol{A}}^{(i)} \cdot \underline{\boldsymbol{B}}_{(j)} = \delta^i_j \quad \Leftrightarrow \quad \underline{\boldsymbol{A}}^{(i)} \cdot \underline{\boldsymbol{B}}_{(j)} = 1, i = j \quad \underline{\boldsymbol{A}}^{(i)} \cdot \underline{\boldsymbol{B}}_{(j)} = 0, i \neq j$$

if $\underline{\boldsymbol{A}}^{(i)} = A^{(i)}_j \underline{\boldsymbol{e}}^j$ and $\underline{\boldsymbol{B}}_{(i)} = B^j_{(i)} \underline{\boldsymbol{e}}_j$, the previous condition implies that:

$$B^i_{(i)} = \frac{A^{(i)}_i}{\left(A^{(i)}_i\right)^2}, \quad B^j_{(i)} = 0 \Rightarrow \qquad \text{[A1.9]}$$

$$\underline{\boldsymbol{A}}_j^{(i)} \cdot \underline{\boldsymbol{B}}_{(i)}^j = A_j^{(i)} (\underline{\boldsymbol{e}}^j \cdot \underline{\boldsymbol{e}}_j) \frac{A_j^{(i)}}{\left(A_j^{(i)}\right)^2} = 1; \quad \underline{\boldsymbol{A}}_j^{(i)} \cdot \underline{\boldsymbol{B}}_{(i)}^k = A_j^{(i)} \underline{\boldsymbol{e}}^j \cdot \underline{\boldsymbol{e}}_k \frac{A_k^{(i)}}{\left(A_k^{(i)}\right)^2} = 0$$

So the reasonable requirement for the inverse v-vector existence for $\underset{\approx}{\underline{\boldsymbol{A}}}$ is:

$$A_j^{(i)} \neq 0 \qquad \text{[A1.10]}$$

The inverse on the s-space v-vector to the v-vector $\underset{\approx}{\underline{\boldsymbol{A}}}$ will be denoted by $\underset{\approx}{\underline{\boldsymbol{A}}}^{-1^s}$, where the small index s recalls that this is an inverse in the s-space. It can be shown that if $\underset{\approx}{\underline{\boldsymbol{A}}}^{-1^s}$ is the inverse of a v-vector $\underset{\approx}{\underline{\boldsymbol{A}}}$ on s-space, then $\underset{\approx}{\underline{\boldsymbol{A}}}^{-1^s}$ is the inversed v-vector on tensor space and vice versa:

$$\underset{\approx}{\underline{\boldsymbol{A}}} \cdot \underset{\approx}{\underline{\boldsymbol{A}}}^{-1^s} = \underset{\approx}{\underline{\mathrm{I}}} \quad \Leftrightarrow \quad \underset{\approx}{\underline{\boldsymbol{A}}} \circ \underset{\approx}{\underline{\boldsymbol{A}}}^{-1^s} = \underline{\underline{\boldsymbol{I}}}$$

Let us split the second equality:

$$\begin{aligned} \underset{\approx}{\underline{\boldsymbol{A}}} \circ \underset{\approx}{\underline{\boldsymbol{A}}}^{-1^s} &= (\underline{\boldsymbol{A}}^{(i)} \underset{\sim}{\underline{\mathrm{e}}}_i) \circ (\underset{\sim}{\underline{\mathrm{e}}}^j \{\underline{\boldsymbol{A}}^{-1^s}\}_{(j)}) = \\ &= (A_k^{(i)} \underline{\boldsymbol{e}}^k \underset{\sim}{\underline{\mathrm{e}}}_i) \circ (\underset{\sim}{\underline{\mathrm{e}}}^j \{A^{-1^s}\}_{(j)}^m \underline{\boldsymbol{e}}_m) = \\ &= ((A_k^{(i)} \underset{\sim}{\underline{\mathrm{e}}}_i \circ \{A^{-1^s}\}_{(j)}^m \underset{\sim}{\underline{\mathrm{e}}}^j) \underline{\boldsymbol{e}}^k \otimes \underline{\boldsymbol{e}}_m \end{aligned} \qquad \text{[A1.11]}$$

to get a unit tensor, we should require the following:

$$((A_k^{(i)} \underset{\sim}{\underline{\mathrm{e}}}_i \circ \{A^{-1^s}\}_{(j)}^m \underset{\sim}{\underline{\mathrm{e}}}^j) = \delta_m^k$$

which is equivalent to:

$$((A_k^{(i)} \underset{\sim}{\underline{\mathrm{e}}}_i \circ \{A^{-1^s}\}_{(j)}^k \underset{\sim}{\underline{\mathrm{e}}}^j) = 1; \quad ((A_k^{(i)} \underset{\sim}{\underline{\mathrm{e}}}_i \circ \{A^{-1^s}\}_{(j)}^m \underset{\sim}{\underline{\mathrm{e}}}^j) = 0, m \neq k$$

$$A_k^{(i)} \{A^{-1^s}\}_{(i)}^k = 1; \quad A_k^{(i)} \{A^{-1^s}\}_{(i)}^m = 0, m \neq k$$

which according to [A1.9] is for $k = m$

$$A_k^{(i)} \frac{A_k^{(i)}}{\left(A_k^{(i)}\right)^2} = 0 + \cdots + 0 + A_k^{(k)} \frac{A_k^{(k)}}{\left(A_k^{(k)}\right)^2} + 0 + \cdots + 0 = 1;$$

and for $k \neq m$

$$A_k^{(i)} \frac{A_m^{(i)}}{\left(A_m^{(i)}\right)^2} = 0 + \cdots + 0 + \overbrace{A_k^{(k)}}^{\neq 0} \overbrace{\frac{A_m^{(k)}}{\left(A_m^{(k)}\right)^2}}^{=0;\ m\neq i} + \cdots + \overbrace{A_k^{(m)}}^{=0;\ m\neq i} \overbrace{\frac{A_m^{(m)}}{\left(A_m^{(m)}\right)^2}}^{\neq 0}$$
$$+0 + \cdots + 0 = 0$$

Thus, it is demonstrated that the inverse v-vector on s-space is the inverse on tensor space. Since all transitions are sufficient and necessary, the inverse statement is also true. From now on, we will note $\underset{\sim}{\underline{\boldsymbol{A}}}^{-1}$ all inverse v-vectors; if such a v-vector exists, the following statements are true:

$$\underset{\sim}{\underline{\boldsymbol{A}}} \circ \underset{\sim}{\underline{\boldsymbol{A}}}^{-1} = \underline{\underline{\boldsymbol{I}}}\,, \qquad \underset{\sim}{\underline{\boldsymbol{A}}} \cdot \underset{\sim}{\underline{\boldsymbol{A}}}^{-1} = \underset{\approx}{\mathrm{I}}$$

Since $\underset{\approx}{\mathrm{I}} = \underset{\approx}{\mathrm{I}}^{\intercal}$ and $\underline{\underline{\boldsymbol{I}}} = \underline{\underline{\boldsymbol{I}}}^{\intercal}$:

$$\underset{\sim}{\underline{\boldsymbol{A}}} \circ \underset{\sim}{\underline{\boldsymbol{A}}}^{-1} = \underset{\sim}{\underline{\boldsymbol{A}}}^{-1} \circ \underset{\sim}{\underline{\boldsymbol{A}}} \quad \Leftrightarrow \quad \underset{\sim}{\underline{\boldsymbol{A}}} \cdot \underset{\sim}{\underline{\boldsymbol{A}}}^{-1} = \underset{\sim}{\underline{\boldsymbol{A}}}^{-1} \cdot \underset{\sim}{\underline{\boldsymbol{A}}}$$

A1.6.6. *Isomorphism of s-space and tensor space*

If the dimensions of the s-space and the tensor space are equivalent $n = m$, then they are isomorphic, that is for each element of the s-space of dimension n and order k there is only one element of the kth order tensor space of dimension n and vice versa. All structures and operations are also preserved. Isomorphism between vectors and v-scalars is ensured by v-vector $\underset{\sim}{\underline{\boldsymbol{A}}} \in {}_1^n\mathbb{S}_1^n$, which can be considered as a bijective linear function:

$$\underset{\sim}{\underline{\boldsymbol{A}}}\colon {}_1^n\mathbb{S}_0^n \to \mathbb{T}_1^n \quad \text{and} \quad \underset{\sim}{\underline{\boldsymbol{A}}}\colon \mathbb{T}_1^n \to {}_1^n\mathbb{S}_0^n$$

Not all v-vectors can establish an isomorphism. $\underset{\sim}{\underline{\boldsymbol{A}}}$ should be defined such that:

$$\text{if } \mathrm{Ker}\underset{\sim}{\underline{\boldsymbol{A}}} \equiv {}_1^n\mathbb{S}_0^n, \text{ then } \mathrm{Im}\underset{\sim}{\underline{\boldsymbol{A}}} \equiv \mathbb{T}_1^n$$

$$\text{if } \mathrm{Ker}\underset{\sim}{\underline{\boldsymbol{A}}} \equiv \mathbb{T}_1^n, \text{ then } \mathrm{Im}\underset{\sim}{\underline{\boldsymbol{A}}} \equiv {}_1^n\mathbb{S}_0^n$$

It means that n linear independent vectors (or v-scalars) are transformed into n linear independent v-scalars (or vectors).

THEOREM.– *If* $\underset{\sim}{\underline{\boldsymbol{A}}} \in {}^{n}_{1}\mathbb{S}^{n}_{1}$ *and* $\underset{\sim}{\underline{\boldsymbol{A}}} = \underline{\boldsymbol{A}}_{(i)} \underset{\sim}{\mathrm{e}}^{i}$*, where* $\underline{\boldsymbol{A}}_{(i)}$ *are* n *linearly independent vectors and* $\underset{\sim}{\mathrm{e}}^{i}$ *are* n *linearly independent v-scalars, then* $\underset{\sim}{\underline{\boldsymbol{A}}}$ *is a bijection from the v-scalar (vector) space to the vector (v-scalar space) space and the unique inverse bijection* $\underset{\sim}{\underline{\boldsymbol{B}}}$ *from the vector (v-scalar space) space to the v-scalar (vector space) space exists, such that* $\underset{\sim}{\underline{\boldsymbol{B}}} = \underset{\sim}{\underline{\boldsymbol{A}}}^{-1}$.

PROOF.– Let

$$\forall \underset{\sim}{\mathrm{x}} \in {}^{n}_{1}\mathbb{S}^{n}_{0} \mid \underset{\sim}{\mathrm{x}} = x^{i} \underset{\sim}{\mathrm{e}}_{i}, \forall x^{i} \neq 0,$$

where the v-scalars $\underset{\sim}{\mathrm{e}}_{i}$ are linearly independent, then $\underset{\sim}{\underline{\boldsymbol{A}}}$ is a bijection:

$$\underset{\sim}{\underline{\boldsymbol{A}}} : {}^{n}_{1}\mathbb{S}^{n}_{0} \rightarrow \mathbb{T}^{n}_{1},$$

if and only if

$$\exists \underline{\boldsymbol{y}} \in \mathbb{T}^{n}_{1},\ \underline{\boldsymbol{y}} = y^{k} \underline{\boldsymbol{e}}_{k}, y^{k} \neq 0,$$

where $\underline{\boldsymbol{e}}_{k}$ are linearly independent vectors. The bijection $\underset{\sim}{\underline{\boldsymbol{A}}}$ is as follows:

$$\underline{\boldsymbol{y}} = \underset{\sim}{\underline{\boldsymbol{A}}} \circ \underset{\sim}{\mathrm{x}} \quad \Leftrightarrow \quad y^{k} \underline{\boldsymbol{e}}_{k} = \underline{\boldsymbol{A}}_{(k)} \underset{\sim}{\mathrm{e}}^{k} \circ x^{i} \underset{\sim}{\mathrm{e}}_{i} \quad \Leftrightarrow \quad y^{k} \underline{\boldsymbol{e}}_{k} = \underline{\boldsymbol{A}}_{(k)} x^{k}$$

if $y^{k} = 0$, then:

$$\underline{\boldsymbol{A}}_{(k)} x^{k} = 0$$

since all x^{k} are non-zero by default, then vectors $\underline{\boldsymbol{A}}_{(k)}$ are linearly dependent, which contradicts the condition of theorem, so $y^{k} \neq 0$ and $\underset{\sim}{\underline{\boldsymbol{A}}}$ is a bijection from ${}^{n}_{1}\mathbb{S}^{n}_{0}$ to $\mathbb{T}^{n}_{1}$.

Let an inverse bijection $\underset{\sim}{\underline{\boldsymbol{B}}}$ exists such that:

$$\underset{\sim}{\underline{\boldsymbol{B}}}: {}^{n}_{1}\mathbb{S}^{n}_{0} \to \mathbb{T}^{n}_{1},$$

then it transforms elements:

$$\underset{\sim}{\mathrm{x}}' = \underset{\sim}{\underline{\boldsymbol{B}}} \cdot \underline{\boldsymbol{y}}$$

Substituting $\underline{\boldsymbol{y}}$ as image of $\underset{\sim}{\mathrm{x}}$ gives:

$$\underset{\sim}{\mathrm{x}}' = \underset{\sim}{\underline{\boldsymbol{B}}} \cdot (\underset{\sim}{\underline{\boldsymbol{A}}} \circ \underset{\sim}{\mathrm{x}}),$$

to get $\underset{\sim}{\mathrm{x}}' = \underset{\sim}{\mathrm{x}}$, we require that $\underset{\sim}{\underline{\boldsymbol{B}}} \cdot \underset{\sim}{\underline{\boldsymbol{A}}} = \underset{\approx}{\mathrm{I}}$, and by definition $\underset{\sim}{\underline{\boldsymbol{B}}} = \underset{\sim}{\underline{\boldsymbol{A}}}^{-1}$. The theorem is proved.

A1.6.6.1. *Unit v-vector*

At first glance, it *seems* to be meaningful to introduce a special kind of bijective function – a unit v-vector $\underset{\approx}{\underline{\underline{\boldsymbol{I}}}}$ – which is its own inverse. The first form for this v-vector which crosses on mind can be defined only if $n = m$ in the following way:

$$\underset{\sim}{\underline{\boldsymbol{I}}} = \frac{1}{2} (\underline{\boldsymbol{e}}_i \underset{\sim}{\mathrm{e}}^{i} + \underline{\boldsymbol{e}}^{i} \underset{\sim}{\mathrm{e}}_{i}), \qquad \text{[A1.12]}$$

where $\underline{\boldsymbol{e}}_i$, $\underset{\sim}{\mathrm{e}}_i$ are vectors and v-scalars of bases and $\underline{\boldsymbol{e}}^i$, $\underset{\sim}{\mathrm{e}}^{i}$ are vectors and v-scalars of dual bases in vector space and s-space, respectively. Then, we require that for any vector $\underline{\boldsymbol{a}} \in \mathbb{T}^{n}_{1}$ and v-scalar $\underset{\sim}{\alpha} \in {}^{m}_{1}\mathbb{S}^{n}_{0}$:

$$\underline{\boldsymbol{a}} = \underset{\sim}{\underline{\boldsymbol{I}}} \circ \underset{\sim}{\alpha} \qquad \underset{\sim}{\alpha} = \underset{\sim}{\underline{\boldsymbol{I}}} \cdot \underline{\boldsymbol{a}} \qquad \underset{\sim}{\underline{\boldsymbol{I}}} = \underset{\sim}{\underline{\boldsymbol{I}}}^{-1}$$

Let us prove that $\underset{\sim}{\underline{\boldsymbol{I}}}$ defined like in [A1.12] is its own inverse:

$$\underset{\sim}{\underline{\boldsymbol{I}}} \cdot \underset{\sim}{\underline{\boldsymbol{I}}} = \underset{\approx}{\mathrm{I}}$$

$$\underset{\sim}{\underline{\boldsymbol{I}}} \cdot \underset{\sim}{\underline{\boldsymbol{I}}} = \tfrac{1}{4}\,(\,\underline{\boldsymbol{e}}_i \underset{\sim}{\mathrm{e}}^{\,i} + \underline{\boldsymbol{e}}^i \underset{\sim}{\mathrm{e}}_i\,) \cdot (\,\underline{\boldsymbol{e}}_j \underset{\sim}{\mathrm{e}}^{\,j} + \underline{\boldsymbol{e}}^j \underset{\sim}{\mathrm{e}}_j\,) = \tfrac{1}{4}\,\Big(\underline{\boldsymbol{e}}_i \underset{\sim}{\mathrm{e}}^{\,i} \cdot \underline{\boldsymbol{e}}_j \underset{\sim}{\mathrm{e}}^{\,j} + \underline{\boldsymbol{e}}_i \underset{\sim}{\mathrm{e}}^{\,i} \cdot \underline{\boldsymbol{e}}^j \underset{\sim}{\mathrm{e}}_j +$$
$$+\,\underline{\boldsymbol{e}}^i \underset{\sim}{\mathrm{e}}_i \cdot \underline{\boldsymbol{e}}_j \underset{\sim}{\mathrm{e}}^{\,j} + \underline{\boldsymbol{e}}^i \underset{\sim}{\mathrm{e}}_i \cdot \underline{\boldsymbol{e}}^j \underset{\sim}{\mathrm{e}}_j\Big) = \tfrac{1}{4}\,\Big([A_{jk}][S^{jm}]\underline{\boldsymbol{e}}_i \cdot \underline{\boldsymbol{e}}^k \underset{\sim}{\mathrm{e}}^{\,i} \boxtimes \underset{\sim}{\mathrm{e}}_m + \qquad [\text{A1.13}]$$
$$+\delta^j_i \underset{\sim}{\mathrm{e}}^{\,i} \boxtimes \underset{\sim}{\mathrm{e}}_j + \delta^i_j \underset{\sim}{\mathrm{e}}^{\,i} \boxtimes \underset{\sim}{\mathrm{e}}_+ [A^{ik}][S_{im}]\underline{\boldsymbol{e}}_k \cdot \underline{\boldsymbol{e}}^j \underset{\sim}{\mathrm{e}}^{\,m} \boxtimes \underset{\sim}{\mathrm{e}}_j\Big)$$

If $[A^{ik}][S_{kj}] = \delta^i_j$ and $[S^{ik}][A_{kj}] = \delta^i_j$, then

$$\underset{\sim}{\underline{\boldsymbol{I}}} \cdot \underset{\sim}{\underline{\boldsymbol{I}}} = \frac{1}{4}\,\Big([S_{ji}][S^{jm}]\underset{\sim}{\mathrm{e}}^{\,i} \boxtimes \underset{\sim}{\mathrm{e}}_m + [S^{ij}][S_{im}]\underset{\sim}{\mathrm{e}}^{\,m} \boxtimes \underset{\sim}{\mathrm{e}}_j\Big) + \frac{1}{4}\,\Big(\delta^j_i + \delta^i_j\Big)\,\underset{\sim}{\mathrm{e}}^{\,i} \boxtimes \underset{\sim}{\mathrm{e}}_j$$

But since $[A^{ij}]$ and $[S^{ij}]$ are independent metric matrices in different spaces, there is no connection between them; so the unit v-vector can be defined in spaces with equal metric in each point. Under this condition, the following statement is true:

$$\underset{\sim}{\underline{\boldsymbol{I}}} \cdot \underset{\sim}{\underline{\boldsymbol{I}}} = \frac{1}{4}\,4\underset{\approx}{\mathrm{I}} = \underset{\approx}{\mathrm{I}}.$$

For arbitrary tensor space and s-space, the question of the unit v-vector remains open.

A1.6.6.2. *Isomorphism between sub-spaces of s-space and tensor space*

A more interesting case arises when the tensor space and the s-space are of different dimensions, which is, by the way, the case considered in this book: the s-space, which relates to the surface, is 2D and the tensor space is 3D.

Let us consider an isomorphism between an m-dimensional s-space and a sub-space of vector space of dimension $\mathbb{T}^m_1 \subset \mathbb{T}^n_1$, $m < n$. Then there exists a v-vector $\underset{\sim}{\underline{\boldsymbol{S}}} \in {}^m_1\mathbb{S}^n_1$ ensuring a bijective projection from one space to another:

$$\underset{\sim}{\underline{\boldsymbol{S}}}\colon {}^m_1\mathbb{S}^n_1 \to \mathbb{T}^n_1$$

and its inverse $\underset{\sim}{\underline{\boldsymbol{S}}}^{-1} \in {}^m_1\mathbb{S}^n_1$ ensuring the inverse projection:

$$\underset{\sim}{\underline{\boldsymbol{S}}}^{-1}\colon \mathbb{T}^n_1 \to {}^m_1\mathbb{S}^n_1$$

such that:

$$\underset{\sim}{\underline{\boldsymbol{S}}} \cdot \underset{\sim}{\underline{\boldsymbol{S}}}^{-1} = \underset{\approx}{\mathrm{I}}$$

Let us consider a sub-basis $\underline{\boldsymbol{e}}_{i'} \in \mathbb{T}_1^m \subset \mathbb{T}_1^n$, which allows us to express any vector $\underline{\boldsymbol{y}}'$ in this subspace:

$$\underline{\boldsymbol{y}}' = y^{i'} \underline{\boldsymbol{e}}_{i'}$$

then there exists an isomorphism with a bijection function $\underset{\sim}{\underline{\boldsymbol{S}}}$ such that for any $\underset{\sim}{\mathrm{x}} \in {}_1^m\mathbb{S}_0^n$:

$$\underline{\boldsymbol{y}}' = \underset{\sim}{\underline{\boldsymbol{S}}} \circ \underset{\sim}{\mathrm{x}}$$

If such a bijection exists, then the inverse also exists, such that:

$$\underset{\sim}{\mathrm{x}} = \underset{\sim}{\underline{\boldsymbol{S}}}^{-1} \cdot \underline{\boldsymbol{y}}'$$

and

$$\underset{\sim}{\underline{\boldsymbol{S}}} \circ \underset{\sim}{\underline{\boldsymbol{S}}}^{-1} = \underset{\approx}{\mathrm{I}}$$

but obviously

$$\underset{\sim}{\underline{\boldsymbol{S}}} \cdot \underset{\sim}{\underline{\boldsymbol{S}}}^{-1} \neq \underline{\underline{\boldsymbol{I}}}$$

A1.6.7. *Tensor product of v-vectors*

The tensor product of two v-vectors or double tensor product (by analogy with double scalar product) implies that the tensor product is evaluated both between v-scalars and vectors. This product associates a t-tensor for each ordered pair of v-vectors:

$$\{ \overset{\boxtimes}{\otimes} \} : {}^{m}_{1}\mathbb{S}^{n}_{1} \times {}^{m}_{1}\mathbb{S}^{n}_{1} \to {}^{m}_{2}\mathbb{S}^{n}_{2}$$

Let $\underset{\sim}{\underset{\sim}{\boldsymbol{a}}}, \underset{\sim}{\underset{\sim}{\boldsymbol{b}}} \in {}^{m}_{1}\mathbb{S}^{n}_{1}$ and $\underset{\sim}{\underset{\sim}{\underset{\sim}{\boldsymbol{C}}}} \in {}^{m}_{2}\mathbb{S}^{n}_{2}$, then:

$$\underset{\sim}{\underset{\sim}{\boldsymbol{a}}} \overset{\boxtimes}{\otimes} \underset{\sim}{\underset{\sim}{\boldsymbol{b}}} = \underset{\approx}{\underset{\approx}{\underset{\approx}{\boldsymbol{C}}}}$$

This operation can be introduced as:

$$\underset{\sim}{\underset{\sim}{\boldsymbol{a}}} \overset{\boxtimes}{\otimes} \underset{\sim}{\underset{\sim}{\boldsymbol{b}}} = \underline{\boldsymbol{a}}^{(i)} \underline{\boldsymbol{e}}_i \overset{\boxtimes}{\otimes} \underline{\boldsymbol{b}}^{(j)} \underline{\boldsymbol{e}}_j = \underline{\boldsymbol{a}}^{(i)} \otimes \underline{\boldsymbol{b}}^{(j)} \underline{\boldsymbol{e}}_i \boxtimes \underline{\boldsymbol{e}}_j = \underset{\approx}{\underset{\approx}{\underset{\approx}{\boldsymbol{C}}}}$$

To demonstrate that the resulting t-tensor is invariant in s-space, it is sufficient and necessary to show that:

$$\underline{\boldsymbol{a}}^{(i)} \otimes \underline{\boldsymbol{b}}^{(j)} \underline{\boldsymbol{e}}_i \boxtimes \underline{\boldsymbol{e}}_j = \underline{\boldsymbol{a}}_{(i)} \otimes \underline{\boldsymbol{b}}^{(j)} \underline{\boldsymbol{e}}^i \boxtimes \underline{\boldsymbol{e}}_j = \underline{\boldsymbol{a}}^{(i)} \otimes \underline{\boldsymbol{b}}_{(j)} \underline{\boldsymbol{e}}_i \boxtimes \underline{\boldsymbol{e}}^j = \underline{\boldsymbol{a}}_{(i)} \otimes \underline{\boldsymbol{b}}_{(j)} \underline{\boldsymbol{e}}^i \boxtimes \underline{\boldsymbol{e}}^j$$

which according to [A1.6] rewrites:

$$\begin{aligned} & \underline{\boldsymbol{a}}^{(i)} \otimes \underline{\boldsymbol{b}}^{(j)} \underline{\boldsymbol{e}}_i \boxtimes \underline{\boldsymbol{e}}_j = [S_{ik}] \underline{\boldsymbol{a}}^{(k)} \otimes \underline{\boldsymbol{b}}^{(j)} \underline{\boldsymbol{e}}_l \boxtimes \underline{\boldsymbol{e}}_j [S^{il}] = \\ = \quad & [S_{jk}] \underline{\boldsymbol{a}}^{(i)} \otimes \underline{\boldsymbol{b}}^{(k)} \underline{\boldsymbol{e}}_i \boxtimes \underline{\boldsymbol{e}}_l [S^{jl}] = [S_{ik}][S_{jl}] \underline{\boldsymbol{a}}_{(k)} \otimes \underline{\boldsymbol{b}}_{(l)} \underline{\boldsymbol{e}}_p \boxtimes \underline{\boldsymbol{e}}_q [S^{ip}][S^{jq}] \end{aligned} \qquad [A1.14]$$

since $[S_{ik}][S^{kj}] = \delta^j_i$, the invariance of the double tensor product is demonstrated.

A1.7. Reduced form of s-structures

In Chapter 2, we made use of the reduced form of s-structures. The reduced form of s-structure presents a matrix filled with scalars, vectors, and tensors. To define operations between matrices, the transposition operation has to be introduced. If the matrix is filled with tensors of second- and higher order, two transposition operations should be distinguished. Since the matrix is a two index construction, the use of the reduced form of s-structures is *limited* to second-order structures. So, formally, this form is of limited use, see remark 2.5. Here the main rules and forms of reduced s-structures are given.

For two v-vectors $\underset{\sim}{\underline{\boldsymbol{a}}}, \underset{\sim}{\underline{\boldsymbol{b}}} \in {}^{m}_{1}\mathbb{S}^{n}_{1}$, two matrices of vectors $[\underset{\sim}{\underline{\boldsymbol{a}}}]_{\{1\times m\}}, [\underset{\sim}{\underline{\boldsymbol{b}}}]_{\{1\times m\}}$ are defined, then two scalar products are defined as (here and further, the $\sim$ symbol means the equivalence between different representations):

$$\boxed{\alpha = \underset{\sim}{\underline{\boldsymbol{a}}} \overset{\circ}{\cdot} \underset{\sim}{\underline{\boldsymbol{b}}}} \quad \sim$$

$$\alpha = [\underset{\sim}{\underline{\boldsymbol{a}}}]^{\intercal} \cdot [\underset{\sim}{\underline{\boldsymbol{b}}}] \quad \sim \quad \alpha = \underline{\boldsymbol{a}}^{(i)} \cdot \underline{\boldsymbol{b}}^{(i)},\ i = 1, m$$

$$\boxed{\underset{\approx}{\mathrm{A}} = \underset{\sim}{\underline{\boldsymbol{a}}} \overset{\boxtimes}{\cdot} \underset{\sim}{\underline{\boldsymbol{b}}}} \quad \sim$$

$$[\underset{\approx}{\mathrm{A}}] = [\underset{\sim}{\underline{\boldsymbol{a}}}] \cdot [\underset{\sim}{\underline{\boldsymbol{b}}}]^{\intercal} \quad \sim \quad A^{ij} = \underline{\boldsymbol{a}}^{i} \cdot \underline{\boldsymbol{b}}^{j},\ i, j = 1, m$$

Note that an orthonormal basis in s-space is required. Remark also that:

$$[\underset{\sim}{\underline{\boldsymbol{a}}}] \cdot [\underset{\sim}{\underline{\boldsymbol{b}}}]^{\intercal} = \left[[\underset{\sim}{\underline{\boldsymbol{b}}}] \cdot [\underset{\sim}{\underline{\boldsymbol{a}}}]^{\intercal} \right]^{\intercal}$$

For example, t-scalar, v-tensor and t-tensor:

$$\underset{\approx}{\mathrm{D}} \in {}^{m}_{2}\mathbb{S}^{n}_{0}, \quad \underset{\sim\sim}{\underline{\underline{\boldsymbol{C}}}} \in {}^{m}_{1}\mathbb{S}^{n}_{2}, \quad \underset{\approx}{\underline{\underline{\boldsymbol{E}}}} \in {}^{m}_{2}\mathbb{S}^{n}_{2}$$

for which the following matrices are defined:

$$[\underset{\approx}{\mathrm{D}}]_{\{m\times m\}}, [\underset{\sim\sim}{\underline{\underline{\boldsymbol{C}}}}]_{\{1\times m\}}, \quad [\underset{\approx}{\underline{\underline{\boldsymbol{E}}}}]_{\{m\times m\}},$$

then the products with a v-vector can be presented in a reduced form as follows:

$$\boxed{\underset{\sim}{\underline{\boldsymbol{d}}} = \underset{\sim}{\underline{\boldsymbol{a}}} \circ \underset{\approx}{\mathrm{D}}} \quad \sim$$

$$[\underset{\sim}{\underline{\boldsymbol{d}}}] = [\underset{\sim}{\underline{\boldsymbol{a}}}]^{\intercal}[\underset{\approx}{\mathrm{D}}] \quad \sim \quad \underline{\boldsymbol{d}}^j = \underline{\boldsymbol{a}}^i D^{ij},\ i,j = 1,m$$

$$[\underset{\sim}{\underline{\boldsymbol{d}}}] = [\underset{\approx}{\mathrm{D}}]^{\intercal}[\underset{\sim}{\underline{\boldsymbol{a}}}] \quad \sim \quad \underline{\boldsymbol{d}}^j = D^{ji}\underline{\boldsymbol{a}}^i,\ i,j = 1,m$$

$$\boxed{\underset{\sim}{\underline{\boldsymbol{d}}} = \underset{\sim}{\underline{\boldsymbol{a}}} \overset{\circ}{\cdot} \underset{\sim}{\underline{\underline{\boldsymbol{C}}}}} \quad \sim$$

$$\underline{\boldsymbol{d}} = [\underset{\sim}{\underline{\boldsymbol{a}}}]^{\intercal} \cdot [\underset{\sim}{\underline{\underline{\boldsymbol{C}}}}] \quad \sim \quad \underline{\boldsymbol{d}} = \underline{\boldsymbol{a}}^i \cdot \underline{\underline{\boldsymbol{C}}}^i, \quad i = 1,m$$

$$\underline{\boldsymbol{d}} = [\underset{\sim}{\underline{\underline{\boldsymbol{C}}}}^{\intercal}] \cdot [\underset{\sim}{\underline{\boldsymbol{a}}}] \quad \sim \quad \underline{\boldsymbol{d}} = \underline{\underline{\boldsymbol{C}}}^{i\intercal} \cdot \underline{\boldsymbol{a}}^i, \quad i = 1,m$$

$$\boxed{\underset{\sim}{\underline{\boldsymbol{d}}} = \underset{\sim}{\underline{\boldsymbol{a}}} \overset{\circ}{\cdot} \underset{\approx}{\underline{\underline{\boldsymbol{E}}}}} \quad \sim$$

$$[\underset{\sim}{\underline{\boldsymbol{d}}}] = [\underset{\sim}{\underline{\boldsymbol{a}}}]^{\intercal} \cdot [\underset{\approx}{\underline{\underline{\boldsymbol{E}}}}] \quad \sim \quad \underline{\boldsymbol{d}}^j = \underline{\boldsymbol{a}}^i \cdot \underline{\underline{\boldsymbol{E}}}^{ij}, \quad i,j = 1,m$$

$$[\underset{\sim}{\underline{\boldsymbol{d}}}] = [\underset{\approx}{\underline{\underline{\boldsymbol{E}}}}^{\intercal}]^{\intercal} \cdot [\underset{\sim}{\underline{\boldsymbol{a}}}] \quad \sim \quad \underline{\boldsymbol{d}}^j = \underline{\underline{\boldsymbol{E}}}^{\intercal ji} \cdot \underline{\boldsymbol{a}}^i, \quad i,j = 1,m$$

For $\underset{\approx}{\mathrm{A}}, \underset{\approx}{\mathrm{B}}, \underset{\approx}{\mathrm{C}} \in {}_2^m\mathbb{S}_0^n$, the s-dot product in the reduced representation is defined as follows:

$$\boxed{\underset{\approx}{\mathrm{A}} = \underset{\approx}{\mathrm{B}} \circ \underset{\approx}{\mathrm{C}}} \quad \sim$$

$$[\underset{\approx}{\mathrm{A}}] = [\underset{\approx}{\mathrm{B}}][\underset{\approx}{\mathrm{C}}] \quad \sim \quad A^{ij} = B^{ik}C^{kj}$$

For $\underset{\approx}{\underset{\approx}{\boldsymbol{D}}}, \underset{\approx}{\underset{\approx}{\boldsymbol{E}}} \in {}_2^m\mathbb{S}_1^n$, the double dot product is defined as:

$$\boxed{\underset{\approx}{\underset{\approx}{\mathrm{A}}} = \underset{\approx}{\underset{\approx}{\boldsymbol{B}}} \overset{\circ}{\cdot} \underset{\approx}{\underset{\approx}{\boldsymbol{C}}}} \quad \sim$$

$$[\underset{\approx}{\underset{\approx}{\mathrm{A}}}] = [\underset{\approx}{\underset{\approx}{\boldsymbol{B}}}] \cdot [\underset{\approx}{\underset{\approx}{\boldsymbol{C}}}] \quad \sim \quad A^{ij} = \underset{\approx}{\boldsymbol{B}}^{ik} \cdot \underset{\approx}{\boldsymbol{C}}^{kj}$$

And so on for other combinations, for example:

$$\underset{\approx}{\underset{\approx}{\boldsymbol{A}}} \in {}_2^m\mathbb{S}_1^n, \underset{\approx}{\underset{\approx}{\underset{\approx}{\boldsymbol{B}}}} \in {}_2^m\mathbb{S}_2^n, \quad \underset{\approx}{\underset{\approx}{\boldsymbol{A}}} \overset{\circ}{\cdot} \underset{\approx}{\underset{\approx}{\underset{\approx}{\boldsymbol{B}}}} = \underset{\approx}{\underset{\approx}{\boldsymbol{C}}} \in {}_2^m\mathbb{S}_1^n$$

Formally, in the linear algebra, the following operations are forbidden:

$$[\underset{\sim}{\boldsymbol{a}}] \cdot [\underset{\sim}{\boldsymbol{b}}], \quad [\underset{\sim}{\boldsymbol{a}}] \cdot [\underset{\approx}{\underset{\approx}{\boldsymbol{B}}}], \quad [\underset{\approx}{\underset{\approx}{\boldsymbol{B}}}] \cdot [\underset{\sim}{\boldsymbol{a}}]^{\mathsf{T}}$$

but regardless of this restriction, we used them keeping in mind that behind these matrix notations there exist higher order s-structures, see remark 2.5.

Appendix 2

Variations of Geometrical Quantities

A2.1. First-order variations

This appendix summaries the derivations of first- and second-order variations of geometrical quantities, whose final forms are given in section 2.3. The details of the s-structure formalism, that is extensively used here, can be found in Appendix 1.

Remark A2.1. On variations

By variation of a function $f(t, x(t))$ at point $\{t_0, x(t_0)\}$ we mean the following:

$$\delta f(t_0, x(t_0)) = \lim_{\delta t \to 0} \left(f(t_0 + \delta t, x(t_0)) - f(t_0, x(t_0)) \right) = \left. \frac{\partial f}{\partial t} \right|_{t_0} \delta t.$$

The last equality is valid if the function f is at least C^1-smooth by t within a certain neighborhood of the point t_0. In the considered framework, for example, the variation of the projection point $\underline{\boldsymbol{\rho}}$ is given by:

$$\delta \underline{\boldsymbol{\rho}}(t_0) = \lim_{\delta t \to 0} \left(\underline{\boldsymbol{\rho}}(t_0 + \delta t, \underset{\sim}{\xi}(t_0)) - \underline{\boldsymbol{\rho}}(t_0, \underset{\sim}{\xi}(t_0)) \right).$$

For the full variation of a function $f(t, x(t))$ we get:

$$\bar{\delta} f(t_0, x(t_0)) = \lim_{\delta t \to 0} \left(f(t_0 + \delta t, x(t_0 + \delta t)) - f(t_0, x(t_0)) \right)$$

$$= \left. \frac{\partial f}{\partial t} \right|_{t_0} \delta t + \left. \frac{\partial f}{\partial x} \right|_{t_0} \delta x = \delta f + \left. \frac{\partial f}{\partial x} \right|_{t_0} \delta x.$$

The second equality is valid if the function f is at least C^1-smooth by t and x within a certain neighborhood of the point $\{t_0, x(t_0)\}$.

A2.1.1. *Normal projection case*

The slave-point vector is represented by the sum of the projection vector and the normal vector multiplied by the normal gap:

$$\underline{\boldsymbol{r}}_s = \underline{\boldsymbol{\rho}} + g_n \underline{\boldsymbol{n}}. \qquad [A2.1]$$

The full variation of equation [A2.1] gives:

$$\bar{\delta} \underline{\boldsymbol{r}}_s = \bar{\delta} \underline{\boldsymbol{\rho}} + \delta g_n \underline{\boldsymbol{n}} + g_n \bar{\delta} \underline{\boldsymbol{n}}, \qquad [A2.2]$$

where $\bar{\delta}$ denotes a full variation and δ denotes a simple variation (see remark A2.1). It can be shown that $\bar{\delta} g_n = \delta g_n$; for that we have to take a partial derivative of expression [A2.1] with respect to $\underset{\sim}{\xi}$ and take a dot product with $\underline{\boldsymbol{n}}$. Thus, g_n can be considered as one of the independent coordinates of the slave-point in the local master basis (the first two coordinates are given by $\underset{\sim}{\xi}$). Expanding the full variations in [A2.2] gives:

$$\delta \underline{\boldsymbol{r}}_s = \delta \underline{\boldsymbol{\rho}} + \frac{\partial \underline{\boldsymbol{\rho}}}{\partial \underset{\sim}{\xi}}^{\mathsf{T}} \delta \underset{\sim}{\xi} + \delta g_n \underline{\boldsymbol{n}} + g_n \left(\delta \underline{\boldsymbol{n}} + \frac{\partial \underline{\boldsymbol{n}}}{\partial \underset{\sim}{\xi}}^{\mathsf{T}} \delta \underset{\sim}{\xi} \right). \qquad [A2.3]$$

As $\underline{\boldsymbol{r}}_s$ and $\underset{\sim}{\xi}$ and g_n depend only on time, their full variations $\bar{\delta} *$ coincide with their simple variations $\delta *$.

The scalar product of the expression [A2.3] with the normal vector $\underline{\boldsymbol{n}}$ gives directly the first variation of the normal gap g_n:

$$\boxed{\delta g_n = \underline{\boldsymbol{n}} \cdot (\delta \underline{\boldsymbol{r}}_s - \delta \underline{\boldsymbol{\rho}})}, \qquad [A2.4]$$

because

$$\underline{\boldsymbol{n}} \cdot \frac{\partial \underline{\underline{\boldsymbol{\rho}}}}{\partial \underset{\sim}{\xi}} = 0; \quad \underline{\boldsymbol{n}} \cdot \delta \underline{\boldsymbol{n}} = 0 \quad \text{and} \quad \underline{\boldsymbol{n}} \cdot \frac{\partial \underline{\boldsymbol{n}}}{\partial \underset{\sim}{\xi}} = 0. \tag{A2.5}$$

The dot product of equation [A2.3] with the covariant basis v-vector gives:

$$\frac{\partial \underline{\underline{\boldsymbol{\rho}}}}{\partial \underset{\sim}{\xi}} \cdot (\delta \underline{\boldsymbol{r}}_s - \delta \underline{\boldsymbol{\rho}}) = \frac{\partial \underline{\underline{\boldsymbol{\rho}}}}{\partial \underset{\sim}{\xi}} \cdot \frac{\partial \underline{\underline{\boldsymbol{\rho}}}^{\mathsf{T}}}{\partial \underset{\sim}{\xi}} \delta \underset{\sim}{\xi} + g_n \left(\frac{\partial \underline{\underline{\boldsymbol{\rho}}}}{\partial \underset{\sim}{\xi}} \cdot \delta \underline{\boldsymbol{n}} + \frac{\partial \underline{\underline{\boldsymbol{\rho}}}}{\partial \underset{\sim}{\xi}} \cdot \frac{\partial \underline{\boldsymbol{n}}^{\mathsf{T}}}{\partial \underset{\sim}{\xi}} \delta \underset{\sim}{\xi} \right),$$

expressing $\delta \underset{\sim}{\xi}$, we get:

$$\delta \underset{\sim}{\xi} = \left[\frac{\partial \underline{\underline{\boldsymbol{\rho}}}}{\partial \underset{\sim}{\xi}} \cdot \frac{\partial \underline{\underline{\boldsymbol{\rho}}}^{\mathsf{T}}}{\partial \underset{\sim}{\xi}} + g_n \frac{\partial \underline{\underline{\boldsymbol{\rho}}}}{\partial \underset{\sim}{\xi}} \cdot \frac{\partial \underline{\boldsymbol{n}}^{\mathsf{T}}}{\partial \underset{\sim}{\xi}} \right]^{-1} \cdot \left(\frac{\partial \underline{\underline{\boldsymbol{\rho}}}}{\partial \underset{\sim}{\xi}} \cdot (\delta \underline{\boldsymbol{r}}_s - \delta \underline{\boldsymbol{\rho}}) - g_n \frac{\partial \underline{\underline{\boldsymbol{\rho}}}}{\partial \underset{\sim}{\xi}} \cdot \delta \underline{\boldsymbol{n}} \right), \tag{A2.6}$$

where the first term in square brackets is the first fundamental surface metric matrix (t-scalar)

$$\underset{\approx}{\mathrm{A}} = \frac{\partial \underline{\underline{\boldsymbol{\rho}}}}{\partial \underset{\sim}{\xi}} \cdot \frac{\partial \underline{\underline{\boldsymbol{\rho}}}^{\mathsf{T}}}{\partial \underset{\sim}{\xi}} \tag{A2.7}$$

and the second term should be transformed to get rid of the normal vector's derivative[1], so

$$\frac{\partial \underline{\underline{\boldsymbol{\rho}}}}{\partial \underset{\sim}{\xi}} \cdot \underline{\boldsymbol{n}} = 0 \Rightarrow \frac{\partial}{\partial \underset{\sim}{\xi}} \left(\frac{\partial \underline{\underline{\boldsymbol{\rho}}}}{\partial \underset{\sim}{\xi}} \cdot \underline{\boldsymbol{n}} \right) = 0 \Leftrightarrow \frac{\partial \underline{\underline{\boldsymbol{\rho}}}}{\partial \underset{\sim}{\xi}} \cdot \frac{\partial \underline{\boldsymbol{n}}^{\mathsf{T}}}{\partial \underset{\sim}{\xi}} = -\frac{\partial^2 \underline{\underline{\boldsymbol{\rho}}}}{\partial \underset{\sim}{\xi}^2} \cdot \underline{\boldsymbol{n}} \tag{A2.8}$$

which is the second fundamental surface matrix (t-scalar) with minus sign:

$$\underset{\approx}{\mathrm{H}} = \frac{\partial^2 \underline{\underline{\boldsymbol{\rho}}}}{\partial \underset{\sim}{\xi}^2} \cdot \underline{\boldsymbol{n}}. \tag{A2.9}$$

1 We avoid the variation of the normal vector, because in the finite element framework it is hard to express it from the variation of nodal positions. It is more convenient to work with variations of the local basis vectors.

The last term in [A2.6] should also be transformed to avoid the variation of the normal. Similar to [A2.8], we get:

$$\frac{\partial \underline{\boldsymbol{\rho}}}{\partial \underset{\sim}{\xi}} \cdot \underline{\boldsymbol{n}} = 0 \Rightarrow \delta \left(\frac{\partial \underline{\boldsymbol{\rho}}}{\partial \underset{\sim}{\xi}} \cdot \underline{\boldsymbol{n}} \right) = 0 \Leftrightarrow \frac{\partial \underline{\boldsymbol{\rho}}}{\partial \underset{\sim}{\xi}} \cdot \delta \underline{\boldsymbol{n}} = -\delta \frac{\partial \underline{\boldsymbol{\rho}}}{\partial \underset{\sim}{\xi}} \cdot \underline{\boldsymbol{n}}. \qquad [A2.10]$$

Substituting [A2.7], [A2.9] and [A2.10] into [A2.6] gives us the expression for the variation of the local coordinate:

$$\boxed{\delta \underset{\sim}{\xi} = \left[\underset{\approx}{\mathrm{A}} - g_n \underset{\approx}{\mathrm{H}} \right]^{-1} \left(\frac{\partial \underline{\boldsymbol{\rho}}}{\partial \underset{\sim}{\xi}} \cdot (\delta \underline{\boldsymbol{r}}_s - \delta \underline{\boldsymbol{\rho}}) + g_n \underline{\boldsymbol{n}} \cdot \delta \frac{\partial \underline{\boldsymbol{\rho}}}{\partial \underset{\sim}{\xi}} \right)}. \qquad [A2.11]$$

This is the classical expression originally obtained in [LAU 92] and [LAU 93]. Often, the normal gap is assumed to be relatively small and is neglected, which gives a simpler expression:

$$\delta \underset{\sim}{\xi} = \bar{\underset{\approx}{\mathrm{A}}} \frac{\partial \underline{\boldsymbol{\rho}}}{\partial \underset{\sim}{\xi}} \cdot (\delta \underline{\boldsymbol{r}}_s - \delta \underline{\boldsymbol{\rho}}) = \overline{\frac{\partial \underline{\boldsymbol{\rho}}}{\partial \underset{\sim}{\xi}}} \cdot (\delta \underline{\boldsymbol{r}}_s - \delta \underline{\boldsymbol{\rho}}). \qquad [A2.12]$$

Note also that using this form [A2.12] for huge separations/penetrations makes the numerical procedure more stable [WRI 06].

A2.1.2. *Shadow-projection case: infinitely remote emitter*

To obtain derivatives for the shadow-projection and an infinitely remote emitter, we start from the expression connecting the slave-point $\underline{\boldsymbol{r}}_s$ and its shadow-projection $\underline{\boldsymbol{\rho}}$ through the shadow gap g_s and the unit vector $\underline{\boldsymbol{e}}$ pointing to the emitter:

$$\underline{\boldsymbol{r}}_s = \underline{\boldsymbol{\rho}} + g_s \underline{\boldsymbol{e}},$$

the variation of this expression gives:

$$\delta \underline{\boldsymbol{r}}_s = \delta \underline{\boldsymbol{\rho}} + \frac{\partial \underline{\boldsymbol{\rho}}}{\partial \underset{\sim}{\xi}}^{\mathsf{T}} \delta \underset{\sim}{\xi} + \delta g_s \underline{\boldsymbol{e}}. \qquad [A2.13]$$

The scalar product of [A2.13] with the vector $\underline{\boldsymbol{e}}$ yields:

$$\delta g_s = \underline{\boldsymbol{e}} \cdot \left[(\delta \underline{\boldsymbol{r}}_s - \delta \underline{\boldsymbol{\rho}}) - \frac{\partial \underline{\boldsymbol{\rho}}^{\mathsf{T}}}{\partial \underset{\sim}{\xi}} \delta \underset{\sim}{\xi} \right]. \qquad [A2.14]$$

To obtain δg_s we need to evaluate $\delta \underset{\sim}{\xi}$; for that, we take a dot product of [A2.13] with a v-vector containing two orthonormal vectors $\underline{\boldsymbol{s}}_1$ and $\underline{\boldsymbol{s}}_2$ orthogonal to the vector $\underline{\boldsymbol{e}}$:

$$\underset{\sim}{\boldsymbol{s}} = \begin{bmatrix} \underline{\boldsymbol{s}}_1 \\ \underline{\boldsymbol{s}}_2 \end{bmatrix}, \; \underline{\boldsymbol{s}}_1 \cdot \underline{\boldsymbol{s}}_2 = 0, \; \underset{\sim}{\boldsymbol{s}} \cdot \underline{\boldsymbol{e}} = 0$$

$$\underset{\sim}{\boldsymbol{s}} \cdot (\delta \underline{\boldsymbol{r}}_s - \delta \underline{\boldsymbol{\rho}}) = \underset{\sim}{\boldsymbol{s}} \cdot \frac{\partial \underline{\boldsymbol{\rho}}^{\mathsf{T}}}{\partial \underset{\sim}{\xi}} \delta \underset{\sim}{\xi},$$

from which it follows:

$$\delta \underset{\sim}{\xi} = \underset{\approx}{\mathrm{P}} \underset{\sim}{\boldsymbol{s}} \cdot (\delta \underline{\boldsymbol{r}}_s - \delta \underline{\boldsymbol{\rho}}), \qquad [A2.15]$$

with

$$\underset{\approx}{\mathrm{P}} = \left[\underset{\sim}{\boldsymbol{s}} \cdot \frac{\partial \underline{\boldsymbol{\rho}}^{\mathsf{T}}}{\partial \underset{\sim}{\xi}} \right]^{-1}. \qquad [A2.16]$$

It is worth mentioning that expression [A2.15] in comparison with [A2.11] does not contain, at least explicitly, any gap g_n or g_s.

The product $\underset{\approx}{\mathrm{P}} \underset{\sim}{\boldsymbol{s}}$ can be represented in the following form:

$$\underset{\approx}{\mathrm{P}} \underset{\sim}{\boldsymbol{s}} = \overline{\frac{\partial \underline{\boldsymbol{\rho}}}{\partial \underset{\sim}{\xi}}} \cdot \left[\underline{\underline{\boldsymbol{I}}} - \frac{\underline{\boldsymbol{e}} \otimes \underline{\boldsymbol{n}}}{\underline{\boldsymbol{e}} \cdot \underline{\boldsymbol{n}}} \right] \qquad [A2.17]$$

To prove it we express the v-vector $\underset{\sim}{\boldsymbol{s}}$ through the surface basis vectors:

$$\underset{\sim}{\boldsymbol{s}} = \underset{\approx}{\mathrm{a}} \overline{\frac{\partial \underline{\boldsymbol{\rho}}}{\partial \underset{\sim}{\xi}}} + \underset{\sim}{\mathrm{b}} \underline{\boldsymbol{n}} \qquad [A2.18]$$

Dot products of [A2.17] with the contravariant basis v-vector and the normal vector give, respectively:

$$\underset{\approx}{\mathrm{a}} = \underset{\sim}{\boldsymbol{s}} \cdot \frac{\partial \underline{\boldsymbol{\rho}}^{\mathsf{T}}}{\partial \underset{\sim}{\xi}}, \quad \underset{\sim}{\mathrm{b}} = \underset{\sim}{\boldsymbol{s}} \cdot \underline{\boldsymbol{n}}, \tag{A2.19}$$

as

$$\overline{\frac{\partial \underline{\boldsymbol{\rho}}}{\partial \underset{\sim}{\xi}}} \cdot \frac{\partial \underline{\boldsymbol{\rho}}}{\partial \underset{\sim}{\xi}} = \underset{\approx}{\mathrm{I}}, \ \underline{\boldsymbol{n}} \cdot \frac{\partial \underline{\boldsymbol{\rho}}^{\mathsf{T}}}{\partial \underset{\sim}{\xi}} = 0 \ \text{ and } \ \overline{\frac{\partial \underline{\boldsymbol{\rho}}}{\partial \underset{\sim}{\xi}}} \cdot \underline{\boldsymbol{n}} = 0$$

Now equation [A2.16] can be rewritten using [A2.17] and [A2.19]:

$$\underset{\approx}{\mathrm{P}}\, \underset{\sim}{\boldsymbol{s}} = \left[\underset{\sim}{\boldsymbol{s}} \cdot \frac{\partial \underline{\boldsymbol{\rho}}^{\mathsf{T}}}{\partial \underset{\sim}{\xi}} \right]^{-1} \left[\underset{\sim}{\boldsymbol{s}} \cdot \frac{\partial \underline{\boldsymbol{\rho}}^{\mathsf{T}}}{\partial \underset{\sim}{\xi}} \right] \overline{\frac{\partial \underline{\boldsymbol{\rho}}}{\partial \underset{\sim}{\xi}}} + \left[\underset{\sim}{\boldsymbol{s}} \cdot \frac{\partial \underline{\boldsymbol{\rho}}^{\mathsf{T}}}{\partial \underset{\sim}{\xi}} \right]^{-1} \left[\underset{\sim}{\boldsymbol{s}} \cdot \underline{\boldsymbol{n}} \right] \underline{\boldsymbol{n}}, \tag{A2.20}$$

where the first pair of square brackets gives a unit t-scalar $\underset{\approx}{\mathrm{I}}$, and the second pair of square brackets can be replaced by $\underset{\sim}{\mathrm{c}}$:

$$\begin{aligned} &\left(\underset{\sim}{\boldsymbol{s}} \cdot \frac{\partial \underline{\boldsymbol{\rho}}^{\mathsf{T}}}{\partial \underset{\sim}{\xi}} \right)^{-1} (\underset{\sim}{\boldsymbol{s}} \cdot \underline{\boldsymbol{n}}) = \underset{\sim}{\mathrm{c}} \quad \Leftrightarrow \quad \underset{\sim}{\boldsymbol{s}} \cdot \underline{\boldsymbol{n}} = \left(\underset{\sim}{\boldsymbol{s}} \cdot \frac{\partial \underline{\boldsymbol{\rho}}^{\mathsf{T}}}{\partial \underset{\sim}{\xi}} \right) \underset{\sim}{\mathrm{c}} \quad \Leftrightarrow \\ &\Leftrightarrow \quad \underset{\sim}{\boldsymbol{s}} \cdot \left(\underline{\boldsymbol{n}} - \frac{\partial \underline{\boldsymbol{\rho}}^{\mathsf{T}}}{\partial \underset{\sim}{\xi}} \underset{\sim}{\mathrm{c}} \right) = 0 \Leftrightarrow \underline{\boldsymbol{n}} - \frac{\partial \underline{\boldsymbol{\rho}}^{\mathsf{T}}}{\partial \underset{\sim}{\xi}} \underset{\sim}{\mathrm{c}} = \beta \underline{\boldsymbol{e}}, \end{aligned} \tag{A2.21}$$

where β is another coefficient. The left dot product of the last term with the covariant basis v-vector gives the expression for $\underset{\sim}{\mathrm{c}}$:

$$\underset{\sim}{\mathrm{c}} = -\beta \underset{\approx}{\bar{\mathrm{A}}} \frac{\partial \underline{\boldsymbol{\rho}}}{\partial \underset{\sim}{\xi}} \cdot \underline{\boldsymbol{e}} = -\beta \overline{\frac{\partial \underline{\boldsymbol{\rho}}}{\partial \underset{\sim}{\xi}}} \cdot \underline{\boldsymbol{e}}. \tag{A2.22}$$

Substituting [A2.22] in [A2.20] yields:

$$\underset{\approx}{\mathrm{P}}\, \underset{\sim}{\boldsymbol{s}} = \overline{\frac{\partial \underline{\boldsymbol{\rho}}}{\partial \underset{\sim}{\xi}}} - \beta \left(\overline{\frac{\partial \underline{\boldsymbol{\rho}}}{\partial \underset{\sim}{\xi}}} \cdot \underline{\boldsymbol{e}} \right) \underline{\boldsymbol{n}}.$$

Finally, to evaluate the coefficient β, we take the dot product of the latter equation with vector $\underline{\boldsymbol{e}}$:

$$\left(\overline{\frac{\partial \underline{\boldsymbol{\rho}}}{\partial \underset{\sim}{\xi}}} \cdot \underline{\boldsymbol{e}}\right)(1 - \beta \underline{\boldsymbol{n}} \cdot \underline{\boldsymbol{e}}) = 0 \Rightarrow \beta = \frac{1}{\underline{\boldsymbol{n}} \cdot \underline{\boldsymbol{e}}}.$$

So equation [A2.17] is proven. Using the latter equalities, the variation of the surface parameter [A2.15] can be rewritten as:

$$\boxed{\delta \underset{\sim}{\xi} = \overline{\frac{\partial \underline{\boldsymbol{\rho}}}{\partial \underset{\sim}{\xi}}} \cdot \left[\underline{\underline{\boldsymbol{I}}} - \frac{\underline{\boldsymbol{e}} \otimes \underline{\boldsymbol{n}}}{\underline{\boldsymbol{e}} \cdot \underline{\boldsymbol{n}}}\right] \cdot (\delta \underline{\boldsymbol{r}}_s - \delta \underline{\boldsymbol{\rho}})}. \qquad \text{[A2.23]}$$

Remark A2.2. On the special projection operator

In equation [A2.23] $\left[\underline{\underline{\boldsymbol{I}}} - \frac{\underline{\boldsymbol{e}} \otimes \underline{\boldsymbol{n}}}{\underline{\boldsymbol{e}} \cdot \underline{\boldsymbol{n}}}\right]$ *is a special non-symmetric projection operator. The left dot product with a vector* $\underline{\boldsymbol{a}}$ *projects this vector on a plane orthogonal to the normal vector* $\underline{\boldsymbol{n}}$*; the right dot product projects this vector on a plane orthogonal to the pointer vector* $\underline{\boldsymbol{e}}$*, see Figure A2.1. If the vector standing on right hand is collinear to the pointer* $\underline{\boldsymbol{e}}$*, then the projection operator gives zero, if vector standing on left hand is collinear with the normal* $\underline{\boldsymbol{n}}$*, the projection operator also gives zero.*

$$\left[\underline{\underline{\boldsymbol{I}}} - \frac{\underline{\boldsymbol{e}} \otimes \underline{\boldsymbol{n}}}{\underline{\boldsymbol{e}} \cdot \underline{\boldsymbol{n}}}\right] \cdot \underline{\boldsymbol{a}} = \underline{\boldsymbol{b}} \Rightarrow \underline{\boldsymbol{b}} \cdot \underline{\boldsymbol{n}} = 0 \quad \textit{and} \quad \underline{\boldsymbol{a}} \cdot \left[\underline{\underline{\boldsymbol{I}}} - \frac{\underline{\boldsymbol{e}} \otimes \underline{\boldsymbol{n}}}{\underline{\boldsymbol{e}} \cdot \underline{\boldsymbol{n}}}\right] = \underline{\boldsymbol{c}} \Rightarrow \underline{\boldsymbol{c}} \cdot \underline{\boldsymbol{e}} = 0$$

$$\textit{if} \quad \underline{\boldsymbol{a}} = \alpha \underline{\boldsymbol{e}} \quad \textit{then} \quad \left[\underline{\underline{\boldsymbol{I}}} - \frac{\underline{\boldsymbol{e}} \otimes \underline{\boldsymbol{n}}}{\underline{\boldsymbol{e}} \cdot \underline{\boldsymbol{n}}}\right] \cdot \underline{\boldsymbol{a}} = 0$$

$$\textit{if} \quad \underline{\boldsymbol{a}} = \alpha \underline{\boldsymbol{n}} \quad \textit{then} \quad \underline{\boldsymbol{a}} \cdot \left[\underline{\underline{\boldsymbol{I}}} - \frac{\underline{\boldsymbol{e}} \otimes \underline{\boldsymbol{n}}}{\underline{\boldsymbol{e}} \cdot \underline{\boldsymbol{n}}}\right] = 0.$$

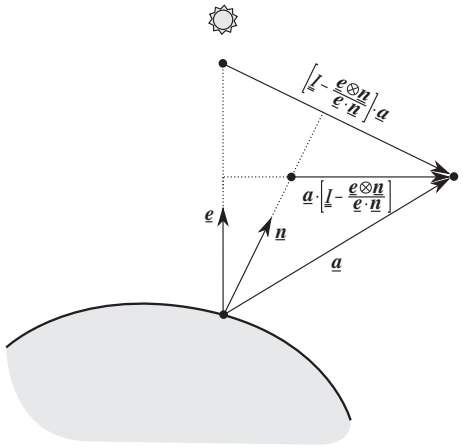

Figure A2.1. *Representation of the projection operator*

Substituting [A2.23] into [A2.14] yields the expression for the shadow gap's variation:

$$\delta g_s = \left\{ \underline{\boldsymbol{e}} - \underline{\boldsymbol{e}} \cdot \left[\frac{\partial \underline{\boldsymbol{\rho}}^{\mathsf{T}}}{\partial \underset{\sim}{\xi}} \otimes \overline{\frac{\partial \underline{\boldsymbol{\rho}}}{\partial \underset{\sim}{\xi}}} \right] \cdot \left(\underline{\underline{\boldsymbol{I}}} - \frac{\underline{\boldsymbol{e}} \otimes \underline{\boldsymbol{n}}}{\underline{\boldsymbol{e}} \cdot \underline{\boldsymbol{n}}} \right) \right\} \cdot (\delta \underline{\boldsymbol{r}}_s - \delta \underline{\boldsymbol{\rho}}). \qquad [A2.24]$$

It can be shown that the term in square brackets is a symmetric projection operator on the basis (tangential) plane:

$$\begin{aligned} &\underline{\boldsymbol{a}} \cdot \left[\frac{\partial \underline{\boldsymbol{\rho}}^{\mathsf{T}}}{\partial \underset{\sim}{\xi}} \otimes \overline{\frac{\partial \underline{\boldsymbol{\rho}}}{\partial \underset{\sim}{\xi}}} \right] = \left[\frac{\partial \underline{\boldsymbol{\rho}}^{\mathsf{T}}}{\partial \underset{\sim}{\xi}} \otimes \overline{\frac{\partial \underline{\boldsymbol{\rho}}}{\partial \underset{\sim}{\xi}}} \right] \cdot \underline{\boldsymbol{a}} = \underline{\boldsymbol{a}} - \underline{\boldsymbol{a}} \cdot \underline{\boldsymbol{n}} \otimes \underline{\boldsymbol{n}} \Leftrightarrow \\ &\left[\overline{\frac{\partial \underline{\boldsymbol{\rho}}}{\partial \underset{\sim}{\xi}}}^{\mathsf{T}} \otimes \frac{\partial \underline{\boldsymbol{\rho}}}{\partial \underset{\sim}{\xi}} \right] = \left[\frac{\partial \underline{\boldsymbol{\rho}}^{\mathsf{T}}}{\partial \underset{\sim}{\xi}} \otimes \overline{\frac{\partial \underline{\boldsymbol{\rho}}}{\partial \underset{\sim}{\xi}}} \right] = \underline{\underline{\boldsymbol{I}}} - \underline{\boldsymbol{n}} \otimes \underline{\boldsymbol{n}}, \end{aligned} \qquad [A2.25]$$

carrying this form, [A2.24] transforms into the final form for the first variation of the shadow gap:

$$\boxed{\delta g_s = \frac{\underline{\boldsymbol{n}}}{\underline{\boldsymbol{n}} \cdot \underline{\boldsymbol{e}}} \cdot (\delta \underline{\boldsymbol{r}}_s - \delta \underline{\boldsymbol{\rho}}).} \qquad [A2.26]$$

A2.1.3. *Shadow-projection case: close emitter*

In case of shadow-projection due to a close emitter, we start from:

$$\underline{\boldsymbol{r}}_s = \underline{\boldsymbol{\rho}} + g_s \underline{\boldsymbol{e}}, \qquad \text{[A2.27]}$$

the difference from the previous case is that vector $\underline{\boldsymbol{e}}$ is not constant and takes the following form:

$$\underline{\boldsymbol{e}} = \frac{\underline{\boldsymbol{r}}_e - \underline{\boldsymbol{r}}_s}{\| \underline{\boldsymbol{r}}_e - \underline{\boldsymbol{r}}_s \|} = \frac{\underline{\boldsymbol{r}}_e - \underline{\boldsymbol{r}}_s}{d_{se}},$$

where $d_{se} = \| \underline{\boldsymbol{r}}_e - \underline{\boldsymbol{r}}_s \|$ is the distance between the slave-point and the emitter; variation of this vector is:

$$\delta \underline{\boldsymbol{e}} = -\delta \underline{\boldsymbol{r}}_s^{\mathrm{S}}, \qquad \text{[A2.28]}$$

where $\delta \underline{\boldsymbol{r}}_s^{\mathrm{S}}$ is a normalized projection of the vector $\delta \underline{\boldsymbol{r}}_s$ on a plane orthogonal to $\underline{\boldsymbol{e}}$:

$$\delta \underline{\boldsymbol{r}}_s{}^S = \left(\underline{\underline{\boldsymbol{I}}} - \underline{\boldsymbol{e}} \otimes \underline{\boldsymbol{e}} \right) \cdot \frac{\delta \underline{\boldsymbol{r}}_s}{d_{se}} = \underset{\sim}{\underline{\boldsymbol{s}}}^{\mathsf{T}} \otimes \underset{\sim}{\underline{\boldsymbol{s}}} \cdot \frac{\delta \underline{\boldsymbol{r}}_s}{d_{se}} = \underset{\sim}{\underline{\boldsymbol{s}}} \overset{\circ}{\otimes} \underset{\sim}{\underline{\boldsymbol{s}}} \cdot \frac{\delta \underline{\boldsymbol{r}}_s}{d_{se}}. \qquad \text{[A2.29]}$$

The variation of [A2.27] gives:

$$\delta \underline{\boldsymbol{r}}_s = \delta \underline{\boldsymbol{\rho}} + \frac{\partial \underline{\boldsymbol{\rho}}^{\mathsf{T}}}{\partial \underset{\sim}{\xi}} \delta \underset{\sim}{\xi} + \delta g_s \underline{\boldsymbol{e}} + g_s \delta \underline{\boldsymbol{e}}. \qquad \text{[A2.30]}$$

As $\delta \underline{\boldsymbol{e}} \cdot \underline{\boldsymbol{e}} = 0$, the dot product of expression [A2.30] with vector $\underline{\boldsymbol{e}}$ gives exactly the same expression as [A2.14]:

$$\delta g_s = \underline{\boldsymbol{e}} \cdot \left[(\delta \underline{\boldsymbol{r}}_s - \delta \underline{\boldsymbol{\rho}}) - \frac{\partial \underline{\boldsymbol{\rho}}^{\mathsf{T}}}{\partial \underset{\sim}{\xi}} \delta \underset{\sim}{\xi} \right], \qquad \text{[A2.31]}$$

the dot product of [A2.30] with v-vector $\underset{\sim}{\underline{\boldsymbol{s}}}$ together with [A2.28] gives:

$$\underset{\sim}{\underline{\boldsymbol{s}}} \cdot \frac{\partial \underline{\boldsymbol{\rho}}^{\mathsf{T}}}{\partial \underset{\sim}{\xi}} \delta \underset{\sim}{\xi} = \underset{\sim}{\underline{\boldsymbol{s}}} \cdot (\delta \underline{\boldsymbol{r}}_s - \delta \underline{\boldsymbol{\rho}}) + g_s \underset{\sim}{\underline{\boldsymbol{s}}} \cdot \delta \underline{\boldsymbol{r}}_s{}^S, \qquad \text{[A2.32]}$$

and carrying that $\underset{\sim}{\boldsymbol{s}} \cdot (\underset{\sim}{\boldsymbol{s}}^{\mathsf{T}} \otimes \underset{\sim}{\boldsymbol{s}}) = \underset{\sim}{\boldsymbol{s}}$ from [A2.16], [A2.17] and [A2.29] we obtain the first variation for the surface parameter:

$$\boxed{\delta\underset{\sim}{\xi} = \overline{\frac{\partial \underline{\boldsymbol{\rho}}}{\partial \underset{\sim}{\xi}}} \cdot \left[\underset{\equiv}{\boldsymbol{I}} - \frac{\underline{\boldsymbol{e}} \otimes \underline{\boldsymbol{n}}}{\underline{\boldsymbol{e}} \cdot \underline{\boldsymbol{n}}}\right] \cdot \left[\left(1 + \frac{g_s}{d_{se}}\right) \delta\underline{\boldsymbol{r}}_s - \delta\underline{\boldsymbol{\rho}}\right]}. \qquad [A2.33]$$

This expression reduces to [A2.23] for a far emitter $d_{se} \gg 1$ or for small gaps $g_s \approx 0$. Substituting the surface parameter variation [A2.33] in [A2.31] gives:

$$\delta g_s = \frac{\underline{\boldsymbol{n}}}{\underline{\boldsymbol{e}} \cdot \underline{\boldsymbol{n}}} \cdot (\delta\underline{\boldsymbol{r}}_s - \delta\underline{\boldsymbol{\rho}}) - \frac{g_s}{d_{se}} \underline{\boldsymbol{e}} \cdot \frac{\partial \underline{\boldsymbol{\rho}}^{\mathsf{T}}}{\partial \underset{\sim}{\xi}} \otimes \overline{\frac{\partial \underline{\boldsymbol{\rho}}}{\partial \underset{\sim}{\xi}}} \cdot \left[\underset{\equiv}{\boldsymbol{I}} - \frac{\underline{\boldsymbol{e}} \otimes \underline{\boldsymbol{n}}}{\underline{\boldsymbol{e}} \cdot \underline{\boldsymbol{n}}}\right] \cdot \delta\underline{\boldsymbol{r}}_s. \qquad [A2.34]$$

And finally, using [A2.25] we obtain the first variation of the shadow gap:

$$\boxed{\delta g_s = \frac{\underline{\boldsymbol{n}}}{\underline{\boldsymbol{e}} \cdot \underline{\boldsymbol{n}}} \cdot \left[\left(1 + \frac{g_s}{d_{se}}\right) \delta\underline{\boldsymbol{r}}_s - \delta\underline{\boldsymbol{\rho}}\right] - \frac{g_s}{d_{se}} \underline{\boldsymbol{e}} \cdot \delta\underline{\boldsymbol{r}}_s}. \qquad [A2.35]$$

Assuming small gaps $g_s \approx 0$ or a far emitter $d_{se} \gg 1$ results in the expression obtained for an infinitely remote emitter [A2.26].

A2.2. Second-order variations

A2.2.1. *Normal projection case*

To get second-order variations ($\Delta\delta g_n$ and $\Delta\delta\underset{\sim}{\xi}$), we start by taking the full second variation $\bar{\Delta}$ of [A2.3]:

$$\begin{aligned} \bar{\Delta}\delta\underline{\boldsymbol{r}}_s \quad &= \Delta\delta\underline{\boldsymbol{r}}_s = \Delta\delta\underline{\boldsymbol{\rho}} + \delta\frac{\partial \underline{\boldsymbol{\rho}}^{\mathsf{T}}}{\partial \underset{\sim}{\xi}} \Delta\underset{\sim}{\xi} + \Delta\frac{\partial \underline{\boldsymbol{\rho}}^{\mathsf{T}}}{\partial \underset{\sim}{\xi}} \delta\underset{\sim}{\xi} + \Delta\underset{\sim}{\xi}^{\mathsf{T}} \frac{\partial^2 \underline{\boldsymbol{\rho}}}{\partial \underset{\sim}{\xi}^2} \delta\underset{\sim}{\xi} \\ &+ \underline{\frac{\partial \underline{\boldsymbol{\rho}}^{\mathsf{T}}}{\partial \underset{\sim}{\xi}} \Delta\delta\underset{\sim}{\xi}} + \underline{\underline{\Delta\delta g_n \underline{\boldsymbol{n}}}} + \underline{\delta g_n \bar{\Delta}\underline{\boldsymbol{n}}} + \underline{\Delta g_n \bar{\delta}\underline{\boldsymbol{n}}} + g_n \bar{\Delta}\bar{\delta}\underline{\boldsymbol{n}}. \end{aligned} \qquad [A2.36]$$

The first term is zero by default, because $\underline{\boldsymbol{r}}_s = \underline{\boldsymbol{r}}_s(t) \Rightarrow \Delta\delta\underline{\boldsymbol{r}}_s = 0$; it can also be shown that the second term is zero ($\Delta\delta\underline{\boldsymbol{\rho}} = 0$); but a rather similar term $\Delta\delta\underline{\boldsymbol{n}} \neq 0$. The underlined terms in [A2.36] are orthogonal to the normal vector; the double-underlined term is orthogonal to the tangential plane of the surface basis.

In a dot product of equation [A2.36] with the normal vector, the underlined terms vanish:

$$\Delta\delta g_n = -\underline{\boldsymbol{n}} \cdot \delta\frac{\partial \underline{\boldsymbol{\rho}}^{\mathsf{T}}}{\partial \underset{\sim}{\xi}} \Delta\underset{\sim}{\xi} - \underline{\boldsymbol{n}} \cdot \Delta\frac{\partial \underline{\boldsymbol{\rho}}^{\mathsf{T}}}{\partial \underset{\sim}{\xi}} \delta\underset{\sim}{\xi} - \Delta\underset{\sim}{\xi}^{\mathsf{T}}\underline{\boldsymbol{n}} \cdot \frac{\partial^2 \underline{\boldsymbol{\rho}}}{\partial \underset{\sim}{\xi}^2}\delta\underset{\sim}{\xi} - g_n\underline{\boldsymbol{n}} \cdot \bar{\Delta}\bar{\delta}\underline{\boldsymbol{n}}, \quad \text{[A2.37]}$$

where the third term in the right-hand part contains the second fundamental surface matrix (t-scalar):

$$\underline{\boldsymbol{n}} \cdot \frac{\partial^2 \underline{\boldsymbol{\rho}}}{\partial \underset{\sim}{\xi}^2} = \underset{\approx}{\mathrm{H}}, \quad \text{[A2.38]}$$

and the last term can be expanded as:

$$-\underline{\boldsymbol{n}} \cdot \bar{\Delta}\bar{\delta}\underline{\boldsymbol{n}} = \bar{\Delta}\underline{\boldsymbol{n}} \cdot \bar{\delta}\underline{\boldsymbol{n}}, \quad \text{[A2.39]}$$

because

$$\underline{\boldsymbol{n}} \cdot \bar{\delta}\underline{\boldsymbol{n}} = 0 \Rightarrow \bar{\Delta}(\underline{\boldsymbol{n}} \cdot \bar{\delta}\underline{\boldsymbol{n}}) = 0 \Leftrightarrow -\underline{\boldsymbol{n}} \cdot \bar{\Delta}\bar{\delta}\underline{\boldsymbol{n}} = \bar{\Delta}\underline{\boldsymbol{n}} \cdot \bar{\delta}\underline{\boldsymbol{n}}.$$

A derivative of a unit vector is orthogonal to the vector itself. It means that the derivative of the normal vector is a combination of in-plane basis vectors, so it can be written in the following form:

$$\frac{\partial \underline{\boldsymbol{n}}}{\partial \underset{\sim}{\xi}} = \underset{\approx}{\mathrm{B}}\frac{\partial \underline{\boldsymbol{\rho}}}{\partial \underset{\sim}{\xi}}. \quad \text{[A2.40]}$$

The right dot product with the transposed basis v-vector gives:

$$\frac{\partial \underline{\boldsymbol{n}}}{\partial \underset{\sim}{\xi}} \cdot \frac{\partial \underline{\boldsymbol{\rho}}^{\mathsf{T}}}{\partial \underset{\sim}{\xi}} = \underset{\approx}{\mathrm{B}}\frac{\partial \underline{\boldsymbol{\rho}}}{\partial \underset{\sim}{\xi}} \cdot \frac{\partial \underline{\boldsymbol{\rho}}^{\mathsf{T}}}{\partial \underset{\sim}{\xi}} = \underset{\approx}{\mathrm{B}}\,\underset{\approx}{\mathrm{A}}, \quad \text{[A2.41]}$$

where the last term is a product of the t-scalar $\underset{\approx}{\mathrm{B}}$ with the first fundamental surface metric matrix $\underset{\approx}{\mathrm{A}}$ and the first term can be transformed as:

$$\underline{\boldsymbol{n}} \cdot \frac{\partial \underline{\boldsymbol{\rho}}}{\partial \underset{\sim}{\xi}} = 0 \Rightarrow \frac{\partial}{\partial \underset{\sim}{\xi}}\left(\underline{\boldsymbol{n}} \cdot \frac{\partial \underline{\boldsymbol{\rho}}}{\partial \underset{\sim}{\xi}}\right) = 0 \Leftrightarrow \frac{\partial \underline{\boldsymbol{n}}}{\partial \underset{\sim}{\xi}} \cdot \frac{\partial \underline{\boldsymbol{\rho}}^{\mathsf{T}}}{\partial \underset{\sim}{\xi}} = -\underline{\boldsymbol{n}} \cdot \frac{\partial^2 \underline{\boldsymbol{\rho}}}{\partial \underset{\sim}{\xi}^2} = -\underset{\approx}{\mathrm{H}}, \quad \text{[A2.42]}$$

which is nothing but the second fundamental surface matrix. From [A2.41] and [A2.42] it follows that:

$$\underset{\approx}{\mathrm{B}} = -\underset{\approx}{\mathrm{H}}\,\underset{\approx}{\mathrm{A}}^{-1} = -\underset{\approx}{\mathrm{H}}\,\underset{\approx}{\bar{\mathrm{A}}},$$

substituting this expression into [A2.40] yields:

$$\frac{\partial \underline{\boldsymbol{n}}}{\partial \underset{\sim}{\xi}} = -\underset{\approx}{\mathrm{H}}\,\underset{\approx}{\bar{\mathrm{A}}}\,\frac{\partial \underline{\boldsymbol{\rho}}}{\partial \underset{\sim}{\xi}} \quad \Rightarrow \quad \frac{\partial \underline{\boldsymbol{n}}}{\partial \underset{\sim}{\xi}} = -\underset{\approx}{\mathrm{H}}\,\overline{\frac{\partial \underline{\boldsymbol{\rho}}}{\partial \underset{\sim}{\xi}}}. \qquad [A2.43]$$

The same procedure can be carried out for the variation of the normal vector:

$$\left\{\begin{array}{l} \delta\underline{\boldsymbol{n}} = \underset{\sim}{\mathrm{b}}^{\mathsf{T}}\,\overline{\frac{\partial \underline{\boldsymbol{\rho}}}{\partial \underset{\sim}{\xi}}} \Rightarrow \delta\underline{\boldsymbol{n}} \cdot \overline{\frac{\partial \underline{\boldsymbol{\rho}}^{\mathsf{T}}}{\partial \underset{\sim}{\xi}}} = \underset{\sim}{\mathrm{b}}^{\mathsf{T}}\,\underset{\approx}{\mathrm{A}} = \underset{\approx}{\mathrm{A}}\,\underset{\sim}{\mathrm{b}} \\ \delta\left(\underline{\boldsymbol{n}} \cdot \overline{\frac{\partial \underline{\boldsymbol{\rho}}}{\partial \underset{\sim}{\xi}}}\right) = 0 \Leftrightarrow \delta\underline{\boldsymbol{n}} \cdot \overline{\frac{\partial \underline{\boldsymbol{\rho}}}{\partial \underset{\sim}{\xi}}} = -\underline{\boldsymbol{n}} \cdot \delta\overline{\frac{\partial \underline{\boldsymbol{\rho}}}{\partial \underset{\sim}{\xi}}} \end{array}\right. \Rightarrow$$
$$\Rightarrow \underset{\sim}{\mathrm{b}} = -\underset{\approx}{\bar{\mathrm{A}}}\left(\underline{\boldsymbol{n}} \cdot \delta\overline{\frac{\partial \underline{\boldsymbol{\rho}}}{\partial \underset{\sim}{\xi}}}\right) \Leftrightarrow \delta\underline{\boldsymbol{n}} = -\left(\underline{\boldsymbol{n}} \cdot \delta\overline{\frac{\partial \underline{\boldsymbol{\rho}}}{\partial \underset{\sim}{\xi}}}\right)^{\mathsf{T}} \overline{\frac{\partial \underline{\boldsymbol{\rho}}}{\partial \underset{\sim}{\xi}}}. \qquad [A2.44]$$

Finally,

$$\delta\underline{\boldsymbol{n}} = -\left(\underline{\boldsymbol{n}} \cdot \delta\frac{\partial \underline{\boldsymbol{\rho}}}{\partial \underset{\sim}{\xi}}\right)^{\mathsf{T}} \overline{\frac{\partial \underline{\boldsymbol{\rho}}}{\partial \underset{\sim}{\xi}}} \quad \text{and} \quad \bar{\delta}\underline{\boldsymbol{n}} = -\left(\underline{\boldsymbol{n}} \cdot \bar{\delta}\frac{\partial \underline{\boldsymbol{\rho}}}{\partial \underset{\sim}{\xi}}\right)^{\mathsf{T}} \overline{\frac{\partial \underline{\boldsymbol{\rho}}}{\partial \underset{\sim}{\xi}}}. \qquad [A2.45]$$

According to equation [A2.45], we can transform [A2.39]:

$$\bar{\Delta}\underline{\boldsymbol{n}} \cdot \bar{\delta}\underline{\boldsymbol{n}} = \left(\underline{\boldsymbol{n}} \cdot \bar{\Delta}\frac{\partial \underline{\boldsymbol{\rho}}}{\partial \underset{\sim}{\xi}}\right)^{\mathsf{T}} \overline{\frac{\partial \underline{\boldsymbol{\rho}}}{\partial \underset{\sim}{\xi}}} \cdot \overline{\frac{\partial \underline{\boldsymbol{\rho}}}{\partial \underset{\sim}{\xi}}}^{\mathsf{T}} \left(\underline{\boldsymbol{n}} \cdot \bar{\delta}\frac{\partial \underline{\boldsymbol{\rho}}}{\partial \underset{\sim}{\xi}}\right) = \left(\underline{\boldsymbol{n}} \cdot \bar{\Delta}\frac{\partial \underline{\boldsymbol{\rho}}}{\partial \underset{\sim}{\xi}}\right)^{\mathsf{T}} \underset{\approx}{\bar{\mathrm{A}}} \left(\underline{\boldsymbol{n}} \cdot \bar{\delta}\frac{\partial \underline{\boldsymbol{\rho}}}{\partial \underset{\sim}{\xi}}\right),$$

Expanding the full variations and using [A2.38] results in

$$\begin{aligned} \bar{\Delta}\underline{\boldsymbol{n}} \cdot \bar{\delta}\underline{\boldsymbol{n}} &= \left(\underline{\boldsymbol{n}} \cdot \Delta\frac{\partial \underline{\boldsymbol{\rho}}}{\partial \underset{\sim}{\xi}} + \underset{\approx}{\mathrm{H}}\,\Delta\underset{\sim}{\xi}\right)^{\mathsf{T}} \underset{\approx}{\bar{\mathrm{A}}} \left(\underline{\boldsymbol{n}} \cdot \delta\frac{\partial \underline{\boldsymbol{\rho}}}{\partial \underset{\sim}{\xi}} + \underset{\approx}{\mathrm{H}}\,\delta\underset{\sim}{\xi}\right) \\ &= \Delta\underset{\sim}{\xi}^{\mathsf{T}}\,\underset{\approx}{\mathrm{H}}\,\underset{\approx}{\bar{\mathrm{A}}}\,\underset{\approx}{\mathrm{H}}\,\delta\underset{\sim}{\xi} + \left(\underline{\boldsymbol{n}} \cdot \Delta\frac{\partial \underline{\boldsymbol{\rho}}}{\partial \underset{\sim}{\xi}}\right)^{\mathsf{T}} \underset{\approx}{\bar{\mathrm{A}}}\,\underset{\approx}{\mathrm{H}}\,\delta\underset{\sim}{\xi} + \Delta\underset{\sim}{\xi}^{\mathsf{T}}\,\underset{\approx}{\mathrm{H}}\,\underset{\approx}{\bar{\mathrm{A}}} \left(\underline{\boldsymbol{n}} \cdot \delta\frac{\partial \underline{\boldsymbol{\rho}}}{\partial \underset{\sim}{\xi}}\right) \qquad [A2.46] \\ &+ \left(\underline{\boldsymbol{n}} \cdot \Delta\frac{\partial \underline{\boldsymbol{\rho}}}{\partial \underset{\sim}{\xi}}\right)^{\mathsf{T}} \underset{\approx}{\bar{\mathrm{A}}} \left(\underline{\boldsymbol{n}} \cdot \delta\frac{\partial \underline{\boldsymbol{\rho}}}{\partial \underset{\sim}{\xi}}\right). \end{aligned}$$

Substituting [A2.38], [A2.39] and the contracted form of [A2.46] in [A2.37] gives the second variation of the normal gap:

$$\boxed{\begin{aligned}\Delta\delta g_n = \quad & -\underline{\boldsymbol{n}}\cdot\left(\delta\frac{\partial\underline{\boldsymbol{\rho}}^{\intercal}}{\partial\underset{\sim}{\xi}}\Delta\underset{\sim}{\xi}+\Delta\frac{\partial\underline{\boldsymbol{\rho}}^{\intercal}}{\partial\underset{\sim}{\xi}}\delta\underset{\sim}{\xi}\right)-\Delta\underset{\sim}{\xi}^{\intercal}\underset{\approx}{\mathrm{H}}\,\delta\underset{\sim}{\xi}\\ & +g_n\left(\Delta\underset{\sim}{\xi}^{\intercal}\underset{\approx}{\mathrm{H}}+\underline{\boldsymbol{n}}\cdot\Delta\frac{\partial\underline{\boldsymbol{\rho}}^{\intercal}}{\partial\underset{\sim}{\xi}}\right)\underset{\approx}{\bar{\mathrm{A}}}\left(\underline{\boldsymbol{n}}\cdot\delta\frac{\partial\underline{\boldsymbol{\rho}}}{\partial\underset{\sim}{\xi}}+\underset{\approx}{\mathrm{H}}\,\delta\underset{\sim}{\xi}\right)\end{aligned}}\quad\text{[A2.47]}$$

The same form has been obtained in [LAU 92]. If we assume a small gap $g_n \approx 0$, we get a simpler expression:

$$\Delta\delta g_n = -\underline{\boldsymbol{n}}\cdot\left(\delta\frac{\partial\underline{\boldsymbol{\rho}}^{\intercal}}{\partial\underset{\sim}{\xi}}\Delta\underset{\sim}{\xi}+\Delta\frac{\partial\underline{\boldsymbol{\rho}}^{\intercal}}{\partial\underset{\sim}{\xi}}\delta\underset{\sim}{\xi}\right)-\Delta\underset{\sim}{\xi}^{\intercal}\underset{\approx}{\mathrm{H}}\,\delta\underset{\sim}{\xi}. \qquad \text{[A2.48]}$$

To derive the second variation of the surface parameter $\Delta\delta\underset{\sim}{\xi}$, we compute the dot product of [A2.36] with the surface basis v-vector; only the term underlined twice in [A2.36] vanishes:

$$\begin{aligned}0 = & \frac{\partial\underline{\boldsymbol{\rho}}}{\partial\underset{\sim}{\xi}}\cdot\delta\frac{\partial\underline{\boldsymbol{\rho}}^{\intercal}}{\partial\underset{\sim}{\xi}}\Delta\underset{\sim}{\xi}+\frac{\partial\underline{\boldsymbol{\rho}}}{\partial\underset{\sim}{\xi}}\cdot\Delta\frac{\partial\underline{\boldsymbol{\rho}}^{\intercal}}{\partial\underset{\sim}{\xi}}\delta\underset{\sim}{\xi}+\Delta\underset{\sim}{\xi}^{\intercal}\boxed{\frac{\partial\underline{\boldsymbol{\rho}}}{\partial\underset{\sim}{\xi}}\cdot\frac{\partial^2\underline{\boldsymbol{\rho}}}{\partial\underset{\sim}{\xi}^2}}^{*}\delta\underset{\sim}{\xi}\\ & +\frac{\partial\underline{\boldsymbol{\rho}}}{\partial\underset{\sim}{\xi}}\cdot\frac{\partial\underline{\boldsymbol{\rho}}^{\intercal}}{\partial\underset{\sim}{\xi}}\Delta\delta\underset{\sim}{\xi}+\delta g_n\frac{\partial\underline{\boldsymbol{\rho}}}{\partial\underset{\sim}{\xi}}\cdot\bar{\Delta}\underline{\boldsymbol{n}}+\Delta g_n\frac{\partial\underline{\boldsymbol{\rho}}}{\partial\underset{\sim}{\xi}}\cdot\bar{\delta}\underline{\boldsymbol{n}}+g_n\frac{\partial\underline{\boldsymbol{\rho}}}{\partial\underset{\sim}{\xi}}\cdot\bar{\Delta}\bar{\delta}\underline{\boldsymbol{n}}.\end{aligned}\qquad\text{[A2.49]}$$

Remark A2.3. On simplified form of s-structures

As we can see, the boxed term in equation [A2.49] *is strange from the point of view of linear algebra, since the product of non-consistent matrices and vectors is forbidden. Formally, in linear algebra, we can choose between two possibilities:*

$$\frac{\partial\underline{\boldsymbol{\rho}}^{\intercal}}{\partial\underset{\sim}{\xi}}\cdot\frac{\partial^2\underline{\boldsymbol{\rho}}}{\partial\underset{\sim}{\xi}^2}=\underset{\sim}{\bullet}^{\intercal}\quad\textit{or}\quad\frac{\partial^2\underline{\boldsymbol{\rho}}}{\partial\underset{\sim}{\xi}^2}\cdot\frac{\partial\underline{\boldsymbol{\rho}}}{\partial\underset{\sim}{\xi}}=\underset{\sim}{\bullet}.$$

Here, contrary to the rules of linear algebra, this product will imply the third-order t-scalar $2 \times 2 \times 2$

$$\frac{\partial^2 \underset{\sim}{\boldsymbol{\rho}}}{\partial \underset{\sim}{\xi}^2} \cdot \frac{\partial \underset{\sim}{\boldsymbol{\rho}}^{\mathsf{T}}}{\partial \underset{\sim}{\xi}} = \overset{3}{\underset{\approx}{\bullet}} \quad \textit{and} \quad \frac{\partial \underset{\sim}{\boldsymbol{\rho}}}{\partial \underset{\sim}{\xi}} \cdot \frac{\partial^2 \underset{\sim}{\boldsymbol{\rho}}}{\partial \underset{\sim}{\xi}^2} = \overset{3}{\underset{\approx}{\bullet}}. \qquad (*)$$

This non-consistency appears due to the fact that reduced s-structures, which are used here for simplicity, do not allow us to pass to higher order s-structures.

The apparatus developed for full s-structures (see Appendix 1) is consistent and rigorous, but notions are more complicated. So in this chapter, the reduced form of s-structures is used and it will be simply supposed that operations $(*)$ *are permitted.*

Let us consider the last term in [A2.49]:

$$\frac{\partial \underset{\sim}{\boldsymbol{\rho}}}{\partial \underset{\sim}{\xi}} \cdot \bar{\Delta}\bar{\delta}\underline{\boldsymbol{n}},$$

it can be expressed by taking the second variation of the expression:

$$\begin{aligned}
&\frac{\partial \underset{\sim}{\boldsymbol{\rho}}}{\partial \underset{\sim}{\xi}} \cdot \underline{\boldsymbol{n}} = 0 \Rightarrow \bar{\Delta}\bar{\delta}\left(\frac{\partial \underset{\sim}{\boldsymbol{\rho}}}{\partial \underset{\sim}{\xi}} \cdot \underline{\boldsymbol{n}}\right) = 0 \quad \Leftrightarrow \bar{\Delta}\left(\bar{\delta}\frac{\partial \underset{\sim}{\boldsymbol{\rho}}}{\partial \underset{\sim}{\xi}} \cdot \underline{\boldsymbol{n}} + \frac{\partial \underset{\sim}{\boldsymbol{\rho}}}{\partial \underset{\sim}{\xi}} \cdot \bar{\delta}\underline{\boldsymbol{n}}\right) = 0 \quad \Leftrightarrow \\
&\bar{\Delta}\bar{\delta}\frac{\partial \underset{\sim}{\boldsymbol{\rho}}}{\partial \underset{\sim}{\xi}} \cdot \underline{\boldsymbol{n}} + \bar{\delta}\frac{\partial \underset{\sim}{\boldsymbol{\rho}}}{\partial \underset{\sim}{\xi}} \cdot \bar{\Delta}\underline{\boldsymbol{n}} + \bar{\Delta}\frac{\partial \underset{\sim}{\boldsymbol{\rho}}}{\partial \underset{\sim}{\xi}} \cdot \bar{\delta}\underline{\boldsymbol{n}} + \frac{\partial \underset{\sim}{\boldsymbol{\rho}}}{\partial \underset{\sim}{\xi}} \cdot \bar{\Delta}\bar{\delta}\underline{\boldsymbol{n}} = 0 \quad \Leftrightarrow \qquad [A2.50] \\
&\frac{\partial \underset{\sim}{\boldsymbol{\rho}}}{\partial \underset{\sim}{\xi}} \cdot \bar{\Delta}\bar{\delta}\underline{\boldsymbol{n}} = -\bar{\Delta}\bar{\delta}\frac{\partial \underset{\sim}{\boldsymbol{\rho}}}{\partial \underset{\sim}{\xi}} \cdot \underline{\boldsymbol{n}} - \bar{\delta}\frac{\partial \underset{\sim}{\boldsymbol{\rho}}}{\partial \underset{\sim}{\xi}} \cdot \bar{\Delta}\underline{\boldsymbol{n}} - \bar{\Delta}\frac{\partial \underset{\sim}{\boldsymbol{\rho}}}{\partial \underset{\sim}{\xi}} \cdot \bar{\delta}\underline{\boldsymbol{n}}.
\end{aligned}$$

The variations of the normal vector have to be avoided; so they are replaced by [A2.45] which yields:

$$\frac{\partial \underset{\sim}{\boldsymbol{\rho}}}{\partial \underset{\sim}{\xi}} \cdot \bar{\Delta}\bar{\delta}\underline{\boldsymbol{n}} = -\bar{\Delta}\bar{\delta}\frac{\partial \underset{\sim}{\boldsymbol{\rho}}}{\partial \underset{\sim}{\xi}} \cdot \underline{\boldsymbol{n}} + \bar{\delta}\frac{\partial \underset{\sim}{\boldsymbol{\rho}}}{\partial \underset{\sim}{\xi}} \cdot \overline{\frac{\partial \underset{\sim}{\boldsymbol{\rho}}}{\partial \underset{\sim}{\xi}}}^{\mathsf{T}} \left(\underline{\boldsymbol{n}} \cdot \bar{\Delta}\frac{\partial \underset{\sim}{\boldsymbol{\rho}}}{\partial \underset{\sim}{\xi}}\right) + \bar{\Delta}\frac{\partial \underset{\sim}{\boldsymbol{\rho}}}{\partial \underset{\sim}{\xi}} \cdot \overline{\frac{\partial \underset{\sim}{\boldsymbol{\rho}}}{\partial \underset{\sim}{\xi}}}^{\mathsf{T}} \left(\underline{\boldsymbol{n}} \cdot \bar{\delta}\frac{\partial \underset{\sim}{\boldsymbol{\rho}}}{\partial \underset{\sim}{\xi}}\right). \qquad [A2.51]$$

The next two terms in equation [A2.49] contain variations of the normal vector that also have to be replaced:

$$\frac{\partial \underset{\sim}{\boldsymbol{\rho}}}{\partial \underset{\sim}{\xi}} \cdot \underline{\boldsymbol{n}} = 0 \Rightarrow \bar{\delta}\left(\frac{\partial \underset{\sim}{\boldsymbol{\rho}}}{\partial \underset{\sim}{\xi}} \cdot \underline{\boldsymbol{n}}\right) = 0 \Leftrightarrow \frac{\partial \underset{\sim}{\boldsymbol{\rho}}}{\partial \underset{\sim}{\xi}} \cdot \bar{\delta}\underline{\boldsymbol{n}} = -\underline{\boldsymbol{n}} \cdot \bar{\delta}\frac{\partial \underset{\sim}{\boldsymbol{\rho}}}{\partial \underset{\sim}{\xi}}. \qquad [A2.52]$$

Substituting [A2.51], [A2.52] in [A2.49] and replacing its fourth term by the first fundamental metric matrix gives:

$$\begin{aligned} 0 \quad &= \frac{\partial \underline{\boldsymbol{\rho}}}{\partial \underset{\sim}{\xi}} \cdot \delta \frac{\partial \underline{\boldsymbol{\rho}}^{\mathsf{T}}}{\partial \underset{\sim}{\xi}} \Delta \underset{\sim}{\xi} + \frac{\partial \underline{\boldsymbol{\rho}}}{\partial \underset{\sim}{\xi}} \cdot \Delta \frac{\partial \underline{\boldsymbol{\rho}}^{\mathsf{T}}}{\partial \underset{\sim}{\xi}} \delta \underset{\sim}{\xi} + \Delta \underset{\sim}{\xi}^{\mathsf{T}} \frac{\partial \underline{\boldsymbol{\rho}}}{\partial \underset{\sim}{\xi}} \cdot \frac{\partial^2 \underline{\boldsymbol{\rho}}}{\partial \underset{\sim}{\xi}^2} \delta \underset{\sim}{\xi} + \underset{\approx}{\mathrm{A}} \Delta \delta \underset{\sim}{\xi} \\ &- \delta g_n \underline{\boldsymbol{n}} \cdot \bar{\Delta} \frac{\partial \underline{\boldsymbol{\rho}}}{\partial \underset{\sim}{\xi}} - \Delta g_n \underline{\boldsymbol{n}} \cdot \bar{\delta} \frac{\partial \underline{\boldsymbol{\rho}}}{\partial \underset{\sim}{\xi}} - g_n \boxed{\bar{\Delta} \bar{\delta} \frac{\partial \underline{\boldsymbol{\rho}}}{\partial \underset{\sim}{\xi}} \cdot \underline{\boldsymbol{n}}} \\ &+ g_n \bar{\delta} \frac{\partial \underline{\boldsymbol{\rho}}}{\partial \underset{\sim}{\xi}} \cdot \overline{\frac{\partial \underline{\boldsymbol{\rho}}}{\partial \underset{\sim}{\xi}}}^{\mathsf{T}} \left(\underline{\boldsymbol{n}} \cdot \bar{\Delta} \frac{\partial \underline{\boldsymbol{\rho}}}{\partial \underset{\sim}{\xi}} \right) + g_n \bar{\Delta} \frac{\partial \underline{\boldsymbol{\rho}}}{\partial \underset{\sim}{\xi}} \cdot \overline{\frac{\partial \underline{\boldsymbol{\rho}}}{\partial \underset{\sim}{\xi}}}^{\mathsf{T}} \left(\underline{\boldsymbol{n}} \cdot \bar{\delta} \frac{\partial \underline{\boldsymbol{\rho}}}{\partial \underset{\sim}{\xi}} \right). \end{aligned} \qquad \text{[A2.53]}$$

Expanding the boxed term and carrying that

$$\Delta \delta \underline{\boldsymbol{\rho}} = 0 \Rightarrow \Delta \delta \frac{\partial \underline{\boldsymbol{\rho}}}{\partial \underset{\sim}{\xi}} = 0$$

gives:

$$\bar{\Delta} \bar{\delta} \frac{\partial \underline{\boldsymbol{\rho}}}{\partial \underset{\sim}{\xi}} \cdot \underline{\boldsymbol{n}} = \underline{\boldsymbol{n}} \cdot \delta \frac{\partial^2 \underline{\boldsymbol{\rho}}}{\partial \underset{\sim}{\xi}^2} \Delta \underset{\sim}{\xi} + \left(\underline{\boldsymbol{n}} \cdot \Delta \frac{\partial^2 \underline{\boldsymbol{\rho}}}{\partial \underset{\sim}{\xi}^2} + \Delta \underset{\sim}{\xi}^{\mathsf{T}} \underline{\boldsymbol{n}} \cdot \frac{\partial^3 \underline{\boldsymbol{\rho}}}{\partial \underset{\sim}{\xi}^3} \right) \delta \underset{\sim}{\xi} + \underline{\boldsymbol{n}} \cdot \frac{\partial^2 \underline{\boldsymbol{\rho}}}{\partial \underset{\sim}{\xi}^2} \Delta \delta \underset{\sim}{\xi}. \qquad \text{[A2.54]}$$

The last term contains the second fundamental matrix $\underset{\approx}{\mathrm{H}}$; remember that:

$$\frac{\partial^3 \underline{\boldsymbol{\rho}}}{\partial \underset{\sim}{\xi}^3} = \overset{3}{\underset{\approx}{\bullet}}$$

substituting equation [A2.54] in [A2.53] allows us to group terms containing the second variation of the surface parameter:

$$\begin{aligned} &(g_n \underset{\approx}{\mathrm{H}} - \underset{\approx}{\mathrm{A}}) \Delta \delta \underset{\sim}{\xi} = \frac{\partial \underline{\boldsymbol{\rho}}}{\partial \underset{\sim}{\xi}} \cdot \left(\delta \frac{\partial \underline{\boldsymbol{\rho}}^{\mathsf{T}}}{\partial \underset{\sim}{\xi}} \Delta \underset{\sim}{\xi} + \Delta \frac{\partial \underline{\boldsymbol{\rho}}^{\mathsf{T}}}{\partial \underset{\sim}{\xi}} \delta \underset{\sim}{\xi} \right) + \Delta \underset{\sim}{\xi}^{\mathsf{T}} \left(\frac{\partial \underline{\boldsymbol{\rho}}}{\partial \underset{\sim}{\xi}} \cdot \frac{\partial^2 \underline{\boldsymbol{\rho}}}{\partial \underset{\sim}{\xi}^2} \right) \delta \underset{\sim}{\xi} \\ &\underbrace{- \underline{\boldsymbol{n}} \cdot \left(\bar{\Delta} \frac{\partial \underline{\boldsymbol{\rho}}}{\partial \underset{\sim}{\xi}} \delta g_n + \bar{\delta} \frac{\partial \underline{\boldsymbol{\rho}}}{\partial \underset{\sim}{\xi}} \Delta g_n \right)}_{\text{term 1}} - g_n \underline{\boldsymbol{n}} \cdot \left(\delta \frac{\partial^2 \underline{\boldsymbol{\rho}}}{\partial \underset{\sim}{\xi}^2} \Delta \underset{\sim}{\xi} + \Delta \frac{\partial^2 \underline{\boldsymbol{\rho}}}{\partial \underset{\sim}{\xi}^2} \delta \underset{\sim}{\xi} \right) \\ &- g_n \Delta \underset{\sim}{\xi}^{\mathsf{T}} \left(\underline{\boldsymbol{n}} \cdot \frac{\partial^3 \underline{\boldsymbol{\rho}}}{\partial \underset{\sim}{\xi}^3} \right) \delta \underset{\sim}{\xi} \\ &\underbrace{+ g_n \left(\bar{\delta} \frac{\partial \underline{\boldsymbol{\rho}}}{\partial \underset{\sim}{\xi}} \cdot \overline{\frac{\partial \underline{\boldsymbol{\rho}}}{\partial \underset{\sim}{\xi}}}^{\mathsf{T}} \right) \left(\underline{\boldsymbol{n}} \cdot \bar{\Delta} \frac{\partial \underline{\boldsymbol{\rho}}}{\partial \underset{\sim}{\xi}} \right)}_{\text{term 2}} + \underbrace{g_n \left(\bar{\Delta} \frac{\partial \underline{\boldsymbol{\rho}}}{\partial \underset{\sim}{\xi}} \cdot \overline{\frac{\partial \underline{\boldsymbol{\rho}}}{\partial \underset{\sim}{\xi}}}^{\mathsf{T}} \right) \left(\underline{\boldsymbol{n}} \cdot \bar{\delta} \frac{\partial \underline{\boldsymbol{\rho}}}{\partial \underset{\sim}{\xi}} \right)}_{\text{term 3}}. \end{aligned} \qquad \text{[A2.55]}$$

The last step is to expand the full derivatives in the marked terms on the right hand:

$$
\begin{aligned}
\text{Term 1:}\quad & \underline{\boldsymbol{n}} \cdot \left(\bar{\Delta} \frac{\partial \underline{\boldsymbol{\rho}}}{\partial \underset{\sim}{\xi}} \delta g_n + \bar{\delta} \frac{\partial \underline{\boldsymbol{\rho}}}{\partial \underset{\sim}{\xi}} \Delta g_n \right) = \\
& \underline{\boldsymbol{n}} \cdot \left(\Delta \frac{\partial \underline{\boldsymbol{\rho}}}{\partial \underset{\sim}{\xi}} \delta g_n + \frac{\partial^2 \underline{\boldsymbol{\rho}}}{\partial \underset{\sim}{\xi}^2} \Delta \underset{\sim}{\xi} \delta g_n + \delta \frac{\partial \underline{\boldsymbol{\rho}}}{\partial \underset{\sim}{\xi}} \Delta g_n + \frac{\partial^2 \underline{\boldsymbol{\rho}}}{\partial \underset{\sim}{\xi}^2} \delta \underset{\sim}{\xi} \Delta g_n \right) \\
& = \underline{\boldsymbol{n}} \cdot \left(\Delta \frac{\partial \underline{\boldsymbol{\rho}}}{\partial \underset{\sim}{\xi}} \delta g_n + \delta \frac{\partial \underline{\boldsymbol{\rho}}}{\partial \underset{\sim}{\xi}} \Delta g_n \right) + \underset{\approx}{\mathrm{H}} \left(\Delta \underset{\sim}{\xi} \delta g_n + \delta \underset{\sim}{\xi} \Delta g_n \right) \\
\text{Term 2:}\quad & g_n \left(\bar{\delta} \frac{\partial \underline{\boldsymbol{\rho}}}{\partial \underset{\sim}{\xi}} \cdot \overline{\frac{\partial \underline{\boldsymbol{\rho}}}{\partial \underset{\sim}{\xi}}}^{\mathsf{T}} \right) \left(\underline{\boldsymbol{n}} \cdot \bar{\Delta} \frac{\partial \underline{\boldsymbol{\rho}}}{\partial \underset{\sim}{\xi}} \right) = \\
& g_n \left(\delta \frac{\partial \underline{\boldsymbol{\rho}}}{\partial \underset{\sim}{\xi}} + \frac{\partial^2 \underline{\boldsymbol{\rho}}}{\partial \underset{\sim}{\xi}^2} \delta \underset{\sim}{\xi} \right) \cdot \left(\underset{\approx}{\bar{\mathrm{A}}} \frac{\partial \underline{\boldsymbol{\rho}}}{\partial \underset{\sim}{\xi}} \right)^{\mathsf{T}} \left(\underline{\boldsymbol{n}} \cdot \Delta \frac{\partial \underline{\boldsymbol{\rho}}}{\partial \underset{\sim}{\xi}} + \underset{\approx}{\mathrm{H}} \Delta \underset{\sim}{\xi} \right) \\
\text{Term 3:}\quad & \text{expands as term 2.}
\end{aligned}
\qquad [A2.56]
$$

These terms inserted in expression [A2.54] give the ultimate expression for the second-order variation of the surface parameter:

$$
\begin{aligned}
\Delta \delta \underset{\sim}{\xi} \quad = & (g_n \underset{\approx}{\mathrm{H}} - \underset{\approx}{\mathrm{A}})^{-1} \left\{ \frac{\partial \underline{\boldsymbol{\rho}}}{\partial \underset{\sim}{\xi}} \cdot \left(\delta \frac{\partial \underline{\boldsymbol{\rho}}^{\mathsf{T}}}{\partial \underset{\sim}{\xi}} \Delta \underset{\sim}{\xi} + \Delta \frac{\partial \underline{\boldsymbol{\rho}}^{\mathsf{T}}}{\partial \underset{\sim}{\xi}} \delta \underset{\sim}{\xi} \right) \right. \\
& + \Delta \underset{\sim}{\xi}^{\mathsf{T}} \left(\frac{\partial \underline{\boldsymbol{\rho}}}{\partial \underset{\sim}{\xi}} \cdot \frac{\partial^2 \underline{\boldsymbol{\rho}}}{\partial \underset{\sim}{\xi}^2} \right) \delta \underset{\sim}{\xi} \\
& - \underline{\boldsymbol{n}} \cdot \left(\Delta \frac{\partial \underline{\boldsymbol{\rho}}}{\partial \underset{\sim}{\xi}} \delta g_n + \delta \frac{\partial \underline{\boldsymbol{\rho}}}{\partial \underset{\sim}{\xi}} \Delta g_n \right) - \underset{\approx}{\mathrm{H}} \left(\Delta \underset{\sim}{\xi} \delta g_n + \delta \underset{\sim}{\xi} \Delta g_n \right) \\
& - g_n \underline{\boldsymbol{n}} \cdot \left(\delta \frac{\partial^2 \underline{\boldsymbol{\rho}}}{\partial \underset{\sim}{\xi}^2} \Delta \underset{\sim}{\xi} + \Delta \frac{\partial^2 \underline{\boldsymbol{\rho}}}{\partial \underset{\sim}{\xi}^2} \delta \underset{\sim}{\xi} \right) - g_n \Delta \underset{\sim}{\xi}^{\mathsf{T}} \left(\underline{\boldsymbol{n}} \cdot \frac{\partial^3 \underline{\boldsymbol{\rho}}}{\partial \underset{\sim}{\xi}^3} \right) \delta \underset{\sim}{\xi} \\
& + g_n \left(\delta \frac{\partial \underline{\boldsymbol{\rho}}}{\partial \underset{\sim}{\xi}} + \frac{\partial^2 \underline{\boldsymbol{\rho}}}{\partial \underset{\sim}{\xi}^2} \delta \underset{\sim}{\xi} \right) \cdot \frac{\partial \underline{\boldsymbol{\rho}}^{\mathsf{T}}}{\partial \underset{\sim}{\xi}} \underset{\approx}{\bar{\mathrm{A}}} \left(\underline{\boldsymbol{n}} \cdot \Delta \frac{\partial \underline{\boldsymbol{\rho}}}{\partial \underset{\sim}{\xi}} + \underset{\approx}{\mathrm{H}} \Delta \underset{\sim}{\xi} \right) \\
& \left. + g_n \left(\Delta \frac{\partial \underline{\boldsymbol{\rho}}}{\partial \underset{\sim}{\xi}} + \frac{\partial^2 \underline{\boldsymbol{\rho}}}{\partial \underset{\sim}{\xi}^2} \Delta \underset{\sim}{\xi} \right) \cdot \frac{\partial \underline{\boldsymbol{\rho}}^{\mathsf{T}}}{\partial \underset{\sim}{\xi}} \underset{\approx}{\bar{\mathrm{A}}} \left(\underline{\boldsymbol{n}} \cdot \delta \frac{\partial \underline{\boldsymbol{\rho}}}{\partial \underset{\sim}{\xi}} + \underset{\approx}{\mathrm{H}} \delta \underset{\sim}{\xi} \right) \right\}.
\end{aligned}
\qquad [A2.57]
$$

Grouping terms with δg_n and Δg_n gives a shorter expression:

$$\begin{aligned}\Delta\delta\underset{\sim}{\xi} = (g_n \underset{\approx}{\mathrm{H}} - \underset{\approx}{\mathrm{A}})^{-1} \Bigg\{ & \frac{\partial \underline{\boldsymbol{\rho}}}{\partial \underset{\sim}{\xi}} \cdot \left(\delta \frac{\partial \underline{\boldsymbol{\rho}}}{\partial \underset{\sim}{\xi}}^{\mathsf{T}} \Delta\underset{\sim}{\xi} + \Delta \frac{\partial \underline{\boldsymbol{\rho}}}{\partial \underset{\sim}{\xi}}^{\mathsf{T}} \delta\underset{\sim}{\xi} \right) + \Delta\underset{\sim}{\xi}^{\mathsf{T}} \left(\frac{\partial \underline{\boldsymbol{\rho}}}{\partial \underset{\sim}{\xi}} \cdot \frac{\partial^2 \underline{\boldsymbol{\rho}}}{\partial \underset{\sim}{\xi}^2} \right) \delta\underset{\sim}{\xi} \\ & - g_n \underline{\boldsymbol{n}} \cdot \left(\delta \frac{\partial^2 \underline{\boldsymbol{\rho}}}{\partial \underset{\sim}{\xi}^2} \Delta\underset{\sim}{\xi} + \Delta \frac{\partial^2 \underline{\boldsymbol{\rho}}}{\partial \underset{\sim}{\xi}^2} \delta\underset{\sim}{\xi} \right) - g_n \Delta\underset{\sim}{\xi}^{\mathsf{T}} \left(\underline{\boldsymbol{n}} \cdot \frac{\partial^3 \underline{\boldsymbol{\rho}}}{\partial \underset{\sim}{\xi}^3} \right) \delta\underset{\sim}{\xi} \\ & + \left[g_n \left(\delta \frac{\partial \underline{\boldsymbol{\rho}}}{\partial \underset{\sim}{\xi}} + \frac{\partial^2 \underline{\boldsymbol{\rho}}}{\partial \underset{\sim}{\xi}^2} \delta\underset{\sim}{\xi} \right) \cdot \frac{\partial \underline{\boldsymbol{\rho}}}{\partial \underset{\sim}{\xi}}^{\mathsf{T}} \underset{\approx}{\bar{\mathrm{A}}} - \delta g_n \underset{\approx}{\mathrm{I}} \right] \left(\underline{\boldsymbol{n}} \cdot \Delta \frac{\partial \underline{\boldsymbol{\rho}}}{\partial \underset{\sim}{\xi}} + \underset{\approx}{\mathrm{H}} \Delta\underset{\sim}{\xi} \right) \\ & + \left[g_n \left(\Delta \frac{\partial \underline{\boldsymbol{\rho}}}{\partial \underset{\sim}{\xi}} + \frac{\partial^2 \underline{\boldsymbol{\rho}}}{\partial \underset{\sim}{\xi}^2} \Delta\underset{\sim}{\xi} \right) \cdot \frac{\partial \underline{\boldsymbol{\rho}}}{\partial \underset{\sim}{\xi}}^{\mathsf{T}} \underset{\approx}{\bar{\mathrm{A}}} - \Delta g_n \underset{\approx}{\mathrm{I}} \right] \left(\underline{\boldsymbol{n}} \cdot \delta \frac{\partial \underline{\boldsymbol{\rho}}}{\partial \underset{\sim}{\xi}} + \underset{\approx}{\mathrm{H}} \delta\underset{\sim}{\xi} \right) \Bigg\}. \end{aligned}$$

[A2.58]

This expression coincides with the one originally obtained in [LAU 92]; it contains a third derivative of the master-surface vector $\underline{\boldsymbol{\rho}}$, which imposes a more strict condition on the smoothness of the master. However, the approximation of this variation for small gaps $g_n \approx 0$, leading to a simpler form, does not contain this derivative:

$$\begin{aligned}\Delta\delta\underset{\sim}{\xi} = \underset{\approx}{\bar{\mathrm{A}}} \Bigg\{ & \delta g_n \left(\underline{\boldsymbol{n}} \cdot \Delta \frac{\partial \underline{\boldsymbol{\rho}}}{\partial \underset{\sim}{\xi}} + \underset{\approx}{\mathrm{H}} \Delta\underset{\sim}{\xi} \right) + \Delta g_n \left(\underline{\boldsymbol{n}} \cdot \delta \frac{\partial \underline{\boldsymbol{\rho}}}{\partial \underset{\sim}{\xi}} + \underset{\approx}{\mathrm{H}} \delta\underset{\sim}{\xi} \right) \\ & - \frac{\partial \underline{\boldsymbol{\rho}}}{\partial \underset{\sim}{\xi}} \cdot \left(\delta \frac{\partial \underline{\boldsymbol{\rho}}}{\partial \underset{\sim}{\xi}}^{\mathsf{T}} \Delta\underset{\sim}{\xi} + \Delta \frac{\partial \underline{\boldsymbol{\rho}}}{\partial \underset{\sim}{\xi}}^{\mathsf{T}} \delta\underset{\sim}{\xi} \right) - \Delta\underset{\sim}{\xi}^{\mathsf{T}} \left(\frac{\partial \underline{\boldsymbol{\rho}}}{\partial \underset{\sim}{\xi}} \cdot \frac{\partial^2 \underline{\boldsymbol{\rho}}}{\partial \underset{\sim}{\xi}^2} \right) \delta\underset{\sim}{\xi} \Bigg\}. \end{aligned}$$

[A2.59]

A2.2.2. *Shadow-projection case: infinitely remote emitter*

It is much easier to compute the second-order variations in case of the shadow-projection. A variation of equation [A2.13] gives:

$$0 = \bar{\Delta}\bar{\delta}\underline{\boldsymbol{\rho}} + \Delta\delta g_s \underline{\boldsymbol{e}},$$

expanding the full variations yields:

$$\Delta\delta g_s \underline{\boldsymbol{e}} = -\delta \frac{\partial \underline{\boldsymbol{\rho}}}{\partial \underset{\sim}{\xi}}^{\mathsf{T}} \Delta\underset{\sim}{\xi} - \Delta \frac{\partial \underline{\boldsymbol{\rho}}}{\partial \underset{\sim}{\xi}}^{\mathsf{T}} \delta\underset{\sim}{\xi} - \Delta\underset{\sim}{\xi}^{\mathsf{T}} \frac{\partial^2 \underline{\boldsymbol{\rho}}}{\partial \underset{\sim}{\xi}^2} \delta\underset{\sim}{\xi} - \frac{\partial \underline{\boldsymbol{\rho}}}{\partial \underset{\sim}{\xi}}^{\mathsf{T}} \Delta\delta\underset{\sim}{\xi}, \qquad [A2.60]$$

the dot product with vector $\underline{\boldsymbol{e}}$ gives:

$$\Delta\delta g_s = -\underline{\boldsymbol{e}}\cdot\left(\delta\frac{\partial\underline{\boldsymbol{\rho}}}{\partial\underset{\sim}{\xi}}^{\mathsf{T}}\Delta\underset{\sim}{\xi}+\Delta\frac{\partial\underline{\boldsymbol{\rho}}}{\partial\underset{\sim}{\xi}}^{\mathsf{T}}\delta\underset{\sim}{\xi}+\Delta\underset{\sim}{\xi}^{\mathsf{T}}\frac{\partial^2\underline{\boldsymbol{\rho}}}{\partial\underset{\sim}{\xi}^2}\delta\underset{\sim}{\xi}\right)-\underline{\boldsymbol{e}}\cdot\frac{\partial\underline{\boldsymbol{\rho}}}{\partial\underset{\sim}{\xi}}^{\mathsf{T}}\Delta\delta\underset{\sim}{\xi}, \quad \text{[A2.61]}$$

where the last term can be determined by the dot product of [A2.60] with v-vector $\underline{\boldsymbol{s}}$:

$$\left(\underset{\sim}{\boldsymbol{s}}\cdot\frac{\partial\underline{\boldsymbol{\rho}}}{\partial\underset{\sim}{\xi}}^{\mathsf{T}}\right)\Delta\delta\underset{\sim}{\xi}=-\underset{\sim}{\boldsymbol{s}}\cdot\delta\frac{\partial\underline{\boldsymbol{\rho}}}{\partial\underset{\sim}{\xi}}^{\mathsf{T}}\Delta\underset{\sim}{\xi}-\underset{\sim}{\boldsymbol{s}}\cdot\Delta\frac{\partial\underline{\boldsymbol{\rho}}}{\partial\underset{\sim}{\xi}}^{\mathsf{T}}\delta\underset{\sim}{\xi}-\Delta\underset{\sim}{\xi}^{\mathsf{T}}\underset{\sim}{\boldsymbol{s}}\cdot\frac{\partial^2\underline{\boldsymbol{\rho}}}{\partial\underset{\sim}{\xi}^2}\delta\underset{\sim}{\xi},$$

using notation $\underset{\approx}{\mathrm{P}}$ from [A2.16], we have the expression for the second variation of the surface parameter:

$$\boxed{\Delta\delta\underset{\sim}{\xi}=-\overline{\frac{\partial\underline{\boldsymbol{\rho}}}{\partial\underset{\sim}{\xi}}}\cdot\left[\underline{\underline{\boldsymbol{I}}}-\frac{\underline{\boldsymbol{e}}\otimes\underline{\boldsymbol{n}}}{\underline{\boldsymbol{e}}\cdot\underline{\boldsymbol{n}}}\right]\cdot\left(\delta\frac{\partial\underline{\boldsymbol{\rho}}}{\partial\underset{\sim}{\xi}}^{\mathsf{T}}\Delta\underset{\sim}{\xi}+\Delta\frac{\partial\underline{\boldsymbol{\rho}}}{\partial\underset{\sim}{\xi}}^{\mathsf{T}}\delta\underset{\sim}{\xi}+\Delta\underset{\sim}{\xi}^{\mathsf{T}}\frac{\partial^2\underline{\boldsymbol{\rho}}}{\partial\underset{\sim}{\xi}^2}\delta\underset{\sim}{\xi}\right)}, \quad \text{[A2.62]}$$

where the operator in square brackets is discussed in Remark 2.3. Substituting [A2.62] in [A2.61] gives:

$$\begin{aligned}\Delta\delta g_s = \quad & -\left[\underline{\boldsymbol{e}}-\left(\underline{\boldsymbol{e}}\cdot\frac{\partial\underline{\boldsymbol{\rho}}}{\partial\underset{\sim}{\xi}}\right)\otimes\overline{\frac{\partial\underline{\boldsymbol{\rho}}}{\partial\underset{\sim}{\xi}}}\cdot\left(\underline{\underline{\boldsymbol{I}}}-\frac{\underline{\boldsymbol{e}}\otimes\underline{\boldsymbol{n}}}{\underline{\boldsymbol{e}}\cdot\underline{\boldsymbol{n}}}\right)\right]\\ & \left(\delta\frac{\partial\underline{\boldsymbol{\rho}}}{\partial\underset{\sim}{\xi}}^{\mathsf{T}}\Delta\underset{\sim}{\xi}+\Delta\frac{\partial\underline{\boldsymbol{\rho}}}{\partial\underset{\sim}{\xi}}^{\mathsf{T}}\delta\underset{\sim}{\xi}+\Delta\underset{\sim}{\xi}^{\mathsf{T}}\frac{\partial^2\underline{\boldsymbol{\rho}}}{\partial\underset{\sim}{\xi}^2}\delta\underset{\sim}{\xi}\right),\end{aligned} \quad \text{[A2.63]}$$

where the expression in square brackets is the same as in equation [A2.24], so the second variation of the shadow gap can be rewritten as:

$$\boxed{\Delta\delta g_s=-\frac{\underline{\boldsymbol{n}}}{\underline{\boldsymbol{e}}\cdot\underline{\boldsymbol{n}}}\cdot\left(\delta\frac{\partial\underline{\boldsymbol{\rho}}}{\partial\underset{\sim}{\xi}}^{\mathsf{T}}\Delta\underset{\sim}{\xi}+\Delta\frac{\partial\underline{\boldsymbol{\rho}}}{\partial\underset{\sim}{\xi}}^{\mathsf{T}}\delta\underset{\sim}{\xi}+\Delta\underset{\sim}{\xi}^{\mathsf{T}}\frac{\partial^2\underline{\boldsymbol{\rho}}}{\partial\underset{\sim}{\xi}^2}\delta\underset{\sim}{\xi}\right)}. \quad \text{[A2.64]}$$

A2.2.3. *Shadow-projection case: close emitter*

In this case, we take the variation of expression [A2.30]:

$$\begin{aligned}0= \quad & \delta\frac{\partial\underline{\boldsymbol{\rho}}}{\partial\underset{\sim}{\xi}}^{\mathsf{T}}\Delta\underset{\sim}{\xi}+\Delta\frac{\partial\underline{\boldsymbol{\rho}}}{\partial\underset{\sim}{\xi}}^{\mathsf{T}}\delta\underset{\sim}{\xi}+\Delta\underset{\sim}{\xi}^{\mathsf{T}}\frac{\partial^2\underline{\boldsymbol{\rho}}}{\partial\underset{\sim}{\xi}^2}\delta\underset{\sim}{\xi}+\frac{\partial\underline{\boldsymbol{\rho}}}{\partial\underset{\sim}{\xi}}^{\mathsf{T}}\Delta\delta\underset{\sim}{\xi}\\ + \quad & \Delta\delta g_s\underline{\boldsymbol{e}}+\delta g_s\Delta\underline{\boldsymbol{e}}+\Delta g_s\delta\underline{\boldsymbol{e}}+g_s\Delta\delta\underline{\boldsymbol{e}}\,.\end{aligned} \quad \text{[A2.65]}$$

The dot product with vector $\underline{\boldsymbol{e}}$ and account of the following equality $\delta\underline{\boldsymbol{e}}\cdot\underline{\boldsymbol{e}}=0$ gives:

$$\Delta\delta g_s=-\underline{\boldsymbol{e}}\cdot\left(\delta\frac{\partial\underline{\underline{\boldsymbol{\rho}}}^{\mathsf{T}}}{\partial\underset{\sim}{\xi}}\Delta\underset{\sim}{\xi}+\Delta\frac{\partial\underline{\underline{\boldsymbol{\rho}}}^{\mathsf{T}}}{\partial\underset{\sim}{\xi}}\delta\underset{\sim}{\xi}+\Delta\underset{\sim}{\xi}^{\mathsf{T}}\frac{\partial^2\underline{\underline{\boldsymbol{\rho}}}}{\partial\underset{\sim}{\xi}^2}\delta\underset{\sim}{\xi}\right)-\underline{\boldsymbol{e}}\cdot\frac{\partial\underline{\underline{\boldsymbol{\rho}}}^{\mathsf{T}}}{\partial\underset{\sim}{\xi}}\Delta\delta\underset{\sim}{\xi}-g_s\underline{\boldsymbol{e}}\cdot\Delta\delta\underline{\boldsymbol{e}}, \tag{A2.66}$$

where, due to the orthogonality of a unit vector to its variation and according to [A2.28] and [A2.29], the last term becomes:

$$\underline{\boldsymbol{e}}\cdot\Delta\delta\underline{\boldsymbol{e}}=-\delta\underline{\boldsymbol{e}}\cdot\Delta\underline{\boldsymbol{e}}=-\frac{(\delta\underline{\boldsymbol{r}}_s\cdot\underline{\underline{\boldsymbol{s}}}^{\mathsf{T}})(\underline{\underline{\boldsymbol{s}}}\cdot\Delta\underline{\boldsymbol{r}}_s)}{d_{se}^2}. \tag{A2.67}$$

The dot product of [A2.65] with v-vector $\underline{\underline{\boldsymbol{s}}}$ allows us to evaluate the second variation of the surface parameter:

$$\begin{aligned}\Delta\delta\underset{\sim}{\xi}\;&=-\left(\underline{\underline{\boldsymbol{s}}}\cdot\frac{\partial\underline{\underline{\boldsymbol{\rho}}}^{\mathsf{T}}}{\partial\underset{\sim}{\xi}}\right)^{-1}\underline{\underline{\boldsymbol{s}}}\cdot\left(\delta\frac{\partial\underline{\underline{\boldsymbol{\rho}}}^{\mathsf{T}}}{\partial\underset{\sim}{\xi}}\Delta\underset{\sim}{\xi}+\Delta\frac{\partial\underline{\underline{\boldsymbol{\rho}}}^{\mathsf{T}}}{\partial\underset{\sim}{\xi}}\delta\underset{\sim}{\xi}+\Delta\underset{\sim}{\xi}^{\mathsf{T}}\frac{\partial^2\underline{\underline{\boldsymbol{\rho}}}}{\partial\underset{\sim}{\xi}^2}\delta\underset{\sim}{\xi}\right)\\&\quad-\left(\underline{\underline{\boldsymbol{s}}}\cdot\frac{\partial\underline{\underline{\boldsymbol{\rho}}}^{\mathsf{T}}}{\partial\underset{\sim}{\xi}}\right)^{-1}\underline{\underline{\boldsymbol{s}}}\cdot(\delta g_s\Delta\underline{\boldsymbol{e}}+\Delta g_s\delta\underline{\boldsymbol{e}})-g_s\left(\underline{\underline{\boldsymbol{s}}}\cdot\frac{\partial\underline{\underline{\boldsymbol{\rho}}}^{\mathsf{T}}}{\partial\underset{\sim}{\xi}}\right)^{-1}\underline{\underline{\boldsymbol{s}}}\cdot\Delta\delta\underline{\boldsymbol{e}}.\end{aligned} \tag{A2.68}$$

Let us consider the right part of the last term using [A2.28] and [A2.29]:

$$\begin{aligned}&\underline{\underline{\boldsymbol{s}}}\cdot\Delta\delta\underline{\boldsymbol{e}}=-\underline{\underline{\boldsymbol{s}}}\cdot\Delta\left[\left(\underline{\underline{\boldsymbol{I}}}-\underline{\boldsymbol{e}}\otimes\underline{\boldsymbol{e}}\right)\cdot\tfrac{\delta\underline{\boldsymbol{r}}_s}{d_{se}}\right]=\\&-\underline{\underline{\boldsymbol{s}}}\cdot\left[(\Delta\underline{\boldsymbol{e}}\otimes\underline{\boldsymbol{e}}+\underline{\boldsymbol{e}}\otimes\Delta\underline{\boldsymbol{e}})\cdot\tfrac{\delta\underline{\boldsymbol{r}}_s}{d_{se}}+\left(\underline{\underline{\boldsymbol{I}}}-\underline{\boldsymbol{e}}\otimes\underline{\boldsymbol{e}}\right)\cdot\delta\underline{\boldsymbol{r}}_s\Delta\tfrac{1}{d_{se}}\right]\\&=\tfrac{1}{d_{se}^2}\underline{\underline{\boldsymbol{s}}}\cdot(\Delta\underline{\boldsymbol{r}}_s\otimes\underline{\boldsymbol{e}}\cdot\delta\underline{\boldsymbol{r}}_s+\delta\underline{\boldsymbol{r}}_s\otimes\underline{\boldsymbol{e}}\cdot\Delta\underline{\boldsymbol{r}}_s),\end{aligned} \tag{A2.69}$$

in a similar manner, it is easy to show that:

$$\underline{\underline{\boldsymbol{s}}}\cdot\delta\underline{\boldsymbol{e}}=-\underline{\underline{\boldsymbol{s}}}\cdot\frac{\delta\underline{\boldsymbol{r}}_s}{d_{se}}. \tag{A2.70}$$

Substituting [A2.69] and [A2.70] in [A2.68] and carrying [A2.17] gives:

$$\boxed{\begin{aligned}\Delta\delta\underset{\sim}{\xi}\;&=-\overline{\frac{\partial\underline{\underline{\boldsymbol{\rho}}}}{\partial\underset{\sim}{\xi}}}\cdot\left[\underline{\underline{\boldsymbol{I}}}-\frac{\underline{\boldsymbol{e}}\otimes\underline{\boldsymbol{n}}}{\underline{\boldsymbol{e}}\cdot\underline{\boldsymbol{n}}}\right]\cdot\left\{\delta\frac{\partial\underline{\underline{\boldsymbol{\rho}}}^{\mathsf{T}}}{\partial\underset{\sim}{\xi}}\Delta\underset{\sim}{\xi}+\Delta\frac{\partial\underline{\underline{\boldsymbol{\rho}}}^{\mathsf{T}}}{\partial\underset{\sim}{\xi}}\delta\underset{\sim}{\xi}+\Delta\underset{\sim}{\xi}^{\mathsf{T}}\frac{\partial^2\underline{\underline{\boldsymbol{\rho}}}}{\partial\underset{\sim}{\xi}^2}\delta\underset{\sim}{\xi}\right.\\&\qquad\left.-\tfrac{1}{d_{se}}(\Delta g_s\delta\underline{\boldsymbol{r}}_s+\delta g_s\Delta\underline{\boldsymbol{r}}_s)+\tfrac{g_s}{d_{se}^2}(\Delta\underline{\boldsymbol{r}}_s\otimes\underline{\boldsymbol{e}}\cdot\delta\underline{\boldsymbol{r}}_s+\delta\underline{\boldsymbol{r}}_s\otimes\underline{\boldsymbol{e}}\cdot\Delta\underline{\boldsymbol{r}}_s)\right\}.\end{aligned}} \tag{A2.71}$$

Assuming small gaps $g_s \approx 0$ results in a shorter expression:

$$\begin{aligned}\Delta\delta\underset{\sim}{\xi} \quad &= -\overline{\frac{\partial\underline{\boldsymbol{\rho}}}{\partial\underset{\sim}{\xi}}}\cdot\left[\underline{\underline{\boldsymbol{I}}}-\frac{\underline{\boldsymbol{e}}\otimes\underline{\boldsymbol{n}}}{\underline{\boldsymbol{e}}\cdot\underline{\boldsymbol{n}}}\right]\cdot\left\{\delta\frac{\partial\underline{\boldsymbol{\rho}}}{\partial\underset{\sim}{\xi}}^{\mathsf{T}}\Delta\underset{\sim}{\xi}+\Delta\frac{\partial\underline{\boldsymbol{\rho}}}{\partial\underset{\sim}{\xi}}^{\mathsf{T}}\delta\underset{\sim}{\xi}+\Delta\underset{\sim}{\xi}^{\mathsf{T}}\frac{\partial^2\underline{\boldsymbol{\rho}}}{\partial\underset{\sim}{\xi}^2}\delta\underset{\sim}{\xi}\right.\\ &\left.-\tfrac{1}{d_{se}}\left(\Delta g_s\delta\underline{\boldsymbol{r}}_s+\delta g_s\Delta\underline{\boldsymbol{r}}_s\right)\right\}.\end{aligned} \tag{A2.72}$$

Substituting [A2.71] and [A2.67] in [A2.66] gives:

$$\begin{aligned}&\Delta\delta g_s=-\underline{\boldsymbol{e}}\cdot\left(\delta\frac{\partial\underline{\boldsymbol{\rho}}}{\partial\underset{\sim}{\xi}}^{\mathsf{T}}\Delta\underset{\sim}{\xi}+\Delta\frac{\partial\underline{\boldsymbol{\rho}}}{\partial\underset{\sim}{\xi}}^{\mathsf{T}}\delta\underset{\sim}{\xi}+\Delta\underset{\sim}{\xi}^{\mathsf{T}}\frac{\partial^2\underline{\boldsymbol{\rho}}}{\partial\underset{\sim}{\xi}^2}\delta\underset{\sim}{\xi}\right)\\ &+\left\{\underline{\boldsymbol{e}}\cdot\frac{\partial\underline{\boldsymbol{\rho}}}{\partial\underset{\sim}{\xi}}^{\mathsf{T}}\otimes\overline{\frac{\partial\underline{\boldsymbol{\rho}}}{\partial\underset{\sim}{\xi}}}\cdot\left[\underline{\underline{\boldsymbol{I}}}-\frac{\underline{\boldsymbol{e}}\otimes\underline{\boldsymbol{n}}}{\underline{\boldsymbol{e}}\cdot\underline{\boldsymbol{n}}}\right]\right\}\\ &\cdot\left[\delta\frac{\partial\underline{\boldsymbol{\rho}}}{\partial\underset{\sim}{\xi}}^{\mathsf{T}}\Delta\underset{\sim}{\xi}+\Delta\frac{\partial\underline{\boldsymbol{\rho}}}{\partial\underset{\sim}{\xi}}^{\mathsf{T}}\delta\underset{\sim}{\xi}+\Delta\underset{\sim}{\xi}^{\mathsf{T}}\frac{\partial^2\underline{\boldsymbol{\rho}}}{\partial\underset{\sim}{\xi}^2}\delta\underset{\sim}{\xi}-\tfrac{1}{d_{se}}\left(\Delta g_s\delta\underline{\boldsymbol{r}}_s+\delta g_s\Delta\underline{\boldsymbol{r}}_s\right)\right.\\ &\left.+\tfrac{g_s}{d_{se}^2}\left(\Delta\underline{\boldsymbol{r}}_s\otimes\underline{\boldsymbol{e}}\cdot\delta\underline{\boldsymbol{r}}_s+\delta\underline{\boldsymbol{r}}_s\otimes\underline{\boldsymbol{e}}\cdot\Delta\underline{\boldsymbol{r}}_s\right)\right]+\tfrac{g_s}{d_{se}^2}(\delta\underline{\boldsymbol{r}}_s\cdot\underset{\sim}{\underline{\boldsymbol{s}}}^{\mathsf{T}})(\underset{\sim}{\underline{\boldsymbol{s}}}\cdot\Delta\underline{\boldsymbol{r}}_s),\end{aligned} \tag{A2.73}$$

where the expression in braces can be rewritten as:

$$\underline{\boldsymbol{e}}\cdot\frac{\partial\underline{\boldsymbol{\rho}}}{\partial\underset{\sim}{\xi}}^{\mathsf{T}}\otimes\overline{\frac{\partial\underline{\boldsymbol{\rho}}}{\partial\underset{\sim}{\xi}}}\cdot\left[\underline{\underline{\boldsymbol{I}}}-\frac{\underline{\boldsymbol{e}}\otimes\underline{\boldsymbol{n}}}{\underline{\boldsymbol{e}}\cdot\underline{\boldsymbol{n}}}\right]=\underline{\boldsymbol{e}}-\frac{\underline{\boldsymbol{n}}}{\underline{\boldsymbol{n}}\cdot\underline{\boldsymbol{e}}}=-\frac{\underline{\boldsymbol{n}}}{\underline{\boldsymbol{n}}\cdot\underline{\boldsymbol{e}}}\cdot\underset{\sim}{\underline{\boldsymbol{s}}}^{\mathsf{T}}\otimes\underset{\sim}{\underline{\boldsymbol{s}}},$$

consequently [A2.73], transforms into:

$$\boxed{\begin{aligned}\Delta\delta g_s \quad &= -\frac{\underline{\boldsymbol{n}}}{\underline{\boldsymbol{n}}\cdot\underline{\boldsymbol{e}}}\cdot\left(\delta\frac{\partial\underline{\boldsymbol{\rho}}}{\partial\underset{\sim}{\xi}}^{\mathsf{T}}\Delta\underset{\sim}{\xi}+\Delta\frac{\partial\underline{\boldsymbol{\rho}}}{\partial\underset{\sim}{\xi}}^{\mathsf{T}}\delta\underset{\sim}{\xi}+\Delta\underset{\sim}{\xi}^{\mathsf{T}}\frac{\partial^2\underline{\boldsymbol{\rho}}}{\partial\underset{\sim}{\xi}^2}\delta\underset{\sim}{\xi}\right.\\ &\quad -\frac{\underset{\sim}{\underline{\boldsymbol{s}}}^{\mathsf{T}}\otimes\underset{\sim}{\underline{\boldsymbol{s}}}}{d_{se}}\cdot\left(\Delta g_s\delta\underline{\boldsymbol{r}}_s+\delta g_s\Delta\underline{\boldsymbol{r}}_s\right)\\ &\quad \left.+\frac{g_s}{d_{se}^2}\underset{\sim}{\underline{\boldsymbol{s}}}^{\mathsf{T}}\left(\underset{\sim}{\underline{\boldsymbol{s}}}\cdot\Delta\underline{\boldsymbol{r}}_s\underline{\boldsymbol{e}}\cdot\delta\underline{\boldsymbol{r}}_s+\underset{\sim}{\underline{\boldsymbol{s}}}\cdot\delta\underline{\boldsymbol{r}}_s\otimes\underline{\boldsymbol{e}}\cdot\Delta\underline{\boldsymbol{r}}_s\right)\right)\\ &\quad +\frac{g_s}{d_{se}^2}(\delta\underline{\boldsymbol{r}}_s\cdot\underset{\sim}{\underline{\boldsymbol{s}}}^{\mathsf{T}})(\underset{\sim}{\underline{\boldsymbol{s}}}\cdot\Delta\underline{\boldsymbol{r}}_s).\end{aligned}} \tag{A2.74}$$

Assuming small gaps $g_s \approx 0$ results in a shorter expression:

$$\begin{aligned}\Delta\delta g_s \quad &= -\frac{\underline{\boldsymbol{n}}}{\underline{\boldsymbol{n}}\cdot\underline{\boldsymbol{e}}} \cdot \left(\delta\frac{\partial \underline{\boldsymbol{\rho}}^{\mathsf{T}}}{\partial \underset{\sim}{\xi}} \Delta\underset{\sim}{\xi} + \Delta\frac{\partial \underline{\boldsymbol{\rho}}^{\mathsf{T}}}{\partial \underset{\sim}{\xi}} \delta\underset{\sim}{\xi} + \Delta\underset{\sim}{\xi}^{\mathsf{T}} \frac{\partial^2 \underline{\boldsymbol{\rho}}}{\partial \underset{\sim}{\xi}^2} \delta\underset{\sim}{\xi} \right. \\ &\quad \left. -\frac{\underset{\sim}{\underline{\boldsymbol{s}}}^{\mathsf{T}} \otimes \underset{\sim}{\underline{\boldsymbol{s}}}}{d_{se}} \cdot (\Delta g_s \delta\underline{\boldsymbol{r}}_s + \delta g_s \Delta\underline{\boldsymbol{r}}_s) \right).\end{aligned} \qquad [A2.75]$$

In the case of an infinitely remote emitter ($d_{se} \to \infty$), we get the same expressions as in the previous section, both for the surface parameter [A2.62] and the shadow gap [A2.64].

Bibliography

[ABA 07] ABAQUS release notes, Abaqus release 6.7, 2007.

[ALA 88] ALART P., Multiplicateurs 'augmentés' et méthode de Newton généralisée pour contact avec frottement, Report, Document LMA-DME-EPFL, Lausanne, 1988.

[ALA 91] ALART P., CURNIER A., "A mixed formulation for frictional contact problem prone to Newton like solution methods", *Computer Method in Applied Mechanics and Engineering*, vol. 92, pp. 353–375, 1991.

[ALA 97] ALART P., "Méthode de Newton généralisée en mécanique du contact", *Journal de Mathématiques Pures et Appliqués*, vol. 76, pp. 83–108, 1997.

[ALA 04] ALART P., BARBOTEU M., GRIL J., "A numerical modelling of nonlinear 2D-frictional multicontact problems: application to post-buckling in cellular media", *Computational Mechanics*, vol. 34, pp. 298–309, 2004.

[ALE 83] ALEXANDROV V.M., MHITARYAN S.M., *Contact Problems for Bodies with Thin Coatings and Interlayers*, Nauka, Moscow, 1983.

[ANS 05] ANSYS Contact technology guide, ANSYS release 10, August 2005.

[ARR 58a] ARROW K., HURWICZ L., UZAWA H., *Studies in Nonlinear Programming*, Stanford University Press, 1958.

[ARR 58b] ARROW K.J., SOLOW R.M., "Gradient methods for constrained maxima, with weakened assumptions", in ARROW K., HURWICZ L., UZAWA H. (eds) *Studies in Linear and Nonlinear Programming*, Stanford University Press, pp. 166–176, 1958.

[BAB 95] BABUŠKA I., IHLENBURG F., PAIK E.T., SAUTER S.A., "A generalized finite element method for solving the Helmholtz equation in two dimensions with minimal pollution", *Computer Methods in Applied and Mechanical Engineering*, vol. 128, pp. 325–359, 1995.

[BAR 99] BARBOTEU M., Contact, frottement et techniques de calcul parallèle, PhD Thesis, University of Montpellier, France.

[BAR 02] BARBOTEU M., ALART P., PAGANO S., "Modélisation de problèmes non linéaires de grande taille: grandes déformations et autocontact dans un milieu cellulaire", *Revue européenne des éléments finis*, vol. 11, pp. 447–461, 2002.

[BAT 96] BATHE K.-J., *Finite Element Procedures*, Prentice Hall, 1996.

[BEC 03] BECKER R., HANSBO P., STENBERG R., "A finite element method for domain decomposition with non-matching grids", *Mathematical Modelling and Numerical Analysis*, vol. 37, pp. 209–225, 2003.

[BEL 98] BELGACEM F.B., HILD P., LABORDE P., "The mortar finite element method for contact problems", *Mathematical and Computer Modelling*, vol. 28, pp. 263–271, 1998.

[BEL 08] BELYTSCHKO T., KAM LIU W., MORAN B., *Nonlinear Finite Elements for Continua and Structures*, John Wiley & Sons, Hoboken, NJ, 2008.

[BEN 90] BENSON D.J., HALLQUIST J.O., "A single surface contact algorithm for the post-buckling analysis of shell structures", *Computer Methods in Applied Mechanics and Engineering*, vol. 78, pp. 141–163, 1990.

[BEN 07] BENSON D.J., *The History of LS-DYNA*, University of California, San Diego, 2007.

[BER 81] BERTSEKAS D.P., Augmented Lagrangian and differentiable exact penalty methods, Technical report LIDS-P; 1113, Laboratory for Information and Decision Systems, Massachusetts Institute of Technology, 1981.

[BER 84] BERTSEKAS D.P., *Constrained Optimization and Lagrange Multiplier Methods*, Academic Press, 1984.

[BER 90] BERNARDI C., DEBIT N., MADAY Y., "Coupling finite element and spectral methods: first results", *Mathematics of Computation*, vol. 54, pp. 21–39, 1990.

[BER 03] BERTSEKAS D.P., NEDIC A., OZDAGLAR A.E., *Convex Analysis and Optimization*, Athena Scientific, 2003.

[BES 97] BESSON J., FOERCH R., "Large scale object-oriented finite element code design", *Computer Methods in Applied Mechanics and Engineering*, vol. 142, pp. 165–187, 1997.

[BHA 02] BHASHYAM G.R., ANSYS Mechanical – a powerful nonlinear simulation tool, Report , 2002. Available at http://ansys.net/collection/824.

[BON 06] BONNANS J.F., GILBERT J.C., LEMARÉCHAL C., SAGASTIZÁBAL C.A., *Numerical Optimization, Theoretical and Numerical Aspect*, 2nd ed., Springer, 2006.

[BOW 50] BOWDEN F.P., TABOR D., *The Friction and Lubrication of Solids*, Oxford University Press, UK, 1950.

[BRO 00] BROWN K., ATTAWAY S., PLIMPTON S., HENDRICKSON B., "Parallel strategies for crash and impact simulations", *Computer Methods in Applied Mechanics and Engineering*, vol. 184, pp. 375–390, 2000.

[BRU 02] BRUNEEL H.C.J., DE RYCKE I., "QuickTrace: a fast algorithm to detect contact", *International Journal for Numerical Methods in Engineering*, vol. 54, pp. 299–316, 2002.

[BUS 09] BUSSETTA P., MARCEAU D., PONTHOT J.-P., "Résolution du problème de contact mécanique frottant: méthode du lagrangien augmenté adapté", *Proceedings of 9th National Symposium on Computational Structural Mechanics*, vol. 2, Giens, France, pp. 623–628, 25–29 May 2009.

[CAM 82] CAMPOS L.T., ODEN J.T., KIKUCHI N., "A numerical analysis of the class of contact problems with friction in elastostatics", *Computer Methods in Applied and Mechanical Engineering*, vol. 34, pp. 821–845, 1982.

[CHA 04] CHAMORET D., SAILLARD P., RASSINEUX A., BERGHEAU J.-M., "New smoothing procedures in contact mechanics", *Journal of Computational and Applied Mathematics*, vol. 168, pp. 107–116, 2004.

[CHA 76] CHAND R., HAUG E.J., RIM K., "Analysis of unbonded contact problems by means of quadratic programming", *Journal of Optimization Theory and Applications*, vol. 20, pp. 171–189, 1976.

[COC 84] COCU M., "Existence of solutions of Signorini problems with friction", *International Journal of Engineering Science*, vol. 22, pp. 567–575, 1984.

[COM 10] COMSOL Multiphysics 4.1 Release notes, 2010.

[COU 57] COURTNEY-PRATT J.S., EISNER E., "the effect of a tangential force on the contact of metallic bodies", *Proceedings of the Royal Society of London A*, vol. 238, SME Press, Dearborn, MI, pp. 529-550, 1957.

[CRI 00a] CRISFIELD M.A., *Non-linear Finite Element Analysis of Solids and Structures, Volume 1: Essentials*, John Wiley & Sons, Hoboken, NJ, 2000.

[CRI 00b] CRISFIELD M.A., *Non-linear Finite Element Analysis of Solids and Structures, Volume 2: Advanced Topics*, John Wiley & Sons, Hoboken, NJ, 2000.

[CRI 00c] CRISFIELD M.A., "Re-visiting the contact patch test", *International Journal for Numerical Methods in Engineering*, vol. 48, pp. 435–449, 2000.

[CUR 84] CURNIER A., "A theory of friction", *International Journal of Solids and Structures*, vol. 20, pp. 637–647, 1984.

[CUR 88] CURNIER A., ALART P., "A generalized Newton method for contact problem with friction", *Journal de mécanique théorique et appliquée*, Special Issue: *Numerical Methods in Mechanics of Contact Involving Friction*, pp. 67–82, 1988.

[CUR 95] CURNIER A., HE Q.-C., KLARBRING A., "Continuum mechanics modeling of large deformation contact with friction", in RAOUS M., JEAN M., MOREAU J., (eds), *Contact Mechanics*, Plenum, pp. 145–158, 1995.

[DE 98] DE SAXCE G., BOUSSHINE L., "Limit analysis theorems for implicit standard materials: application to the unilateral contact with dry friction and the non-associated flow rules in soils and rocks", *International Journal of Mechanical Sciences*, vol. 40, pp. 387–398, 1998.

[DIC 06a] DICK T., CAILLETAUD G., "Analytic and FE based estimations of the coefficient of friction of composite surfaces", *Wear*, vol. 260, pp. 1305–1316, 2006.

[DIC 06b] DICK T., CAILLETAUD G., "Fretting modelling with a crystal plasticity model of Ti6Al4V", *Computational Materials Science*, vol. 38, pp. 113–125, 2006.

[DIC 08] DICK T., BASSEVILLE S., CAILLETAUD G., "Fatigue modelling in fretting contact with a crystal plasticity model", *Computational Materials Science*, vol. 43, pp. 36–42, 2008.

[DRU 53] DRUCKER D.C., Coulomb friction, plasticity, and limit loads, Report no. 85, Office of Naval Research, January 1953.

[DUV 71] DUVAUT G., LIONS J.L., "Elasticité avec frottement", *Journal de Mécanique*, vol. 10, pp. 409–420, 1971.

[DUV 76] DUVAUT G., LIONS J.L., *Inequalities in Mechanics and Physics*, Springer-Verlag, 1976.

[FAR 94] FARHAT C., ROUX F.-X., "Implicit parallel processing in structural mechanics", *Computational Mechanics Advances*, vol. 2, pp. 1–24, 1994.

[FIC 63] FICHERA G., "Sul problema elastostatico di Signorini con ambigue condizioni al contorno", *Atti della Accademia Nazionale dei Lincei, Serie Ottava, Rendiconti, Classe di Scienze Fisiche, Matematiche e Naturali*, vol. 34, pp. 138–142, 1963.

[FIC 64] FICHERA G., "Problemi elastostatici con vincoli unilaterali: Il problema di Signorini con ambigue condizioni al contorno", *Atti della Accademia Nazionale dei Lincei. Memorie. Classe di Scienze Fisiche, Matematiche e Naturali*, vol. 7, pp. 91–140, 1964.

[FIC 72] FICHERA G., "Boundary value problems of elasticity with unilateral constraints", in TRUESDELL C., (ed.), *Mechanics of Solids*, vol. 2, Springer-Verlag, pp. 391–424, 1972.

[FIS 05] FISCHER K.A., WRIGGERS P., "Frictionless 2d contact formulations for finite deformations based on the mortar method", *Computational Mechanics*, vol. 36, pp. 226–244, 2005.

[FIS 06] FISCHER K.A., WRIGGERS P., "Mortar based frictional contact formulation for higher order interpolations using the moving friction cone", *Computer Methods in Applied Mechanics and Engineering*, vol. 195, pp. 5020–5036, John H. Argyris Memorial Issue, Part I, 2006.

[FLE 70] FLETCHER R., "A class of methods in nonlinear programming with termination and convergence properties", in ABADIE J. (ed.), *Integer and Nonlinear Programming*, North-Holland Publishing Company, 1970.

[FLE 77] FLETCHER R., FREEMAN T.L., "A modified Newton method for minimization", *Journal of Optimization Theory and Applications*, vol. 23, Springer, pp. 357–372, 1977.

[FOR 76] FORTIN M., "Minimization of some non-differentiable functionals by the augmented Lagrangian method of Hestenes and Powell", *Applied Mathematics and Optimization*, vol. 2, pp. 236–250, 1976.

[FRA 75] FRANCAVILLA A., ZIENKIEWICZ O.C., "A note on numerical computation of elastic contact problems", *International Journal for Numerical Methods in Engineering*, vol. 9, pp. 913–924, 1975.

[FRI 04] FRITZ A., HÜEBER S., WOHLMUTH B.I., "A comparison of mortar and Nitsche techniques for linear elasticity", *CALCOLO*, vol. 41, pp. 115–137, 2004.

[FUJ 00] FUJUN W., JIANGANG C., ZHENHAN Y., "A contact searching algorithm for contact-impactor problems", *Acta Mechanica Sinica (English series)*, vol. 16, pp. 374–382, 2000.

[FUJ 01] FUJUN W., JIANGANG C., ZHENHAN Y., "FFS contact searching algorithm for dynamic finite element analysis", *International Journal for Numerical Methods in Engineering*, vol. 52, pp. 655–672, 2001.

[GAL 53] GALIN L.A., *Contact Problems is Elasticity*, GosTechTeorIzdat, Moscow, 1953.

[GAL 76] GALIN L.A., *Development of the Contact Theory in USSR*, Nauka, Moscow, 1976.

[GIA 89] GIANNAKOPOULOS A.E., "The return mapping method for the integration of friction constitutive relations", *Computers & Structures*, vol. 32, pp. 157–167, 1989.

[GIB 84] GIBBS J.W., *Elements of Vector Analysis*, New Haven, CT, 1884.

[GIB 60] GIBBS J.W., WILSON E.B., *Vector Analysis: A Textbook for the Use of Students of Mathematics and Physics*, Founded Upon the Lectures of J. Willard Gibbs, Dover, 1960.

[GLO 89] GLOWINSKI R., LE TALLEC P., *Augmented Lagrangians and Operator-Splitting Methods in Nonlinear Mechanics*, SIAM, Philadelphia, 1989.

[GOR 98] GORYACHEVA I.G., *Contact Mechanics in Tribology*, Springer, 1998.

[GOR 01] GORYACHEVA I.G., *Mechanics of Frictional Interaction*, Nauka, Moscow, 2001.

[GOS 06] GOSSELET P., REY C., "Non-overlapping domain decomposition methods in structural mechanics", *Archives of Computational Methods in Engineering*, vol. 13, pp. 515–572, 2006.

[GRI 07] GRIEBEL M., KNAPEK S., ZUMBUSCH G., *Numerical Simulation in Molecular Dynamics*, Springer-Verlag, 2007.

[HAL 85] HALLQUIST J.O., GOUDREAU G.L., BENSON D.J., "Sliding interfaces with contact-impact in large-scale Lagrangian computations", *Computer Methods in Applied Mechanics and Engineering*, vol. 51, no. 1–3, pp. 107–137, 1985.

[HAN 90] HANSSON E., KLARBRING A., "Rigid contact modelled by CAD surface", *Engineering Computations*, vol. 7, pp. 344–348, 1990.

[HAR 09] HARTMANN S., OLIVER J., CANTE J.C., WEYLER R., HERNÁNDEZ J.A., "A contact domain method for large deformation frictional contact problems. Part 2: numerical aspects", *Computer Methods in Applied Mechanics and Engineering*, vol. 198, pp. 2607–2631, 2009.

[HEE 93] HEEGAARD J.-H., CURNIER A., "An augmented Lagrangian method for discrete large-slip contact problems", *International Journal for Numerical Methods in Engineering*, vol. 36, pp. 569–593, 1993.

[HEE 96a] HEEGAARD J.-H., CURNIER A., "Geometric properties of 2D and 3D unilateral large slip contact operators", *Computer Methods in Applied Mechanics and Engineering*, vol. 131, pp. 263–286, 1996.

[HEE 96b] HEEGE A., ALART P., "A frictional contact element for strongly curved contact problems", *International Journal for Numerical Methods in Engineering*, vol. 39, pp. 165–184, 1996.

[HER 82] HERTZ H., "Ueber die Berührung fester elastische Körper", *Journal für die reine und angewandte Mathematik*, vol. 92, pp. 156–171, 1882.

[HES 69] HESTENES M.R., "Survey paper: multipliers and gradient methods", *Journal of Optimization Theory and Applications*, vol. 4, pp. 303–320, 1969.

[HEY 89] HEYLIGER P.R., KRIZ R.D., "Stress intensity factors by enriched mixed finite elements", *International Journal for Numerical Methods in Engineering*, vol. 28, pp. 1461–1473, 1989.

[HUG 77] HUGHES T.R.J., TAYLOR R.L., KANOKNUKULCHAI W., "A finite element method for large displacement contact and impact problems", in BATHE K., ODEN J., WUNDERLICH W., WILSON E. (eds), *Formulations and Computational Algorithms in FE Analysis*, MIT Press, pp. 468–495, 1977.

[JAR 99] JARUSEK J., ECK C., "Dynamic contact problems with small Coulomb friction for viscoelastic bodies; existence of solutions", *Mathematical Models and Methods in Applied Sciences*, vol. 9, pp. 11–34, 1999.

[JEA 95] JEAN M., "Frictional contact in collections of rigid or deformable bodies: numerical simulation of geomaterial motions", *Studies in Applied Mechanics*, vol. 42, pp. 463–486, 1995.

[JOH 94] JOHNSON K.L., *Contact Mechanics*, Cambridge University Press, 1994.

[KAG 47] KAGAN V.F., *Basics of Surface Theory in Tensor Form*, vol. 1, M-L: OGIZ, 1947 [In Russian].

[KAN 48] KANTOROVICH L.V., "Functional analysis and applied mathematics", *Uspehi Matematicheskih Nauk*, vol. 3, pp. 89–185, 1948.

[KIK 88] KIKUCHI N., ODEN J.T., *Contact Problems in Elasticity: A Study of Variational Inequalities and Finite Element Methods*, SIAM, Philadelphia, 1988.

[KLA 79] KLANG M., On interior contact under friction between cylindrical elastic bodies, PhD Thesis, Linköping University, 1979.

[KLA 86] KLARBRING A., "A mathematical programming approach to three-dimensional contact problems with friction", *Computer Methods in Applied Mechanics and Engineering*, vol. 58, pp. 175–200, 1986.

[KLA 88] KLARBRING A., "On discrete and discretized nonlinear elastic structures in unilateral contact (stability, uniqueness and variational principles)", *International Journal of Solids and Structures*, vol. 24, pp. 459–479, 1988.

[KLA 90] KLARBRING A., "Examples of non-uniqueness and non-existence of solutions to quasistatic contact problems with friction", *Ingenieur-Archiv (Archive of Applied Mechanics)*, vol. 60, pp. 529–541, 1990.

[KON 05] KONYUKHOV A., SCHWEIZERHOF K., "Covariant description for frictional contact problems", *Computational Mechanics*, vol. 35, pp. 190–213, 2005.

[KON 06a] KONYUKHOV A., SCHWEIZERHOF K., "On a geometrical approach in contact mechanics", in PFEIFFER F., WRIGGERS P. (eds), *Analysis and Simulation of Contact Problems*, Lecture Notes in Applied and Computational Mechanics, vol. 27, Springer, pp. 23–30, 2006.

[KON 06b] KONYUKHOV A., SCHWEIZERHOF K., "A special focus on 2D formulations for contact problems using a covariant description", *International Journal for Numerical Methods in Engineering*, vol. 66, pp. 1432–1465, 2006.

[KON 07a] KONYUKHOV A., SCHWEIZERHOF K., "On a continuous transfer of history variables for frictional contact problems based on interpretations of covariant derivatives as a parallel translation", in EBERHARD P. (ed.), *IUTAM Symposium on Multiscale Problems in Multibody System Contacts*, IUTAM Bookseries, vol. 1, Springer, pp. 95–101, 2007.

[KON 07b] KONYUKHOV A., SCHWEIZERHOF K., "Symmetrization of various friction models based on an augmented Lagrangian Approach", in WRIGGERS P., NACKENHORST U. (eds), *IUTAM Symposium on Computational Methods in Contact Mechanics*, vol. 3 of IUTAM Bookseries, vol. 3, Springer, pp. 97–111, 2007.

[KON 08] KONYUKHOV A., SCHWEIZERHOF K., "On the solvability of closest point projection procedures in contact analysis: analysis and solution strategy for surfaces of arbitrary geometry", *Computer Methods in Applied Mechanics and Engineering*, vol. 197, pp. 3045–3056, 2008.

[KON 09] KONYUKHOV A., SCHWEIZERHOF K., "Incorporation of contact for high-order finite elements in covariant form", *Computer Methods in Applied Mechanics and Engineering*, vol. 198, pp. 1213–1223, 2009.

[KRS 02] KRSTULOVIĆ-OPARA L., WRIGGERS P., KORELC J., "A C1-continuous formulation for 3D finite deformation frictional contact", *Computational Mechanics*, vol. 29, pp. 27–42, 2002.

[LAU 92] LAURSEN T.A., Formulation and treatment of frictional contact problems using finite elements, PhD Thesis, Department of Mechanical Engineering, Stanford University, 1992.

[LAU 93] LAURSEN T.A., SIMO J.C., "A continuum-based finite element formulation for the implicit solution of multibody, large deformation frictional contact problems", *International Journal for Numerical Methods in Engineering*, vol. 36, pp. 3451–3485, 1993.

[LAU 94] LAURSEN T.A., "The convected description in large deformation frictional contact problems", *International Journal of Solids and Structures*, vol. 31, pp. 669–681, 1994.

[LAU 02] LAURSEN T.A., *Computational Contact and Impact Mechanics: Fundamentals of Modeling Interfacial Phenomena in Nonlinear Finite Element Analysis*, Springer-Verlag, 2002.

[LOU 01] LOUNESTO P., *Clifford Algebras and Spinors*, Cambridge University Press, UK, 2001.

[LUE 03] LUENBERGER D.G., *Linear and Nonlinear Programming*, 2nd ed., Kluwer Academic Publishers, 2003.

[LUR 70] LURIE A.I., *Theory of Elasticity*, Nauka, Moscow, 1970.

[MAR 87] MARTINS J.A.C., ODEN J.T., "Existence and uniqueness results for dynamic contact problems with nonlinear normal and friction interface laws", *Nonlinear Analysis, Theory, Methods and Applications*, vol. 11, pp. 407–428, 1987.

[MAR 94] MARTINS J.A.C., MONTEIRO MARQUES M.D.P., GASTALDI F., "On an example of non-existence of solutions to a quasistatic frictional contact problem", *European Journal of Mechanics A/Solids*, vol. 13, pp. 113–133, 1994.

[MCD 00] MCDEVITT T.W., LAURSEN T.A., "A mortar-finite element formulation for frictional contact problems", *International Journal for Numerical Methods in Engineering*, vol. 48, pp. 1525–1547, 2000.

[MEL 96] MELENK J.M., BABUŠKA I., "The partition of unity finite element method: basic theory and applications", *Computer Methods in Applied Mechanics and Engineering*, vol. 139, pp. 289–314, 1996.

[MIC 78] MICHALOWSKI R., MRÓZ Z., "Associated and non-associated sliding rules in contact friction problems", *Archives of Mechanics*, vol. 30, pp. 259–276, 1978.

[MID 85] MIDDLETON J., PANDE G. (eds), *Penalty and Augmented Lagrangian Formulation for Contact Problems*, Elsevier, 1985.

[MIJ 00] MIJAR A.R., ARORA J.S., "Review of formulations for elastostatic frictional contact problems", *Structural and Multidisciplinary Optimization*, vol. 20, pp. 167–189, Springer, 2000.

[MIJ 04a] MIJAR A.R., ARORA J.S., "An augmented Lagrangian optimization method for contact analysis problems, 1: formulation and algorithm", *Structural and Multidisciplinary Optimization*, vol. 28, pp. 99–112, 2004.

[MIJ 04b] MIJAR A.R., ARORA J.S., "An augmented Lagrangian optimization method for contact analysis problems, 2: numerical evaluation", *Structural and Multidisciplinary Optimization*, vol. 28, pp. 113–126, 2004.

[MOË 99] MOËS N., DOLBOW J., BELYTSCHKO T., "A finite element method for crack growth without remeshing", *International Journal for Numerical Methods in Engineering*, vol. 46, pp. 131–150, 1999.

[MUR 88] MURTY K.G., *Linear Complementarity, Linear and Nonlinear Programming*, Helderman-Verlag, 1988. Available at http://ioe.engin.umich.edu/people/fac/books/murty/linear_complementarity_webbook/.

[MUS 66] MUSKHELISHVILI N.I., *Some Basic Problems in the Mathematical Theory of Elasticity*, 5th ed., Nauka, Moscow, 1966.

[OAT 07] OATIS D., "Getting in touch with ANSYS contact", *The Focus, Journal of Phoenix Analysis and Design Technologies*, no. 58, pp. 1–4, 2007.

[OLD 94] OLDENBURG M., NILSSON L., "The position code algorithm for contact searching", *International Journal for Numerical Methods in Engineering*, vol. 37, pp. 359–386, 1994.

[OLI 09] OLIVER J., HARTMANN S., CANTE J.C., WEYLER R., HERNÁNDEZ J.A., "A contact domain method for large deformation frictional contact problems. Part 1: theoretical basis", *Computer Methods in Applied Mechanics and Engineering*, vol. 198, pp. 2591–2606, 2009.

[OLI 10] OLIVER J., HARTMANN S., CANTE J., WEYLER R., HERNÁNDEZ J., "On a new 3D contact domain method for large deformation contact problems", *Plenary Lecture at IV European Conference on Computational Mechanics*, Congress Centre, France, 16–21 May 2010. Available at http://www.eccm2010.org/cv/pdf/oliver.pdf.

[PAD 01] PADMANABHAN V., LAURSEN T.A., "A framework for development of surface smoothing procedures in large deformation frictional contact analysis", *Finite Elements in Analysis and Design*, vol. 37, pp. 173–198, 2001.

[PAN 85] PANAGIOTOPOULOS P.D., *Inequality Problems in Mechanics, Convex and Nonconvex Energy Functions*, Birkhäuser, 1985.

[PAR 89] PARISCH H., "A consistent tangent stiffness matrix for three-dimensional non-linear contact analysis", *International Journal for Numerical Methods in Engineering*, vol. 28, pp. 1803–1812, 1989.

[PIE 97] PIETRZAK G., Continuum mechanics modelling and augmented Lagrangian formulation of large deformation frictional contact problems, PhD Thesis, École Polytechnique Fédérale de Lausanne, 1997.

[PIE 99] PIETRZAK G., CURNIER A., "Large deformation frictional contact mechanics: continuum formulation and augmented Lagrangian treatment", *Computer Methods in Applied Mechanics and Engineering*, vol. 177, pp. 351–381, 1999.

[POW 69] POWELL M.J.D., "A method for nonlinear constraints in minimization problems", in FLETCHER R. (ed.), *Optimization*, Academic Press, London, pp. 283–298, 1969.

[POW 78] POWELL M.J.D., "Algorithms for nonlinear constraints that use Lagrangian functions", in *Mathematical Programming*, vol. 14, North-Holland Publishing Company, pp. 224–248, 1978.

[PUS 02] PUSO M.A., LAURSEN T.A., "A 3D contact smoothing method using gregory patches", *International Journal for Numerical Methods in Engineering*, vol. 54, pp. 1161–1194, 2002.

[PUS 03] PUSO M.A., LAURSEN T.A., "Mesh tying on curved interfaces in 3D", *Engineering Computations*, vol. 20, pp. 305–319, 2003.

[PUS 04] PUSO M.A., "A 3D mortar method for solid mechanics", *International Journal for Numerical Methods in Engineering*, vol. 59, pp. 315–336, 2004.

[RAB 65] RABINOWICZ E., *Friction and Wear of Materials*, Wiley, 1965.

[RAB 86] RABIER P.J., MARTINS J.A.C., ODEN J.T., CAMPOS L., "Existence and local uniqueness of solutions to contact problems in elasticity with nonlinear friction laws", *International Journal of Engineering Science*, vol. 24, pp. 1755–1768, 1986.

[ROC 70] ROCKAFELLAR R.T., *Convex Analysis*, Princeton University Press, 1970.

[ROC 73a] ROCKAFELLAR R.T., "A dual approach to solving nonlinear programming problems by unconstrained optimization", *Mathematical Programming*, vol. 5, North-Holland Publishing Company, pp. 354–373, 1973.

[ROC 73b] ROCKAFELLAR R.T., "The multiplier method of Hestenes and Powell applied to convex programming", *Journal of Optimization Theory and Applications*, vol. 12, pp. 555–562, 1973.

[ROU 09] ROUSSELIER G., BARLAT F., YOON J.W., "A novel approach for anisotropic hardening modeling. Part I: theory and its application to finite element analysis of deep drawing", *International Journal of Plasticity*, vol. 25, pp. 2383–2409, 2009.

[SIG 33] SIGNORINI A., "Sopra alcune questioni di elastostatica", *Atti della Societa Italiana per Il Progresso delle Scienze*, 1933.

[SIG 59] SIGNORINI A., "Questioni di elasticità non linearizzata e semilinearizzata", *Rendiconti di Mathematica e dell sue Apllicazioni, V. Ser.*, vol. 18, pp. 95–139, 1959.

[SIM 85] SIMO J., WRIGGERS P., TAYLOR R., "A perturbed Lagrangian formulation for the finite element solution of contact problems", *Computer Methods in Applied Mechanics and Engineering*, vol. 50, pp. 163–180, 1985.

[SIM 92] SIMO J.C., LAURSEN T.A., "An augmented Lagrangian treatment of contact problems involving friction", *Computers & Structures*, vol. 42, pp. 97–116, 1992.

[SIM 98] SIMO J.C., HUGHES T. J.R., *Computational Inelasticity*, Springer, 1998.

[SPE 75] SPENCE D.A., "The Hertz contact problem with finite friction", *Journal of Elasticity*, vol. 5, pp. 297–319, 1975.

[TAY 91] TAYLOR R.L., PAPADOPOULOS O., "On a patch test for contact problems in two dimensions", in WRIGGERS P., WAGNER W. (eds), *Nonlinear Computational Mechanics*, Springer, pp. 690–702, 1991.

[TOS 05] TOSELLI A., WIDLUND O., *Domain Decomposition Methods – Algorithms and Theory*, Springer-Verlag, 2005.

[VOR 01] VOROVICH I.I., ALEXANDROV V.M. (eds), *Mechanics of Contact Interactions*, PhysMatLit, Moscow, 2001.

[WEB 90] WEBER G., ANAND L., "Finite deformation constitutive equations, and a time integration procedure for isotropic, hyperelastic viscoplastic solids", *Computer Methods in Applied Mechanics and Engineering*, vol. 79, pp. 173–202, 1990.

[WIE 71] WIERZBICKI A.P., "A penalty function shifting method in constrained static optimization and its convergence properties", *Archiwum Automatyki i Telemechaniki*, vol. 16, pp. 395–416, 1971.

[WIL 64] WILKINS M.L., "Calculation of elastic–plastic flow", *Methods of Computational Physics 3*, Academic Press, New York, NY, 1964.

[WIL 99] WILLIAMS J.R., O'CONNOR R., "Discrete element simulation and the contact problem", *Archives of Computational Methods in Engineering*, vol. 6, pp. 279–304, 1999.

[WOH 01] WOHLMUTH B.I., *Discretization Methods and Iterative Solvers Based on Domain Decomposition*, Springer, 2001.

[WRI 90] WRIGGERS P., VU VAN T., STEIN E., "Finite element formulation of large deformation impact-contact problems with friction", *Computers & Structures*, vol. 37, pp. 319–331, 1990.

[WRI 01] WRIGGERS P., KRSTULOVIĆ-OPARA L., KORELC J., "Smooth C1-interpolations for two-dimensional frictional contact problems", *International Journal for Numerical Methods in Engineering*, vol. 51, pp. 1469–1495, 2001.

[WRI 06] WRIGGERS P., *Computational Contact Mechanics*, 2nd ed., Springer-Verlag, 2006.

[WRI 08] WRIGGERS P., ZAVARISE G., "A formulation for frictionless contact problems using a weak form introduced by Nitsche", *Computational Mechanics*, vol. 41, Springer, pp. 407–420, 2008.

[WRO 94] WRONSKI M., Couplage du contact et du frottement avec la mécanique non linéaire des solides en grandes déformations, PhD Thesis, University of Technology of Compiègne France, 1994.

[YAN 05] YANG B., LAURSEN T.A., MENG X., "Two dimensional mortar contact methods for large deformation frictional sliding", *International Journal for Numerical Methods in Engineering*, vol. 62, pp. 1183–1225, 2005.

[YAN 08a] YANG B., LAURSEN T.A., "A contact searching algorithm including bounding volume trees applied to finite sliding mortar formulations", *Computational Mechanics*, vol. 41, pp. 189–205, 2008.

[YAN 08b] YANG B., LAURSEN T.A., "A large deformation mortar formulation of self contact with finite sliding", *Computer Methods in Applied Mechanics and Engineering*, vol. 197, pp. 756–772, 2008.

[YAS 11a] YASTREBOV V.A., CAILLETAUD G., FEYEL F., "Enrichment of the contact geometry within the finite element method", *Proceedings of 10th National Symposium* in Calculation of Structures, Giens, France, 9–13, May 2011.

[YAS 11b] YASTREBOV V.A., CAILLETAUD G., FEYEL F., "A local contact detection technique for very large contact and self-contact problems: sequential and parallel implementations", in ZAVARISE G., WRIGGERS P. (eds), *Trends in Computational Contact Mechanics*, Lecture Notes in Applied and Computational Mechanics, vol. 58, Springer, pp. 227–251, 2011.

[ZAV 98] ZAVARISE G., WRIGGERS P., "A segment-to-segment contact strategy", *Mathematical and Computer Modelling*, vol. 28, pp. 497–515, 1998.

[ZAV 09a] ZAVARISE G., DE LORENZIS L., "A modified node-to-segment algorithm passing the contact patch test", *International Journal for Numerical Methods in Engineering*, vol. 79, pp. 379–416, 2009.

[ZAV 09b] ZAVARISE G., DE LORENZIS L., "The node-to-segment algorithm for 2D frictionless contact: classical formulation and special cases", *Computer Methods in Applied Mechanics and Engineering*, vol. 198, pp. 3428–3451, 2009.

[ZHI 01] ZHILIN P.A., *Vectors and Second-order Tensors in Three Dimensional Space*, Nestor, Saint-Petersburg, 2001.

[ZHO 88] ZHONG W.X., SUN S.M., "A finite element method for elasto-plastic structure and contact problem by parametric quadratic programming", *International Journal for Numerical Methods in Engineering*, vol. 26, pp. 2723–2738, 1988.

[ZIE 00a] ZIENKIEWICZ O.C., TAYLOR R.L., *The Finite Element Method, Volume 1: The Basis*, 5th ed., Butterworth-Heinemann, 2000.

[ZIE 00b] ZIENKIEWICZ O.C., TAYLOR R.L., *The Finite Element Method, Volume 2: Solid Mechanics*, 5th ed., Butterworth-Heinemann, 2000.

Index

A

Active set, active set strategy, 144, 166-170
Adhesion, adherence, 118
Asperity, 119, 144
Augmented Lagrangian method, 7, 170, 174, 179
  convergence, convergence types, 188, 275-276
  history, 7, 170
  method of multipliers, the multiplier method of Hestenes and Powell, 170
  residual vector, 239, 241
  tangent matrix, 240, 244
  update of the penalty parameter, 263
  Uzawa's algorithm, 8, 171, 173, 174, 188, 203
Axial vector, 302

B, C

Babuška-Brezzi conditions, 4, 222
Cartesian, cylindrical or spherical basis, 110, 124
Closest point
  on curve, 28-30
  on face, 26, 27
Contact
  bilateral, multi-body, 5, 18, 135-136
  complementary condition, 108, 129
  contact pressure, 106, 143
  equivalence of the friction contact to partial Dirichlet-Neumann boundary conditions, 121, 132 (OR, interpretation of frictional constraints)
  equivalence of the normal contact to partial Dirichlet-Neumann boundary conditions, 109, 130 (OR, interpretation of contact constraints)
  Hertz-Signorini-Moreau conditions, 107, 129, 145, 176
  Karush-Kuhn-Tucker conditions, 107
  kinematic constraint, 105
  non-penetration conditions, 125
  potential contact zone, 105
  Signorini's problem, 110, 124
  slip constraint, 112

static constraint, 106
stick constraint, 112
unilateral, 17, 103, 124
Contact discretization
contact domain method, 12, 221
contact element, 9, 45, 73, 216, 217
mortar method, 12, 220
Nitsche method, 12, 220
node-to-node, 4, 10-11, 220
node-to-segment, 4, 10-11, 72, 223
segment-to-segment, 4, 10-11

D

Detection, 9
all-to-all, 73, 76
blind spot, 80 (text+fig), 81
bounding box, 74-75, 78, 79
bucket sort, 84
closest node approach, 75
failure of the closest node approach, 83(fig), 84(remark), 85(fig 3.7+fig 3.8)
for explicit integration, 71
for implicit integration, 72, 75, 167
maximal detection distance (MDD), 75, 76, 86
MDMR, 97, 99-100
neighbouring cells, 90
parallel detection, 97, 264
passing by nodes, 81 (text+fig), 82
proximal volume, 82
SDMR, 97
self-contact, 93-94(text+fig)
spatial/global search , 73
Drucker-Prager yield criterion, 118

E

Einstein summation, 301
Examples
augmented Lagrangian method for a one-dimensional problem, 183
contact detection, 87-89
enriched geometry, 65-68
Lagrange multiplier method for a one-dimensional problem, 164
parallel detection test, 100
penalty method for a one-dimensional problem, 148
rheology of a one-dimensional frictional system on a sinusoidal rigid substrate, 133
rheology of a one-dimensional frictional system, 119
slip and stick paths, 116
tangent matrix and residual vector for a contact problem, 226

F

Finite element method, 212
parent space, 45, 214
shape functions, 44, 213
Friction, 111
analogy with plastic flow, 117, 204
Coulomb's cone, 111, 114, 115, 154
Coulomb's disk, 177
Coulomb's friction, 111, 142, 153, 162, 177, 205
discontinuous slip, 135(fig)
heterogeneous friction, 263-264
microsliding, 144
non-associativity, 111
pure stick, 119
slip state, 112, 156
slip surface, 117, 177, 204
slip-in-stick, 155, 207
stick state, 112, 154
work of friction, 141

G

Gap function, 21, 126
asymmetry of the gap, 16, 127-128

discontinuity of the normal projection, 31
distance functional, 22
gap vector, 128
non-uniqueness of the gap, 16, 28, 29
normal gap, 15, 21, 22, 126, 138
normal projection, 22, 80
shadow gap, 35, 127, 138-139
Geometry
basis and dual basis, 303
continuous description, 15, 17
convective coordinates, convective parameter, 37, 214
covariant and contravariant objects, 304, 307
enriched contact geometry, 51, 64-65
first fundamental surface matrix, 19, 20, 304
invariant objects, 307-308
second fundamental surface matrix, 20
transformation matrix, pushforward transformation matrix and pullback transformation matrix, 306, 317

H, I

Hessian, , 195
Ill-conditioning of the matrix, 17, 86, 196

J, K

Jacobian,106,195
generalized Jacobian, 201
Kantorovich theorem, 195, 198, 202

L, M

Linearly independent vectors, 305
Lipschitz continuity, 193, 195-197
Matrix condition number, 187, 196, 241
Matrix's eigenvalues, 196
Method of Lagrange multipliers, 157
initial guess, 263
Method of partial Dirichlet-Neumann boundary conditions, PDN, 251
active search strategy, 254
Min-max problem, 160, 173
Multi-face contact elements, 91-92, 250-251, 262
Multi-point constraints, 252

N

Newton's method, Newton-Raphson's method, 18, 27, 31, 32, 64, 165, 167, 169, 171, 173, 191-201, 227
generalized Newton method, 173, 200-203
multi-dimensional, 193
one-dimensional, 190
Nodal normal vector, 95-96

P

Partial boundary conditions, 109
Penalty method, 145
linear penalty, 146
nonlinear penalty, 151-152
residual vector, 227, 231
tangent matrix, 228, 235
Plasticity, 117
Polar vector, 302
Primal and dual variables, 171

Q, R

Quasi-potential, 178,
Reference frame , 301
Return mapping algorithm, 205
Roughness, 51, 119

S

S-structures, 20, 327
  invariance of v-vectors , 335
  inverse v-vector, 341
  reduced form , 351, 367-368
  v-scalar, 329
  v-tensors, 330
  v-vector, 330
Shadow projection, 32
Sliding/slip
  relative sliding velocity, 36, 37
  sliding path, 38
Static balance of momentum, 136
Strong form, 2, 136
Subdifferential, Subgradient, 175, 198-200

T

Tangent contact matrix, 227, 228, 230, 237, 242
Tangent stiffness matrix, stiffness matrix, 195, 228
transformation matrix, 308, 319,
  diad, 298, 315
  divergence, 310
  gradient, 310
  Gradient or Hamilton's operator, 309
  Laplace operator or Laplacian, 311
  metric matrix, 304
  rotor, 310
  sub-basis, 312
  sub-gradient (over sub-basis), 313
  tensor, 314, 315
    determinant, 323
    inverse tensor, 324
    projection tensor, 321
    spherical and deviatoric tensors, 322
    symmetric and antisymmetric, 318
    tensor's invariants, 321
    trace of a tensor, 319
    vector invariant of a tensor, 320
  triad, 298
Two-pass technique, 11, 223

V

Variation of geometrical quantities
  normal projection
    first order variation of the normal gap, 38, 47
    first order variation of the surface parameter, 38, 48
    second order variation of the normal gap, 40, 49
    second order variation of the surface parameter, 40, 50
  normal projection for enriched contact geometry
    first order variation of the normal gap, 62
    first order variation of the surface parameter, 62
    second order variation of the normal gap, 63
    second order variation of the surface parameter, 63
  shadow projection, close emitter
    first order variation of the shadow gap, 39
    first order variation of the surface parameter, 40
    second order variation of the shadow gap, 41
    second order variation of the surface parameter, 41
  shadow projection, far emitter
    first order variation of the shadow gap, 39

first order variation of the surface parameter, 39
second order variation of the shadow gap, 41
second order variation of the surface parameter, 41
validation, 42-44
Variational equality, 7, 13, 144
Variational inequalities, 3, 5, 6, 141

W

Weak form, 2, 3, 13, 137